SPATIAL ANALYTICS FOR URBAN LIVEABILITY

Applied methodologies for urban planning and ecological practices

---

School and research area

Architecture and Design Doctorate (ADD) School, Architecture Curricula, Strategies and technologies for sustainability and systemic design, XXXVIIIth Doctorate Cycle

Department of Architecture and Design (DAD), University of Genoa,

Stradone di Sant'Agostino 37, 16124, Genoa, Italy

Candidate

Gabriele Oneto

Doctorate supervision

Adriano Magliocco[1] – Supervisor

Maria Canepa[1], **Anne Mimet**[2], **Katia Perini**[1] – Co-supervisors

1. Department of Architecture and Design, University of Genoa, Italy

2. Laboratoire BiodivAG, University of Angers, France

Università di Genova | DAD DIPARTIMENTO ARCHITETTURA E DESIGN

Abstract

Cities are the established primary human habitats and are projected to increase in both population density and surface extension. The process of continuous urbanization is one of the characteristics of Anthropocene, a geological epoch defined by the impact of human activities in influencing Earth's geology and ecosystems, leading to widespread environmental changes and challenges. Unsustainable urban growth, climate change-induced impacts, and mismanaged urban planning expose cities to increased threats to the liveability conditions of urban habitats, such as increased health risks and reduced living comfort. Although cities are primarily human habitats, the negative effects of Anthropocene influence both human and non-human urban inhabitants. The same negative effects are reflected on the conditions of the built and natural environment that compose urban and peri-urban landscapes, having influenced the cultural identity of cities and driven the development of both ecological conservation practices and urban planning. Thus, cities must deal with the transformation or conservation of the built and natural environment, balancing the needs of liveability of urban inhabitants. In practice, contemporary administrations still face numerous challenges while translating multi-disciplinary directives into effective long-term, locally effective, planning strategies and ecological practices. This includes the difficulty of integrating ecological knowledge, climate adaptation requirements, and socio-economic constraints into coherent planning frameworks. New tools and methodologies that account for the holistic structure of cities and its multiple inhabitants would enable planners and researchers to rethink the implementation and effectiveness of urban planning and ecological practices in light of novel perspectives.

This thesis confronts two of the most influential contemporary threats to urban liveability that influence the built and natural environment, namely the loss of biodiversity and increased urban heat. The thesis presents two different novel methodologies, one for each thematic, that enable the description and comparison of urban landscapes conditions. The goal is to support the implementation and definition of urban planning and ecological practices, by building the methodological and technical backgrounds to develop interactive tools and dashboards or fostering cooperation between researchers and practitioners and facilitate evidence-based decision making.

The outcome of the first methodology is called Cohabscapes (from Co-Habitative landScapes) and consists in a classification of urban landscapes for determining liveability conditions of human and non-human inhabitants, such as plants and animals. This classification is based on geospatial and remote sensing data, and through unsupervised machine learning produces a set of raster layers that gives information on urban form, anthropic imprint, and biophysical conditions. A first version of the methodology was applied on three case studies, i.e. Vienna, Munich, and Genoa,

within the FET H2020 project ECOLOPES. An application with 30 bird species open data showcases the usage of Cohabscapes in retrieving useful patterns for ecological research and biodiversity-informed urban planning. Then, the roadmap to extending Cohabscapes for major European cities is presented, bringing cities comparison at the continental scale. This tool will support the exchange of spatial knowledge and ecological insights within and between cities, providing planners, architects, and ecologists with a shared analytical basis to design and evaluate green urbanism strategies and biodiversity-sensitive interventions, such as Nature-Based Solutions.

The second methodology consists of a site-selection criterion to estimate the most suitable urban areas for introducing mitigation strategies against urban heat islands. This methodology uses opensource satellite, geospatial, and census data, through a combination of morphometric spatial analysis and multicriteria ranking to obtain its results. The methodology was developed within the PRIN project URBAN GENERATION and applied to the case studies of Genoa and Turin. An application of this methodology is presented, by using the site characterization data to generalize the design of green mitigation strategies, such as Nature-Based Solutions, with machine learning techniques. To enable the application, a conversion model is developed to downscale urban data at the building scale, transforming the study into a multiscale problem. This application highlights an effective way to deal with multiscalarity in urban planning, supporting the implementation of known strategies as effective countermeasure to urban heat.

The thesis is conducted in support with the Chair of Terrestrial Ecology, Technical University of Munich, Germany; Laboratoire BioadivAG, University of Angèrs, France; CIMA Foundations, Savona, Italy; contributing in the FET H2020 project ECOLOPES (ECOLOgical building enveloPES; https://ecolopes.org/) and PNRR-PRIN project URBAN GENERATION (https://ecosystemics.eu/research/projects/urban-generation/).

In the long term, the results of this thesis are intended to support the development of integrated planning frameworks, inform policy-making, and guide the design of adaptive, biodiversity-supportive, and climate-resilient urban environments. The methodologies provide replicable, scalable, and transparent approaches that can be expanded, updated, and integrated into future research, digital platforms, and decision-support systems.

Keywords

Geospatial analysis; landscape ecology; climate change adaptation; unsupervised classification; regression analysis

Index and synthesis of contents

INTRODUCTION

PART 1. LIVEABILITY AND THE EFFECTS OF URBAN PLANNING AND ECOLOGICAL PRACTICES

<u>**Chapter 1**. Liveability in urban environments: what threatens who?</u>

Review research chapter. This chapter establishes the thesis's theoretical foundations. Cities, as the dominant human habitat, are expanding rapidly, intensifying environmental pressures of the Anthropocene. Urbanization, climate change, and weak planning threaten liveability for people and ecosystems. The chapter reviews key concepts and policies in sustainable urban development, exposing gaps such as biased decision-making and the lack of harmonized multi-scalar approaches.

<u>**Chapter 2**. Descriptive analytical tools for urban systems</u>

Review research chapter. This chapter reviews the evolution of tools for studying urban systems, from urban morphology to spatial analysis methods such as space syntax, GIS, and contemporary data-driven approaches. Despite progress, spatial analysis still emphasizes built form over ecological dimensions, limiting its capacity to address challenges like biodiversity loss and urban overheating. In response, the thesis introduces two contributions that will be covered in Part 2 and Part 3.

PART 2. URBAN ENVIRONMENT AND BIODIVERSITY LOSS

Chapter 3. A step toward understanding urban habitats for human and non-human inhabitants: the Cohabscapes classification

Experimental research chapter. The concept of "Cohabscapes" introduces an innovative classification system for urban landscapes, aimed at supporting liveability studies and practices for both human and non-human inhabitants, including plants and animals. This classification leverages geospatial and remote sensing data, employing unsupervised machine learning to generate raster layers at high definition that provide insights into urban form, human impact, and biophysical conditions. The methodology presented in this chapter was tested in three case studies, i.e., Vienna, Munich, and Genoa, within the framework of the FET H2020 project ECOLOPES, and applied on bird species data to showcase its usage in deriving useful patterns for biodiversity-sensitive design. This tool facilitates the exchange of knowledge both between and within cities, fostering collaboration between architects and ecologists to promote urban liveability through green urbanism.

Chapter 4. Attaining continental-scale Cohabscapes: the road forward to bringing co-habitative urban landscapes classifications to all European Functional Urban Areas

Experimental research chapter. The previous presented methodology will be expanded to all European Functional Urban Areas, numbering 753 cities different cities. The previous Cohabscapes methodology is used, applying minor modification on the previously developed methodologies. The modifications allow for a more effective classification, from a theoretical perspective (variables used and sub-classifications definition) and technical perspective (clustering effectiveness).

PART 3. URBAN ENVIRONMENT AND OVERHEATING

Chapter 5. Mitigating urban heat risk to improve urban liveability: a site-selection methodology for determining optimal sites for intervention

Experimental research chapter. The rising temperature in cities is another important matter while addressing liveability in cities. Green solutions are known to be an effective countermeasure to urban heat, providing shading shelter and lowering surface heat capacity. This chapter introduces a site-selection framework designed to identify the most suitable urban areas for implementing mitigation strategies against urban heat islands. By combining opensource satellite, geospatial, and census data with morphometric spatial analysis and multicriteria ranking, this approach generates targeted results. The methodology was applied to case studies in Genoa and Turin, as part of the PRIN project Urban Generation. The strength of such methodology is to use computational techniques, and opensource data, to generate accurate and high-resolution vectorial information on urban areas ideal for urban renovation. Moreover, the generated knowledge can be used to generalize findings on the performance of mitigation strategies, such as Nature-Based solutions, and help the spread of green urbanism.

Chapter 6. Downscaling spatial analysis to the streetscape level: obtaining 3D urban canyons from opensource data enhancing multiscale simulations

Experimental research chapter. Urban morphology plays a decisive role in shaping microclimatic conditions and pedestrian comfort. This chapter develops a computational workflow to classify and analyse urban canyons, integrating building geometry, street orientation, and height-to-width ratios. By applying spatial analysis over building geometries, the cases of Genoa and Turin are confronted. The workflow leverages open geospatial datasets and modular helpers to generate interpretable outputs, both raster and tabular. Ultimately, the chapter demonstrates how morphometric diagnostics can guide targeted interventions, supporting sustainable urban design via the downscale of city-wide analysis.

Chapter 7. Morphological optimization of Nature-Based Solutions for heat mitigation

Experimental research chapter. Building on simulated data, this chapter evaluates mitigation strategies through scenario modelling and comparative analysis. Nature-Based Solutions, such as trees, are tested against canyon typologies to assess cooling potential via shading. The methodology combines multicriteria optimization with predictive machine learning, ensuring that interventions are both spatially precise and performance-driven. Genoa and Turin serve again as case studies, illustrating how localized strategies can scale to broader urban contexts. The chapter emphasizes reproducibility and adaptability, ensuring that findings can be generalized across Italian cities.

PART 4. CONCLUSIONS

Chapter 8. Synthesis of the contribution and take-away highlights

Concluding chapter. Urban planning and ecological practices can shape cities in a positive way, driving humanity in the coming decades in a sustainable approach. The description of built and natural environments presented in this research thesis acknowledged the potential and responsibility of researchers and practitioners to act. By providing both with tools and methodologies to extract knowledge on cities, liveability for all urban inhabitants can foster through sustainable urban development. In this chapter, the primary outcomes of the thesis are summarised and confronted in relation to the research objectives, together with the methodological and conceptual innovations and possibilities for future developments.

PART 5. RESEARCH DATA AND SUPPORTING INFORMATION

Data availability

Annex A (Chapter 3) – Variable tables, methodologies, and data origin

Annex B (Chapter 3) – Principal Component Analysis (PCA) for the four layers

Annex C (Chapter 3) – Unsupervised Classification scores

Annex D (Chapter 3) – Clusters definitions

Annex E (Chapter 3) – External validations, contingency matrixes

Annex F (Chapter 3) – Birds species data in-depth analysis

Annex G (Chapter 5) – SUHI analysis for remote sensing data

Annex H (Chapter 5) – Correlation analysis for MCDM-derived risk

Annex I (Chapter 5) – Cluster analysis (k value)

Annex J (Chapter 5) – Cluster analysis (cluster content)

Annex K (Chapter 7) – Optimization and ML algorithms comparison

INTRODUCTION

Research objectives

Premise

Cities have become the primary socio-ecological systems of the Anthropocene, where most demographic expansion, land-use intensification, and climate-driven pressures converge. (IPCC, 2022). These pressures amplify ecological and climatic stresses, including biodiversity loss, habitat fragmentation, and the intensification of urban heat, trends widely documented in urban ecology and climate science (Alberti et al., 2023; Elmqvist et al., 2019; IPCC, 2022). Yet despite the urgency of these challenges, contemporary planning systems remain constrained by analytical, institutional, and methodological limitations that prevent ecological and climatic knowledge from being translated into operational decision-making (Frantzeskaki et al., 2024; Pickett et al., 2016).

A central problem identified across the main body of the thesis is the lack of harmonized, scalable, and reproducible analytical tools capable of integrating ecological, climatic, and morphological information across cities. Existing planning instruments rely on heterogeneous datasets, such as cadastral layers, local ecological inventories, Urban Atlas, CORINE, and ad-hoc surveys, each with different resolutions, classifications, and update cycles (European Environment Agency, 2021; Zhu et al., 2020). This heterogeneity greatly prevents cross-city comparison, undermines evidence-based prioritization, and limits the capacity of planners to diagnose ecological degradation or anticipate climate-related risks (McPhearson et al., 2022). As a result, biodiversity considerations remain peripheral in zoning and development control, while climate adaptation strategies often lack spatial precision and fail to account for microclimatic performance (Kabisch et al., 2017; Santamouris, 2015).

These limitations are compounded by methodological fragmentation. Urban morphology research has produced powerful descriptors of built form (e.g., LCZ, morphometric indicators), but these are rarely integrated with ecological indicators or climatic variables (Stewart, 2024; Zhu et al., 2020). Remote sensing and machine learning have advanced rapidly, yet their outputs often remain confined to academic contexts due to computational rigidity, including lack of technical transparency such as insufficient documentation or low methodological flexibility (Zhang & Hu, 2025; Liu et al., 2022). Ecological assessments, meanwhile, are frequently site-specific and non-standardized, making them difficult to scale or integrate into planning workflows (Szulkin et al., 2020). This fragmentation mirrors what the thesis describes as "the difficulty of translating multidisciplinary knowledge into operational planning tools and the absence of harmonized, scalable approaches for comparing urban conditions across cities".

The consequences are visible across European cities:

i. Biodiversity indicators are inconsistently mapped and rarely linked to morphological conditions (Khorrami et al., 2020).

ii. Urban heat assessments rely on coarse-resolution thermal imagery that cannot inform design-level interventions (Zhang & Gu, 2025).

iii. Nature-Based Solutions, i.e. ecologically informed designs that emulate natural physiologies and mechanisms, are deployed without robust evidence of their performance across different canyon typologies (Santamouris, 2015).

iv. Planning authorities lack reproducible workflows that can be adapted to local contexts while remaining comparable across regions (Acuto et al., 2018).

The main contributions of the thesis, i.e. Chapters 3-7, demonstrate that these analytical gaps directly translate into policy failures, or fallacies. Without harmonized classifications, planners cannot identify which urban conditions support multispecies liveability. Without multiscale heat-risk diagnostics, municipalities cannot prioritize interventions or evaluate the performance of mitigation strategies. Without reproducible workflows, ecological and climatic evidence cannot be institutionalized within planning instruments, limiting the long-term impact of sustainability policies.

To guide the reader, the thesis is structured in five complementary parts. Chapters 1 and 2 (Part I) establish the conceptual and analytical foundations. Topics such as the Anthropocene framing, the limitations of contemporary planning, and the role of morphology, ecology, and climate in shaping urban liveability are introduced and augmented from multiple perspectives. Chapters 3–7 form the experimental core, each organized with by introduction–method–results–discussion sections.

Chapters 3–4 (Part II) develop and validate a novel biodiversity-sensitive classification with examples of application, while Chapters 5–7 (Part III) introduce and test a novel multiscale heat-mitigation site-selection and performance-assessment framework.

Chapter 8 (Part IV) synthesizes the findings, articulating their implications for governance, research, planning, and design, and outlining pathways for institutional adoption and future development.

Finally, the Annexes A-K (Part V) corroborate the findings of the thesis with detailed analytical and conceptual information. The online complementary documentation includes detailed and comment Jupyter notebook, together with custom libraries and virtual environments information to facilitate the verification and reproduction of the results.

This thesis positions itself within this systemic problem by arguing that sustainable urban transformation requires open, harmonized, and scalable methodologies that integrate morphology, ecology, and climate into a unified analytical framework. The development of the novel methodologies responds directly to this need, offering tools designed not only for scientific robustness but also for institutional uptake, cross-city comparability, and long-term reproducibility.

Aim and objectives

The overarching aim of this thesis is to develop, validate, and operationalize harmonized, scalable, and reproducible spatial-analytical methodologies that integrate urban morphology, ecological conditions, and climatic processes to support biodiversity-sensitive planning and targeted heat-mitigation interventions. This aim responds directly to the systemic limitations identified in contemporary planning practice, namely the fragmentation of data sources, the lack of cross-city comparability, and the difficulty of translating ecological and climatic knowledge into actionable planning tools (Elmqvist et al., 2019; McPhearson et al., 2022; IPCC, 2022). By grounding the methodological development in open data, transparent workflows, and multiscale analytical logic, the thesis seeks to bridge the persistent gap between scientific evidence and planning implementation (Frantzeskaki et al., 2024; Acuto et al., 2018).

Notably the focus of the thesis is not to appeal to only technical readers and emphasize the computational aspects of the work. Rather, the methodologies come from tangible gaps and are discussed in light of needs and application of researchers and practitioners that operate in urban areas.

The thesis strives to achieve its aim by addressing six objectives:

i. <u>Critically examine how planning systems address ecological sustainability and liveability in the Anthropocene. *(Ch. 1)*</u>

This objective synthesizes the theoretical, policy, and empirical literature on urban sustainability, biodiversity decline, and climate-related risks, with particular attention to the structural limitations of planning systems (Pickett et al., 2016; Kabisch et al., 2017). It examines how governance fragmentation, sectoral silos, and inconsistent data infrastructures hinder the integration of ecological and climatic evidence into planning instruments, and how the Anthropocene framing reshapes expectations for anticipatory, multispecies, and evidence-driven planning (Alberti et al., 2020; Elmqvist et al., 2019). Urban planning can integrate ecological sustainability and liveability in the Anthropocene, through a state-of-the-art review highlighting the strength and weakness of contemporary urban development practices.

ii. <u>Investigate how urban morphology and spatial analytical techniques can generate integrative, quantifiable insights into urban form. *(Ch. 2)*</u>

This objective evaluates the capacity of morphological descriptors, including Local Climate Zones, morphometric indicators, and landscape metrics, to capture the spatial structure of cities in ways that are relevant for ecological and climatic processes (Stewart, 2024; Zhu et al., 2020). It identifies the limitations of existing classification systems, particularly their lack of harmonization and limited ecological sensitivity, and explores opportunities for integrating morphology with biodiversity and microclimatic indicators (Zhu et al., 2020; Khorrami et al., 2020).

iii. <u>Define, validate, and test a novel methodology for biodiversity-sensitive urban landscapes classification *(Ch. 3,4)*</u>

This objective develops a harmonized, machine-learning-based classification framework that integrates morphological, ecological, and biophysical variables to describe urban landscape conditions relevant to biodiversity. Validation uses species-occurrence data, citizen-science datasets, and cross-city comparisons, demonstrating the framework's capacity to capture gradients of habitat quality and multispecies liveability (Szulkin et al., 2020; Alberti et al., 2023). The workflow emphasizes reproducibility and scalability, enabling application across European cities with heterogeneous data infrastructures (European Environment Agency, 2021).

iv. Develop and validate a multiscale methodology for selecting and evaluating Nature-Based Solutions for heat mitigation. *(Ch. 5-7)*

This objective integrates thermal remote sensing, morphometric analysis, and multicriteria decision methods to identify priority sites for heat-mitigation interventions. It includes a downscaling framework that translates city-level indicators into street- and building-scale guidance (Oleson et al., 2013; Santamouris, 2015). Machine-learning models predict the performance of Nature-Based Solutions across different canyon typologies, addressing the current lack of evidence-based guidance for microclimatic design (Santamouris et al., 2015; Liu et al., 2023).

methodology capable of selecting the most suitable conditions for lessening urban heat-related risk through the implementation of Nature-Based mitigation measures, including the implementation of multiscale tools and predictive models to assess the performance of such measures.

v. Bridge research and practice by producing and contextualizing tools and workflows. *(Ch. 3-7, synthesized in Ch. 8)*

This objective ensures that the methodologies developed in the thesis are not only scientifically robust but also institutionally actionable. It includes the creation of reproducible workflows, open datasets, and decision-support materials that can be integrated into planning processes. The thesis evaluates governance implications and identifies pathways for embedding biodiversity-sensitive and climate-aware tools into planning regulations, monitoring frameworks, and design guidelines (Frantzeskaki et al., 2024; Acuto et al., 2018).

vi. Assess transferability, limitations, and future directions for the conceptual assumptions and developed methodologies. *(Ch. 8)*

This objective synthesizes the theoretical and empirical findings to evaluate their applicability across different morphological, climatic, and governance contexts. It identifies limitations, proposes improvements, and outlines a research agenda for scaling harmonized ecological-climatic tools to continental monitoring systems and long-term planning instruments (IPCC, 2022; McPhearson et al., 2022).

References

Acuto, M., Parnell, S., & Seto, K. C. (2018). Building a global urban science. *Nature Sustainability, 1*(1), 2–4. https://doi.org/10.1038/s41893-017-0013-9

Alberti, M. (2023). Cities of the Anthropocene: Urban sustainability in an eco-evolutionary perspective. *Philosophical Transactions of the Royal Society B: Biological Sciences, 378*(1883), 20220264. https://doi.org/10.1098/rstb.2022.0264

Alberti, M., Palkovacs, E. P., Des Roches, S., De Meester, L., Brans, K. I., Govaert, L., Grimm, N. B., Harris, N. C., Hendry, A. P., Schell, C. J., Szulkin, M., Munshi-South, J., Urban, M. C., & Verrelli, B. C. (2020). The complexity of urban eco-evolutionary dynamics. *BioScience, 70*(9), 772–793. https://doi.org/10.1093/biosci/biaa079

European Environment Agency (2021). Urban Atlas Land Cover/Land Use 2018 (vector), Europe, 6-yearly, Jul. 2021 [Dataset]. https://doi.org/10.2909/fb4dffa1-6ceb-4cc0-8372-1ed354c285e6

Khorrami, Z., Ye, T., Sadatmoosavi, A., Mirzaee, M., Fadakar Davarani, M. M., & Khanjani, N. (2020). "The indicators and methods used for measuring urban liveability: a scoping review" Reviews on Environmental Health, vol. 36, no. 3, pp. 397-441. https://doi.org/10.1515/reveh-2020-0097

McPhearson, T., Cook, E. M., Berbés-Blázquez, M., Cheng, C., Grimm, N. B., Andersson, E., Barbosa, O., Chandler, D. G., Chang, H., Chester, M. V., Childers, D. L., Elser, S. R., Frantzeskaki, N., Grabowski, Z., Groffman, P., Hale, R. L., Iwaniec, D. M., Kabisch, N., Kennedy, C., … Troxler, T. G. (2022). A social-ecological-technological systems framework for urban ecosystem services. One Earth, 5(5), 505–518. https://doi.org/10.1016/j.oneear.2022.04.007

Oleson, K. W., Monaghan, A., Wilhelmi, O., Barlage, M., Brunsell, N., Feddema, J., Hu, L., & Steinhoff, D. F. (2013). Interactions between urbanization, heat stress, and climate change. *Climatic Change, 129*(3–4), 525–541. https://doi.org/10.1007/s10584-013-0936-8

Santamouris, M. (2015). Analyzing the heat island magnitude and characteristics in one hundred Asian and Australian cities and regions. *Science of the Total Environment, 512–513*, 582–598. https://doi.org/10.1016/j.scitotenv.2015.01.060

Stewart, I. D. (2024). Origins and Evolution of the Local Climate Zone Classification. In R. Wang, M. Cai, C. Ren, & Y. Shi (Eds.), *Local Climate Zone Application in Sustainable Urban Development: Experience from East and Southeast Asian High-Density Cities* (pp. 19–33). Springer International Publishing. https://doi.org/10.1007/978-3-031-56168-9_2

Zhang, J., & Gu, X. (2025). Multi-stakeholder perspectives on urban regeneration: A spatial gradient analysis of heat and pollution effects. International Journal of Biometeorology, 69, 1325–1345. https://doi.org/10.1007/s00484-025-02894-8

Elmqvist, T., Andersson, E., Frantzeskaki, N., McPhearson, T., Olsson, P., Gaffney, O., Takeuchi, K., & Folke, C. (2019). Sustainability and resilience for transformation in the urban century. *Nature Sustainability, 2*(4), 267–273. https://doi.org/10.1038/s41893-019-0250-1

Frantzeskaki, N., Childers, D. L., Pickett, S. T. A., Hoover, F.-A., Anderson, P., Barau, A., Ginsberg, J., Grove, M., Lodder, M., Lugo, A. E., McPhearson, T., Muñoz-Erickson, T. A., Quartier, M., Schepers, S., Sharifi, A., & van de Sijpe, K. (2024). *A transformative shift in urban ecology toward a more active and relevant future for the field and for cities*. Ambio, 53(5), 871–889. https://doi.org/10.1007/s13280-024-01992-y

Pickett, S. T. A., Cadenasso, M. L., Childers, D. L., McDonnell, M. J., & Zhou, W. (2016). Evolution and future of urban ecological science: Ecology in, of, and for the city. *Ecosystem Health and Sustainability, 2*(8), e01229. https://doi.org/10.1002/ehs2.1229

Kabisch, N., Korn, H., Stadler, J., & Bonn, A. (2017). Nature-based solutions to climate change adaptation in urban areas: Linkages between science, policy and practice. Springer. https://doi.org/10.1007/978-3-319-56091-5

Zhang, J., & Gu, X. (2025). Multi-stakeholder perspectives on urban regeneration: A spatial gradient analysis of heat and pollution effects. International Journal of Biometeorology, 69, 1325–1345. https://doi.org/10.1007/s00484-025-02894-8

Liu, Y., Chen, J., Wu, J., & Xu, C. (2022). Urban form, air pollution exposure, and health: A review of the

literature. Environment International, 163, 107236.
https://doi.org/10.1016/j.envint.2022.107236

Zhu, X. X., Hu, J., Qiu, C., Shi, Y., Kang, J., Mou, L., Bagheri, H., Häberle, M., Hua, Y., & al. (2020). So2Sat LCZ42: A benchmark dataset for global local climate zones classification. IEEE Geoscience and Remote Sensing Magazine, 8(3), 76–89.
https://doi.org/10.1109/MGRS.2020.2964708

Overall research methodology

The research is structured in three parts (Fig. 1). The first part covers a general literature review on cities and spatial analytical techniques, focused on identifying what problems affect cities and how can descriptive knowledge to solve those problems can be extracted. This section lays the conceptual foundation for the thesis, exploring the notion of multispecies liveability and reviewing existing frameworks that address urban sustainability in the Anthropocene. It also examines the evolution of spatial analysis, from urban morphology to GIS-based and data-driven approaches, highlighting methodological innovations and persistent gaps. These include the underrepresentation of ecological processes, limited flexibility of existing models, and the lack of harmonized tools for cross-scale comparison.

The second and third parts are experimental sections, each focusing on a different thematic: biodiversity loss and overheating in cities. These two threats are treated as critical dimensions of urban liveability, each requiring tailored analytical approaches and planning responses. In each part, a novel methodology is developed and applied, highlighting opportunities for sustainable development from different data sources and analytical methods.

Part II introduces the Cohabscapes framework, a geospatial and machine learning methodology for classifying urban landscapes based on multispecies liveability. It is applied to three European cities—Vienna, Munich, and Genoa—and extended to the scale of European Functional Urban Areas. The classification supports ecological research and biodiversity-informed planning by integrating remote sensing data, unsupervised clustering, and species richness datasets.

Part III presents a site-selection methodology for mitigating urban overheating through Nature-Based Solutions. It combines morphometric spatial analysis, multicriteria ranking, and predictive modelling to identify suitable intervention areas. The methodology is applied to Genoa and Turin and further refined through a conversion model that downscales city-level data to the urban canyon scale. A final step uses simulated data to derive predictive insights on the performance of mitigation strategies, tested across six Italian cities.

Together, the three parts form a coherent arc, from conceptual framing and review (Part I) to thematic exploration and tool development (Parts II and III). The research integrates ecological and climatic dimensions into spatial analysis, offering scalable, transferable methodologies that support planning, design, and policy aimed at improving urban liveability for both human and nonhuman inhabitants.

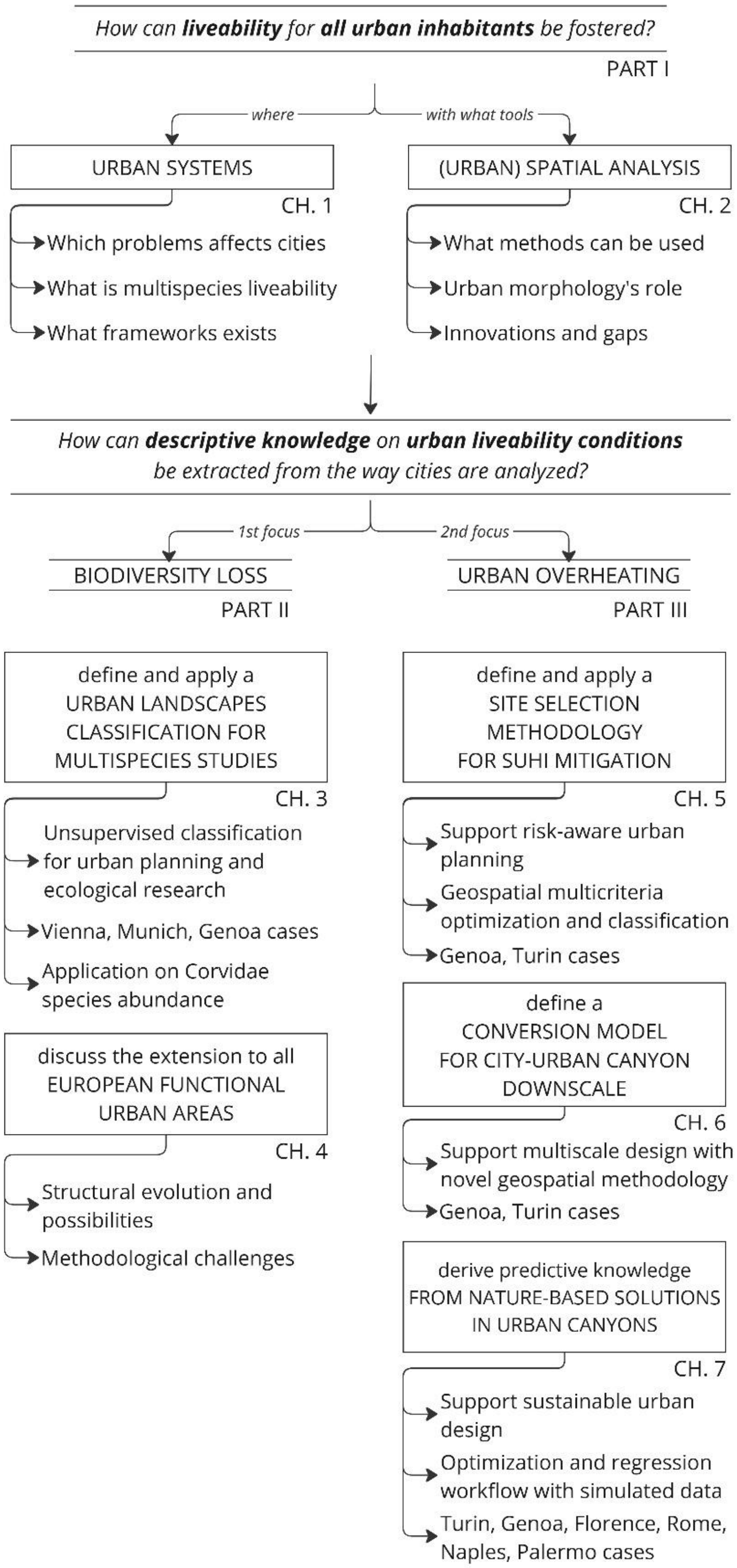

Figure 1. Overall research methodology.

Research partnerships and collaborations throughout the Ph.D.

Through the research, two significant partnerships were achieved to satisfy the requirements of the Scholarship. Specifically, the partnerships were with the Chair of Terrestrial Ecology, Technical University of Munich, Germany, and CIMA Foundation, Savona, Italy.

Visiting Ph.D. student enrolment at Technical University of Munich

The activity at the Technical University of Munich (TUM) was conducted in collaboration with Prof. Wolfgang W. Weisser, Head of the Chair of Terrestrial Ecology, Freising, Germany. In his unit, the research developed methodologies concerning landscape ecology, focusing on analytical and computational side as well as the theoretical background on biodiversity in cities. Through this period, a mentoring with Prof. Anne Mimet (now Laboratoire BioadivAG, University of Angers) was initiated, and following the role evolved into co-tutoring for the present research. Notably, during the visiting period, the usage of High-Performance Computing (HPC) at the Leipzig Research Centre was explored, whose computing capabilities enabled the realization of a portion of the results of the thesis.

The visiting period was conducted in parallel with the collaboration in the FET H2020 project ECOLOPES (ECOLOgical building enveloPES; https://ecolopes.org/). The collaboration in the project reflects the connection between urban planning and applied ecology in Part 2.

Internship at CIMA Foundation

The activity at CIMA Foundation followed the visiting period at TUM, and confronted thematics related to urban overheating. The internship revolved around the PNRR-PRIN URBAN GENERATION project (https://ecosystemics.eu/research/projects/urban-generation/), focusing on the risk assessment and design of mitigation solutions to urban heat. To this end, the internship confronted with the unit specializing in risk and vulnerability assessment (Filippo Fraschini, Ph.D., and Chiara Franciosi, Ph.D.), together with experts in remote sensing and satellite-image processing (Luca Cenci, Ph.D., and Luca Pulvirenti, Ph.D.). The results of the collaboration are contained in Part 3.

Use of generative AI

This paragraph expresses how and in which form generative AI was used in this Ph.D. research thesis.

Microsoft Copilot (GPT-5) was employed exclusively during the revision phase to improve clarity, restructure selected passages, and correct grammar. The scientific content, methodologies, datasets, libraries, and interactive notebooks are entirely authored by the candidate, and all outputs are available for consultation and usage according to the open science requirements of the Ph.D. funding. No images were produced nor modified using generative AI, and AI tools were not involved in the design, execution, or interpretation of the research.

PART 1.

Liveability and the effects of urban planning and ecological practices

Chapter 1.

Liveability in urban environments: what threatens who?

Abstract

This chapter establishes the theoretical foundations of the thesis by examining urban liveability within the context of the Anthropocene and contemporary urbanization. Cities, now the dominant human habitat, continue to expand and intensify pressures on both built and natural environments, generating challenges such as environmental degradation, climate induced hazards, rising temperatures, and biodiversity loss. The chapter frames cities as complex socioecological systems and analyses how these interlinked threats affect humans and nonhuman species alike.

Liveability is introduced and discussed through a multidimensional lens, distinguishing the needs of human populations from the ecological requirements of plants and animals. Patterns of habitat fragmentation, pollution, overheating, and uneven access to resources reveal how urban conditions simultaneously undermine human wellbeing and ecological functioning. The chapter broadens the conventional humancentric definition of liveability by emphasizing the interdependency between species and the ecological processes that sustain urban habitats.

The chapter concludes by reviewing the major international frameworks guiding urban planning and ecological governance. While these frameworks promote sustainability and resilience, persistent gaps (such as weak implementation, skewed perspectives, low flexibility, and lack of harmonization) limit their effectiveness. These shortcomings motivate the thesis's central research question:

How can descriptive knowledge on urban liveability conditions be extracted from the way cities are analysed?

Keywords

urban systems; liveability; sustainable development

1.1. The urban system and its complexity

1.1.1. The urban system

An urban system is a dynamic and interconnected network of people, infrastructure, institutions, and natural environments that collectively shape the functioning and development of cities. At its core, an urban system encompasses human activities, such as economic exchanges, social interactions, and governance, which drive urban growth and transformation over time. The built environment, including transportation networks, residential and commercial structures, and public spaces, interacts with natural features like waterways, vegetation, and climate conditions, creating a complex and evolving spatial organization (Abujder Ochoa et al., 2023). Urban systems are not static; they respond to demographic shifts, technological advancements, policy decisions, and environmental constraints, often exhibiting emergent properties such as socioeconomic stratification, spatial clustering, and adaptive resilience. Understanding the urban system requires a multidisciplinary approach, integrating insights from urban planning, geography, sociology, economics, and environmental science, ensuring cities remain functional, sustainable, and responsive to the needs of their inhabitants (Diemer, 2019).

1.1.2. Complexity in urban systems: time, content, way of behaviour

Complexity refers to the intricate, interdependent nature of systems composed of multiple interacting elements, often exhibiting unpredictable or emergent behaviours (Campbell, Eckerd, & Kim, 2024). Urban systems are inherently complex due to their continuous evolution, diverse components, and the intricate relationships governing their behaviour (Rybski, 2025). Over time, cities expand and transform in response to population growth, economic shifts, technological advancements, and environmental conditions. This temporal dimension is evident in patterns of urbanization, infrastructural development, and socio-spatial restructuring. At their core, urban systems encompass a wide range of elements, including human inhabitants, built environments such as architecture and transportation networks, and natural features like green spaces and waterways. These elements interact in multifaceted ways, giving rise to emergent properties such as economic clustering, migration flows, and land-use dynamics. The correlations between urban features shape behavioural patterns (Wang Yue Dong, 2023). For example, public transportation networks influence mobility choices, socioeconomic disparities impact access to resources, and environmental policies affect sustainability outcomes. Cities exhibit nonlinear and adaptive characteristics, meaning that small interventions can trigger far-reaching consequences, often hard to predict and evaluate in full. The work of architects and practitioners that act in fostering resilient and sustainable urban development must recognize this complexity and carefully approach the topic by steps (UN-Habitat, 2024).

1.1.3. Cities as the primary human habitats

First and foremost, cities are a human phenomenon. Humans built cities as a response to the need for organization, security, and efficiency in sustaining larger populations and advancing civilization. The history of the early settlement is rooted in this functionalist approach. In all recognised cradles of human civilization (the Fertile Crescent, China, and Mesoamerica), the first large settlements emerged near vital resources such as water, fertile land, and later along trade routes, allowing communities to develop agriculture, commerce, and governance structures (Diamond, 2005). As societies expanded, cities became centres of economic activity, cultural exchange, and technological innovation, fostering specialization and collaboration among individuals. Urban environments provided protection through fortified structures and enabled the coordination of administrative, political, and social institutions. Over time, cities evolved into complex systems, integrating infrastructure, transportation, and communication networks to support the diverse needs of inhabitants. To this day, it can be said that cities serve as the primary human habitat due to their concentration of resources, economic opportunities, and social infrastructures that support diverse populations (Espey et al., 2024). In fact, urban areas facilitate human interaction, innovation, and cultural exchange, fostering environments where individuals can access employment, education, healthcare, and essential services. The built environment, including transportation networks, residential structures, and commercial spaces, enhances efficiency and connectivity, enabling societies to function at larger scales. Furthermore, cities exhibit adaptive and self-organizing characteristics, often responding to human influence and needs, such as demographic and economic growth, and technological advancements through urban planning and governance mechanisms. While rural areas continue to play vital roles, cities accommodate most of the global population, shaping contemporary human experiences and societal development. The dynamic interplay between physical infrastructure, socioeconomic structures, and environmental considerations underscores the complexity of urban systems, reinforcing their status as the dominant human habitat (Acuto et al., 2018).

1.1.4. Cities are projected to grow

Cities are projected to experience significant growth in both spatial extent and in functional density (UN Department of Economic and Social Affairs, 2024). Both consequences are due to what is commonly referred to as urbanization. Urbanization refers to the process by which population in cities increases, as well as urban infrastructure, resulting in the growth and densification of urban environments. This growth is especially visible in developing regions, where rising populations demand more housing, services, and infrastructure (Myers, 2021). Economic factors also play a role: cities continue to attract people with opportunities for work, education, and innovation. At the same time, advances in transport, communication, and sustainability help cities adapt to new pressures, some seen as progress, others as challenges. The result is a complex mix of opportunities and problems, such as the urgent need for quality housing and inclusive planning. For local governments and urban practitioners, the challenge lies in managing this growth wisely making decisions that not only respond to immediate needs but also improve long-term wellbeing (Wang et al., 2021).

1.1.5. Anthropocene and cities

The continuous process of decision-making shape human societies and environments, influencing how resources are distributed, how people are threated, and how ecological functions are influenced. This chain of processes and choices is closely linked to Anthropocene, the proposed epoch characterized by humanity's significant impact on Earth's systems. Anthropocene is a proposed geological epoch marking the period when human activities have become the primary force influencing Earth's ecosystems, climate, and geological processes. Unlike past epochs shaped by natural forces, this era highlights humanity's capacity to modify landscapes, biodiversity, and atmospheric conditions (Steffen et al., 2020). Urbanization exemplifies Anthropocene's defining features, as human activities within cities (and more than often, outside cities) drive land-use change, biodiversity loss, pollution, and climate change. The great concentration of populations and industries within urban areas amplifies all the aforementioned phenomena, effecting people lives (Elmqvist et al., 2019). Humans, like other species, actively shape their habitat through continuous interaction with their environment, creating complex ecological relationships that influence both natural and built landscapes. Urbanization represents this dynamic, as cities emerge in response to human needs within defined spatial boundaries. Through modification on cities, urbanization generates feedback loops, where environmental changes, such as rising temperatures, biodiversity loss, and pollution, further influence urban development strategies and societal behaviours (McPhearson et al., 2022). The action of humans in cities have consequences outside of the conventional urban spatial boundaries. In fact, the theory of Anthropocene expresses that human influence extends beyond localized spaces, contributing to planetary-scale transformations such as climate change and ecological shifts. Recognizing this correlation of scale is essential for advancing sustainable approaches to urban planning, ensuring that human habitats can support the future lives of humans (Bai et al., 2018).

1.1.6. Challenges for humans in cities

Anthropocene brings forth several challenges for humans to face, if they want to preserve life in cities as the habitats they are accustomed to (Table 1). Some challenges confront urban degradation, caused by unsustainable land use and active human activity, such as environmental degradation, deforestation, greenhouse gas emissions and water acidification. Other challenges consider effects of the shifting urban climate, such as extreme weather events and rising temperatures. Finally, challenges such as sea level rise are often not caused by urban activity but expose cities to risk to human life.

Table 1. Primary challenges for human's wellbeing in cities.

Challenges drivers...	**...and causal dynamics**	**References**
Environmental degradation arises from the intensive interplay between human activities and natural systems. Urbanization, industrial operations, and escalating resource consumption compromise the integrity of air, water, and soil. The rapid expansion of built environments fragments habitats and disrupts local ecosystems, while vehicular emissions, industrial discharges, and inadequate waste management introduce persistent pollutants.	These processes generate cascading effects that undermine ecological resilience and human wellbeing. Chemical contamination accumulates in soils and waters, weakening ecosystem services and public health. The urban heat island effect amplifies local climatic extremes, further stressing vegetation and biodiversity, and reinforcing feedback loops that intensify environmental stress in cities.	Elmqvist et al., 2019; Bai et al., 2018
Deforestation is connected to the demand for land, construction materials, and agricultural products intensifies, often leading to the conversion of forested areas into built environments or agricultural lands. This transformative land-use change disrupts carbon sequestration processes, compromises biodiversity, and destabilizes local water cycles, thereby exacerbating climatic extremes and undermining ecological resilience.	The ripple effects of deforestation extend to urban habitats, where reduced green space diminishes natural cooling effects and increases vulnerability to air pollution and urban heat islands. Moreover, the loss of forests limits the natural regulation of hydrological and atmospheric systems, worsening flooding or drought conditions that directly impact urban infrastructure and public health.	Foley et al., 2005; Hansen et al., 2013
In cities, **greenhouse gas emissions** stem from concentrated human activities such as industrial production, transportation, and intensive energy use. These processes release large volumes of carbon dioxide, methane, and other gases, which accumulate in the atmosphere and intensify both global climate change and local heat island effects.	The interaction of emissions with urban form creates complex feedbacks. Infrastructure layout, uneven energy consumption, and socioeconomic disparities shape how emissions are produced and managed. These dynamics strain energy systems, alter microclimates, and complicate mitigation strategies, making	Bai et al., 2018; Seto et al., 2014

	emissions control a persistent urban challenge.	
Water acidification in cities is driven by pollutants such as sulphur dioxide and nitrogen oxides from industry, traffic, and energy production. These emissions form acids that fall as acid rain, altering the chemistry of rivers, lakes, and reservoirs. Urban runoff carrying chemical residues from impervious surfaces further intensifies the process.	Lower pH levels disrupt aquatic biological processes, reduce biodiversity, and weaken ecosystem resilience. Acidification also degrades water quality and impairs ecosystem services, creating risks for both ecological systems and human health.	Likens et al., 1996; Kan et al., 2024
Climate change combines with urban form to magnify vulnerabilities, making cities especially prone to extreme weather. As urban areas expand and densify, the frequency and intensity of heat waves, heavy rainfall, and windstorms increase, driven by both global climatic shifts and local amplifiers such as the urban heat island effect and altered hydrological cycles. Impervious surfaces further exacerbate runoff, raising flood risks.	These conditions strain urban systems by overwhelming drainage, stressing energy supplies, and exposing populations to greater health risks. Aging or poorly designed infrastructure magnifies the impact of these events, disrupting transportation, energy, and public services, and reinforcing the cycle of vulnerability within urban environments.	IPCC, 2022; Rosenzweig et al., 2018
Rising temperatures in cities are intensified by the urban heat island effect, where concrete and asphalt absorb and re-emit heat. This amplifies ambient warming, increases energy demand for cooling, and heightens health risks, especially for vulnerable populations. Elevated temperatures also interact with hydrological processes, altering precipitation patterns, water quality, and the resilience of urban green spaces.	These shifts accelerate the degradation of infrastructure and compound existing environmental stressors. The combined pressures highlight the need for adaptive urban planning strategies that expand vegetation cover, integrate sustainable energy solutions, and design resilient systems to mitigate long-term heat impacts.	Santamouris et al., 2015; Oleson et al., 2013
Sea-level rise, driven by global warming and melting ice masses, exposes coastal cities to gradual inundation and episodic storm surges. These processes directly threaten the stability of built environments and critical infrastructure.	Encroaching seawater damages transport, water supply, and housing systems while saltwater intrusion compromises freshwater reserves and urban green spaces. These impacts heighten risks to public safety and weaken ecological balance in coastal urban areas.	Hinkel et al., 2014

1.1.7. In search of solutions

In conclusion, Anthropocene and urbanization are intertwined concepts, and citizens must face multiple challenges that threatens the quality of their habitats, and in turn the quality of their lives. Urban areas, as concentrated nodes of human activity, are increasingly vulnerable to Anthropocene challenges and climate-induced phenomena such as extreme weather events, rising temperatures, and sea-level rise. These environmental stressors exacerbate existing issues such as inadequate infrastructure, housing shortages, and public health concerns. This takes a toll on different urban inhabitants, placing a disproportionate burden on marginalized communities. Furthermore, rapid urbanization fuelled by migration and economic pressures, intensifies resource consumption and environmental degradation, leading to diminished urban green spaces, degraded air quality, and water scarcity. The next step is to correlate these challenges with the need of liveability of urban inhabitants, highlighting what urban habitats need to proliferate and what is threaten.

1.2. Urban liveability

1.2.1. Humans' needs for liveability in cities

Liveability is a multi-dimensional and hierarchical concept which consists of various criteria and may be evaluated in vastly different ways; there is yet no thorough or widely accepted method for its evaluation and still no consensus on its effective indicators (Higgs et al., 2019). In short, human liveability in cities is grounded in the fulfilment of interconnected needs that span the physical, economic, and social dimensions of life (Alsayed, 2024). Nevertheless, the matter of human liveability is an intricate concept where adhering to a single perspective can lead to skewered, or biased, perspectives. The different perspectives on human liveability hold different values, each highlighting a distinct interpretation of what it means to live well (Gonzalez Bohorquez et al., 2024).

From the standpoint of bare functionalism, the emphasis lies on quantifiable essentials such as housing, income, food, commuting, and interpersonal relationships (Jodder et al., 2025). This view prioritizes the systematic provision of basic services and infrastructure that support day-to-day survival and minimize the burdens of urban life. For example, well-planned transportation networks and affordable housing developments are critical for reducing commute times and ensuring that financial resources suffice for a dignified lifestyle. Functionalism, as an approach to human liveability, emphasizes the ecological processes inherent in urban environments by treating cities as complex systems where physical infrastructure, resource flows, and environmental interactions shape daily human existence. At its core, this perspective focuses on measurable and quantifiable aspects of habitability, such as housing quality, transportation efficiency, energy consumption, and the circulation of goods, under the notion that optimizing these ecological processes will inherently improve overall human well-being. However, this approach is not without its biases.

One primary bias is reductionism. By condensing human experience solely into its ecological and functional components, functionalism tends to overlook the nuanced, subjective dimensions of lived experience. For instance, while it may prioritize data on commute times or energy efficiency, it often neglects the culturally shaped perceptions of place and belonging that contribute significantly to a community's identity. This narrow focus can result in urban policies that are efficient on paper but disconnected from the everyday emotional and cultural realities of residents. This detachment can be correlated to low feasibility of implementing new architectural designs and low success rate for novel urban plannings (Zucaro & Agostinho, 2025; Cheshmehzangi et al., 2024).

Another significant bias is the assumption of urban centrism. By initially representing human habitats predominantly as cities, functionalism risks marginalizing non-urban forms of living, such as peri-urban communities, whose ecological processes social dynamics sometimes vastly differ from those in dense urban cores. This perspective may inadvertently mistakenly enforce solutions that are tailored to metropolitan settings to unsuitable areas, thereby reinforcing a divide between urban and non-urban populations (Cheshmehzangi, 2025; Mishra, 2025).

A further bias lies in the quantitative emphasis of the approach. Functionalism privileges metrics that are easily measured, like transportation throughput and housing density, while undervaluing qualitative aspects such as community ties, aesthetic perceptions, or spiritual fulfilment. Such an inherent preference for measurable data can lead to a technocentric mindset in urban planning where the pursuit of efficiency overshadows the broader human need for meaning and social justice (Oliveira & Porta, 2025; Beck & Mitkiewicz, 2025).

While functionalism offers valuable insights into the ecological underscoring of cities as urban habitats, its biases highlight the importance of consider cultural, ethical, and subjective factors to holistically perceive human liveability. A different cultural perspective argues that liveability is also shaped by the shared histories, traditions, and communal practices that provide individuals with a sense of identity and belonging. In urban settings, cultural festivals, museums, and public spaces not only celebrate heritage but also reinforce community ties, which in turn contribute to social cohesion and personal satisfaction. This perspective acknowledges that environments imbued with cultural significance can foster a greater sense of place and pride among inhabitants (Cobbina et al., 2025; Dempsey & newton, 2024).

Differently, the ethical perspective interrogates liveability in terms of justice and equity. This approach questions how resources and opportunities are distributed among various segments of the population. It underscores the necessity of inclusive policies that ensure marginalized groups have equitable access to the essentials of life, thereby asserting that a truly liveable society is one in which fairness and social justice underpin all urban development strategies (Kramer et al., 2024).

Complementing these perspectives is the spiritual perspective. Here, the focus transgresses the tangible and delves into the realm of personal meaning and ethical existence. A spiritually liveable environment might include areas of natural beauty, contemplative spaces, or community rituals that promote reflection and inner peace, elements that are crucial for nurturing emotional well-being and resilience in the face of modern-day stresses (Billet et al., 2025).

In sum, addressing human liveability in cities effectively requires integrating these different perspectives. By considering quantitative and qualitative aspects in urban habitats, the depiction of liveability that is obtained describes not only the basic needs for life but also elevate the quality of life through shared meaning, widespread inclusion, and a deep sense of community. For example, the manifestation of this fulfilment can be associated in secure housing, stable income, accessible nutritious food, efficient commuting systems, and supportive interpersonal relationships. A secure and affordable home is the cornerstone of liveability, providing not only shelter but also a vital sense of stability and community identity. Urban initiatives that focus on mixed-income housing developments have demonstrated how well-planned residential areas can cultivate a sense of belonging and foster community resilience. Complementing the need for a stable home is the necessity of a steady income, which empowers individuals to support themselves and their families while gaining access to essential services such as healthcare and education. In many urban settings, tailored economic policies and employment programs have been crucial in mitigating poverty and expanding opportunities for upward mobility. Access to nutritious food is equally indispensable, as it underpins physical health and cognitive performance. Urban agriculture projects and farmer's markets in city centres serve as practical examples of initiatives that enhance food security and improve community health outcomes. Efficient commuting is another critical element, as reliable and affordable transportation networks enable individuals to navigate urban landscapes, minimize stress, and maintain work-life balance. Cities that invest in comprehensive public transit systems tend to report lower levels of congestion and higher overall satisfaction among residents (Jodder et al., 2025; Reid et al., 2024). Lastly, robust interpersonal relationships are vital for fostering social cohesion, emotional support, and a shared sense of responsibility within communities. Social infrastructures, such as community centres and local clubs, play an essential role in building and sustaining these important bonds (Lauer et al., 2025).

The synergy between a stable home, sufficient income, reliable access to food, efficient commuting, and supportive relationships forms the backbone of liveability, corresponding to an overall healthy well-being in cities.

1.2.2. How human liveability in cities is challenged

Ensuring that the well-being of urban inhabitants is safeguarded in an era defined by its Anthropocene challenges means confronting the correlations and causalities between what humans need to live well and what limits or threatens that. Simply put, it can be said that the uncontrolled development of urban areas intensifies resource consumption, alters natural landscapes, and contributes to the degradation of ecosystem services, which in turn diminish the quality of urban habitats. Although, scientists differ in identifying the consequences and causes for the decrease in quality of life due to the complex nature of cities (Mishra, 2025).

Some examples are clearer, such as that the proliferation of concrete infrastructure not only accentuates the urban heat island effect but also disrupts local climatic patterns, leading to heightened energy demands and increased vulnerability to climate-induced stress. Similarly, rapid urban growth often leaves municipal infrastructures overstretched and citizens exposed to elevated levels of air and noise pollution, which can precipitate a cascade of public health issues such as respiratory disorders and mental health challenges. In both cases, the cascading effect between hazardous phenomenon and threats to the inhabitants are difficult to predict, quantify, and perceive. In the case of urban overheating phenomenon such as the heat island effect, the increased surface and air mean temperatures and heatwaves can constrain the energy system to higher peaks of demands in summer, leading to potential shortages on other systems or full-on blackouts (Yin et al., 2025). This example highlights how focusing on a single matter, i.e. overheating, can leave cities susceptible to other threats. As various components of urban infrastructure and services (heating/cooling, transport, housing, etc.) are interlinked, failure in one sector can trigger broader systemic challenges. This interdependency further destabilizes urban liveability by creating risks that are more difficult to predict and manage (IPCC, 2022).

In case of air and noise pollution due to traffic, it is easier to associate the distress due to prolonged exposure to heavy traffic to respiratory disorders than to poor mental health in vulnerable citizens (Liu et al., 2022; Khan et al., 2018). In this second example, the same matter, i.e. air and noise pollution, can be differently affecting different populations. In both cases, the problem of single inhabitants is sometimes something that is difficult to generalize, and if done incorrectly can lead to incompatibility of design implementation, lowered effectiveness, or worse the solutions can be counter-effective (Arriazu, Ramos et al., 2024). This incompatibility is reflected in evidence from the disparity between different urban group of inhabitants. For example, the IPCC's Differentiated Human Vulnerability highlights that socioeconomic status, planning deficits, and disparities in access to resources mean that some communities, particularly those in unplanned or informal settlements, are at far greater risk. This differentiated vulnerability shows how the same threat can result in very different outcomes regarding human liveability, leaving the most disadvantaged even more exposed (IPCC, 2022).

The process of urbanisation is itself a driver of vulnerability. As cities grow, and especially through unplanned and informal settlements in low- and middle-income nations, the combination of rapid population increase, and limited adaptive capacity leads to heightened exposure. Between 2015 and 2020, urban populations grew by more than 397 million people, with over 90% of that growth occurring in less developed regions. This rapid and uneven growth compounds risks and undermines the liveability of urban environments, as the infrastructure and resources needed to cope with climate hazards struggle to keep pace (IPCC, 2022). In identifying threats to human liveability, numerous frameworks have been developed to quantify the primary factors and processes that create and affect liveability. Albeit some indicators feature prominently (Environmental Friendliness and Sustainability, Socio-Cultural Conditions and Economic Vibrancy and Competitiveness – Khorrami et al., 2020), there are yet many general and site-specific indicators to rank urban liveability (Table 2).

Table 2. Urban liveability indicators.

Liveability indicator	**Description**	**Usage and scope**	**References**
Economist Intelligence Unit (EIU) Global Liveability Index	Annual ranking of 173 global cities, assessing stability, healthcare, education, culture and environment, and infrastructure. Produces a composite score widely used in policy and corporate relocation strategies.	Used by governments for benchmarking competitiveness, and by multinational corporations to guide relocation, investment, and expatriate placement decisions.	Economist Intelligence Unit, 2024
World Health Organization Quality of Life (WHOQOL)	A comprehensive framework measuring individuals' perceptions of their quality of life within cultural and value contexts. Includes WHOQOL-100 and WHOQOL-BREF, covering domains such as physical health, psychological state, independence, social relationships, environment, and spirituality.	Applied in cross-cultural health research, clinical studies, and public health evaluations to assess subjective well-being and compare populations across diverse cultural contexts.	The WHOQOL Group, 1998
OECD How's Life? Report	Flagship OECD publication operationalizing the Well-being Framework. Covers 11 dimensions (income, health, education, environment, security, work-life balance, etc.), integrating objective and subjective indicators. Provides longitudinal and cross-country comparisons for evidence-based policymaking.	Used by policymakers for cross-country benchmarking, long-term monitoring of well-being trends, and designing evidence-based strategies for inclusive growth and resilience.	OECD, 2024
Mercer Quality of Living Survey	Evaluates non-economic aspects of urban living, including political stability, healthcare, education, public services, and recreation. Used by governments and multinational corporations to guide expatriate assignments and relocation policies.	Primarily used by multinational corporations and governments to determine expatriate compensation packages, relocation policies, and risk assessments for international assignments.	Mercer, 2024
Urban Liveability Index (ULI)	Developed in Melbourne, integrates policy-relevant indicators (housing, transport, walkability, access to services) with health outcomes. Spatially sensitive, measuring liveability at neighbourhood scale.	Used in urban health research and planning, especially in Australia, to evaluate built environments and equity.	Higgs et al., 2019

Global Liveable Cities Index (GLCI)	Developed in Singapore, focusing on five domains: economic vibrancy, environmental friendliness, domestic security, socio-cultural conditions, and governance.	Applied in Asia-Pacific contexts for benchmarking cities beyond Western-centric indices.	Khorrami et al., 2020
UN-Habitat Urban Monitoring Framework (UMF)	Global framework aligned with SDG 11 ("Make cities inclusive, safe, resilient and sustainable"). Includes indicators on housing, mobility, environment, governance, and equity.	Used by governments and international organizations to track SDG progress and policy monitoring.	UN-Habitat, 2024
Water Inclusive Sustainability (WIS) Index	Novel framework measuring cities' sustainability through water availability, inclusiveness, innovation, and ecological friendliness.	Applied in China (Yangtze River Economic Belt), but conceptually transferable to global urban sustainability debates.	Gao et al., 2023
Centre for Liveable Cities (CLC) Singapore Liveability Framework	Policy-oriented framework emphasizing integrated planning, environmental sustainability, high-quality built environments, and community well-being.	Used in Singapore and internationally as a governance and planning tool.	Centre for Liveable Cities, 2025

Taken together, these evaluation standards offer data-driven insights that assist urban planners, researchers, and policy makers in recognizing strengths, addressing weaknesses, and benchmarking cities towards more sustainable and inclusive urban futures. Yet, the comparative analysis also reveals that liveability is not a neutral or abstract metric: it is deeply tied to the everyday vulnerabilities and risks that shape human well-being.

At the most immediate level, liveability is undermined when basic human needs are not met. Health concerns, the inability to access a stable home, insufficient income, unreliable access to food, and unsustainable commuting patterns all erode the quality of urban life (Alsayed, 2024). Increased traffic congestion and pollution not only compromise physical health but also reduce time available for social interaction. When cities fail to provide spaces and conditions that enable social gathering, they weaken the very fabric of community, making it harder for individuals to construct and sustain meaningful relationships (Higgs et al., 2019). These deficits highlight that liveability cannot be reduced to infrastructure or economic performance alone; it must be understood as the capacity of urban systems to secure the conditions for human flourishing.

At a broader scale, liveability is threatened by the cumulative responsibility of urban degradation. Unsustainable land use, industrial activity, and environmental exploitation drive processes of deforestation, greenhouse gas emissions, and water acidification. These human-induced pressures amplify the frequency and intensity of extreme weather events, rising temperatures, and the urban heat island effect (Rybski, 2025). Heatwaves, sea level rise, and climate-related hazards pose direct risks to human life and, by extension, to the very possibility of liveability in vulnerable regions (IPCC, 2023). The indicators reviewed in the table provide important benchmarks, but they must be interpreted against this backdrop of systemic environmental stress.

The key point that emerges is that liveability is not only about comparative rankings or abstract well-being frameworks. It is about confronting the dual challenge of ensuring equitable access to health, housing, food, and mobility, while simultaneously addressing the planetary boundaries that urbanization continues to strain. Without tackling both dimensions (i.e., the immediate social determinants of well-being and the long-term ecological sustainability of cities) any measure of liveability risks becoming partial, or even misleading.

The compounded impacts of urbanism necessitate integrative and sustainable planning strategies that harmonize urban development with ecological preservation, ensuring that the well-being of inhabitants is safeguarded in an era defined by its Anthropocene challenges. Yet, by framing urban liveability as a recursive product of cities from all its inhabitants, the concept can be widened to accommodate all its living inhabitants. This means that ecologically cities, as urban habitats, support the life of humans, but also plants and animals. These in turn contributes to the ecological functioning of cities, living both separate and intertwining lives with human inhabitants. A further analysis on the roles of this second type of inhabitants can be done, obtaining an insight on urban complexity and liveability from a different perspective.

1.2.3. Perspective of other urban inhabitants: plants and animals

Cities, as primarily human domains, are interwoven with plant and animal life that contributes to the ecological fabric of urban areas. The development of cities has gone through a complex interplay with the inherent dynamics of local fauna and flora, where the natural attributes of these organisms have significantly influenced the spatial and cultural structures of cities, even as urbanism has in turn modified their evolutionary trajectories (Frantzeskaki et al., 2024).

Historically, the presence of native vegetation and animal communities provided early settlers not only with essential resources but also with natural guidelines for the organization of settlements. For instance, the deliberate selection of settlements featuring abundant trees and water sources often led to the establishment of fruitful agricultural zones and natural gathering places, which later evolved into urban centres (Decocq, 2024). Presence of vegetation and animals was not just a prerogative of also linked to utilitarian factors. In many historical descriptions, cultural and religious practices were connected to specific plants and animals, thus integrating them into the social and ceremonial fabric of communities, thereby influencing city planning and the location of sacred sites (Ives et al., 2024). Such early interactions exemplify how natural elements, through their aesthetic, environmental, and cultural connotations, influenced the structure urban spaces.

Animals have strongly contributed materially and symbolically to city life, serving as both subjects and vehicles for brother interpretation of urban history. Animal presence in cities ranged from the incidental and adversarial (spiders and mice) to the symbiotically (farming and labour). Such presence led to a particular declination of urban space, to accommodate such different presences, such as simple stables to road systems. In fact, it can be argued that various species (including horses, donkeys, camels, even elephants) have been pivotal in shaping the infrastructure of cities through their roles in transportation, labour, and the production of goods. Thanks to these contributions, the current re-evaluation of urban history through interdisciplinary lens has re-integrated animal agency into the story of cities (Brantz, 2020). Therefore, the re-orientation toward an inclusive view of urban history (and planning) opens to a search for new avenues in comparative urban studies and environmental ethics.

The role of non-human inhabitants, intending all living species apart from human (and microbes), is therefore historically tied with the development of urban habitats. Nevertheless, it is pivotal to state that the same urban habitats, whose ecological content is so diverse and rich, have traditionally been described from the human-centred narrative. This fact has never been a particularly strong contender for modifying the trend of urbanism, until safeguarding biodiversity became a priority for administrations (Mahmoud et al., 2025; Rega-Brodsky et al., 2022). From an egalitarian perspective, safeguarding urban liveability means referring to all vulnerable living beings populating the habitat, to the needs of each one and to the interplay between the different populations. In practical terms, biodiversity in cities contributes to regulating microclimates, mitigating urban heat islands, managing stormwater, and improving air quality, while also providing psychological and social benefits through access to green and blue spaces (Kabisch et al., 2017). These functions are not marginal: they directly affect human health and resilience, making biodiversity a cornerstone of sustainable urban governance.

To study this, the discipline of urban ecology arose in the 1990s from the necessity to deepen our comprehension of both the ecological processes and human activities that shape urban ecosystems (McDonnell & Niemelä, 2011). Initially, research in this field concentrated on examining biodiversity, ecosystem functions, and the services provided by urban environments (Botkin & Beveridge, 1997). More recently, however, scholars have expanded their focus by integrating these ecological components with socioeconomic processes, urban management strategies, planning, and design initiatives (James & Douglas, 2023). Research on urban ecology has since started to move away from the focus on describing the patterns of biodiversity in cities, the so-called "low-hanging-fruit" of urban biodiversity research, toward different ecological questions. Specifically, these questions are referring to the contextualization and possibility for comparison between different urban cases; the use of variables capable of capturing vegetation structure, resource availability, social factors; use generalization and comparative studies considering different cities and regions (McDonnell & Hans, 2013). The questions strongly link to urban studies on both function and structure, implying a deep correlation between urban planning and ecological practices.

Parallelly, it has been long found that enriched biodiversity can enhance human well-being (Taylor & Hochuli, 2015) (Table 3). Therefore, a broader narrative of cities that includes human and non-human inhabitants is needed to both increase human liveability and strengthen the overall habitat liveability.

Table 3. Primary contributions of urban biodiversity to human well-being and liveability.

Kind of liveability	**Contribution of biodiversity**	**References**
Physical and mental health	Exposure to biodiverse green spaces reduces stress, improves mental health, lowers risks of cardiovascular disease, and supports immune function.	Wood et al., 2018; Wu et al., 2024; The Lancet Planeraty Health, 2025
Social cohesion and equity	Access to biodiverse environments fosters social interaction, community identity, and equitable well-being. Lack of access exacerbates inequalities.	Jennings & Bamkole, 2019; Jennings et al., 2024; Ayatollahi & Morello, 2025
Ecosystem services & resilience	Biodiversity supports climate regulation, air purification, stormwater management, and pollination, buffering cities against climate risks.	Elmqvist et al., 2019; Wang et al., 2024; Jamal et al., 2025
Cultural and psychological value	Encounters with diverse species enrich cultural identity, aesthetic appreciation, and sense of place, contributing to subjective well-being.	Aerts et al., 2018; Finnerty et al., 2025; Dushkova et al., 2025
Governance planning implications	Integrating biodiversity into planning (e.g., nature-based solutions, ecological corridors) enhances resilience, equity, and long-term liveability.	Frantzeskaki et al., 2019; Mahmoud et al., 2025; Davis, 2025

1.2.4. Urban plants and animals' needs for liveability and threats

The liveability of non-human organisms in cities hinges on a set of fundamental requirements, whose absence contributes to the damage to the ecological functioning of urban habitats. Such requirements collectively determine the capacity of plant and animal population to thrive in both natural and urbanized environments (Humbal et al., 2023). The liveability of plants and animals in cities is challenged by urbanization, driving systemic changes in ecological and evolutionary processes, reshaping biodiversity and ecosystem functions (Pickett et al., 2016). Moreover, urban habitats are influenced by the regional shifts of climate and temperatures, exacerbated by climate-change (Szulkin et al., 2020). Through the lens of this accelerated habitat shift, all aspects of non-human liveability are threatened (Table 4).

Table 4. Liveability needs and threats for plants and animals.

Liveability needs...	**…and threats**	**References**
Adequate **soil quality** and **water availability** are fundamental for plant survival, as they ensure proper nutrient absorption and hydration. Without sufficient access to water and fertile soil, plants struggle to maintain essential biological functions such as photosynthesis and growth.	Urban expansion leads to soil compaction and pollution, reducing fertility and water retention. Climate change exacerbates droughts and extreme weather, further limiting water access.	Cullis et al., 2019; Zango et al, 2022
Accessible **food sources** are crucial for sustaining urban wildlife. Animals must obtain enough energy to support their metabolism, reproduction, and movement. In cities, they rely on various food sources, whether from natural vegetation or available resources in their surroundings such as from human-generated waste.	Urban expansion often results in habitat fragmentation and the replacement of native vegetation with impervious surfaces or ornamental plants, disrupting food networks. Climate change compounds this by shifting phenological patterns, such as flowering and fruiting times, which can desynchronize food availability for pollinators and herbivores. These disruptions reduce the abundance and diversity of food sources, particularly for specialist species (ref).	Theodorou, 2022; Larson & Sander, 2025
Safe **shelter** and nesting sites provide protection and stability for animals. Shelter ensures they can rest, evade predators, and rear their young in a secure environment. Nesting sites are particularly important for birds and small mammals that require specific conditions for breeding and survival.	Urban development simplifies landscapes, removing natural shelters such as tree cavities, underbrush, and wetlands. This loss of structural complexity reduces nesting and refuge opportunities for many species, which are essential for reproduction. Climate change further degrades these microhabitats by increasing temperature extremes and reducing humidity, which is	Chen et al., 2023; Mengiste et al., 2024

	especially detrimental to species with narrow thermal tolerances.	
Air quality and **climate regulation** impact both plant and animal health. Clean air is necessary for respiration, allowing animals to function effectively and reducing stress from harmful pollutants. Likewise, plants depend on favourable climate conditions to maintain biological processes and structural integrity.	Cities are hotspots for air pollution, including particulate matter, nitrogen oxides, and ozone, which negatively affect plant photosynthesis and animal respiratory health. Climate change intensifies these effects by increasing the frequency of heatwaves and stagnant air conditions, which trap pollutants. Vegetation can help mitigate air pollution and regulate microclimates, but urban greenery is often sparse or poorly maintained in densely built environments. This creates feedback loops where poor air quality and extreme temperatures further reduce vegetation health and coverage. For example, urban pollinator populations decline significantly in areas with low native plant diversity and high thermal stress.	Arriazu-Ramos et al., 2024; Liang et al., 2023
Minimized **noise pollution** is essential for species that rely on vocal communication, particularly birds and amphibians. Their ability to transmit messages for mating, navigation, and territory defence can be disrupted in noisy urban environments, affecting their survival and interactions.	Chronic urban noise from traffic, construction, and industry interferes with animal communication, navigation, and predator-prey interactions. Climate change may indirectly amplify noise impacts by altering species distributions and increasing the density of urban populations seeking refuge from climate extremes. For example, birds in noisy environments often shift their vocalizations to higher frequencies, which can reduce mating success and territory defence. These behavioural adaptations are not always sufficient to offset the ecological costs of chronic noise exposure.	McMahon et al., 2017; Rhodes et al., 2023
Minimizing **light pollution** is critical for supporting the ecological rhythms of non-human organisms in cities. Species behaviour depends on natural light cycles. Plants depend on natural nighttime light for their growth and flowering cycles. Animals, instead, depends on dim nighttime lights for movements such as for foraging and migrating and for reproduction.	For animals, especially nocturnal species, constant exposure to artificial light disrupts natural behaviours such as foraging, mating, and predator avoidance. Urban lighting can fragment habitats by creating zones of avoidance, particularly for light-sensitive species like bats and amphibians. Climate change may exacerbate these effects by forcing species into more illuminated urban refuges where survival is compromised. For plants, extended exposure to light can interfere with photoperiodism, delaying flowering or leaf fall and disrupting synchrony with pollinators or seasonal cycles.	McMahon et al., 2017; Smit et al., 2022

Secure **migration pathways** allow animals to move freely within urban areas, ensuring they can find food, shelter, and mates. Many species follow established routes for seasonal migration, dispersal, or daily movement patterns, making connectivity between habitats essential for maintaining populations.	Urbanization leading to habitat fragmentations obstructs traditional migration routes, while climate change forces species to shift their ranges in search of suitable habitats. The combination of physical barriers (e.g., roads, buildings) and ecological mismatches (e.g., altered seasonal biological cues) severely limits the ability of species to adapt to changing conditions. Without functional ecological corridors, many species face local extinctions due to isolation and reduced genetic diversity.	Chen et al., 2023; Chen et al., 2025

Additionally, various species have evolved to meet their liveability needs through behavioural adaptations and ecological interactions that reflect the complexities of the urban environment. Reportedly, urban-driven genetic-changes affects crucial processes like pollination, air purification, and food production (Johnson & Munshi-South, 2017). These changes are relevant to urban liveability since habitat functioning is entirely dependent on the proper functioning of its parts. This evolutionary change feedback effectively damages the urban habitat stability and resilience in the long term (Dakos et al., 2019).

1.2.5. Habitat quality: liveability conditions and built and natural environment features

Habitat quality is a concept that encompasses both the liveability conditions experienced by inhabitants and the characteristics of the built and natural environments in which they live. Habitat quality reflects the degree to which a living environment supports physical health, psychological well-being, and social cohesion (Williams et al., 2020). Key indicators of liveability, such as access to clean air and water, adequate housing, transportation infrastructure, and proximity to essential services, are often proxied or directly considered in habitat quality assessment. For instance, urban neighbourhoods with well-maintained green spaces and efficient public transit systems tend to score higher in terms of (human) liveability, as they promote an active lifestyle that reduces environmental stressors (Khorrami et al., 2020).

The concept of habitat quality plays a crucial role in tying urban liveability conditions to environmental features. In fact, urban liveability is influenced by the spatial and functional characteristics of the living environment where humans and non-humans live, including housing design, land-use patterns, transportation infrastructure, and access to green spaces (Bolzan et al., 2023). For example, high-density, mixed-use developments that integrate residential, commercial, and recreational functions tend to enhance liveability by reducing travel distances, encouraging active mobility, and fostering social interaction (Mellen & Short, 2023). At the same time, the presence of natural elements such as parks, urban forests, and water bodies contributes significantly to mental and physical well-being, offering restorative experiences and ecological benefits like temperature regulation and stormwater management (Kabisch et al., 2015). People living near biodiverse green areas often report lower stress levels and higher life satisfaction (World Health Organization, 2021).

However, the access to liveability in cities is not evenly distributed for two different reasons. First, among socio-economically disadvantaged communities frequently facing environmental deficits, such as poor air quality and limited public amenities, which exacerbate health and social inequalities (Ganzleben & Kazmierczak, 2020). Secondly, the liveability of urban environments for non-human species is often compromised by habitat fragmentation, pollution, and the homogenization of landscapes through ornamental planting and excessive paving (Campos et al., 2024).

Addressing these disparities requires urban planning that prioritizes inclusivity, ensuring that all communities have equitable access to the environmental and infrastructural benefits that support well-being. As cities confront the escalating challenges of urbanization and climate change, this inclusive approach must be coupled with the integration of mitigation strategies such as green infrastructure into the built environment to enhance ecological resilience and mitigate environmental risks (Meerow & Newell, 2017). These interventions not only improve environmental performance and reduce vulnerability to climate-related hazards but also create opportunities to reimagine urban spaces as multifunctional ecosystems (Czechowski et al., 2015). One key aspect of this is the level of acceptance of biodiversity by human citizens. In fact, recent research shows that public acceptance of urban biodiversity is highly species-specific and shaped by both demographic factors and personal experiences with nature. Individuals with higher education levels, gardening habits, or frequent nature interactions tend to tolerate a wider range of species closer to their homes, while pet owners and older residents often prefer greater separation, especially from animals perceived as pests (Sweet & Weisser, 2025), ultimately limiting the effectiveness of urban designs.

Recognizing the dynamic interactions between urban development and biodiversity, planning strategies must evolve beyond static conservation models to embrace adaptive, ecologically informed frameworks (Alberti, 2023). This involves designing green spaces that serve dual purposes: providing recreational and aesthetic value for residents while also functioning as viable habitats for urban flora and fauna. Maintaining ecological corridors, supporting species movement, and incorporating biodiversity-friendly building practices are essential components of this approach. By aligning inclusive urban planning with adaptive ecological design, cities can foster environments that support a broader and more integrated definition of liveability, one that encompasses the health, resilience, and flourishing of both human and non-human life within shared urban habitats.

1.3. International frameworks for urban liveability

As shown in sections 1.1 and 1.2 urbanization, while central to economic growth and development, often comes at the cost of environmental degradation and reduced urban liveability. Climate change further amplifies these issues by intensifying heat, flooding, and biodiversity loss in densely populated areas. As cities expand, the need for sustainable and ecologically sound planning becomes increasingly urgent. Urban planning must evolve to prioritize ecological practices that restore and preserve natural systems within cities, while keeping unsustainable urbanization and climate change-induced effects in check.

The side of urban planning

Urban planning holds a central position in advancing urban liveability, particularly when aligned with global and regional policy frameworks (Table 5).

Table 5. International frameworks for urban liveability and sustainable development.

Framework	**Description**	**References**
Sendai Framework for Disaster Risk Reduction (2015–2030)	Global UN agreement to reduce disaster risk and build resilience. It outlines seven global targets and four priority actions, including understanding disaster risk, strengthening governance, investing in prevention, and enhancing preparedness. It promotes risk-informed development and resilient infrastructure.	United Nations Office for Disaster Risk Reduction (UNDRR), 2015
2030 Agenda for Sustainable Development (SDGs)	Adopted in 2015, the Agenda sets 17 SDGs to eradicate poverty, protect the planet, and ensure prosperity. SDG 11 focuses on sustainable cities and communities, calling for inclusive, safe, resilient, and sustainable urban environments. Urban planning is central to achieving these goals through integrated housing, transport, green space, and resilience policies.	United Nations, 2015
European Green Deal	EU roadmap to climate neutrality by 2050. Promotes decarbonization, biodiversity protection, and circular economy principles. In this light, urban planning is key for sustainable mobility, energy-efficient buildings, and green infrastructure.	European Commission, 2019
New Leipzig Charter (2020)	Updates the previous 2007 Leipzig Charter to address climate change and contemporary urban challenges. Promotes integrated, place-based urban development, multi-level governance, and participatory planning. Aligns	European Ministers responsible for Urban and Territorial Development, 2020

	with EU cohesion policy and the Urban Agenda for the EU.	
OECD Principles on Urban Policy	Strategic framework guiding sustainable urban development. Promotes integrated planning that balances economic growth with environmental protection, encourages green infrastructure and climate adaptation, and stresses multi-level governance and stakeholder engagement. Widely referenced in national urban policy reforms.	OECD, 2019

From such frameworks, urban planners have focused on the inclusion of vegetation in cities in form of ecologically-sound architectural designs. Nature-Based Solutions (NBS) are now widely adopted in urban planning across the globe, supported by a growing body of academic literature and policy frameworks (Mahmoud et al., 2022). Their integration into urban strategies is driven by their capacity to address multiple challenges simultaneously, such as climate adaptation, biodiversity loss, and social inequality, while enhancing ecosystem services and urban resilience (Pinto et al., 2022). Following these descriptions, some frameworks that explicitly reference NBS have been developed (Table 6). Together, they show how NBS have shifted from experimental concepts to mainstream planning tools. The World Bank Catalogue provides project-level guidance; the Urban Nature Platform translates EU biodiversity goals into local greening plans; and the UN-Habitat's New Urban Agenda embeds NBS in global governance. Taken as a whole, these initiatives highlight that NBS are no longer optional add-ons but core strategies for liveability in cities.

Table 6. International frameworks for NBS integration, monitoring, or on NBS benefits.

NBS framework	**Description**	**References**
World Bank – Catalogue of Nature-Based Solutions for Urban Resilience	Provides a structured overview of NBS that enhance urban resilience to climate risks such as flooding, heatwaves, and biodiversity loss. Includes practical examples and guidance for integrating NBS into urban development projects, particularly in low- and middle-income countries. Emphasizes co-benefits such as improved public health, social cohesion, and economic opportunities.	World Bank, 2021
Urban Nature Platform (EU Biodiversity Strategy)	Initiative under the EU Biodiversity Strategy for 2030. Encourages cities to develop Urban Nature Plans (formerly Urban Greening Plans) to restore biodiversity through urban forests, green roofs, and community gardens. Supports cities in designing, funding, and implementing NBS that contribute to climate adaptation and improved quality of life.	European Commission, 2024

UN-Habitat and the Habitat Agenda / New Urban Agenda	Promotes sustainable urban development with strong emphasis on ecological planning and resilience. Encourages adoption of green infrastructure, enhancement of ecosystem services, and integration of NBS into land-use planning. Reinforced through Habitat III and the New Urban Agenda, with a focus on inclusive governance and equitable access to green spaces.	UN-Habitat, 2016

The first globally agreed definition of NBS is: "Nature-Based Solutions are actions to protect, conserve, restore, sustainably use and manage natural or modified terrestrial, freshwater, coastal and marine ecosystems which address social, economic and environmental challenges effectively and adaptively, while simultaneously providing human well-being, ecosystem services, resilience and biodiversity benefits (United Nations Environment Program, 2024). Notably, the UNAP 2024 report opens the role of urban planning to "actions", including not only the act of intervening and transforming cities, but also more passive acts such as conservation, restoration, and use. Therefore, the emphasis on sustainable urban development falls as much on transforming and greening cities, as gathering knowledge on the effectiveness of solutions, the feasibility of implementation, and the conditions of urban habitats.

The side of ecological practices

Parallel to reports and framework that drive urban planning toward sustainable city designs, ecological practices (e.g., laws and directives) instruct on how to better safeguard biodiversity by improving habitat quality (Table 7). These instruments demonstrate that biodiversity protection is a legal obligation embedded in European governance. The EU Climate Law and Environmental Policy Framework establish overarching conditions for sustainability, while the Birds and Habitats Directives provide the legal backbone for species and habitat conservation through the Natura 2000 network. More recent strategies, such as the EU Biodiversity Strategy for 2030 and the Nature Restoration Law, set binding restoration targets and explicitly integrate NBS into urban and regional planning. Taken together, these measures ensure that ecological quality is treated as a prerequisite for liveability, requiring cities to align their development trajectories with biodiversity conservation and long-term resilience.

Table 7. International ecological practices, laws, and directives on biodiversity to improve urban habitat quality.

Ecological practice	Description	References
EU Climate Law (Regulation (EU) 2021/1119)	Legally enshrines the EU's commitment to climate neutrality by 2050, with a binding target of at least 55% net emissions reduction by 2030 (compared to 1990 levels). Establishes a 2040 target process, creates the European Scientific Advisory Board on Climate Change, and requires Member States to develop long-term strategies. Sets overarching conditions for habitat quality at the city level, linking climate neutrality to liveability.	European Parliament & Council, 2021
EU Environmental Policy Framework	Provides the legal and strategic basis for environmental protection across the EU, grounded in principles of prevention, precaution, and the polluter pays. Covers air and water quality, waste management, and climate action. Ensures ecological considerations are integrated into urban planning and development, making sustainability a legal obligation for Member States.	European Parliament, 2025
EU Nature Directives (Birds and Habitats Directives)	Cornerstones of EU biodiversity law. Require Member States to protect species and habitats via the Natura 2000 network. Influence urban planning by restricting harmful development in sensitive areas, promoting ecological connectivity, and supporting green infrastructure. Provide the legal foundation for biodiversity conservation and NBS implementation.	European Commission, 2009; European Commission, 1992
EU Biodiversity Strategy for 2030	Aims to reverse biodiversity loss and restore ecosystems by 2030. Sets targets including protection of at least 30% of EU land and sea, legally binding restoration goals, and large-scale deployment of NBS (urban greening, rewilding, wetland restoration). Introduces the EU Nature Restoration Law to mandate recovery of degraded habitats.	European Commission, 2020
EU Nature Restoration Law (Regulation (EU) 2024/1991)	First continent-wide law mandating ecosystem restoration. Legally binding targets: restore at least 20% of EU land and sea by 2030, all ecosystems in need by 2050. Includes no net loss of urban green space and tree cover by 2030, reversal of pollinator decline, and restoration of wetlands, forests, grasslands, rivers, and marine ecosystems. Requires Member States to prepare national restoration plans and monitor progress with standardized indicators.	European Parliament & Council, 2024

Gaps, what is missing and what could be done better

Despite their ambition and scope, major international and European frameworks on urban planning and ecological sustainability exhibit several critical factors that may hinder their effectiveness in practice. These gaps are exacerbated in applications where urban planning and ecology are tied and are particularly evident in four areas (Fig. 1).

i. Lack of implementation. Ecological frameworks set ambitious goals but falter in practice due to weak enforcement, limited capacity, low public engagement, and poor monitoring.

ii. Skewed perspective. Urban ecological frameworks often privilege technocratic, human-centred metrics, overlooking social equity and non-human needs, which can reinforce inequalities and deliver only superficial biodiversity gains.

iii. Low flexibility. Rigid, top down frameworks limit local adaptation, stifling experimentation and biodiversity sensitive planning.

iv. Lack of harmonization. Fragmented governance and standards create misalignment across scales and sectors, leading to uneven, inefficient, and inequitable ecological outcomes.

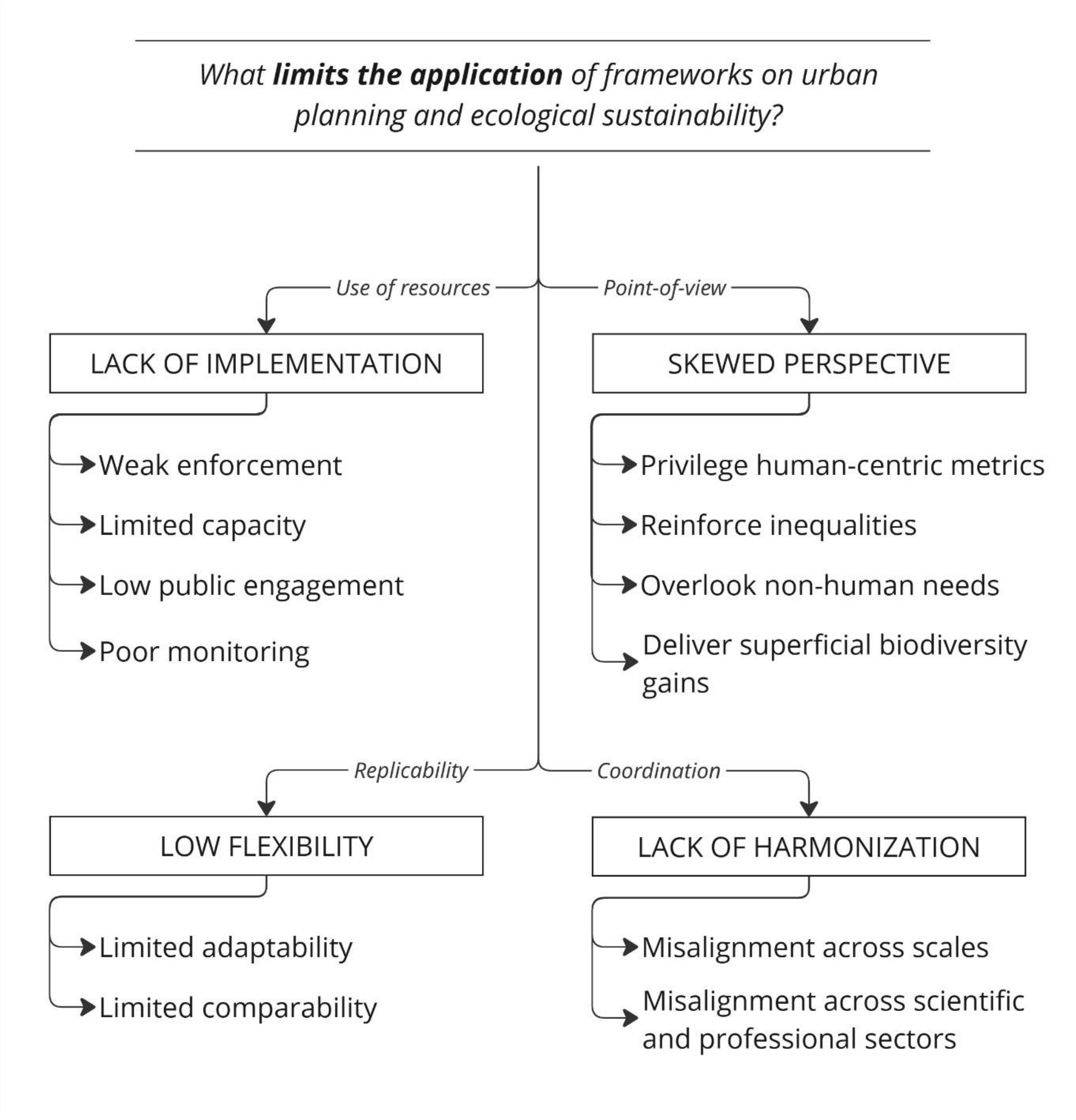

Figure 1. Primary causes of limitation for international frameworks on planning and ecological sustainability.

1.3.3.1. Lack of implementation

While international and regional frameworks such as the EU Biodiversity Strategy and the Nature Restoration Law set ambitious ecological targets, their implementation at the local level remains inconsistent and often symbolic. A key issue is the disconnect between policy ambition and institutional capacity. For example, although NBS are widely promoted in urban policy, their actual deployment is hindered by fragmented governance, lack of technical expertise, and insufficient integration into statutory planning processes (Almenar et al., 2021). Moreover, pilot projects dominate the urban landscapes, often serving as showcases rather than scalable models.

Many NBS initiatives remain isolated experiments, lacking the political and financial support needed for long-term institutionalization (Frantzeskaki et al., 2022). This is compounded by short-term funding cycles, which discourage continuity and limit the ability of local governments to maintain or expand ecological interventions.

Another aspect for the lack of implementation of ecological frameworks is the absence of binding enforcement mechanisms. While frameworks like the EU Climate Law include legally binding targets, others rely heavily on voluntary compliance and soft governance. This results in uneven implementation across member states and cities, with some regions advancing rapidly while others lag behind. This is sometimes shown when urban greening policies fail to reach marginalized communities, revealing a gap between stated goals and capacity for equitable delivery (Langemeyer & Connolly, 2020).

Another barrier to the effective implementation of ecological frameworks is the limited understanding and appreciation of these initiatives by the general public. While policies may be technically sound, their success depends heavily on public support and civic participation. Studies show that when citizens are not adequately informed or engaged, ecological interventions such as NBS are met with indifference or even resistance (Dunlap et al., 2021). Moreover, the lack of environmental literacy among urban populations can lead to misinterpretation of ecological goals, reducing the perceived value of green infrastructure or biodiversity conservation. This disconnect is particularly evident in marginalized communities, where ecological projects may be seen as tools of gentrification rather than inclusive development (Bonney et al., 2016).

Finally, monitoring and evaluation systems are often underdeveloped, making it difficult to assess progress or adapt strategies. Without robust data and feedback loops, implementation remains reactive rather than strategic. This lack of accountability undermines the transformative potential of ecological frameworks and limits their impact on urban sustainability (Kumar et al., 2021).

1.3.3.2. Skewed perspectives

A persistent critique of urban ecological frameworks is their tendency to adopt technocratic and ecological-economic perspectives, often at the expense of social equity, cultural diversity, and local knowledge systems. For example, while some frameworks emphasize metrics such as carbon reduction, ecosystem services, and land restoration, they frequently overlook who benefits from these interventions and who may be excluded or harmed (Anguelovski et al., 2016). Thus, many climate adaptation and greening strategies in cities reproduce existing inequalities by prioritizing affluent areas and sidelining marginalized communities. This is linked to green gentrification, a phenomenon where ecological improvements drive up property values and displace vulnerable populations (Mendonça et al., 2016). Moreover, the framing of NBS as universally beneficial can obscure the political and spatial dynamics of urban development. Planning decisions based solely on environmental indicators can inadvertently exacerbate social vulnerability (Zhang & Gu, 2025).

A different critique regarding perspective is the fact that urban ecological frameworks often prioritize human-centred metrics, such as recreational value or carbon sequestration, while neglecting the ecological needs and spatial experiences of non-human species. This anthropocentric bias results in planning that may appear green but fails to support meaningful biodiversity. For example, green roofs and pocket parks are frequently cited as NBS, yet they often lack the structural complexity, native vegetation, or connectivity required to sustain viable populations of urban fauna and flora (Pickett et al., 2024). Similarly, as for marginalized human communities, most urban planning models rely on remote sensing and land-use classifications that do not account for species-specific liveability needs or ecological interactions (Chen et al., 2025). Moreover, the spatial and temporal rhythms of urban life such as that of artificial lighting and noise pollution, can severely disrupt the life cycles of urban wildlife. For instance, nocturnal species are particularly vulnerable to light pollution, while migratory birds face increasing risks due to the loss of stopover habitats. Yet, these dynamics are rarely integrated into urban ecological assessments or planning tools (Zhang et al., 2024).

1.3.3.3. Low flexibility

Low flexibility in international and European urban planning and ecological sustainability frameworks constitutes a significant gap because it limits the ability of cities to respond dynamically to local environmental and socio-economic conditions. This limit constitutes a rigidity that often stems from the dominance of standardized, top-down policy instruments that prioritize uniformity over contextual responsiveness. For examples, cities can sometimes lack the institutional mechanisms to accommodate local experimentation or adaptive governance, which are essential for addressing complex urban sustainability challenges (Muñoz Gielen & Tasan-Kok, 2010). This limit is also found in regards to climate adaptation, where uncertainty and variability demand iterative and responsive planning. Many European cities are constrained by national and EU-level regulations that do not allow for the trial-and-error approaches necessary for effective climate resilience strategies (Mees et al., 2012). The resulting measures may be misaligned with their specific vulnerabilities or capacities, reducing both the efficiency and equity of sustainability interventions (Oneto & Canepa, 2023).

Low flexibility has another effect in undermining biodiversity conservation efforts, particularly in urban contexts where rigid governance structures often fail to accommodate ecological complexity. Biodiversity in urban areas is highly context-dependent, requiring localized, adaptive strategies that can respond to dynamic environmental and social conditions. However, many planning frameworks remain overly prescriptive, limiting the integration of site-specific ecological knowledge and stakeholder input. Successful biodiversity preservation outcomes in cities strongly depend on recognizing the heterogeneity of urban ecosystems and enabling place-based interventions (Kowarik & von der Lippe, 2018). Rigid planning mechanisms often overlook informal green spaces and spontaneous vegetation, which can serve as critical habitats for native and endangered species. Endangered plant species can be found in unconventional urban habitats such as brownfields and cemeteries, typically excluded from formal planning due to their marginal status. This exclusion is due to prioritization of standardized land-use categories over ecological functions (Planchuelo et al., 2019). Similar cases can be observed animals, such as for rare or endangered bird species (MacGregor-Fors et al., 2020).

1.3.3.4. Lack of harmonization

Harmonization refers to the alignment of policies, standards, and practices across different governance levels and sectors. Its absence often results in contradictions and inefficiencies that undermine the goals of urban planning and ecological practices. This issue is sometimes referred to as multiscalarity, in which the scale refers to both hierarchical levels of administration and analysis resolution, such as landscape, urban, or regional (Ramaswami et al., 2016). Low harmonization, or multiscalarity, is particularly acute in the European Union, where diverse national planning traditions and regulatory systems coexist under overarching EU directives.

One example is the misalignment between EU-level sustainability objectives and local implementation capacities. While cities such as Rotterdam and New York have developed advanced climate governance strategies, their efforts are often constrained by national policies that do not fully support or align with local innovation (Hölscher et al., 2019). This lack of vertical integration, i.e. communication between different steps of governance hierarchy, can lead to regulatory uncertainty and missed opportunities for synergies between climate change adaptation, biodiversity conservation, and urban development. The consequences of this lack of harmonization are evident in the uneven application of NBS across European cities. While some municipalities have successfully mainstreamed these approaches, others struggle due to conflicting regulations or lack of coherent guidance from higher governance level (Chausson et al., 2020). This inconsistency not only hampers ecological effectiveness but also exacerbates social inequalities, as access to green infrastructure becomes dependent on local administrative capacity rather than shared standards.

Horizontal fragmentation, i.e. communication between different administrative bodies at the same level of hierarchical governance, further complicates the implementation of integrated urban sustainability strategies across sectors such as transport, housing, and environmental protection. The compartmentalization of planning responsibilities across different administrative bodies leads to siloed decision-making, which is incompatible with the systemic nature of ecological challenges (Rydin, 2025). In the case of NBS or less complex green infrastructure projects, the design may be hindered by zoning laws or transport policies that do not account for ecological connectivity or multifunctionality.

In either vertical or horizontal case, there is an emphasis on the difficulty of comparison for architectural designs, urban planning solutions, and ecological practices. For example, the scarcity of harmonized methodological frameworks in how cities function as habitat leads to inconsistent data collection and reporting, which in turn hampers cross-city comparisons and the development of best practices (Beloin-Saint-Pierre, 2017). Moreover, the lack of comparability affects the credibility and legitimacy of urban ecological planning. When cities use different indicators or planning criteria, it becomes challenging to benchmark performance or to justify investments in ecological infrastructure. This has long been found as a leading cause to inefficiencies such as duplication of efforts and missed opportunities for collaborative learning (Wilkinson et al., 2013).

Final remarks: cities, liveability, and possibilities for improvement

In conclusion, the challenge of achieving sustainable cities capable of supporting both human and non-human life hinges on the integration of robust urban planning and ecological practices. As urbanization and climate change intensify, cities must evolve into adaptive, inclusive, and ecologically resilient systems. This transformation is currently lead by a robust set of international frameworks, that guide the development of national directives and strategies. However, such frameworks expose urban planning and ecological practices to several potential critical factors: lack of actual implementation, skewed perspectives that prioritize human-centric or sectoral goals, low flexibility in adapting to local contexts, and insufficient harmonization across governance levels and sectors. These shortcomings not only limit the effectiveness of interventions that should favour urban sustainable development but also perpetuate social and ecological inequalities.

This chapter highlighted how urban liveability is challenged and what are the overarching legal frameworks that enforce urban planning and ecological practices in cities. From this knowledge, an alternative path for supporting better integrated urban planning and ecological practices can be formulated. Instead of focusing on improving the legal frameworks from a policy perspective, the thesis will focus on studying the conditions for which urban liveability can be deduced. Indeed, urban features such as built and natural fundamentally shape urban liveability, accounting for both human and non-human needs for a liveable urban environment. Therefore, the research question needs to be refocused and specified, moving from

How can liveability for all urban inhabitants be fostered?

to

How can descriptive knowledge on urban liveability conditions be extracted from the way cities are analysed?

By developing shared frameworks and methodologies that capture the complexity of urban systems, planners and policymakers can foster more coherent and equitable strategies. Such analytical clarity is essential for aligning local actions with global sustainability goals, enabling comparability across different urban environments, and ensuring that both human and ecological needs are met. The next chapter will delve into descriptive analytical tools for describing urban systems. It will explore how spatial data, together with geospatial modelling, can be instrumental in providing quantitative patterns to support the foundation for more informed urban planning and ecological practices.

1.3. References

Abujder Ochoa, W. A., Iarozinski Neto, A., Vitorio Junior, P. C., Palma Calabokis, O., & Ballesteros-Ballesteros, V. (2023). The theory of complexity and sustainable urban development: A systematic literature review. Sustainability, 17(1), 3. https://doi.org/10.3390/su17010003

Acuto, M., Parnell, S., & Seto, K. C. (2018). Building a global urban science. *Nature Sustainability, 1*(1), 2–4. https://doi.org/10.1038/s41893-017-0013-9

Aerts, R., Honnay, O., & Van Nieuwenhuyse, A. (2018). Biodiversity and human health: Mechanisms and evidence of the positive health effects of diversity in nature and green spaces. British Medical Bulletin, 127(1), 5–22. https://doi.org/10.1093/bmb/ldy021

Alberti, M. (2023). Cities of the Anthropocene: Urban sustainability in an eco-evolutionary perspective. *Philosophical Transactions of the Royal Society B: Biological Sciences, 378*(1883), 20220264. https://doi.org/10.1098/rstb.2022.0264

Almenar, J. B., et al. (2021). Nexus between nature-based solutions, ecosystem services and urban challenges. Land Use Policy, 100, 104898. https://doi.org/10.1016/j.landusepol.2020.104898

Alsayed, S. S. (2024). Urban human needs: Conceptual framework to promoting urban city fulfills human desires. Frontiers in Sustainable Cities, 6. https://doi.org/10.3389/frsc.2024.1395980

Anguelovski, I., Shi, L., Chu, E., Gallagher, D., Goh, K., Lamb, Z., Reeve, K., & Teicher, H. (2016). Equity impacts of urban land use planning for climate adaptation: Critical perspectives from the global north and south. Journal of Planning Education and Research, 36(3), 333–348. https://doi.org/10.1177/0739456X16645166

Arriazu-Ramos, A., Santamaría, J. M., Monge-Barrio, A., Bes-Rastrollo, M., Gutiérrez Gabriel, S., Benito Frias, N., & Sánchez-Ostiz, A. (2024). *Health impacts of urban environmental parameters: A review of air pollution, heat, noise, green spaces and mobility*. Sustainability, 17(10), 4336. https://doi.org/10.3390/su17104336

Ayatollahi, A., & Morello, E. (2025). Scoping the emerging role of urban biodiversity in social impact assessment: A systematic review. Frontiers in Sustainable Cities, 7, 1623650. https://doi.org/10.3389/frsc.2025.1623650

Bai, X., Dawson, R. J., Ürge-Vorsatz, D., Delgado, G. C., Barau, A. S., Dhakal, S., Dodman, D., Leonardsen, L., Masson-Delmotte, V., Roberts, D. C., & Schultz, S. (2018). Six research priorities for cities and climate change. *Nature, 555*(7694), 23–25. https://doi.org/10.1038/d41586-018-02409-z

Beck, D., & Mitkiewicz, J. (2025). A systematic literature review of citizen science in urban studies and regional urban planning: Policy, practical, and research implications. Urban Ecosystems, 28, 85. https://doi.org/10.1007/s11252-025-01693-8

Beloin-Saint-Pierre, D., Rugani, B., Lasvaux, S., Mailhac, A., Popovici, E., Sibiude, G., Benetto, E., & Schiopu, N. (2017). A review of urban metabolism studies to identify key methodological choices for future harmonization and implementation. *Journal of Cleaner Production, 163,* S223–S240. https://doi.org/10.1016/j.jclepro.2016.09.014

Billet, J., McPherson, E., Norenzayan, A., & Schaller, M. (2025). *Seeing nature through a spiritual lens: An experimental test of the effects of eco-spirituality on well-being*. Journal of Environmental Psychology, 92, 102321. https://doi.org/10.1016/j.jenvp.2025.102321

Bolzan Wesz, J. G., Miron, L. I. G., Delsante, I., & Tzortzopoulos, P. (2023). Urban quality of life: A systematic literature review. *Urban Science, 7*(2), 56. https://doi.org/10.3390/urbansci7020056

Bonney, R., Phillips, T. B., Ballard, H. L., & Enck, J. W. (2016). Public participation in scientific research: A framework for deliberate design. *Ecology and Society*, 21(2), 7. https://www.jstor.org/stable/26269051

Botkin, D. B., & Beveridge, C. E. (1997). Cities as environments. Urban Ecosystems, 1(1), 3–19, Retrieved from https://web.mit.edu/people/spirn/Public/Granite%20Garden%20Research/Urban%20ecology/Botkin%20&%20Beveridge%201997%20Cities%20as%20Environments.pdf

Brantz, D. (2020). "Animals in Urban-Environmental History". Concepts of Urban-Environmental History, edited by Sebastian Haumann, Martin Knoll and Detlev Mares, Bielefeld, pp. 191-202. https://doi.org/10.1515/9783839443750-013

Campbell, H. E., Eckerd, A., & Kim, Y. (2024). Complexity approach to urban systems. In Green gentrification and environmental injustice (pp. 43–60). Springer. https://doi.org/10.1007/978-3-031-65100-7_3

Campos, C. O., Almeida, S. F. P., Serra, S. R. Q., Calapez, A. R., Silveira, P., & Feio, M. J. (2024). The overlooked margins: How cities impact diversity of plants and terrestrial invertebrates along urban streams. *Urban Ecosystems, 27*, 1751–1766. https://link.springer.com/article/10.1007/s11252-024-01551-z

Centre for Liveable Cities. (2025). Measuring Urban Liveability. Retrieved from https://knowledgehub.clc.gov.sg/liveability-framework/measuring-urban-liveability

Chausson, A., Turner, B., Seddon, D., Chabaneix, N., Girardin, C. A. J., Kapos, V., Key, I., Roe, D., Smith, A., Woroniecki, S., & Seddon, N. (2020). Mapping the effectiveness of nature-based solutions for climate change adaptation. *Global Change Biology, 26*(11), 6134–6155. https://doi.org/10.1111/gcb.15310

Chen, C. Y., Chuang, Y. H., Chen, H. W., & Teng, C. S. (2025). *Optimizing ecological corridors for urban sustainability by using remote sensing and decision modeling*. International Journal of Environmental Science and Technology, 22, 10013–10028. https://doi.org/10.1007/s13762-024-06272-6

Chen, C. Y., Chuang, Y. H., Chen, H. W., & Teng, C.-S. (2025). Optimizing ecological corridors for urban sustainability by using remote sensing and decision modeling. *International Journal of Environmental Science and Technology, 22*, 10013–10028. https://doi.org/10.1007/s13762-024-06272-6

Chen, S., Liu, Y., Patrick, S. C., Goodale, E., Safran, R. J., & Pagani-Núñez, E. (2023). A multidimensional framework to quantify the effects of urbanization on avian breeding fitness. *Ecology and Evolution, 13*(7), ece3.10259. https://doi.org/10.1002/ece3.10259

Chen, S., Liu, Y., Patrick, S. C., Goodale, E., Safran, R. J., & Pagani-Núñez, E. (2023). A multidimensional framework to quantify the effects of urbanization on avian breeding fitness. *Ecology and Evolution, 13*(7), ece3.10259. https://doi.org/10.1002/ece3.10259

Cheshmehzangi, A. (2025). Urban planning for the contemporary age: Navigating complexities and shaping urban futures. Encyclopedia, 5(1), 19. https://doi.org/10.3390/encyclopedia5010019

Cheshmehzangi, A., Allam, Z., & Siew, G. (2024). Diversity in cities and addressing urban sustainability. In Diversity as Catalyst: Economic Growth and Urban Resilience in Global Cityscapes (pp. 1–9). Springer. https://doi.org/10.1007/978-981-97-8776-0_1

Cobbina, E. J., Ametepey, S. O., Aigbavboa, C., Frempong-Jnr, E. Y., Thwala, W. D., Ebekozien, A., & Addy, H. (2025). *The influence of cultural identity on achieving sustainable urban development in developing countries*. Frontiers in Built Environment, 11, 1582670. https://doi.org/10.3389/fbuil.2025.1582670

Cullis, J. D. S., Horn, A., Rossouw, N., Fisher-Jeffes, L., Kunneke, M. M., & Hoffman, W. (2019). Urbanisation, climate change and its impact on water quality and economic risks in a water scarce and rapidly urbanising catchment: Case study of the Berg River Catchment. *H2Open Journal, 2*(1), 146–167. https://doi.org/10.2166/h2oj.2019.027

Czechowski, D., Hauck, T., & Hausladen, G. (Eds.). (2015). *Revising green infrastructure: Concepts between nature and design* (1st ed.). CRC Press. https://doi.org/10.1201/b17639

Dakos, V., Matthews, B., Hendry, A. P., Levine, J., Loeuille, N., Norberg, J., Nosil, P., Scheffer, M., & De Meester, L. (2019). Ecosystem tipping points in an evolving world. *Nature Ecology & Evolution, 3*(3), 355–362. https://doi.org/10.1038/s41559-019-0797-2

Davis, M. (2025). Strengthening urban governance for inclusive and effective nature-based solutions. Open Access Government, 46(11921). https://doi.org/10.56367/OAG-046-11921

Decocq, G. (Ed.). (2024). *Historical ecology: Learning from the past to understand the present and forecast the future of ecosystems*. Wiley. https://www.wiley.com/en-us/Historical+Ecology%3A+Learning+from+the+Past+to+Understand+the+Present+and+Forecast+the+Future+of+Ecosystems-p-9781394169757

Dempsey, N., & Newton, L. (2024). The significance of culture for social sustainability. *Local Environment*, *29*(1), 1–17. https://doi.org/10.1080/13549839.2024.2424427

Diamond, J. M. (2005). Guns, germs, and steel: The fates of human societies. Norton.

Diemer, A. (2019). System dynamics for sustainable urban planning. In Encyclopedia of the UN Sustainable Development Goals. Springer. https://doi.org/10.1007/978-3-319-71061-7_115-1

Dunlap, L., Corris, A., Jacquart, M., Biener, Z., & Potochnik, A. (2021). Divergence of values and goals in participatory research. *Studies in History and Philosophy of Science*, 88, 284–291. https://doi.org/10.1016/j.shpsa.2021.06.015

Dushkova, D., Ignatieva, M., Müller, N., & Nilon, C. (2025). Integrating biodiversity in the urban planning and design processes. Urban Ecosystems, 28(84). https://doi.org/10.1007/s11252-025-01697-4

Economist Intelligence Unit. (2024). The Global Liveability Index 2024. Economist Intelligence Unit. Retrieved from https://www.eiu.com/n/campaigns/global-liveability-index-2024/

Elmqvist, T., Andersson, E., Frantzeskaki, N., McPhearson, T., Olsson, P., Gaffney, O., Takeuchi, K., & Folke, C. (2019). Sustainability and resilience for transformation in the urban century. *Nature Sustainability*, *2*(4), 267–273. https://doi.org/10.1038/s41893-019-0250-1

Elmqvist, T., Andersson, E., Frantzeskaki, N., McPhearson, T., Olsson, P., Gaffney, O., … Folke, C. (2019). Sustainability and resilience for transformation in the urban century. Nature Sustainability, 2(4), 267–273. https://doi.org/10.1038/s41893-019-0250-1

Espey, J., Keith, M., Parnell, S., Schwanen, T., & Seto, K. C. (2024). *Designing policy for Earth's urban future.* Science, 383(6681), 364–367. https://doi.org/10.1126/science.adi6636

European Commission. (1992). *Council Directive 92/43/EEC on the conservation of natural habitats and of wild fauna and flora (Habitats Directive)*. https://eur-lex.europa.eu/eli/dir/1992/43/oj

European Commission. (2009). *Directive 2009/147/EC on the conservation of wild birds (Birds Directive)*. https://eur-lex.europa.eu/eli/dir/2009/147/oj

European Commission. (2019). The European Green Deal. COM(2019) 640 final. https://eur-lex.europa.eu/legal-content/EN/TXT/?uri=CELEX:52019DC0640

European Commission. (2020). *EU Biodiversity Strategy for 2030: Bringing nature back into our lives*. COM(2020) 380 final. https://eur-lex.europa.eu/legal-content/EN/TXT/?uri=CELEX:52020DC0380

European Commission. (2024). *Urban Nature Platform*. Retrieved from https://environment.ec.europa.eu/topics/urban-environment/urban-nature-platform_en

European Ministers responsible for Urban and Territorial Development. (2020). The New Leipzig Charter: The transformative power of cities for the common good. https://www.bmi.bund.de/SharedDocs/downloads/EN/eu-presidency/gemeinsame-erklaerungen/new-leipzig-charta-2020.pdf

European Parliament & Council. (2021). *Regulation (EU) 2021/1119 establishing the framework for achieving climate neutrality (European Climate Law)*. Official Journal of the European Union, L 243, 1–17. https://eur-lex.europa.eu/eli/reg/2021/1119/oj

European Parliament & Council. (2024). *Regulation (EU) 2024/1991 on nature restoration*. Official Journal of the European Union, L 2024/1991. https://eur-lex.europa.eu/eli/reg/2024/1991/oj

European Parliament. (2025). *Environment policy: General principles and basic framework*. European Parliament Fact Sheets. https://www.europarl.europa.eu/factsheets/en/sheet/71/environment-policy-general-principles-and-basic-framework

Finnerty, P. B., Carthey, A. J. R., Banks, P. B., Brewster, R., Grueber, C. E., Houston, D., … van Eeden, L. M. (2025). Urban rewilding to combat global biodiversity decline. BioScience, 75(7), 545–558. https://doi.org/10.1093/biosci/biaf062

Foley, J. A., DeFries, R., Asner, G. P., Barford, C., Bonan, G., Carpenter, S. R., Chapin, F. S., Coe, M. T.,

Daily, G. C., Gibbs, H. K., Helkowski, J. H., Holloway, T., Howard, E. A., Kucharik, C. J., Monfreda, C., Patz, J. A., Prentice, I. C., Ramankutty, N., & Snyder, P. K. (2005). Global consequences of land use. *Science, 309*(5734), 570–574. https://doi.org/10.1126/science.1111772

Frantzeskaki, N., Childers, D. L., Pickett, S. T. A., Hoover, F.-A., Anderson, P., Barau, A., Ginsberg, J., Grove, M., Lodder, M., Lugo, A. E., McPhearson, T., Muñoz-Erickson, T. A., Quartier, M., Schepers, S., Sharifi, A., & van de Sijpe, K. (2024). *A transformative shift in urban ecology toward a more active and relevant future for the field and for cities*. Ambio, 53(5), 871–889. https://doi.org/10.1007/s13280-024-01992-y

Frantzeskaki, N., et al. (2022). Nature-based solutions for urban resilience: A review of barriers and enablers. Environmental Science & Policy, 132, 1–10. https://doi.org/10.1016/j.ufug.2022.127611

Frantzeskaki, N., McPhearson, T., Collier, M. J., Kendal, D., Bulkeley, H., Dumitru, A., … Elmqvist, T. (2019). Nature-based solutions for urban climate change adaptation: Linking science, policy, and practice communities for evidence-based decision-making. BioScience, 69(6), 455–466. https://doi.org/10.1093/biosci/biz042

Ganzleben, C., & Kazmierczak, A. (2020). Leaving no one behind – Understanding environmental inequality in Europe. *Environmental Health, 19*, Article 57. https://doi.org/10.1186/s12940-020-00600-2

Gao, S., Xiong, Q., & Yu, J. (2023). Conceptualization and measurement of water inclusive sustainability of China's cities in the Yangtze River Economic Belt. Sustainable Cities and Society, 92, 104474. https://doi.org/10.1016/j.scs.2023.104474

Gonzalez Bohorquez, N., Stafford, L., McPhail, S. M., Selim, S. M., Kularatna, S., & Malatzky, C. (2024). Disability, equity, and measurements of livability: A scoping review. Disability and Health Journal, 17(1), 101521. https://doi.org/10.1016/j.dhjo.2023.101521

Hansen, M. C., Potapov, P. V., Moore, R., Hancher, M., Turubanova, S. A., Tyukavina, A., Thau, D., Stehman, S. V., Goetz, S. J., Loveland, T. R., Kommareddy, A., Egorov, A., Chini, L., Justice, C. O., & Townshend, J. R. G. (2013). High-resolution global maps of 21st-century forest cover change. *Science, 342*(6160), 850–853. https://doi.org/10.1126/science.1244693

Higgs, C., Badland, H., Simons, K., Knibbs, L. D., & Giles-Corti, B. (2019). The Urban Liveability Index: Developing a policy-relevant urban liveability composite measure and evaluating associations with transport mode choice. International Journal of Health Geographics, 18(1), 14. https://doi.org/10.1186/s12942-019-0178-8

Hinkel, J., Lincke, D., Vafeidis, A. T., Perrette, M., Nicholls, R. J., Tol, R. S. J., Marzeion, B., Fettweis, X., Ionescu, C., & Levermann, A. (2014). Coastal flood damage and adaptation costs under 21st century sea-level rise. *Proceedings of the National Academy of Sciences, 111*(9), 3292–3297. https://doi.org/10.1073/pnas.1222469111

Hölscher, K., Frantzeskaki, N., & Loorbach, D. (2019). Steering transformations under climate change: Capacities for transformative climate governance and the case of Rotterdam, the Netherlands. *Regional Environmental Change, 19*(3), 791–805. https://doi.org/10.1007/s10113-018-1329-3

Humbal, A., Chaudhary, N., & Pathak, B. (2023). Urbanization trends, climate change, and environmental sustainability. In B. Pathak & R. S. Dubey (Eds.), Climate change and urban environment sustainability (pp. 151–166). Springer. https://doi.org/10.1007/978-981-19-7618-6_9

IPCC. (2022). Climate Change 2022: Impacts, adaptation, and vulnerability. Contribution of Working Group II to the Sixth Assessment Report of the Intergovernmental Panel on Climate Change [H.-O. Pörtner, D. C. Roberts, M. Tignor, E. S. Poloczanska, K. Mintenbeck, A. Alegría, M. Craig, S. Langsdorf, S. Löschke, V. Möller, A. Okem, & B. Rama (Eds.)]. Cambridge University Press. https://doi.org/10.1017/9781009325844

Ives, C. D., Kidwell, J. H., Anderson, C. B., Arias-Arévalo, P., Gould, R. K., Kenter, J. O., & Murali, R. (2024). *The role of religion in shaping the values of nature*. Ecology and Society, 29(2), 10. https://doi.org/10.5751/ES-15004-290210

Jamal, S., Atahar, M., & Ahmad, W. S. (2025). Resilience in urban ecosystems: Interdisciplinary perspectives and strategic pathways. GeoJournal, 90(18). https://doi.org/10.1007/s10708-024-11270-9

James, P., & Douglas, I. (2023). Urban ecology: an introduction. Routledge.

Jennings, V., & Bamkole, O. (2019). The relationship between social cohesion and urban green space: An avenue for health promotion. International Journal of Environmental Research and Public Health, 16(3), 452. https://doi.org/10.3390/ijerph16030452

Jennings, V., Rigolon, A., Thompson, J., Murray, A., Henderson, A., & Gragg, R. S. (2024). The dynamic relationship between social cohesion and urban green space in diverse communities. International Journal of Environmental Research and Public Health, 21(6), 800. https://doi.org/10.3390/ijerph21060800

Jodder, P. K., Hossain, M. Z., & Thill, J.-C. (2025). Urban livability in a rapidly urbanizing mid-size city: Lessons for planning in the Global South. Sustainability, 17(4), 1504. https://doi.org/10.3390/su17041504

Johnson, M. T. J., & Munshi-South, J. (2017). Evolution of life in urban environments. *Science, 358*(6363), eaam8327. https://doi.org/10.1126/science.aam8327

Kabisch, N., Korn, H., Stadler, J., & Bonn, A. (Eds.). (2017). Nature-based solutions to climate change adaptation in urban areas: Linkages between science, policy and practice. Springer. https://doi.org/10.1007/978-3-319-56091-5

Kabisch, N., Qureshi, S., & Haase, D. (2015). Human–environment interactions in urban green spaces—A systematic review of contemporary issues and prospects for future research. *Environmental Impact Assessment Review, 50*, 25–34. https://doi.org/10.1016/j.eiar.2014.08.007

Kan, D., & Lv, L. (2024). The impact of new urbanization on water ecological resilience: An empirical study from central China. *PLOS ONE, 19*(12), e0313865. https://doi.org/10.1371/journal.pone.0313865

Khan, J., Ketzel, M., Kakosimos, K., Sørensen, M., & Jensen, S. S. (2018). Road traffic air and noise pollution exposure assessment – A review of tools and techniques. Science of The Total Environment, 634, 661–676. https://doi.org/10.1016/j.scitotenv.2018.03.374

Khorrami, Z., Ye, T., Sadatmoosavi, A., Mirzaee, M., Fadakar Davarani, M. M., & Khanjani, N. (2020). "The indicators and methods used for measuring urban liveability: a scoping review" Reviews on Environmental Health, vol. 36, no. 3, pp. 397-441. https://doi.org/10.1515/reveh-2020-0097

Kowarik, I., & von der Lippe, M. (2018). Plant population success across urban ecosystems: A framework to inform biodiversity conservation in cities. Journal of Applied Ecology, 55(5), 2354–2361. https://doi.org/10.1111/1365-2664.13144

Kramer, J., Silverton, S., & Späth, P. (2024). *Urban governance arrangements for sustainability and justice – linking theory with experience*. Urban Transformations, 6(6), Article 6. https://doi.org/10.1186/s42854-024-00064-4

Kumar, P., Debele, S. E., Sahani, J., Rawat, N., Marti-Cardona, B., Alfieri, S. M., Basu, B., Sarkar Basu, A., Bowyer, P., Charizopoulos, N., Jaakko, J., Loupis, M., Menenti, M., Mickovski, S. B., Pfeiffer, J., Pilla, F., Pröll, J., Pulvirenti, B., Rutzinger, M., Sannigrahi, S., … Zieher, T. (2021). An overview of monitoring methods for assessing the performance of nature-based solutions against natural hazards. *Earth-Science Reviews, 217*, 103603. https://doi.org/10.1016/j.earscirev.2021.103603

Langemeyer, J., & Connolly, J. J. T. (2020). Weaving notions of justice into urban ecosystem services research and practice. Environmental Science & Policy, 109, 1–9. https://doi.org/10.1016/j.envsci.2020.03.021

Larson, R. N., & Sander, H. A. (2025). *Variation in species-specific responses to habitat fragmentation and land cover structure in urban small mammal communities*. Journal of Mammalogy, 106(2), 339–351. https://doi.org/10.1093/jmammal/gyae121

Lauer, S., Wong, K. L. Y., & Yan, M. C. (2025). *Social infrastructure, community organizations, and friendship formation: A scoping review*. Community Development Journal, 60(2), 267–285. https://doi.org/10.1093/cdj/bsae023

Liang, H., He, Y.D., Theodorou, P., & Yang, C.F. (2023). The effects of urbanization on pollinators and pollination: A meta-analysis. Ecology Letters, 26 (9), 1629–1642. https://doi.org/10.1111/ele.14277

Likens, G. E., Driscoll, C. T., & Buso, D. C. (1996). Long-term effects of acid rain: Response and recovery of a forest ecosystem. *Science, 272*(5259), 244–246. https://doi.org/10.1126/science.272.5259.244

Liu, Y., Chen, J., Wu, J., & Xu, C. (2022). Urban form, air pollution exposure, and health: A review of the literature. Environment International, 163, 107236. https://doi.org/10.1016/j.envint.2022.107236

MacGregor-Fors, I., Escobar-Ibáñez, J. F., Schondube, J. E., Zuria, I., Ortega-Álvarez, R., Sosa-López, J. R., Ruvalcaba-Ortega, I., Almazán-Núñez, R. C., Arellano-Delgado, M., Arriaga-Weiss, S. L., Calvo, A., Chapa-Vargas, L., Silvestre Lara, P. X., García-Chávez, J. H., Hinojosa, O., Koller-González, J. M., Lara, C., López de Aquino, S., López-Santillán, D., Maya-Elizarrarás, E., Medina, J. P., Moreno Navarro, J. de J., Murillo García, L. E., Orozco, L., Pineda-López, R., Rodríguez-Ruíz, E. R., Tinajero Hernández, J. R., Torres Abán, L. B., & Vega-Rivera, J. H. (2020). The urban contrast: A nationwide assessment of avian diversity in Mexican cities. *Science of the Total Environment, 748*, 141915. https://doi.org/10.1016/j.scitotenv.2020.141915

Mahmoud, I. H., Morello, E., Lemes de Oliveira, F., & Geneletti, D. (Eds.). (2022). Nature-based solutions for sustainable urban planning: Greening cities, shaping cities

Mahmoud, I., Dubois, G., Liquete, C., & Robuchon, M. (2025). Understanding collaborative governance of biodiversity-inclusive urban planning: Benchmarking results for urban nature plans in 10 European cities. Urban Ecosystems, 28(1), 17. https://doi.org/10.1007/s11252-024-01656-5

Mahmoud, I., Dubois, G., Liquete, C., & Robuchon, M. (2025). Understanding collaborative governance of biodiversity-inclusive urban planning: Benchmarking results for urban nature plans in 10 European cities. Urban Ecosystems, 28(1), 17. https://doi.org/10.1007/s11252-024-01656-5

McDonnell, M. J., & Niemelä, J. (2011). The history of urban ecology. Urban ecology: Patterns, processes, and applications, 5-13.

McDonnell, M.J., Hahs, A.K. (2013). The future of urban biodiversity research: Moving beyond the 'low-hanging fruit'. Urban Ecosystems 16, 397–409. https://doi.org/10.1007/s11252-013-0315-2

McMahon, T. A., Rohr, J. R., & Bernal, X. E. (2017). Light and noise pollution interact to disrupt interspecific interactions. *Ecology, 98*(5), 1290–1299. https://doi.org/10.1002/ecy.1770

McPhearson, T., Cook, E. M., Berbés-Blázquez, M., Cheng, C., Grimm, N. B., Andersson, E., Barbosa, O., Chandler, D. G., Chang, H., Chester, M. V., Childers, D. L., Elser, S. R., Frantzeskaki, N., Grabowski, Z., Groffman, P., Hale, R. L., Iwaniec, D. M., Kabisch, N., Kennedy, C., … Troxler, T. G. (2022). A social-ecological-technological systems framework for urban ecosystem services. One Earth, 5(5), 505–518. https://doi.org/10.1016/j.oneear.2022.04.007

Meerow, S., & Newell, J. P. (2017). Spatial planning for multifunctional green infrastructure: Growing resilience in Detroit. *Landscape and Urban Planning, 159*, 62–75. https://doi.org/10.1016/j.landurbplan.2016.10.005

Mees, H. L. P., Driessen, P. P. J., & Runhaar, H. A. C. (2012). Exploring the scope of public and private responsibilities for climate adaptation. Journal of Environmental Policy & Planning, 14(3), 305–330. https://doi.org/10.1080/1523908X.2012.707407

Mellen, H., & Short, M. (2023). Designing for social interaction in high-density housing: A multiple case analysis of recently completed design-led developments in London. *Frontiers in Sustainable Cities, 4*, Article 1043701. https://doi.org/10.3389/frsc.2022.1043701

Mendonça, R., Roebeling, P., Fidélis, T., & Saraiva, M. (2024). Can policy instruments enhance the benefits of nature-based solutions and curb green gentrification? The case of Genova, Italy. *Environmental Science & Policy, 158*, 1–14. https://doi.org/10.1016/j.envsci.2024.103533

Mengiste, B. M., Shi, W., & Wong, M. S. (2024). *Urban landscape and development effects on city sustainability: A systematic review of empirical studies*. Environment, Development and Sustainability, 26(10), 15421–15445. https://doi.org/10.1007/s10668-024-05405-8

Mercer (2024). Quality of Living City Ranking 2024. Mercer. Retrieved from https://www.mercer.com/insights/total-rewards/talent-mobility-insights/quality-of-living-city-ranking/

Mishra, V. (2025). *Rethinking urban future: Towards sustainable cities and communities*. Anthropocene Science, 4(3), 88. https://doi.org/10.1007/s44177-025-00088-w

Muñoz Gielen, D., & Tasan-Kok, T. (2010). Flexibility in planning and the consequences for public-value capturing in UK, Spain and the Netherlands. *European Planning Studies, 18*(7), 1097–1131. https://doi.org/10.1080/09654311003744191

Myers, G. (2021). Urbanisation in the Global South. In C. M. Shackleton, S. S. Cilliers, E. Davoren, & M. J. du Toit (Eds.), *Urban ecology in the Global South* (pp. 27–49). Springer. https://doi.org/10.1007/978-3-030-67650-6_2

OECD (2019). OECD Principles on Urban Policy. OECD Publishing. Retrieved from https://www.oecd.org/en/about/programmes/oecd-programme-on-national-urban-policy/oecd-principles-on-urban-policy.html

OECD (2024). How's Life? 2024: Well-being and resilience in times of crisis. OECD Publishing. https://doi.org/10.1787/90ba854a-en

Oleson, K. W., Monaghan, A., Wilhelmi, O., Barlage, M., Brunsell, N., Feddema, J., Hu, L., & Steinhoff, D. F. (2013). Interactions between urbanization, heat stress, and climate change. *Climatic Change, 129*(3–4), 525–541. https://doi.org/10.1007/s10584-013-0936-8

Oliveira, V., & Porta, S. (2025). *Quantitative and qualitative analysis in urban morphology: Systematic legacy and latest developments*. Proceedings of the Institution of Civil Engineers – Urban Design and Planning, 178(2), 75–87. https://doi.org/10.1680/jurdp.24.00047

Oneto, G., & Canepa, M. (2023). Addressing sustainable urban flood risk: Reviewing the role and scope of theoretical models and policies. *Water Policy, 25*(8), 797–814. https://doi.org/10.2166/wp.2023.022

Pickett, S. T. A., Cadenasso, M. L., Childers, D. L., McDonnell, M. J., & Zhou, W. (2016). Evolution and future of urban ecological science: Ecology in, of, and for the city. *Ecosystem Health and Sustainability, 2*(8), e01229. https://doi.org/10.1002/ehs2.1229

Pickett, S. T. A., Simone, A. T., Anderson, P., Sharifi, A., Barau, A., Hoover, F.-A., Childers, D. L., McPhearson, T., Muñoz-Erickson, T. A., Pacteau, C., Grove, M., Frantzeskaki, N., Nagendra, H., & Ginsberg, J. (2024). The relational shift in urban ecology: From place and structures to multiple modes of coproduction for positive urban futures. *Ambio, 53*(4), 845–870. https://doi.org/10.1007/s13280-024-02001-y

Pineda-Pinto, M., Frantzeskaki, N., & Nygaard, C. A. (2022). The potential of nature-based solutions to deliver ecologically just cities: Lessons for research and urban planning from a systematic literature review. *Ambio, 51*(1), 167–182. https://doi.org/10.1007/s13280-021-01553-7

Planchuelo, G., von der Lippe, M., & Kowarik, I. (2019). Untangling the role of urban ecosystems as habitats for endangered plant species. *Landscape and Urban Planning, 189,* 320–334. https://doi.org/10.1016/j.landurbplan.2019.05.007

Ramaswami, A., Russell, A. G., Culligan, P. J., Sharma, K. R., & Kumar, E. (2016). Meta-principles for developing smart, sustainable, and healthy cities. *Science, 352*(6288), 940–943. https://doi.org/10.1126/science.aaf7160

Rega-Brodsky, C. C., Aronson, M. F. J., Piana, M. R., Carpenter, E. S., Hahs, A. K., Herrera-Montes, A., Knapp, S., Kotze, D. J., Moretti, M., & Williams, N. S. G. (2022). Urban biodiversity: State of the science and future directions. Urban Ecosystems, 25(5), 1083–1096. https://doi.org/10.1007/s11252-022-01207-w

Reid, S., Kraatz, J., & Caldera, S. (2024). A liveability framework for medium- to high-density social and affordable housing: An Australian housing case study. *Urban Policy and Research*, 42(2), 139–159. https://doi.org/10.1080/08111146.2024.2323013

Rhodes, M. L., Ryder, T. B., Evans, B. S., To, J. C., Neslund, E., Will, C., O'Brien, L. E., & Moseley, D. L. (2023). The effects of anthropogenic noise and urban habitats on song structure in a vocal mimic: The gray catbird (*Dumetella carolinensis*) sings higher frequencies in noisier habitats. *Frontiers in Ecology and*

Evolution, 11, 1252632. https://doi.org/10.3389/fevo.2023.1252632

Rosenzweig, C., Solecki, W., Romero-Lankao, P., Mehrotra, S., Dhakal, S., & Ibrahim, S. A. (Eds.). (2018). *Climate Change and Cities: Second Assessment Report of the Urban Climate Change Research Network (UCCRN ARC3.2).* Cambridge University Press. https://doi.org/10.1017/9781316563878

Rybski, D. (Ed.). (2025). Compendium of urban complexity. Springer. https://doi.org/10.1007/978-3-031-82666-5

Rydin, Y. (2025). *Planning without growth*. Bristol University Press. https://doi.org/10.51952/9781447369790

Santamouris, M. (2015). Analyzing the heat island magnitude and characteristics in one hundred Asian and Australian cities and regions. *Science of the Total Environment, 512–513*, 582–598. https://doi.org/10.1016/j.scitotenv.2015.01.060

Seto, K. C., Dhakal, S., Bigio, A., Blanco, H., Delgado, G. C., Dewar, D., Huang, L., Inaba, A., Kansal, A., Lwasa, S., McMahon, J. E., Müller, D. B., Murakami, J., Nagendra, H., & Ramaswami, A. (2014). Human settlements, infrastructure and spatial planning. In O. Edenhofer et al. (Eds.), *Climate Change 2014: Mitigation of Climate Change. Contribution of Working Group III to the Fifth Assessment Report of the Intergovernmental Panel on Climate Change* (pp. 923–1000). Cambridge University Press.

Smit, J. A. H., Cronin, A. D., van der Wiel, I., Oteman, B., Ellers, J., & Halfwerk, W. (2022). Interactive and independent effects of light and noise pollution on sexual signaling in frogs. *Frontiers in Ecology and Evolution, 10*, 934661. https://doi.org/10.3389/fevo.2022.934661

Steffen, W., Rockström, J., Richardson, K., Lenton, T. M., Folke, C., Liverman, D., Summerhayes, C. P., Barnosky, A. D., Cornell, S. E., Crucifix, M., Donges, J. F., Fetzer, I., Lade, S. J., Scheffer, M., Winkelmann, R., & Schellnhuber, H. J. (2020). The emergence and evolution of Earth System Science. *Nature Reviews Earth & Environment, 1*(1), 54–63. https://doi.org/10.1038/s43017-019-0005-6

Sweet, F. S. T., & Weisser, W. W. (2025). Welcome for thee, but not for me: How demographic parameters and nature experience affect how close to home people accept animals. *Basic and Applied Ecology, 87*, 83–91. Urban & Fischer. https://doi.org/10.1016/j.baae.2025.06.007

Szulkin M, Munshi-South J, Charmantier A. (2020) *Urban evolutionary biology*. New York, NY: Oxford University Press.

Taylor, L., Hochuli, D.F. (2015). Creating better cities: how biodiversity and ecosystem functioning enhance urban residents' wellbeing. Urban Ecosystems, 18, 747–762, https://doi.org/10.1007/s11252-014-0427-3

The Lancet Planetary Health. (2025). A health impact assessment of progress towards urban nature targets in European cities. The Lancet Planetary Health, 9(3), e210–e222. https://doi.org/10.1016/S2542-5196(25)00053-1

The WHOQOL Group. (1998). Development of the World Health Organization WHOQOL-BREF quality of life assessment. Psychological Medicine, 28(3), 551–558. https://doi.org/10.1017/S0033291798006667

Theodorou, P. (2022). The effects of urbanisation on ecological interactions. *Current Opinion in Insect Science, 50*, 100922. https://doi.org/10.1016/j.cois.2022.100922

UN-Habitat. (2016). *The New Urban Agenda*. Quito: United Nations. Retrieved from https://habitat3.org/the-new-urban-agenda/

UN-Habitat. (2024). Urban Monitoring Framework. Retrieved from https://data.unhabitat.org/pages/urban-monitoring-framework

UN-Habitat. (2024). World Cities Report 2024: The urban future. United Nations Human Settlements Programme. Retrieved from https://unhabitat.org/world-cities-report-2024

United Nations Environment Program (2024). Information on the implementation of resolution 5/5 on nature-based solutions for supporting sustainable development (UNEP/EA.6/INF/5). https://documents.un.org/doc/undoc/gen/k24/000/78/pdf/k2400078.pdf

United Nations Office for Disaster Risk Reduction (UNDRR). (2015). Sendai Framework for Disaster Risk Reduction 2015–2030.

https://www.undrr.org/publication/sendai-framework-disaster-risk-reduction-2015-2030

United Nations, Department of Economic and Social Affairs, Population Division. (2024). *World Urbanization Prospects: The 2024 Revision*. New York: United Nations. Retrieved from https://population.un.org/wup/

United Nations. (2012). *General Assembly Official Records, A/C.2/66/SR.31*. Retrieved from UN Official Document

United Nations. (2015). Transforming our world: The 2030 Agenda for Sustainable Development. https://sdgs.un.org/2030agenda

Wang Yue Dong, M. (2023). A critical analysis on complex urban systems and complexity theory. Journal of Complex Networks and Systems, 3(1), 25–39. https://anapub.co.ke/journals/jcns/jcns_pdf/2023/jcns_volume_3-issue_1/JCNS202303003.pdf

Wang, D., Xu, P. Y., An, B. W., & Guo, Q. P. (2024). Urban green infrastructure: Bridging biodiversity conservation and sustainable urban development through adaptive management. Frontiers in Ecology and Evolution, 12, 1440477. https://doi.org/10.3389/fevo.2024.1440477

Wang, Y., Fang, X., Yin, S., & Chen, W. (2021). *Low-carbon development quality of cities in China: Evaluation and obstacle analysis*. Sustainable Cities and Society, 64, 102553. https://doi.org/10.1016/j.scs.2020.102553

Wilkinson, C., Saarne, T., Peterson, G. D., & Colding, J. (2013). Strategic spatial planning and the ecosystem services concept – An historical exploration. *Ecology and Society, 18*(1), 37. https://www.jstor.org/stable/26269278

Williams, A. J., Maguire, K., Morrissey, K., Taylor, T., & Wyatt, K. (2020). Social cohesion, mental wellbeing and health-related quality of life among a cohort of social housing residents in Cornwall: A cross-sectional study. *BMC Public Health, 20*, 985. https://doi.org/10.1186/s12889-020-09078-6

Wood, E., Harsant, A., Dallimer, M., Cronin de Chavez, A., McEachan, R. R. C., & Hassall, C. (2018). Not all green space is created equal: Biodiversity predicts psychological restorative benefits from urban green space. Frontiers in Psychology, 9, 2320. https://doi.org/10.3389/fpsyg.2018.02320

World Bank. (2021). *A Catalogue of Nature-Based Solutions for Urban Resilience*. Washington, DC: World Bank. Retrieved from https://documents.worldbank.org/en/publication/documents-reports/documentdetail/502101636360985715

World Health Organization (WHO). (2021). *Green and blue spaces and mental health: New evidence and perspectives for action*. WHO Regional Office for Europe. Retrieved from https://iris.who.int/handle/10665/342931

Wu, C. C., O'Keefe, J., Ding, Y., & Sullivan, W. C. (2024). Biodiversity of urban green spaces and human health: A systematic review of recent research. Frontiers in Ecology and Evolution, 12, 1467568. https://doi.org/10.3389/fevo.2024.1467568

Yin, C., Yan, J., Yuan, M., Tian, G., Wen, Q., Wang, L., & Li, L. (2025). How does built environment affect the urban heat island effect? A systematic framework integrating land use, building form, and road network. Environment, Development and Sustainability, 27(6), 1–25. https://doi.org/10.1007/s10668-025-06390-2

Zango, B.-S., Seidou, O., Sartaj, M., Nakhaei, N., & Stiles, K. (2022). Impacts of urbanization and climate change on water quantity and quality in the Carp River watershed. *Journal of Water and Climate Change, 13*(2), 786–816. https://doi.org/10.2166/wcc.2021.158

Zhang, J., & Gu, X. (2025). Multi-stakeholder perspectives on urban regeneration: A spatial gradient analysis of heat and pollution effects. International Journal of Biometeorology, 69, 1325–1345. https://doi.org/10.1007/s00484-025-02894-8

Zhang, Y., Li, X., Wang, Y., & Liu, J. (2024). Understanding the association between urban noise and nighttime light in China. *Scientific Reports, 14*, 83125. https://doi.org/10.1038/s41598-024-83125-9

Zucaro, A., & Agostinho, F. (2025). Urban sustainability: Challenges and opportunities for resilient and resource-efficient cities. Frontiers in Sustainable Cities, 7, 1556974. https://doi.org/10.3389/frsc.2025.1556974

Chapter 2.

Descriptive analytical tools for urban systems

Abstract

This second chapter examines how descriptive and analytical tools have evolved to make urban systems measurable, comparable, and interpretable across disciplines. Beginning with early morphological traditions, the chapter shows how manual mapping and typological studies established the first systematic frameworks for describing urban form and its historical development. It then outlines the emergence of configurational analysis through space syntax, which reframed cities as relational spatial systems capable of shaping movement, social encounter, and long-term transformation.

The chapter next traces how the GIS revolution and spatial econometrics introduced data-rich, statistically rigorous methods that allowed urban researchers to quantify relationships among land use, morphology, accessibility, environmental conditions, and socio-economic processes.

Finally, it discusses contemporary data-driven approaches—remote sensing, machine learning, open data integration that enable high-resolution, multi-scalar analyses of urban form and environmental dynamics.

Despite these advances, the chapter identifies four persistent limitations, similar to the ones highlighted in the previous chapter: implementation gaps, skewed perspectives toward built form, low methodological flexibility, and lack of harmonization across scales and governance levels. These gaps explain why current spatial tools remain insufficient for addressing urgent ecological and climatic challenges. This motivates the thesis's core methodological contributions introduced in later chapters. Two methodologies, Cohabscapes, which classifies urban landscapes through geospatial and machine learning data, and a site-selection framework for heat mitigation, together extending spatial analysis into ecological and climatic domains to provide scalable, actionable tools for integrated urban planning.

Keywords

urban morphology; spatial analysis; data-driven methods

2.1. Urban morphology and descriptive knowledge of cities

2.1.1. The discipline of urban morphology

Urban morphology, as a foundational discipline within urban studies, offers a critical lens through which the physical form and spatial structure of cities can be interpreted and contextualized. This chapter begins by situating urban morphology within the broader epistemological landscape of urban knowledge, emphasizing its role in producing descriptive knowledge from the built and natural environment. At its core, urban morphology is concerned with the systematic study of urban form, comprising streets, plots, buildings, and the processes that shape their transformation over time.

Vítor Oliveira (2022) defines urban morphology as both a method and a field of knowledge that bridges architecture, geography, and urban planning, enabling researchers to decode the spatial logic embedded in cities. His work highlights the importance of formal analysis in understanding how cities evolve, not merely as physical entities but as socio-spatial constructs shaped by cultural and economic factors. This analytical perspective on urban studies is derived from the need of simplifying and the complex structure and abundance of information that cities are composed of. In fact, Oliveira introduces the concept of urban morphology as a hierarchical view of cities, in which relationships between different dimensions of cities are structured on physical elements, such as buildings or streets. This layered idea that cities can be composed of relationships between elements is also referred by other authors with names such as urban tissue or urban landscape. Karl Kropf, for example, uses the term urban tissue to define the organic structure in which a set of urban elements is assembled at a specific location and at a specific scale (Kropf, 1996). Generally, all urban tissues are composed of the same kind of elements such as open spaces, parks, streets, buildings, and landmarks. The way in which these same elements are combined characterise a specific city location, giving it a clear objective identification (e.g., the angle in which two streets collide) but also a cultural connotation (e.g., a landscape deemed worthy to be classified as a World Heritage). This concept is extremely valuable for deriving descriptive knowledge of cities, since objective identification can be compared to assess similarities and differences. This, in turn, enables to compare the phenomena that develop underneath the urban tissues, such wellbeing conditions (and the urban liveability threats discussed in Chapter 1).

2.1.2. Relations with urban planning

The objective identification of particular spatial combinations is of extreme use for urban planning due to the translation of requirements for administrations to measurable and operational components of the urban planning and policy process. Transport modelling and land use modelling are clear examples of application. Sergio Porta's work tie urban form and socio-economic activity together by quantifying the spatial configurations of urban elements, specifically streets, to determine the degree of resilience and vitality of urban systems (Porta et al., 2006). His use of street centrality metrics introduced a network-based approach to urban morphology that treats cities as complex spatial systems. By analysing the topological and geometric properties of street networks, Porta demonstrated how centrality correlates with the distribution of economic activities, such as retail and services, in cities like Bologna and Barcelona. This approach not only reveals the structural logic of urban form but also provides a predictive framework for understanding how spatial configuration influences urban vitality. Furthermore, Porta's work on resilience proxies, such as variety, extends this analysis to assess the adaptability of urban form over time. His integration of morphological theory with complex systems science has advanced the operationalization of urban resilience, offering planners a robust set of tools to evaluate and design urban environments (Porta et al., 2017).

Similar approaches include land use modelling to derive and predict transport demand or residential location choice. In Schirmer's case, the novelty lies in his development of a multiscale morphological classification system that translates the complexity of urban form into quantifiable variables usable in behavioural simulation models (Schirmer & Axhausen, 2019). His work demonstrates how morphological features, such as block size and street connectivity, can be systematically integrated into residential location choice models, thereby linking the physical structure of cities to individual decision-making processes. This approach not only enhances the predictive accuracy of urban simulations but also provides planners with a morphologically informed framework for evaluating the long-term impacts of urban design on land use and sustainability.

The cultural connotation of space is emphasized by the temporal continuity and transformation that cities undergo. Indeed, urban form is not static but evolves through identifiable processes that reflects socio-economic and cultural dynamics. J.W.R. Whitehand, through the so called historical-geographical approach, identifies morphological regions as urban areas that exhibit consistent patterns of form through prolonged temporal development (Whitehand, 2001; Oliveira, 2019). While this concept is of value for urban conservation due to its foundation on building types and understanding of how different parts of a city have developed over time, this is also interesting to ground spatial cultural identity in the processes of urban development. One example of morphological region that is often used in contemporary studies is the fringe-belt. This type of region is a zone of mixed land uses that encompasses the edge of built-up areas due to urban expansions, and it is characterized by discontinuous urban features including large scale industrial facilities together with institutional buildings and parks that often resist new development and preserve pre-existing urban structures. This is the case for multiple urban peripheries in Europe and in other areas of the world, where the urbanization in the twentieth and twenty-one century that expanded from the old urban centres expanded over historical assets that once where part of the countryside, such as religious complexes and large estates (Whitehand & Morton, 2003).

Michael Mehaffy has advanced the theoretical foundations of urban morphology by building on the legacy of Christopher Alexander (Alexander et al., 1977). His work explores how the geometry of urban form links morphological thinking with sustainable urbanism and design theory. Mehaffy's key innovation lies in his effort to operationalize Alexander's theories, particularly the idea that urban environments should emerge from bottom-up adaptive processes rather than top-down impositions (Mehaffy et al., 2020). Mehaffy argues how pattern languages as structured sets of design solutions can be used to guide the creation of urban environments that are both human-centred and ecologically responsive. He emphasizes the importance of generative codes, which are rule-based systems that allow urban form to evolve organically, much like natural systems. This approach aligns closely with contemporary concerns in urban resilience and sustainability, as it promotes incremental, context-sensitive development that can adapt over time.

2.1.3. Relations with landscape ecology and biodiversity conservation

The intersection between urban morphology and other fields do not reside only in urban planning. Lars Marcus introduced the concept of spatial capital, as the capacity of urban form to support social and economic activities through its spatial configuration. This concept builds from analytical description of the built environment to deduce the opportunities for improving urban interactions and resilience (Marcus, 2010). One key aspect of spatial capital is the highlights of how spatial configurations can influence the adaptability and sustainability of urban systems. This is explicitly viewed as an opportunity to build a framework to support or constraint the analysis of ecological functions (Marcus & Colding, 2014). Marcus argues that the spatial layout of cities affects the flow of ecological services (i.e., air circulation, water drainage, biodiversity corridors), just as it affects human movement and social interaction. Methodologically, this knowledge translates into quantitatively identifying the spatial resilience of urban form, meaning the degree of opposition that urban form poses to movement and change. The relevance of this principle is particularly evident in relation to landscape ecology, where key concepts such as connectivity and patch dynamics that share similar metrics for spatial resilience (such as connectivity matrixes) are used to study ecological performance. A second contribution of spatial capital is the connection between urban morphology and multi-scalar analysis. Urban and ecological processes operate at different spatial and temporal scales, such as the development of residential housing or nesting to satisfy the need of shelter for both humans and non-humans correlate with the conditions of surrounding built and natural environment. This perspective should encourage researchers to consider how local design decisions (e.g., the building orientation) interact with broader landscape patterns (e.g., green infrastructure network that grow with a particular amount of sunlight) (Marcus et al., 2019).

Other authors extend from this concept of spatial and ecological resilience, empathizing the connection and the intrinsic relationship between urban systems and ecosystems in urban designs and plans that aim to be sustainable and resilient. Alessandra Feliciotti work argues that cities, like natural systems, benefit from diversity and redundancy for evolving without compromising their identity or functionality (Feliciotti et al., 2016). Specifically, Feliciotti explains that the capacity to assess urban form is useful to absorb shocks and stresses to urban systems, while maintaining essential functions, such as in cases of climatic or ecological distress. Thus, the quantitative description of cities typical of urban morphology characterise a reactive (or proactive) response to urban challenges. This same reasoning is the ground statement for other formulations of ecological urban resilience. Johan Colding introduces social-ecological systems as frameworks where human and ecological components are deeply intertwined. In such systems, spatial arrangements have the potential to enhance ecological functions, integrating traditional ecological knowledge into urban planning (Colding & Barthel, 2019).

The spatial and temporal factors that define urban development and are explicit in urban morphology not only contribute to cities evolve, but also how living organism that live in cities adapt. Specifically, urbanization alters ecological processes but also drives evolutionary changes in species. Urban patterns that describe urbanization, such as fragmentation and connectivity, can influence the adaptive traits of organisms such as the response to modified nutrient cycles or climate regulation. In turn, the same urban patterns can help explaining the phenomena and bring new ecological knowledge to the urban planning process (Palazzo, 2022).

Finally, the spatial and temporal factors that define urban development and are explicit in urban morphology not only contribute to how cities evolve, but also to how the living organisms that inhabit them adapt. Marina Alberti's work has been instrumental in revealing how urbanization acts as an evolutionary force, altering not only ecological processes but also the adaptive traits of species (Alberti et al., 2020). Alberti illustrates that urban patterns such as fragmentation and connectivity can drive phenotypic changes in both plant and animal populations, influencing traits like dispersal ability, reproductive timing, and tolerance to pollutants. These changes are not merely side effects of urbanization but are part of a co-evolutionary process in which human and natural systems shape each other. Alberti argues that understanding these dynamics is crucial for urban planning, as the same spatial patterns that influence ecological adaptation can also be used to generate new ecological knowledge. For instance, the configuration of green infrastructure, street networks, and building densities can either support or hinder biodiversity, depending on how they affect habitat connectivity and resource availability. By linking urban morphology with evolutionary ecology, Alberti provides a framework for designing cities that are not only more resilient but also more attuned to the biological realities of urban ecosystems. Her work thus repositions urban planning as a driver of ecological innovation, capable of fostering adaptive capacity in both human and non-human communities.

2.1.4. Knowledge from describing urban features

Urban morphology has proven to be more than a descriptive lens: it offers direct relevance for urban planning, landscape ecology, and biodiversity conservation. By showing how spatial form shapes ecological processes and social interactions, it provides a framework to understand cities as living systems where built and natural structures co-evolve. This perspective positions morphology not only as a tool for interpreting the past but also as a means of identifying opportunities to guide urban development toward resilience and ecological integrity. To make this potential actionable, however, conceptual advances must be coupled with analytical precision. The next chapter turns to spatial analytical techniques, showing how urban features can be quantified and compared to generate knowledge that supports both scientific inquiry and planning practice.

2.2. Spatial analytical techniques for deriving quantifiable knowledge from urban features

2.2.1. Initial approaches

The first systematic attempts to derive quantifiable knowledge from urban features emerged in the 1960s, when urban morphology began to consolidate as a distinct field of inquiry. Researchers at the time were primarily concerned with describing and classifying the physical form of cities, often through typological studies of streets, blocks, and building patterns. This descriptive orientation reflected the influence of geography and architecture, where the city was understood as a material artifact that could be measured, compared, and categorized (Oliveira, 2022). Early studies relied on manual mapping and schematic representation, focusing on recurring forms such as grid layouts, radial structures, or irregular fabrics. These classifications were not only descriptive but also intended to provide a basis for comparative analysis across different urban contexts.

Early studies relied on manual mapping and schematic representation, focusing on recurring forms such as grid layouts, radial structures, or irregular fabrics. These classifications were not only descriptive but also intended to provide a basis for comparative analysis across different urban contexts. The Conzenian school was central in this regard: M. R. G. Conzen's work on Alnwick (1960) introduced the tripartite division of town plan into streets, plots, and buildings, which became a methodological cornerstone for urban morphology. By mapping these elements manually, Conzen demonstrated how the persistence of plot boundaries could reveal long-term processes of urban transformation, even when building fabrics changed. This approach established the principle that urban form could be studied through measurable units, and that these units carried historical depth (Conzen, 1960). The significance of these early approaches lies less in their technical sophistication than in their methodological stance. They established the principle that urban form could be studied through measurable features, and that these features could reveal broader processes of urbanization. This orientation toward systematic description created the conditions for subsequent innovations, including configurational analysis and spatial statistics. In this sense, the 1960s represent the formative stage of spatial analytical techniques, where the descriptive study of morphology began to evolve into a more explicitly analytical and comparative science.

In parallel, Italian scholars such as Saverio Muratori and his school in Rome developed typological methods that emphasized the study of building types and their aggregation into urban tissues. Muratori's *Studi per una operante storia urbana di Venezia* (1960) exemplified this approach, where schematic drawings of building types were used to trace the evolution of the Venetian urban fabric. The typological method was not only descriptive but also normative, as it sought to inform contemporary design practice by identifying enduring structural principles (Muratori, 1960). Similarly, Gianfranco Caniggia extended this line of inquiry by formalizing the concept of "process typology," which explained how urban tissues evolved through incremental transformations of basic building types (Caniggia, 1963).

These early approaches shared a reliance on schematic representation as a way to reduce the complexity of urban form into analyzable categories. Whether through Conzen's cartographic overlays of plots and streets or Muratori's typological diagrams, the aim was to establish reproducible frameworks for comparison. Oliveira (2022) notes that this period marked the transition from impressionistic descriptions of cities to systematic and measurable studies of urban form. The classifications of grid, radial, and irregular fabrics were not merely descriptive labels but analytical tools that allowed scholars to compare cities across different historical and cultural contexts. In this sense, the 1960s represent the formative stage of spatial analytical techniques, where the descriptive rigor of manual mapping and typological analysis laid the groundwork for later computational and configurational methods.

2.2.2. Configurational Approaches: The Emergence of Space Syntax

The emergence of space syntax in the late 1970s and early 1980s represented a decisive shift in the analytical study of urban form. Developed by Bill Hillier and Julienne Hanson, space syntax introduced a configurational perspective, where the focus moved from the classification of individual elements to the relational properties of entire spatial systems. In The Social Logic of Space (Hillier & Hanson, 1984), the authors argued that spatial configuration, defined as the pattern of connections and relations among spaces, plays a fundamental role in shaping patterns of movement, encounter, and social interaction. This marked a departure from earlier morphological approaches, which had emphasized descriptive typologies of plots, blocks, and building types, toward a framework that sought to explain how spatial form generates social effects.

The methodological innovation of space syntax lay in its ability to translate spatial configurations into graph-based representations. By reducing urban layouts to nodes and connections, researchers could measure properties such as integration, choice, and depth, which quantified the accessibility and centrality of spaces within a network. These measures provided a reproducible way to compare different urban systems and to test hypotheses about the relationship between spatial form and human behavior. Early applications demonstrated that highly integrated streets tended to attract more pedestrian movement, while segregated areas were more likely to experience social marginalization (Hillier, 1996).

Configurational analysis has since expanded beyond the street network to include other fundamental elements of urban form. Recent work on plot systems illustrates this extension: Bobkova, Berghauser Pont, and Marcus (2021) developed analytical typologies of plots across five European cities, showing how attributes such as plot size, frontage, and compactness can be translated into configurational measures. Their study demonstrates that plots, like streets, exhibit systematic relational properties that shape urban capacity for diversity, accessibility, and long-term transformation. This reinforces the broader claim of the configurational approach: spatial form, whether at the scale of streets or plots, is not merely a backdrop but an active generator of urban processes.

2.2.3. Quantitative Spatial Analysis and the GIS Revolution

From the 1980s onward, the rise of quantitative spatial analysis transformed the study of urban systems. While earlier morphological and configurational approaches emphasized description and relational structure, the integration of Geographic Information Systems (GIS) introduced a new capacity for handling large datasets, spatial statistics, and multi-scalar comparisons. This shift allowed urban researchers to move beyond schematic representations and to test hypotheses with empirical precision. Anselin's pioneering work on spatial econometrics demonstrated how spatial dependence and spatial autocorrelation could be formally measured, highlighting that urban phenomena such as housing prices, land use, or accessibility are rarely independent but instead clustered and interrelated across space (Anselin, 1988; Anselin, 2022).

The GIS revolution also enabled the systematic mapping of urban features at unprecedented scales. By digitizing cadastral maps, transport networks, and environmental layers, researchers could integrate diverse datasets into a single analytical framework. This integration facilitated studies of accessibility, for example through measures of travel time and service catchments, which became central to transport and planning research. Ertugay and Düzgün (2016) applied GIS-based accessibility modelling in Thessaloniki to evaluate health and shelter service provision under earthquake scenarios, showing how probabilistic road closures could dramatically alter service reach. Such case studies illustrate how GIS-based spatial analysis provided not only descriptive mapping but also decision-support tools for urban resilience.

Housing markets have been another major field of application. Shabrina, Arcaute, and Batty (2022) used geographically weighted regression to analyse the impact of Airbnb on London's housing market, demonstrating how spatial heterogeneity in short-term rental activity contributed to rising housing pressures in specific neighbourhoods. Their study exemplifies how spatial econometric methods can reveal localized effects that would be obscured in traditional global models. Similarly, Tepe and Guldmann (2020) developed parcel-level spatio-temporal models of land-use change, showing how neighbourhood history and proximity effects drive urban development dynamics. These works highlight the versatility of spatial econometrics in capturing both structural and behavioural dimensions of urban change.

Environmental exposure studies further expanded the scope of spatial analysis. Wang and Kwan (2018) introduced a context-based crystal-growth method for environmental exposure assessment, combining GIS with GPS trajectory data to capture individual-level exposure to pollutants in Chicago. Their approach demonstrated how spatial analysis could move beyond static residential measures to account for daily mobility patterns, thereby offering a more accurate picture of environmental inequalities. Similar methods have since been applied to urban heat island studies, where GIS-based spatial statistics are used to link land cover and morphology to localized temperature variations (Guo et al., 2020).

A defining characteristic of this phase was the development of reproducible statistical techniques that could be applied across contexts. Moran's I and related indices of spatial autocorrelation became standard tools for detecting clustering, while regression models incorporating spatial lags and error terms allowed for more accurate estimation of urban processes. These methods provided a bridge between urban morphology and the social sciences, as they enabled the quantification of relationships between spatial form and socioeconomic variables. The quantitative turn thus marked a methodological expansion: from descriptive and configurational analysis to computational and statistical modelling. By embedding urban form within a broader spatial-statistical framework, GIS and spatial econometrics established the conditions for contemporary data-driven approaches, where urban systems are analysed not only as physical structures but also as dynamic, measurable processes.

2.2.4. Data-Driven and Integrative Approaches in Urban Analysis

The contemporary phase of spatial analysis is defined by the integration of machine learning, remote sensing, and open data into urban research. Unlike earlier approaches that relied on manual mapping or statistical models, current methods exploit the availability of high-resolution spatial data and computational power to capture the complexity of urban systems. The distinction between supervised and unsupervised learning has become central in this context. Supervised methods, such as convolutional neural networks (CNNs), are widely used for classification tasks where labelled training data are available, for example in mapping land use or detecting informal settlements (Wurm et al., 2019). Unsupervised methods, including clustering algorithms like k-means or self-organizing maps, are applied when labels are absent, allowing researchers to identify emergent patterns in urban fabrics, such as functional clusters or morphological regions (Zhu et al., 2017). Both approaches extend the descriptive traditions of urban morphology into predictive and adaptive frameworks.

Remote sensing has been a key driver of this transformation. The increasing availability of very high-resolution (VHR) imagery from satellites and drones has enabled the detection of fine-grained urban features, from individual buildings to micro-scale land cover variations. High resolution, however, introduces methodological challenges: raster data (gridded cells) provide continuous coverage but require careful handling of spatial autocorrelation and resolution effects, while vector data (shapes such as parcels or building footprints) allow for precise delineation but often lack temporal depth. Contemporary spatial analysis often combines the two, using raster-based indices (e.g., NDVI, land surface temperature) alongside vector-based morphological measures (e.g., plot compactness, street centrality) to capture both continuous and discrete aspects of urban form (Guan et al., 2021).

The role of open data has also been transformative. Platforms such as OpenStreetMap provide global, freely accessible vector data on streets, buildings, and land use, which can be integrated with remote sensing imagery to enrich urban analysis. Mahabir et al. (2018) demonstrated how open data combined with high-resolution imagery can be used to detect and map informal settlements in Kenya, highlighting the potential of volunteered geographic information to complement Earth observation. Similarly, the So2Sat LCZ42 dataset (Zhu et al., 2020) has become a benchmark for training machine learning models to classify local climate zones worldwide, illustrating how open, standardized datasets accelerate methodological innovation and reproducibility.

These developments have expanded the scope of spatial analysis from descriptive and configurational studies to integrative, predictive, and operational frameworks. By combining supervised and unsupervised learning, remote sensing, and open data, contemporary approaches are capable of addressing both the physical and social dimensions of urban systems. The ability to process high-resolution data in both raster and vector formats ensures that urban analysis can capture the fine-grained heterogeneity of cities while maintaining scalability across regions. This integrative orientation positions spatial analysis not only as a research tool but also as a practical instrument for planning, governance, and resilience.

2.2.5. Gap and research opportunities

Contemporary spatial analysis has advanced rapidly, and yet key urban challenges remain under-addressed. While the literature prioritizes mapping the built form, land cover and use, ecological dimensions (e.g., biodiversity, habitat quality, and ecosystem connectivity) are often secondary. This imbalance limits the capacity of spatial tools to inform planning strategies that engage both human needs and ecological processes, particularly amid intensifying environmental degradation, deforestation, greenhouse gas emissions, water acidification, climate change, and rising temperatures (IPCC, 2023).

These pressures converge most acutely in biodiversity loss and urban overheating, the two focal problems of this thesis. The *IPCC AR6 Synthesis Report* underscores that warming has already reached hazardous levels, with near-term trajectories increasing risks to ecosystems, human health, and urban systems. It stresses the urgency of accelerated action to limit further biodiversity loss and mitigate heat-related impacts in cities (IPCC, 2023). Recent systematic reviews confirm that urban overheating is amplified by built-environment characteristics and requires integrative planning responses (Joshi et al., 2024), while biodiversity monitoring in cities remains fragmented despite advances in remote sensing (Finizio et al., 2024). Adaptation strategies exist, but they are often insufficiently embedded in planning frameworks (An & Dedekorkut-Howes, 2025).

Yet, spatial analysis itself continues to exhibit critical gaps that directly mirror the shortcomings identified in Section 1.3 regarding international frameworks on urban planning and ecological practices.

First, an implementation gap persists. Although high-resolution spatial data and advanced models are increasingly available, their outputs too often remain confined to academic demonstration rather than being embedded in planning practice. This reflects a broader pattern noted in global assessments, where ambitious commitments frequently fail to translate into operational change (UNEP, 2024). Second, skewed perspectives dominate much of the current literature, with emphasis placed either on built form or on ecological indicators in isolation. Reviews of urban biodiversity integration highlight that planning still privileges human-centric or infrastructural priorities, sidelining ecological processes (Dushkova et al., 2025; Prodanovic et al., 2024). Overcoming this imbalance requires integrative approaches that combine heterogeneous variables (e.g. ecological, morphological, demographic, thermal) within the same analytical pipeline, thereby capturing cross-domain dependencies. Third, low flexibility constrains existing methods: many spatial models are computationally intensive, rigid in their assumptions, and difficult to adapt to new datasets or local contexts. Recent work on modular clustering and adaptive urban growth boundaries demonstrates the potential of more flexible, scenario-based approaches (Liu et al., 2025). Finally, a lack of harmonization undermines comparability across scales and governance levels. This weakness is widely acknowledged in both biodiversity and climate governance, where fragmented mandates and overlapping reporting frameworks hinder coherent action (IPCC, 2023; UNEP, 2024). Here, spatial analysis can contribute by aligning outputs with international frameworks (e.g., SDGs, Sendai Framework, EU Green Deal) while tailoring indicators to local planning needs, thus creating a bridge between global reporting requirements and site-specific action.

This gap is particularly evident in the need for integrative frameworks that can simultaneously account for human and non-human liveability, and that can translate high-resolution spatial data into actionable planning tools. The challenge lies in bridging descriptive mapping with normative guidance: moving from identifying patterns to supporting decisions about where and how to intervene. Addressing this gap requires methodologies that combine unsupervised learning for landscape classification with multicriteria analysis for site prioritization, while leveraging open and high-resolution data sources to ensure reproducibility and scalability.

It is within this context that the thesis introduces two novel methodologies in Part 2 and Part 3 respectively. The first, Cohabscapes, develops a classification of urban landscapes that integrates geospatial and remote sensing data with unsupervised machine learning to describe liveability conditions for both human and non-human inhabitants. The second proposes a site-selection criterion for urban heat mitigation, combining morphometric spatial analysis with multicriteria ranking to identify suitable areas for intervention. Together, these contributions address the identified gap by extending contemporary spatial analysis into the ecological and climatic domains, offering tools that support cooperation between researchers and practitioners in fostering urban liveability.

2.3. References

Alberti, M., Palkovacs, E. P., Des Roches, S., De Meester, L., Brans, K. I., Govaert, L., Grimm, N. B., Harris, N. C., Hendry, A. P., Schell, C. J., Szulkin, M., Munshi-South, J., Urban, M. C., & Verrelli, B. C. (2020). The complexity of urban eco-evolutionary dynamics. *BioScience, 70*(9), 772–793. https://doi.org/10.1093/biosci/biaa079

Alexander, C., Ishikawa, S., & Silverstein, M. (1977). *A pattern language: Towns, buildings, construction* (Vol. 2). Oxford University Press.

An, S., & Dedekorkut-Howes, A. (2025). A review of adaptation strategies to increased urban temperatures and the heat island effect. *Discover Cities, 2*(32). https://doi.org/10.1007/s44327-025-00064-4

Anselin, L. (1988). Spatial econometrics: Methods and models. Springer. https://doi.org/10.1007/978-94-015-7799-1

Anselin, L. (2022). Spatial econometrics. In Handbook of spatial analysis in the social sciences (pp. 101–122). Edward Elgar Publishing. https://doi.org/10.4337/9781789903942.00014

Berghauser Pont, M., Stavroulaki, G., Bobkova, E., Gil, J., Marcus, L., & Olsson, J. (2019). The spatial distribution and frequency of street, plot and building types across five European cities. Environment and Planning B: Urban Analytics and City Science, 46(7), 1226–1242. https://doi.org/10.1177/2399808319857720

Bobkova, E., Berghauser Pont, M., & Marcus, L. (2021). Towards analytical typologies of plot systems: Quantitative profile of five European cities. Environment and Planning B: Urban Analytics and City Science, 48(4), 604–620. https://doi.org/10.1177/2399808320909780

Caniggia, G. (1963). Lettura di una città: Como. Centro Studi di Storia Urbanistica.

Colding, J., & Barthel, S. (2019). Exploring the social-ecological systems discourse 20 years later. *Ecology and Society, 24*(1), Article 2. https://doi.org/10.5751/ES-10598-240102

Conzen, M. R. G. (1960). Alnwick, Northumberland: A study in town-plan analysis. Institute of British Geographers.

Dushkova, D., Ignatieva, M., Müller, N., & Nilon, C. (2025). Editorial for special issue "Integrating biodiversity in the urban planning and design processes." *Urban Ecosystems, 28*(84). https://doi.org/10.1007/s11252-025-01697-4

Ertugay, K., & Düzgün, H. Ş. (2016). Accessibility modeling in earthquake case considering road closure probabilities: A case study of health and shelter service accessibility in Thessaloniki, Greece. International Journal of Disaster Risk Reduction, 17, 49–66. https://doi.org/10.1016/j.ijdrr.2016.03.004

Feliciotti, A., Romice, O., & Porta, S. (2016). Design for change: Five proxies for resilience in the urban form. *Open House International, 41*(4), 23–30. https://doi.org/10.1108/OHI-04-2016-B0004

Finizio, M., Pontieri, F., Bottaro, C., Di Febbraro, M., Innangi, M., Sona, G., & Carranza, M. L. (2024). Remote sensing for urban biodiversity: A review and meta-analysis. *Remote Sensing, 16*(23), 4483. https://doi.org/10.3390/rs16234483

Geertman, S., & Stillwell, J. (2009). Planning support systems: Best practice and new methods. Springer. https://doi.org/10.1007/978-1-4020-8952-7

Guan, Q., Zhu, Q., Guo, X., Deng, W., & Zhong, Y. (2021). Land-use/land-cover change detection based on a Siamese global learning framework for high spatial resolution remote sensing imagery. ISPRS Journal of Photogrammetry and Remote Sensing, 184, 63–78. https://doi.org/10.1016/j.isprsjprs.2021.01.015

Guo, A., Yang, J., Xiao, X., Xia, J., Jin, C., & Li, X. (2020). Influences of urban spatial form on urban heat island effects at the community level in China. Sustainable Cities and Society, 53, 101972. https://doi.org/10.1016/j.scs.2019.101972

Hillier, B. (1996). Space is the machine: A configurational theory of architecture. Cambridge University Press.

Hillier, B., & Hanson, J. (1984). The social logic of space. Cambridge University Press.

Intergovernmental Panel on Climate Change (IPCC) (2023). Climate Change 2023: Synthesis Report. Contribution of Working Groups I, II and III to the Sixth Assessment Report of the Intergovernmental Panel on Climate Change [Core Writing Team, H. Lee, & J. Romero (Eds.)]. IPCC. https://doi.org/10.59327/IPCC/AR6-9789291691647

Joshi, K., Khan, A., Anand, P., & Sen, J. (2024). Understanding the synergy between heat waves and the built environment: A three-decade systematic review informing policies for mitigating urban heat island in cities. *Sustainable Earth Reviews, 7*(25). https://doi.org/10.1186/s42055-024-00094-7

Karimi, K. (2018). Space syntax: consolidation and transformation of an urban research field. Journal of Urban Design, 23(1), 1–4. https://doi.org/10.1080/13574809.2017.1407080

Kropf, K. (1996). Urban tissue and the character of towns. *Urban Design International, 1*(3), 247–263. https://doi.org/10.1057/udi.1996.32

Liu, Z., Gong, B., Lü, Z., He, C., Salem, M., Osman, T., & Liu, H. (2025). A framework for creating urban growth boundaries that integrate ecological protection and disaster risk reduction. *Landscape Ecology, 40*(122). https://doi.org/10.1007/s10980-025-02143-8

Mahabir, R., Croitoru, A., Crooks, A., Agouris, P., & Stefanidis, A. (2018). Detecting and mapping slums using open data: A case study in Kenya. International Journal of Digital Earth, 11(1), 1–25. https://doi.org/10.1080/17538947.2017.1349846

Marcus, L. (2010). Spatial capital. *Journal of Space Syntax, 1*(1), 30–40. UCL Space Syntax Laboratory.

Marcus, L., & Colding, J. (2014). Toward an integrated theory of spatial morphology and resilient urban systems. *Ecology and Society, 19*(4), 55. https://doi.org/10.5751/ES-06939-190455

Marcus, L., Berghauser Pont, M., & Barthel, S. (2019). Towards a socio-ecological spatial morphology: Integrating elements of urban morphology and landscape ecology. *Urban Morphology, 23*(2), 115–124.

Mehaffy, M. W., Kryazheva, Y., Rudd, A., Salingaros, N. A., & Gren, A. (2020). *A new pattern language for growing regions: Places, networks, processes*. Sustasis Foundation.

Muratori, S. (1960). Studi per una operante storia urbana di Venezia. Istituto Poligrafico dello Stato.

Oliveira, V. (2022). Urban morphology: An introduction to the study of the physical form of cities (2nd ed.). Springer. https://doi.org/10.1007/978-3-030-92454-6

Oliveira, V. (Ed.). (2019). *J.W.R. Whitehand and the historico-geographical approach to urban morphology*. Springer. https://doi.org/10.1007/978-3-030-00620-4

Palazzo, E. (2022). Bridging urban morphology and urban ecology: A framework to identify morpho-ecological periods and patterns in the urban ecosystem. *Journal of Urban Ecology, 8*(1), juac007. https://doi.org/10.1093/jue/juac007

Porta, S., Crucitti, P., & Latora, V. (2006). The network analysis of urban streets: A dual approach. *Physica A: Statistical Mechanics and its Applications, 369*(2), 853–866. https://doi.org/10.1016/j.physa.2005.12.063

Porta, S., Romice, O., Feliciotti, A., & Slade, G. (2017). Plot-based urbanism and the design of urban form. *Urban Morphology, 21*(1), 1–14.

Prodanovic, V., Bach, P. M., & Stojkovic, M. (2024). Urban nature-based solutions planning for biodiversity outcomes: Human, ecological, and artificial intelligence perspectives. *Urban Ecosystems, 27*, 1795–1806. https://doi.org/10.1007/s11252-024-01558-6

Schirmer, P. M., & Axhausen, K. W. (2019). A multiscale clustering of the urban morphology for use in quantitative models. In C. B. Jones & J. M. Portugali (Eds.), *The mathematics of urban morphology* (pp. 355–382). Springer International Publishing. https://doi.org/10.1007/978-3-030-12381-9_16

Shabrina, Z., Arcaute, E., & Batty, M. (2022). Airbnb and its potential impact on the London housing market. Urban Studies, 59(1), 197–221. https://doi.org/10.1177/00420980211014820

Tepe, E., & Guldmann, J. M. (2020). Spatio-temporal multinomial autologistic modeling of land-use change: A parcel-level approach. Environment and

Planning B: Urban Analytics and City Science, 47(3), 473–488. https://doi.org/10.1177/2399808318785630

United Nations Environment Programme. (2024). *Multilateral Environmental Agreements Negotiator's Handbook* (3rd ed.). UNEP. https://wedocs.unep.org/bitstream/handle/20.500.11822/7496/Guide_for_MEAs_final.pdf

Wang, J., & Kwan, M. P. (2018). An innovative context-based crystal-growth activity space method for environmental exposure assessment: A study using GIS and GPS trajectory data collected in Chicago. International Journal of Environmental Research and Public Health, 15(4), 703. https://doi.org/10.3390/ijerph15040703

Whitehand, J. W. R. (2001). British urban morphology: The Conzenian tradition. *Urban Morphology, 5*(2), 103–109.

Whitehand, J. W. R., & Morton, N. J. (2003). Fringe belts and the recycling of urban land: An academic concept and planning practice. *Environment and Planning B: Planning and Design, 30*(6), 819–839. https://doi.org/10.1068/b12997

Wurm, M., Stark, T., Zhu, X. X., Weigand, M., & Taubenböck, H. (2019). Semantic segmentation of slums in satellite images using transfer learning on fully convolutional neural networks. ISPRS Journal of Photogrammetry and Remote Sensing, 150, 59–69. https://doi.org/10.1016/j.isprsjprs.2019.02.006

Zhu, X. X., Hu, J., Qiu, C., Shi, Y., Kang, J., Mou, L., Bagheri, H., Häberle, M., Hua, Y., & al. (2020). So2Sat LCZ42: A benchmark dataset for global local climate zones classification. IEEE Geoscience and Remote Sensing Magazine, 8(3), 76–89. https://doi.org/10.1109/MGRS.2020.2964708

Zhu, X. X., Tuia, D., Mou, L., Xia, G. S., Zhang, L., Xu, F., & Fraundorfer, F. (2017). Deep learning in remote sensing: A comprehensive review and list of resources. IEEE Geoscience and Remote Sensing Magazine, 5(4), 8–36. https://doi.org/10.1109/MGRS.2017.2762307

PART 2.

Urban environment and biodiversity loss

Chapter 3.

A step toward understanding urban habitats for human and non-human inhabitants: the Cohabscapes classification

Abstract

This chapter presents a novel methodological framework for classifying urban landscapes through the lens of cohabitation, with a focus on the spatial dynamics that sustain both human and non-human life. Urban liveability is increasingly recognised as a function of spatial and ecological qualities, yet existing frameworks rarely provide a species-generic classification that combines high spatial resolution with multidimensionality. This gap limits the translation of ecological insights into actionable planning strategies, including Nature-Based Solutions (NBS).

To address this Cohabscapes (from Co-Habitative landScapes) is introduced, a framework designed to classify urban landscapes at 10-metre resolution across four complementary dimensions: Local and Landscape Urban Fabric, Anthropic Imprint, and Biophysical Conditions. The method relies exclusively on open-access geospatial and remote sensing data, processed through automated pipelines that integrate Principal Component Analysis with unsupervised K-Means clustering, ensuring scalability and adaptability to diverse urban contexts.

Applied within the H2020 ECOLOPES project to Vienna, Munich, and Genoa, Cohabscapes produced 32 distinct classes, enabling nuanced differentiation between core and peri-urban areas. Comparative validation with Urban Atlas and Morphological Settlement Zones confirmed that Cohabscapes achieves stronger integration of socio-economic and biophysical data, offering a more comprehensive representation of urban liveability. As a socio-ecological and planning application, we link Cohabscapes classes to citizen-science observation on 30 bird species to identify urban conditions supporting human-nature interactions. The results pinpoint sets of conditions that can inform targeted NBS objective to promote multispecies liveability in cities. The outcomes of this chapter are threefold:

i. A transferable, open-access framework that bridges urban ecology and planning through a species-generic, high-resolution classification.

ii. Enhanced integration of socio-economic and biophysical dimensions, surpassing existing frameworks in representing urban liveability.

iii. Exemplified the ecological relevance, by correlating data from 30 bird species to Cohabscapes layers, enabling more inclusive and effective NBS strategies.

By framing urban space as a shared habitat, Cohabscapes advances ecological research and sustainable urban planning through a practical, adaptable mapping tool for designing resilient and liveable cities.

Keywords

urban landscape; cohabitation; unsupervised classification

Acknowledgements

The author gratefully acknowledges the fruitful discussions between the ECOLOPES consortium members that improved and shaped the initial versions of this Chapter.

The author acknowledges with appreciation the stimulating discussion held with the Chair of Terrestrial Ecology (TUM) researchers, particularly Rafael Achury, Andrew Fairbairn, Victoria Culshaw, Robert Kunast, Sebastian Meyer, Annika Neuhaus, Lisa Merkens, Fabio Sweet, Wolfgang Weisser, and Laura Windorfer.

The author gratefully notes that this Chapter's content was presented at URBIS24 (Rome, Tor Vergata University, under the European Space Agency framework) (16/09/2024), at the 54th Annual Conference of the *Gesellschaft für Ökologie* (GfÖ) in Freising, and during seminars at Chair of Terrestrial Ecology, TUM, Freising (19/03/2024), and the Laboratoire BioadivAG, University of Angers (06/03/2025). These occasions provided valuable feedback that helped refine the work.

This Chapter has been prepared using European Union's Copernicus Land Monitoring Service information. The DOI links are in the References section.

Preliminary research results that served as the backbone of this Chapter are currently published as preprint at https://doi.org/10.1101/2024.11.11.622937, and as technical article for the ECOLOPES project found at https://ecolopes.org/wp-content/uploads/2025/01/Oneto-et-al_Urban-classification.pdf. Further research results, especially related to a larger pool of 195 European bird species and a deeper quantitative analysis, have led to an additional research paper (*Cities, Elsevier*, under review).

3.1. Introduction

3.1.1. The ECOLOPES project and characterising urban landscapes for ecologically-sound designs

The ECOLOPES project (ECOlogical building enveLOPES: a game-changing design approach for regenerating urban ecosystems; https://ecolopes.org/) represents a significant attempt to rethink the relationship between architecture, ecology, and urban form by proposing envelopes of buildings that function as ecological interfaces rather than inert boundaries. Its central aim is to integrate biodiversity and ecological processes into the very fabric of urban landscapes, moving beyond the traditional dichotomy between built and natural environments. Recent scholarship has highlighted how urban morphology can be redefined through ecological design strategies that embed habitats within façades, roofs, and transitional spaces, thereby creating conditions for species coexistence in dense metropolitan contexts (Perini & Magliocco, 2014). For example, experimental prototypes developed within ECOLOPES explore how vegetated building skins can provide microhabitats for pollinators and birds while simultaneously regulating thermal performance, thus linking ecological and technical functions (Stavric et al., 2021). This approach resonates with broader debates in landscape urbanism, where the city is increasingly understood as a hybrid ecosystem requiring careful calibration of spatial, material, and biological variables (Steiner, 2020). Characterising urban landscapes for such ecologically-sound designs requires not only mapping vegetation cover or species presence but also assessing flows of energy, water, and human activity that influences the liveability of the city for urban dwelling species. Recent studies on urban ecological networks demonstrate that fragmented green areas can be reconnected through corridors integrated into architectural envelopes, thereby enhancing resilience against climate stressors (Haaland & van den Bosch, 2021). The ECOLOPES framework thus contributes to a methodological shift: instead of treating ecological performance as an afterthought, it positions it as a generative principle of design. In conclusion, characterising urban landscapes through the lens of ecological functionality allows architects and planners to move toward a more systemic integration of biodiversity, where buildings are not isolated objects but active participants in the metabolism of the city.

3.1.2. The challenge of planning, designing, and researching multispecies liveability

Human health and well-being are fundamentally connected to natural systems, a relationship acknowledged in policy and practice (Felappi et al., 2020; Audusseau et al., 2024). European cities are increasingly adopting designs and management approaches that support, rather than exclude, biodiversity (Shingne, 2020). Nature-Based Solutions (NBS) have been promoted to integrate natural elements into urban fabrics and enhance liveability for people and other species (Eggermont et al., 2015; Sowińska-Świerkosz and García, 2022). Despite this, NBS encounter obstacles across multiple development stages that limit their full potential (Apfelbeck et al., 2020). Consequently, the urban ecology of many non-human species, such as covering behaviour, habitat use, and interspecific interactions (including with humans), remains poorly understood (Alberti, 2015; Moreno-García et al., 2025). Where knowledge does exist, it is often specific to individual cities, and its transferability across different cities and species is largely untested (Moreno-García et al., 2025; Pickett et al., 2016). This gap is compounded at the planning level, where the integration of ecological and sociological knowledge into design solutions is limited, revealing weak coordination between disciplines (Finnerty et al., 2025; Wang et al., 2024). Addressing this challenge requires building disciplinary bridges that enable the creation and transfer of knowledge. This Chapter proposes one such bridge: a common descriptive framework of urban conditions that underpin liveability for synanthropic species, including humans, and that can inform the range of disciplines involved in NBS, from fundamental ecological and sociological research (suitable for any species) to design, planning, and governance.

The proposed urban description is founded on a multidimensional, local account of the urban environment that spans purely abiotic conditions (climate, topography, hydrology) through urban fabric and anthropic use (Rega-Brodsky et al., 2022).

3.1.3. Local conditions and ecological opportunities

Local conditions determine the ecological opportunities available to species according to their niches, thereby shaping the distribution, movement, and well-being of humans, plants, and animals (Hutchinson, 1957; Wong & Candolin, 2019; Alberti et al., 2015). Consequently, a city's liveability depends on the conditions organisms encounter during their daily activities (Raymond et al., 2025). These conditions arise from interactions among features and from their spatial arrangement. Thus a single element such as a tree can affect liveability differently when isolated versus when it is part of a larger wooded area. A growing body of work shows that local conditions (microclimate, resource availability, shelter, and disturbance levels) emerge from the regional setting (topography, climate, native species) together with urban structure and management practices (Eggermont et al., 2015; Aronson et al., 2016). Buildings, vegetation, water bodies, and management practices, such as lighting or traffic control, modify local temperature, moisture, connectivity, and resource distribution; these altered conditions determine whether organisms can establish, move, feed, and reproduce (Fischer & Lindenmayer, 2006; McPhearson et al., 2022). Because species differ in physiology and ecology, the same location can be favourable to one taxon and hostile to another; this taxon specificity is well documented and underlines the need for multispecies urban descriptions that are broadly applicable yet precise enough to capture species-specific responses (Mimet et al., 2013; Marrec et al., 2020). Beyond niche availability, urban liveability for a species also depends on the presence of interacting species-competitors, predators, or mutualists, each governed by their own ecological conditions, creating interdependencies that shape community composition. Therefore, a multispecies urban description enables the study of species interactions and community assembly across ecological organization levels, from individual niche responses to community dynamics.

3.1.4. Describing the context for multispecies interaction

3.1.4.1. Continuous gradients and spatial interactions

The liveability conditions described above do not appear as abrupt, discrete changes tied to single urban features (trees, streets, buildings), but rather as continuous gradients that emerge from the relational interactions among those features. For example, local temperature and humidity beneath a tree depend on the tree's characteristics (broadleaf versus coniferous, size, species) and the point's position relative to the crown, but also on surrounding elements such as soil moisture, pavement cover, and nearby shading from other trees or buildings. These interactions affect humans as well as non-human inhabitants, since conditions at any location result from the combination of elements at varying distances and their spatial arrangement (Pickett et al., 2017). This behaviour motivates a continuous, fine-scale description of the urban environment rather than an object-oriented one (Fischer & Lindenmayer, 2006; Aronson et al., 2016; Mimet et al., 2013).

3.1.4.2. Four dimensions of urban liveability

The local conditions that shape urban liveability can be organised along four separable dimensions, building on the hierarchical filters identified by Aronson et al. (2016) as governing species distribution in cities. At the broadest level, regional abiotic conditions (climate, topography, hydrology) set the baseline environmental context. These are modulated by the structural fabric of the city (vegetation, buildings, water bodies), by landscape context (connectivity, patch configuration, spatial arrangement of elements), and finally by anthropic signals (management practices, lighting, and traffic) which operate at the finest and most dynamic scale.

Explicitly separating these dimensions allows each driver to be examined and acted on independently (Heymans et al., 2019; Zhao et al., 2024). Returning to earlier examples, a street tree simultaneously modifies local microclimate (abiotic), provides nesting and foraging substrate (fabric), enhances connectivity between green patches (landscape), and alters pedestrian use and lighting needs (anthropic) (Aronson et al., 2016).

Conversely, a city square concentrates heat and runoff (abiotic), reduces shelter and food resources (fabric), fragments movement corridors for small fauna (landscape), and concentrates human activity and management interventions (anthropic) (Stewart & Oke, 2012; EEA, 2022). Such a framework enables planners and researchers to identify which urban condition classes support or limit biodiversity and to prioritise NBS interventions accordingly. Treating these dimensions as distinct but combinable layers preserves disciplinary detail while reducing misalignment between ecological analysis and planning practice (McPhearson et al., 2022), keeping the specific drivers of any observed pattern identifiable and actionable (Zhao et al., 2024; Heymans et al., 2019).

3.1.5. Existing classification systems and gaps

Implementing a continuous, multidimensional, species-generic description of urban conditions requires assessing whether existing urban classification systems already provide the necessary tools. Cities are currently described through several methods: land-use taxonomies, morphological typologies, climate-oriented morphologies, functional zoning, and green infrastructure inventories (Table 1). These descriptions employ different semantics, units, and scales, producing spatial mismatches (parcels versus rasters, coarse administrative polygons versus fine ecological gradients) and pursuing divergent objectives (planning, climate modelling, biodiversity conservation). This diversity complicates the translation of ecological knowledge into actionable NBS (Eggermont et al., 2015; Sowińska-Świerkosz & García, 2022). Existing systems contribute useful elements but do not jointly fulfil the requirements of a comprehensive, multidimensional, high-resolution, and transferable description. Local Climate Zones capture morphology relevant to heat studies but are not designed for multispecies inference; functional zoning incorporates socioeconomic information but remains largely anthropocentric. Green infrastructure taxonomies add ecological detail but often omit spatial configuration and anthropic signals (EEA, 2022; Pesaresi & Panagiotis, 2023; Stewart & Oke, 2012; Morpurgo et al., 2023). These gaps create demand for common descriptive building blocks that are computable from open data and interpretable across disciplines (Li et al., 2019; Shouhang et al., 2024; Fleischmann & Arribas-Bel, 2022). For example, Urban Functional Zone (UFZ) approaches represent an important body of work for characterising dominant human uses of urban space, often relying on points-of-interest, mobility data, and remote sensing (Lu et al., 2022; Du et al., 2024). This aspect is also common to Spatial Signatures (Fleischmann & Arribas-Bel, 2022). These approaches primarily address the functional organisation of cities from an anthropocentric perspective and generally do not represent the combined biophysical, structural, and anthropic conditions that shape multispecies liveability.

Table 1. Current main urban classification systems organised for direct comparison. Columns: System; Primary focus; Dimensional coverage (Abiotic; Fabric; Anthropic); Typical resolution; Geographic scope.

System	Primary focus	Dimensional coverage (Abiotic; Fabric; Anthropic)	Typical resolution	Geographic scope
Urban Atlas (EEA, 2022)	Land use mapping for planning and monitoring	Abiotic: low; Fabric: medium; Anthropic: medium	Vector polygons (MMU 0.25 ha); derivatives at 10 m	Europe
Morphological Settlement Zones (MSZ) (Pesaresi & Panagiotis, 2023)	Built-up continuity for sprawl and density analysis	Abiotic: low; Fabric: high; Anthropic: low	Built-up raster inputs ~10 m; neighbourhood aggregates ~100 m	Europe / Global (GHSL)
Urban Functional Zones (UFZ) (Shouhang et al., 2024)	Functional zoning and mobility from POI and remote sensing	Abiotic: low; Fabric: medium; Anthropic: high	Variable (polygonal or grid outputs)	Increasingly global
Local Climate Zones (LCZ) (Stewart & Oke, 2012)	Urban morphology for climate and heat island studies	Abiotic: high; Fabric: high; Anthropic: low	Standard LCZ unit commonly represented at ~100 m	Global
WorldPop Settlement Patterns (Jochem et al., 2021)	Building footprint patterns for population and growth modelling	Abiotic: low; Fabric: high; Anthropic: medium	Often aggregated to 100 m grids; building footprints finer	Global
MODUM (Alexiou et al., 2016)	Density and accessibility for compact city and transport planning	Abiotic: low; Fabric: high; Anthropic: medium	Small-area units; derived metrics at ~10–100 m	Europe
Spatial Signatures (Fleischmann & Arribas-Bel, 2022)	Morphology and function for typology and analytics	Abiotic: low; Fabric: high; Anthropic: medium	Fine urban tessellation units aggregated to signatures	National / scalable
Urban Morphological Zones (UMZ) (EEA, 2013)	Built-up proximity for urban-rural gradient and planning	Abiotic: low; Fabric: medium; Anthropic: low	Polygonal zones; MMU similar to Urban Atlas	Europe
Global Urban Footprint (GUF) (DLR, 2014)	SAR imagery for global urbanization and risk assessment	Abiotic: low; Fabric: high; Anthropic: low	Binary raster, native ~12 m	Global
Urban Expansion Typologies (Angel et al., 2016)	Historical growth typologies from satellite imagery	Abiotic: low; Fabric: medium; Anthropic: low	Temporal satellite mosaics; resolution depends on imagery	Global
Consolidated Urban Green Infrastructure Classification (CUGIS) (Morpurgo et al., 2023)	Vegetation and land use for ecosystem and biodiversity planning	Abiotic: medium; Fabric: high; Anthropic: medium	Vegetation-focused classes; mapping unit variable	Global applicability

3.1.6. Aim and objectives

The aim of this work is to develop a transferable, species-generic classification method that represents urban conditions at fine grain (10-metre resolution) across four complementary dimensions: Local Urban Fabric, Landscape Urban Fabric, Anthropic Imprint, and Biophysical Conditions. The objectives are as follows.

i. Operationalise local condition descriptors using open geospatial data and moving-window summaries.

ii. Derive independent sub-classifications for each environmental dimension and recombine them into integrated condition classes.

iii. Evaluate the framework through internal optimisation and external comparison with established systems.

iv. Demonstrate the ecological and planning relevance of the framework by linking the Cohabscapes classes to detection levels for a range of bird species, identifying classes that best support human–nature interactions and could therefore guide targeted NBS interventions.

Achieving these goals requires methods that represent space continuously at fine grain, summarise local composition and configuration at scales relevant to how organisms use urban space, and preserve separability across the four dimensions. The resulting framework is intended to bridge ecological insight and urban planning practice, supporting NBS that account for interactions among features, among species, and between species and their environment.

3.2. Methodology

3.2.1. Overall Cohabscapes methodology

The Cohabscapes (from Co-Habitative landScapes) is a classification methodology introduced to delineate urban environments for multiple inhabitants, employing four distinct sub-classifications to organise data and enable a more detailed analysis of different urban dimensions. The first and second sub-classifications, grouped under Urban Form, describe urban morphology at both local and landscape scales. The Anthropic Imprint sub-classification captures human interactions with urban areas, including land-use policies, anthropogenic emissions, services, and economic orientation. The Biophysical Conditions sub-classification refers to abiotic attributes (e.g., climate, orography) that shape urban conditions and dynamics.

The Cohabscapes methodology is structured in four steps. Following city selection, it (1) defines urban boundaries, classification units, and scales; (2) compiles datasets for each sub-classification; (3) preprocesses the data; and (4) applies unsupervised clustering (Fig. 1). The methodology is implemented in Python using established geospatial libraries (see Annex A for details)

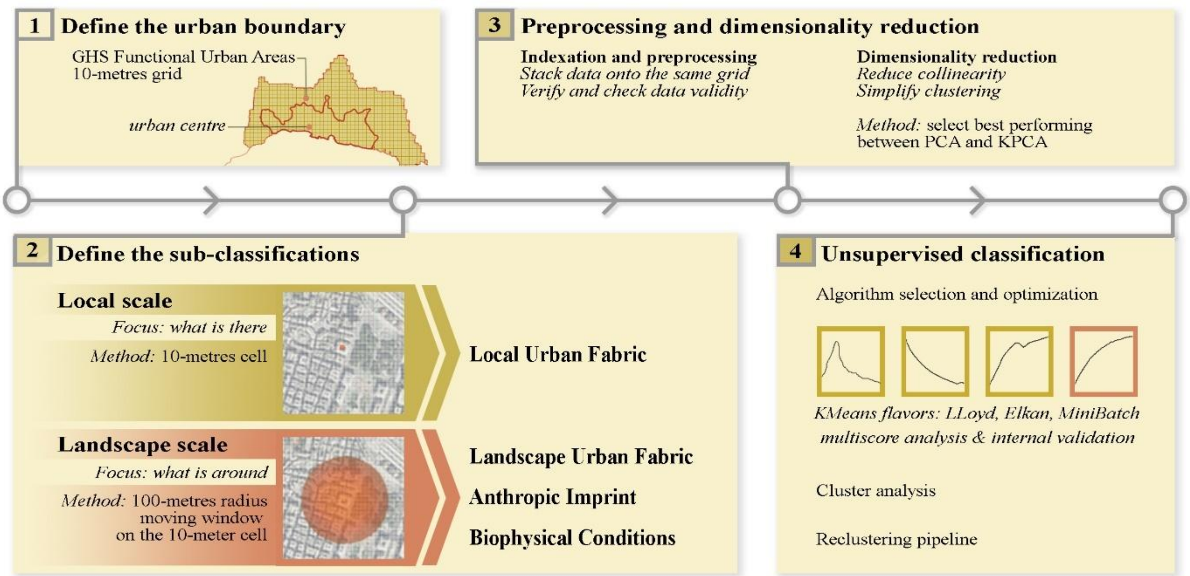

Figure 1: Steps of the Cohabscapes methodology. The first step regards setting the computation spatial limits (i.e., the urban boundary) and the resolution. The second step involves selecting relevant variables for each sub-classification, selecting opensource data repositories and computing variables descriptive of the local and landscape-scales conditions. The third step preprocesses data in terms of standardization techniques and dimensionality reduction to extract intra-subclassification dimensions and smooth the classification process. The fourth and last step consists of the clustering of the 10-metres cells through unsupervised classification, optimisation and cluster content analysis to characterize and name the resulting classes

3.2.2. Step 1: Defining the urban boundary, the classification units, and the classification scales

3.2.2.1. Urban boundaries

Urban areas are delineated according to the Global Human Settlement Layer Functional Urban Areas (Schiavina et al., 2023), developed under the auspices of the Organisation for Economic Co-operation and Development (https://www.oecd.org/en.html) and the European Union (Dijkstra et al., 2019). This approach integrates satellite-derived settlement data with population density and commuting patterns to define urban centres and their functional extents. Within the context of multispecies liveability, this delineation provides a consistent spatial unit suitable for comparing ecological and social conditions across regions.

3.2.2.2. Classification units

Classification units are defined as 10 m resolution cells, based on an equiareal global grid projected onto the Mollweide coordinate system (ESRI:54009; further details in Annex A). Unlike irregular polygons, which lack inherent scale and are difficult to relate to ecological or socio-economic processes, raster cells offer a consistent, scale-explicit framework. This is particularly relevant because many ecological and social processes are scale-dependent, and both humans and other species perceive and interact with their environments at different spatial resolutions (Wu, 2004). A uniform 10 m grid represents a practical compromise: it is sufficiently detailed to capture ecological structures, landscape heterogeneity, and urban features, while remaining computationally feasible and supported by available datasets, ensuring scalability across large areas and applicability across domains.

3.2.2.3. Local and landscape scales

The classification framework operates at two spatial scales: local and landscape. The local scale is defined by individual 10 m grid cells and captures the immediate characteristics of the urban fabric. The landscape scale summarises the surrounding context within a 100 m radius of each cell, representing a generic neighbourhood setting rather than species-specific movement ranges.

The 100 m radius was chosen as a compromise supported by literature to capture how nearby elements such as vegetation structure, built density, disturbance, and microclimate, shape local urban conditions that affect multiple taxa and human perception at a fine spatial grain (McCaffrey & Mannan, 2012; Mitchell et al., 2016; González Gómez et al., 2022). Recent findings indicate that environmental predictors act across a wide range of characteristic radii depending on the process considered, with several predictors (topographic, transport, vegetation) and some edaphic factors favouring a 100 m extent (Collart et al., 2025). This evidence supports a layered rather than a single-scale approach.

Accordingly, the framework adopts the highest feasible spatial resolution and the smallest transferable neighbourhood extent, enabling later aggregation to broader scales for downstream analyses.

3.2.3. Step 2: Defining the sub-classifications

To organise the drivers of the social and ecological processes that shape urban multispecies liveability, variables were grouped into four sub-classifications following the hierarchical filter logic of Aronson et al. (2016). Local Urban Fabric and Landscape Urban Fabric act as structural filters, describing built and natural elements that determine habitat structure and spatial configuration at local and neighbourhood scales. Anthropic Imprint captures human activities and management signals that function as dynamic filters on disturbance and resource availability. Biophysical Conditions cover abiotic constraints (climate, topography, and hydrology) that set baseline environmental limits. Separating variables in this way preserves ecological meaning while supporting planning-oriented interpretation and targeted intervention. Variables were chosen from the literature for their relevance to core ecological and social processes affecting urban liveability and for their availability in open, globally consistent datasets. Each variable was assigned uniquely to one sub-classification according to its primary role within the hierarchical filter logic to avoid redundancy. Data quality checks addressing noise and related issues were performed (see Annex A and the commented Jupyter notebooks for details). It should be noted that correlations between variables across sub-classifications are to be expected in urban systems and reflect interacting structural, anthropic, and biophysical processes rather than analytical bias.

3.2.3.1. Local Urban Fabric

Nine variables were selected to describe both built features (e.g., built-up fraction, imperviousness degree) (Boeing, 2018) and vegetation conditions (e.g., tree cover density, water presence) (Wentz et al., 2018) (Table 2).

Table 2. Variables for Urban Form local sub-classification.

Category	**Variable**	**Data source**	**Native resolution**	**Reference**
Artificial features	Built-up fraction	GHS Built-S layer	10 metres	Pesaresi M. & Panagiotis P. 2023a
	Building height	GHS Built-C layer Morphological Settlement Zones; Urban Atlas Building Height 2012	100 metres; 10 metres	Pesaresi M. & Panagiotis P. 2023b; EEA, 2022
	Mayor transport route presence	OSM; GHS Built-C layer Morphological Settlement Zones	Vectorial; 10 metres	http://www.openstreetmap.org/; Pesaresi M. & Panagiotis P. 2023b

	Imperviousness density	CLMS HRL Imperviousness	10 metres	EEA, 2020a
Natural features	Tree cover density	CLMS HRL Tree cover density	10 metres	EEA, 2020b
	Grassland presence	CLMS HRL Grassland	10 metres	EEA, 2020c
	Shrub presence	CLMS HRL Small woody features	10 metres	EEA, 2020d
	Agricultural land presence	European Space Agency WorldCoverV2 2021	10 metres	Zanaga et al., 2022
	Aquatic surface presence	CLMS HRL Water and wetness	10 metres	EEA 2023
	Count of different land covers	All the above	-	-

3.2.3.2. Landscape Urban Fabric

This sub-classification incorporates landscape composition, diversity, and configuration. To maintain consistency with the local scale, 24 variables were derived from the local urban form sub-classification. Composition variables were calculated from the Principal Component (PC) values of each cell in the local urban form PCA, expressed as the mean and standard deviation of the 10 PCs within the 100 m landscape radius (moving window approach[1]). This approach accounts for quantitative differences in cell composition along the PCs. Landscape diversity and configuration were derived from local urban form classes by computing Shannon's Diversity Index and the contagion index, using FragStats 4.2 (https://fragstats.org/; McGarigal et al., 2023).

[1] The moving window (also called sliding window) is a way of looking at data step by step, in small portions. Formally, a moving/sliding window is a fixed-size subset of sequential data that moves one step (or more) at a time across the dataset. At each position, computations are performed only on the elements inside the window. This approach reduces complexity by localizing operations, making it useful in signal processing (e.g., moving averages) and algorithm design (e.g., substring search, maximum/minimum problems). The efficiency comes from reusing partial results as the window shifts, rather than recalculating from scratch. In this application, the window size is also carefully defined as a matrix of size R x R, where R = 11 cells equalling a radius of 110 metres, as for the analysis requirements. The matrix itself serves as a inscribed circular kernel of radius R/2, centred on (R/2; R/2).

3.2.3.3. Anthropic Imprint

For Anthropic Imprint 13 variables were selected at the landscape scale to capture demographic characteristics, service accessibility, urban policy, and anthropic emissions (Table 3). Demography and land use directly reflect human activity in urban areas: the former provides a direct measure, while the latter represents passive human activities such as intensive industrial operations or park regulations (Clifton et al., 2008). Passive anthropic emissions, including nighttime light pollution and heat release, are also included due to their documented effects on urban wildlife (Crippa et al.,2021).

Table 3. Variables for Anthropic Imprint sub-classification.

Category	Variable	Data source	Native resolution	Reference
Demographics	Population Density	GHS Population	100 metres	Schiavina et al., 2023
	Age Structures: 0-15	WorldPop Age and Gender structured	100 metres	Bondarenko et al. 2020
	Age Structures: 20-35			
	Age Structures: 40-60			
	Age Structures: 65-85			
Land use: Services, accessibility, policy	Commercial Area Ratio	OSM	Vectorial	www.openstreetmap.org
	Industrial Area Ratio			
	Public Services Area Ratio			
	Recreational Area Ratio			
	Cultural Location Ratio			
	Public Green Proportion	OSM; CLMS HRL Tree cover density, CLMS HRL Grassland, CLMS HRL Small woody features	Vectorial; 10 metres; 10 metres; 10 metres	www.openstreetmap.org; EEA, 2020b; EEA 2020c; EEA, 2020d
	Preservation Policy Ratio	World Database on Protected Areas	Vectorial	United Nations Environment Programme - World Conservation Monitoring Centre, 2019
	Average Distance to Public Transport	OSM	Vectorial	www.openstreetmap.org

Anthropic emissions	Nighttime light Pollution	Luojia 1-A	130 metres	Chen et al., 2022
	Anthropogenic Heat Flux	Average Anthropic Heat Emission	1000 metres	Varquez et al., 2021

3.2.3.4. Biophysical Conditions

This sub-classification captures hydrological, topographical, pedological, and climatic conditions at the landscape scale. To represent both central tendencies and variability, 19 variables were derived from the mean and standard deviation of the input data (Table 4). A key challenge was to reflect both large-scale climatic differences (e.g., between Genoa and Vienna) and city-scale variations (e.g., local effects of topography and urbanisation). This was addressed by extracting both absolute and city-relative climate variables, with the latter calculated by weighting cell values against city-wide means. Standard deviation was excluded for climate data, as preliminary analyses showed that the coarse native resolution of 1000 m produced strong gridded patterns that negatively affected clustering.

Table 4. Variables for Biophysical Conditions sub-classification.

Category	**Variable**	**Data source**	**Native resolution**	**Reference**
Hydrology	Permanent water ratio	CLMS HRL Water and wetness	10 metres	EEA, 2020d
	Temporary water ratio			
Topography	Mean Altitude	TanDEM-X 30m Edited Digital Elevation Model	30 metres	González et al., 2020
	Standard deviation Altitude			
	Mean Slope			
	Standard deviation Slope			
	Mean Aspect			
	Standard deviation Aspect			
	Mean Curvature			
	Standard deviation Curvature			
Soil	Soil wetness ratio	CLMS HRL Water and wetness	10 metres	EEA, 2020d
Climate	Absolute max of air temperature, mean value	CHELSA BIOCLIM+ v2.1	1000 metres	Karger et al., 2017

	Relative max of air temperature, mean value			
	Absolute min of air temperature, mean value			
	Relative min of air temperature, mean value			
	Absolute precipitations, mean value			
	Relative precipitations, mean value			
	Wind speed at 10m, mean value	Global Wind Atlas	250 metres	Davis et al., 2023
	Wind speed at 200m, mean value			

All data was downloaded, reprojected, partitioned, and processed according to the requirements of the different sub-classifications. Detailed descriptions of data preparation methodologies and processing pipelines are detailed in Annex A.

3.2.4. Step 3: Preprocessing and dimensionality reduction

3.2.4.1. Indexation and preprocessing

For each sub-classification, raster datasets were merged by masking out pixels outside the buffered Functional Urban Areas. Pixel coordinates were obtained by loading each city and storing the coordinates separately, linked to a universal index later used during data shuffling and sampling.

3.2.4.2. Dimensionality reduction

Dimensionality reduction and collinearity management were addressed through feature reduction techniques, which are known to enhance clustering performance (Li et al., 2019; Paumelle et al., 2023). Two alternative approaches were tested for each sub-classification: Principal Component Analysis (PCA)[2] and Kernel Principal Component Analysis (KPCA)[3]. A grid search

[2] Principal Component Analysis (PCA) is a linear dimensionality reduction technique that identifies orthogonal directions (principal components) capturing the greatest variance in the data. Mathematically, this involves solving the eigenvalue problem for the covariance matrix $C = \frac{1}{n} X^\top X$, where the leading eigenvectors define the directions of maximal variance. This reduces dimensionality while retaining the most informative structure.

[3] Kernel PCA (KPCA) generalizes PCA by applying the kernel trick: instead of working directly in the input space, data are implicitly mapped into a higher-dimensional feature space via a kernel function $k(x_i, x_j)$. In this space,

was conducted to identify the optimal kernel and hyperparameters, comparing linear, polynomial, radial basis function, and additive chi-squared kernels, with 50 components modelled using the Nystroem approximation in sklearn[4]. Both PCA and KPCA analyses were implemented with sklearn's PCA method, Nystroem kernel approximation, and gridsearchcv pipelines (Pedregosa et al., 2011). Results were then compared by plotting outputs, contrasting standard PCA with 0.95 explained variance against the best KPCA approximation. The method that achieved the same variance with fewer axes was selected. Prior to fixing the explained variance threshold, scree plots and cumulative variance curves were inspected for PCA and KPCA solutions, and input datasets were curated using documented accuracy layers and manual consistency checks (see Annex B for preprocessing and scree plots).

3.2.5. Step 4: Unsupervised Classification

3.2.5.1. Algorithm selection *and optimisation*

Following dimensionality reduction, the most suitable clustering algorithm and number of classes were determined based on the PCA output. Preliminary tests compared several unsupervised clustering algorithms, including Hierarchical Agglomeration, DBSCAN, HDBSCAN, OPTICS, and Random Forest. Ultimately, variants of the KMeans algorithm were selected, with optimisation limited to the Lloyd, Elkan, and MiniBatch implementations[5] available in sklearn (Annex C). Although less complex than other algorithms, the KMeans family produced robust results. The primary reason for this choice was computational feasibility, as the dataset encompassed more than 60 million cells at 10 m resolution, despite the

---

nonlinear relationships can be captured as linear ones, and the eigenvalue problem is solved on the kernel matrix K. However, computing and storing K for large datasets is computationally expensive, as it scales quadratically with the number of samples.

[4] The Nyström approximation addresses the KPCA by sampling a subset of $m \ll n$landmark points. It constructs a smaller kernel submatrix

$K_{mm}$and cross-kernel K_{nm}, then approximates the full kernel matrix as:

$$K \approx K_{nm} K_{mm}^{-1} K_{mn}.$$

This yields a low-rank representation of the kernel, reducing computational complexity from $O(n^3)$to $O(nm^2)$. The approximation preserves much of the spectral structure of the original kernel, making KPCA feasible for large-scale applications.

[5] The KMeans algorithm partitions data into k clusters by iteratively assigning points to the nearest centroid and updating centroids as the mean of their assigned points, with the objective of minimizing the within-cluster sum of squared distances. The standard implementation, known as Lloyd's algorithm, follows this straightforward iterative refinement but can be computationally intensive for large datasets. To improve efficiency, Elkan's algorithm leverages the triangle inequality to reduce the number of exact distance computations, maintaining bounds that allow many assignments to be skipped while still converging to the same solution. For very large-scale problems, MiniBatch KMeans introduces a stochastic approximation by updating centroids using small random subsets of the data rather than the full dataset, significantly reducing computational cost and memory requirements at the expense of some accuracy.

relatively small and collinear set of variables within each sub-classification.

Algorithm performance was evaluated using the Silhouette score as the primary indicator of internal validation, complemented by the Calinski-Harabasz and Davies-Bouldin indices as secondary measures. Inertia plots were also generated to apply the Elbow Method as an additional validation criterion[6].

The different KMeans variants were tested across a range of 6–30 possible class numbers (k), with results plotted for each evaluation metric. The final selection was based on comparative performance across the three indices, with the Elbow Method serving as a qualitative reference. A three-fold multicriteria comparison was applied: for each k, the difference between its score and the best score was calculated across all indices. Summing these differences identified the k value that most consistently approximated the optimal solutions.

3.2.5.2. Class interpretation

The content of the classes was interpreted using the Principal Component values associated with each class (Fig. 2). Boxplot visualisations were employed to display the normalised Principal Components, scaled from –1 to 1. Data spread and median values were categorised into high (>|0.6|), medium (|0.6|–|0.3|), and low (|0.3|–|0.1|) ranges. This procedure directly linked Principal Component distributions and medians to covariances with the original variables, thereby identifying which variables exerted the strongest influence on each class. The analysis was particularly tailored to highlight classes along axes with narrow box distributions. A complete analysis of the boxplots and the associated reasoning is provided in Annex D. After assigning class names, values were remapped to enhance readability (Fig. 2).

[6] The Silhouette score is a geometric measure that evaluates how similar an object is to its own cluster compared to other clusters, defined for each point as the difference between its average intra-cluster distance and the lowest average inter-cluster distance, normalized to lie between −1and 1. The Calinski–Harabasz index (also known as the Variance Ratio Criterion) quantifies clustering quality by computing the ratio of between-cluster dispersion to within-cluster dispersion, with higher values indicating more distinct partitions. The Davies–Bouldin index expresses the average similarity between each cluster and its most similar counterpart, based on the ratio of intra-cluster scatter to inter-cluster separation, where lower values correspond to greater distinctness. The Elbow Method, in turn, is a heuristic based on plotting the inertia (the sum of squared distances of samples to their closest cluster center) as a function of the number of clusters, identifying the point where marginal gains in compactness begin to diminish.

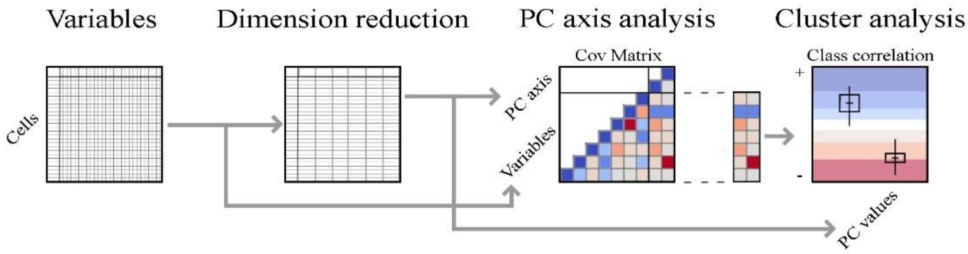

Fig. 2: Class interpretation is based on to the correlation values between each PC and the input variables. After feature reductions, the principal components and variable covariance is calculated. These values, split between high, medium and low correlation, are visualised and interpreted through boxplots for each class.

3.2.5.3. Adapted pipeline for the Urban form sub-classification

Within the Local Urban Form sub-classification, the clustering pipeline applied directly to the FUAs demonstrated limited effectiveness in distinguishing features within city cores, as these conditions were under-represented. Specifically, the initial clustering was unable to differentiate streets from buildings or to distinguish forms based on building height. To address this limitation, an additional pipeline was introduced, involving a second round of unsupervised classification to reprocess classes dominated by urban features. Classes were selected for re-clustering based on their variation along Principal Components associated with urban variables of interest. The selection criterion required at least |0.5| covariance between a class and the relevant PCs, restricting the process to classes representing artificial features. After extracting the pixels for the selected classes, the same optimisation procedure was applied, with the k range limited to between the existing number of classes plus one and up to five times that number. The newly generated classes were then merged with the original set.

The clustering process was further adapted for the two urban form sub-classifications to improve the treatment of water cells. Given the limited extent of water in urban environments, water pixels were excluded from the clustering pipeline and instead used to create a stable water layer. This layer was subsequently incorporated into the local classification at the final stage, forming a distinct water class.

3.2.6. Validation

The combined local–landscape scale approach and the use of multiple sub-classifications result in a methodology that is not directly comparable with existing classification systems. Following the precedent of Fleischmann and Arribas-Bel (2022), results were compared with established classifications using statistical methods. Comparisons were based on contingency matrices and Pearson's χ^2 test to determine whether observed and reference class frequencies differed significantly. The strength of association was further quantified using Cramér's V. Two reference classifications were used for comparison: the Urban Atlas (EEA, 2021) and the GHS Morphological Settlement Zones (MSZ) (Pesaresi and Panagiotis, 2023b), selected due to similarities with Cohabscapes in data composition, FUA extension, and immediate data availability.

3.2.7. Case study

A case study was conducted to illustrate the application of the Cohabscape classification across three European cities: Vienna (Austria), Munich (Germany), and Genoa (Italy). These case studies were developed within the framework of the H2020 ECOLOPES project, which focuses on designing multi-species, computationally derived green building envelopes. Within this context, Cohabscapes serves as a tool to describe and compare urban site conditions. The methodology can be integrated at multiple stages of the workflow, offering a fine-resolution, comprehensive, and multidimensional framework that facilitates the identification of analogous conditions and the visualisation of key differences among cities.

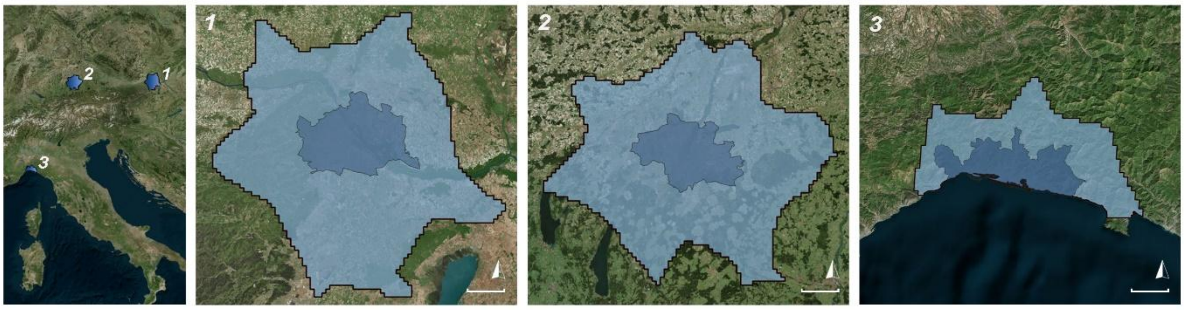

Fig. 3: Localization of the three case studies (left to right 1 Vienna, 2 Munich, and 3 Genoa), highlighting the different analysed boundaries: the Functional Urban Area (FUA, in cyan), and the core city centre corresponding to the municipality (blue). The white scale bar corresponds to 10000-metres.

The classification's capacity to differentiate urban contexts was demonstrated both across and within the three case study cities (Fig. 4). To achieve this, the frequency of class combinations across the four sub-classifications was analysed. The approach consisted of two steps:

i. Inter-city comparison. Sub-classifications were compared across Functional Urban Areas (FUAs) to identify regional patterns in class frequency. Radar plots were used to visualise the distributions, highlighting both similarities and differences among cities and demonstrating the classification's ability to detect analogues as well as variations.

ii. Intra-city comparison. Urban centres (central municipalities) were contrasted with surrounding peri-urban areas, delineated using OSM administrative boundaries (Fig. 5). Results were visualised through twelve heatmaps, covering all pairwise sub-classification combinations across the three cities. This analysis showcased how Cohabscape captures internal diversity within FUAs, revealing contrasts between central and peripheral urban contexts.

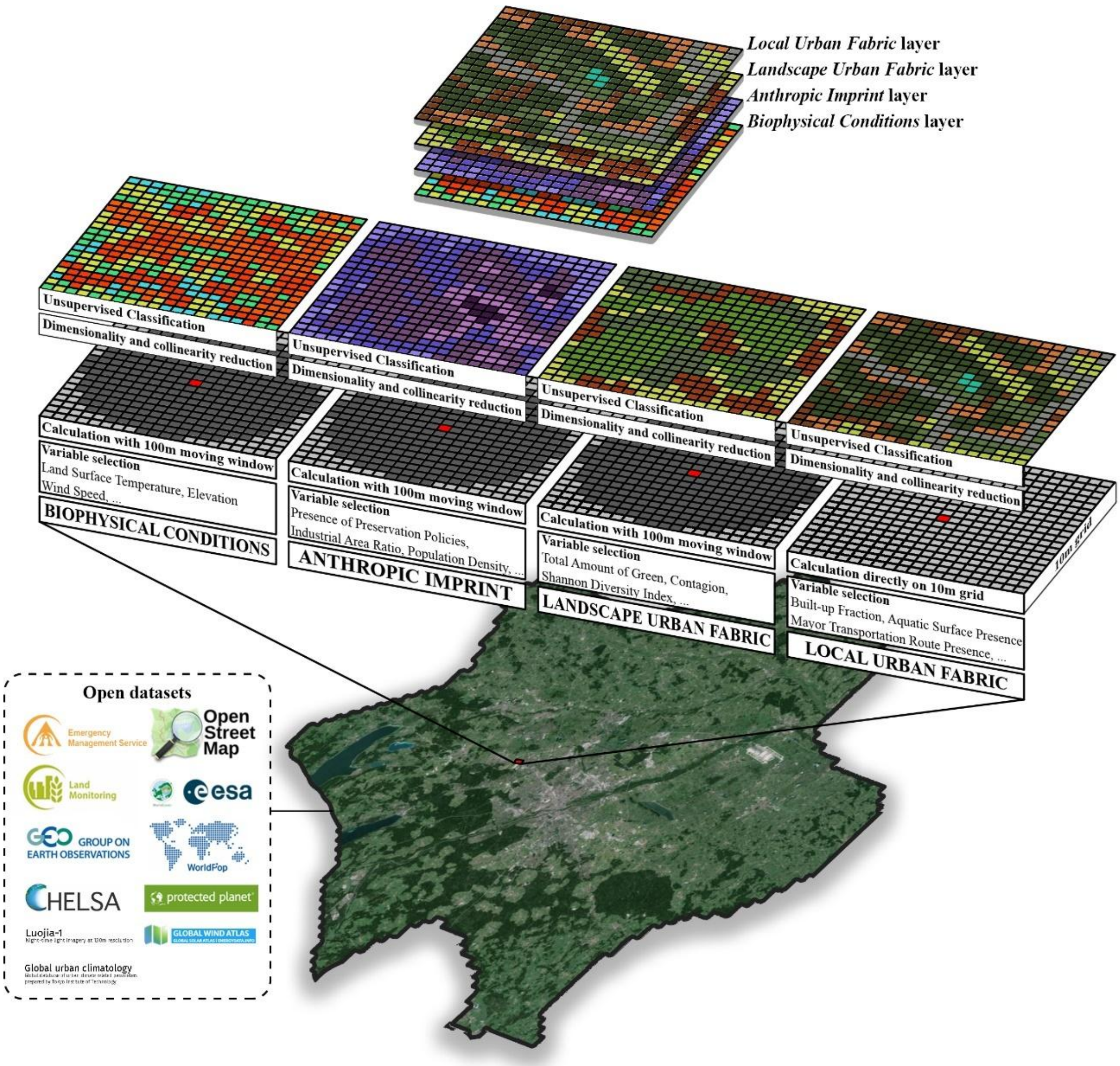

Fig. 4: Application of the Urban Cohabscape classification to the Munich case study, from the bottom: definition of the city boundary through FUA, data collection and computation for each layer, dimensionality reduction and clustering, resulting in four rasters at 10 metres resolution.

3.2.8. From species observation to site selection: using Cohabscapes for social-ecological NBS planning

The planning utility of Cohabscapes is demonstrated by analysing citizen-science bird records from the eBird Observation Dataset (EOD) across the condition classes to identify those that concentrate species detections. Such records reflect both the ecological suitability of a site for a given species and observers' preferences and availability. Consequently, classes with high detection densities can be interpreted as favourable for human–nature interactions and thus serve as practical targets for NBS interventions aimed at promoting urban biodiversity and its accessibility to residents. For each condition class, landscape availability and species observation electivity were computed using Jacobs' D index, which quantifies preference or avoidance of a class relative to its availability in the landscape (Eq. 1). The analysis focuses on the 30 most abundant bird species in Vienna, Munich, and Genoa, to reveal common observation patterns across the cities.

$$D = \frac{r - p}{r + p - 2rp} \quad (1)$$

Where r denotes the proportion of use and p the proportion of availability, ranging from −1 (strong avoidance) to +1 (strong preference). For each city and species, class availability and use were computed across the four Cohabscape dimensions. Class-level D values were then derived and concatenated into unified species profiles. Cells with low counts were masked (counts <4) prior to further analysis.

Cross-city consistency was assessed by computing pairwise Pearson correlation coefficients ρbetween species' concatenated Dprofiles; results are reported as $|\rho|$ together with associated p-values. For each species, only the intersection of class columns present in both cities was used, and low-count cells were masked as above. The number of paired class columns retained for a species is denoted the effective sample size n_{eff}.

Two measures of variance were computed on the concatenated paired D values: **variance (abs.)**, defined as the sample variance s^2 of those paired D values, and **variance (rel.)**, obtained by rescaling the absolute variance to the maximum observed absolute variance across the dataset for comparability (Eq. 2).

$$variance\ (rel.) = \frac{s^2}{\max\{s^2\}}$$

Additionally, mean D reports the net direction of selection (positive = net over-detection), while mean |D| and median |D| report effect magnitude irrespective of sign, preventing cancellation between positive and negative values.

Further methodological details, such as the computational implementation, can be found in the supplementary material (Annex F).

3.3. Results

3.3.1. The four sub-classifications

Based on the selected variables, open-source data were retrieved and processed through four separate pipelines, each corresponding to one sub-classification. Data from all cities were integrated, preprocessed, and classified, and the results are presented below.

Local Urban Fabric produced 13 classes (Fig. 5.1). Most classes were dominated by natural features (nine), while fewer were characterised by artificial features (four). Dimensionality reduction was performed using KPCA, resulting in the selection of six principal components. Unsupervised clustering was applied twice, using an adapted pipeline to re-cluster classes by extracting KPCA axes strongly correlated with artificial features. The two clustering runs employed Elkan KMeans with $k = 10$ and Elkan KMeans with $k = 4$, the latter applied to three reprocessed classes.

Landscape Urban Fabric yielded seven classes (Fig. 5.2). As with the local scale, natural-dominated classes (five) outnumbered those strongly influenced by artificial features (two). The classification was derived from the local-scale results, using KPCA outputs as inputs. Dimensionality reduction through PCA reduced the 24 variables to six components, which were then grouped using the Elkan KMeans algorithm.

Anthropic Imprint resulted in six classes (Fig. 5.3). The division was balanced between landscapes dominated by anthropic uses and functions, and those with limited human presence. Dimensionality reduction was carried out using PCA, producing five principal components. Clustering with Elkan KMeans then generated six distinct classes.

Biophysical Conditions also produced six classes (Fig. 5.4). In this case, the classes did not clearly separate anthropic from natural landscapes. The urban–rural perimeter could not be unambiguously defined, and the resulting classes primarily reflected regional climatic trends along with the presence of reliefs and hills. Dimensionality reduction using PCA produced eight principal components, which were subsequently grouped into six classes using Elkan KMeans.

3.3.2. Comparing city contexts

Maps were plotted and visually compared to identify the spatial distribution and frequency of classes across the three cities (Fig. 5). In most sub-classifications, Genoa emerged as an outlier. For both Local and Landscape Urban Form, the continental case studies (Munich and Vienna) displayed higher frequencies of classes associated with agriculture and grasslands, which were almost absent in Genoa.

From the perspective of the Anthropic Imprint, differences between cities were relatively minor, although Genoa showed fewer industrial and commercial areas compared to Munich and Vienna. By contrast, the Biophysical Conditions sub-classification revealed markedly different class distributions across all three cities.

These regional contrasts are exemplified in the case of urban parks (Fig. 6), which illustrate how the classification framework captures differences at both regional and finer scales. For instance, significant variation was observed in the Anthropic Imprint regarding accessibility to regulated natural areas (class 3), which was more limited in Genoa than in Munich and Vienna. Similarly, the Biophysical Conditions highlighted distinct patterns, with Genoa standing out due to locally warmer areas, where the city was primarily distinguished by temperature.

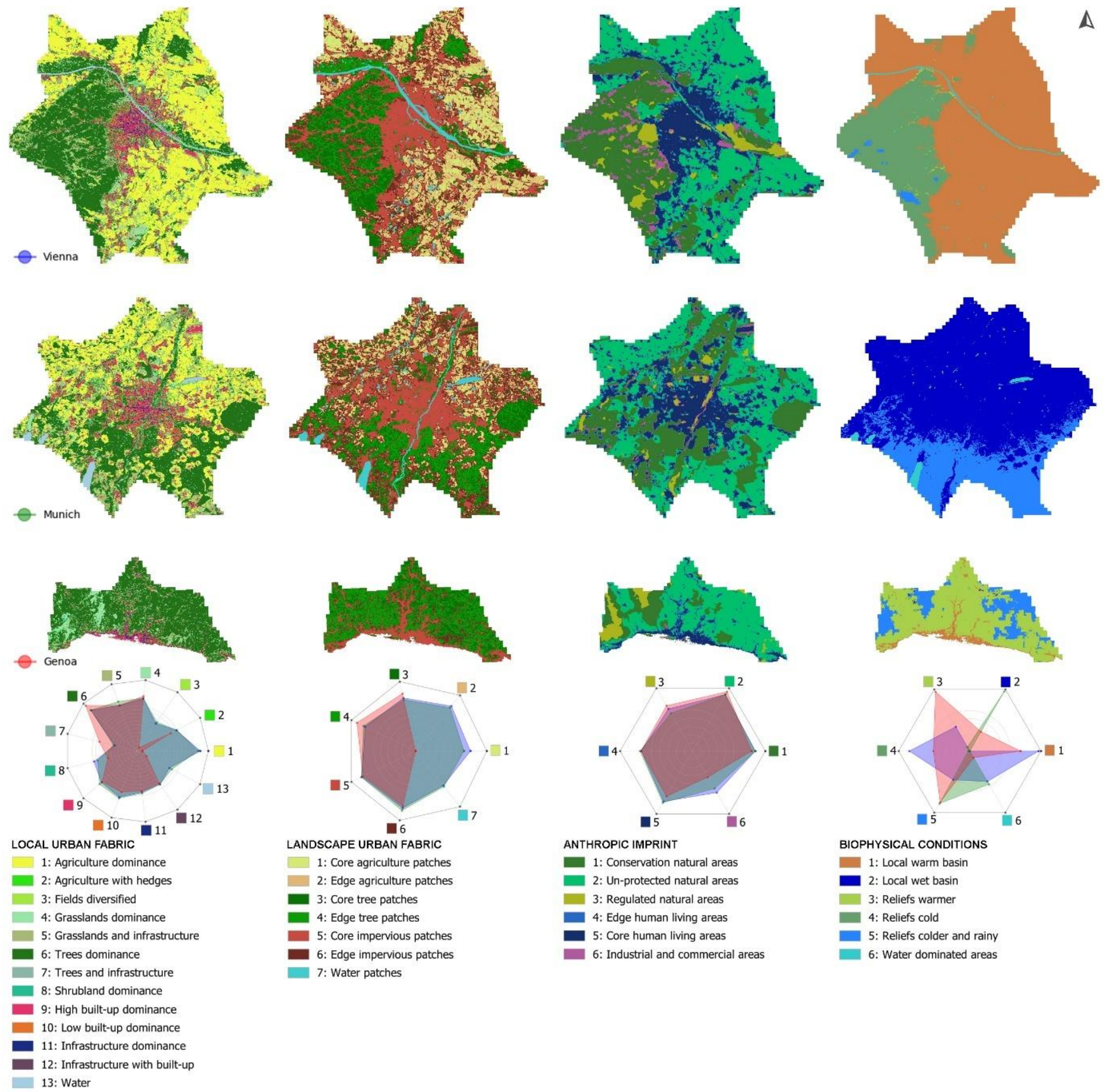

Fig. 5.1 to 5.4: The Cohabscape methodology applied to the case studies of Vienna, Munich, and Genoa. For each sub-classification, the spread of class frequencies across the cities is shown using logarithmic scale log10. Continental cities such as Vienna and Munich share numerous Urban Form features in the peri-urban area, such as vast agricultural areas that are not present in the narrow coastal city of Genoa. On the Anthropic Imprint, the cities behave more similarly, with the only class with different values being areas with large industrial use that are less present in Genoa. Finally, the most evident sub-classification in term of regional difference is the Biophysical Conditions, indicating underlying differences even among the cities that appeared more similar from a climatic point of view (Vienna and Munich).

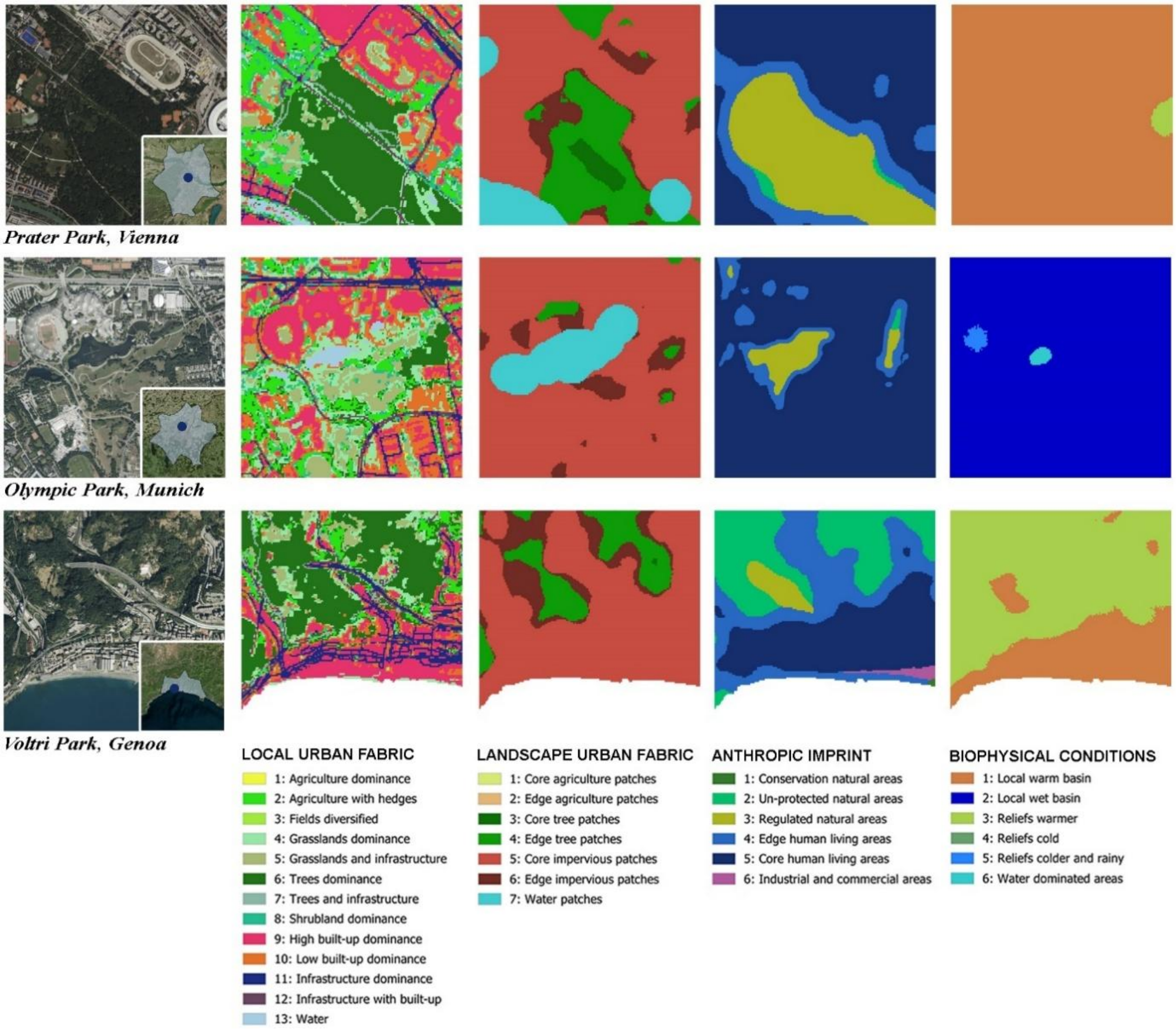

Fig 6: The Cohabscape methodology, zoomed-in view for three different urban parks in Vienna, Munich, and Genoa, at 1:10000 scale.

3.3.3. Comparing centre and peri-urban contexts

The intra-city comparison was structured by distinguishing between urban centres and surrounding peri-urban areas, with the former representing only 15% of the total FUA. To simplify interpretation, classes within each sub-classification were grouped according to their dominant variables. Local Urban Form was grouped into agricultural, grasslands, trees, artificial, and water classes. Landscape Urban Form was grouped into agricultural, trees, impervious, and water. Anthropic Imprint was divided into natural- and human-centric categories. Biophysical Conditions were grouped into low topography, high topography, and water (Fig. 7).

The correlations between urban centres and peri-urban areas revealed distinct behaviours across the different sub-classifications. These included variations in the concentration of natural- versus artificial-dominated classes, the juxtaposition of natural and impervious patches at core and edge locations, differences in human presence as reflected in human- versus natural-centred classes, and contrasting distributions of local temperatures and topographical features.

Urban centres appeared more heterogeneous than peri-urban areas when assessed through the Local Urban Form sub-classification (Fig. 7, upper). In contrast, when Local Urban Form was not the primary discriminating factor, urban centres exhibited less heterogeneity compared to peri-urban areas (Fig. 7, bottom).

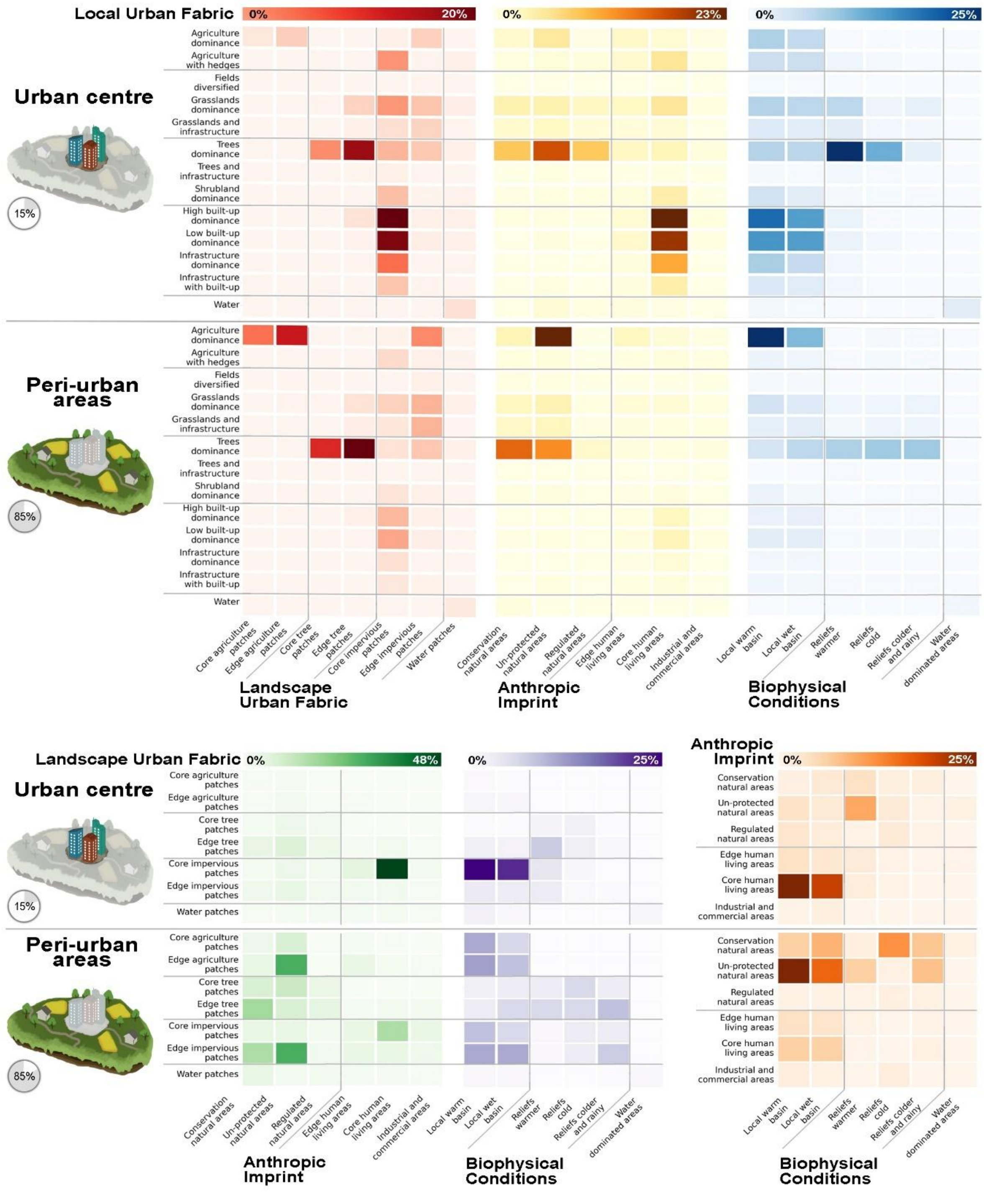

Fig. 7: Pairwise combinations between the different sub-classifications classes frequencies of occurrences, of all case studies jointed together. Each row confronts local Urban Form with one different sub-classification between Urban Form at landscape scale, Anthropic Imprint, Biophysical Conditions. The rows are divided between the total amount in the total amount of cells in urban centres (15%), and total amount in peri-urban areas (85%).

3.3.4. Validation

To focus on the main results, the Chapter presents the association analysis here, while the contingency matrices are provided in the supplementary material (Annex E).

3.3.4.1. Confront with Urban Atlas

The Urban Atlas (UA) offers harmonized, high-resolution land cover and land use data for FUAs across Europe. The spatial extent of FUAs in UA differs slightly from the GHS FUAs: UA boundaries strictly follow administrative limits, whereas GHS FUAs extend beyond them. UA includes 27 land-use classes within a single classification, covering both urban form (e.g., built-up areas, green spaces, infrastructure) and human presence or functions (e.g., residential, commercial, industrial areas).

Each Cohabscapes sub-classification was compared with UA. The UA data were rasterised and reprojected to match Cohabscapes, enabling raster-based calculations. The resulting statistics (Table 5) show that all layers are statistically significant ($\varrho = 0.000$), indicating that associations are unlikely to occur by chance. Form Local Urban Fabric produced the highest χ^2 statistic (1.6×10^8) and degrees of freedom (dof = 312), with a relatively high Cramér's V (V = 0.462). This outcome aligns with expectations, as both layers capture fine-grained morphological patterns. Landscape Urban Fabric yielded a slightly lower χ^2 (1.1×10^8) but a higher Cramér's V (V = 0.535), suggesting stronger alignment at broader scales, likely due to generalised landform patterns. The Anthropic Imprint sub-classification, while producing the lowest χ^2 (5.6×10^7), still showed a moderate-to-strong association (V = 0.423), possibly influenced by the inclusion of OSM data in both layers, particularly for functional land uses such as industrial and commercial zones. Finally, Biophysical Conditions achieved the highest Cramér's V (V = 0.554) despite a mid-range χ^2 (9.63×10^7), indicating that natural land cover and ecological gradients are strongly structured and play a significant role in shaping urban–rural transitions.

A visual comparison of UA over Cohabscapes can be seen in Figure 8.

Table 5. Pearson's χ^2 and Cramér's V between UA and Cohabscapes sub-classifications.

Cohabscapes sub-classification	χ^2 statistic	ϱ value	Degrees of freedom (dof)	Cramér's V	Comment
Local Urban Fabric	1.6+E8	0.000	312	0.462	Statistically significant (ϱ), moderate-strong association (V), highest χ^2 and dof.
Landscape Urban Fabric	1.1+E8	0.000	156	0.535	Statistically significant (ϱ), high association (V).
Anthropic Imprint	5.6+E7	0.000	130	0.423	Statistically significant (ϱ), moderate-strong association (V), the weakest.
Biophysical Conditions	9.6+E7	0.000	130	0.554	Statistically significant (ϱ), highest association (V).

3.3.4.2. Confront with Morphological Settlement Zones

The Morphological Settlement Zones (MSZ) classification delineates settlement extent and internal structure at 100 m resolution, based on built-up surface fraction and spatial morphology. It integrates built form, vegetation, water, roads, and building height to characterise settlement patterns and their functional and environmental context. Developed from the GHS FUAs, MSZ is the most comparable existing classification to Cohabscapes in terms of spatial extent, though it relies on fewer data dimensions.

Distributed in raster format, MSZ is spatially compatible with Cohabscapes after reprojection. The resulting statistics (Table 6) confirm that all layers are statistically significant (ϱ = 0.000). Local Urban Fabric produced the highest χ^2 (8.6×10^6) and dof (168), leading to the highest Cramér's V (V = 0.251). This result is expected, as MSZ is itself a morphological classification, making Local Urban Fabric the most directly comparable layer. The remaining sub-classifications showed weaker associations, though Anthropic Imprint scored highest among them, likely for reasons similar to UA, given the shared reliance on OSM data.

A visual comparison of MSZ with Cohabscapes can be seen in Figure 8.

Table 6. Pearson's χ^2 and Cramér's V between MSZ and Cohabscapes sub-classifications.

Cohabscapes sub-classification	χ^2 statistic	ϱ value	Degrees of freedom (dof)	Cramér's V	Comment
Urban Form Local	8.6+E6	0.000	168	0.251	Statistical significance (ϱ), weak-moderate association (V), highest significance (χ^2) and highest complexity (dof).
Urban Form Landscape	1.8+E6	0.000	84	0.165	Statistical significance (ϱ), weak association (V).
Anthropic Imprint	1.7+E6	0.000	70	0.177	Statistical significance (ϱ), weak association (V).
Biophysical Conditions	1.4+E6	0.000	70	0.158	Statistical significance (ϱ), weakest association (V).

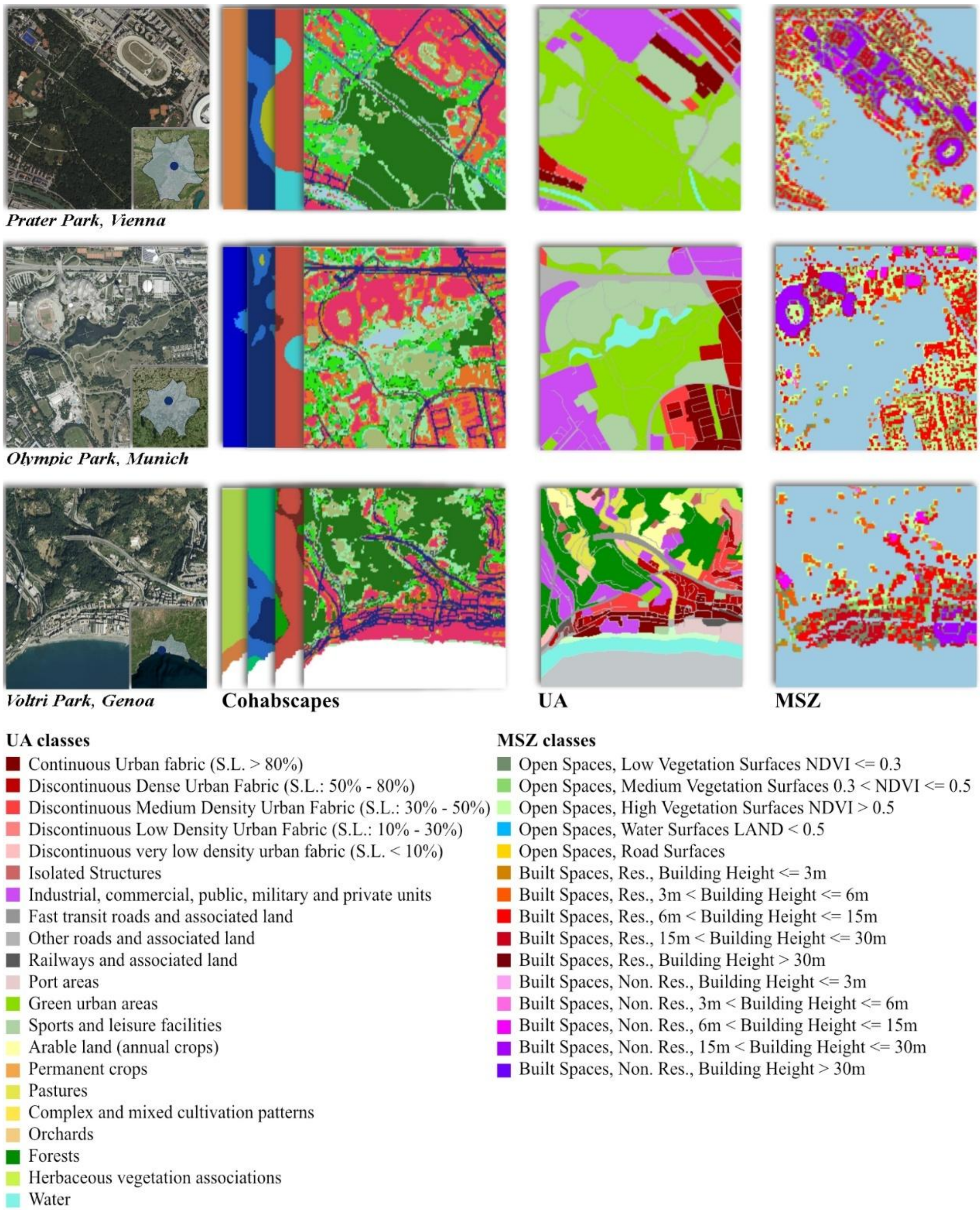

Fig. 8: Zoomed-in comparison of Cohabscapes Urban Fabric Local subclassification (showing the highest correlation levels) vs UA and vs MSZ, using the same areas as Fig. 6.

3.3.5. Ecological NBS planning from (bird) data-driven site selection

To summarise observation patterns across Cohabscape classes and to identify those that facilitate or constrain human–nature interactions, detailed results are presented for five representative species, with full results provided in the supplementary material (Annex F). The selected species illustrate contrasting urban ecologies and planning relevance: *Corvus corone* (highly adaptable omnivore, synanthropic), *Turdus merula* (urban-tolerant thrush), *Parus major* and *Cyanistes caeruleus* (small insectivorous, cavity-nesting passerines dependent on vegetation structure), and *Sitta europaea* (forest-associated cavity nester, indicator of mature tree continuity) (Murgui & Hedblom, 2017). Owing to the very low number of observations in Genoa, the analysis focuses on Vienna and Munich to examine classes that concentrate bird detections and are therefore relevant to human–nature interactions and planning (Fig. 9).

Tree-dominant and low-built/mixed-green subclasses exhibit strong, stable detections (high D, low uncertainty) for woodland and generalist species, identifying them as priority classes for NBS aimed at enhancing everyday human–nature interactions. In contrast, highly built and industrial classes favour synanthropic species and require different management or restoration approaches, consistent with existing ecological knowledge (Murgui & Hedblom, 2017).

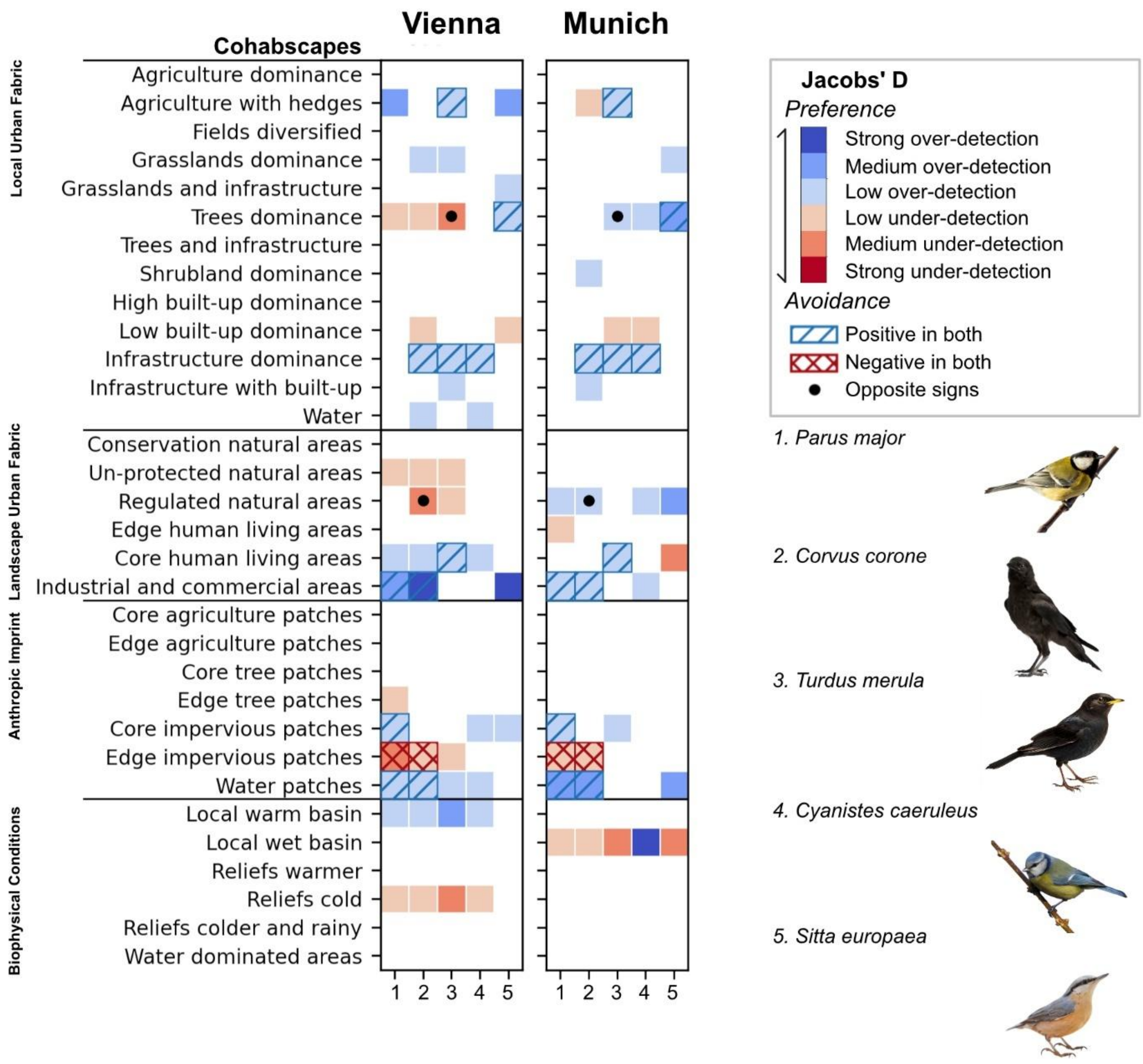

Fig. 9. Jacobs' D for the five selected species by Cohabscapes classes, for Vienna and Munich. Blue values show over-detection, while red show under-detection. Hatched cells show equal trends (preference vs avoidance) in both cities, while dotted values show cells with opposite trends.

Correlation and variance analyses revealed a strong level of agreement across the three cities between Corvidae abundance patterns in both the 1D and 2D classes, underscoring comparable associations between Corvidae abundance and the Cohabscape classes across cities (Table 7). Computed metrics in the subset of cells that contained enough observations (Table 4) summarize how repeatable detections map onto the same Cohabscapes classes in Vienna and Munich, informing human-nature interactions. The first row shows the overall Vienna-Munich comparison across species, setting a comparative threshold. Relative to this, *Corvus corone* and *Parus major* show correlation at or above the overall level, where other species fall below or are marginal, so their species-level transferability should be interpreted with caution. *Corvus corone* and *Parus major* show the strongest cross-city consistency, Corvus with the highest |ρ| (≈0.578) and Parus with a moderate |ρ| (≈0.381), indicating that for these species class-level D patterns are more transferable between cities. Both also show positive mean D, meaning detections are concentrated in few Cohabscapes classes rather than uniformly distributed. *Turdus merula* has a weak |ϱ| (≈0.157) despite a positive mean D, so its class associations are less consistent between cities. *Cyanistes caeruleus* (|ϱ| ≈ 0.072, n = 9) and *Sitta europaea* (|ϱ| ≈ 0.101, n = 5) have low |ϱ| and few paired cells, giving low-confidence. Low correlations may reflect either real differences between cities in class relevance or from sampling noise.

Table 4. Intersection summary of Jacobs' D (Vienna vs Munich), showing the n° of paired cells, abs. Pearson's ρ with p-value, variance (abs. and rel.), mean D, and magnitude of summaries (mean |D|, median |D|). D cells with counts <4 were masked. Rows with few paired cells (<10) are low-confidence.

Species	**Paired cells**	**Pearson's ϱ (abs.)**	**Pearson p**	**Variance (abs.)**	**Variance (rel.)**	**Mean D**	**Mean |D|**	**Median |D|**
Overall	27	0.522	0.005	0.044	0.048	0.270	0.284	0.260
Parus major	17	0.381	0.030	0.074	0.214	0.091	0.231	0.171
Corvus corone	14	0.578	0.132	0.100	0.288	0.064	0.267	0.210
Turdus merula	9	0.157	0.686	0.079	0.229	0.121	0.278	0.283
Cyanistes caeruleus	9	0.072	0.853	0.042	0.120	0.067	0.175	0.148
Sitta europaea	5	0.101	0.871	0.118	0.342	0.170	0.307	0.286

3.4. Discussion

The discussion is organised into three parts. First, the outcomes are compared with existing classifications in relation to previously identified gaps. Second, potential applications are explored, particularly in supporting ecological understanding of liveability conditions and interspecies interactions in urban design. Finally, the study's limitations are addressed.

3.4.1. Comparison with existing classifications

The results of the Cohabscapes classification highlight its ability to integrate urban form, function, ecological structure, and anthropic presence into a single framework. This multidimensional approach enables detailed spatial analysis of liveability across species and urban contexts. In contrast, existing classification systems often isolate specific dimensions. For example, MSZ and LCZ focus on physical morphology but lack socio-ecological integration. Urban Atlas and UFZ provide functional coverage but overlook biophysical variability. CUGIS offers ecological insight but remains disconnected from built form and human activity. WorldPop contributes demographic detail but lacks environmental context. Even multidimensional systems such as MODUM and Spatial Signatures, while layered in structure, do not fully capture the ecological and co-habitative complexity addressed by Cohabscapes.

This comparison underscores the added value of a classification that balances resolution, dimensionality, and scalability. Cohabscapes provides a more holistic perspective on urban liveability, particularly in contexts where human and non-human needs intersect.

3.4.2. Applications in ecological research and urban design and planning

For urban design and NBS planning, the four sub-classifications offer a practical, layered lens for site selection, scenario comparison and performance evaluation. Planners can, for example, prioritise tree-dominant and low-built/mixed-green classes for parks and street-tree planting, target core/edge tree and agricultural patches to strengthen connectivity or applying greening retrofits in highly built classes to improve thermal comfort and human-nature contact (Čeplová et al., 2017). Cohabscapes thus supports both broad, place-based interventions and more focused, taxa-specific follow-ups, mixing urban data with socio-ecological data. Researchers can overlay species or trait data or use the classes as covariates or strata in model-based analyses to investigate how particular taxa respond within those strata (Hughes et al., 2021; Martin et al., 2023).

The ecological relevance of Cohabscapes has been exemplified by the application with bird data, describing urban conditions for multispecies liveability in term of where human-nature interactions are likely, occasional, or absent. This has implications for broad planning and monitoring in complex settings (Likens & Lindenmayer, 2012; Mimet et al., 2014). Table 4 shows how metrics translate detection patterns into signals useful for planning. Where mean D is consistently positive and ϱ is moderate–high (for example, *Parus major*, *Corvus corone*), planners can target the specific classes that support repeatable encounters for protection, greening, or design interventions. Low-ϱ or low-sample cases require city-specific mapping and checks for sampling bias before generalizing. High variance flags class-specific associations that benefit from fine-scale interventions (for example, enhancing tree-dominant or mixed-green patches, improving connectivity of core/edge tree patches, or retrofitting highly built classes). Because these metrics reflect detection patterns rather than full ecological processes, Cohabscapes is best used as a planning-oriented complementary lens for site selection, monitoring and targeted surveys. Species-level ecological inference should be reserved for studies with dedicated sampling or experimental designs. Additionally, when species data are sparse, Cohabscapes can supports modelling and decision making while flagging under-sampled classes for targeted surveys (Kattwinkel et al., 2009).

In the context of the ECOLOPES project, Cohabscapes derived its strong connection with integrated ecological design, where the objective is to create urban environments that support the liveability of both human and non-human inhabitants. Designing for multiple stakeholders simultaneously is challenging, particularly when their interactions are considered together. Cohabscapes addresses this by providing a harmonised, transdisciplinary framework that bridges ecological, morphological, and functional dimensions. It supports the planning and evaluation of NBS by identifying urban conditions conducive to biodiversity, climate adaptation, and ecosystem service provision. For instance, plant species can be selected based on their performance across Cohabscape classes to optimise stormwater retention and thermal comfort. Similarly, animal connectivity can be assessed by aligning species' home ranges with landscape patterns identified through the classification, as demonstrated in the bird species case study. As urban areas face increasing pressure to accommodate diverse forms of life, Cohabscapes offers a valuable tool for advancing co-habitative, biophilic urban design.

3.4.3. Limitations

The classification has several practical limitations. Variables were selected from the literature as broad ecological drivers and species occurrences were deliberately excluded to preserve transferability and to enable the framework to function as a predictive downstream tool for liveability assessment. This choice maintains neutrality but prevents direct use of the classification as a biodiversity distribution mapping tool until empirical relationships between classes and biodiversity are established; once those relationships are quantified, Cohabscapes can be used to interpret and compare biodiversity patterns while remaining independent of species data. In the example application, owing to the nature and relatively small size of the eBird dataset in the three cities, the analysis focused on the capacity of classes to support human–nature interactions rather than on modelling species occurrences. Nevertheless, the example indicates that participatory datasets, when combined with appropriate species distribution modelling methods, can be used to model species distributions within cities and to evaluate the capacity of classes to support urban-dwelling species.

The pipeline currently describes the urban environment at two scales: local (the contents of a 10 m cell) and landscape (composition and configuration of 10 m cells within a 100 m radius). The 10 m resolution reflects the finest feasible grain achievable with broadly available datasets. The 100 m neighbourhood extent was chosen on environmental and ecological scaling grounds as a consensus, higher-resolution neighbourhood scale supported in the literature. It is acknowledged that a two-scale description may omit processes operating at finer or broader extents. Cohabscapes is designed to allow users to upscale or reaggregate the 10 m classifications to compute metrics at broader, user-defined scales (as already implemented for the urban fabric landscape classification). The Local Urban Fabric classification summarises finer-resolution information within each 10 m cell. Integration of additional scales (for example, a regional scale to capture broad biogeographical and cultural variation that drives cross-country heterogeneity) is under consideration. Preliminary sensitivity tests with alternative radii were conducted during variable and data selection; these indicated the potential value of additional scales (e.g., regional extents that capture species-level connectivity) but also revealed substantial data and computational demands (Collart et al., 2025).

A further scale-related limitation concerns variables with coarse spatial or temporal resolution, such as some climate layers. Downscaling these layers to 10 m does not increase their intrinsic information content, and therefore their explanatory power for fine-grain temperature variation or rapid urban change remains limited.

Only published, validated datasets were used to characterise the classifications, and quality filters were applied to retain variables with clear relevance to urban conditions. Nonetheless, residual misalignments persist (for example, UA versus GHS FUA boundaries and differing native resolutions), which are evident in validation and in the bird-data application. These data mismatches, together with thematic groupings that can produce collinear signals (e.g., built-up density versus commercial area ratio), complicate fine-scale interpretation. Collinearity is explicitly addressed through PCA/KPCA prior to clustering.

Dimensionality reduction via PCA/KPCA streamlines analysis but can obscure direct, intuitive links between individual variables and resulting classes. Although covariance thresholds guided interpretation, class naming relied on analogies, which may reduce clarity for end users. Case studies were limited to Central Europe, introducing geographic bias; while the methodology is transferable, the current model is not directly generalisable beyond this region and requires retraining with local urban data. A deterministic nomenclature for classes is recommended as the framework expands to new cities. Coastal contexts pose an additional issue: water pixels were excluded (sea areas omitted) and several layers (elevation, temperature) are ambiguous over water. Buffer zones were used to mitigate distortions in nearby pixels, but omission of the sea may affect landscape-scale interpretations in coastal settings.

Future developments should address these limitations by incorporating a more comprehensive pool of high-quality data and additional liveability drivers as they become available. Such enhancements would increase the sensitivity and robustness of the classification for capturing drivers relevant to a broader range of species (including urban avoiders), social and ecological processes, and interspecific cohabitation. Chapter 4 tries to develop theoretical and computational considerations on these limitations, proposing conceptual and technical solutions.

3.5. Conclusions

3.5.1. Closing summary

This chapter presents a novel urban classification designed to capture the liveability conditions of multiple inhabitants, namely humans, plants, and animals, across different urban dimensions. The main conclusions are as follows:

i. The Cohabscapes methodology achieves a species-generic description of cities by incorporating variables and modelling criteria that reflect the liveability requirements of multiple inhabitants, such as resource availability and mobility, across multiple scales. The code is openly distributed and can be applied to other European FUAs or adapted to data-scarce regions with minimal modifications.

ii. The methodology was applied to three European case studies, demonstrating the process of producing classifications consistent with the Cohabscapes framework. Results are openly available in raster format, alongside the full PCA/KPCA datasets for all sub-classifications in parquet table format, enabling immediate use in research and design.

iii. Cohabscapes shows partial comparability with existing systems such as Urban Atlas and Morphological Settlement Zones. A key distinction lies in its stronger integration of data across multiple urban dimensions, including urban form and socioeconomics, facilitated by the sub-classification structure.

iv. An application using bird species data (30 individual species) demonstrated the utility of Cohabscapes in ecological research. With the addition of further datasets through data stacking, this approach could enhance understanding of urban liveability and support the design of more effective NBS.

3.6. References

Alberti, M. (2015). Eco-evolutionary dynamics in an urbanizing planet. *Trends in Ecology & Evolution, 30*(2), 114–126. https://doi.org/10.1016/j.tree.2014.11.007

Alberti, M. (2023). Cities of the Anthropocene: urban sustainability in an eco-evolutionary perspective, Philos Trans R Soc Lond B Biol Sci., https://doi.org/10.1098/rstb.2022.0264

Alexiou, Singleton & Longley (2016) Alexiou, A., Singleton, A., & Longley, P. A. (2016). A classification of multidimensional open data for urban morphology. Built Environment, 42(3), 382–395. https://doi.org/10.2148/benv.42.3.382

Angel, S., Blei, A. M., Parent, J., Lamson-Hall, P., & Galarza Sánchez, N. (2016). Atlas of urban expansion—2016 edition (Vols. 1–2). Lincoln Institute of Land Policy; UN-Habitat; New York University. https://www.lincolninst.edu/publications/other/atlas-urban-expansion-2016-edition

Aronson, M.F.J., Nilon, C.H., Lepczyk, C.A., Parker, T.S., Warren, P.S., Cilliers, S.S., Goddard, M.A., Hahs, A.K., Herzog, C., Katti, M., La Sorte, F.A., Williams, N.S.G., & Zipperer, W. (2016). Hierarchical filters determine community assembly of urban species pools, Ecology 97, 2952–2963. https://doi.org/10.1002/ecy.1535

Arribas-Bel, D., Fleischmann, M. (2022). Spatial Signatures - Understanding (urban) spaces through form and function. Habitat International 128, 102641. https://doi.org/10.1016/j.habitatint.2022.102641

Audusseau, H., Schmucki, R., Croci, S., Dubreuil, V. (2024). Sustainable urban planning needs stronger interdisciplinarity and better co-designing: How ecologists and climatologists can fully leverage climate monitoring data. Wiley Interdisciplinary Reviews: Climate Change. https://doi.org/10.1002/wcc.912

Beck, H.E., Zimmermann, N.E., McVicar, T.R., Vergopolan, N., Berg, A., Wood, E.F. (2018). Present and future Köppen-Geiger climate classification maps at 1-km resolution. Sci Data 5, 180214. https://doi.org/10.1038/sdata.2018.214

Beevers, L., McClymont, K., Bedinger, M. (2022). A hazard-agnostic model for unpacking systemic impacts in urban systems. Civil Engineering and Environmental Systems 39, 224–241. https://doi.org/10.1080/10286608.2022.2083112

Bolliger, J., Lischke, H., & Green, D. G. (2005). Simulating the spatial and temporal dynamics of landscapes using generic and complex models. Ecological Complexity, 2(2), 107–116. https://doi.org/10.1016/j.ecocom.2004.11.005

Čeplová, N., Kalusová, V., Lososová, Z. (2017). Effects of settlement size, urban heat island and habitat type on urban plant biodiversity. Landscape and Urban Planning 159, 15–22. https://doi.org/10.1016/j.landurbplan.2016.11.004

Clifton, K., Ewing, R., Knaap, G., & Song, Y. (2008). Quantitative analysis of urban form: A multidisciplinary review. Journal of Urbanism: International Research on Placemaking and Urban Sustainability, 1(1), 17–45. https://doi.org/10.1080/17549170801903496

Collart, F., Rey, P.-L., Altermatt, F., Külling, N., Guisan, A., & Adde, A. (2025). *On the use of neighboring habitats as predictors of species distributions.* Oikos. https://doi.org/10.1002/oik.11963

Coutard, O., Florentin, D. (2024). Researching infrastructures and cities: origins, debates, openings, in: Coutard, O., Florentin, D. (Eds.), Handbook of Infrastructures and Cities, Geography, Planning and Tourism 2024. Edward Elgar Publishing, pp. 1–49. https://doi.org/10.4337/9781800889156.00009

Crippa, M., Guizzardi, D., Pisoni, E., Solazzo, E., Guion, A., Muntean, M., Florczyk, A., Schiavina, M., Melchiorri, M., Hutfilter, A.F. (2021). Global anthropogenic emissions in urban areas: patterns, trends, and challenges. Environ. Res. Lett. 16, 074033. https://doi.org/10.1088/1748-9326/ac00e2

Dijkstra, L., H. Poelman and P. Veneri (2019). The EU-OECD definition of a functional urban area.OECD Regional Development Working Papers, No. 2019/11, OECD Publishing, Paris. https://doi.org/10.1787/d58cb34d-en.

EEA Urban Morphological Zones dataset European Environment Agency. (2013). Urban morphological zones (vector), version 2013. EEA. https://sdi.eea.europa.eu/data/8ab00854-d08f-43b1-b78f-447ce13857d1

Eggermont, H., Balian, E., Azevedo, J. M. N., Beumer, V., Brodin, T., Claudet, J., Fady, B., Grube, M., Keune, H., Lamarque, P., Reuter, K., Smith, M., Van Ham, C., Weisser, W. W., & Le Roux, X. (2015). Nature-based Solutions: New Influence for Environmental Management and Research in Europe. GAIA - Ecological Perspectives for Science and Society, 24(4), 243–248. https://doi.org/10.14512/gaia.24.4.9

Esch, T., Marconcini, M., Marmanis, D., Zeidler, J., Elsayed, S., Metz, A., Müller, A., & Dech, S. (2014). Dimensioning urbanization: An advanced procedure for characterizing human settlement properties and patterns using spatial network analysis. Applied Geography, 55, 212–228. https://doi.org/10.1016/j.apgeog.2014.09.009

Ettinger, A.K., Buhle, E.R., Feist, B.E., Howe, E., Spromberg, J.A., Scholz, N.L., Levin, P.S. (2021). Prioritizing conservation actions in urbanizing landscapes. Sci Rep 11, 818. https://doi.org/10.1038/s41598-020-79258-2

European Environment Agency (2021). Urban Atlas Land Cover/Land Use 2018 (vector), Europe, 6-yearly, Jul. 2021 [Dataset]. https://doi.org/10.2909/fb4dffa1-6ceb-4cc0-8372-1ed354c285e6

Felappi, J.F., Sommer, J.H., Falkenberg, T., Terlau, W., Kötter, T. (2020). Green infrastructure through the lens of "One Health": A systematic review and integrative framework uncovering synergies and trade-offs between mental health and wildlife support in cities. Science of The Total Environment 748, 141589. https://doi.org/10.1016/j.scitotenv.2020.141589

Finnerty, P. B., Carthey, A. J. R., Banks, P. B., Brewster, R., Grueber, C. E., Houston, D., Martin, J. M., McManus, P., Roncolato, F., van Eeden, L. M., Wauchope, M., & Newsome, T. M. (2025). *Urban rewilding to combat global biodiversity decline.* BioScience, 75(7), 545–558. https://doi.org/10.1093/biosci/biaf062

Fleischmann, M., & Arribas-Bel, D. (2022). Geographical characterisation of British urban form and function using the spatial signatures framework. Scientific Data, 9, 546. https://doi.org/10.1038/s41597-022-01640-8

GBIF.org (24 January 2025) GBIF Occurrence Download https://doi.org/10.15468/dl.cd3bpu

González-Gómez, K., Rollins, D.K., Castro, M. (2022). Modeling Urban Road Scenarios to Evaluate Intersection Visibility. Sustainability 14, 354. https://doi.org/10.3390/su14010354

Halstead, M., Ahmadi, A., Smitt, C., Schmittmann, O., McCool, C. (2021). Crop Agnostic Monitoring Driven by Deep Learning. Frontiers in Plant Science 12.

Heymans, A., Breadsell, J., Morrison, G. M., Byrne, J. J., & Eon, C. (2019). Ecological urban planning and design: A systematic literature review. Sustainability, 11(13), 3723. https://doi.org/10.3390/su11133723

Hughes, A.C., Orr, M.C., Ma, K., Costello, M.J., Waller, J., Provoost, P., Yang, Q., Zhu, C., Qiao, H. (2021). Sampling biases shape our view of the natural world. Ecography 44, 1259–1269. https://doi.org/10.1111/ecog.05926

Hutchinson, E. (1957). Concluding remarks. Cold Spring Harbor Symposia on Quantitative Biology 22:415–427.

Jacobs, J. (1974). Quantitative measurement of food selection. *Oecologia, 14*, 413–417. https://doi.org/10.1007/BF00384581

Jochem, W. C., & Tatem, A. J. (2021). Tools for mapping multi-scale settlement patterns of building footprints: An introduction to the R package foot. PLOS ONE, 16(2), Article e0247535. https://doi.org/10.1371/journal.pone.0247535

Katabaro, J. M., Yan, Y., Hu, T., Yu, Q., & Cheng, X. (2022). A review of the effects of artificial light at night in urban areas on the ecosystem level and the remedial measures. Frontiers in Public Health, 10. https://doi.org/10.3389/fpubh.2022.969945

Kropf, K. (2009). Aspects of urban form. Urban Morphology 13, 105–120. https://doi.org/10.51347/jum.v13i2.3949

Labadi, S., Giliberto, F., Rosetti, I., Shetabi, L., & Yildirim, E. (2021). Heritage and the sustainable development goals: Policy guidance for heritage and development actors. International Journal of Heritage Studies.

Li, E., Parker, S.S., Pauly, G.B., Randall, J.M., Brown, B.V., Cohen, B.S. (2019). An Urban Biodiversity Assessment Framework That Combines an Urban Habitat Classification Scheme and Citizen Science Data. Frontiers in Ecology and Evolution 7. https://doi.org/10.3389/fevo.2019.00277

Likens, G.E., Lindenmayer, D.B. (2012). Integrating approaches leads to more effective conservation of biodiversity. Biodivers Conserv 21, 3323–3341. https://doi.org/10.1007/s10531-012-0364-5

Luo, Y., Lü, Y., Liu, L., Liang, H., Li, T., Ren, Y. (2020). Spatiotemporal scale and integrative methods matter for quantifying the driving forces of land cover change. Science of The Total Environment 739, 139622. https://doi.org/10.1016/j.scitotenv.2020.139622

Majchrowska, S., Mikołajczyk, A., Ferlin, M., Klawikowska, Z., Plantykow, M.A., Kwasigroch, A., Majek, K. (2022). Deep learning-based waste detection in natural and urban environments. Waste Management 138, 274–284. https://doi.org/10.1016/j.wasman.2021.12.001

Marrec, R., Abdel Moniem, H.E., Iravani, M., Hricko, B., Kariyeva, J., Wagner, H.H. (2020). Conceptual framework and uncertainty analysis for large-scale, species-agnostic modelling of landscape connectivity across Alberta, Canada. Sci Rep 10, 6798. https://doi.org/10.1038/s41598-020-63545-z

Martin, T. E., Bennett, G. C., Fairbairn, A., & Mooers, A. O. (2023). 'Lost' taxa and their conservation implications. Animal Conservation, 26(1), 14-24. https://doi.org/10.1111/acv.12788

McCaffrey, R.E., Mannan, R.W. (2012). How scale influences birds' responses to habitat features in urban residential areas. Landscape and Urban Planning 105, 274–280. https://doi.org/10.1016/j.landurbplan.2011.12.022

McPhearson, T., Cook, E. M., Berbés-Blázquez, M., Cheng, C., Grimm, N. B., Andersson, E., Barbosa, O., Chandler, D. G., Chang, H., Chester, M. V., Childers, D. L., Elser, S. R., Frantzeskaki, N., Grabowski, Z., Groffman, P., Hale, R. L., Iwaniec, D. M., Kabisch, N., Kennedy, C., … Troxler, T. G. (2022). A social-ecological-technological systems framework for urban ecosystem services. One Earth, 5(5), 505–518. https://doi.org/10.1016/j.oneear.2022.04.007

Mendoza Beltran, A., Padró, R., La Rota-Aguilera, M.J., Marull, J., Eckelman, M.J., Cirera, J., Giocoli, A., Villalba, G. (2023). Displaying geographic variability of peri-urban agriculture environmental impacts in the Metropolitan Area of Barcelona: A regionalized life cycle assessment. Sci. Total Environ. 858. https://doi.org/10.1016/j.scitotenv.2022.159519

Mimet, A., Maurel, N., Pellissier, V., Simon, L., & Julliard, R. (2014). Towards a unique landscape description for multi-species studies: A model comparison with common birds in a human-dominated French region. Ecological Indicators 36, 19–32. https://doi.org/10.1016/j.ecolind.2013.06.029

Mitchell, M.G.E., Wu, D., Johansen, K., Maron, M., McAlpine, C., Rhodes, J.R. (2016). Landscape structure influences urban vegetation vertical structure. Journal of Applied Ecology 53, 1477–1488. https://doi.org/10.1111/1365-2664.12741

Moreno-García, P., Savage, A., Salgado, A. L., Tartaglia, E. S., Cocciardi, J. M., Aronson, M. F. J., Jarzyna, M. A., Alberti, M., & Li, D. (2025). *The effects of urbanization on species interactions.* Nature Cities, 2, 693–702. https://doi.org/10.1038/s44284-025-00288-w

Morpurgo, J., Remme, R.P., Van Bodegom, P.M. (2023). CUGIC: The Consolidated Urban Green Infrastructure Classification for assessing ecosystem services and biodiversity. Landscape and Urban Planning 234, 104726. https://doi.org/10.1016/j.landurbplan.2023.104726

Murgui, E., & Hedblom, M. (Eds.). (2017). Ecology and conservation of birds in urban environments. Springer. https://doi.org/10.1007/978-3-319-43314-1

Nielsen, A. B., van den Bosch, M., Maruthaveeran, S., & van den Bosch, C. K. (2014). Species abundance in urban parks and its drivers: A review of empirical evidence. Urban Ecosystems, 17(1), 305–327. https://doi.org/10.1007/s11252-013-0316-1

Olgyay, V. (2015). Design with Climate: Bioclimatic Approach to Architectural Regionalism - New and expanded Edition. Princeton University Press. https://doi.org/10.1515/9781400873685

Oliveira, V. (2022). Urban Morphology: An Introduction to the Study of the Physical Form of Cities, The Urban Book Series. Springer International Publishing, Cham. https://doi.org/10.1007/978-3-030-92454-6

Opdam, P., Luque, S., Nassauer, J., Verburg, P.H., & Wu, J. (2018). How can landscape ecology contribute to sustainability science? Landscape Ecol 33, 1–7. https://doi.org/10.1007/s10980-018-0610-7

Paumelle, M., Occelli, F., Wakim, L.M., Brousmiche, D., Bouhadj, L., Ternynck, C., Lanier, C., Cuny, D., Deram, A. (2023). Description of the multi-dimensional environment at the territorial scale: A holistic framework using cluster analysis and open data in France. Ecological Indicators 154, 110562. https://doi.org/10.1016/j.ecolind.2023.110562

Pedregosa, F., Varoquaux, G., Gramfort, A., Michel, V., Thirion, B., Grisel, O., Blondel, M., Prettenhofer, P., Weiss, R., Dubourg, V., Vanderplas, J., Passos, A., Cournapeau, D., Brucher, M., Perrot, M., & Duchesnay, É. (2011). Scikit-learn: Machine Learning in Python. Journal of Machine Learning Research, 12(85), 2825–2830.

Pesaresi M., & Panagiotis P. (2023). GHS-BUILT-C R2023A - GHS Settlement Characteristics, derived from Sentinel2 composite (2018) and other GHS R2023A data. European Commission, Joint Research Centre (JRC) [Dataset] https://doi.org/10.2905/3C60DDF6-0586-4190-854B-F6AA0EDC2A30

Pickett, S. T. A., Cadenasso, M. L., Rosi-Marshall, E. J., Belt, K. T., Groffman, P. M., Grove, J. M., Irwin, E. G., Kaushal, S. S., LaDeau, S. L., Nilon, C. H., Swan, C. M., & Warren, P. S. (2017). *Dynamic heterogeneity: A framework to promote ecological integration and hypothesis generation in urban systems.* Urban Ecosystems, 20, 1–14. https://doi.org/10.1007/s11252-016-0574-9

Potter, J. D., Brooks, C., Donovan, G., Cunningham, C., & Douwes, J. (2023). A perspective on green, blue, and grey spaces, biodiversity, microbiota, and human health. Science of The Total Environment, 892, 164772. https://doi.org/10.1016/j.scitotenv.2023.164772

Puchol-Salort, P., O'Keeffe, J., van Reeuwijk, M., Mijic, A.(2021). An urban planning sustainability framework: Systems approach to blue green urban design. Sustainable Cities and Society 66, 102677. https://doi.org/10.1016/j.scs.2020.102677

Raymond, C. M., Rautio, P., Fagerholm, N., Aaltonen, V. A., Andersson, E., Celermajer, D., Christie, M., Hällfors, M., Saari, M. H., Mishra, H. S., Lechner, A. M., Pineda-Pinto, M., & Schlosberg, D. (2025). *Applying multispecies justice in nature-based solutions and urban sustainability planning: Tensions and prospects.* npj Urban Sustainability, 5(2). https://doi.org/10.1038/s42949-025-00191-2

Raymond, C. M., Rautio, P., Fagerholm, N., Aaltonen, V. A., Andersson, E., Celermajer, D., Christie, M., Hällfors, M., Saari, M. H., Mishra, H. S., Lechner, A. M., Pineda-Pinto, M., & Schlosberg, D. (2025). Applying multispecies justice in nature-based solutions and urban sustainability planning: Tensions and prospects. *npj Urban Sustainability, 5*(1), Article 2. https://doi.org/10.1038/s42949-025-00191-2

Rega-Brodsky, C. C., Aronson, M. F. J., Piana, M. R., Carpenter, E.-S., Hahs, A. K., Herrera-Montes, A., Knapp, S., Kotze, D. J., Lepczyk, C. A., Moretti, M., Salisbury, A. B., Williams, N. S. G., Jung, K., Katti, M., MacGregor-Fors, I., La Sorte, F. A., Sheel, V., Threfall, C. G., & Nilon, C. H. (2022). *Urban biodiversity: State of the science and future directions.* Urban Ecosystems, 25, 1083–1096. https://doi.org/10.1007/s11252-022-01207-w

Sharifi, A., & Yamagata, Y. (2016). Urban Resilience Assessment: Multiple Dimensions, Criteria, and Indicators. In Y. Yamagata & H. Maruyama (Eds.), Urban Resilience: A Transformative Approach (pp. 259–276). Springer International Publishing. https://doi.org/10.1007/978-3-319-39812-9_13

Shouhang Du et al. (2024) Du, S., Zhang, X., Lei, Y., Huang, X., Tu, W., Liu, B., Meng, Q., & Du, S. (2024). Mapping urban functional zones with remote sensing and geospatial big data: A systematic review. GIScience & Remote Sensing, 61(1), 1–28. https://doi.org/10.1080/15481603.2024.2404900

Soberon, J., & A. T. Peterson. (2005). Interpretation of Models of Fundamental Ecological Niches and Species' Distributional Areas. Biodiversity Informatics 2:1–10.

Sowińska-Świerkosz, B., García, J. (2022). What are Nature-based solutions (NBS)? Setting core ideas for concept clarification. Nature-Based Solutions 2, 100009. https://doi.org/10.1016/j.nbsj.2022.100009

Stewart & Oke (2012) Stewart, I. D., & Oke, T. R. (2012). Local climate zones for urban temperature studies. Bulletin of the American Meteorological Society, 93(12), 1879–1900. https://doi.org/10.1175/BAMS-D-11-00019.1

Stokes, E.C., Seto, K.C. (2019). Characterizing and measuring urban landscapes for sustainability. Environ. Res. Lett. 14, 045002. https://doi.org/10.1088/1748-9326/aafab8

Verrelli, B.C., Alberti, M., Des Roches, S., Harris, N.C., Hendry, A.P., Johnson, M.T.J., Savage, A.M., Charmantier, A., Gotanda, K.M., Govaert, L., Miles, L.S., Rivkin, L.R., Winchell, K.M., Brans, K.I., Correa, C., Diamond, S.E., Fitzhugh, B., Grimm, N.B., Hughes, S., Marzluff, J.M., Munshi-South, J., Rojas, C., Santangelo, J.S., Schell, C.J., Schweitzer, J.A., Szulkin, M., Urban, M.C., Zhou, Y., Ziter, C. (2022). A global horizon scan for urban evolutionary ecology. Trends in Ecology & Evolution 37, 1006–1019. https://doi.org/10.1016/j.tree.2022.07.012

Wang, D. D., Xu, P.-Y., An, B.-W., & Guo, Q.-P. (2024). *Urban green infrastructure: Bridging biodiversity conservation and sustainable urban development through adaptive management approach.* Frontiers in Ecology and Evolution, 12. https://doi.org/10.3389/fevo.2024.1440477

Weisser, W.W., Hensel, M., Barath, S., Culshaw, V., Grobman, Y.J., Hauck, T.E., Joschinski, J., Ludwig, F., Mimet, A., Perini, K., Roccotiello, E., Schloter, M., Shwartz, A., Hensel, D.S., Vogler, V. (2023). Creating ecologically sound buildings by integrating ecology, architecture and computational design. People and Nature 5, 4–20. https://doi.org/10.1002/pan3.10411

Wentz, E. A., York, A. M., Alberti, M., Conrow, L., Fischer, H., Inostroza, L., Jantz, C., Pickett, S. T. A., Seto, K. C., & Taubenböck, H. (2018). Six fundamental aspects for conceptualizing multidimensional urban form: A spatial mapping perspective. Landscape and Urban Planning, 179, 55–62. https://doi.org/10.1016/j.landurbplan.2018.07.007

Wong, B. B. M., & Candolin, U. (2015). *Behavioral responses to changing environments*. Behavioral Ecology, 26(3), 665–673. https://doi.org/10.1093/beheco/aru183

WorldPop (www.worldpop.org - School of Geography and Environmental Science, University of Southampton; Department of Geography and Geosciences, University of Louisville; Departement de Geographie, Universite de Namur) and Center for International Earth Science Information Network (CIESIN), Columbia University (2018). Global High Resolution Population Denominators Project - Funded by The Bill and Melinda Gates Foundation (OPP1134076). [dataset] https://dx.doi.org/10.5258/SOTON/WP00646

Wu, J. (2004). Effects of changing scale on landscape pattern analysis: Scaling relations. Landscape Ecology, 19(2), 125–138. https://doi.org/10.1023/B:LAND.0000021711.40074.ae

Zhang, P., Ghosh, D., & Park, S. (2023). Spatial measures and methods in sustainable urban morphology: A systematic review. Landscape and Urban Planning, 237, 104776. https://doi.org/10.1016/j.landurbplan.2023.104776

Zhao, W., Liu, D., Niu, J., He, J., & Xu, F. (2024). Spatial Heterogeneity Analysis of the Multidimensional Characteristics of Urban Green Spaces in China—A Study Based on 285 Prefecture-Level Cities. Land, 13(7), Article 7. https://doi.org/10.3390/land13071050

Zhou, W., Pickett, S. T. A., & Cadenasso, M. L. (2017). Shifting concepts of urban spatial heterogeneity and their implications for sustainability. Landscape Ecology, 32(1), 15–30. https://doi.org/10.1007/s10980-016-0432-4

Chapter 4.

Attaining continental-scale Cohabscapes: the road forward to bringing co-habitative urban landscapes classifications to all European Functional Urban Areas

Abstract

This chapter advances the Cohabscapes methodology introduced in Chapter 3 by critically examining its current limitations and the future development ways for achieving continental expansion. The focus is twofold:

i. First by assessing the methodological constraints that arise from variable selection, dimensionality reduction, clustering strategies, and available open data.

ii. Second, by exploring how the framework can be scaled to encompass all European Functional Urban Areas (FUAs).

Particular attention is given to the challenges of harmonizing diverse datasets, integrating multiscale dimensions, and ensuring comparability across heterogeneous urban systems. The chapter also situates Cohabscapes within the geographic context of European FUAs, highlighting disparities in population, area, and urban core–periphery ratios, while proposing a structured sampling strategy to capture climatic and morphological diversity that should in turn strengthen the unsupervised training. While modelled data for continental application are already available, the integration of machine learning components remains a future step. Overall, the chapter positions Cohabscapes as a conceptual and computational scaffold for pan-European urban ecology, capable of providing a shared language for biodiversity-informed planning and cross-city comparison.

Keywords

unsupervised classification; Functional Urban Areas; scale-up process

4.1. Introduction

The Cohabscapes classification framework, introduced in Chapter 3, represents a novel attempt to describe cities as co-habitative landscapes through a species-generic lens. Its potential lies in providing a shared language for biodiversity-informed planning, capable of harmonizing ecological and morphological knowledge across diverse urban contexts. Extending this methodology to the continental scale would open new opportunities: enabling cross-city comparisons, supporting European-level monitoring frameworks, and guiding interventions that balance ecological resilience with urban liveability.

Therefore, this Chapter explores how Cohabscapes can (in practice) evolve beyond its initial scope. Rather than focusing solely on technical constraints, the discussion highlights the broader impacts of scaling: the implication on focusing on the notion of species-generality, the possibility of identifying common ecological patterns across Europe, and of integrating climatic and socioeconomic diversity into a unified classification. While methodological refinements are necessary, the emphasis here is on the pathways forward and the transformative role Cohabscapes could play as a pan-European infrastructure for ecological knowledge exchange.

Generally, these limitations and constrains arise from design choices took during the conceptualization, data availability, and computational strategies, and they highlight areas where refinement is needed before scaling the methodology to continental applications. Table 1 summarizes the main limitations and outlines potential directions for improvement.

Table 1. Main challenges deriving from the limitations of the Cohabscapes methodology, and possible solutions.

Limitation	**Description**	**Argument in favour or in contrast of the limitation, including possible solutions**
Variable selection	Reliance on species generality excluded indicators such as species abundance. This reduced species-specific bias but could weaken ecological sensitivity.	This is a main property of the classification. Integrating abundance or diversity metrics and maintaining safeguards against overfitting is challenging.
Layer subdivision and collinearity	Variables were grouped into four thematic layers, which increased flexibility but introduced collinearities (e.g., Built-up Density from Local Urban Fabric vs. Commercial Area Ratio from Anthropic Imprint).	Additional preprocessing such as applying collinearity diagnostics and variable reduction before classification to improve interpretability could lead to a better subdivision. Otherwise, the restructuring of the four subclassifications could solve the problems at the root by introducing a different subdivision of information.
Dimensionality reduction	PCA/KPCA simplified the dataset but obscured intuitive links between variables and classes.	The application on a small city set (Vienna, Munich, Genoa) lead to a skewed and difficult to assess cluster analysis, that probably is unfit

and class naming	Class naming relied on analogical interpretation, limiting transparency.	to represent the continental scale as is. Establishing a standardized naming protocol based on measurable thresholds could ease the process especially during a scaling-up approach.
Clustering algorithm	K-means (in its canonical variants) was used for classification. While computationally efficient, it assumes spherical clusters and does not account for spatial association, potentially oversimplifying urban patterns.	Explore spatially explicit clustering methods (e.g., spatially constrained k-means, density-based clustering, graph-based clustering, or hierarchical-based clustering) to capture spatial dependencies and irregular cluster shapes. This consideration should take into account the computational constraint and availability. The previous version of the classification was optimized for parallel processing and execution in High Performance Computing environments, but additional care in optimization should be considered, especially when working at continental scale.
Geographic scope	Case studies were concentrated in Central Europe, introducing regional bias.	Retrain the methodology with datasets from diverse European regions to improve generalisability. The goal is to satisfy the needs of European scientists and administrations by aligning with the definitions of the Organization of Economic Development (OECD), following the Functional Urban Areas defined by Schiavina et al., 2023.
Data resolution	Variables such as temperature were limited in spatial and temporal resolution. The fixed 10 m resolution restricted the ability to capture seasonal or rapid urban change.	The strive toward high resolution contrast with the actuality in data availability, especially in relation to time-series. Simplifications might occur, especially during a scaling-up approach where some data layer may fail to comply simply because of spatial incompatibility (e.g., remote images over a continental scale would need to be taken at different times and sky conditions).
Exclusion of sea areas	Marine areas were excluded, with only buffer zones applied to mitigate distortion, limiting coastal applicability.	The previous version of the classification operated on a large 200m boundary that enabled to compute landscape metrics with enough confidence of not dealing with edge errors. Sea is different, because while many data layers (e.g., elevation) provide data for submarine pixels, other do not or do it with low accuracy (e.g., temperature over sea or lake surfaces). Ultimately, coastal zones are problematic as much as lakes since the means of retrieving information (such as from remote sensing) is different, and usually not considered in urban planning. For example, NDVI classifies terrestrial pixels that are vegetated or non-vegetated (both as positive values) and classifies all water pixels together

		(as negative values). Ultimately, for data that is non accurate over water pixels, the easiest approach would be to consider the indirect influence of that pixel over the neighbouring, keeping this fallacy as an intrinsic weakness of coastal areas.

4.1.1. Variables and classification structure at (European) continental scale

4.1.1.1. On species generality and the spectres of prior imaginaries

One of the defining properties of the Cohabscapes classification system is its reliance on species generality. By design, the framework excludes species specific indicators such as abundance or diversity metrics. This choice reduces the risk of bias toward some taxa and ensures that the classification remains broadly applicable across different ecological and cultural contexts. However, the tradeoff is a potential weakening of ecological sensitivity, since ecological indicators hold particular significance, for example insects' abundance patterns often provide early signals of environmental change (Chowdhury et al., 2023).

A counter-argument is that this limitation is not a flaw but rather a benefit of the system. Integrating abundance or diversity metrics at continental scale would require safeguards against overfitting and context-specific distortions, which are difficult to maintain in a continent-spanning framework (Mathers et al., 2024). For rare or locally extinct species, the exclusion of abundance is unproblematic, as their absence is already captured by broader environmental descriptors (Mace et al., 2018). For very abundant species, however, the omission may obscure important ecological dynamics since dominant populations often drive ecosystem processes and their fluctuations can signal broader environmental change (Hillebrand et al., 2018).

From an architectural perspective, there is also a form of design ingenuity in excluding species. By not privileging any organism, the classification allows urban designs to be conceived as spaces for all "urban citizens" whether human or non-human, without being pre-defined by species-specific requirements (Canepa et al., 2023). This introduces a form of species agnosticism, where the classification takes no sides in describing cities through the lens of any taxa (Zeller et al., 2024). Instead, it provides a neutral scaffold that can accommodate multiple ecological interpretations, enabling planners to imagine urban coexistence beyond anthropocentric or other species-centrism paradigms (Heymans et al., 2019).

Species agnosticism, however, is not merely a technical manoeuvre in classification; it can be understood as a philosophical position. By refusing to anchor urban design in any single species, the framework resists essentialism and opens the city to a plurality of ecological narratives. In this sense, the scaffold becomes a generative device: neutral, flexible, and capable of hosting diverse ecological interpretations rather than prescribing them in advance. It is precisely this openness that allows urban design to be imagined as a site of multi-species futures (Zari et al., 2020).

Yet, neutrality is never absolute. Drawing on Derrida's notion of hauntology (Derrida, 1994), this framework can be read as haunted by prior ecological imaginaries. In urban design, hauntology functions less as a technical term than as a philosophical lens, collecting much of the discourse in urban environmental philosophy on how past species hierarchies continue to shape present possibilities (Sterling, 2022; Lown, 2025). Thus, even as the classification claims impartiality, it carries with it the spectral presence of prior ecological imaginaries, such as species once privileged in conservation discourse, cultural symbols of urban nature, or historical absences that continue to resonate in contemporary design. Species agnosticism, therefore, cannot fully escape the ghosts of the paradigms it seeks to transcend (Davis, 2005).

So, rather than undermining agnosticism, these hauntings can be seen as productive tensions. The scaffold is not simply neutral nor haunted, but a palimpsest, i.e., a layered structure where new ecological narratives are inscribed over traces of older ones (Huyssen, 2003; Edensor, 2005). This palimpsestic quality means that urban design is simultaneously a site of coexistence and remembrance, where planners negotiate between opening space for future multi-species relations and acknowledging the spectral presence of past hierarchies (Corboz, 1983). In this sense, species agnosticism is both enabling and limited. While neutrality creates room for diverse ecological futures, it also risks flattening ecological difference and cannot fully escape the ghosts of prior imaginaries (Bennett, 2010). And precisely in this tension lies its generative potential, as hauntology ensures that futures remain entangled with cultural and ecological pasts without assigning heritage value, but simply recognizing the layered legacies that shape urban design.

4.1.1.2. Translating species-generality into the multidimensional classification system

The challenge that arises from addressing species-generality at the foundation of the classification lies in addressing the structure of the system, and how much "humanness" can truly be left in.

Presently, Cohabscapes partially addresses this challenge with multidimensionality, i.e., dividing information between complementary layers, and in this case urban fabric, anthropic imprint, and biophysical conditions. This structure ensures that the classification captures not only the physical configuration of settlements but also the human and environmental processes that shape them. Nevertheless, it is apparent that the three dimensions are not equally distanced from human agency.

Biophysical conditions are relatively unproblematic, since species respond to climate and environmental gradients in their own ways (Pearson & Dawson, 2003). Yet, in the Anthropocene, humans also shape urban climates indirectly through greenhouse gas emissions, heat island effects, and land-use change (IPCC, 2023). For this reason, biophysical conditions can still be treated as a relatively neutral lens for describing cities: they provide a baseline grounded in ecological gradients, even if those gradients are increasingly modulated by human influence (Forman, 2014; Pickett et al., 2013).

Urban fabric is more complex. It is the direct expression of human action on the environment, but its outcomes are not exclusively human. Buildings, streets, and infrastructures are used by humans, but also by birds, rodents, insects, and spontaneous vegetation. Historically, urban form is rooted in settlement development, shaping human ways of life as much as it is shaped by them. In this sense, urban form is both a cultural artifact and an ecological substrate (Rossi, 1982; Spirn, 1984). As Rossi argues, the city's architecture embodies collective memory, embedding cultural practices and identified into its form. At the same time, Spirn demonstrated that urban fabric functions ecologically, providing hatibats and flows that extend beyond human use. Thus, the cultural development of cities is inseparable from their physical form. Streets and squares are stages for social life, while infrastructures and buildings anchor identify through continuity and change. Urban fabric gives a city its identify precisely because it is layered. In this way, the city is not only a human artifact but also a living substrate, and its identify emerges as much from the dynamic interplay of its cultural memory as from its ecological adaptation.

Anthropic imprint is the most anthropocentric dimension, and it's inherently related to the dominant role of humans in the urban environment and in Earth's ecosystems at large (Vitousek et al., 1997). Indicators such as population density could be criticized as a fallacy, since they effectively measure the abundance of a single species: humans. To address this, the focus is not on humans per se, but on their imprint, i.e., the ways in which human presence and activity shape urban environments, both actively (e.g., land uses, transport networks) and passively (e.g., designation of parks, conservation areas) (Fuller & Irvine, 2012). This framing treats socioeconomics as a record of human legacy rather than a value-laden description of human society. It acknowledges that humans are the apex organism of the urban habitat, and that accounting for their imprint is both logical and necessary (Grimm et al., 2008). Importantly, this perspective resonates with the earlier discourse on ecological legacy and hauntology: human settlements are haunted by past decisions, infrastructures, and spatial hierarchies that continue to shape ecological developments. By focusing on imprint rather than direct human actions, the focus lies into capturing enduring traces of human agency such as roads and zoning that persist even when daily flows of traffic or patterns of use change. This distinction is crucial as it shifts the attention from the ephemeral "live feed" of humana activities to the structural legacies that define urban environments over time (Shackleton & Gwedla, 2021; Heymans et al., 2019).

Taken together, these considerations reaffirm the classification's species-generic stance while clarifying its treatment of human influence. By balancing ecological neutrality with recognition of human imprint, the system remains flexible enough to operate at continental scale while avoiding species-specific biases, such as anthropocentric, that could undermine its generality. Nevertheless, the argumentation for multiscalary needs further clarification.

4.1.1.3. Considerations on the multiscalarity of the classification

A central challenge in developing a robust classification framework lies in achieving multidimensionality while also accounting for multiscalarity, meaning the representation of different layers of urban data that can be complementary horizontally (i.e., at the same scale) and vertically (i.e., at different scales).

Presently, the four sub-classification system operates at two scales: Local, describing the contents of 10-metres cell with no influence of outside information, and Landscape, describing the surrounding environment of each cell in a 100-metres buffer. However, the current system is constrained by the resolution of available data. Urban fabric data, derived from high-resolution spatial sources, can be meaningfully expressed at both the local and landscape scales. In contrast, anthropic imprint indicators and biophysical variables are typically available only at coarser resolutions, which restricts their application to the sole landscape scale. This imbalance has led to a system of four sub-classifications across two scales, but it also exposes a number of weaknesses:

i. Urban fabric is over-represented, as it can be expressed at multiple scales, while the anthropic imprint and biophysical dimensions are under-represented.

ii. Key differentiating variables such as GDP, employment rates, mean annual temperature, and precipitations are excluded because they operate at scales coarser than the landscape, from 1000-metres resolution up to a single value for any city.

iii. The result is a classification that is internally consistent but limited in its ability to capture macro-regional differences between cities across Europe.

If the objective is to extend Cohabscapes across European FUAs and build a pan-European classification, it becomes necessary to incorporate these broader-scale variables. This requires introducing a third level of scale: the Regional scale, defined here as a dimensionless classification that operates on one-dimensional array, where values are representative of the entire city rather than of individual cells or groups of cells. By doing so, the classification system can integrate both fine-grained local detail and coarse-grained regional context, thereby balancing multidimensionality with multiscalarity. The expanded framework would therefore consist of six sub-classifications across three scales:

i. Urban Fabric at the Local (10 m cell) and Landscape (100 m radius) scales, reflecting the high-resolution data available for built and natural features and their spatial configuration.

ii. Anthropic Imprint (representing socioeconomic conditions) at the Landscape and Regional (city-level array) scales, incorporating both city-level indicators and broader metrics such as GDP and employment.

iii. Biophysical Conditions at the Landscape and Regional scales, combining medium-resolution environmental data with coarse climatic variables such as mean annual temperature and precipitations.

This expansion addresses the weaknesses of the current system by ensuring that each dimension is represented at the most appropriate scale of analysis. It also enhances the capacity of the classification to differentiate between cities not only based on their morphology but also in terms of their socioeconomic and environmental contexts at continental scale.

4.2. Computation considerations on preprocessing and clustering

4.2.1. Dimensionality reduction

4.2.1.1. PCA/KPCA pipeline

Dimensionality reduction is a practical and effective step in classification problems because it lowers the complexity of the clustering[7] (Florczyk et al., 2019), and Cohabscapes already integrates this step. Principal Component Analysis (PCA) and Kernel PCA (KPCA) provide compact representations of high-dimensional, heterogeneous inputs while preserving most of the information needed for downstream interpretation and clustering. KPCA is especially useful when optimizing the kernel choice to capture non-linear structure. For example, polynomial kernels can model curved decision boundaries, while χ^2 kernels are appropriate for histogram-like or non-negative feature distributions typical of spatial and ecological variables (Schölkopf, Smola, & Müller, 1998). Kernel selection guided by validation metrics and interpretability checks helps align the reduced space with the phenomena of interest.

As said before, the usage of dimensionality reduction algorithms can lower the workload of further analysis, especially when applied to large datasets. Here, a workflow in batches can be formed. Incremental PCA allows streaming large datasets in mini-batches, avoiding the need to load the entire matrix into memory and enabling consistent scaling onto a common axis before clustering (Ross, 2008). Analogous strategies can be applied to KPCA via out-of-core approximations such as the Nyström method (Fowlkes et al., 2004), or by fitting on representative subsets with careful feature standardization, then projecting new batches consistently. This approach supports continental-scale processing, where city-level tiles and temporal slices can be reduced and merged without sacrificing reproducibility (Fauvel et al., 2013; Florczyk et al., 2019).

Additionally, once the Incremental PCA model has been fitted to the entire matrix, the resulting principal components axes are globally consistent. This means that clustering can subsequently be performed city-by-city, with each local dataset projected

[7] Dimensionality reduction decreases the number of variables while retaining most of the relevant information. By projecting data into a lower-dimensional space, it reduces redundancy and noise, thereby simplifying the clustering task. This improves computational efficiency and enhances the stability of the resulting groups. For example, instead of characterizing vegetation by hundreds of overlapping indicators (e.g., leaf area index, canopy cover, biomass density, and NDVI), dimensionality reduction can combine these into a smaller set of composite measures that still capture the essential patterns of vegetation structure and function. Clustering then operates on these clearer, more compact descriptors rather than on a noisy, redundant set of raw variables.

onto the same PCA space. In practice, this ensures that the reduced features are directly comparable across cities, while significantly reducing the computational burden of the heavier classification tasks (Zhao et al., 2019)

4.2.1.2. Explained variance

One variable to consider is the explained variance, i.e., the proportion of the total variability in a dataset that is captured by a statistical model or by a reduced set of components[8]. Explained variance thresholds provide a clear stopping rule for component selection. Retaining approximately 95% of variance, as is done in Cohabscapes, can be done in applied PCA because it removes noise and redundancy while preserving the bulk of information relevant to spatial and ecological structure (Jolliffe & Cadima, 2016). In any case, there is no prescription of universal threshold, as the number of components is ultimately context-dependant. Lowering the threshold could directly simplify the calculation, by further reducing the data that is clustered, albeit at a cost of precision. For example, in exploratory sciences such as ecology and psychology a threshold of 0.5 is commonly adopted because the data is usually very noisy and the goal is interpretability rather than reconstruction (Peres-Neto et al., 2005). In other fields, such as in engineering and image analysis (or geospatial classification, as for Cohabscapes), a higher threshold is more common because the goal is to preserve fine-grained structure for downstream tasks such as clustering (Fauvel et al., 2013).

4.2.2. Clustering

4.2.2.1. Confronting alternative clustering algorithms in urban classifications

At the core of the Cohabscapes methodology lies a problem of unsupervised classification. Although this data comes from various sources (geospatial, demographic, climate to name a few), it is ultimately spatially linked to urban spaces.

The previous version of Cohabscapes used K-Means to solve this problem, due to its computational efficiency and ease of implementation. Its centroid-based formulation allowed rapid partitioning of very large datasets into a predefined number of clusters, making it well-adapted to continental-scale processing where scalability was a primary concern. However, while K-Means performs well on convex and relatively homogeneous clusters, it is less effective at capturing irregular spatial structures or incorporating explicit spatial constraints such as the ones that are present with urban data. These limitations motivate the exploration of alternative clustering approaches that can better account for spatial

[8] In the context of PCA or KPCA, explained variance measures how much of the original data's variance is retained by each principal component. Formally, it is the ratio between the variance accounted for by a given component (its eigenvalue) and the total variance of all components. Summing across the first k components gives the cumulative explained variance, which indicates how much of the dataset's overall information is preserved when reducing dimensionality.

dependencies and complex geometries (Steinley et al., 2010).

Density-based methods, such as DBSCAN and its hierarchical extension HDBSCAN, identify clusters as contiguous regions of high point density separated by areas of lower density. Unlike K-Means, they do not assume convex cluster shapes and can therefore capture irregular morphologies, such as fragmented urban patches or ecological corridors. They also explicitly identify noise points, which is valuable in heterogeneous spatial datasets. The main drawbacks are their sensitivity to parameter choices (e.g., neighbourhood radius, minimum points) and their heavier computational cost, which can become significant at continental scale (Campello et al., 2013).

Graph-based approaches represent spatial units as nodes connected by edges that encode similarity or adjacency. Clustering is then achieved through graph partitioning techniques such as spectral clustering or community detection. This framework is highly flexible, as it allows spatial contiguity to be encoded directly in the graph structure, ensuring that resulting clusters respect geographic adjacency. Graph-based methods are particularly effective at capturing complex spatial dependencies and multi-criteria similarity (e.g., urban form and socio-ecological attributes). However, they are memory-intensive and computationally demanding, especially when applied to continental-scale graphs, since spectral methods require eigen-decomposition of large matrices (Yang et al., 2016).

Hierarchical clustering builds a nested tree (dendrogram) of clusters by either iteratively merging smaller groups (agglomerative) or splitting larger ones (divisive). This produces a full hierarchy of partitions, allowing analysis at multiple spatial scales without fixing the number of clusters in advance. When spatial constraints are added, merges can be restricted to adjacent units, ensuring geographic contiguity. The main advantage of hierarchical methods is their interpretability and flexibility in exploring multi-scale patterns. However, their computational complexity is high (often quadratic in the number of observations), which makes them challenging to apply directly at continental scale without approximation or sampling strategies (Murtagh & Contreras, 2017)

Beyond classical algorithms, recent work has introduced deep learning–based approaches that combine representation learning with clustering. Autoencoder-based methods (Xie et al., 2016) learn compact latent spaces where clusters are more separable, while variational extensions (Jiang et al., 2017) add probabilistic structure for greater robustness. In image and spatial analysis, deep clustering frameworks (Caron et al., 2018) integrate convolutional networks with clustering objectives, improving performance on high-dimensional data.

Another trend is the combination of manifold learning and density-based clustering. For example, UMAP (McInnes et al., 2018) provides non-linear dimensionality reduction that preserves local structure, and when paired with HDBSCAN (McInnes et al., 2017), it yields stable clusters in noisy, irregular datasets. These pipelines are increasingly used in ecology and geospatial analysis.

The main characteristics of these methods are illustrated in Table 2.

Table 2. Confronting different clustering methodologies based on their properties.

Method	**Cluster shape**	**Spatial constraints**	**Scalability**	**Noise handling**	**k-required**
K-Means	Convex, spherical	Optional (via spatial K-Means)	Excellent (HPC-friendly)	Poor (sensitive to outliers)	Yes
Density-based (DBSCAN / HDBSCAN)	Arbitrary, irregular	Implicit via density neighborhoods	Moderate (parameter tuning + heavier computation)	Explicit (labels noise separately)	No
Graph-based (Spectral / Community detection)	Arbitrary, flexible	Directly encoded in adjacency graph	Heavy (eigen-decomposition, memory-intensive)	Possible (depends on similarity definition)	Depends on method
Hierarchical (Agglomerative / Divisive)	Nested, multi-scale	Possible (spatially constrained merges)	Poor ($O(n^2)$), unless approximated	Limited	No (cut dendrogram at chosen level)
Deep Embedded Clustering (DEC, VaDE)	Arbitrary (latent space)	Implicit (depends on embedding)	Moderate–High (GPU required)	Often robust (latent denoising)	No
Deep Clustering (CNN-based, e.g. DeepCluster)	Arbitrary (image/feature embeddings)	Implicit	High (GPU-accelerated, scalable to large images)	Moderate	No
UMAP + HDBSCAN	Arbitrary, non-linear manifolds	Implicit (via manifold structure)	Moderate (scales well with optimizations)	Strong (HDBSCAN robust to noise)	No

Accurate testing should be conducted to determine the most effective ML algorithm, while maintaining computational efficiency due to the large size of the dataset.

4.2.2.2. DBSCAN and HDBSCAN

A definite choice of clustering algorithm requires comprehensive testing across the full scale of the training data. Nonetheless, some considerations can be made a priori and through a smaller-scale inquiry.

From a ML perspective, K-Means (the algorithm used for the first version of Cohabscapes) remains efficient and HPC-friendly, but it reliance on convex cluster shapes and sensitivity to outlies makes it unsuitable for complex datasets (MacQueen, 1967; Baligodugula & Amsaad, 2025). These reasons enforce the necessity of searching for alternative clustering criteria, balancing the complexity of the task with the need for accuracy.

As highlighted before (Table 2), numerous alternatives exist. Graph-based methods such as spectral clustering or community detection offer flexibility in cluster definition, yet their dependence on eigen decomposition renders them computationally heavy and difficult to scale to continental raster datasets (Ng et al., 2002). Hierarchical clustering provides nested, multi-scale insights but suffers from poor scalability (Murtagh & Contreras, 2012). Deep clustering approaches (such as CNN-based) are powerful in latent spaces but require GPU acceleration and introduce methodological opacity, complicating reproducibility (Xie et al., 2016; Jiang et al., 2017). UMAP combined with HDBSCAN shows promise for manifold learning, though it adds complexity in parameter tuning (McInnes, Healy, & Melville, 2018).

An interesting avenue to explore is the DBSCAN (Density-Based Spatial Clustering of Applications with Noise) family of algorithms, considering also HDBSCAN (Hierarchical DBSCAN). These algorithms detect arbitrary, irregular cluster shapes without requiring a predefined number of clusters, explicitly labelling noise to avoid forcing assignment of outliers, and handle heterogeneous densities. This last property is especially critical for distinguishing compact urban cores from diffuse peripheries (Ester et al., 1996; Campello et al., 2013). Comparative studies confirm that density-based clustering consistently outperform centroid-based methods in robustness and interpretability, especially in spatial and high-dimensional datasets in today's ML environment (Schubert et al., 2017). Applications of density-based clustering in urban contexts demonstrate its versatility. For example, in Wuhan, China, DBSCAN was applied to classify production, living, and ecological spaces, by using point-of-interest data, successfully identifying irregular urban clusters and separating noise, thereby confirming its suitability for complex urban contexts where traditional centroid-based methods fail (Tu et al., 2022). Similarly, in Bavaria, Germany, a data-driven approach combined DBSCAN with feature engineering to delineate urban areas from multi-source geospatial data. This study highlighted DBSCAN's ability to improve precision compared to conventional Open Street Maps-based delineations, underscoring its value in large-scale urban planning tasks (Fang et al., 2025). Extending to smart city applications, HDBSCAN has been applied in Italy to detect multi-density urban hotspots, effectively distinguishing compact centres from diffuse peripheral activity. This case illustrates HDBSCAN's robustness in handling heterogeneous densities and its relevance for contemporary smart city planning and management (Cesario et al., 2023).

Conceptually, DBSCAN works by defining clusters as contiguous regions of high density separated by regions of low density. This makes DBSCAN particularly well-suited for spatial data and irregularly shaped clusters, which are common in urban and ecological contexts, as shown in previous examples. The algorithm relies on two parameters: ε (eps) and minimum points.

The ε parameter defines the radius of a neighbourhood around a point, while minimum points specify the minimum requirement of points within that neighbourhood for the point to be considered a core point (Ester et al., 1996). Thus, points are classified into three categories:

i. Core points, which have at least "minimum points" neighbours within ε.

ii. Border points, which fall within neighbourhood of a core point but do not themselves meet the minimum point threshold.

iii. Noise points, which are neither core nor border points and remain unflustered. This category is what allows DBSCAN to distinguish dense clusters from sparse region and explicitly label outliers.

DBSCAN begins by selecting an unvisited point and checking whether it qualifies as a core point. If it does, the algorithm expands a cluster by recursively including all points that are density-reachable from the core. Border points are attached to clusters but do not expand them further. Points that cannot be reached from any core point are labelled as noise. This iterative process continues until all points are visited, resulting in clusters of arbitrary shape and size, along with a set of noise points.

The main strength of DBSCAN lies in its ability to discover clusters of irregular shape and to handle noise explicitly. It does not require the number of clusters to be specified in advance, which is a major advantage in exploratory analysis. However, DBSCAN is sensitive to parameter selection: a single ε value may not capture clusters with varying densities, and inappropriate choices can lead to either fragmented clusters or overly large ones. This limitation is addressed by HDBSCAN, which generalizes DBSCAN by varying ε across scales and selecting stable clusters automatically.

HDBSCAN was developed as a natural extension of DBSCAN to overcome its sensitivity to parameter choice (Campello et al., 2013). While DBSCAN requires a single fixed ε radius, HDBSCAN generalizes the concept of density by building a hierarchy of clusters across multiple density thresholds, allowing the algorithm to adapt to datasets where clusters vary in density, which is common in urban and ecological contexts.

The algorithm computes mutual reachability distances between points, which incorporate both the core distance of each point and their pairwise separation. From these distances, HDBSCAN constructs a minimum spanning tree that represents the connectivity of the dataset. This is further condensed into a hierarchy of clusters at different density levels. Instead of forcing a single ε value, HDBSCAN explores the full tree and identifies clusters that persist across scales. The final step is cluster selection, where the algorithm chooses the most stable clusters, i.e. those that remain coherent across a wide range of density levels. Similarly, as DBSCAN, points that do not belong to any stable cluster are labelled as noise. Its only parameter is the minimum cluster size, which defines the smallest grouping of points that can be considered a valid cluster. This makes HDBSCAN robust in datasets with heterogeneous densities, but it is more intensive DBSCAN. Nevertheless, it is worth stating that the complexity of DBSCAN and HDBSCAN while the scale-up process can be lessened up through parallelization and smart data pipelining.

4.2.2.3. Strategy for introducing spatial association

Spatial association is critical because clustering algorithms like DBSCAN rely on density and proximity. Without associating raster cells to their spatial context, the algorithm risks treating each cell as independent, leading to fragmented (or worse, spatially misleading) clusters. By embedding information about location and adjacency, spatial association allows the detection of coherent urban structures, while supporting comparability across different cities and ensuring that clusters reflect meaningful morphological patterns rather than random pixel distributions. In practice, this makes it possible to identify dense cores, peripheral zones, and transitional areas in a way that is consistent across the European urban system (Fang. et al., 2025). This rational is commonly associated with urban morphology studies, where capturing the structural coherence of cities is essential.

However, introducing spatial association also carries risks. By embedding information about the surrounding cells into each raster unit, the analysis may inadvertently impose artificial coherence. And for ecological applications, this can lead to biases, as the algorithm may overemphasize contiguity and underrepresent ecological heterogeneity. For example, fragmented habitats or discontinuous green spaces may be forced into clusters that appear denser than they truly are, obscuring ecological variability (Tu et al., 2022; Xiao et al., 2022).

Methodologically, spatial association can be introduced in DBSCAN/HDBSCAN. This is achieved through a three-step normalization strategy:

i. First, each city's raster grid is cantered on its local barycentre.

ii. Second, these normalized grids are aligned to a general reference grid, enabling inter-city comparison.

iii. Third, derived measures, such as presence within FUA/UC or distances from the barycentre, are calculated to provide consistent indicators of spatial contiguity.

This normalization ensures that DBSCAN's ε encodes adjacency in a way that is comparable across cities, allowing clusters to be detected as dense urban formations rather than fragmented noise. Parameter ε can be further be seen as a measure of "rook" (horizontally and vertical adjacency, $\varepsilon = cell\ size$) or "queen" contiguity (adding diagonal adjacency, $\varepsilon = cell\ size \times \sqrt{2}$). While usually queen contiguity better reflects built-up contiguity (especially in dense fabrics), rook contiguity might be preferable in ecological analysis as diagonal connections can artificially smooth fragmentation (Anselin & Rey, 2014). To fully incorporate spatial association, the x/y coordinates of each cell can be added to the feature array used for clustering. However, coordinates are measured in units (metres) that are often vasrlt different in scale compared to other attributes (which in this case are normalized Principal Component axis). If left unadjusted, the coordinate values would dominate the clustering process, biasing results toward spatial proximity rather than attribute similarity. Thus, a final step of standardization is required, applying z-score standardization to x and y so each has mean 0 and standard deviation 1 before concatenating with PCs. Additional tuning and scaling would be required depending on the actual data ranges.

4.2.3.4. On the definition of Urban Centre

The definition of UC is central for ensuring comparability across cities, and to properly weight internally the clusters based on the disproportionate weight of peripheral areas and core areas. Three methodological approaches are considered:

i. UCDB R2024A: This dataset provides the built-in UC definitions for GHSL FUAs. It represents the official Eurostat/OECD methodology, harmonized across Europe, and is widely used in policy and statistical contexts (Melchiorri et al., 2024).

ii. OSM Municipality Boundaries: In the first version of Cohabscapes, municipal boundaries from OSM were used to approximate urban extents (https://www.openstreetmap.org). This approach leverages volunteered geographic information, offering flexibility and local detail, but introduces variability in coverage and quality across regions. Additionally, it can introduce back a bias of anthropocentric design that was originally left out by selecting the GHSL FUAs.

iii. ESA Land Cover Pixel Kernel Estimation: This method defines UCs by clustering built-up pixels from ESA World Land Cover raster (ESA, 2021), using kernel estimation of the first level to identify contiguous urban patches. It is morphology-driven and ecologically general, reflecting disturbance patterns rather than administrative boundaries.

Albeit UCDB are the de facto default option, and OSM boundaries are already tested in Cohabscapes, further care should be taken. In fact, the difference in defining the UC would represent a discrepant barycentre, thus a mismatch for x/y coordinates used in the normalized spatial association. While this could be negligible in centric FUAs, peculiar cases where the UC is not easily identified or shifted from the barycentre of the FUA could introduce anomalies, disturbing the clustering process.

4.2.3.5. Considerations on scalability and parallelization

Scalability is a methodological requirement even when potent hardware is available, as large-scale raster datasets exceed the limits of single-machine computation. The pipeline therefore combines Incremental PCA/KPCA for dimensionality reduction, with DBSCAN/HDBSCAN for clustering. This can further be supported by parallelization strategies and enhanced algorithmic variants. During the Ph.D., experimentations with High-Performance Computing (HPC) systems (Leibniz Research Centre, Technical University of Munich; NHR@FAU, Erlangen-Nurnberg) lead to testing and familiarization with HPC architectures and parallelization techniques, fundamental for optimizing large-scale geospatial workflows.

The Incremental PCA requires projection tasks to be decoupled across multiple processors or nodes to reduce runtime through iterative batches. Clustering, if done from aligned principal components, can be simplified as an embarrassingly parallel task, i.e., one where little or no effort is needed to split the problem into several parallel tasks, as clusters do not depend on other cities and can be fully distributed as separate jobs while maintaining full consistency.

Existing frameworks can support this scalability through distributed computing environments. For example, Dask provides parallel arrays and dataframes, enabling DBSCAN/HDBSCAN to be executed across large datasets while maintaining consistency with the global PCA space (Rocklin et al., 2015). In HPC contexts, OpenMP and MPI can parallelize the neighbourhood search step, which is the most computationally demanding part of density-based clustering (Velarde Martínez, 2022). GPU acceleration, such as RAPIDS cuML, further reduces runtime by implementing DBSCAN and HDBSCAN on modern accelerators, allowing millions of points to be processed efficiently (Nolet & Gala, 2021). Although, some frameworks can be rigid and limit the implementation of algorithmic implementations such as custom kernels (e.g., for configuration metrics computation in a moving rounded window)

Additionally, enhanced variants can improve scalability while preserving methodological coherence. For example, Hybrid approaches combine the strengths of DBSCAN and HDBSCAN for cluster selection. In practice, this reduces the formation of micro-clusters in high-density regions, which can otherwise fragment the analysis. At the same time, robustness is maintained in sparse areas, where density variations are more subtle. This balance makes hybrid strategies particularly useful for urban morphology, where dense cores and diffuse peripheries coexist (Malzer & Baum, 2021). Other optimizations can be obtained from approximating nearest neighbour's queries. In fact, neighbourhood queries are the most computationally demanding step in DBSCAN/HDBSCAN, especially in high-dimensional PCA spaces. Libraries such as FAISS (Johnson et al., 2019) or Annoy (Bernhardsson, 2018) accelerate this process by trading exactness for speed. They provide efficient indexing structures that allow rapid retrieval of candidate neighbours, drastically reducing runtime while maintaining sufficient accuracy for clustering. Further optimization can be made by using spatial indexing structures such as KD-trees or ball trees. These data structures partition the feature space, allowing queries to be resolved in logarithmic rather than linear time. In practice, this reduces computational complexity when clustering large datasets projected into multiple principal components. This technique is especially effective in conjunction with approximation of nearest neighbour methods (Muja & Lowe, 2009). Additionally, for extremely large rasters, clustering can be performed in overlapping tiles rather than on the entire dataset at once. Each tile is clustered independently, and results are later merged to ensure consistency across boundaries. This approach reduces memory load and allows parallel execution, while overlapping ensures that clusters crossing tile boundaries are not artificially fragmented (Vartholomaios, 2025). Finally, on the same family of DBSCAN is the SS-DBSCAN (Stratified Sampling DBSCAN), that uses sampling and parameter optimization to improve scalability. This algorithm functions by stratifying the dataset into representative subsets and performing clustering on reduced samples without losing global structure. Parameter optimization then ensures that ε and the minimum points are tuned to each stratum, improving clustering quality (Monko & Kimura, 2025).

4.3. The geographic context: European FUAs under the lens

4.3.1. Choosing the right FUA system

Cohabscapes adopt the Global Human Settlement Layer (GHSL) Functional Urban Areas (FUA) (EC JRC, 2024a) as a standardized way to delineate commuting zones around urban centres, and its use in the scope of Cohabscapes to discriminate between urban and non-urban areas. FUAs were originally defined for the 2015 commuting epoch, using an automated OECD (Organization for Economic Cooperation and Development) aligned procedure that integrates travel time to urban centres, urban centre size, local population, and country GDP per capita. This approach allows for global comparability without relying on national administrative boundaries or detailed commuting matrices, which are often unavailable outside Europe. While the FUAs themselves remain tied to 2015 commuting conditions, the supporting GHSL ecosystem has been updated in 2024, including the Urban Centre Database (UCDB R2024A, Melchiorri et al., 2024), which is aligned with GHS-SMOD R2023A (EC JRC, 2023a), and refreshed country statistics (R2024A, EC JRC, 2024b). This creates a methodological tension: the functional delineation is temporally static, while the underlying settlement and population layers evolve, requiring careful acknowledgement of the mismatch between commuting and population data epochs.

The GHSL FUA introduces several benefits, by providing a globally consistent and automated classification that enables cross-country comparison, while avoiding the arbitrariness of administrative delineations. It integrates Earth Observation (EO) derived GHSL layers such as UCDB, GHS-POP (EC JRC, 2019), and GHS-BUILT-S (EC JRC, 2023b) with OECD concepts[9], making it suitable for monitoring indexes such as Sustainable Development Goals and international policies frameworks. It also scales to countries lacking detailed commuting data by using modelled proxies,

[9] The OECD concepts behind FUAs are a methodological framework jointly developed by the OECD and the European Commission to define cities and their commuting zones in a consistent way across countries. An urban centre is identified as a contiguous area of high population density (at least 1,500 inhabitants per km²) with a minimum population of 50’000 people. Around these centres, a commuting zone is delineated by including surrounding areas where a significant share of the workforce (typically 15% or more) commutes into the centre. FUAs are thus defined as labour market areas rather than administrative units, and they can be polycentric, meaning multiple centres can form a single commuting zone. These principles ensure that FUAs reflect functional socio-economic integration rather than political boundaries, and GHSL operationalizes them globally by applying Earth Observation data and proxies (travel time, UC size, population, GDP per capita) to approximate commuting flows where detailed national data are not available (OECD, 2012; Dijkstra et al., 2019).

thereby extending coverage beyond OECD-only contest. However, weaknesses remain. The reliance on the 2015 commuting epoch means that FUAs do not capture more recent dynamics such as urban sprawl or shifts in commuting patterns due to remote work (Kurek et al., 2019). Proxy-based delineation can also misrepresent complex polycentric or cross-border labour markets, and many bias in urban centre detection propagates directly into FUA extents and downstream indicators (Schiavina et al., 2019). Additionally, the temporal mismatch between static FUAs and updated GHSL datasets complicates trend analysis and requires explicit normalization. The dimension of FUAs also constrains the data available for analysis. Because FUAs act as spatial containers, only datasets that overlap with their boundaries can be used directly. This excludes peri-urban or exurban areas where commuting flows may extend beyond the FUA borders. Larger FUAs risk averaging out fine-grained heterogeneity, while smaller FUAs may truncate wider functional systems, affecting comparability of data such as densities or land cover or land uses.

Additionally, GHSL FUAs are not the only widely adopted system for European cities. The Urban Atlas (UA) FUAs (EEA, 2021), produced within the Copernicus Land Monitoring Service (CLMS), represent a complementary approach that differs substantially in scope and methodology. Whereas GHSL FUAs are globally defined through an automated procedure that relies on EO data and modelled proxies for commuting zones, UA FUAs are EU-specific operational products tied to Eurostat and OECD harmonization. They serve as containers for high-resolution land-use polygons, enabling detailed analyses of urban morphology, land-use efficiency, and activity patterns. GHSL FUAs provide standardized global coverage but lack intra-urban detail, while UA FUAs offer rich land-use classes within European FUAs, making them highly relevant for local policy and planning but limited in geographic scope. Data lineage also diverges: GHSL FUAs are EO-derived models built on standardized methodologies, whereas UA FUAs integrate administrative and functional decisions together with official statistics, with population figures downscaled to detailed land-use parcels.

It is worth noting that FUAs are not an exclusive of Europe, and beyond these two systems, other FUA frameworks exist, such as the U.S. Metropolitan Statistical Areas (albeit not directly called FUAs, but conceptually very similar) (Office of Management and Budget, 2010) or Japan's Metropolitan Employment Areas (Kanemoto et al., 2006), each system reflecting different priorities, such as local comparability or national specificity.

4.3.2. GHSL FUAs for pan-European Cohabscapes

As discussed in Chapter 3, the choice for GHSL FUA is primarily due the fact that the urban areas are not constrained by administrative boundaries. Unlike anthropocentric subdivisions such as municipalities or counties (or UA FUAs, notably), GHSL FUAs are delineated based on commuting flows and settlement morphology. This functional approach captures the actual spatial footprint of human activity and mobility, which is more relevant for ecological processes such as habitat fragmentation, species dispersal, and urban–rural gradients (Isola et al., 2024). By avoiding administrative bias, FUAs open the possibility of species-generic considerations, enabling analyses that apply across taxa without privileging human governance structures.

The ecological relevance of FUAs lies in their ability to represent the intensity and connectivity of settlements. Urban expansion affects bird migration corridors, insect pollination networks, and mammal dispersal patterns regardless of municipal borders. FUAs therefore provide a consistent spatial framework for studying biodiversity impacts and environmental pressures. Their harmonized global methodology also allows for cross-national comparisons, which are critical for ecological studies that require consistent units of analysis. Similar approaches have been adopted in recent research: Pesaresi et al. (2024) demonstrate how GHSL products integrate EO and census data to support global urban–environmental analysis, while Melchiorri et al. (2022) highlight GHSL's role in SDG monitoring, explicitly linking FUAs to society–environment interactions.

Following through with Cohabscapes methodology, the choice of GHSL FUAs for the EU coverage must comply with the CLMS framework and its data availability, including data from the High-Resolution Suite of products, which is EU-centric. This compliance requirement defines the geographic scope of the research and excludes countries not covered by CLMS datasets, such as Armenia, Azerbaijan, Belarus, Kazakhstan, Russia, and Ukraine. FUAs in these regions cannot be incorporated into analyses requiring CLMS inputs. Additionally, Vatican City is also excluded as an independent unit, since it is fully embedded within Rome's FUA.

With these compliance notes, the sample of the study includes 753 cities across Albania, Andorra, Austria, Belgium, Bosnia and Herzegovina, Bulgaria, Croatia, Cyprus, Czech Republic, Denmark, Estonia, Finland, France, Georgia, Germany, Greece, Hungary, Iceland, Ireland, Italy, Kosovo, Latvia, Liechtenstein, Lithuania, Luxembourg, Malta, Moldova, Monaco, Montenegro, Netherlands, North Macedonia, Norway, Poland, Portugal, Romania, San Marino, Serbia, Slovakia, Slovenia, Spain, Sweden, Switzerland, Turkey, and the United Kingdom. The selected subset of European cities can be seen in Figure 1.

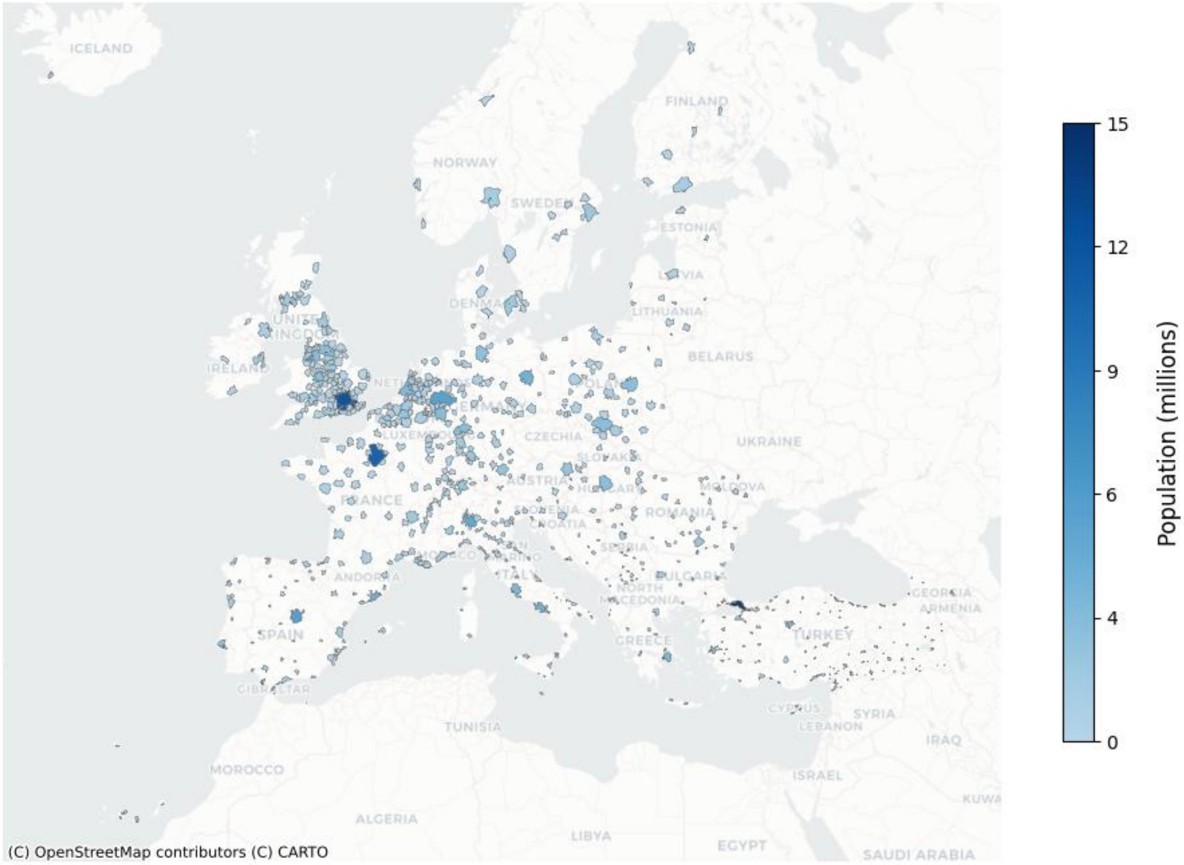

Figure 1. European FUAs, coloured by population count (2015).

This dataset presents several disparities in term of country, population count, area, and FUA/UC differences. These four topics can be unpacked separately and together should form a basis for consideration in building a coherent and comparable pan-European classification system.

The distribution of FUAs across European countries reveals striking disparities in how urban systems are classified (Fig. 2). Countries such as Turkey (123 FUAs), the United Kingdom (91), Italy (79), Germany (70), Spain (66), and France (65) dominate the dataset, while smaller states such as Luxembourg, Malta, Montenegro, and Iceland register only a single FUA. This imbalance reflects not only differences in territorial size and population but also methodological biases inherent in counting FUAs as discrete units.

This trend presents firstly a skew toward countries with numerous FUAs that could introduce distortions when comparing urban systems across Europe, as nations with many FUAs encompass a wide range of climatic zones and regional contexts. For example, Spain's FUAs span Mediterranean, Atlantic, and semi-arid regions, while Turkey's FUAs extend from coastal temperate zones to continental interiors. In contrast, countries with only one or two FUAs, such as Luxembourg or Malta, are represented by a single climatic and regional profile. This creates a disproportionate weight in comparative studies: countries with many FUAs appear more diverse and complex, while smaller states are reduced to singular cases, limiting the analytical depth of cross-national comparisons.

Secondly, the methodology of counting FUAs tends to privilege large, polycentric countries. Germany, Italy, and Spain, with their historically decentralized urban hierarchies, naturally produce dozens of FUAs. Conversely, countries with centralized systems, such as Greece or Bulgaria, appear underrepresented despite the significance of their capital cities. This bias can obscure the role of primate cities in shaping national development, while exaggerating the apparent diversity of polycentric systems. As a result, comparative classifications risk conflating the number of FUAs with the strength or resilience of urban systems.

Beyond climate and regionality, the dataset raises questions about demographic concentration and economic geography, shifting the imbalance on other urban dimensions. Countries with numerous FUAs often exhibit balanced territorial development, with multiple secondary cities supporting national cohesion. In contrast, countries with few FUAs may experience over-concentration of population and resources in a single metropolitan area, leading to spatial inequalities. Furthermore, the classification highlights the tension between statistical representation and lived urban realities: the presence of many FUAs does not necessarily equate to equitable development, nor does the absence of multiple FUAs imply a lack of urban dynamism (Brezzi & Veneri, 2014; OECD 2024).

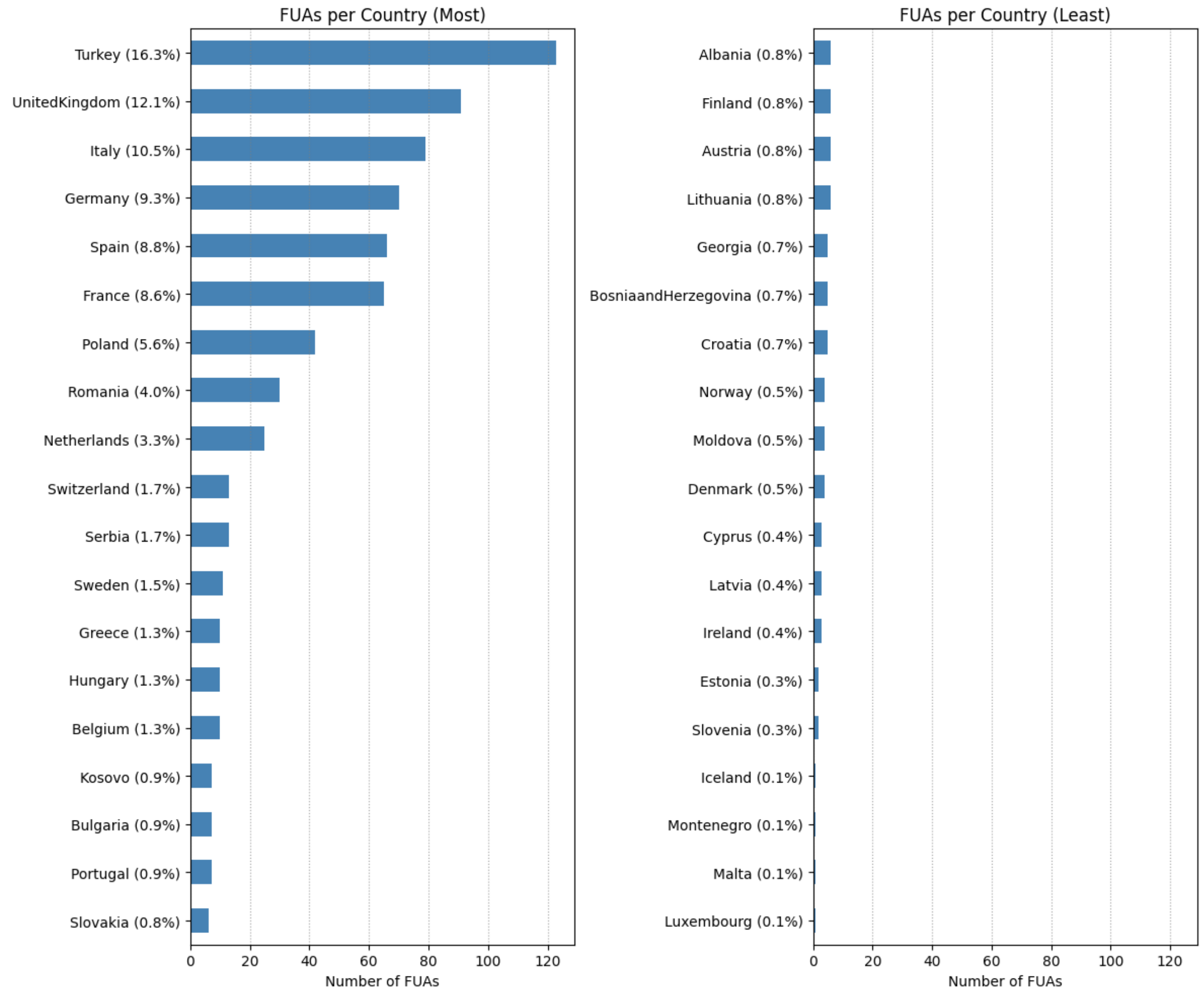

Figure 2. European FUAs, divided and ordered between countries.

Shifting the focus on population and the FUA/UC dualism, the dataset reveals the overwhelming presence of a handful of mega-cities that dominate the European urban landscape. Istanbul, with nearly 14.8 million inhabitants in its FUA, stands as the largest metropolitan region, followed closely by London (12.6 million) and Paris (11.2 million). Other FUAs such as Madrid (6.1 million), Barcelona (4.6 million), Naples (4.0 million), Rome (3.5 million), Manchester (3.2 million), Birmingham (2.9 million), and Ankara (3.3 million) reinforce this pattern of continental giants. Each of these FUAs anchors its national economy and exerts influence far beyond its immediate region.

In contrast to the dominance of single capitals, several countries exhibit polycentric urban systems. Germany is the clearest example, with Berlin (4.3 million), Hamburg (2.6 million), Munich (2.4 million), Frankfurt (3.0 million), Cologne (3.1 million), and Stuttgart (2.2 million) all functioning as major FUAs. Italy follows a similar pattern, with Milan (5.1 million), Rome (3.5 million), Naples (4.0 million), Turin (1.7 million), and Palermo (954,000) forming a distributed hierarchy. Spain also demonstrates polycentricity, with Madrid and Barcelona as primate cities but Valencia, Seville, Bilbao, and Zaragoza acting as strong secondary centres.

The United Kingdom likewise shows a dense network of FUAs: London dominates, but Manchester, Birmingham, Leeds, Glasgow, Liverpool, and Newcastle all exceed one million inhabitants. Turkey, though heavily dominated by Istanbul, also contains multiple FUAs above one million, including Ankara, Izmir, Bursa, and Gaziantep.

Smaller states such as Luxembourg, Malta, Montenegro, and Iceland present a very different picture. Each is represented by a single FUA: Luxembourg City (442,000), Valletta (383,000), Podgorica (135,000), and Reykjavik (209,000). In these contexts, the capital city is essentially synonymous with the national urban system. This primacy reflects limited territorial extent and population size.

Other medium-sized states, such as Albania, Bulgaria, and Greece, also show strong primacy. Tirana, Sofia, and Athens each dwarf their secondary FUAs, concentrating political and economic functions in a single metropolitan region.

The dataset's distinction between FUA population and UC population allows us to examine the balance between core cities and their peripheries (Figure 3).

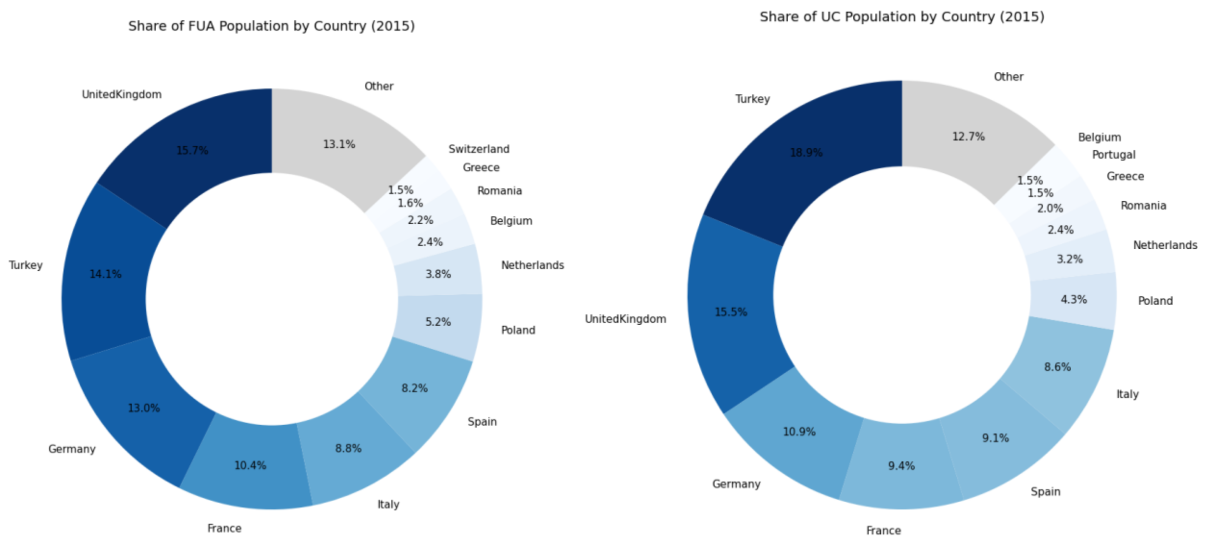

Figure 3. Share of population in the FUA (left) and Urban Centre (right), divided by country.

Going into detail, for many large FUAs suburbanization is extensive. Madrid's FUA population of 6.1 million contrasts with its UC population of 5.0 million, meaning nearly one fifth of its inhabitants live outside the core. Dortmund shows an even starker difference, with 5.8 million in the FUA versus 3.7 million in the UC, a suburban share of almost 40 percent. Naples, Lisbon, and Berlin also demonstrate significant metropolitan spread, with suburban populations accounting for 15–25 percent of the total. By contrast, smaller FUAs often remain compact. Cities such as Trani, Bisceglie, and Andria in Italy, or Liepaja in Latvia and Pejë in Kosovo, have UC populations that account for 90–95 percent of the FUA total. In these cases, the functional region closely matches the city boundary, indicating limited suburban zones and compact urban forms. Paris and London occupy an intermediate position: both have extensive suburban belts, but their UC populations still account for most of the metropolitan total.

Taken together, the dataset highlights a dual model of European urbanization. On one side are the mega-cities with extensive peripheries, where suburban populations account for 15–30 percent of the metropolitan total. On the other side are compact FUAs, where the core city nearly equals the FUA population. Large, polycentric countries dominate the dataset, skewing comparative analysis toward diverse climates and regions. Spain, Italy, Germany, the UK, and Turkey encompass multiple climatic zones and regional identities, while smaller states such as Malta or Luxembourg are represented by a single profile. This creates a classification bias: countries with many FUAs appear more diverse and complex, while smaller states are reduced to singular cases. This distinction is central to understanding the weight of peri-urban areas in the classification. Chapter 3, in fact, showed that between Vienna, Munich, and Genoa, almost 15% of all pixels were obtained from the core urban areas, producing unbalanced clusters that favoured the identification of patterns in the peripheral areas and drowned urban cores.

A similar point can be made regarding area, and its different distribution between FUAs and UC (Fig. 4). Across countries, the overall trend in the FUA/UC ratios shows clear contrasts: Northern and Central European nations often display very high ratios, with FUAs stretching far beyond their dense cores due to dispersed settlement and extensive peri-urban areas, while Mediterranean countries tend to have lower ratios, reflecting more compact urban centres relative to their metropolitan footprints. Large capitals such as London, Paris, Madrid, and Warsaw consistently show FUAs several times larger than their UCs, whereas cities in Italy, Spain, and Turkey frequently present denser cores that occupy a greater share of their total classified area.

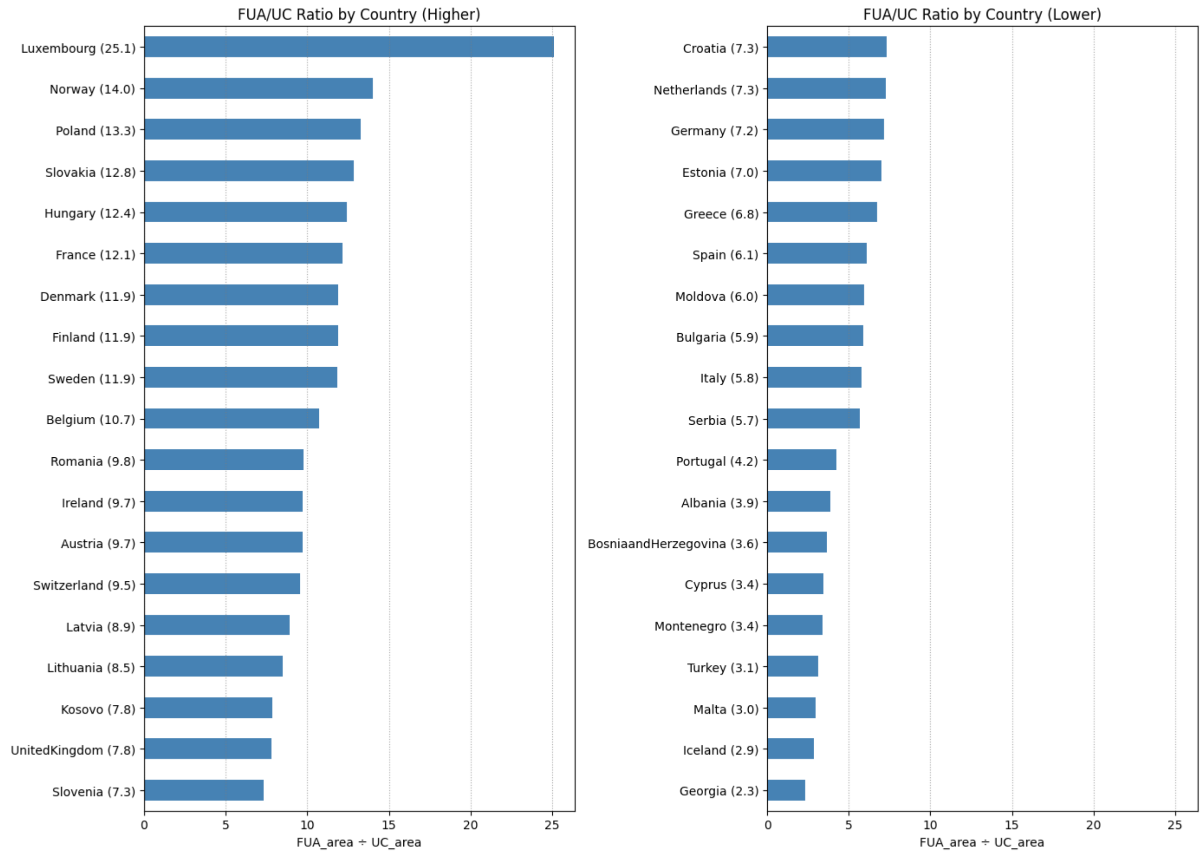

Figure 4. Ratio of area between FUA and UC, divided by countries.

Going into details, some cities show a relatively balanced relationship for FUA/UC ratio. Naples, for example, has a ratio of about 2.4, meaning its dense urban centre makes up a substantial share of the metropolitan footprint. Istanbul is even more compact, with a ratio below 2. These cases reflect cities where the dense core dominates, and peri-urban spread is less pronounced in the classification. By contrast, Oslo presents a striking disparity. Its FUA is over 17 times larger than its UC, which points to a city heavily influenced by dispersed settlement patterns and peri-urban lands. Katowice in Poland shows a similar phenomenon, with a ratio above 8, reflecting a fragmented urban landscape where multiple centres and industrial belts inflate the FUA boundary far beyond the dense UC core. Large capitals such as London, Paris, and Madrid all have FUAs several times larger than their UCs. London's ratio is about 3, Paris around 4, and Madrid above 5. These values highlight how peri-urban belts and commuting zones expand the classified FUA, even though the UC itself is massive. Meanwhile, Berlin and Frankfurt show ratios around 4–6, again pointing to FUAs that extend well beyond the dense UC.

For smaller cities, ratios can swing dramatically depending on how peri-urban pixels are classified. Valletta in Malta, for example, has a relatively small FUA but a UC that makes up a large share, producing a low ratio. Conversely, places like Oslo or Katowice show how the classification can exaggerate the FUA footprint when peri-urban land is abundant. These disparities highlight the spatial bias inherent in pixel-based classification: compact cities appear dense and balanced, while dispersed settlement regions inflate the FUA far beyond the UC. This shows that not only are the ratios not uniform, but the very delineation of UC can deeply influence the proportion of pixels, thus classes, that the system can identify.

4.3.3. Learning from European FUAs diversity to structure the training set

The 753 cities in the study are very different, and as shown by the previous distributions. To build a classification that is representative of European diversity, simply sampling a random number of cities is insufficient. The sampling must learn from this diversity and be designed accordingly. It must be structured from different perspectives: size, population, and regionality, including climatic diversity.

To capture climatic diversity in a systematic way, mean annual air temperature was selected as one of the key metrics. This choice reflects the importance of climate as a structuring factor for urban form, population distribution, and regional differentiation. The methodology for calculating mean annual temperature was based on TerraClimate, a high-resolution global dataset that provides monthly maximum and minimum air temperature fields from 1958 onwards (Abatzoglou et al., 2018). Annual means were derived by averaging across maximum and minimum yearly values, for each year between the last ten available (2015 to 2024). Finally, the multi-year mean annual temperature was calculated by concatenating the annual means across the ten-year period and averaging them, resulting in a single continuous raster representing the period-average Mean Annual Temperature (MAT).

This raster was explicitly tagged with EPSG:4326 and reprojected to the working coordinate reference system to ensure spatial alignment with the FUA geometries. Each FUA polygon was then clipped against the raster, and the mean value of the clipped area was extracted. In cases where no data were available within the bounds of a city polygon, the value was recorded as missing rather than excluded, thereby preserving the integrity of the dataset and allowing reporting of coverage gaps. The cities that were excluded for this reason are: 'Heerlen', 'Ruse', 'Donostia / San Sebastián', 'Elx / Elche', 'Alacant / Alicante', 'Geneva', 'Biel/Bienne', 'Basel', and 'Londonderry/Derry'. Notably, this does not exclude these cities from the classification but leaves them into a separate cluster of cities which does not have explicit information of MAT and thus can be sampled accordingly together with the others.

Alongside mean annual temperature, two additional metrics were selected to characterize urban diversity: the ratio between FUA and UC area, and population density, both calculated from the GHSL FUA dataset. The FUA/UC ratio captures the relative extent of functional urban areas compared to their urban cores, while population density provides a measure of demographic intensity. Population density was log-transformed to account for skewness and to enable more balanced binning.

Together, these three metrics (FUA/UC ratio, log-transformed population density, and mean annual temperature) were used to construct a hierarchical equal-count binning system. Cities were first partitioned into tertiles based on the FUA/UC ratio, then subdivided within each tertile according to population density, and finally further divided by mean annual temperature. This procedure produced a three-dimensional cube of 27 bins, each representing a distinct combination of urban form, demographic intensity, and climatic conditions (Fig. 5). Labels were assigned to each bin to indicate whether a city fell into low, medium, or high ranges for each metric. The resulting classification allowed cities to be visualized in an interactive three-dimensional scatter plot, where each point was positioned according to its values for the three metrics and coloured by its bin assignment.

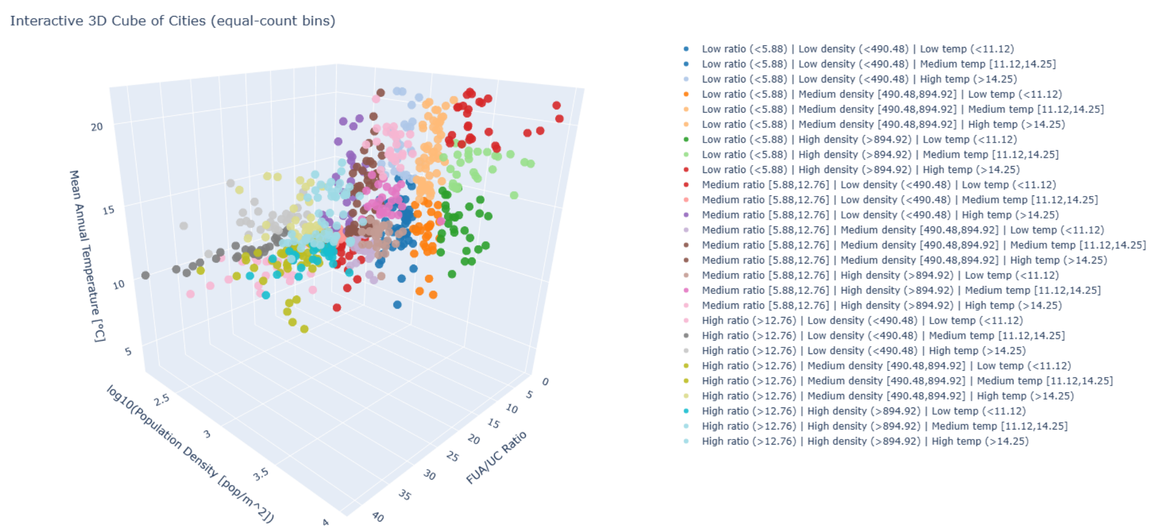

Figure 5. 3D scatter plot of FUAs according to FUA/UC ratios, population density, and MAT.

This leaves the FUA dataset divided into 27 groups of equal count, representing different conditions. Thus, to the standard approach of subdividing the dataset in training and testing subsets can be done in parallel for each group, following the feature-aware splitting method (Liu & Cocea, 2017). Additionally, the mismatched cities without MAT can be added as a separate 28th group.

4.4. Conclusions

This chapter discussed the potential, and the challenges, of the Cohabscapes classification for expanding to all European FUAs. While the strength of a unified species-generic framework has been discussed, both from a theoretical and philosophical perspective and from a methodological and computational side, there is still space for testing and verifying that the process is scalable and capable of achieving the result. Particularly, several observations can be made.

i. Conceptually, at its foundation Cohabscapes adopts a species-generic approach, deliberately excluding abundance or diversity metrics to avoid privileging particular taxa. This neutrality is not only a technical choice but also a philosophical position: it resists anthropocentrism and species-centrism, opening urban design to multiple ecological narratives. Yet neutrality is never absolute. The framework is haunted by prior imaginaries and ecological legacies, which shape how cities are understood. Nonetheless the tension is productive, since it allows Cohabscapes to function as a scaffold for multi-species futures while acknowledging the cultural and ecological pasts embedded in urban form.

ii. The classification is organized into three complementary dimensions, with urban fabric, anthropic imprint, and biophysical conditions, each with different proximities to human agency. Expanding from two scales (local and landscape) to three (adding regional) strengthens the framework's ability to capture both fine-grained urban detail and macro-regional differences. This multiscale design should help the framework differentiate cities not only by morphology but also by socioeconomic and climatic context, making continental comparability more effective.

iii. Scaling Cohabscapes requires efficient yet sensible computation. PCA/KPCA pipelines reduce complexity while preserving comparability across cities, enabling continental datasets to be processed consistently. Alternative clustering methods were critically assessed: while K-Means remains efficient, density-based approaches such as DBSCAN and HDBSCAN offer greater robustness for irregular urban morphologies and heterogeneous densities. Embedding spatial association and adopting parallelization strategies (such as with using dedicated HPC architectures) further enhance scalability, ensuring that continental processing is technically achievable without sacrificing methodological coherence.

iv. The choice of GHSL FUAs provides a globally harmonized, non-administrative framework aligned with OECD and EU monitoring needs. FUAs capture functional urban regions relevant for ecological processes, but disparities in their distribution, population concentration, and FUA/UC ratios introduce biases. Large polycentric countries dominate the dataset, while smaller states are reduced to singular cases. Mega-cities with extensive peripheries skew classification toward suburban pixels, whereas compact cities emphasize dense cores. This balance must be addressed, and a structured sampling strategy based on different metrics (FUA/UC ratio, population density, and MAT) partitioning the dataset into 27 representative bins should improve the training accuracy by reflecting Europe's climatic and morphological diversity.

Taken together, these reflections clarify that Cohabscapes is more than a technical classification. It is a conceptual and infrastructural project: a species-agnostic, multiscale, and computationally robust system that can harmonize ecological knowledge across Europe. Its impact lies in providing cities with a shared language to describe their habitats, enabling cross-city comparisons, and supporting planners and ecologists in designing interventions that are both locally grounded and continentally coherent. By embedding biodiversity into standardized spatial units and computationally scalable workflows, Cohabscapes positions itself as a European infrastructure for ecological and planning collaboration.

As of the writing of the thesis, variables concerning the Local Urban Fabric have been computed, following the protocols discussed in Chapter 3, and are ready to be pre-processed and clustered to stress-test the methodology over a single sub-classification. Further analysis would present weaknesses and instruct on how to adjust the path forward to achieving a pan-European Cohabscapes classification system. Yet the pathway is clear, as the Cohabscapes framework can evolve from a localized methodological experiment into a continental scaffold for multi-species urban futures, where biodiversity and liveability are understood as shared responsibilities across cities and nations.

4.5. References

Abatzoglou, J. T., S. Z. Dobrowski, S. A. Parks, and K. C. Hegewisch, (2018). TerraClimate, a high-resolution global dataset of monthly climate and climatic water balance from 1958–2015. Scientific Data, 5, https://doi.org/10.1038/sdata.2017.191.

Anselin, L., & Rey, S. J. (2014). *Modern spatial econometrics in practice: A guide to GeoDa, GeoDaSpace and PySAL*. GeoDa Press. Retrieved from https://sergerey.org/giasp16/pdfs/anselin_rey_weights.pdf

Baligodugula, V. V., & Amsaad, F. (2025). *Unsupervised learning: Comparative analysis of clustering techniques on high-dimensional data* (arXiv:2503.23215v1 [cs.LG]). arXiv. https://arxiv.org/abs/2503.23215

Bennett, J. (2010). Vibrant matter: A political ecology of things. Duke University Press. https://doi.org/10.1215/9780822391623

Bernhardsson, E. (2018). *Annoy: Approximate nearest neighbors in C++/Python*. GitHub repository. https://github.com/spotify/annoy

Brezzi, M., & Veneri, P. (2014). *Assessing polycentric urban systems in the OECD: Country, regional and metropolitan perspectives*. OECD Publishing. https://doi.org/10.1787/5jz5mpdkmvnr-en

Campello, R. J. G. B., Moulavi, D., & Sander, J. (2013). Density-based clustering based on hierarchical density estimates. *Advances in Knowledge Discovery and Data Mining (PAKDD)*, 160–172. https://doi.org/10.1007/978-3-642-37456-2_14

Campello, R. J. G. B., Moulavi, D., & Sander, J. (2013). Density-based clustering based on hierarchical density estimates. *Pacific-Asia Conference on Knowledge Discovery and Data Mining (PAKDD)*, 160–172. https://doi.org/10.1007/978-3-642-37456-2_14

Canepa, M., Mosca, F., Barath, S., Changenet, A., Hauck, T. E., Ludwig, F., Roccotiello, E., Pianta, M., Uthaya Selvan, S., Vogler, V., & Perini, K. (2022). Ecolopes, beyond greening: A multi-species approach for urban design. Agathón | International Journal of Architecture, Art and Design, 11, 238–245. https://doi.org/10.19229/2464-9309/11212022

Caron, M., Bojanowski, P., Joulin, A., & Douze, M. (2018). Deep clustering for unsupervised learning of visual features. In V. Ferrari, M. Hebert, C. Sminchisescu, & Y. Weiss (Eds.), *Computer Vision – ECCV 2018* (pp. 132–149). Springer. https://doi.org/10.1007/978-3-030-01264-9_9

Cesario, E., Lindia, P., & Vinci, A. (2023). Detecting multi-density urban hotspots in a smart city: Approaches, challenges and applications. Big Data and Cognitive Computing, 7(1), 29. https://doi.org/10.3390/bdcc7010029"

Chowdhury, S., Dubey, V. K., Choudhury, S., Das, A., Jeengar, D., Sujatha, B., Kumar, A., Kumar, N., & Semwal, A. (2023). *Insects as bioindicator: A hidden gem for environmental monitoring*. *Frontiers in Environmental Science, 11*, 1146052. https://doi.org/10.3389/fenvs.2023.1146052

Corboz, A. (1983). The land as palimpsest. Diogenes, 31(121), 12–34. https://doi.org/10.1177/039219218303112102

Davis, C. (2005). Hauntology, spectres and phantoms. *French Studies, 59*(3), 373–379. https://doi.org/10.1093/fs/kni143

Derrida, J. (1994). Specters of Marx: The state of the debt, the work of mourning, and the new international (P. Kamuf, Trans.). New York: Routledge.

Dijkstra, L., Poelman, H., & Veneri, P. (2019). The EU-OECD definition of a functional urban area. OECD Regional Development Working Papers, 2019/11. OECD Publishing. https://doi.org/10.1787/d58cb34d-en

Edensor, T. (2005). Industrial ruins: Space, aesthetics and materiality. Berg.

Ester, M., Kriegel, H.-P., Sander, J., & Xu, X. (1996). A density-based algorithm for discovering clusters in large spatial databases with noise. *Proceedings of the Second International Conference on Knowledge Discovery and Data Mining (KDD)*, 226–231. https://dl.acm.org/doi/10.5555/3001460.3001507

European Commission, Joint Research Centre. (2019). *GHS-POP R2019A – Global Human Settlement Population Grid*. European Commission. https://human-settlement.emergency.copernicus.eu/ghs_pop2019.php

European Commission, Joint Research Centre. (2023b). *GHS-BUILT-S R2023A – Global built-up surface grid, 1975–2030*. European Commission. https://human-settlement.emergency.copernicus.eu/ghs_buS2023.php

European Commission, Joint Research Centre. (2023b). *GHS-SMOD R2023A – Degree of Urbanisation classification, 1975–2030*. European Commission. https://human-settlement.emergency.copernicus.eu/ghs_smod2023.php

European Commission, Joint Research Centre. (2024a). *GHS-FUA R2024A: Global Human Settlement – Functional Urban Areas dataset*. European Union, JRC Data Catalogue. Retrieved from https://data.jrc.ec.europa.eu/collection/ghsl

European Commission, Joint Research Centre. (2024b). *Global Human Settlement Layer – Settlement Model Layer (GHS-SMOD R2024A)*. European Commission. https://human-settlement.emergency.copernicus.eu/datasets.php

European Environment Agency. (2021). *Urban Atlas Land Cover/Land Use 2018 (vector), Europe, 6-yearly*. Copernicus Land Monitoring Service (CLMS). https://land.copernicus.eu/en/products/urban-atlas/urban-atlas-2018

European Space Agency. (2021). *ESA WorldCover 10 m 2021 v200* [Data set]. European Space Agency. https://esa-worldcover.org/en/data-access

Fang, C., Zhou, L., Gu, X., Liu, X., & Werner, M. (2025). A data-driven approach to urban area delineation using multi-source geospatial data. Scientific Reports, 15, 93366. https://doi.org/10.1038/s41598-025-93366-x

Fauvel, M., Tarabalka, Y., Benediktsson, J. A., Chanussot, J., & Tilton, J. C. (2013). Advances in spectral-spatial classification of hyperspectral images. *Proceedings of the IEEE*, *101*(3), 652–675. https://doi.org/10.1109/JPROC.2012.2197589

Florczyk, A. J., Corbane, C., Ehrlich, D., Freire, S., Kemper, T., Maffenini, L., Melchiorri, M., Pesaresi, M., Politis, P., Schiavina, M., Sabo, S., & Zanchetta, L. (2019). GHSL Data Package 2019. *Publications Office of the European Union.* https://doi.org/10.2760/290498

Forman, R. T. T. (2014). *Urban ecology: Science of cities.* Cambridge University Press. https://doi.org/10.1017/CBO9781139030472

Fowlkes, C., Belongie, S., Chung, F., & Malik, J. (2004). Spectral grouping using the Nyström method. IEEE Transactions on Pattern Analysis and Machine Intelligence, 26(2), 214–225. https://doi.org/10.1109/TPAMI.2004.1262185

Fuller, R. A., & Irvine, K. N. (2012). Interactions between people and nature in urban environments. In K. J. Gaston (Ed.), *Urban ecology* (pp. 134–171). Cambridge University Press. https://doi.org/10.1017/CBO9780511778483.008

Grimm, N. B., Faeth, S. H., Golubiewski, N. E., Redman, C. L., Wu, J., Bai, X., & Briggs, J. M. (2008). Global change and the ecology of cities. *Science, 319*(5864), 756–760. https://doi.org/10.1126/science.1150195

Liu, H. & Cocea, M. (2017). Semi-random partitioning of data into training and test sets in granular computing context. *Granular Computing*, 2, 357–386. https://doi.org/10.1007/s41066-017-0049-2

Heymans, A., Breadsell, J., Morrison, G. M., Byrne, J. J., & Eon, C. (2019). Ecological urban planning and design: A systematic literature review. *Sustainability*, *11*(13), 3723. https://doi.org/10.3390/su11133723

Hillebrand, H., Blasius, B., Borer, E. T., Chase, J. M., Downing, J. A., Eriksson, B. K., … & Ryabov, A. B. (2018). Biodiversity change is uncoupled from species richness trends: Consequences for conservation and monitoring. *Journal of Applied Ecology*, *55*(1), 169–184. https://doi.org/10.1111/1365-2664.12959

Huyssen, A. (2003). Present pasts: Urban palimpsests and the politics of memory. Stanford University Press.

Intergovernmental Panel on Climate Change (IPCC) (2023). Climate Change 2023: Synthesis Report. Contribution of Working Groups I, II and III to the

Sixth Assessment Report of the Intergovernmental Panel on Climate Change [Core Writing Team, H. Lee, & J. Romero (Eds.)]. IPCC. https://doi.org/10.59327/IPCC/AR6-9789291691647

Isola, F., Lai, S., Leone, F., & Zoppi, C. (2024). Urban green infrastructure and ecosystem service supply: A study concerning the functional urban area of Cagliari, Italy. Sustainability, 16(19), 8628. https://doi.org/10.3390/su16198628

Jiang, Z., Zheng, Y., Tan, H., Tang, B., & Zhou, H. (2017). *Variational deep embedding: An unsupervised and generative approach to clustering* (arXiv:1611.05148). arXiv. https://doi.org/10.48550/arXiv.1611.05148

Jiang, Z., Zheng, Y., Tan, H., Tang, B., & Zhou, H. (2017). Variational deep embedding: An unsupervised and generative approach to clustering. *Proceedings of the 26th International Joint Conference on Artificial Intelligence (IJCAI 2017)*, 1965–1972. https://doi.org/10.24963/ijcai.2017/273

Johnson, J., Douze, M., & Jégou, H. (2019). *Billion-scale similarity search with GPUs*. *IEEE Transactions on Big Data, 7*(3), 535–547. https://doi.org/10.1109/TBDATA.2019.2921572

Jolliffe, I. T., & Cadima, J. (2016). Principal component analysis: A review and recent developments. *Philosophical Transactions of the Royal Society A: Mathematical, Physical and Engineering Sciences, 374*(2065), 20150202. https://doi.org/10.1098/rsta.2015.0202

Kanemoto, Y., Tokuoka, K., & Kurima, R. (2006). *Metropolitan Employment Areas (MEA) dataset based on the 2010 Population Census of Japan*. Research Institute of Economy, Trade and Industry (RIETI). Retrieved from https://www.arcgis.com/home/item.html?id=9c0d06ca8bea4356aa6def459fa438d0

Kurek, S., Wójtowicz, M., & Gałka, J. (2019). Functional urban areas: Theoretical background. In *Functional Urban Areas in Poland* (pp. 11–31). Springer. https://doi.org/10.1007/978-3-030-31527-6_2

Lown, J. (2025). Spectres of gentrification: Towards a hauntological framework for exploring the impacts of gentrification. *Urban Studies, 62*(11). https://doi.org/10.1177/00420980241306087

Mace, G. M., Barrett, M., Burgess, N. D., Cornell, S. E., Freeman, R., Grooten, M., & Purvis, A. (2018). Aiming higher to bend the curve of biodiversity loss. *Nature Sustainability, 1*(9), 448–451. https://doi.org/10.1038/s41893-018-0130-0

MacQueen, J. (1967). Some methods for classification and analysis of multivariate observations. In L. M. Le Cam & J. Neyman (Eds.), Proceedings of the Fifth Berkeley Symposium on Mathematical Statistics and Probability (Vol. 1, pp. 281–297). University of California Press. https://projecteuclid.org/euclid.bsmsp/1200512992

Malzer, C., & Baum, M. (2021). *A hybrid approach to hierarchical density-based cluster selection*. *arXiv preprint arXiv:1911.02282*. https://arxiv.org/abs/1911.02282

Mathers, K. L., Robinson, C. T., Hill, M., Kowarik, C., Heino, J., Deacon, C., & Weber, C. (2024). How effective are ecological metrics in supporting conservation and management in degraded streams? *Biodiversity and Conservation, 33*(18), 3981–4002. https://doi.org/10.1007/s10531-024-02933-7

McInnes, L., Healy, J., & Astels, S. (2017). hdbscan: Hierarchical density based clustering. *Journal of Open Source Software, 2*(11), 205. https://doi.org/10.21105/joss.00205

McInnes, L., Healy, J., & Melville, J. (2018). *UMAP: Uniform manifold approximation and projection for dimension reduction* (arXiv:1802.03426). arXiv. https://doi.org/10.48550/arXiv.1802.03426

McInnes, L., Healy, J., & Melville, J. (2018). UMAP: Uniform Manifold Approximation and Projection for dimension reduction. *arXiv preprint arXiv:1802.03426*. https://arxiv.org/abs/1802.03426

Melchiorri, M., et al. (2022). The global human settlement layer sets a new standard for global urban data reporting with the urban centre database. Frontiers in Environmental Science, 10, 1003862. https://doi.org/10.3389/fenvs.2022.1003862

Melchiorri, M., Mari Rivero, I., Florio, P., Schiavina, M., Krasnodebska, K., Politis, P., Uhl, J., Pesaresi, M., Maffenini, L., Sulis, P., Crippa, M., Guizzardi, D., Pisoni, E., Belis, C., Oom, D., Branco, A., Mwaniki, D., Githira, D., Kochulem, E., Tommasi, P., Carioli, A., Ehrlich, D., Kemper, T., & Dijkstra, L. (2024). *Stats in the City – the GHSL Urban Centre*

Database 2025 (GHS-UCDB R2024A). Publications Office of the European Union. https://publications.jrc.ec.europa.eu/repository/handle/JRC139768

Monko, G., & Kimura, M. (2025). Enhanced stratified sampling–density-based spatial clustering of applications with noise (SS-DBSCAN) for high-dimensional data. *Data Science, 8*(2), 1–19. https://doi.org/10.1177/24518492251349080

Muja, M., & Lowe, D. G. (2009). Fast approximate nearest neighbors with automatic algorithm configuration. In Proceedings of the International Conference on Computer Vision Theory and Applications (VISAPP'09) (pp. 331–340). INSTICC Press. Retrieved from https://www.cs.ubc.ca/~lowe/papers/09muja.pdf

Murtagh, F., & Contreras, P. (2012). Algorithms for hierarchical clustering: An overview. *Wiley Interdisciplinary Reviews: Data Mining and Knowledge Discovery*, *2*(1), 86–97. https://doi.org/10.1002/widm.53

Murtagh, F., & Contreras, P. (2017). Algorithms for hierarchical clustering: An updated review. *Wiley Interdisciplinary Reviews: Data Mining and Knowledge Discovery*, *7*(6), e1219. https://doi.org/10.1002/widm.1219

Ng, A. Y., Jordan, M. I., & Weiss, Y. (2002). On spectral clustering: Analysis and an algorithm. *Advances in Neural Information Processing Systems (NeurIPS)*, 14, 849–856.

Nolet, C., & Gala, D. (2021). *GPU-accelerated hierarchical DBSCAN with RAPIDS cuML – Let's get back to the future*. NVIDIA Technical Blog. https://developer.nvidia.com/blog/gpu-accelerated-hierarchical-dbscan-with-rapids-cuml-lets-get-back-to-the-future

OECD. (2012). Redefining "urban": A new way to measure metropolitan areas. OECD Publishing. https://doi.org/10.1787/9789264174108-en

OECD. (2024). *OECD regions and cities at a glance 2024*. OECD Publishing. https://doi.org/10.1787/f42db3bf-en

Office of Management and Budget. (2010). *Standards for defining metropolitan and micropolitan statistical areas*. Federal Register, 75(123), 37246–37252. https://doi.org/10.1037/e648842012-001

Pearson, R. G., & Dawson, T. P. (2003). Predicting the impacts of climate change on the distribution of species: Are bioclimate envelope models useful? *Global Ecology and Biogeography, 12*(5), 361–371. https://doi.org/10.1046/j.1466-822X.2003.00042.x

Pedersen Zari, M., Connolly, P., & Southcombe, M. (Eds.). (2020). *Ecologies Design: Transforming Architecture, Landscape, and Urbanism.* Routledge. https://doi.org/10.4324/9780429279904

Peres-Neto, P. R., Jackson, D. A., & Somers, K. M. (2005). How many principal components? Stopping rules for determining the number of non-trivial axes revisited. *Computational Statistics & Data Analysis, 49*(4), 974–997. https://doi.org/10.1016/j.csda.2004.06.015

Pesaresi, M., et al. (2024). Advances on the Global Human Settlement Layer by joint assessment of Earth Observation and population survey data. International Journal of Digital Earth, 17(1). https://doi.org/10.1080/17538947.2024.2390454

Pickett, S. T. A., Cadenasso, M. L., & McGrath, B. (2013). *Resilience in ecology and urban design: Linking theory and practice for sustainable cities.* Springer. https://doi.org/10.1007/978-94-007-5341-9

Rocklin, M. (2015). *Dask: Parallel computation with blocked algorithms and task scheduling*. In *Proceedings of the 14th Python in Science Conference* (pp. 130–136). https://doi.org/10.25080/Majora-7b98e3ed-013

Ross, D. A., Lim, J., Lin, R. S., & Yang, M. H. (2008). Incremental learning for robust visual tracking. *International Journal of Computer Vision, 77*(1–3), 125–141. https://doi.org/10.1007/s11263-007-0075-7

Schiavina M., Freire S., Carioli A., MacManus K. (2023). GHS-POP R2023A - GHS population grid multitemporal (1975-2030).European Commission, Joint Research Centre (JRC) [Dataset]. https://doi.org/10.2905/2FF68A52-5B5B-4A22-8F40-C41DA8332CFE

Schiavina, M., Moreno-Monroy, A., Maffenini, L., & Veneri, P. (2019). *GHSL-OECD Functional Urban Areas: Public release of GHS-FUA R2019A* (EUR 30001 EN). Publications Office of the European Union. https://ghsl.jrc.ec.europa.eu/documents/GHSL_FUA_2019.pdf

Schölkopf, B., Smola, A., & Müller, K.-R. (1998). Nonlinear component analysis as a kernel eigenvalue problem. *Neural Computation, 10*(5), 1299–1319. https://doi.org/10.1162/089976698300017467

Schubert, E., Sander, J., Ester, M., Kriegel, H.-P., & Xu, X. (2017). DBSCAN revisited, revisited: Why and how you should (still) use DBSCAN. *ACM Transactions on Database Systems, 42*(3), 19. https://doi.org/10.1145/3068335

Shackleton, C. M., & Gwedla, N. (2021). The legacy effects of colonial and apartheid imprints on urban greening in South Africa: Spaces, species, and suitability. *Frontiers in Ecology and Evolution, 8,* 579813. https://doi.org/10.3389/fevo.2020.579813

Steinley, D. (2010). K-means clustering: A half-century synthesis. *British Journal of Mathematical and Statistical Psychology, 59*(1), 1–34. https://doi.org/10.1348/000711005X48266

Sterling, C. (2022). Becoming hauntologists: A new model for critical-creative heritage practice. *Heritage & Society, 14*(1), 67–86. https://doi.org/10.1080/2159032X.2021.2016049

Tu, X., Fu, C., Huang, A., Chen, H., & Ding, X. (2022). DBSCAN spatial clustering analysis of urban "production–living–ecological" space based on POI data: A case study of central urban Wuhan, China. International Journal of Environmental Research and Public Health, 19(9), 5153. https://doi.org/10.3390/ijerph19095153

Vartholomaios, A. (2025). Detection and clustering of urban form types with machine learning: Insights into Thessaloniki's urban planning and evolution. *Computational Urban Science, 5*(51). https://doi.org/10.1007/s43762-025-00206-9

Velarde Martínez, A. (2022). *Parallelization of array method with hybrid programming: OpenMP and MPI. Applied Sciences, 12*(15), 7706. https://doi.org/10.3390/app12157706

Vitousek, P. M., Mooney, H. A., Lubchenco, J., & Melillo, J. M. (1997). Human domination of Earth's ecosystems. *Science, 277*(5325), 494–499. https://doi.org/10.1126/science.277.5325.494

Xiao, T., Wan, Y., Jin, R., Qin, J., & Wu, T. (2022). Integrating Gaussian mixture dual-clustering and DBSCAN for exploring heterogeneous characteristics of urban spatial agglomeration areas. *Remote Sensing, 14*(22), 5689. https://doi.org/10.3390/rs14225689

Xie, J., Girshick, R., & Farhadi, A. (2016). *Unsupervised deep embedding for clustering analysis*. In M. F. Balcan & K. Q. Weinberger (Eds.), *Proceedings of the 33rd International Conference on Machine Learning (ICML)* (Vol. 48, pp. 478–487). PMLR. https://proceedings.mlr.press/v48/xieb16.html

Xie, J., Girshick, R., & Farhadi, A. (2016). Unsupervised deep embedding for clustering analysis. *Proceedings of the 33rd International Conference on Machine Learning (ICML 2016)*, 478–487. PMLR. Retrieved from https://proceedings.mlr.press/v48/xieb16.html

Yang, Z., Algesheimer, R., & Tessone, C. J. (2016). A comparative analysis of community detection algorithms on artificial networks. *Scientific Reports, 6*, 30750. https://doi.org/10.1038/srep30750

Zeller, K. A., Compton, B. W., Finn, S. P., & Palm, E. C. (2024). Measuring ecological connectivity with ecological distance and dynamic resistant kernels. *Landscape Ecology, 39,* Article 95. https://doi.org/10.1007/s10980-024-01890-4

Zhao, F., Rekik, I., Lee, S.-W., Liu, J., Zhang, J., & Shen, D. (2019). Two-phase incremental kernel PCA for learning massive or online datasets. *Complexity, 2019,* Article 5937274. https://doi.org/10.1155/2019/5937274

PART 3.

Urban environment and overheating

Chapter 5.

Mitigating urban heat risk to improve urban liveability: a site-selection methodology for determining optimal sites for intervention

Abstract

Urban heat risk arises from the interaction between urban form (morphology, density) and function (land use, sociodemographic vulnerability), yet most assessment methods use spatial units that do not match how architects and planners perceive and change urban space. This reduces their value for design practice, which operates at the scale of plots and blocks that capture spatial form but often miss functional factors crucial to heat vulnerability.

To overcome this challenge, the Chapter present a quantitative method that combines form and function to aid site selection. It uses a multicriteria ranking built on over fifty variables representing exposure, vulnerability, and hazard, and a site-characterization step that groups areas with similar spatially lagged form- and function-related features. The workflow merges morphogenetic spatial modules, objective MCDM weighting, and clustering, and is tested in Genoa and Turin to assess how different spatial units, algorithms, and weighting choices affect outcomes. The method improves fine-scale assessment and supports comparison across varied urban contexts for planning and design. The chapter achieves several outcomes:

i. Improved accuracy in SUHI risk detection through the integration of morphological spatial modules, with Enclosed Tessellation coupled with TOPSIS emerging as particularly effective.

ii. Strengthening usability for both researchers and practitioners, since results are directly linked to urban form structure and activity-based urban functions, making them actionable for decision-making and design.

iii. The development of a transferable and adaptable framework, showing potential for application in diverse urban contexts beyond the case studies.

iv. Evidence of strong within-city insights, where the methodology successfully identifies priority areas for intervention in the case study cities.

Although cross-city comparability proved limited (only 4% of high-risk areas shared comparable features), this finding underscores the importance of tailoring mitigation strategies to local conditions rather than relying on generic solutions.

Keywords

Data-driven urban planning; surface urban heat island; morphometrics; spatial analysis;

remote sensing; multicriteria risk assessment.

Acknowledgements

The author expresses sincere thanks to Luca Cenci, Filippo Fraschini, and Luca Pulvirenti from CIMA Foundation, Savona, for their attentive and caring support.

The author extends gratitude to the consortium of the URBAN GENERATION project (https://ecosystemics.eu/research/projects/urban-generation/) for their valuable and insightful collaboration.

The author acknowledges and gratefully thanks Martin Fleischmann for the support and the use of the Neatnet package (https://github.com/uscuni/neatnet) during the alpha stage of development.

This Chapter has been prepared using European Union's Copernicus Land Monitoring Service information. The DOI links are in the References section.

Preliminary results of this Chapter were consolidated in a research paper (*City, Territory, Architecture, Elsevier,* currently under review).

5.1. Introduction

5.1.1. The PRIN URBAN GENERATION project

The PRIN URBAN GENERATION project (2023–2025) investigates adaptive and mitigative design strategies for climate-resilient urban environments. Framed within the broader discourse on metropolitan vulnerability and ecological transition, the research addresses the dual role of cities as both primary emitters of greenhouse gases and loci of climate-related risk. Through a multi-scalar, design-oriented methodology, the project explores how spatial configurations, nature-based solutions (NBS), can reduce anthropogenic pressures (particularly those linked to urban heat mitigation) while enhancing ecosystem health and social liveability. The initiative is grounded in Italian urban contexts and contributes to the operationalization of global frameworks such as the SDGs (United Nations, 2015) and the EU Green Deal (European Commission, 2019).

5.1.2. Urban Heat Island and Nature-Based strategies for mitigation

Urban heat is an urgent problem for cities, as rising temperatures from climate change increase the frequency and intensity of extreme heat events (Santamouris, 2022). A major part of this issue is the Surface Urban Heat Island (SUHI) effect, which describes the temperature gap between urban areas and nearby rural zones. SUHI arises from the interplay of land cover, the built environment, and human activities (IPCC, 2022), creating uneven thermal patterns that strain public health, energy systems, and urban infrastructure (Zhao et al., 2021; Mora et al., 2017). This has driven demand for analytical tools that can pinpoint where heat risk concentrates and how it connects to the city's physical and functional characteristics (Melis et al., 2023).

5.1.2.1. The spatiality of urban heat: comparing methodologies and patterns

Capturing patterns from SUHI is challenging. SUHI depends on a city's physical form, including building density, vegetation cover, elevation, and street layout, as well as social factors like demographic vulnerability and exposure (Gao et al., 2022). Because of this mix, heat risk is inherently multidimensional, shaped by both formal (morphological) and functional (activity-based) drivers of urban climate (You et al., 2023). The problem is especially pronounced in dense or topographically varied cities, where thermal differences occur at fine spatial scales that matter for planning and design (Mansouri & Zarghami, 2025). As cities pursue interventions such as NBS, shading, or microclimate improvements, there is a growing need for spatial heat representations that are actionable at neighbourhood, block, and site scales (Mosca et al., 2024). For planners and designers, these representations must combine formal and functional attributes to reflect how design practice shapes urban space (Kang et al., 2022).

5.1.2.2. Limitations of current approaches

Remote sensing has been central to SUHI research. Satellite-derived Land Surface Temperature (LST) from missions like Landsat 8/9 and Sentinel-3 has allowed systematic mapping of urban thermal patterns (Stewart, 2024). These datasets are widely used to locate hotspots and study links between thermal behaviour, land cover, and morphology (Kim & Brown, 2021; Sidiqui et al., 2022; Assaf & Assaad, 2024). Yet, the typical use of LST often creates a mismatch with the spatial scales and categories used in planning and design. Classification systems such as Local Climate Zones (LCZs) provide a shared vocabulary for connecting morphology and climate, but their broad typologies often miss the microscale variability that drives thermal behaviour in complex urban areas (Stewart, 2024). Consequently, while remote sensing is essential for understanding thermal patterns, its outputs do not always align with the spatial logic planners and designers use to interpret, regulate, and change urban space.

A major source of this misalignment is the spatial units used in SUHI studies. Many analyses use administrative or statistical units or census blocks (Ascencio et al., 2023; Assaf & Assaad, 2024), street networks (Chen et al., 2022; Liu et al., 2024), or districts (Sidiqui et al., 2022) because they ease demographic integration and policy reporting. However, these units were not created to represent the built environment. Their boundaries often cut across coherent morphological structures, mixing building types, densities, and land uses in ways that hide the links between form and thermal behaviour (Chen et al., 2023). This problem is worsened by the Modifiable Areal Unit Problem (MAUP), which can change correlations, rankings, and hotspot detection depending on how data are aggregated (Chen et al., 2023). In practice, this means that identified "high risk areas" may reflect the geometry of the chosen units rather than true thermal conditions. As a result, many SUHI assessments are hard to translate into design-relevant insights, especially when planners and architects work at scales different from those used in the analysis (Keith et al., 2023).

An urban morphological perspective can help address these limits. Morphometric and morphogenetic methods create spatial modules based on the city's internal structure by capturing configurational features like barriers and connectivity and linking them to functional and environmental data (Dibble et al., 2019; Wang et al., 2023; Arribas-Bel & Fleischmann, 2022). By basing analysis on morphology instead of administrative boundaries, these approaches align thermal assessment with the spatial frameworks that guide design practice and territorial governance (Chen et al., 2023).

Heat risk assessment is multidimensional and can be broken down into hazards, exposure, and vulnerability, which interact across variables that differ in scale, behaviour, and epistemic status. Multicriteria Decision-Making (MCDM) methods offer a structured way to combine such diverse data, producing objective and reproducible rankings (Rahman & Pekkat, 2024). Their flexibility has made them common in environmental risk assessment and climate adaptation planning (Reyes-Norambuena et al., 2024). Still, MCDM results are sensitive to methodological choices. For example, weighting schemes can be subjective, algorithmic approaches may yield different outcomes, and the effect of spatial units on rankings is seldom tested (Qi et al., 2023). These concerns are especially important for site selection, where methodological artifacts can be mistaken for real territorial conditions.

Taken together, these points highlight three persistent gaps. First, SUHI studies often use spatial units that do not match how planners and designers organize or change urban space, reducing the usefulness of results (Chen et al., 2023; Keith et al., 2023). Second, formal and functional drivers of heat are often studied separately, preventing a relational view of how thermal risk arises from their interaction (Gao et al., 2022; Dibble et al., 2019; Wang et al., 2023). Third, methodological choices in MCDM workflows, such as with spatial units, weighting schemes, algorithmic logic, rarely undergo sensitivity analysis, making it hard to tell robust territorial patterns apart from analytical artifacts (Rahman & Pekkat, 2024; Reyes Norambuena et al., 2024; Qi et al., 2023).

5.1.3. Objective and case study

This Chapter addresses these gaps by proposing a framework that situates heat risk assessment within the relational structure of urban form and function. It does so by pursuing three aims:

i. Identify where SUHI-related risk emerges by combining morphogenetic spatial modules, objective MCDM weighting, and spatially lagged clustering, by formulating a data-driven methodology.

ii. Assess how methodological choices, especially the selection of spatial units, influence the identification of priority sites for climate-adaptation measures. This aim is supported by sensitivity analysis to the different parameters.

iii. Show how spatially aligned data can be used to describe and compare different sites by grouping them into homogeneous clusters.

Through these aims, the Chapter seeks to provide a more spatially coherent and operational approach to site selection for urban design.

5.2. Methodology

5.2.1. Overall methodology

The methodology for selecting and characterising urban areas for SUHI mitigation is structured into six steps (Fig. 1):

i. Data selection, by identifying relevant variables and retrieving data from open-source datasets.

ii. Data modelling, by generalizing spatial modules and computing SUHI and other variables.

iii. Spatial association, building autocorrelation of spatial data based on the size and location of each spatial module.

iv. Site selection, ranking modules using MCDM criteria, supported by sensitivity analysis.

v. Assessment of relative differences between spatial approaches by quantitatively comparing them.

vi. Site characterisation, by clustering urban areas into homogeneous groups to enable comparison within and between cities.

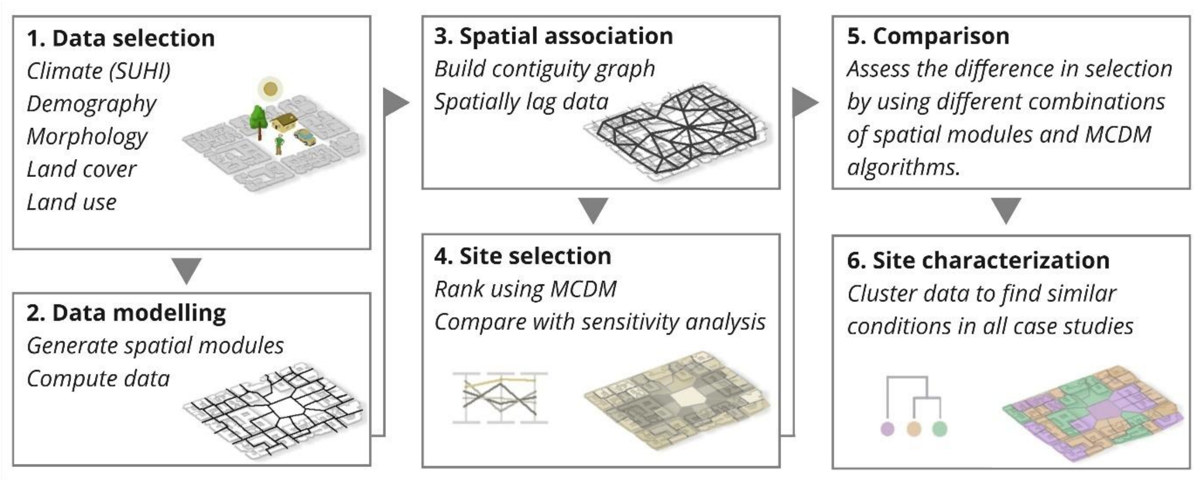

Figure 1. Six steps of the methodology.

The methodology is tested on two Italian case studies with contrasting morphologies and climates:

i. Genoa, a coastal city enclosed by steep forested hills, with narrow urban canyons, high humidity, 559,000 residents in 240 km², and an annual average temperature of 15 °C.

ii. Turin, a compact city on the Po plain, surrounded by the western Alpine arc, with 851,000 residents in 130 km² and an annual average temperature of 12 °C.

To ensure comparability, the analysis focuses on periods with low cloud cover, consistent acquisition times, and seasonal relevance, using shared data layers. An aerial overview of the two study areas (Fig. 2) highlights their morphological contrasts and provides context for interpreting results.

Figure 2. Aerial view of the case studies: Genoa (left) and Turin (right).

5.2.2. Data selection

SUHI-related risk for citizens is conceptualised as the product of hazard, exposure, and vulnerability. Based on the literature, variables shown to influence SUHI risk were selected, spanning multiple urban dimensions: weather and climate, demography, morphology, land cover, and land use (Table 1). This ensures that the analysis captures the multidimensional complexity of urban conditions (Pena Acosta et al., 2023). For each polygon, both internal and surrounding conditions were considered by calculating mean and standard deviation zonal statistics.

Table 1. Variables used for modelling SUHI risk, capturing hazards, exposures, and vulnerabilities through climate, demography, morphology, land cover, and land use variables.

Urban dimension	**Variable and risk category**	**Zonal statistics**	**Data source**	**Data resolution**	**Reasoning**
Climate	50 percentile Surface Heat Island (Hazard)	Mean, standard deviation	Landsat 8 and 9, images acquisition at 10:00-10:30 GMT with almost clear sky conditions for Genoa (01/07, 02/07, 09/07, 10/07, 17/07/, 18/07, 03/08, 10/08,11/08) and Turin (01/07, 08/07, 09/07, 16/07, 24/07, 25/07, 01/08,02/08, 09/08)	- Spatial Resolution (GSD): 100 meters - Pixel size: 30 meters;	(Sidiqui et al., 2022; Ascencio et a., 2023)
	Wind speed at 10/50/100/150/2		Global Wind Atlas (Davis et al., 2023)	300 meters	(Abbassi et al., 2022;

	00 meters (Hazard)				Hou et al., 2023)
Demography (indirect source)	Vulnerable young citizen (0-5) (Vulnerability)	Mean, standard deviation	Italy 100m Age and structure in 2020 (Bondarenko et al., 2020)	100 meters	(Sidiqui et al., 2022; Ascencio et a., 2023)
	Vulnerable elderly citizen (65+) (Vulnerability)				(Sidiqui et al., 2022; Ascencio et a., 2023)
	Population density (Vulnerability)		GHS-POP R2023A, tiles "R4_C19", "R4_C20", "R5_C19", "R5_C20", (Schiavina et al., 2023)		(Sidiqui et al., 2022; Ascencio et a., 2023)
Demography (direct source)	Population resident (Vulnerability)	Majority	Italian census data, tables R01_11, R07_11 (ISTAT, 2021)	Vector (census blocks)	(Sidiqui et al., 2022; Ascencio et a., 2023)
	Vulnerable young citizen (0-5) (Vulnerability)				(Sidiqui et al., 2022; Ascencio et a., 2023 ; Szagri et al, 2023)
	Vulnerable elderly citizen (65+) (Vulnerability)				(Sidiqui et al., 2022; Ascencio et a., 2023; Szagri et al, 2023)
	Citizen with low or no education (Vulnerability)				(Sidiqui et al., 2022; Ascencio et a., 2023; Szagri et al, 2023)
	Citizen with degrees (Vulnerability)				(Sidiqui et al., 2022; Ascencio et a., 2023; Szagri et al, 2023)
	Citizen employed (Vulnerability)				(Sidiqui et al., 2022; Ascencio et a., 2023; Szagri et al, 2023)
	Citizen from Extra EU				(Sidiqui et al., 2022;

	counties (Vulnerability)				Ascencio et a., 2023; Szagri et al, 2023)
	Citizen living alone (Vulnerability)				(Sidiqui et al., 2022; Ascencio et a., 2023; Szagri et al, 2023)
Morphology	Elevation (Exposure)	Mean, standard deviation	Tinitaly 1.1 DEM, tiles: w49535, w49540, w49045, w49050 (Tarquini et al., 2023)	10 meters	(Hou et al., 2023; Xu et al., 2024)
	Slope (Exposure)				(Hou et al., 2023)
	Roughness (Exposure)				(Hou et a., 2023; Xu et a., 2024)
	Building height (Exposure)		Urban Atlas Building Height 2012 (CLMS, 2022)		(Gao et a., 2022; Xu et a., 2024)
	Built-up ratio (Exposure)	Average	Urban Atlas Building Height 2012 (CLMS, 2022), Open Street Maps (www.openstreetmaps.org)		(Gao et a., 2022; Xu et a., 2024)
Land cover	Impervious density (Exposure)	Mean, standard deviation	Copernicus High Resolution Layers (HRL) Imperviousness (2020a)	10 meters	(Gao et a., 2022; Xu et al., 2024)
	Tree cover density (Exposure)		HRL Tree Cover Density (EEA, 2020b)		(Gao et a., 2022; Xu et al., 2024)
	Ratio of shrublands (Exposure)		HRL Small Vegetated Feature (EEA, 2023)		(Gao et a., 2022; Xu et al., 2024)
	Ratio of grasslands (Exposure)		HRL Grassland (EEA, 2020d)		(Gao et a., 2022; Xu et al., 2024)
	Ratio of surface waters (Exposure)		HRL Water and Wetness (EEA, 2020e)		(Gao et a., 2022; Xu et al., 2024)
	Ratio of surface wetness (Exposure)				(Almeida et al., 2021; Gao et a., 2022)
Land use	Distance from transports (Vulnerability)	-	OSM	Vectorial (OSM features)	(Gao et a., 2022; Xu et a., 2024)

	Distance from public services (Vulnerability)				(Sidiqui et al., 2022)
	Distance from emergency facilities (Vulnerability)				(Sidiqui et al., 2022; Szagri et al., 2023)
	Distance from green amenities (Vulnerability)				(Gao et a., 2022; Xu et al., 2024)
	Distance from non-green amenities (Vulnerability)				(Gao et a., 2022; Sidiqui et a., 2022)

5.2.3. Data Modelling

The modelling stage combines the construction of spatial modules with the computation of SUHI intensity and other explanatory variables. This step is central to the methodology, as it defines the analytical units and ensures that all relevant dimensions of urban form and environment are captured consistently across the two case studies.

5.2.3.1. Generating the spatial modules

To evaluate the influence of spatial design on SUHI risk, two different modules were employed: Enclosed Tessellations (ET) and Census Blocks (CB).

i. Enclosed Tessellations (ET) represent a morphometric approach, where contiguous polygons are derived directly from the physical structure of the city. They are built from features that act as barriers or enclosures in the urban fabric (streets, building plots, railways, and waterways). These features were extracted from OpenStreetMap (OSM) using the OSMnx library (Boeing, 2024). Preprocessing was carried out with Momepy (Fleischmann, 2019) and Shapely (Gillies et al., 2007), while the Neatnet package (Fleischmann et al., 2025) was used to simplify dense intersections such as traffic stops and train stations. The final tessellations were generated around each building plot, producing a fine-scale, morphology-driven representation of urban space.

ii. Census Blocks (CB), by contrast, represent a more traditional administrative unit. They were obtained from the Italian cadastre (2011) and are compatible with the most recent census data (ISTAT, 2021). While less directly tied to urban form, CBs provide a useful benchmark for comparing the added value of morphometric modules since CB's contribution in defining SUHI related risk is already documented (Ascencio et al., 2023; Assaf & Assaad, 2024).

5.2.3.2. Computing SUHI from satellite data

SUHI intensity was calculated for Genoa and Turin during the anomalously hot summer of 2022 (NOAA, 2023), using Landsat 8 and 9 imageries acquired between 1 July and 15 August 2022. Landsat was chosen over coarser resolution missions such as Sentinel3 because of its finer spatial resolution and effective revisit time of less than eight days under clear sky conditions. Only morning overpasses (10:00–10:30 GMT) were used, and images with high cloud cover were excluded (Table 2).

Preprocessing involved masking residual clouds and shadows using the QA_PIXEL band, and subsetting each scene to an Area of Interest (AOI) defined by municipal boundaries extended with buffers from the GHS-FUA layer (Schiavina et al., 2023). LST values were converted to Celsius, stacked for each AOI, and aggregated using the pixel-wise 50th percentile (50p), producing representative maps for summer 2022.

SUHI intensity was then derived following the "buffer area around the city" method (Raj & Yun, 2023). Urban pixels were classified as "Artificial Surfaces" (CLC, 2018), comprised "Agricultural" and "Forest/seminatural" classes. Wetlands and water bodies were excluded, as their thermal behaviour differs substantially from terrestrial surfaces and could bias the estimation of land-based urban–rural temperature contrasts. The CLC raster (100 m) was resampled to the Landsat grid, and SUHI was computed as the difference between the mean rural LST and each urban pixel within municipal boundaries.

5.2.3.3. Computing other variables

All other explanatory variables were processed through automated pipelines to ensure reproducibility. Wind speed, elevation, building height, land cover, and demographic data were loaded as rasters, with mean and standard deviation extracted via zonal statistics. Built-up area was derived from OSM building data (used in ET construction) and Urban Atlas building height data. Demographic information was obtained from the Italian cadastre, extracted from CB units and resampled. Land use was expressed in terms of distances, calculated from OSM and Urban Atlas features using a K-Neighbours Tree.

All workflows are documented in supplementary Jupyter notebooks, which include the computational environment required to reproduce the results.

5.2.4. Spatial association

To reinforce the morphological connection of urban data, we introduce spatial association, which embeds mathematical relationships into the dataset based on the dimensions and vicinity of all polygons. This step is crucial for highlighting differences between spatial patterns, as it allows us to confront both geometric entities and their associated attributes (Long & Robertson, 2018).

Spatial weights were assigned to each polygon according to contiguity, i.e. the degree of adjacency between a polygon and its neighbours. Specifically, we employed a queen contiguity weight matrix, calculated from polygon centroids. Queen contiguity was selected because it captures both edge- and corner-based adjacency, making it particularly suitable for modelling SUHI risk at the building scale. Since SUHI is ultimately experienced by human inhabitants, and urban planning and regulation operate at this fine scale, queen contiguity provides a meaningful spatial weight for linking morphology to risk.

5.2.5. Site selection

5.2.5.1. MCDM algorithms

The identification of priority sites was carried out using two Multicriteria Decision-Making (MCDM) algorithms: TOPSIS and VIKOR. These were chosen to compare different approaches to risk ranking (Shekhovtsov & Sałabun, 2020).

TOPSIS (Technique for Order Preference by Similarity to Ideal Solution) evaluates alternatives based on their closeness to the ideal solution and distance from the worst solution. The best alternative is the one with the highest relative closeness to the ideal. It is defined as follows. Given a decision matrix $X = [x_{ij}]$ with m alternatives and n criteria:

i. The data is normalized into dimensionless values so that criteria with different units can be compared.

$$r_{ij} = \frac{x_{ij}}{\sqrt{\sum_{i=1}^{m} x_{ij}^2}}$$

ii. The weighted normalized matrix is obtained, by applying weights to reflect the relative importance of each criterion. The weights are specified in the next section (See "Site selection – Weighting Criteria").

$$v_{ij} = w_j \cdot r_{ij}, j = 1, \dots, n$$

ii. Ideal and negative ideal solutions are defined for each criterion.

$$A^+ = \{v_1^+, v_2^+, \dots, v_n^+\}, v_j^+ = \max_i \quad v_{ij}$$

$$A^- = \{v_1^-, v_2^-, \dots, v_n^-\}, v_j^- = \min_i \quad v_{ij}$$

iii. The distance of each alternative is calculated from the ideal and worst solutions.

$$S_i^+ = \sqrt{\sum_{j=1}^{n} (v_{ij} - v_j^+)^2}, S_i^- = \sqrt{\sum_{j=1}^{n} (v_{ij} - v_j^-)^2}$$

iv. Finally, the closeness coefficient is determined, which determines the ranking by the relative closeness to the ideal solution. Alternatives are ranked in descending order of C_i.

$$C_i = \frac{S_i^-}{S_i^+ + S_i^-}, 0 \leq C_i \leq 1$$

VIKOR (VlseKriterijumska Optimizacija I Kompromisno Resenje), in contrast, identifies a compromise solution that balances proximity to the ideal with stability and acceptable advantage conditions. Thus, the compromise solution sits between the overall group utility (benefit of the majority) and the individual regret (worst-case dissatisfaction).

i. Best and worst values are established and form the reference points for each criterion.

$$f_j^* = \max_i x_{ij} \ ; \ f_j^- = \min_i x_{ij}$$

The Utility measure (S) is calculated, evaluating the overall performance of each alternative across all criteria. The weights are specified in the next section (See "Site selection – Weighting Criteria").

$$S_i = \sum_{j=1}^{n} w_j \cdot \frac{f_j^* - x_{ij}}{f_j^* - f_j^-}$$

ii. Then the Regret measure (R) captures the worst performance of each alternative on any single criterion.

$$R_i = \max_j \left[w_j \cdot \frac{f_j^* - x_{ij}}{f_j^* - f_j^-} \right]$$

iii. Finally, the VIKOR index (Q) combines group utility and individual regret into a single ranking index. Alternatives are ranked in ascending order of Q_i.

$$Q_i = \frac{v(S_i - S^*)}{S^- - S^*} + (1 - v) \cdot \frac{R_i - R^*}{R^- - R^*}$$

Where:

- $S^* = \min S_i \ ; \ S^- = \max S_i$
- $R^* = \min R_i \ ; \ R^- = \max R_i$
- v is the weight of the "majority rule" (commonly $v = 0.5$).

5.2.5.2. Weighting criteria

To meet the requirements of the MCDM algorithms, objective weighting methods were applied: the Entropy method, which measures the importance of criteria based on variability or uncertainty, and the Gini method, which evaluates inequality or dispersion of values. Using objective weights reduces redundancy caused by collinearity and ensures that dependent variables (e.g., "citizens with low or no education" vs. "citizens with degrees") are rescaled appropriately. Implementations of TOPSIS, VIKOR, and the weighting schemes were run using the pymcdm library (Kizielewicz et al., 2023).

Entropy weighting assigns weights to criteria based on the degree of variability or uncertainty in the data. A criterion with greater variation across alternatives carries more information and therefore receives a higher weight. Conversely, criteria with little variation are considered less informative and receive lower weights.

iv. The decision matrix (i.e., the array of alternatives) is normalized, converting raw values into proportions so that each criterion is comparable.

$$p_{ij} = \frac{x_{ij}}{\sum_{i=1}^{m} x_{ij}}, i = 1, \dots, m; \ j = 1, \dots, n$$

v. The entropy value for each criterion is calculated, measuring the degree of disorder or uncertainty in the distribution of values.

$$e_j = -k \sum_{i=1}^{m} p_{ij} \ln(p_{ij}), k = \frac{1}{\ln(m)}$$

vi. Then the degree of diversification is retrieved, capturing how much useful information a criterion provides (higher when entropy is lower).

$$d_j = 1 - e_j$$

vii. Finally, the entropy weight is calculated by assigning weights proportionally to the information content of each criterion.

$$w_j = \frac{d_j}{\sum_{j=1}^{n} d_j}$$

Gini weighting assigns weights by measuring the inequality or dispersion of criterion values across alternatives. A criterion with higher inequality (greater spread of values) is considered more discriminative and thus receives a higher weight.

i. Gini coefficient (G) for each criterion is calculated, quantifying the inequality by comparing all pairwise differences in values.

$$G_j = \frac{\sum_{i=1}^{m} \sum_{k=1}^{m} | x_{ij} - x_{kj} |}{2m^2 \cdot \bar{x}_j}$$

Where $\bar{x}_j$is the mean of criterion j.

ii. The corresponding weight is obtained by normalizing the coefficients so that weights sum to one.

$$w_j = \frac{G_j}{\sum_{j=1}^{n} G_j}$$

5.2.5.3. Variables selection for optimization

From the original variable matrix, only variables with a monotone correlation with SUHI were extracted (Liu et al., 2022), allowing them to be assigned positive or negative optimisation criteria (Table 2). These variables compose the decision matrix for the MCDM problem. The resulting scores were mapped to produce risk surfaces, highlighting areas more prone to SUHI risk as well as those with lower vulnerability. The same process was repeated for subsets of variables corresponding to hazard, exposure, and vulnerability, enabling us to disentangle the contribution of each dimension to overall risk.

Table 2. Subset of variables for MCDM, corresponding to the decision matrix and criteria types, divided between benefits (exacerbate SUHI risk) and costs (limit SUHI risk).

Optimization criteria	Risk category	Criteria type	Reasoning
Mean 50 percentile SUHI	Hazard	Benefit (+1)	The warmer the area, the higher SUHI risk (Hou et a., 2023).
Mean wind speed at 10/50/100/150/200 meters	Hazard	Cost (-1)	Strong ventilation can dissipate surface heat (Abbassi et al., 2022).
Mean vulnerable young citizen (0-5), indirect source	Vulnerability	Benefit (+1)	Presence of vulnerable stakeholders adds to the risk (Szagri et al., 2023).
Mean vulnerable elderly citizen (65+), indirect source	Vulnerability	Benefit (+1)	
Mean population density, indirect source	Vulnerability	Benefit (+1)	
Mean vulnerable young citizen (0-5), direct source	Vulnerability	Benefit (+1)	
Mean vulnerable elderly citizen (65+), direct source	Vulnerability	Benefit (+1)	
Citizen with low or no education	Vulnerability	Benefit (+1)	Vulnerable citizen that may be less receptive to risk mitigation strategies (such as public alarms, emergency drills and evacuations, acceptance to mitigation strategies) (Szagri et al., 2023).
Citizen from Extra EU counties	Vulnerability	Benefit (+1)	
Citizen living alone	Vulnerability	Benefit (+1)	
Citizen with degrees	Vulnerability	Cost (-1)	Citizen that may be more receptive to risk mitigation strategies. (Szagri et al., 2023).
Citizen employed	Vulnerability	Cost (-1)	
Mean elevation	Exposure	Cost (-1)	High elevation typically features lesser temperatures (Hou et a., 2023).
Mean slope	Exposure	Cost (-1)	Rugged terrain features can impede ventilation and non-uniformly exposure to heat (Hou et al., 2023).
Mean roughness	Exposure	Cost (-1)	
Mean rugosity	Exposure	Cost (-1)	
Mean building height	Exposure	Benefit (+1)	Often considered as proxy for SUHI exposure (Chen et al., 2022).
Average built up ratio	Exposure	Benefit (+1)	
Mean impervious density	Exposure	Benefit (+1)	
Mean tree cover density	Exposure	Cost (-1)	Green features lower SUHI (Eggermont et al., 2015).
Mean ratio of shrublands	Exposure	Cost (-1)	
Mean ratio of grasslands	Exposure	Cost (-1)	
Distance from transports	Vulnerability	Cost (-1)	Access points to public and private transport networks enable more connectivity and lessen isolation for stakeholders (Chen et al., 2022).
Distance from public services	Vulnerability	Benefit (+1)	Risk grows with increasing distance to and from public services (schools, town halls) and
Distance from emergency facilities	Vulnerability	Benefit (+1)	

			emergency facilities (hospitals, clinics) (Szagri et al., 2023).
Distance from green amenities	Vulnerability	Benefit (+1)	Close distance with parks and urban greenery lowers SUHI risk (Chen et al., 2022).
Distance from non-green amenities	Vulnerability	Cost (-1)	Grey amenities (e.g., shopping malls, luna parks) are often impervious surfaces with high stakeholder density, thus adding to SUHI risk (Chen et al., 2022).

5.2.5.4. Sensitivity analysis

To assess how the different combination of spatial modules fare in identifying risk, as well as for operative robustness, a sensitivity analysis was conducted. This involved calculating the standard deviation of scores across methods and comparing rankings using Kernel Density Estimation and pairwise plots under different weighting schemes (Stević et al., 2022). The most stable and consistent weighting criteria were then selected as the basis for final site selection by looking at stability and overall performance between the cases, ultimately basing the site selection.

Finally, risk and its components (hazard, exposure, vulnerability) were divided into quartiles, with the highest quartile forming the focus of subsequent analyses. Correlation analysis was then applied to identify how individual variables influenced overall risk and its sub-components. This step demonstrates the capacity of MCDM not only to rank sites but also to steer the interpretation of risk drivers, providing actionable insights for urban planning and SUHI mitigation.

5.2.6. Comparison between spatial modules and MCDM algorithms

To evaluate the consistency of results across different spatial modules and decision-making approaches, Enclosed Tessellations (ET) and Census Blocks (CB) were compared using a random sample of 1,000 shared points from the case studies. For each point, we examined the difference in scores produced by the two MCDM algorithms (TOPSIS and VIKOR) and quantified their association. The distribution of differences was visualised through kernel density plots, which provide an overview of the overall behaviour of each combination.

Beyond score differences, the stability of results was assessed across the case studies by comparing ET and CB preferences for all algorithm combinations. By plotting algorithm preferences at each sample location, we were able to identify which urban areas were more frequently classified as at risk by specific methods. This analysis highlights not only where ET and CB produce similar rankings, but also where they diverge, offering insights into the consistency and robustness of SUHI risk identification across spatial modules and algorithms.

5.2.7. Site characterization

The final step of the methodology focuses on characterising urban areas according to their SUHI risk. The goal is to identify groups of polygons with similar features and SUHI scores, thereby defining site conditions that are comparable both within and between cities. To achieve this, all data ranked in the highest quartile of SUHI risk was selected and clustered the associated spatially lagged variables to generate urban typologies.

To reduce collinearity and simplify the feature space, Principal Component Analysis (PCA) was applied, retaining the minimum number of components required to explain 95% of the total variance. The reduced dataset was then used as input for Hierarchical Agglomerative Clustering (HAC), implemented with the scikit-learn library (Pedregosa et al., 2011). HAC was computed across a broad range of cluster numbers (k = 2 to 30), with the optimal solution selected using the Silhouette Score and further validated visually through a clustergram, which illustrates the closeness of PCA-weighted cluster means.

Finally, to interpret the content of each cluster, the mean, standard deviation, and Pearson's correlation coefficient (ϱ) were computed for all variables. This step allows to describe the defining characteristics of each urban typology, linking them back to SUHI risk conditions and providing a basis for comparing mitigation strategies across different morphological and climatic contexts.

5.3. Results

This section presents the outputs of the spatial-MCDM workflow applied to Genoa and Turin, highlighting how different methodological choices influence SUHI-related risk identification. The emphasis is on data output and interpretation, contextualizing outcomes on the effect that different choices have at the planning level.

5.3.1. Site selection outputs

Data was extracted for Genoa and Turin, producing Enclosed Tessellations (ET) with 33’052 polygons in Genoa and 20’449 polygons in Turin, each of varying size. The application of the Neatnet algorithm simplified the street and railway networks by a factor of 10:1, substantially reducing complexity in dense areas such as train stations and major intersections. A s intended, many of the simplified polygons corresponded to these highly complex nodes, improving the comparability between ET and Census Blocks (CB). This preprocessing step ensures that subsequent analyses are less affected by artefacts of network density and more reflective of meaningful urban morphology.

The spatial weights analysis confirmed significant associations between polygons, providing a robust foundation for the MCDM steps. One variable, Surface Water Capacity, was excluded due to its near absence in Genoa, which prevented entropy weight computation. MCDM analysis generated site preferences and rankings for TOPSIS and VIKOR, using entropy and Gini weighting criteria, applied to ET and CB (Fig. 3).

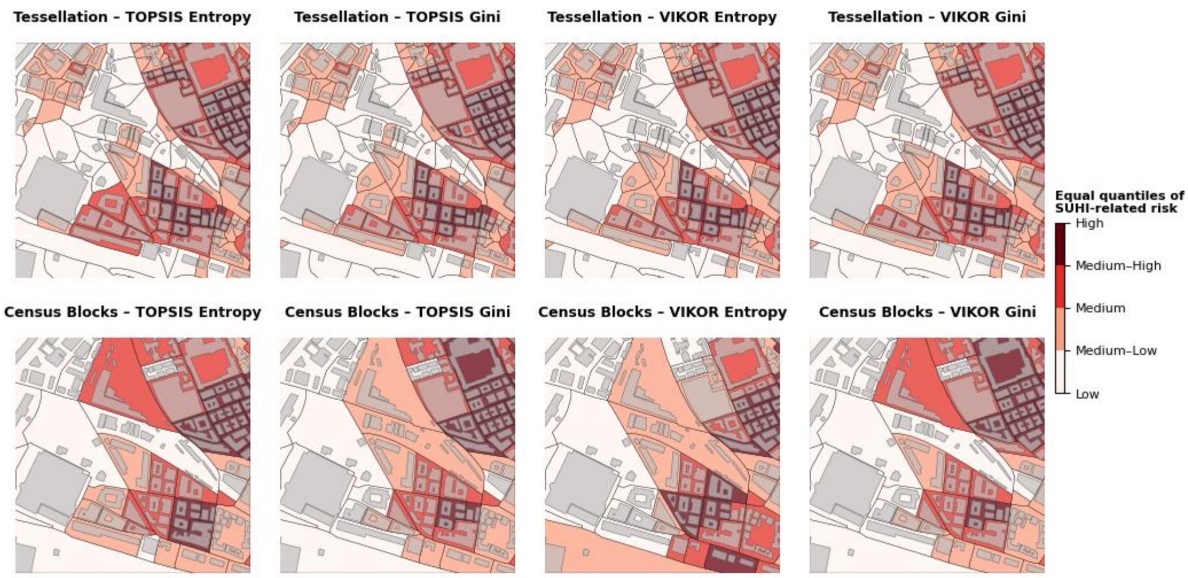

Figure 3. Excerpts from Genoa (Cornigliano) site selection process, including all possible combinations of spatial modules, MCDM, and weights.

5.3.2. Sensitivity and stability analysis outcomes

The MCDM analysis generated site preferences and rankings using both TOPSIS and VIKOR, combined with Entropy and Gini weighting criteria, applied to both ET and CB. From this, four main observations emerged:

i. the sensitivity of results to algorithm choice and weighting scheme,

ii. the relative stability of rankings across modules,

iii. the identification of high-priority sites for intervention, and

iv. the comparability of outputs across case studies.

The resulting scores highlight the highest priority sites for intervention in both Genoa and Turin, forming the basis for subsequent site characterisation.

5.3.2.1. Sensitivity analysis on MCDM algorithms and weights

The sensitivity analysis examined the standard deviation of MCDM scores, revealing that location, spatial module, and algorithm each influenced variation by similar margins (Table 3).

i. The similarity between standard deviations of MCDM preferences was consistently high, always above 83%.

ii. The lowest similarity was observed in Genoa using VIKOR with CB (83.5%), while the highest was in Genoa using TOPSIS (99.7%).

iii. On average, similarity exceeded 91% (95.2% for TOPSIS combinations and 91.1% for VIKOR).

These results indicate that TOPSIS tends to produce more stable outcomes, as shown by lower standard deviations across combinations and higher similarity between weighting schemes. However, no single weighting methodology unequivocally favoured a particular combination of location, spatial module, and algorithm.

The differences between the lowest and second-lowest mean standard deviations for TOPSIS (Entropy method) and VIKOR (Gini method) were both under 0.02, which we consider not significant. Thus, while the analysis confirms the overall stability of the approaches (with TOPSIS generally more stable in Genoa and VIKOR in Turin) it does not provide sufficient evidence to declare one method universally superior.

Table 3. Standard deviation of scores (algorithm preferences) for sensitivity analysis, run by changing the weighting criteria between the different MCDM algorithms, spatial modules, and locations.

Location, Spatial module	**TOPSIS scores Entropy std**	**TOPSIS scores Gini std**	**TOPSIS scores std similarity [%]**	**VIKOR scores Entropy std**	**VIKOR scores Gini std**	**VIKOR scores std similarity [%]**
Genoa, ET	0.048868	0.048994	99.7428	0.128735	0.144918	88.8330
Genoa, CB	0.056312	0.055580	98.6994	0.107624	0.089849	83.4837

Turin, ET	0.043501	0.049806	87.3403	0.130364	0.132861	98.1205
Turin, CB	0.039854	0.041953	94.9958	0.097849	0.092119	94.1441
Mean	0.047134	0.049083	95.1946	0.116143	0.114937	91.1453

5.3.2.2. Ranking distribution

As a second observation, we analysed the differences in ranking distributions (Fig. 4). Across all cases, two major poles emerged at the extremes of the distributions: one around the lowest and one around the highest differences in weighting criteria. These poles correspond to urban areas consistently ranked either very high or very low by all algorithm–weighting combinations. In other words, while there are variations in intermediate rankings, the best and worst urban areas are identified similarly across methods.

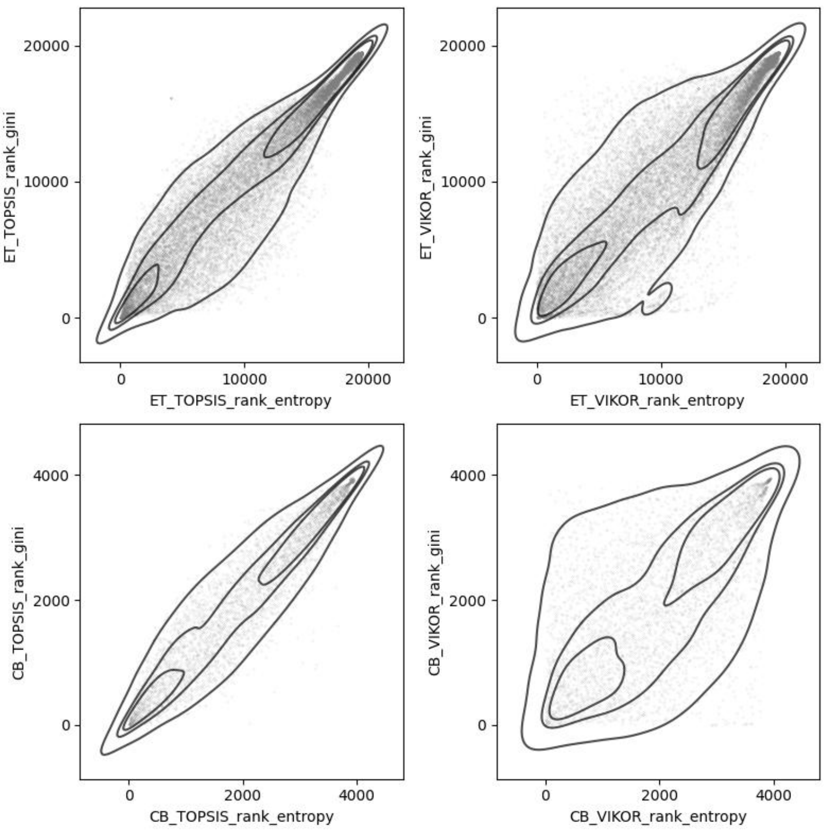

Figure 4. Pairwise plots of rankings for sensitivity analysis for the combined locations (Genoa and Turin), between the combinations of weighting criteria between the different MCDM algorithms and spatial modules (ET and CB). A superimposed Kernel Density Estimation of four levels identifies the poles.

When comparing spatial modules, the differences observed with ET were generally smaller than those with CB, reflecting a narrower spread of ranking variation. This is notable given that ET polygons are more than three times as numerous as CB polygons. Despite the larger number of features, ET produced lower ranking variability when algorithms and weighting criteria were changed, suggesting that morphometric units provide more stable results.

Furthermore, in both ET and CB cases, the use of entropy weighting reduced ranking differences compared with Gini weighting, particularly when combined with VIKOR. Taken together with the earlier sensitivity analysis of score standard deviations, these findings support the selection of the entropy method as the preferred objective weighting scheme, due to its greater stability across modules and algorithms.

5.3.2.3. Comparisons between spatial modules and MCDM algorithms

In the comparison based on random samples, both optimization algorithms behaved consistently across the two spatial modules (ET and CB) (Fig. 5). This finding aligns with the previous observations, confirming that the choice of spatial unit does not fundamentally alter the ranking logic of the algorithms.

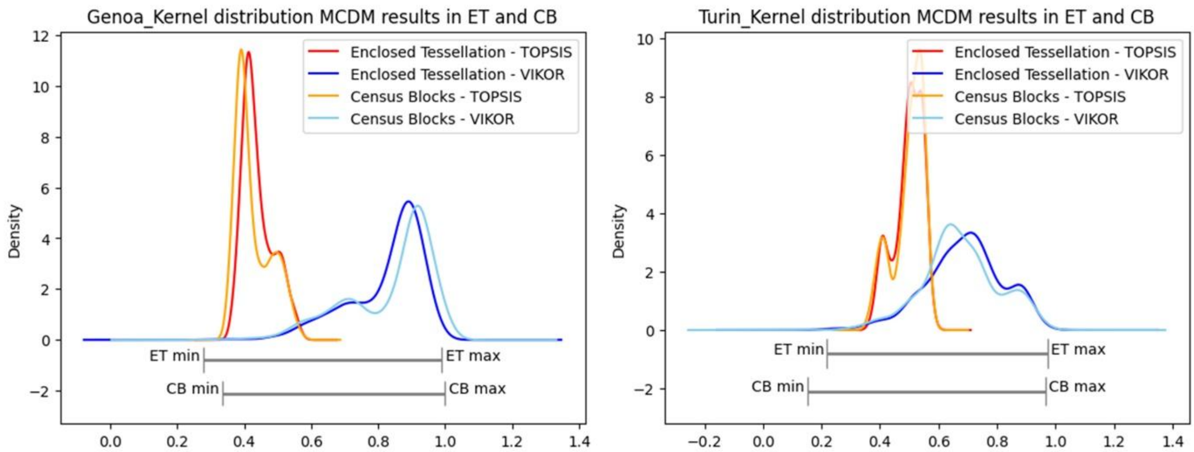

Figure 5. Kernel distribution for MCDM scores in Genoa (left) and Turin (right). Each combination of spatial module (ET and CB) and algorithm (TOPSIS and VIKOR) is considered, while highlighting the maximum and minimum values for consideration.

Nevertheless, a systematic difference emerged in the preference scores: for both Genoa and Turin, VIKOR produced higher scores than TOPSIS, with the effect more pronounced in Genoa. Importantly, this does not imply that VIKOR identified areas at greater risk than TOPSIS. Instead, it reflects the internal logic of the algorithms. While TOPSIS evaluates closeness to an ideal solution and penalises alternatives that fail to meet all criteria simultaneously, VIKOR emphasises compromise solutions and tends to assign higher values to sites that balance trade-offs among criteria.

This distinction is evident in the score ranges: TOPSIS never produced values above 0.7, where 1 would represent the ideal case in which all criteria are fully satisfied. By contrast, VIKOR's scoring framework allowed higher preference values, even when no single site met all criteria perfectly. Thus, although both algorithms ranked sites in a broadly similar order, their scoring scales diverge, with VIKOR producing higher absolute values and TOPSIS remaining more conservative.

5.3.2.4. Spatial differences in algorithm preference

Finally, the spatial distribution of algorithm preferences within the same set of sampled points was examined (Fig. 6). The analysis shows that TOPSIS produces only very small differences between ET and CB within each city, suggesting that its results are relatively insensitive to the geometric attributes of the spatial modules. This stability holds even in cities with markedly different morphologies, such as Genoa and Turin.

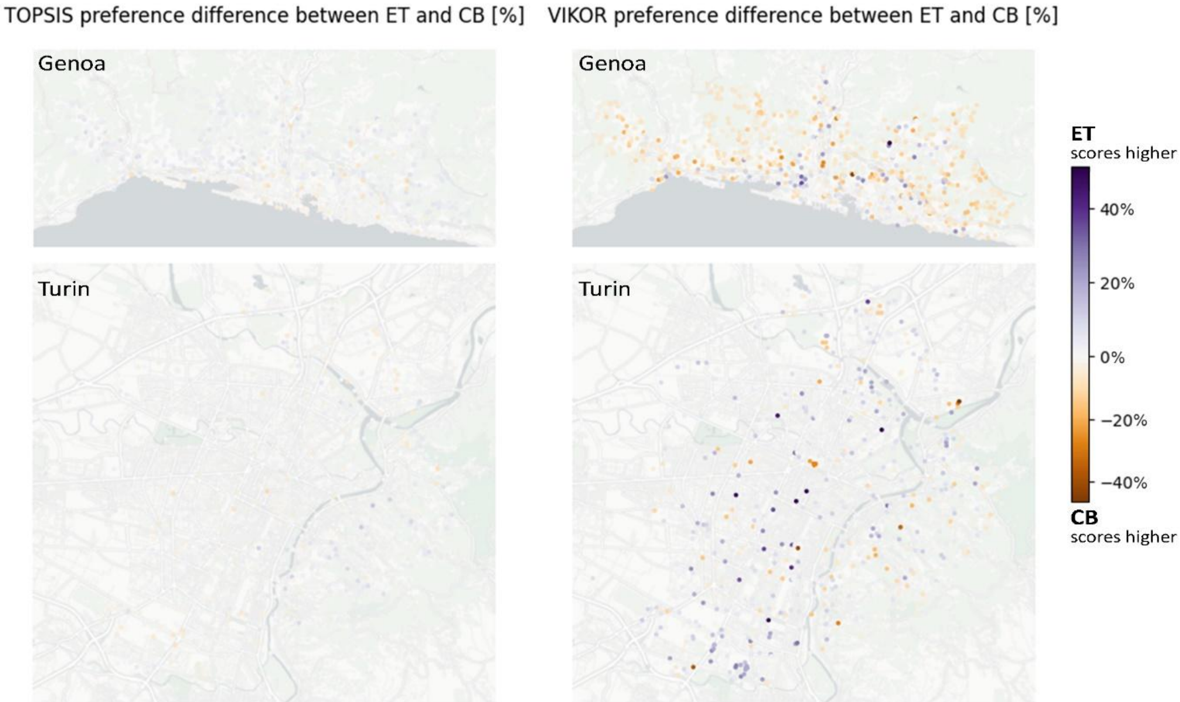

Fig. 6. Spatial comparison between TOPSIS and VIKOR in Genoa (top) and Turin (bottom). TOPSIS (left) notably reduces the difference between the two spatial modules, while VIKOR (right) is more prone to prefer one spatial module to the other between different urban areas.

By contrast, VIKOR exhibits greater variability, with differences between ET and CB more pronounced and less consistent across cities. This indicates that VIKOR is more dependent on the geometric characteristics of the spatial modules, and therefore less stable when applied across contrasting urban contexts.

While this outcome is consistent with previous observations, it provides additional nuance for interpreting the practical use of TOPSIS and VIKOR. It was observed that VIKOR can be more stable in representing SUHI risk patterns in Turin, yet its predictions showed inconsistencies when comparing neighbouring areas. This suggests that VIKOR may be more sensitive to local morphological heterogeneity, whereas TOPSIS maintains greater consistency across both modules and cities.

5.3.2.5. Exemplification of the site selection process

The site selection process builds directly on the results of the previous analyses. Based on the stability tests, the combination of ET with TOPSIS and entropy weights was selected as the most reliable configuration and mapped the resulting scores for both Genoa (Fig. 6) and Turin (Fig. 7). The maps illustrate how each risk component contributes to the combined score, and these effects can be traced back to specific variables through correlation analysis.

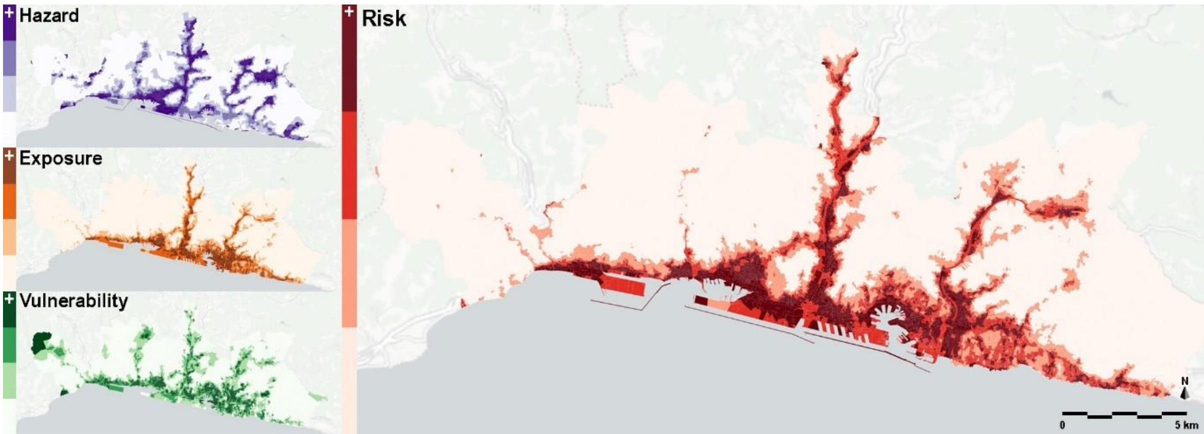

Fig. 7. SUHI related risk for human health, assessment for Genoa, with decomposed maps separately presenting the hazard, exposure, and vulnerability components obtained with the same combination of ET, TOPSIS, entropy weights.

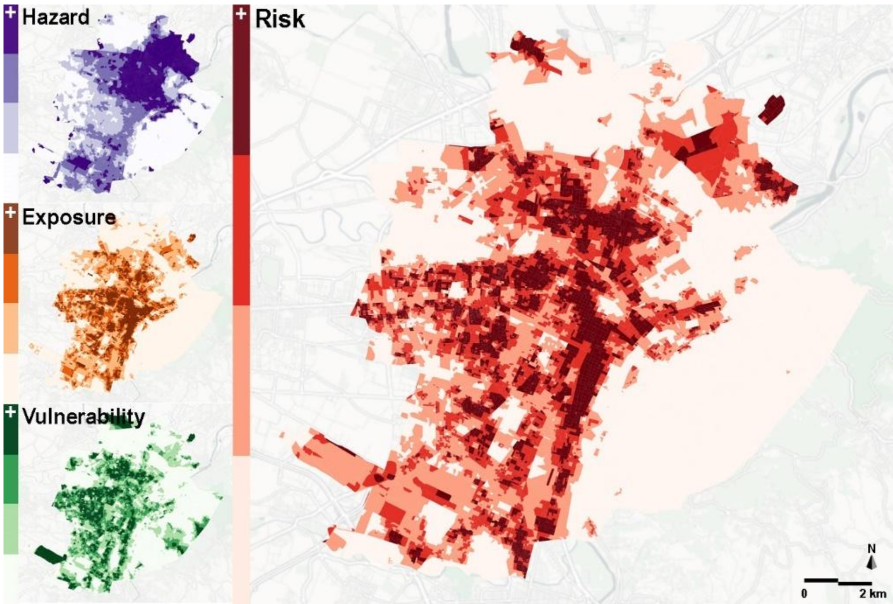

Fig. 8. SUHI related risk for human health, assessment for Turin, with decomposed maps separately presenting the hazard, exposure, and vulnerability components obtained with the same combination of ET, TOPSIS, entropy weights.

To quantify these relationships, Pearson's correlation coefficients (ϱ) was computed for all variables (Fig. 8; full results in Annex H). The correlation matrix reveals that in both Genoa and Turin, exposure is the dominant driver of risk (ϱ = +0.96), underscoring the critical role of urban density and human presence in shaping vulnerability to SUHI. Hazard and vulnerability also contribute meaningfully, with Genoa showing slightly higher sensitivity to risk-related factors compared to Turin.

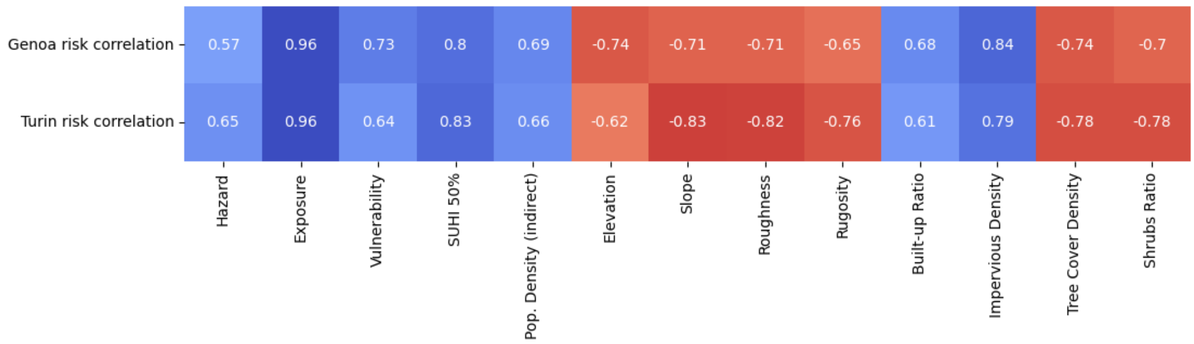

Fig. 8. Pearson's ρ correlation analysis of risk in Genoa and Turin with risk components and highly correlated variables (|ρ|≥+0.6).

As expected, climatic variables such as SUHI intensity exhibit strong positive correlations with risk ($\varrho = +0.80$ in Genoa; $\varrho = +0.83$ in Turin), confirming that thermal stress is a key amplifier of urban risk. By contrast, morphological characteristics (including elevation, slope, and terrain roughness) are negatively correlated with risk, particularly in Turin, suggesting that more rugged or elevated landscapes may provide natural buffering effects. Similarly, vegetation coverage shows an inverse relationship with risk, reinforcing the protective role of green infrastructure in mitigating heat exposure.

Overall, the results demonstrate that while hazard intensity contributes to urban risk, it is exposure and environmental context that are most decisive in shaping SUHI-related vulnerability in both cities. These findings not only align with patterns observed in other densely built urban contexts (Sangiorgio et al., 2020; Gao et al., 2022) but also highlight the importance of integrating morphological and ecological factors into risk-based planning for effective mitigation.

5.3.3. Comparison with existing studies

In Genoa and Turin, the spatial-MCDM framework indicates that SUHI risk is most pronounced in areas with limited vegetation, dense urbanization, and socio-economic vulnerability. Similar patterns have been reported elsewhere: Morabito et al. (2015) mapped elderly heat risk in Italian cities and showed that vulnerability factors can outweigh temperature extremes, while Pappalardo et al. (2023) highlighted how socio-demographic disadvantage shapes risk distribution in Padua from a climate-justice perspective. In Genoa, Morabito explicitly identified Cornigliano (an industrial and densely built district with limited green space) as the highest-risk area, and our analysis confirmed that this neighbourhood remains a critical hotspot. For Turin, Morabito's maps pointed to elevated risk in the central urban districts, where high surface temperatures overlap with a dense elderly population; our results found similar patterns. Additionally, our sensitivity analysis found that entropy weight with TOPSIS provided clear discrimination, whereas VIKOR produced more stable rankings in Turin. These differences echo earlier approaches: Morabito et al. used statistical downscaling to refine LST estimates, while Pappalardo et al. applied composite GIS indices to capture equity concerns. Public-health studies further support the need for validation. For example, Ghirardi et al. (2015) linked heat waves to emergency visits across age groups, and Cremonini & Georgiadis (2025) stressed elderly vulnerability under climate change. Taken together, these comparisons suggest our framework is consistent with existing evidence but would benefit from further testing against health outcomes and broader adaptation strategies. For practical use by planners, results must be screened against regulations that may restrict interventions, e.g. conservation policies in historic centres, or physical constraints such as street geometry (Privitera & Jelo, 2025). The system allows such filters to be added either as masking layers or as variables before MCDM ranking.

5.3.4. Site characterisation outputs

Data from Genoa and Turin was grouped, corresponding to the highest quartile of risk scores identified in the site selection step. To reduce dimensionality PCA was applied, which reduced the number of features from 57 to 17. Subsequently, HAC was performed to classify the data into distinct groups. The optimal number of clusters was determined as k = 8, based on both the Silhouette Score (SS = 0.176) and visual inspection of the clustergram (Annex I). Each cluster's content was extracted from the spatially lagged variables and analysed in detail (Annex J).

The resulting clusters represent distinct typologies of high-risk urban areas, each defined by a unique combination of climatic, demographic, morphological, land cover, and land use characteristics. In total, six clusters were obtained in Genoa (Fig. 10) and three clusters in Turin (Fig. 11).

Figure 10. Site characterization by clustering the highest quartile of areas under SUHI risk in Genoa, grouping areas with similar profiles in terms of climate, demography, morphology, land cover, and land use. Percentages show the occurrences of each cluster in Genoa.

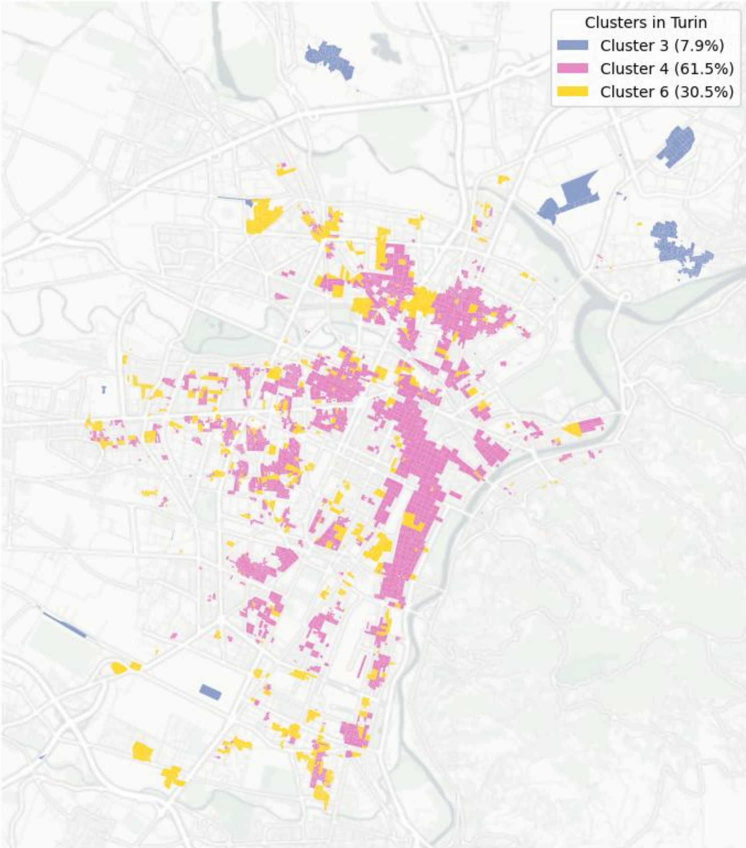

Figure 11. Site characterization by clustering the highest quartile of areas under SUHI risk in Turin, grouping areas with similar profiles in terms of climate, demography, morphology, land cover, and land use. Percentages show the occurrences of each cluster in Turin.

The clustering shown if Fig. 10 (Genoa) and Fig. 11 (Turin) reveals clear differences in the spatial structure of the highest-risk SUHI areas and carries direct implications for intervention priorities. Thus, two main findings can be analysed.

i. Regarding cluster complexity and dominance, Genoa exhibits six distinct clusters, with Cluster 1 covering 45.0% of the highest-risk quartile and other clusters distributed across coastal corridors and inland valleys (Cluster 2 24.8%, Cluster 5 11.5%, Cluster 7 14.1%, Cluster 8 3.0%, Cluster 3 1.6%). Turin shows a simpler pattern with three clusters, dominated by Cluster 4 at 61.5%, followed by Cluster 6 30.5% and Cluster 3 7.9%. These proportions indicate a fragmented, heterogeneous risk landscape in Genoa versus a more homogeneous, city-wide concentration of high-risk conditions in Turin. This indicates that some risk-prone typologies are not marginal but structurally embedded in the cities' morphology.

ii. On the cross-city overlap, only Cluster 3 appears in both cities, representing 1.6% of Genoa's and 7.9% of Turin's high-risk areas (about 4% of the combined sample). Where overlap exists, areas are characterised by high variability in SUHI intensity, imperviousness, land use, and demographic exposure, but low variability in building height. Spatially, these shared sites are typically located outside central cores (along Genoa’s seaside corridors and in Turin’s peri-urban zones) pointing to similar functional and environmental pressures despite differing morphologies.

5.4. Discussion

5.4.1. Implications of the use of spatial analysis and MCDM for site selection

An integrated methodology was developed to support the selection of critical sites for SUHI mitigation, combining spatial analysis with multicriteria decision-making (MCDM). The results indicate that the site selection process obtained through this approach can yield accurate outputs even at very high resolution. Moreover, the findings align with previous studies showing that SUHI risk is exacerbated by limited vegetation, dense urbanisation, and socio-economic vulnerability (Gao et al., 2022; Pena Acosta et al., 2023).

The application demonstrates how MCDM techniques can be coupled with spatial analysis to address site selection problems, namely the identification of urban areas most at risk. Sensitivity analysis indicated that the most stable configuration combined Enclosed Tessellations (ET) as spatial modules, entropy weighting, and the TOPSIS algorithm. However, the relatively small differences between combinations suggest that alternative MCDM techniques may be appropriate for different objectives. For instance, TOPSIS emphasises discrepancies between each condition and the best-performing condition, whereas VIKOR may be more suitable in contexts where compromise solutions are preferable.

Further testing could clarify these differences. One possible extension would be the introduction of a fourth risk category, adaptive capacity, to capture the ability of urban systems to adjust to heat stress, mitigate potential damage, and cope with adaptation strategies (NOAA, 2023). It was also observed that VIKOR can provide more stable representations in certain neighbourhoods of Turin, suggesting that algorithm choice may depend on local context. The iterative nature of the methodology allows for such refinements, enabling future research to focus on narrower city sections or alternative parameter settings.

5.4.2. Application of site selection and characterisation for SUHI mitigation

The site selection framework is directly applicable to workflows requiring in-depth analysis of SUHI-related risk, such as identifying priority areas for NBS. For practical use by local administrations, however, the selection must be complemented by a screening of normative regulations that may restrict interventions. For example, NBS may not be permitted in conservation areas or historical centres (Privitera & Jelo, 2025), and street geometry may limit the feasibility of tree planting. The system is designed to accommodate such constraints by allowing the introduction of masking layers at the end of the process or the inclusion of new variables before MCDM ranking.

The site characterisation step complements site selection by grouping high-risk areas into urban typologies. This enables immediate description of local site conditions and their relation to surrounding areas. Such typologies are particularly valuable for designing NBS, as they allow multi-scalar approaches to the planning and forecasting of mitigation potential (UNDRR & UNU-EHS, 2023).

For example, the urban canyon, defined as the cross-section of two buildings and the street between them (Aliabadi et al., 2019), is a common framework for SUHI analysis in dense cities. Because ET modules are derived from buildings and streets, they are inherently compatible with this concept. Moreover, the spatial association between polygons (See the section "Data Modelling – Spatial association") enables the retrieval of urban canyons geometries and their integration into the analysis, further expanding the applicability of the methodology (further explored in the next Chapter).

Regarding the case study, the spatial patterns imply different strategic priorities that are ultimately very context dependent. Genoa requires a mosaic of targeted, site-specific interventions tailored to diverse local conditions; Turin can benefit from broader area-based measures complemented by targeted actions where smaller clusters indicate concentrated vulnerabilities. The limited cross-city overlap underscores that transferability of interventions should be guided by local cluster profiles rather than by broad city-level analogies.

5.4.3. Methodological limitations

This study focused on two case studies, Genoa and Turin, to simplify the selection of LST images and ensure temporal consistency. While this approach allowed for detailed analysis, it limits the generalisability of the findings. The "best-performing combination" of spatial module and MCDM algorithm may differ in other regions, as spatial analytical methods are highly dependent on urban form. Similarly, site characterisation may yield more clusters when applied to a larger set of cities.

Regarding data, the study used the most recent publicly available datasets with the highest spatial resolution. However, some datasets differ in acquisition year, with the Building Height UA layer dating back to 2012. Ultimately, the study prioritised spatial resolution over temporal consistency, which may introduce minor errors due to land cover change.

Finally, the sea was excluded from the analysis due to incompatibility with the spatial methodology. While coastal polygons indirectly capture some buffering effects of water, the influence of the sea on SUHI is not explicitly quantified here.

5.5. Conclusions

This Chapter developed and tested a spatial method that weights different form-based strategies in support to heat-risk planning through a process of site selection and characterisation. The approach aligns risk assessment with how planners and architects read urban space, linking SUHI related risk to familiar urban forms and functions. The main findings, aligned with the Chapter objectives, are as follows.

i. The most critical urban features influencing SUHI risk were identified, aligning with current findings in the literature. Across Genoa and Turin, vegetation cover, built up density, and demographic indicators emerged as the most influential drivers of SUHI related risk.

ii. By testing spatial modules (Enclosed Tessellations, Census Blocks), MCDM algorithms (TOPSIS, VIKOR), and weighting schemes (Entropy, Gini), a stable and reproducible workflow was established for ranking urban areas and understanding the drivers of prioritisation. Enclosed Tessellation combined with TOPSIS produced the clearest and most stable site selection results, while the framework remains flexible enough to adapt to different planning objectives.

iii. An almost fully automated process was developed, capable of handling heterogeneous datasets to produce SUHI risk rankings for Italian cities. Extension to other European contexts is feasible with minor adjustments, although SUHI data availability and resolution remain barriers to full automation. Future work should focus on integrating higher-resolution and more temporally consistent thermal datasets to overcome this constraint.

iv. Clustering supports planning by characterizing urban sites, distinguishing local urban forms and functional conditions with similar SUHI related risk. This approach revealed distinct and internally consistent high-risk clusters within each city, allowing for comparisons across recurring urban typologies rather than isolated locations. Only a small fraction of high-risk areas was comparable across cities, highlighting the local nature of heat risk patterns and the need for cautious, typology-based generalisation. Nevertheless, internally consistent clusters emerged within each city, providing a basis for targeted implementation of NBS.

Overall, this chapter presented a replicable framework for evidence-based site selection and characterisation in SUHI mitigation planning. The adaptability of the methodology, combined with anticipated improvements in SUHI data availability, offers strong potential for scaling to broader geographic contexts and for supporting the integration of NBS into urban climate adaptation strategies.

5.6. References

Abbassi, Y., Ahmadikia, H., & Baniasadi, E. (2022). Impact of wind speed on urban heat and pollution islands, Urban Climate, 44, 101200. https://doi.org/10.1016/j.uclim.2022.101200

Aliabadi, A.A., Moradi, M., Clement, D. et al. (2019). Flow and temperature dynamics in an urban canyon under a comprehensive set of wind directions, wind speeds, and thermal stability conditions. Environmental Fluid Mechanics, 19, 81–109. https://doi.org/10.1007/s10652-018-9606-8

Almeida, A.T., Alencar, M.H., Garcez, T.V., & Ferreira, R.J.P. (2017). A systematic literature review of multicriteria and multi-objective models applied in risk management, IMA Journal of Management Mathematics, 28(2), 153–184 https://doi.org/10.1093/imaman/dpw021

Almeida, C. R. de, Teodoro, A. C., & Gonçalves, A. (2021). Study of the Urban Heat Island (UHI) Using Remote Sensing Data/Techniques: A Systematic Review. *Environments*, *8*(10), Article 10. https://doi.org/10.3390/environments8100105

Assaf, G., & Assaad, R. H. (2024). Using Data-Driven Feature Engineering Algorithms to Determine the Most Critical Factors Contributing to the Urban Heat Island Effect Associated with Global Warming. 1055–1062. https://doi.org/10.1061/9780784485248.126

Balk D, Leyk S, Jones B, Montgomery MR, Clark A. (2018) Understanding urbanization: A study of census and satellite-derived urban classes in the United States, 1990-2010. PLoS ONE 13(12): e0208487. https://doi.org/10.1371/journal.pone.0208487

Boeing, G. (2024). "Modeling and Analyzing Urban Networks and Amenities with OSMnx." Working paper. Retrieved from https://geoffboeing.com/publications/osmnx-paper/

Bondarenko M., Kerr D., Sorichetta A., and Tatem, A.J. (2020). Estimates of 2020 total number of people per grid square broken down by gender and age groupings using Built-Settlement Growth Model (BSGM) outputs. WorldPop, University of Southampton, UK. https://doi.org/10.5258/SOTON/WP00695

Cenci, L., Pampanoni, V., Laneve, G., Santella, C., & Boccia, V. (2021). Presenting a Semi-Automatic, Statistically-Based Approach to Assess the Sharpness Level of Optical Images from Natural Targets via the Edge Method. Case Study: The Landsat 8 OLI–L1T Data. Remote Sensing, 13(8), 1593. https://doi.org/10.3390/rs13081593

Chen, TH.K., Prishchepov, A.V., Sabel, C.E. (2023). Detecting Urban form Using Remote Sensing: Spatiotemporal Research Gaps for Sustainable Environment and Human Health. In: Wen, TH., Chuang, TW., Tipayamongkholgul, M. (eds) Earth Data Analytics for Planetary Health. Atmosphere, Earth, Ocean & Space. Springer, Singapore. https://doi.org/10.1007/978-981-19-8765-6_10

Chen, Y., Shan, B., & Yu, X. (2022). Study on the spatial heterogeneity of urban heat islands and influencing factors. *Building and Environment*, *208*, 108604. https://doi.org/10.1016/j.buildenv.2021.108604

Cremonini, L., & Georgiadis, T. (2025). Urban effects of climate change on elderly population and the need for implementing urban policies. Encyclopedia, 5(3), 140. https://doi.org/10.3390/encyclopedia5030140

Copernicus Land Monitoring Service. (2012). Urban Atlas Building Height 2012 (raster 10 m), Europe [Dataset]. European Environment Agency. https://doi.org/10.2909/42690e05-edf4-43fc-8020-33e130f620231

Copernicus Land Monitoring Service. (2020). *CORINE Land Cover 2018 (raster 100 m), Europe, 6-yearly* [Data set]. European Environment Agency. https://doi.org/10.2909/960998c1-1870-4e82-8051-6485205ebbac

Cumming, G. S. (2011). Spatial resilience: Integrating landscape ecology, resilience, and sustainability. *Landscape Ecology*, *26*(7), 899–909. https://doi.org/10.1007/s10980-011-9623-1

Dibble, J., Prelorendjos, A., Romice, O., Zanella, M., Strano, E., Pagel, M., & Porta, S. (2019). On the origin of spaces: Morphometric foundations of urban form evolution. *Environment and Planning B: Urban Analytics* *and City Science*, *46*(4), 707–730. https://doi.org/10.1177/2399808317725075

Eggermont, H., Balian, E., Azevedo, J. M. N., Beumer, V., Brodin, T., Claudet, J., Fady, B., Grube, M., Keune, H., Lamarque, P., Reuter, K., Smith, M., Van Ham, C., Weisser, W. W., & Le Roux, X. (2015). Nature-based Solutions: New Influence for Environmental Management and Research in Europe. *GAIA - Ecological Perspectives for Science and Society*, *24*(4), 243–248. https://doi.org/10.14512/gaia.24.4.9

European Commission. (2019). The European Green Deal. COM (2019) 640 final. https://eur-lex.europa.eu/legal-content/EN/TXT/?uri=CELEX:52019DC0640

European Environment Agency (2020a). Grassland 2018 (raster 10 m), Europe, 3-yearly, Aug. 2020 [Dataset]. https://doi.org/10.2909/60639d5b-9164-4135-ae93-fb4132bb6d83

European Environment Agency (2020b). Imperviousness Density 2018 (raster 10 m), Europe, 3-yearly, Aug. 2020 [Dataset]. https://doi.org/10.2909/3bf542bd-eebd-4d73-b53c-a0243f2ed862

European Environment Agency (2020c). Tree Cover Density 2018 (raster 10 m), Europe, 3-yearly, Sep. 2020 [Dataset]. https://doi.org/10.2909/486f77da-d605-423e-93a9-680760ab6791

European Environment Agency (2020d). Water and Wetness 2018 (raster 10 m), Europe, 3-yearly - version 2, Nov. 2020 [Dataset]. https://doi.org/10.2909/7992f641-bf77-47b7-b0c1-74fc832b78b1

European Environment Agency (2022). Urban Atlas Building Height 2012 (raster 10 m), Europe - version 3, Oct. 2022 [Dataset]. https://doi.org/10.2909/42690e05-edf4-43fc-8020-33e130f62023

European Environment Agency (2023). Small Woody Features 2018 (raster 5 m), Europe, 3-yearly, May 2023 [Dataset]. https://doi.org/10.2909/a8e683b1-2f96-45c8-827f-580a79413018

European Environment Agency (2024). Web report no. 20/2024: The impacts of heat on health: surveillance and preparedness in Europe. ISBN: 978-92-9480-696-3, ISSN: 2467-3196, https://doi.org/10.2800/8167140

Feliciotti, A., Romice, O., & Porta, S. (2016). Design for Change: Five Proxies for Resilience in the Urban Form. *Open House International*, *41*(4), 23–30. https://doi.org/10.1108/OHI-04-2016-B0004

Feliciotti, A., Romice, O., & Porta, S. (2018). From system ecology to urban morphology: towards a theory of urban form resilience. Paper presented at International Forum on Urbanism, Barcelona, Spain. https://sciforum.net/manuscripts/5993/manuscript.pdf

Fleischmann, M. (2019) 'momepy: Urban Morphology Measuring Toolkit', Journal of Open Source Software, 4(43), p. 1807. https://doi.org/10.21105/joss.01807.

Fleischmann, M., Romice, O., Porta, S. (2021). Measuring urban form: Overcoming terminological inconsistencies for a quantitative and comprehensive morphologic analysis of cities. Environment and Planning B: Urban Analytics and City Science 48, 2133–2150. https://doi.org/10.1177/2399808320910444

Fleischmann, M., Vybornova, A., & Gaboardi, J.D. (2025). uscuni/neatnet. Zenodo. https://doi.org/10.5281/zenodo.14765801

Gallotti, R., Sacco, P., & De Domenico, M. (2021). Complex Urban Systems: Challenges and Integrated Solutions for the Sustainability and Resilience of Cities. *Complexity*, *2021*, e1782354. https://doi.org/10.1155/2021/1782354

Gao, Y., Zhao, J., & Han, L. (2022). Exploring the spatial heterogeneity of urban heat island effect and its relationship to block morphology with the geographically weighted regression model. *Sustainable Cities and Society*, *76*, 103431. https://doi.org/10.1016/j.scs.2021.103431

Ghirardi, L., Bisoffi, G., Mirandola, R., Ricci, G., & Baccini, M. (2015). The impact of heat on an emergency department in Italy: Attributable visits among children, adults, and the elderly during the warm season. PLOS ONE, 10(10), e0141054. https://doi.org/10.1371/journal.pone.0141054

Gillies, S., & al. (2007). Shapely: manipulation and analysis of geometric objects. Retrieved from https://github.com/Toblerity/Shapely

Hayes, A. T., Jandaghian, Z., Lacasse, M. A., Gaur, A., Lu, H., Laouadi, A., Ge, H., & Wang, L. (2022). Nature-Based Solutions (NBSs) to Mitigate Urban Heat Island (UHI) Effects in Canadian Cities. Buildings, 12(7), 925. https://doi.org/10.3390/buildings12070925

Healey, P. (2004). The Treatment of Space and Place in the new Strategic Spatial Planning in Europe. In B. Müller, S. Löb, & K. Zimmermann (Eds.), *Steuerung und Planung im Wandel: Festschrift für Dietrich Fürst* (pp. 297–329). VS Verlag für Sozialwissenschaften. https://doi.org/10.1007/978-3-322-80583-6_17

Heris, M. P., Muller, B., & Wilson, A. M. (2023). Why Does Planning Matter in Microclimate Management and Urban Heat Mitigation? *Journal of Planning Education and Research*, *43*(2), 371–387. https://doi.org/10.1177/0739456X19883000

Hou, H., Su, H., Yao, C., & Wang, Z (2023), Spatiotemporal patterns of the impact of surface roughness and morphology on urban heat island, Sustainable Cities and Society, 92, 104513, https://doi.org/10.1016/j.scs.2023.104513.

IPCC (2022). Climate Change 2022: Impacts, Adaptation, and Vulnerability. Contribution of Working Group II to the Sixth Assessment Report of the Intergovernmental Panel on Climate Change [H.-O. Pörtner, D.C. Roberts, M. Tignor, E.S. Poloczanska, K. Mintenbeck, A. Alegría, M. Craig, S. Langsdorf, S. Löschke, V. Möller, A. Okem, B. Rama (eds.)]. Cambridge University Press. Cambridge University Press, Cambridge, UK and New York, NY, USA, 3056 pp., https://doi,org/10.1017/9781009325844

Istituto Nazionale di Statistica (ISTAT) (2021). Italian population and housing census for 2021. [Dataset] https://esploradati.censimentopopolazione.istat.it/databrowser/#/it

Kabisch, N., Korn, H., Stadler, J., & Bonn, A. (2017). Nature-based solutions to climate change adaptation in urban areas: Linkages between science, policy and practice. Springer. https://doi.org/10.1007/978-3-319-56091-5

Kim, S. W., & Brown, R. D. (2021). Urban heat island (UHI) intensity and magnitude estimations: A systematic literature review. *Science of The Total Environment*, *779*, 146389. https://doi.org/10.1016/j.scitotenv.2021.146389

Kizielewicz, B., Shekhovtsov, A., & Sałabun, W. (2023). pymcdm—The universal library for solving multi-criteria decision-making problems. SoftwareX, 22, 101368. https://doi.org/10.1016/j.softx.2023.101368

Kotharkar, R., & Ghosh, A. (2022). Progress in extreme heat management and warning systems: A systematic review of heat-health action plans (1995-2020). *Sustainable Cities and Society*, *76*, 103487. https://doi.org/10.1016/j.scs.2021.103487

Liu, Z., Ma, X., Hu, L., Liu, Y., Lu, S., Chen, H., & Tan, Z. (2022). Nonlinear Cooling Effect of Street Green Space Morphology: Evidence from a Gradient Boosting Decision Tree and Explainable Machine Learning Approach. Land, 11(12). https://doi.org/10.3390/land11122220

Long, J., & Robertson, C. (2018). Comparing spatial patterns. *Geography Compass*, *12*(2), e12356. https://doi.org/10.1111/gec3.12356

Luo, J., Yao, Y., & Yin, Q. (2023). Analysis of Long Time Series of Summer Surface Urban Heat Island under the Missing-Filled Satellite Data Scenario. *Sensors*, *23*(22), 9206. https://doi.org/10.3390/s23229206

Meerow, S., & Newell, J. P. (2017). Spatial planning for multifunctional green infrastructure: Growing resilience in Detroit. Landscape and Urban Planning, 159, 62–75. https://doi.org/10.1016/j.landurbplan.2016.10.005

Morabito, M., Crisci, A., Gioli, B., Gualtieri, G., Toscano, P., Di Stefano, V., Orlandini, S., & Gensini, G. F. (2015). Urban-hazard risk analysis: Mapping of heat-related risks in the elderly in major Italian cities. PLOS ONE, 10(6), e0127277. https://doi.org/10.1371/journal.pone.0127277

Mosca, F., Calbi, M., Roccotiello, E., & Perini, K (2025). A computational approach to assess the effects of ecological building envelopes on outdoor thermal comfort, Sustainable Cities and Society, 120, 106170, https://doi.org/10.1016/j.scs.2025.106170

National Centers for Environmental Information (NOAA) (2024). Annual 2023 Global Climate Report. https://www.ncei.noaa.gov/access/monitoring/monthly-report/global/202313

Oliveira, V. (2022). *Urban Morphology: An Introduction to the Study of the Physical Form of Cities*. Springer International Publishing. https://doi.org/10.1007/978-3-030-92454-6

Pappalardo, S. E., Zanetti, C., & Todeschi, V. (2023). Mapping urban heat islands and heat-related risk during heat waves from a climate justice perspective: A case study in the municipality of Padua (Italy) for inclusive adaptation policies. Landscape and Urban Planning, 243, 104831. https://doi.org/10.1016/j.landurbplan.2023.104831

Patil, J., Maithani, S. & Sharma, S.K. (2025) Enhancing spatial resolution of Landsat derived land surface temperature: A novel downscaling approach using an extreme learning machine. *J Earth Syst Sci* **134**, 3, https://doi.org/10.1007/s12040-024-02457-2

Pedregosa, F., Varoquaux, G., Gramfort, A., Michel, V., Thirion, B., Grisel, O., Blondel, M., Prettenhofer, P., Weiss, R., Dubourg, V., Vanderplas, J., Passos, A., Cournapeau, D., Brucher, M., Perrot, M., Duchesnay, E. (2011). Journal of Machine Learning Research, 12, pp. 2825—2830. Retrieved from https://dl.acm.org/doi/10.5555/1953048.2078195

Pena Acosta, M., Dikkers, M., Vahdatikhaki, F., Santos, J., & Dorée, A. G. (2023). A comprehensive generalizability assessment of data-driven Urban Heat Island (UHI) models. *Sustainable Cities and Society*, *96*, 104701. https://doi.org/10.1016/j.scs.2023.104701

Privitera, R., & Jelo, G. (2025). Built Heritage Preservation and Climate Change Adaptation in Historic Cities: Facing Challenges Posed by Nature-Based Solutions. *Sustainability*, 17(13), 5693. https://doi.org/10.3390/su17135693

Rahman, A., & Pekkat, S. (2024). Identifying and ranking of CMIP6-global climate models for projected changes in temperature over Indian subcontinent. *Scientific Reports*, *14*(1), 3076. https://doi.org/10.1038/s41598-024-52275-1

Raj, S., & Yun, G. Y. (2023). Influence of selection of rural reference area for quantifying the surface urban heat islands intensity in major South Korean cities. *Architectural Science Review*, *67*(4), 345–356. https://doi.org/10.1080/00038628.2023.2290740

Reyes-Norambuena, P., Martinez-Torres, J., Nemati, A., Hashemkhani Zolfani, S., & Antucheviciene, J. (2024). Towards Sustainable Urban Futures: Integrating a Novel Grey Multi-Criteria Decision Making Model for Optimal Pedestrian Walkway Site Selection. *Sustainability*, *16*(11), 4437. https://doi.org/10.3390/su16114437

Sangiorgio, V., Fiorito, F., & Santamouris, M. (2020). Development of a holistic urban heat island evaluation methodology. *Scientific Reports*, *10*(1), 17913. https://doi.org/10.1038/s41598-020-75018-4

Santamouris, M. (2022). The Impact and Influence of Mitigation Technologies on Heat-Related Mortality in Overheated Cities. In N. Aghamohammadi & M. Santamouris (Eds.), *Urban Overheating: Heat Mitigation and the Impact on Health* (pp. 155–169). Springer Nature. https://doi.org/10.1007/978-981-19-4707-0_7

Schiavina, M., Moreno-Monroy, A., Maffenini, L., & Veneri P. (2023). GHS-FUA R2019A - GHS functional urban areas, derived from GHS-UCDB R2019A, (2015), R2019A.European Commission, Joint Research Centre (JRC) [Dataset] https://doi.org/10.2905/347F0337-F2DA-4592-87B3-E25975EC2C95

Schiavina, M., Moreno-Monroy, A., Maffenini, L., & Veneri P. (2023). GHS-FUA R2019A - GHS functional urban areas, derived from GHS-UCDB R2019A, (2015), R2019A.European Commission, Joint Research Centre (JRC) [Dataset] https://doi.org/10.2905/347F0337-F2DA-4592-87B3-E25975EC2C95

Setfane, H., Touhami, N.O. (2025). GIS and Multi-criteria Decision Analysis for Sustainable Urban Planning and Governance. In: Lagmiri, S.N., Lazaar, M., Amine, F.M. (eds) Smart Business and Technologies. ICSBT 2024. Lecture Notes in Networks and Systems, vol 1330. Springer, Cham. https://doi.org/10.1007/978-3-031-86698-2_47

Shekhovtsov, A., & Sałabun, W. (2020). A comparative case study of the VIKOR and TOPSIS rankings similarity. *Procedia Computer Science*, *176*, 3730–3740. https://doi.org/10.1016/j.procs.2020.09.014

Sidiqui, P., Roös, P. B., Herron, M., Jones, D. S., Duncan, E., Jalali, A., Allam, Z., Roberts, B. J., Schmidt, A., Tariq, M. A. U. R., Shah, A. A., Khan, N. A., & Irshad, M. (2022). Urban Heat Island vulnerability mapping using advanced GIS data and tools. *Journal of Earth System Science*, *131*(4), 266. https://doi.org/10.1007/s12040-022-02005-w

Stević, Ž., Subotić, M., Tanackov, I., Sremac, S., Ristić, B., & Simić, S. (2022). EVALUATION OF TWO-LANE ROAD SECTIONS IN TERMS OF TRAFFIC RISK USING AN INTEGRATED MCDM MODEL. *Transport*, *37*(5), Article 5. https://doi.org/10.3846/transport.2022.18243

Stewart, I. D. (2024). Origins and Evolution of the Local Climate Zone Classification. In R. Wang, M. Cai, C. Ren, & Y. Shi (Eds.), *Local Climate Zone Application in Sustainable Urban Development: Experience from East and Southeast Asian High-Density Cities* (pp. 19–33). Springer International Publishing. https://doi.org/10.1007/978-3-031-56168-9_2

Stewart, I. D., & Oke, T. R. (2012). Local Climate Zones for Urban Temperature Studies. *Bulletin of the American Meteorological Society*, *93*(12), 1879–1900. https://doi.org/10.1175/BAMS-D-11-00019.1

Szagri, D., Nagy, B., & Szalay, Z. (2023). How can we predict where heatwaves will have an impact? – A literature review on heat vulnerability indexes. *Urban Climate*, *52*, 101711. https://doi.org/10.1016/j.uclim.2023.101711

Tarquini S., I. Isola, M. Favalli, A. Battistini, & G. Dotta (2023). TINITALY, a digital elevation model of Italy with a 10 meters cell size (Version 1.1). Istituto Nazionale di Geofisica e Vulcanologia (INGV). https://doi.org/10.13127/tinitaly/1.1.

UNDRR and UNU-EHS (2023), Nature-based Solutions for Comprehensive Disaster and Climate Risk Management, United Nations Office for Disaster Risk Reduction. Retrieved from https://www.undrr.org/publication/nature-based-solutions-comprehensive-disaster-and-climate-risk-management

United Nations. (2015). *Transforming our world: The 2030 Agenda for Sustainable Development* (A/RES/70/1). United Nations General Assembly. https://sdgs.un.org/goals

Wang, J., Fleischmann, M., Venerandi, A., Romice, O., Kuffer, M., & Porta, S. (2023). EO + Morphometrics: Understanding cities through urban morphology at large scale. *Landscape and Urban Planning*, *233*, 104691. https://doi.org/10.1016/j.landurbplan.2023.104691

Wong, N. H., Tan, C. L., Kolokotsa, D. D., & Takebayashi, H. (2021). Greenery as a mitigation and adaptation strategy to urban heat. Nature Reviews Earth & Environment, 2(3), 166–181. https://doi.org/10.1038/s43017-021-00133-5

Zhou, D., Xiao, J., Bonafoni, S., Berger, C., Deilami, K., Zhou, Y., Frolking, S., Yao, R., Qiao, Z., & Sobrino, J. A. (2019). Satellite Remote Sensing of Surface Urban Heat Islands: Progress, Challenges, and Perspectives. *Remote Sensing*, *11*(1), 48. https://doi.org/10.3390/rs11010048

Chapter 6.

Downscaling spatial analysis to the streetscape level: obtaining 3D urban canyons from opensource data enhancing multiscale simulations

Abstract

This chapter introduces a reproducible conversion model that downscales city-scale urban data to the streetscape level, generating three-dimensional canyon geometries suitable for building-scale analyses such as CFD-based microclimate simulations. Two methodologies for canyon extraction are compared: a street-based approach, which derives canyon profiles from OpenStreetMap data using momepy, and a building-based approach, which identifies canyons through spatial relationships between building façades. The chapter makes two key contributions:

i. A systematic benchmarking of both algorithms across two case studies (Genoa and Turin), showing that the building-based approach produces richer outputs without added computational complexity.

ii. The introduction of a classification scheme that discretizes canyon geometries into nine height–width classes, enabling comparative morphological analysis and integration with microclimate modelling.

By embedding canyon extraction within a reproducible framework, the chapter advances the linkage between urban morphology and climate simulations, offering a scalable pathway from city-level indicators to localized canyon analyses and supporting multiscale approaches to urban heat mitigation. Additionally, the inputs and outputs of this chapter respectively feed from and are fed into the pipelines from Chapter 5 and 7, demonstrating their immediate application and the functionality of the developed components.

Keywords

urban canyon; downscaling; graph analysis

Acknowledgements

Preliminary results of the Chapter were presented at the Mediterranean Green Forum (MDF26, Florence, 09/04/2026).

6.1. Introduction

Urban morphology provides the conceptual and methodological foundation for deriving three-dimensional canyon geometries from city-scale datasets. The geometry of street canyons, defined by building height, street width, and orientation, directly influences solar access, ventilation, and thermal exchanges. Classical morphological indicators such as the height-to-width ratio (H/W), sky view factor (SVF), and building view factor (BVF) remain central to the characterization of canyon form and its climatic implications (Gong, 2025). These parameters not only describe the enclosure of the canyon but also determine the radiative and aerodynamic regimes that govern microclimatic conditions.

The derivation of 3D canyon geometries increasingly relies on open-source geospatial data and automated modelling workflows. Building footprints and heights from repositories such as OpenStreetMap can be extruded into volumetric representations, while digital surface models and LiDAR acquisitions provide higher-resolution inputs for capturing façade complexity and roof structures. GIS-based methods, including the use of the *r.sun* (https://grass.osgeo.org/grass-stable/manuals/r.sun.html) module in GRASS GIS, enable the integration of morphological parameters with solar radiation modelling, thereby linking canyon geometry to energy and comfort outcomes (Anselmo et al., 2024).

Parametric modelling environments further expand the capacity to generate and manipulate canyon geometries. Grasshopper, integrated with Rhinoceros 3D, allows for the rapid prototyping of canyon cross-sections and their systematic variation across morphological parameters. The Ladybug Tools suite extends this functionality by embedding validated environmental engines within the design environment, enabling reproducible workflows that couple geometry generation with simulation (Sadeghipour Roudsari et al., 2013). Such parametric approaches are particularly valuable for sensitivity analyses, where multiple canyon configurations can be tested against climatic indicators.

The methodological challenge lies in ensuring that these 3D canyon models remain consistent across scales. While city-scale models emphasize aggregated morphological descriptors, CFD-based analyses require explicit canyon geometries with sufficient resolution to capture flow separation, turbulence, and radiative exchanges. Validation studies, such as those employing transect measurements across intra-urban canyons, demonstrate the importance of aligning morphological derivation with observed microclimatic variability (De Quadros et al., 2024).

In sum, the creation of 3D canyons from urban morphology involves a multi-step process: (i) extraction of building and street geometries from open data, (ii) derivation of morphological indicators, (iii) extrusion and volumetric modelling of canyon forms, and (iv) integration with simulation environments. This workflow provides a reproducible bridge between urban morphology and microclimate modelling, ensuring that canyon-scale processes are represented within multiscale urban analyses.

This chapter introduces a conversion model designed to downscale urban data obtained in Chapter 5 to the streetscape level, producing three-dimensional canyon geometries suitable for CFD-based microclimate simulations. The approach emphasizes methodological reproducibility, aiming to bridge the gap between city-scale indicators and localized canyon modelling. The following sections outline the methodology for this conversion, while the subsequent chapter (Chapter 7) demonstrates its application for microclimate simulations.

6.2. Methodology

6.2.1. Definition of an Urban Canyon

An *urban canyon* is the linear void space formed by buildings along a street, bounded laterally by façades and vertically by building heights. Its geometry and radiative properties are described through a set of parameters that influence microclimate, energy exchange, and pollutant dispersion. Table 1 describes the parameters that are commonly used in urban climate literature.

Table 1. Urban canyon parameters often used in urban microclimate modelling.

Parameter	Mathematical expression	Notes
Height-to-width ratio (H/W). The ratio between average building height and street width, used to quantify the degree of enclosure. A higher H/W ratio typically reduces solar access and wind penetration, intensifying heat retention and pollutant concentration (Oke, 1988; Grimmond & Oke, 1999).	$\frac{H}{W}$	H = average building height. W = street width perpendicular to façades.
Length and **continuity**. The longitudinal extent of the canyon and its morphological consistency. Finite canyons with interruptions (e.g. intersections, setbacks) exhibit different ventilation and dispersion dynamics compared to idealized infinite canyons (Eliasson, 1996).	$L = \sum_{i=1}^{n} l_i$ $C_i \in \{0,1\}$	L = total canyon length. C_i = binary indicator for uninterrupted segments.
Orientation. The azimuthal alignment of the canyon axis, which governs the timing and intensity of solar exposure. East–west canyons receive more direct sunlight during midday, while north–south orientations experience more diffuse and seasonal variation (Eliasson, 1996).	$\theta = \arctan\left(\frac{\Delta y}{\Delta x}\right)$	θ = Azimuthal angle of the street axis, typically measured from North.
Sky View Factor (SVF). The proportion of visible sky from a point within the canyon, expressed as a fraction of the hemispherical dome. SVF is a key indicator of radiative exchange, influencing nocturnal cooling, longwave radiation loss, and thermal comfort (Unger, 2004; Yang & Li, 2015).	$SVF = \cos^2\left(\arctan\frac{H}{W}\right)$	The SVF is computed as the fraction of the hemisphere that remains visible relative to the observation point (in this simplified formula, at pedestrian eye height equal to ~ 1.5-2m above ground).

Tree View Factor (TVF). The proportion of the view obstructed by vegetation, particularly tree canopies. TVF affects shading, evapotranspiration, and pollutant absorption, and is increasingly used to assess ecosystem services in urban streetscapes (Gong et al., 2018).	$TVF = \frac{A_{tree}}{A_{hemisphere}}$	A_{tree} = projected area of the tree canopy visible in the hempispherical dome. $A_{hemisphere}$ = total hemispherical area.
Building View Factor (BVF). The fraction of the hemispherical field of view occupied by building façades. BVF complements SVF by quantifying radiative trapping and longwave emission from built surfaces, especially in high-density environments (Gong et al., 2018).	$BVF = 1 - SVF - TVF$	Assuming hemispherical closure so that sky + tree + building = 1.
Openness. A perceptual and geometric measure of how "open" the canyon appears, often derived from SVF or modified aspect ratios. Openness influences pedestrian comfort, visual permeability, and perceived safety (Yang & Li, 2015).	$O_{geometric} = \frac{W}{H}$ $O_{perceptual} = \frac{1}{1 + e^{-\alpha(SVF-\beta)}}$	Can be geometric (inverse of H/W) or perceptual (SVF-based). SVF ∈ [0,1]; $\alpha$is a sensitivity parameter (steepness of the curve); β is a perceptual threshold (the SVF value at which openness is perceived as "balanced").

These parameters together provide a multidimensional description of canyon morphology, enabling more realistic microclimate modelling and CFD simulations.

6.2.2. Input data and preprocessing

The data used in this Chapter is tied to the results of the previous Chapter (Table 2). Specifically, streets and building data that was optimized through a pruning and cleaning process (e.g., using Neatnet algorithms to simplify the networks). Notably, data on building height was averaged through the spatial modules used in the previous chapter. While this information is valuable at urban scale, it's not precise enough to downscale. Therefore, the same data (Urban Atlas Building Height 2012 layer at 10m resolution) is used, by directly associating buildings in vector shape via zonal statistics to get accurate measurements.

Table 2. Data used in the canyon conversion model.

Parameter	Methodological notes on preprocessing	Reference
Streets geometry	Graph network of streets, simplified through the use of the Neatnet algorithms.	Open Street Maps /streets (mayor streets only, no tunnels)
Buildings plots	Vector shapes of buildings plots.	Open Street Maps /buildings
Building height	Raster data at 10m, reprojected and extracted through mean zonal statistics on Buildings plots.	Urban Atlas Building Height 2012 (CLMS, 2022)
Masking geometry	Urban tissues defined in Chapter 4 that act as masking tools to identify relevant areas. In the case of Chapter 4 and this application, areas with high risk related to Surface Urban Heat Island are considered.	Chapter 4 of this thesis.

With this data, two methodologies are presented and confronted to retrieve urban canyons. The first uses a simplified methodology rooted around OSM street geometry to associate a 3D canyon to each street segment with surrounding buildings. The second methodology conversely assumes that street geometries are unnecessary to define canyon; therefore, it considers the space between opposing edges of buildings as canyon using a neighbouring graph.

6.2.3. Street-based approach – Using momepy’s Street Profile

The first approach relies on the momepy package to retrieve urban canyons through street profiles. A street profile is a cross-sectional representation of the built environment along a street axis. It describes the spatial relationship between the street centreline (the canyon ”bed”) and the adjacent building façades (the canyon “walls”).

The procedure begins with a preparation step in which the input layers (urban tissue derived from Chapter 4 used as masking geometry, building footprints, street centrelines, and building height data) are harmonized into a consistent spatial framework. To reduce computational load, a sampling percentage can be applied so that only a subset of polygons is processed.

Once the geometry is prepared, the momepy.street_profile function is applied. This tool generates cross-sections perpendicular to the street axis at regular intervals (here, every 10 metres). Each cross-section extends up to a fixed maximum width of 40 metres, ensuring comparability with canyon simulations used in Chapter 7. For every tick, the function measures the distance between opposing façades and records the corresponding building heights. These measurements are then aggregated to produce a statistical profile of each street segment.

The resulting descriptors (width, openness, width deviation, height, height deviation, height-to-width-ratio) are written back into the street dataset. In this way, each street segment is enriched with a compact set of morphological indicators that describe its canyon geometry. Both the street and building layers are then saved in parquet format, ready for visualization or further analysis.

6.2.4. Building-based approach – Using the neighbourhood graph

In this second approach, the urban canyon is derived from the spatial relationships between buildings, rather than from the street network. The assumption tries to go beyond the network dependency of the street-based-method by considering previously unnoticed canyons, while also providing a more accurate representation of the canyon bed shape.

The building-based approach begins by constructing a neighbourhood graph that represents the spatial relationships between all buildings in the study area (considering masked-off areas and building data as for the previous method). This is achieved through a Delaunay triangulation of building centroids, which ensures that each building is connected to its nearest neighbours. The resulting graph provides a dense web of potential canyon axes, unconstrained by the presence or absence of mapped streets (Fig. 1).

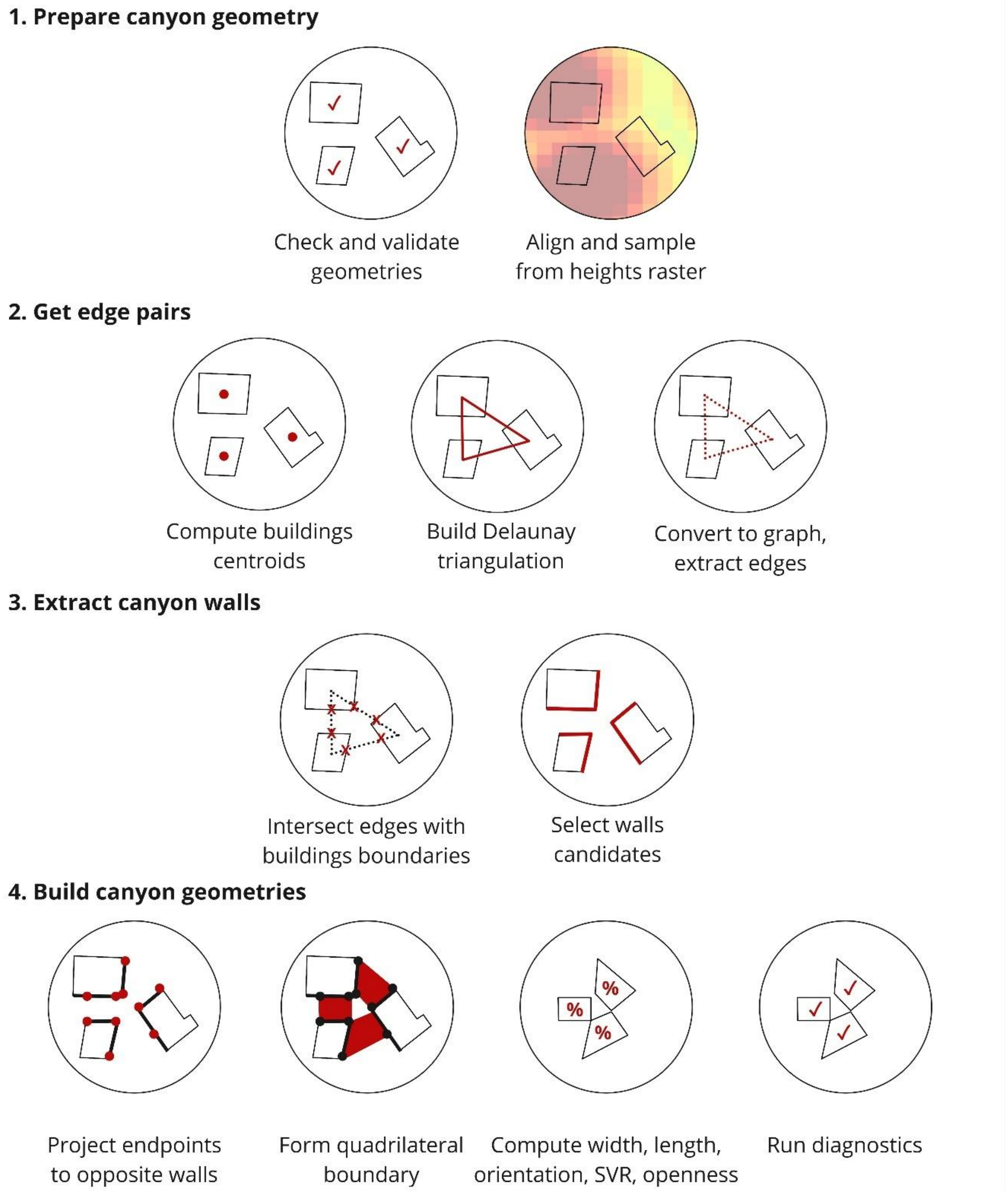

Figure 1. Building-based approach methodology.

From the neighbourhood graph, each edge connecting two building centroids is treated as a candidate axis for a potential canyon (i.e., the axis parallel to a canyon width). For every such pair, the algorithm does not simply assume a uniform façade alignment; instead, it explicitly searches the polygonal boundaries of both buildings to identify the two wall segments that are most likely to act as opposing canyon walls. This is achieved by iterating through all polygon edges of each building, calculating the minimum distance between candidate segments, and testing their relative orientation. Only those pairs of edges that are approximately parallel (within a specified angular tolerance[10]) are retained, ensuring that the resulting canyon reflects a realistic geometric enclosure rather than an arbitrary connection.

Once the two facing walls are identified, they are projected against one another to construct a closed quadrilateral that represents the canyon cross-section. This quadrilateral is not constrained to be rectangular: because the method works directly with the actual geometry of building façades, it can accommodate irregular alignments, skewed orientations, and non-orthogonal intersections. As a result, the approach can capture canyon-like spaces that deviate from the idealized "street canyon" form, including tapered alleys, angled courtyards, or asymmetric passages.

Within this constructed geometry, the principal canyon descriptors are then derived. The width is measured as the distance between the midpoints of the opposing walls, while the length is calculated along the axis defined by the centroid-to-centroid connection. The orientation of the canyon is expressed as the azimuth of this axis, normalized to the range [0,180). Building heights are retrieved for each pair, allowing the computation of an average height and the corresponding height-to-width ratio. Additionally, both SVF and Openness are computed following the formulae in Table 1, based on mean height and width. To ensure robustness, the method incorporates diagnostic checks that flag invalid geometries (e.g. self-crossing quadrilaterals), zero dimensions, or missing wall segments.

[10] In practice, two walls are facing one another when their orientations are sufficiently close to parallel. This is assessed by comparing the azimuth of each façade segment and allowing for a small margin of deviation, typically set at around 10 degrees. In other words, a façade oriented at 90° (east–west) can be paired with another oriented anywhere between 80° and 100°, or equivalently between 260° and 280°. This tolerance ensures that façades which are not perfectly aligned but still broadly parallel can be paired, reflecting the irregularities of real urban form where buildings rarely follow exact orthogonal grids. By applying this criterion, the algorithm can identify opposing walls even when they are slightly skewed, enabling the construction of canyon geometries that are not limited to idealized rectangles but also encompass trapezoidal, angled, or otherwise non-rectangular spaces.

6.3. Results and discussion

6.3.1. Confronting the two approaches

Although the street-based approach was supposed to be more rapid than the building-based approach, since it only utilized the momepy.street_profile function, the resulting runtime proved different. The functions were run ten times each, and the average runtime was calculated. This step took into consideration the fact that both functions are deterministic and accounting for system-level noise, following established micro-benchmarking methodologies (Laaber, 2021). By testing the algorithms on Genoa's and Turin's streets networks and buildings, the combined average runtime was 10m43s for the street-based approach (319s for Genoa and 321s for Turin), and 9m27s for the building-based approach (4m44s for Genoa and 4m43s for Turin), thus making the building-based approach the faster algorithm, albeit by a small factor (643s/567s). Nevertheless, it is worth further investigating the differences between the two approaches separately.

6.3.2.1. Street-based approach

The street-based approach is less efficient due to its longer runtime, and it is shaped by several structural assumptions that restrict its scope. The most fundamental is its dependence on the street network. The method only identifies canyons where two buildings face one another across a mapped street segment. This means that many canyon-like spaces such as courtyards, plazas, or pedestrian alleys, are excluded if they are not represented as streets in the source data. The approach therefore privileges the linearity of the street system, while other forms of urban enclosure remain invisible.

A second limitation is the fixed maximum width threshold. In this implementation, cross sections are capped at 40 metres, a value chosen to ensure consistency with subsequent simulation frameworks. While this facilitates comparability, it also truncates very wide boulevards or open avenues, underrepresenting their geometry. The issue is not unique to the chosen threshold: any fixed maximum width imposes a simplification on spaces that may be broader and more complex.

The method is also sensitive to the quality and alignment of the street network data. Bejcause widths are measured relative to the street axis, misplaced or incomplete street lines can directly bias results. This sensitivity is greater than in building-based approaches, where the façades themselves provide the reference. If the street line is offset from the actual physical bed of the canyon, the calculated widths may be systematically distorted.

Another important constraint is the reduction of geometry to averages and deviations. The street profile condenses complex cross-sections into mean widths, mean heights, and their respective variabilities. While this produces a compact descriptor, it inevitably smooths out local irregularities such as setbacks, arcades, balconies, or overhangs, which may be climatically or socially significant but are not explicitly represented in the output.

Finally, the method's network dependency limits its ability to capture the full diversity of urban voids. Because all profiles are tied to mapped street segments, the approach cannot detect canyon-like spaces that fall outside the street graph. As a result, the method provides a robust but partial view of urban morphology: it excels at describing conventional street canyons, but it systematically excludes other forms of enclosure that may be equally relevant to urban climate or design studies.

6.3.2.2. Building-based approach

The building-based method approach offers greater flexibility than the street-based method. Nevertheless, it is still accompanied by several important limitations. The algorithm can elevate the number of considered canyons by studying the potential canyon relationships between all neighbouring buildings, while remaining less time- and memory-demanding than the street-based approach. The following figures show urban canyons obtained with this methodology in Genoa (Fig. 2) and Turin (Fig. 3).

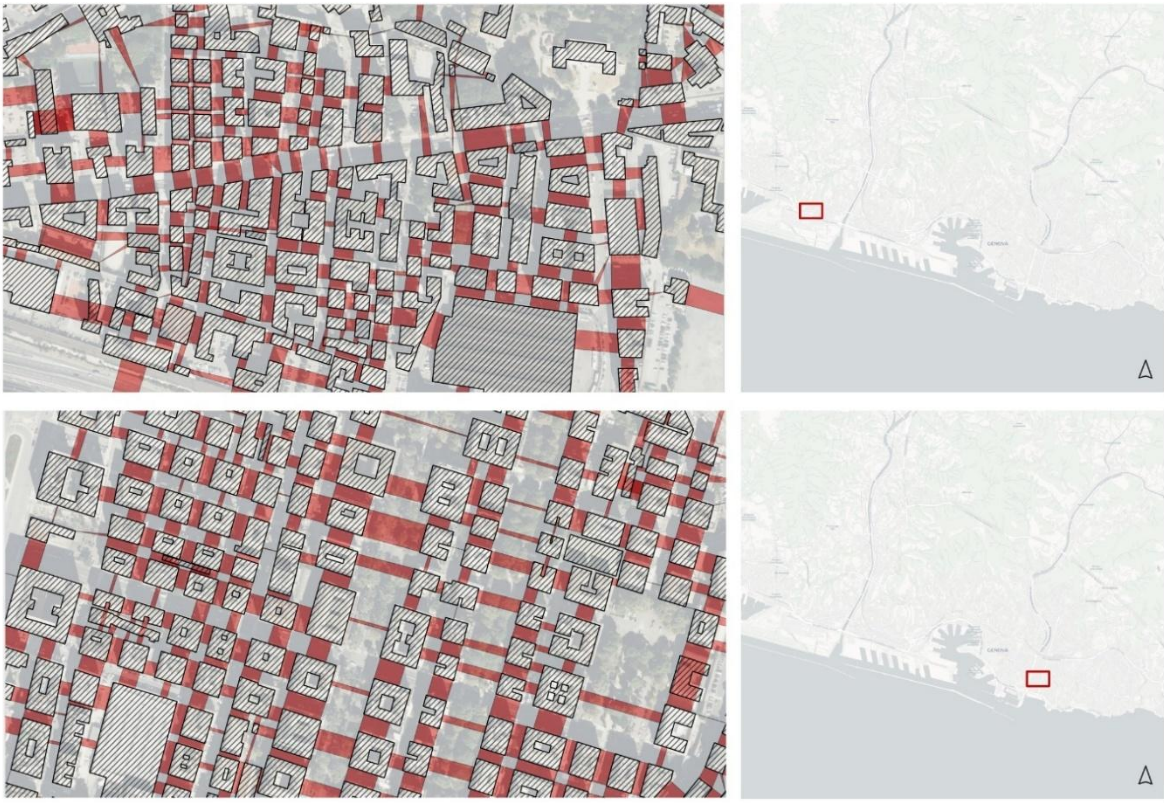

Figure 2. Canyons in Genoa, in Cornigliano area (top) and Foce (bottom), both areas marked as "high risk" as for the site selection methodology introduced in Chapter 5.

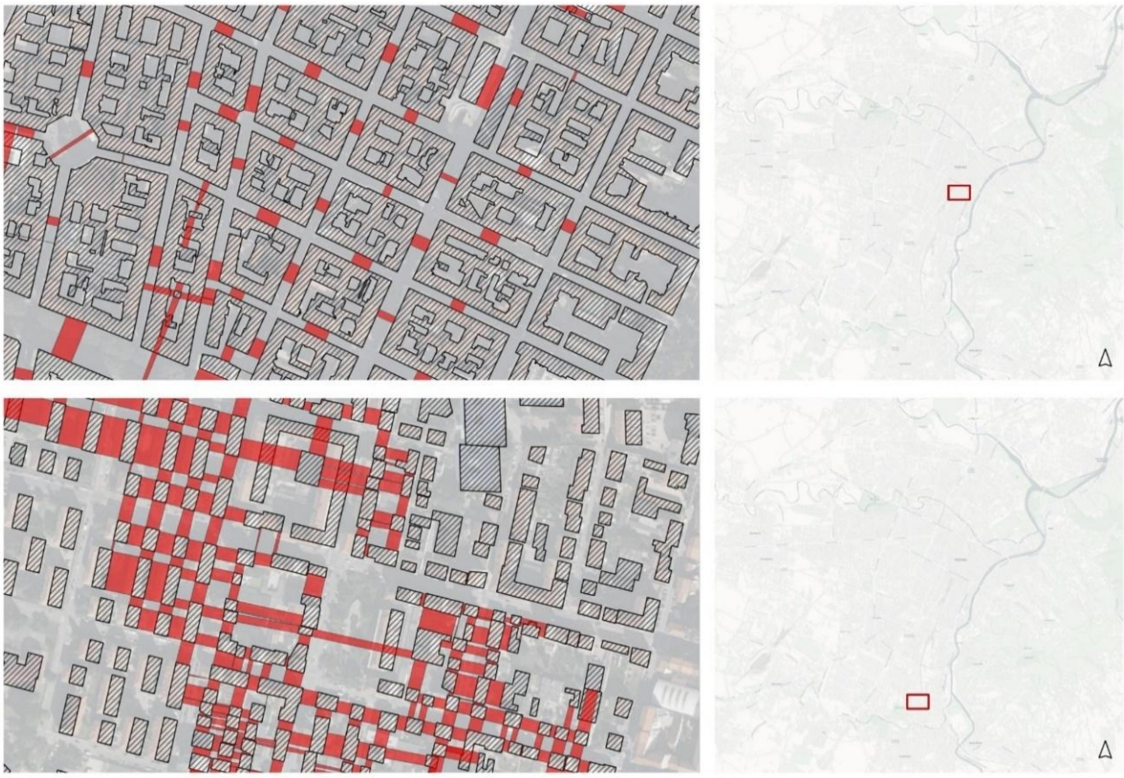

Figure 3. Canyons in Turin, in San Salvario area (top) and Lingotto (bottom), both areas marked as "high risk" as for the site selection methodology introduced in Chapter 5.

The approach outputs are richer than the one from the street-based method. The u_line and v_line (respectively the parallel and perpendicular directives of the canyon), together with the canyon 2D bed are provided, instead of the sole u_line. Additionally, the output works with discrete measurements, giving the modelling true height and width values of the walls.

Nevertheless, a crucial limitation lies in its sensitivity to parameter choices, particularly the angular tolerance used to define "facing" walls. If the tolerance is set too narrowly, valid canyons may be excluded; if it is too broad, the algorithm may generate spurious pairings between façades that are not truly parallel. Similarly, the reliance on Delaunay triangulation means that some centroid-to-centroid connections may not correspond to meaningful urban spaces, requiring careful filtering and diagnostic checks. This can be partially solved by putting a cap to canyon width, ultimately pruning all Delaunay edges that are too long in practice.

The method also produces outputs of greater geometric complexity. Because it is not tied to the street graph, it can identify overlapping or nested canyon geometries. For example, a courtyard within a block may be detected alongside a larger canyon enclosing the same space. While this richness captures the diversity of urban form, it also complicates interpretation and may require post-processing to avoid redundancy. And, as with all morphometric techniques, the approach is highly dependent on data quality. Inaccuracies in building footprints or height attributes propagate directly into canyon descriptors, potentially biasing results.

6.3.2. Downscaling to the street-level

The results in this chapter obtained geospatial information on urban canyon geometry. As for this chapter objective, this information can be fed into street-scale, directly providing accurate morphological information for building urban canyon models. Here, the results are grouped into classes by separating canyons using the mean height (H) and width (W) using thresholds (Table 3).

Table 3. Thresholds for canyon classification based on H_avg and W

	W10 (≤ 17.5 m)	**W25** (17.5–32.5 m)	**W40** (> 32.5 m)
H10 (≤ 17.5 m)	H10-W10	H10-W25	H10-W40
H25 (17.5–32.5 m)	H25-W10	H25-W25	H25-W40
H40 (> 32.5 m)	H40-W10	H40-W25	H40-W40

These thresholds are further explored in Chapter 7 as they represent the parameters for urban canyon-scale shading simulations. The following figures shows the canyons in Genoa (Fig. 4) and Turin (Fig. 5).

The results can be visualized by counting the canyons in Genoa and Turin and grouping them by classes value (Fig. 6).

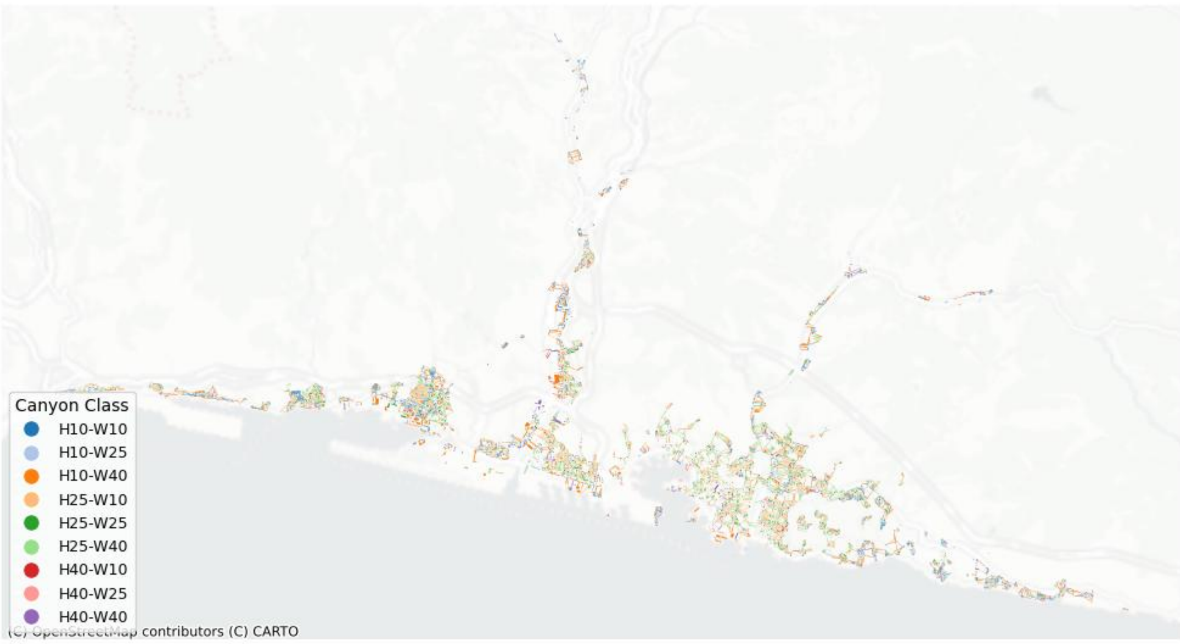

Figure 4. Canyons in Genoa high-risk areas for SUHI-related health risks, classified by W and H_avg values.

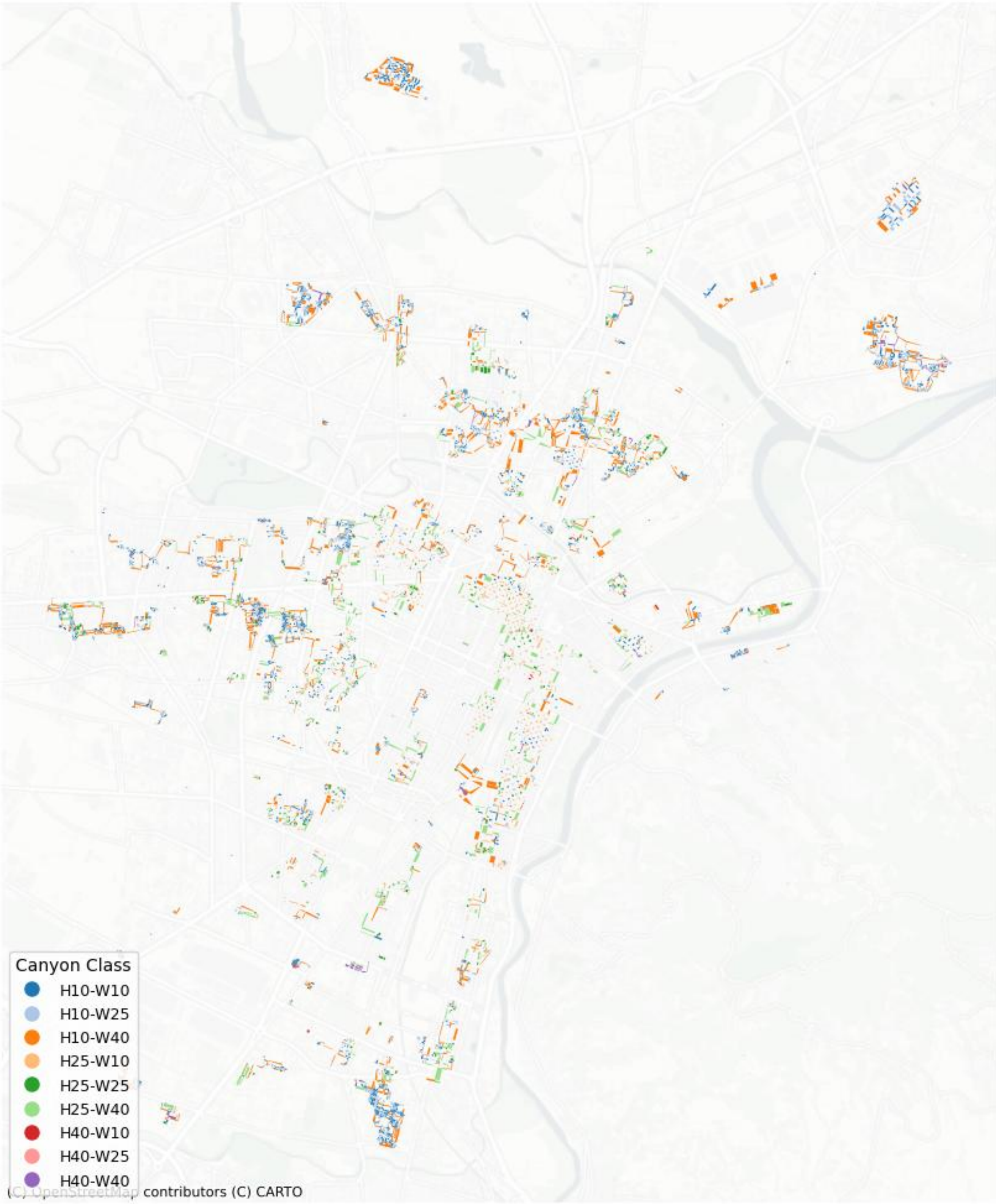

Figure 5. Canyons in Turin high-risk areas for SUHI-related health risks classified by W and H_avg values.

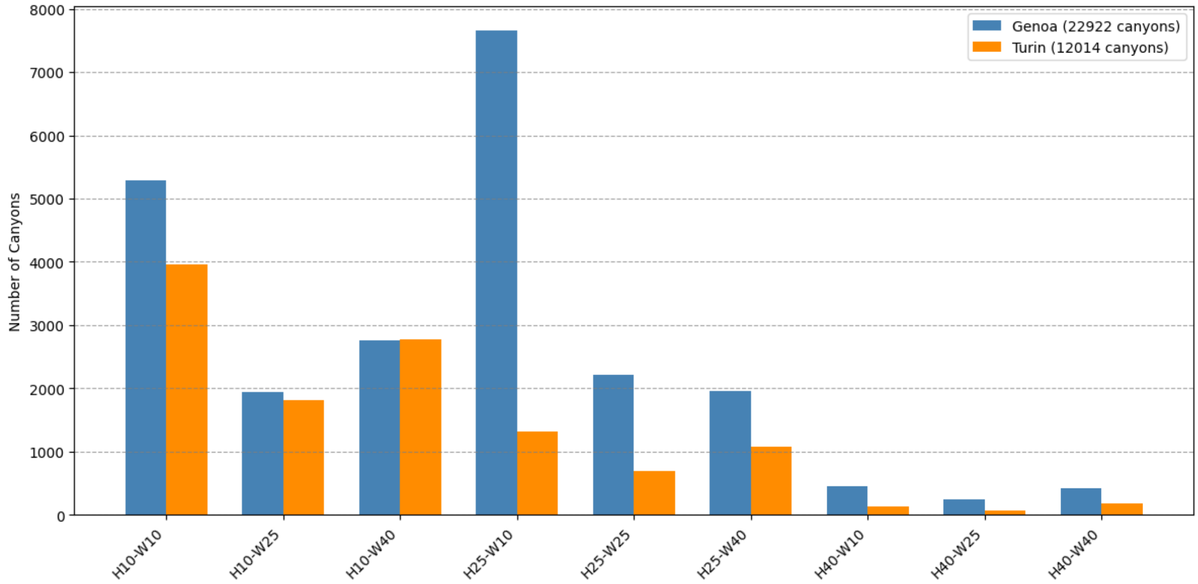

Figure 6. Canyon classes distribution in Genoa (blue) and Turin (Orange)

The analysis of canyon in high-risk areas for SUHI-related health risk distributions reveals marked differences between Genoa and Turin, reflecting their distinct urban morphologies. In Genoa, where a total of 22,922 canyons were identified, the most frequent configuration is H25-W10 (7,656 canyons), pointing to a prevalence of medium-rise buildings aligned along narrow street corridors. This dominance is complemented by substantial shares of H10-W10 (5,292) and H10-W40 (2,753), which highlight the persistence of low-rise canyons in both compact and wider forms. Overall, Genoa's profile suggests a dense and vertically constrained morphology, consistent with its hillside urban structure. Turin, by contrast, with 12,014 canyons, is characterized by a predominance of H10-W10 (3,957 canyons), underscoring the prevalence of low-rise, narrow canyons. While low-rise categories (H10-*) are well represented, medium-rise canyons (H25-*) are comparatively scarce, amounting to only about 3,000 cases against nearly 12,000 in Genoa. Tall canyons (H40-*) remain rare in both cities, though Genoa exhibits proportionally more. Taken together, these distributions illustrate how Genoa's compact, medium-rise canyon typology contrasts with Turin's flatter, more open street morphology, reflecting the relative influence of urban forms.

6.4. Conclusions

This chapter introduced a conversion model designed to bridge city-scale indicators and localized canyon geometries, enabling downscaling for building-scale analysis such as CFD-based microclimate simulations. Two methodologies were confronted: a street-based approach, which derives canyons from OSM street profiles, and a building-based approach, which identifies canyons through spatial relationships between building façades. While the street-based method offers a straightforward link to mapped street segments, its dependence on the network, fixed width thresholds, and sensitivity to data alignment limit its scope and efficiency. The building-based method, conversely, proved more flexible without added computational complexity, producing richer outputs that capture a wider diversity of urban voids, though at the cost of greater geometric complexity and sensitivity to parameter choices. This process underscores the importance of introducing flexibility in downscaling approaches, enabling simple building-scale selection of important simulation data within a reproducible framework. Thus, the chapter naturally follows the city-scale analysis of Chapter 5, laying the groundwork for the street-scale simulations presented in the next chapter.

This chapter introduced a conversion model for downscaling city-scale morphology to streetscape-level canyon geometries, directly applying it by inserting it in the analytical pipeline brought forth by Chapter 5 and 7 bridging urban indicators and building-scale simulation. By confronting a street-based approach (momepy street profiles) with a building-based approach (neighbourhood graph of façades), the work clarifies what each method affords, how their constraints shape outputs, and why canyon modelling matters for multiscale urban climate analysis. Thus, several considerations arise:

i. The street-based method, implemented through momepy profiles, provides standardized descriptors of conventional corridors. It is effective for rapid prototyping and for capturing the geometry of mapped street segments, but its reliance on the street network and fixed width thresholds limits its scope. Wider areas such as boulevards and plazas, or specifically non-mapped spaces are underrepresented, and the reduction of complex cross-sections into averages smooths out local irregularities.

ii. The building-based method, derived from neighbourhood graphs of façades, produces richer outputs. It captures true height and width values, identifies irregular canyon forms such as alleys and courtyards, and proved slightly faster in runtime. However, it is sensitive to parameter choices, particularly angular tolerance, and requires careful filtering to avoid spurious connections. Its geometric richness can also complicate interpretation, sometimes producing overlapping or nested canyon geometries.

iii. A discretization into nine height–width classes transform raw canyon geometries into interpretable categories. This scheme enables systematic comparison across cities and provides simulation-ready inputs for microclimate analysis workflows (Chapter 7). By bridging morphological analysis with modelling requirements, it ensures that canyon-scale processes can be consistently integrated into multiscale urban climate studies.

iv. The application to Genoa and Turin revealed distinct morphological profiles. Genoa is dominated by medium-rise, narrow canyons (H25–W10), reflecting its dense hillside structure, while Turin shows a prevalence of low-rise, narrow canyons (H10–W10), consistent with its flatter, more open street morphology. These contrasts highlight how canyon typologies expose climatic diversity and influence heat risk distributions.

The conversion model establishes a reproducible bridge from city-scale indicators to localized canyon simulations, strengthening the integration of urban morphology and climate modelling, and supporting (but not limited to) heat-mitigation strategies. Future refinements should focus on parameter calibration and filtering of canyon geometries, as well as validation across diverse urban areas.

6.5. References

Anselmo, S., Safaeianpour, A., Torabi Moghadam, S., & Ferrara, M. (2024). GIS-based solar radiation modelling for photovoltaic potential in cities: A sensitivity analysis for the evaluation of output variability range. Energy Reports, 12, 4656–4669. https://doi.org/10.1016/j.egyr.2024.10.031

De Quadros, B. M., Pigliautile, I., Pisello, A. L., Krüger, E., & Mizgier, M. O. (2024). Reliability of urban microclimate simulations: Spatio-temporal validation through intra-urban canyon transects for outdoor thermal comfort analysis. International Journal of Biometeorology, 68(9), 2715–2729. https://doi.org/10.1007/s00484-024-02784-5

Eliasson, I. (1996). Urban nocturnal temperatures, street geometry and land use. *Atmospheric Environment*, *30*(3), 379–392. https://doi.org/10.1016/1352-2310(95)00033-X

Gong, F. Y., Zeng, Z. C., Zhang, F., Li, X., Ng, E., & Norford, L. K. (2018). Mapping sky, tree, and building view factors using Google Street View images. *Building and Environment*, *134*, 90–100. https://doi.org/10.1016/j.buildenv.2018.02.042

Gong, F.-Y. (2025). Urban canyon morphology and solar radiation dynamics. In Street Sensing (pp. 15–28). Springer. https://doi.org/10.1007/978-3-031-92005-9_2

Grimmond, C. S. B., & Oke, T. R. (1999). Aerodynamic properties of urban areas derived from analysis of surface form. *Journal of Applied Meteorology*, *38*(9), 1262–1292. https://doi.org/10.1175/1520-0450(1999)038<1262:APOUAD>2.0.CO;2

Laaber, C. (2021). *Deliberate microbenchmarking of software systems* (Doctoral dissertation, University of Zurich). University of Zurich. https://capuana.ifi.uzh.ch/publications/PDFs/21054_cl-phd-thesis-final.pdf

Oke, T. R. (1988). Street design and urban canopy layer climate. *Energy and Buildings, 11*(1–3), 103–113. https://doi.org/10.1016/0378-7788(88)90026-6

Sadeghipour Roudsari, M., Pak, M., & Smith, A. (2013). Ladybug: A parametric environmental plugin for Grasshopper to help designers create an environmentally-conscious design. *Proceedings of Building Simulation 2013: 13th Conference of IBPSA*, 3128–3135. International Building Performance Simulation Association. https://doi.org/10.26868/25222708.2013.2499

Unger, J. (2004). Intra-urban relationship of air temperature and sky view factor. *Climate Research, 27*(3), 253–263. https://doi.org/10.3354/cr027253

Yang, X., & Li, Y. (2015). The impact of building density and building height heterogeneity on average urban albedo and street surface temperature. *Building and Environment*, *90*, 146–156. https://doi.org/10.1016/j.buildenv.2015.03.037

Chapter 7.

Multiscale optimization of Nature-Based Solutions for heat mitigation

Abstract

Urban areas are increasingly exposed to climate change, with heatwaves posing some of the most severe risks to ecosystems, infrastructure, and human health. These risks are particularly acute in urban canyons, i.e., the street corridors formed by buildings, where geometry and orientation amplify overheating and reduce thermal comfort. Nature-Based Solutions (NBS) are promoted internationally as effective strategies to mitigate these impacts and enhance resilience. Yet their deployment is often constrained by limited planning frameworks and insufficient evidence of performance. Existing simulation tools, while informative, require high computational resources and site-specific modelling of NBS configurations, making them difficult to scale. This chapter applies Machine Learning (ML) to reduce reliance on repeated simulations and to generalize performance outcomes across the Italian territory. In doing so, the chapter achieves the following outcomes:

i. Identification and extension of correlations between urban canyon morphology, site geography, and the effectiveness of NBS through computational simulations.

ii. Reduction of simulation dependence, by demonstrating how Machine Learning (ML) can reduce reliance on repeated, resource-intensive simulations by generalizing performance outcomes across the Italian territory.

iii. Identification of the most effective NBS (limiting to trees-based designs), for different combinations of canyon geometries and geographic location.

iv. The results can be combined with the site selection methodology introduced in Chapter 5 and 6, employing a network-based framework structured around street networks and buildings to directly link site characterization with urban canyon geometry. This integration positions the approach as a pathway toward more scalable and integrated planning for urban climate adaptation and resilience.

Keywords

urban heat mitigation; multicriteria optimization; regression analysis

Acknowledgements

The author expresses sincere thanks to Francesca Mosca (Department of Architecture and Design, University of Genoa) for her continuous support and her valuable contribution to the conceptualization and shaping of the methodology, as well as for the inspiring discussions that brought both clarity and delight to the development of this work.

The author also gratefully acknowledges Silvia Villa (MalGA, University of Genoa) for her expertise in critically reviewing the machine learning outcomes and for the stimulating mathematical discussions that not only strengthened the work but also gave the author great satisfaction.

Preliminary results from this Chapter have been published as research articles (https://dx.doi.org/10.36253/techne-16560; https://doi.org/10.1016/j.ufug.2026.129457). Additionally, results were presented at the Networks Markets People symposium (NMP26, Reggio Calabria, 29/05/2026).

7.1. Introduction

7.1.1. Outdoor thermal comfort in urban canyons and mitigation strategies

Urban environments today are increasingly characterized by complex and interrelated challenges that stem from anthropogenic activities and the global expansion of cities (United Nations, 2018). The rapid pace of urbanization has intensified pressures on land use (Zhou & Chen, 2018), contributed to rising greenhouse gas emissions ("Greenhouse Gas Emissions from Energy Use in Buildings in Europe," 2023), and reshaped urban morphology (Zhang et al., 2023). These processes have simultaneously reduced vegetation cover (Tan et al., 2021), thereby diminishing the ecological functions that underpin urban liveability (Waitt & Knobel, 2018) and accelerating anthropogenic climate change (Ahmadi et al., 2022).

Among the many consequences of climate change, the increase in urban temperatures and the intensification of heatwaves stand out as particularly critical (Thompson et al., 2023; European Commission. Directorate General for Climate Action, 2023). These phenomena exert profound impacts on both ecological systems (Singh et al., 2020a) and human health (Heaviside et al., 2017; Singh et al., 2020b), making them urgent priorities for urban adaptation strategies.

Nature-Based Solutions (NBS), defined as interventions inspired or supported by natural processes (Castellar et al., 2021), have emerged as promising strategies to enhance the quality of urban canyons and regulate microclimatic conditions. Their capacity to deliver ecosystem services (Babí Almenar et al., 2021; Pedersen Zari, 2015) positions them as central tools in mitigating heatwave impacts. By reintroducing vegetation across multiple scales, and particularly within urban canyons (e.g., NBS can moderate local climates through shading), which reduces mean radiant temperatures, and evapotranspiration, which enhances cooling (Jones, 2013; Gu & Goto, 2024; Sun et al., 2025).

Despite these benefits, planning and implementation strategies for NBS remain underdeveloped. In particular, site-specific quantification and prediction of NBS performance are rarely integrated into urban canyon design (Mosca, 2024). This gap limits the ability of planners to fully leverage NBS in mitigating the Urban Heat Island (UHI) effect (Albert et al., 2021). Moreover, the effectiveness of NBS is highly context-dependent, shaped by local climatic conditions (Gulyás et al., 2006), land use patterns (Zhou & Chen, 2018), topography, and built morphology (Allen-Dumas et al., 2020). Consequently, simulations and analyses tailored to specific sites are often required to accurately assess potential benefits and limitations (Peters & Peters, 2018).

Computational simulations have long been employed to evaluate NBS performance, enabling designers to compare alternative configurations. However, these simulations are resource-intensive, requiring bespoke models for each project and significant computational power (Peters & Peters, 2018). Integrating iterative NBS design processes into standard workflows remains challenging (Canepa et al., 2022; Mosca et al., 2025).

Machine Learning (ML) offers a promising alternative. ML systems can identify patterns in training datasets and apply them to predict outcomes for new scenarios, combining accuracy with adaptability (Koutra & Ioakimidis, 2022). In complex, data-rich urban contexts, ML can reduce reliance on ad hoc simulations by learning from datasets that link specific urban characteristics to effective NBS interventions. This approach is particularly relevant in the face of increasing environmental unpredictability (Li et al., 2022). While ML has been widely applied to climate-related phenomena (Yoo, 2018; Miniandi et al., 2025; Ghorbany et al., 2024), its use in optimizing NBS performance remains largely unexplored (Gutierrez Caloir et al., 2023; Zou et al., 2025).

7.1.2. Objectives of the chapter

Considering the current research landscape and the gaps identified in NBS design, the following objectives are confronted in this Chapter:

i. Develop a comprehensive training dataset by establishing a flexible methodology for analysing urban canyons in terms of microclimatic conditions and NBS performance using computational simulations.

ii. Identify optimal NBS configurations through a multi-criteria decision-making (MCDM) framework that ranks simulated solutions based on climatic and geographic variables, urban canyon geometry, and tree species selection; assess the influence of latitude and canyon morphology on performance outcomes.

iii. Predict the most effective NBS strategies for any combination of latitude and urban canyon geometry using ML algorithms and demonstrate applicability through a selected case study.

iv. Validate the proposed methodology across diverse geographic contexts and evaluate the utility of solar radiation metrics during early design phases for microclimate regulation analysis.

7.2. Methodology

The methodological framework was designed around the four research objectives outlined earlier. It combines computational simulations, multi-criteria decision-making (MCDM), ML techniques, and validation and testing into a single workflow. Each step builds on the previous one, ensuring that the study progresses from data generation to predictive modelling and validation in a structured manner (Fig. 1):

i. Identify key urban canyon and NBS features, establish evaluation criteria, and set up the operative workflow for computational simulations of urban canyon configurations to generate the training dataset.

ii. Apply the selected MCDM methodology to determine the best-performing NBS configuration for specific sites and canyon geometries.

iii. Compare alternative ML methods using the training dataset, select the most suitable algorithm, and implement it to predict NBS performance for a given site and canyon through a case study analysis.

iv. Validate ML predictions and the overall workflow against computational simulations for canyon/NBS combinations not included in the training dataset, thereby assessing effectiveness and applicability across different geographical contexts.

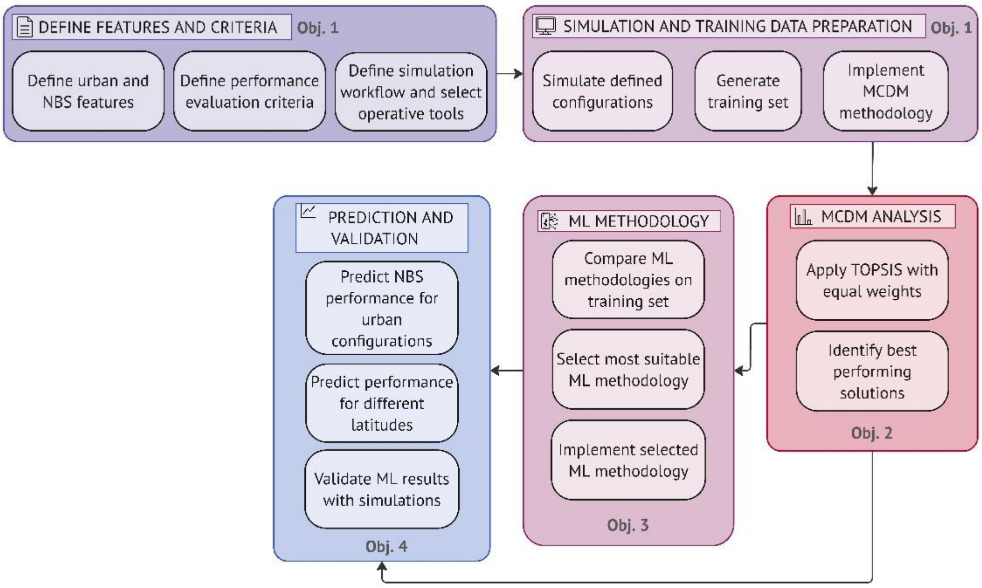

Figure 1. Overview of the methodological steps of the study.

7.2.1. Training set definition and simulation settings

In this Chapter, ML models are trained on datasets containing spatial and urban parameters. During training, the model learns relationships between inputs (e.g., canyon features and design criteria) and outputs (e.g., vegetation characteristics). Once trained, the model can predict outcomes for new scenarios, enabling rapid evaluation of design alternatives without requiring full simulations. Thus, the first step involves defining variables for the characterization of urban areas and NBS to define the training dataset.

The urban canyon model was selected as the baseline representation of urban form. This model is widely used in urban studies because it captures the essential features of built environments while remaining computationally manageable (Yola, 2020; Zhong et al., 2020; Evola et al., 2020; Lobaccaro & Acero, 2015). By varying canyon dimensions, orientations, and vegetation configurations, it was possible to generate a dataset that reflects a wide range of realistic urban conditions.

Input variables included canyon geometry (height, length, orientation), distance between buildings (equal to the canyon width) (Table 1), and vegetation parameters such as tree height, crown radius, crown shape, and trunk volume (Table 2). These variables were chosen based on their relevance in the literature and their direct influence on shading and thermal performance (Muniz-Gäal et al., 2020). Thresholds for each variable were defined to ensure that the simulations covered both typical and extreme conditions.

Table 1. List of input variables for urban canyon features and related thresholds for simulations.

Input variables - Canyon	**Values**	**Unit**
Building distance (canyon width)	10	m
	25	
	40	
Building lenght (canyon lenght)	40	m
Building height (canyon height)	10	m
	25	
	40	
Orientation	0	° (degrees from North)
	90	
Grid size	1.5	m
Latitude (Turin, Genoa, Florence, Rome, Naples, Palermo)	45°04′13″ N	°
	44°25′35″ N	
	43°46′45″ N	
	41°53′30″ N	
	40°51′08″ N	
	38°07'55" N	

Table 2. List of input variables for NBS features and related thresholds for simulations (NBS features corresponding to medium values for Abies Alba; Tallo, 2025).*

Input variables - NBS	Values	Unit
Trunk radius	0.05	m
	0.15*	
	0.30	
Crown radius	0.5	m
	3*	
	5	
NBS height	2	m
	10	
	20*	
Crown height	1/4h*	m (fractions of NBS height)
	2/4h	
	3/4h	
NBS type	Single tree	-
	Single row	
	Double row	
NBS shape	Sphere	-
	Cylinder	
	Cone	
	Reverse cone*	
Number of trees	Low (1/8 possible locations)	-
	Medium (1/4 possible locations)	
	High (1/2 possible locations)	

Output parameters were then established to serve as optimization criteria (Table 3). The primary objective was to improve microclimatic conditions, but operational considerations such as maintenance requirements were also included (Mosca et al., 2025). To balance computational efficiency with accuracy, shading capacity was quantified through solar radiation reduction rather than Mean Radiant Temperature (MRT). Although MRT provides a more detailed measure of thermal comfort, it is computationally demanding. Solar radiation, by contrast, offers a reliable proxy for shading performance and can be calculated more efficiently (Alexandri & Jones, 2008; Alzahrani & Gadi, 2024; Acero & Herranz-Pascual, 2015; Aghamolaei et al., 2022; Liu et al., 2022).

Table 3. Criteria for the optimization of simulations results and related directions

Output variables – Optimization criteria	**Values**	**Unit**
% shaded street	Maximise	%
% shaded building		%
Tree crown volume		m^3
Trunk volume	Minimise	m^3
Number of trees		n

The simulation pipeline was implemented using Rhinoceros 3D (McNeel, 2025) and its parametric plug-in Grasshopper, chosen for their flexibility and precision in modelling complex geometries. Two additional plug-ins were integrated: Ladybug Tools, an open-source suite for environmental analysis (Nicholson et al., 2024; Sadeghipour Roudsari et al., 2013), and Colibri, which automates design space exploration by generating and recording all variable combinations. Weather data were sourced from georeferenced .epw files, with simulations run for a typical summer condition (21 June, 2 PM). In total, the study generated:

6 cities × 3 NBS types × 4 tree types = 72 scenarios

Each scenario produced multiple simulation outputs, which were exported as .csv files to form the training dataset for subsequent analysis.

7.2.2. Multi-criteria Decision-Making analysis

Simulation outputs were analysed to identify best-performing configurations for given canyon conditions. The TOPSIS method (Technique for Order of Preference by Similarity to Ideal Solution) was selected due to its robustness and wide applicability (Pandey et al., 2023). TOPSIS ranks alternatives by measuring their closeness to an ideal solution, maximizing benefits and minimizing costs, while distancing from the negative ideal (Celik & Ogus Binatli, 2018). The process involves data normalization, weighting criteria, calculating distances, and deriving a closeness index. In this study, entropy weights were applied to avoid unbalanced results (Chen, 2021). This approach ensured that the selected NBS configurations maximized benefits (e.g., shading) while minimizing costs (e.g., maintenance), and avoided skewed results caused by unbalanced weighting.

7.2.3. Machine Learning implementation

The third stage focused on predictive modeling. Several ML regression algorithms were tested to determine which could most effectively learn from the training dataset and generalize to new urban contexts. The models included Linear Regression (LR), Kernel Ridge Regression (KRR), Random Forest (RF), Support Vector Regression (SVR), and Multi-Layer Perceptron Regression (MLP) (Demir & Sahin, 2024; Oukhouya & Himdi, 2023). The main differences between all five algorithms are explored in Table 4, and explained in the following paragraphs.

Table 4. Confronts between the five selected ML algorithms.

Algorithm	**Core Principle**	**Strengths**	**Limitations**	**Computational Complexity**	**Suitability for NBS Prediction**
Linear Regression (LR)	Models the relationship between input variables and output as a linear function.	- Simple and interpretable - Fast to train - Provides baseline performance	- Assumes linearity - Poor with non-linear or complex interactions - Sensitive to multicollinearity	Very low (O(n·p), where n = samples, p = features)	Useful as a baseline model; limited for complex, non-linear NBS–canyon interactions.
Kernel Ridge Regression (KRR)	Combines ridge regression with kernel methods to capture non-linear relationships.	- Handles non-linear data well - Regularization reduces overfitting - Flexible kernel choice (e.g., RBF, polynomial)	- Computationally expensive for large datasets - Requires careful kernel and parameter tuning	Moderate to high (depends on kernel; scales poorly with large n)	Suitable for capturing non-linear NBS–geometry effects; best for medium-sized datasets.
Random Forest (RF)	Ensemble of decision trees; predictions are averaged across trees.	- Captures complex non-linear relationships - Robust to noise and overfitting - Provides feature importance	- Less interpretable - Can overfit small datasets - Requires tuning of tree depth and number	Moderate (depends on number of trees; parallelizable)	Strong candidate for NBS prediction; handles mixed variables well but may overfit with limited data.

Support Vector Regression (SVR)	Uses support vectors and kernel functions to fit regression within a margin of tolerance.	- Effective in high-dimensional spaces - Flexible kernel choice - Good generalization	- Sensitive to parameter selection (C, ε, kernel) - Computationally heavy for large datasets - Less scalable	High (training scales ~$O(n^2–n^3)$)	Well-suited for smaller datasets; provides smooth predictions, valuable for NBS performance generalization.
Multi-Layer Perceptron Regression (MLP)	Neural network with multiple hidden layers; learns complex non-linear mappings.	- Highly flexible - Can approximate any function - Captures intricate interactions	- Requires large datasets - Sensitive to hyperparameters - Risk of overfitting - Less interpretable	High (depends on architecture; requires GPU for efficiency)	Potentially powerful for NBS prediction if dataset size increases; currently limited by small training set.

jLinear Regression (LR) is one of the most fundamental techniques in statistical modelling and ML. It assumes a linear relationship between independent variables (predictors) and the dependent variable (outcome). The model estimates coefficients that minimize the sum of squared residuals, providing a straightforward interpretation of how each predictor contributes to the outcome. Its strengths lie in simplicity, interpretability, and computational efficiency. However, LR is limited when relationships are non-linear or when predictors are highly correlated, which can lead to instability in coefficient estimates. Despite these limitations, LR remains a valuable baseline model, offering a benchmark against which more complex algorithms can be compared. In the context of regressions tasks such as NBS prediction, LR provides a good starting benchmark, but cannot capture the non-linear interactions that may arise between variables (Harrell, 2016).

Kernel Ridge Regression (KRR) combines the principles of ridge regression with kernel methods, allowing it to capture non-linear relationships between input and output variables. Ridge regression introduces a regularization term that penalizes large coefficients, thereby reducing overfitting and improving stability. By embedding this within a kernel framework, KRR can project data into higher-dimensional spaces where complex patterns become linearly separable. The choice of kernel (e.g., radial basis function, polynomial) determines the flexibility of the model, enabling it to adapt to different types of non-linearity. In practice, KRR is well suited to medium-sized datasets where non-linear interactions are important but computational resources are limited. Its main drawback lies in scalability: kernel methods require storing and manipulating large kernel matrices, which becomes computationally expensive as dataset size grows. For regressions tasks such as NBS prediction, KRR offers a balance between interpretability and predictive power, and can be particularly useful when the dataset is not large enough to justify deep learning approaches but too complex for purely linear models (Singh & Vijaykumar, 2025).

Random Forest (RF) is an ensemble learning method that builds multiple decision trees and aggregates their predictions. Each tree is trained on a random subset of the data and features, which introduces diversity and reduces the risk of overfitting. The final prediction is obtained by averaging (for regression, as in this case) or voting (for classification) across all trees. RF excels at capturing complex, non-linear relationships and interactions between variables. It is robust to noise, handles mixed data types, and provides measures of feature importance, which can be valuable for interpreting which variables most strongly influence outcomes. However, RF models can become less interpretable as the number of trees increases, and they may overfit when applied to small datasets if hyperparameters such as tree depth are not carefully tuned. Computationally, RF is more demanding than linear models but benefits from parallelization. In the context of NBS prediction, RF is attractive because it can model intricate interactions between canyon and NBS variables. Its ability to highlight variable importance also supports design decisions (Breiman, 2001)

Support Vector Regression (SVR) extends the principles of Support Vector Machines to regression tasks. Instead of fitting a line through all data points, SVR seeks a function that predicts within a specified margin of tolerance (ε), focusing only on support vectors (i.e., data points that lie outside the margin). This makes SVR robust to outliers and capable of generalizing well. The use of kernel functions (e.g., radial basis function, polynomial) allows SVR to capture non-linear relationships by implicitly mapping data into higher-dimensional spaces. The flexibility of SVR comes at the cost of computational intensity, as training scales poorly with large datasets. Performance is highly sensitive to parameter choices (C, ε, kernel type), requiring careful tuning. For NBS prediction, SVR is particularly suitable because the dataset is relatively small and the relationships between variables are non-linear. SVR produces smoother predictions than RF, which is critical when extrapolating to unseen latitudes or canyon geometries (Awad & Khanna, 2015).

Multi-Layer Perceptron Regression (MLP) is a type of feedforward artificial neural network composed of an input layer, one or more hidden layers, and an output layer. Each layer consists of nodes (neurons) connected by weighted edges, with non-linear activation functions enabling the network to approximate complex mappings between inputs and outputs. In theory, MLPs can approximate any continuous function given sufficient depth and training data. The strength of MLP lies in its flexibility: it can capture highly non-linear and hierarchical relationships that simpler models cannot. However, this flexibility comes with significant challenges. MLPs require large datasets to train effectively, are sensitive to hyperparameter choices (e.g., learning rate, number of layers, activation functions), and are prone to overfitting when data is limited. Training is computationally intensive and often requires GPU acceleration. In the context of NBS prediction, MLP represents a powerful but currently impractical option. With the relatively small dataset available, MLP risks overfitting and producing unstable results. As datasets expand and become more complex, such as when incorporating more cities and new indicators, MLP could become a valuable tool for capturing the full complexity of NBS performance (Kruse et al., 2022).

All models were implemented using scikit-learn (Pedregosa et al., 2011). Hyperparameters were optimized through grid-search cross-validation, except for LR, which does not require tuning. To address the relatively small dataset size, the Repeated K-fold method was introduced, improving robustness by averaging results across multiple splits (Lumumba et al., 2024). SVR, typically designed for scalar regression, was adapted for multi-output prediction, enabling it to handle multiple performance indicators simultaneously (Wang et al., 2024).

The dataset was divided into training (70%), validation (15%), and testing (15%) subsets. Model performance was evaluated using R^2 scores, with the most accurate and reliable algorithm selected for further application.

7.2.4. Case studies selection and validation

To analyse the performance of different NBS configurations, a series of case studies were defined that directly addressed the research objectives.

To identify the best-performing NBS for a specific urban site and canyon configuration, a subset of configurations from the training dataset was selected. The city of Genoa (44°25′35″ N) served as the reference case. Eighteen canyon combinations were examined, varying in height and width (10 m, 25 m, and 40 m) and considering both orientations (0° and 90°). This analysis provided a detailed understanding of how canyon geometry and orientation influenced the effectiveness of NBS strategies in a real urban context. The identification of the most performing predictive model will be carried out quantitatively by confronting R^2 scores, and qualitatively by assessing the distribution of predicted data over an array of interpolated values ranging from the maximum to the minimum possible values for canyon geometries and latitudes.

The testing of ML results relied on the reserved testing set, corresponding to 15% of the total number of best simulations. This dataset enabled a direct comparison between predicted and simulated outcomes, ensuring that the methodology was evaluated against unseen data. Robustness was further assessed through a sensitivity analysis of the MCDM algorithm. In this step, the results obtained with TOPSIS were compared with those generated using VIKOR, another widely adopted method in optimization tasks. The comparison was conducted by paralleling all processes performed with TOPSIS and evaluating the differences in scores through the standard deviation metric (Stević et al., 2022). This dual analysis provided insight into the stability of the optimization framework and highlighted the extent to which methodological choices influenced the identification of best-performing NBS configurations.

7.3. Results and Discussion

7.3.1. Simulation output

A total of 314,928 simulations were produced across 72 scenarios, each differentiated by city latitude, NBS shape, and NBS type. This extensive dataset provided a solid empirical basis for examining how vegetation configurations interact with urban canyon geometries under varying climatic contexts. The analysis of these simulations revealed clear and systematic trends in NBS performance across geographical locations and canyon configurations (Fig. 2). When the results were organized into the 18 combined city–NBS scenarios, most configurations displayed consistent performance patterns within each city (rows) and across NBS types (columns).

A particularly noteworthy finding is that every scenario yielded at least one solution with a very high TOPSIS score (>0.9). This demonstrates that, regardless of location or canyon morphology, context-specific optimal NBS configurations can be identified under the defined criteria. Moreover, the simulation outcomes are consistent with established literature on the shading performance of trees in urban environments as a function of latitude and geographical context (Del Campo-Hitschfeld et al., 2023; Kumakura et al., 2011; Palme et al., 2020).

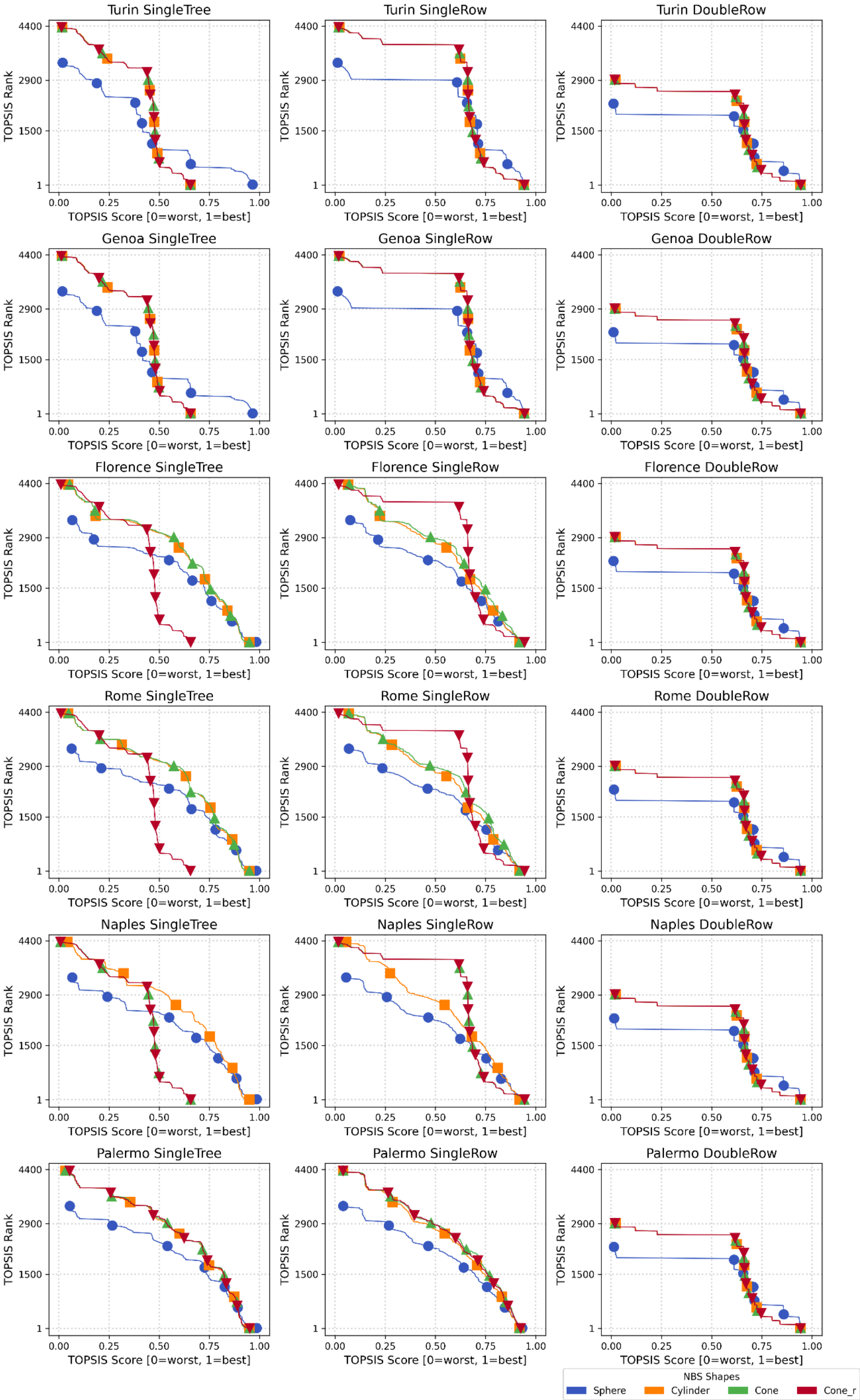

Figure 2. NBS simulated data, divided in 72 scenarios of different city, NBS Shape (Sphere, Cylinder, Cone, Reversed cone), and NBS Type (Single Tree, Single Row, Double Row). A TOPSIS Score of "1" is equal to the ideal solution, and a Rank of "1" is the highest ranking.

Studying the feature influences over the TOPSIS-based performance revealed nuanced patterns (Fig. 3). Several continuous features display clear directional effects, such as Building Distance and Crown Radius that both transition from strongly negative Z-Scores (defined as Zi = (xi- μ)/σ, where xi is the observed value, μ is the mean, and σ is the standard deviation, expressing each feature in units of standard deviations from the mean) at low values (-1.14 and –1.09 respectively) to distinctly positive values near +0.75 to +0.87 at their upper range, indicating that larger distances and crown radii consistently improve performance. Building Height and Crown Height show the opposite trend, with high values associated with Z-Scores near -0.9 to –1.0, suggesting diminishing performance as height increases. City Latitude exhibits the widest spread, ranging from +1.59 to –1.05, highlighting substantial sensitivity to geographic location. Among categorical variables, Tree Shape shows the strongest contrast, with “Sphere” outperforming “Cone Reversed” by more than two standard deviations, and Row declining sharply from the first to the third row. These patterns indicate that geometric and spatial configuration variables exert the strongest influence on the TOPSIS distance to the ideal solution. When contrasted with the VIKOR results (Annex K) the TOPSIS curves appear sharper and more polarized, reflecting TOPSIS’s emphasis on consistent proximity to the ideal solution rather than compromise across criteria.

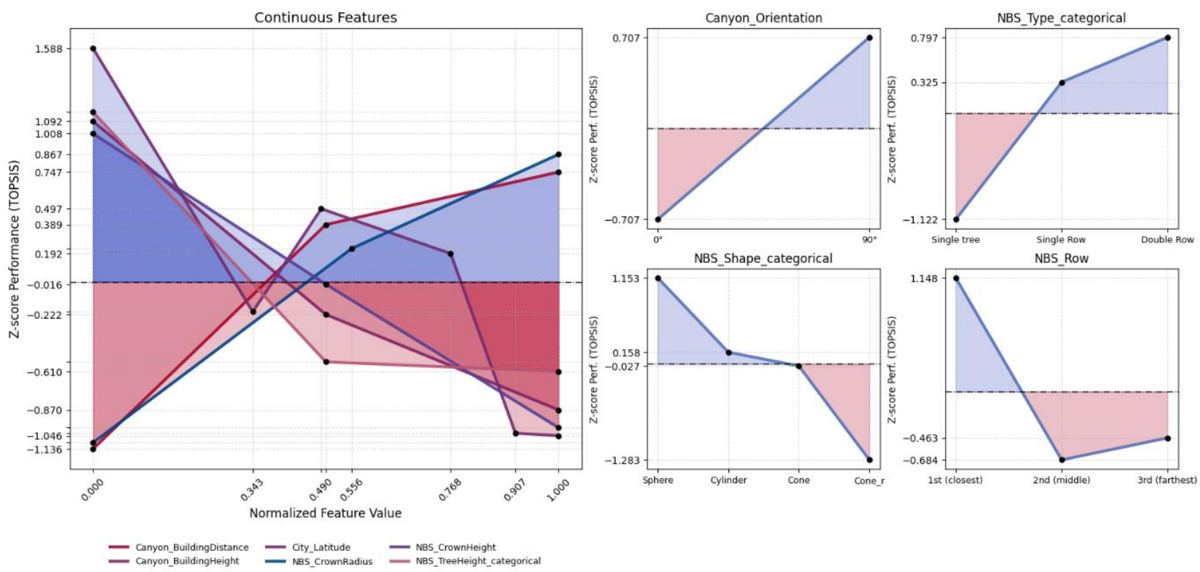

Figure 3. Influencing factors trends over TOPSIS-based standardized performance using the Z-Score. A Z-Score of 0 indicates average performance, while values around +1 or –1 reflect substantially better- or worse-than-average behaviour, respectively.

Correlation analysis between the input variables and the optimization criteria (Fig. 4) revealed several structural patterns in the dataset. The Number of Trees and Tree Trunk Volume exhibited a strong positive correlation (ϱ = +0.62), which indicates that these two criteria are not independent but rather rely on overlapping variables. This relationship becomes clearer when considering their association with NBS Type (ϱ = +0.88 and ϱ = +0.36, respectively) and Tree Quantity (ϱ = +0.79 for both). In practice, this means that the definition of an NBS type (e.g., single tree, row of trees, double row) inherently constrains both the number of trees that can be introduced and the cumulative trunk volume, creating a structural linkage between these parameters.

The Tree Crown Volume generally followed the same collinearity pattern as Number of Trees and Trunk Volume, but diverged when correlated with Crown Radius (ϱ = +0.67). This divergence reflects a geometric trade-off: increasing the crown radius enlarges the canopy of individual trees, thereby increasing crown volume, but simultaneously reduces the number of trees that can be accommodated within a given canyon width. As a result, overall green cover decreases even as individual canopy size expands. This trade-off between canopy size and tree density is well documented in ecological studies, which show strong correlations between crown radius and trunk volume (O'Brien et al., 1995; Pretzsch & Dieler, 2012; Zhu et al., 2021). The consistency of these relationships in the simulation dataset reinforces the relevance of the selected parameters for tree modeling and performance quantification.

For shading-related criteria, Shading on Building Surfaces and Shading on Street Surfaces showed medium-to-high correlations (ϱ = +0.39 and ϱ = +0.69, respectively). The primary influencing factor in both cases was Building Distance, which determines the available space for tree placement and the angle of solar obstruction. This finding is consistent with previous studies that emphasize the role of canyon geometry, particularly the Canyon Ratio (Width/Height), in shaping shading outcomes (Takebayashi & Moriyama, 2012; Andreou, 2014).

Street shading also displayed a negative correlation with Building Height (ϱ = –0.51). Taller buildings reduced the effective shading contribution of trees at street level, as the canyon geometry restricted solar penetration. By contrast, Building Shading showed no correlation with Height. This lack of association is explained by the fixed solar radiation conditions used in the simulations, which standardized building-to-building shading effects and left NBS as the primary source of variation.

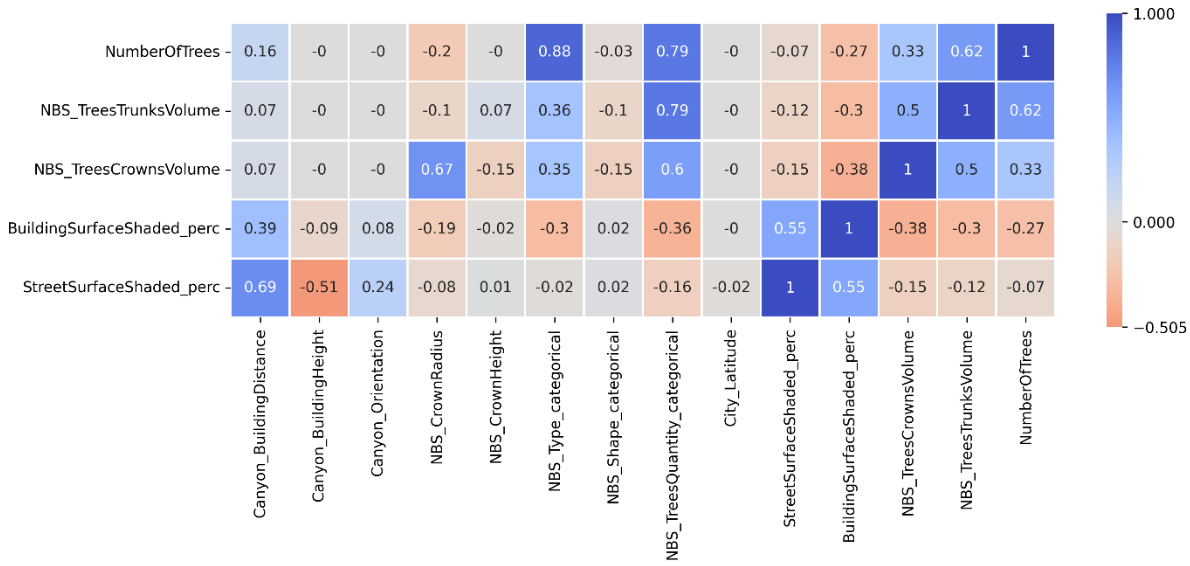

Figure 4. Correlation analysis using Spearman's ρ between simulation variables and optimization criteria. Scores of "1" equal to a perfect positive correlation, while scores of "-1" equal to perfect negative correlation.

Finally, the relationship between geographic location and canyon characteristics was examined by systematically selecting the highest-scoring NBS configuration for each city across the full set of eighteen simulated canyon combinations. These combinations varied in height, depth, and orientation, thereby capturing the principal geometric parameters that define canyon morphology. In total, this procedure generated 72 individual scenarios (Fig. 5), each representing the intersection of a specific latitude with a distinct canyon geometry.

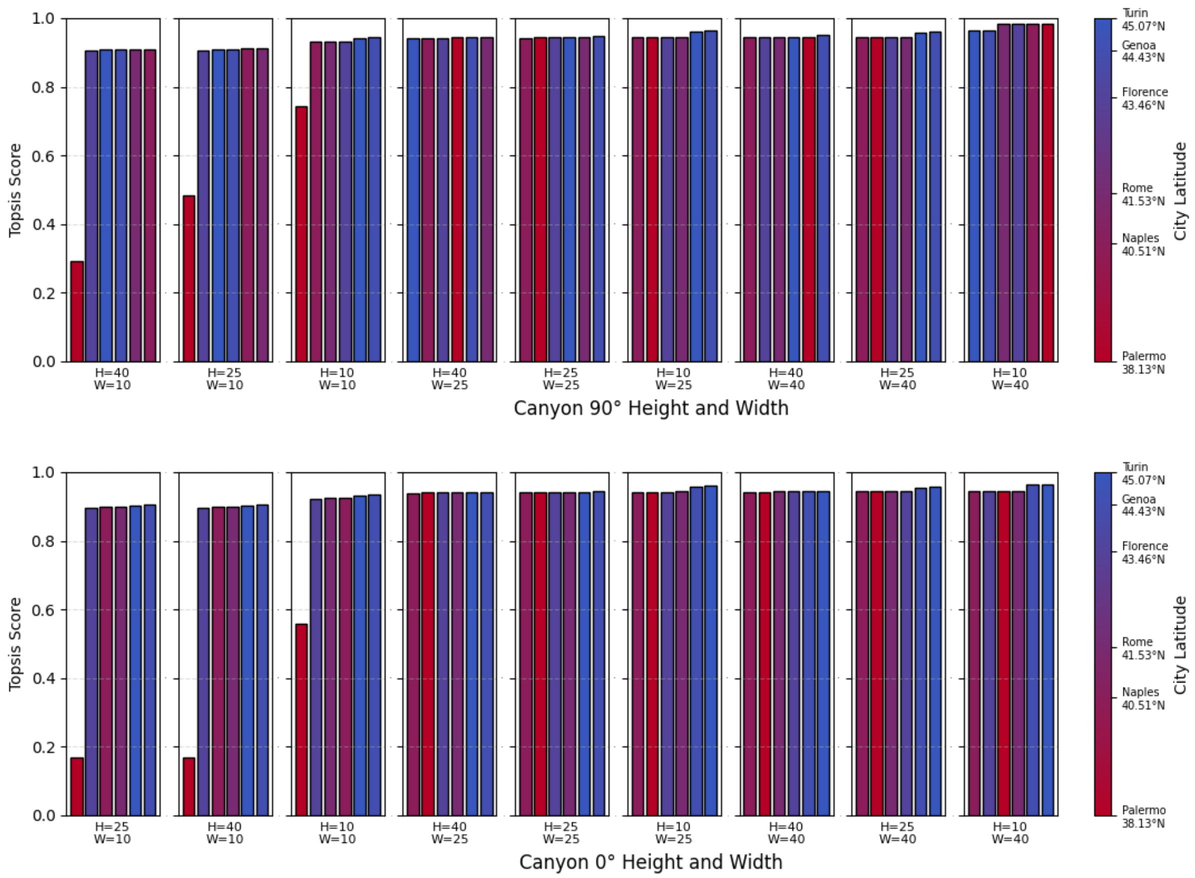

Figure 5. Bar graph of the best NBS from each canyon configuration data for each city, Figure 4a (top) refers to canyons with 90° orientation, Figure 4b (bottom) refers to canyons with 0° orientation.

Through this analysis, it was possible to deduce that all canyons in Turin, Genoa, Florence, Rome, and Naples contained at least one NBS configuration achieving a TOPSIS score greater than 0.9. This confirms that in each of these cities, optimal solutions were consistently identified under the defined criteria. In addition, canyons with a width of W = 40 m generally produced the highest scores, enabling the identification of the best-performing NBS overall, with scores exceeding 0.97 in both orientations.

The performance of NBS gradually decreased with decreasing latitude in 0° canyons, with Palermo consistently showing the lowest values, particularly in narrow canyons (W = 10 m). A similar behaviour was observed in 90° canyons, although with an important distinction: at lower latitudes, performance increased in both the least favourable canyon conditions (W = 10 m) and the most favourable ones (W = 40 m). For the lowest latitude considered in the study (Palermo, 38.13° N), the TOPSIS scores were lower overall due to the larger latitude gap compared to the other selected cities. This difference is directly correlated with the solar angle, as latitude strongly influences solar radiation incidence. As demonstrated in the literature (Kopp, 2023), geographical coordinates, specifically latitude and longitude, as well as the timeframe of quantification, exert a significant impact on solar radiation calculations.

In a second phase, a more detailed analysis was conducted for the city of Genoa, examiningj the best-performing NBS across different canyon configurations and simulated latitudes (Fig. 5). This analysis highlighted that the "optimal" NBS configuration varied depending on canyon type. In narrow canyons, a single tree proved particularly effective, while wider canyons benefited from single or double rows of trees. In terms of tree shape, the optimal configurations included spherical, conical, and reverse-conical geometries. These results emphasize the critical role of crown surface area and volume in enhancing shading and improving microclimatic conditions within urban canyons. This finding is consistent with previous studies (Sharmin et al., 2023; Kuuluvainen & Pukkala, 1987; Franceschi et al., 2022), which demonstrated the strong relationship between tree shape, especially crown distribution and volume, and the capacity to regulate local microclimates.

Notably, across all canyon dimensions, orientations, NBS types, and tree shapes, the optimal crown radius consistently measured 5 metres, which corresponded to the maximum value included in the training dataset. This uniformity suggests that crown radius acted as a limiting factor in the optimization process. Furthermore, analysis of NBS variation under different optimization objectives revealed the adaptability of the methodology. It can be tailored to meet specific design goals or environmental constraints, demonstrating both the flexibility of the approach and the versatility of NBS in addressing diverse criteria.

A closer examination of the results presented in Figure 5, focusing on the best-performing NBS across different canyon types, revealed two additional points:

i. The number of trees varied significantly depending on canyon orientation. This confirmed that building shadows exert a strong influence on shading conditions within the canyon.

ii. In both orientations, under conditions of low buildings and wide canyons, it was expected that the number of trees would increase due to reduced building shading. However, the opposite was observed. This outcome likely reflects the fact that the optimization process considered multiple parameters, not only those directly related to shading (such as crown volume, trunk volume, and tree quantity).

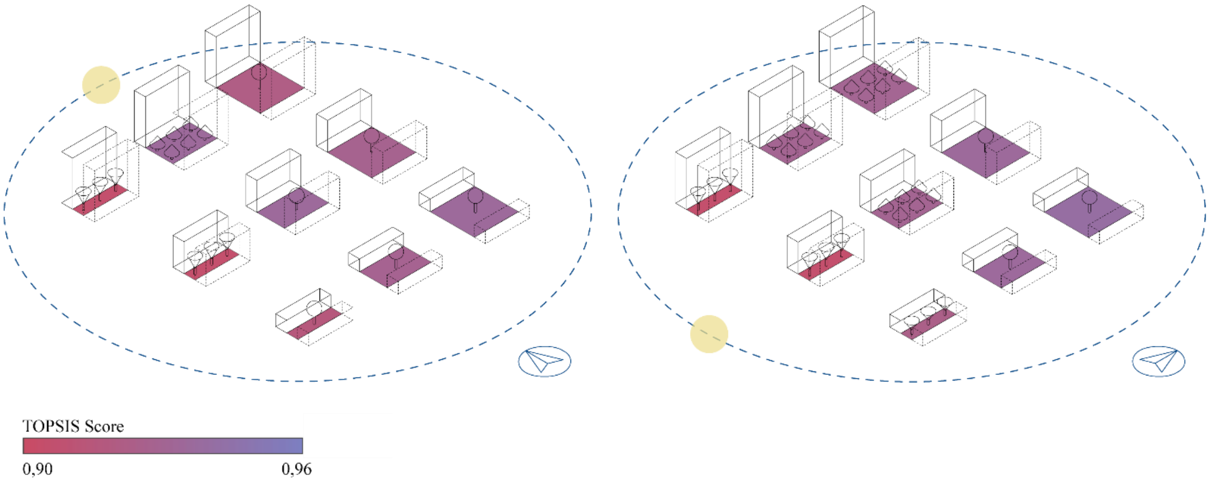

Fig. 6 – Best performing NBS in Genoa for the nine types of urban canyon considered at 0° (left) and 90° (right), with equal weights assigned to all the optimization criteria.

These results demonstrate that boundary conditions are decisive in shaping optimization outcomes. The explanation lies in the behaviour of the optimization algorithm, particularly in how input variables are associated with optimization criteria. For shading-related variables, correlations were observed with both canyon parameters (boundary conditions) and NBS parameters. By contrast, for non-shading variables, correlations were found only with NBS characteristics. As a result, to satisfy all optimization criteria simultaneously, the algorithm was more constrained by non-shading characteristics, since they relied on fewer input variables that carried greater weight (Fig. 3). Consequently, shading was primarily addressed through canyon parameters rather than NBS parameters.

Future developments should investigate strategies to reduce the weight of boundary conditions in the selection of optimal solutions. This would allow shading-related variables to play a more balanced role in the optimization process and improve the capacity of the methodology to identify solutions that maximize shading performance without being disproportionately constrained by non-shading criteria.

The methodology also provides a framework for the quantification and optimization of additional environmental benefits associated with the integration of urban trees, particularly those linked to biomass. Beyond shading and microclimatic regulation, the same workflow can be extended to evaluate ecosystem services that are increasingly recognized as critical in urban sustainability. For example, the simulations and optimization procedures can support the assessment of the carbon sequestration and storage capacity of urban trees (Jin et al., 2023), thereby linking microclimatic performance to broader climate mitigation strategies. Similarly, the methodology can be applied to quantify contributions to air quality improvement, such as the absorption of particulate matter and the release of oxygen (Haq et al., 2024). In addition, the integration of trees within urban canyons can be evaluated in terms of their role in supporting local biodiversity, by providing nutrients, nesting areas, and habitats for insects, birds, and other organisms (Atkins, 2018). These extensions highlight the versatility of the approach, enabling a more holistic evaluation of NBS performance across multiple environmental dimensions.

It is also important to emphasize that, within both the optimization process and the subsequent learning phase, NBS features such as height and crown radius are not directly correlated. This distinction means that species selection does not need to be fixed at the outset of the analysis. Instead, the methodology allows the definition of optimal NBS shapes and dimensional features first, based on performance criteria, and only then links these configurations to specific tree species. In practice, this sequencing ensures that species choice is guided by the geometric and functional characteristics identified as optimal, rather than being constrained prematurely by biological parameters. This separation between geometric optimization and species selection enhances the adaptability of the workflow, making it possible to tailor final design recommendations to both ecological performance and local planting feasibility.

7.3.2. ML training outcomes

The highest-scoring NBS from each of the 72 scenarios were extracted and used as the training dataset for five machine learning algorithms. This dataset provided a structured basis for evaluating how different regression approaches could learn from the simulated configurations and generalize to new urban contexts. Model performance was assessed using R^2 scores (Fig. 7), which quantified the proportion of variance explained by each algorithm and served as a consistent metric for comparison.

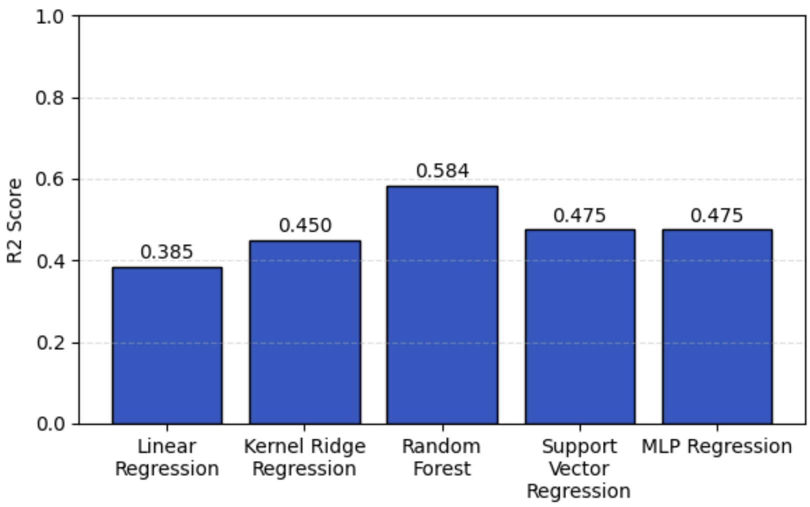

Figure 7. Bar plot indicating the R^2 scores for the different ML models trained on the best-performing simulated data, and the behaviour of the selected methodology (SVR).

Among the tested models, Random Forest (RF) achieved the highest accuracy, with an R^2 value of 0.584. RF's ensemble structure allowed it to capture complex non-linear relationships in the dataset. However, despite its superior accuracy, Support Vector Regression (SVR) was selected as the preferred model. Although SVR achieved a slightly lower R^2 score (0.475, the second-best result), it produced smoother predictions for unobserved data, a property that is particularly valuable when extrapolating performance to latitudes and canyon geometries not included in the training set. This behaviour has been documented in similar applications, where SVR demonstrated strong generalization capacity despite modest accuracy scores (Chou & Bui, 2014).

The comparative evaluation of all five algorithms is presented in detail in the supplementary material (Annex H).

7.3.3. Case studies and validation

The internal validation conducted with 15% of the dataset yielded fluctuating R^2 results, reflecting variability in predictive accuracy across different splits. Notably, the R^2 scores obtained during grid-search optimization were consistently higher than those obtained when predicting the validation set. While small dataset effects may partially explain this discrepancy, a more plausible factor is the presence of optimism bias in the grid-search procedure. In grid-search, models are evaluated multiple times across different folds, which tends to inflate performance estimates. By contrast, internal validation relies on a single split, and if that split contains outliers or atypical patterns, the resulting R^2 values appear lower (Arlot & Celisse, 2010). This distinction highlights the sensitivity of performance metrics to dataset partitioning and underscores the importance of robust validation strategies.

The methodology was then tested by comparing the predicted data generated by the machine learning models with the simulated data produced through the computational pipeline used to define the training set. The testing process concentrated on predictions across different latitudes, since latitude is one of the most influential parameters affecting solar elevation angle and solar radiation. By focusing on this dimension, the analysis directly addressed how geographic variation shapes NBS performance.

All cases for the five machine learning models, along with a sensitivity analysis of the MCDM optimization, are documented in the supplementary material (Annex H). For clarity, four representative urban canyons sampled from the testing set are presented in Table 5, illustrating differences in NBS design configurations. These comparisons show that the methodology remained overall consistent, with only minor discrepancies observed in parameters such as tree height, where predictions tended to underestimate relative to simulated outcomes.

Table 5. Comparison of the features of four sampled canyons between prediction and testing sets.

Location	**Canyon variables**			**Prediction set**		**Testing set**	
	W	H	O	NBS	TOPSIS score	NBS	TOPSIS score
Florence	40m	25m	0°	Double row (1st and 3rd row, 6 trees) Cone 5m crown radius 20m tree height 1/4h crown height (e.g. Abies Alba)	0.944	Double row (1st and 3rd row, 6 trees) Cone 5m crown radius 10m tree height 1/4h crown height	0.954
Rome	25m	25m	0°	Double row (2st and 3rd row, 6 trees) Cone 5m crown radius 2m tree height 1/4h crown height (e.g. Salix Arbutifolia)	0.942	Double row (1st and 3rd row, 6 trees) Cone 5m crown radius 10m tree height 1/4h crown height	0.958
Naples	25m	10m	0°	Double row (2st and 3rd row, 6 trees) Cone 5m crown radius 20m tree height 1/4h crown height (e.g. Platanus Hispanica)	0.942	Double row (2st and 3rd row, 6 trees) Cone 5m crown radius 20m tree height 1/4h crown height	0.942
Palermo	10m	25m	0°	Single row (2nd row, 3 trees) Cone reversed 5m crown radius 2m tree height 1/4h crown height (e.g. Populus Alba)	0.169	Single row (2nd row, 3 trees) Cone reversed 5m crown radius 10m tree height 1/4h crown height	0.179

The approach demonstrated greater robustness when the training set was expanded from four to six cities, with the inclusion of Florence and Naples. This expansion improved stability in the outcomes, suggesting that increasing geographic diversity in the training data strengthens model generalization. However, at specific latitudes such as Palermo, performance deteriorated. This decline is likely attributable to the influence of the solar irradiation angle, which differs significantly at lower latitudes (Kopp, 2023). The results indicate that further enrichment of the training set would enhance predictive robustness. Such enrichment could be achieved either by adding more cities, thereby increasing consistency across latitudes, or by adjusting the timeframe of solar irradiation simulations, which would alter the solar angle and provide a broader basis for prediction.

The sensitivity analysis of the MCDM algorithms revealed that the differences in standard deviation scores between the two methods were very small, indicating a high degree of consistency in their outputs. When comparing results across both seen and unseen datasets, TOPSIS produced slightly lower standard deviation values (–0.011 and –0.020) compared to VIKOR (–0.012 and –0.022). Although the numerical differences were marginal, this outcome highlights that TOPSIS maintained a slightly more stable performance across datasets. The implication of these results is that both algorithms provided reliable rankings of NBS configurations, but TOPSIS exhibited a modest advantage in terms of stability and consistency. This finding is important because it confirms that the optimization framework is not overly sensitive to the choice of MCDM method, while also suggesting that TOPSIS may be preferable when prioritizing robustness in contexts where datasets include both familiar and unfamiliar conditions.

The development of reliable methods for NBS selection can be seen as part of an operative methodology that can be replicated in different geographical contexts to support the improvement of microclimate conditions of urban sites towards climate adaptation through planning and design actions (Fig. 7). The key steps of the operative workflow for its application can be summarized in phases (2) and (3) as the key contribution of this Chapter. The process starts with the identification of the urban site along with its geographical and climatic conditions (step 1, covered in Chapter 5 and 6), that can be select according to site-specific needs, e.g. urban regeneration initiatives, or based on the application of methodologies aimed at defining areas with high risks for citizens in relation to the UHI effect (Sidiqui et al., 2022, Assaf & Assaad 2024).

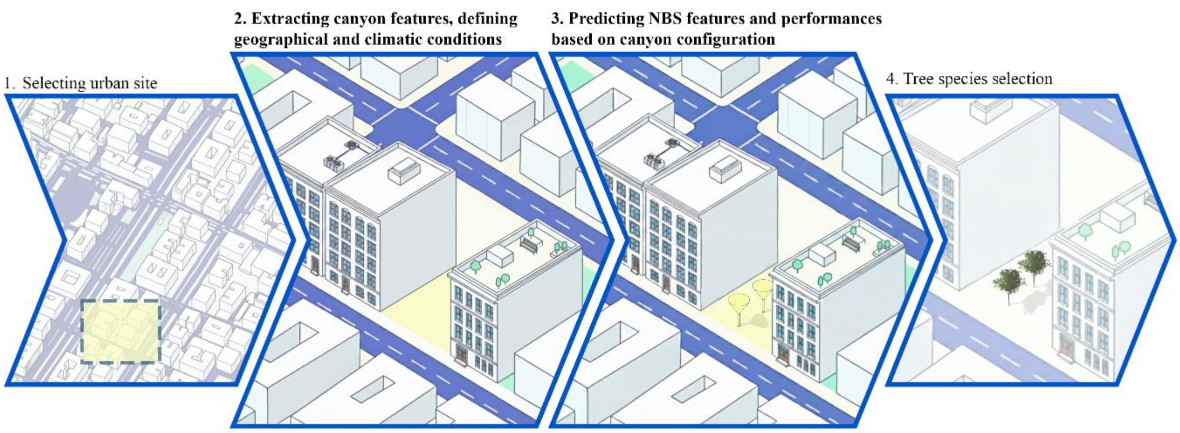

Figure 7. Operative workflow for the application of the proposed methodology in real world applications.

7.4. Conclusions

This Chapter proposed a novel methodology to optimize and predict the performance of NBS in urban canyons, focusing on shading provision as a key parameter for microclimate regulation. The approach demonstrated that it can be applied across different geographical contexts, offering a versatile tool for early-stage design and planning. The work highlights the wide applicability of the methodology and its potential to support the transition of urban areas towards resilience. Importantly, it establishes a foundation for further development, enabling the inclusion of a broader range of NBS performances such as carbon sequestration capacity, air quality improvement, and stormwater retention, thereby contributing to the optimization of urban design for climate change adaptation. In relation to the study objectives, the following conclusions can be drawn:

i. The study produced a comprehensive dataset integrating detailed information on urban canyon geometries and NBS characteristics. This dataset is representative of typical urban street conditions and common plant species used in urban design, ensuring broad applicability across diverse contexts. It also enables correlations to be established between urban morphology, geographical conditions, and NBS performance.

ii. Using a multi-criteria decision-making (MCDM) approach, optimal NBS configurations were identified across different canyon geometries and geographical locations. The methodology allows the selection of best-performing NBS tailored to site-specific requirements and objectives, including maximizing shading at both street and building levels.

iii. The selected ML algorithms demonstrated that NBS performance is strongly influenced by tree shape, canyon geometry, and latitude, with latitude playing the most significant role. The methodology provides a framework to simulate urban canyon conditions, learn from them, and derive best-performing NBS types and related tree features, thereby improving predictive accuracy.

iv. The methodology was tested across six different cities, confirming its usefulness for early-stage design analysis based on solar radiation as a key parameter for outdoor shading. However, predicting NBS performance remains complex, as reflected in the R^2 values. Expanding the dataset in terms of latitudes and timeframes would improve reliability and strengthen predictive robustness.

Despite these key results, several limitations remain. The training dataset was restricted, characterized by limited shading hours, simplified geometric dimensions, and a narrow selection of cities. Computational constraints also posed challenges, including non-optimized GPU processing, the exclusion of MRT analysis, and the sensitivity of both MCDM and ML approaches.

Future developments should focus on the integration of other ecosystem services, such as carbon sequestration, reduction of rainwater runoff in dense urban areas, and biodiversity enhancement. Additional parameters could be implemented to improve the quality of NBS performance prediction. Expanding the dataset to include different hours of the day (as illustrated in the Palermo TOPSIS results), exploring alternative microclimatic indicators such as MRT, and adopting more advanced computational frameworks would further enhance scalability, efficiency, and applicability.

7.5. References

Acero, Juan A., and Karmele Herranz-Pascual. (2015). A Comparison of Thermal Comfort Conditions in Four Urban Spaces by Means of Measurements and Modelling Techniques. *Building and Environment* 93 (November): 245–57. https://doi.org/10.1016/j.buildenv.2015.06.028.

Aghamolaei, Reihaneh, Mohammad Mehdi Azizi, Behnaz Aminzadeh, and James O'Donnell. (2022). A Comprehensive Review of Outdoor Thermal Comfort in Urban Areas: Effective Parameters and Approaches. *Energy & Environment*, August 2, 0958305X221116176. https://doi.org/10.1177/0958305X221116176.

Ahmadi, H., O. Bozorg-Haddad, S. Lucas, V. Prodanovic, and K. Zhang. (2022). Climate Change Drivers. *Springer Water*, 59–93. Scopus. https://doi.org/10.1007/978-981-19-1898-8_3.

Albert, Christian, Mario Brillinger, Paulina Guerrero, et al. (2021). Planning Nature-Based Solutions: Principles, Steps, and Insights. *Ambio* 50 (8): 1446–61. https://doi.org/10.1007/s13280-020-01365-1.

Alexandri, Eleftheria, and Phil Jones. (2008). Temperature Decreases in an Urban Canyon Due to Green Walls and Green Roofs in Diverse Climates. Building and Environment, Part Special: Building Performance Simulation, vol. 43 (4): 480–93. https://doi.org/10.1016/j.buildenv.2006.10.055.

Alzahrani, Ali, and Mohamed Gadi. (2024). Assessment of Modeled Mean Radiant Temperature in Hot and Dry Environments: A Case Study in Saudi Arabia. *Climate* 12 (7): 91. https://doi.org/10.3390/cli12070091.

Arlot, S., & Celisse, A. (2010). A survey of cross-validation procedures for model selection. *Statistics Surveys*, 4, 40–79. https://doi.org/10.1214/09-SS054

Atkins, E. (2018). Green Streets as Habitat for Biodiversity. In *Nature Based Strategies for Urban and Building Sustainability*. Elsevier. https://doi.org/10.1016/B978-0-12-812150-4.00023-9.

Awad, M., & Khanna, R. (2015). Support vector regression. In *Efficient learning machines* (pp. 67–80). Springer. https://doi.org/10.1007/978-1-4302-5990-9_4

Babí Almenar, Javier, Thomas Elliot, Benedetto Rugani, et al. (2021). Nexus between Nature-Based Solutions, Ecosystem Services and Urban Challenges. *Land Use Policy* 100 (January): 104898. https://doi.org/10.1016/j.landusepol.2020.104898.

Breiman, L. (2001). Random forests. *Machine Learning, 45*(1), 5–32. https://doi.org/10.1023/A:1010933404324

Canepa, M., Mosca, F., Barath, S., Changenet, A., Hauck, T.E., Ludwig, F., Pianta, M., Roccotiello, E., Uthaya Selvan, S., Vogler, Verena, & Perini, K. (2022). Ecolopes, beyond greening. A multi-species approach for urban design. *Agathòn 11*, 238. https://doi.org/10.19229/2464-9309/11212022.

Castellar, J.A.C., L.A. Popartan, J. Pueyo-Ros, et al. (2021). Nature-Based Solutions in the Urban Context: Terminology, Classification and Scoring for Urban Challenges and Ecosystem Services. *Science of The Total Environment* 779 (July): 146237. https://doi.org/10.1016/j.scitotenv.2021.146237.

Celik, Serdar, and Ayla Ogus Binatli. (2018). Energy Savings and Economic Impact of Green Roofs: A Pilot Study. *Emerging Markets Finance and Trade* 54 (8): 1778–92.

Chen, P. (2021). Effects of the Entropy Weight on TOPSIS. *Expert Systems with Applications* 168 (April): 114186. https://doi.org/10.1016/j.eswa.2020.114186.

Chou, J. S., & Bui, D. K. (2014). Modeling heating and cooling loads by artificial intelligence for energy-efficient building design. *Energy and Buildings, 82, 437–446.* https://doi.org/10.1016/j.enbuild.2014.07.036

Del Campo-Hitschfeld, María Luisa, Nicolás Arenas, Marco Rivera, and Pablo Ballesteros-Pérez. (2023). Application of Spectrometry for Determining the Solar Radiation of Deciduous Trees' Shade: A Passive Energy Conservation Approach for Mediterranean Climates. *Buildings* 13 (5): 1130. https://doi.org/10.3390/buildings13051130.

Demir, S., & Sahin, E. K. (2024). The effectiveness of data pre-processing methods on the performance of machine learning techniques using RF, SVR, Cubist and SGB: a study on undrained shear strength prediction. *Stochastic Environmental Research and Risk*

Assessment, 38, 3273–3290. https://doi.org/10.1007/s00477-024-02745-9

EEA (2023). Greenhouse Gas Emissions from Energy Use in Buildings in Europe. https://www.eea.europa.eu/en/analysis/indicators/greenhouse-gas-emissions-from-energy.

European Commission. Directorate General for Climate Action. (2023). *EU-Level Technical Guidance on Adapting Buildings to Climate Change: Best Practice Guidance.* Publications Office. https://data.europa.eu/doi/10.2834/585141.

Evola, G, Costanzo, V., Magrì, C., Margani, G., Marletta, L., & Naboni, E. (2020). A Novel Comprehensive Workflow for Modelling Outdoor Thermal Comfort and Energy Demand in Urban Canyons: Results and Critical Issues. *Energy and Buildings* 216 (June): 109946. https://doi.org/10.1016/j.enbuild.2020.109946.

Franceschi, E, Moser-Reischl, A., Rahman, M., Pauleit, S., Pretzsch, H., & Rötzer, T. (2022). Crown Shapes of Urban Trees-Their Dependences on Tree Species, Tree Age and Local Environment, and Effects on Ecosystem Services. *Forests* 13 (5): 748. https://doi.org/10.3390/f13050748.

Ghorbany, S., Hu, M., Yao, S., & and Wang., C. (2024). Towards a Sustainable Urban Future: A Comprehensive Review of Urban Heat Island Research Technologies and Machine Learning Approaches. *Sustainability* 16 (11): 4609. https://doi.org/10.3390/su16114609.

Gu, X, & Goto, E. (2024). Evaluation of Plant Canopy Microclimates with Realistic Plants in Plant Factories with Artificial Light Using a Computational Fluid Dynamics Model. *Building and Environment* 264 (October): 111876. https://doi.org/10.1016/j.buildenv.2024.111876.

Gutierrez, C., Emma, B., Abayneh Abebe, Y., Vojinovic, Z., et al. (2023). Combining Machine Learning and Spatial Data Processing Techniques for Allocation of Large-Scale Nature-Based Solutions. *Blue-Green Systems* 5 (2): 186–99. https://doi.org/10.2166/bgs.2023.040.

Haq, A, Bakshi, B.R., Kodamana, H., & Ramteke, M. (2024). Assessing the Effectiveness of Improving Urban Air Quality with Solutions Based on Technology, Nature and Policy. *Sustainable Cities and Society* 110 (September): 105549. https://doi.org/10.1016/j.scs.2024.105549.

Harrell, F. E., Jr. (2016). *Regression modeling strategies*. Springer International Publishing. https://doi.org/10.1007/978-3-319-19425-7

Heaviside, C., Macintyre, H., & Sotiris Vardoulakis, S. (2017). The Urban Heat Island: Implications for Health in a Changing Environment. *Current Environmental Health Reports* 4 (3): 296–305.

Jin, S., Zhang, E., Guo, H., Hu, C., Zhang, Y., & Yan, D. (2023). Comprehensive Evaluation of Carbon Sequestration Potential of Landscape Tree Species and Its Influencing Factors Analysis: Implications for Urban Green Space Management. *Carbon Balance and Management* 18 (1): 17. https://doi.org/10.1186/s13021-023-00238-w.

Jones, H.G. (2013). *Plants and Microclimate: A Quantitative Approach to Environmental Plant Physiology*. 3rd ed. Cambridge University Press. https://doi.org/10.1017/CBO9780511845727.

Koutra, S., & Ioakimidis, C.S. (2022). Unveiling the Potential of Machine Learning Applications in Urban Planning Challenges. *Land* 12 (1): 83. https://doi.org/10.3390/land12010083.

Kruse, R., Mostaghim, S., Borgelt, C., Braune, C., & Steinbrecher, M. (2022). Multi-layer perceptrons. In *Computational intelligence* (pp. 53–124). Springer. https://doi.org/10.1007/978-3-030-42227-1_5

Kumakura, E., Furuya, K., & Kunii, Y. (2011). Numerical Analysis of Solar Shading Ratio of a Deciduous Tree for Seasonal Change. *Journal of The Japanese Institute of Landscape Architecture* 74 (5): 637–40. https://doi.org/10.5632/jila.74.637.

Kuuluvainen, T., & Pukkala, T. (1987). "Effect of Crown Shape and Tree Distribution on the Spatial Distribution of Shade." *Agricultural and Forest Meteorology* 40 (3): 215–31. https://doi.org/10.1016/0168-1923(87)90060-8.

Li, P., Xu, T., Wei, S., & Wang, Z.H. (2022). Multi-Objective Optimization of Urban Environmental System Design Using Machine Learning. *Computers, Environment and Urban Systems* 94 (June): 101796. https://doi.org/10.1016/j.compenvurbsys.2022.101796.

Liu, K., Lian, Z., Dai, X., & Lai, D. (2022). Comparing the Effects of Sun and Wind on Outdoor Thermal Comfort: A Case Study Based on Longitudinal Subject Tests in Cold Climate Region. *Science of The Total Environment* 825 (June): 154009. https://doi.org/10.1016/j.scitotenv.2022.154009.

Lobaccaro, G., & Acero, J.A. (2015). Comparative Analysis of Green Actions to Improve Outdoor Thermal Comfort inside Typical Urban Street Canyons. *Urban Climate* 14 (December): 251–67. https://doi.org/10.1016/j.uclim.2015.10.002.

Lumumba, V. W., Kiprotich, D., Mpaine, M. L., Makena, N. G., & Kavita, M. D. (2024). Comparative Analysis of Cross-Validation Techniques: LOOCV, K-folds Cross-Validation, and Repeated K-folds Cross-Validation in Machine Learning Models. *American Journal of Theoretical and Applied Statistics*, 13(5), 123–135. https://doi.org/10.11648/j.ajtas.20241305.13

Miniandi, N.D., Hidayat Jamal, M., Idlan Muhammad, M.K., Sharrar, L., & Shahid, S. (2025). Machine Learning in Modeling Urban Heat Islands: A Data-Driven Approach for Kuala Lumpur. *Earth Systems and Environment* 9 (2): 1037–60. https://doi.org/10.1007/s41748-025-00584-4.

Mosca, F., Oneto, G., Guasco, M., & Perini, K. (2025). Data Reasoning to Shape Tree Patches: Optimising Climate Change Adaptation in Urban Canyons. *TECHNE - Journal of Technology for Architecture and Environment* 29 (1): 219–28. https://doi.org/10.36253/techne-16560.

Mosca, F. (2024). *A Conceptual Framework for the Optimization of Environmentally Sustainable Nature-Based Solutions*. Wichmann Verlag. https://doi.org/10.14627/537752017.

Muniz-Gäal, L.P., Cotrim Pezzuto, C., Henriques de Carvalho, M.F., & Toledo Moreira Mota, L. (2020). Urban Geometry and the Microclimate of Street Canyons in Tropical Climate. Building and Environment 169 (February): 106547. https://doi.org/10.1016/j.buildenv.2019.106547.

Nicholson, S., Nikolopoulou, M., Watkins, R., Löve, M., & Ratti, C. (2024). Data Driven Design for Urban Street Shading: Validation and Application of Ladybug Tools as a Design Tool for Outdoor Thermal Comfort.vUrban Climate 56 (July): 102041. https://doi.org/10.1016/j.uclim.2024.102041.

O'Brien, S.T., Hubbell, S.P., Spiro, P. Condit, R., & Foster., R.B. (1995). Diameter, Height, Crown, and Age Relationship in Eight Neotropical Tree Species. *Ecology* 76 (6): 1926–39. https://doi.org/10.2307/1940724.

Oukhouya, H., & El Himdi, K. (2023). Comparing Machine Learning Methods—SVR, XGBoost, LSTM, and MLP—For Forecasting the Moroccan Stock Market. *Computer Sciences & Mathematics Forum*, 7(1), 39. https://doi.org/10.3390/IOCMA2023-14409

Pandey, V.K., & Dincer, H. (2023). A Review on TOPSIS Method and Its Extensions for Different Applications with Recent Development. *Soft Computing* 27 (23): 18011–39. https://doi.org/10.1007/s00500-023-09011-0.

Pedersen Zari, M. (2015). Ecosystem Services Analysis: Mimicking Ecosystem Services for Regenerative Urban Design. *International Journal of Sustainable Built Environment* 4 (1): 145–57. https://doi.org/10.1016/j.ijsbe.2015.02.004

Pedregosa, F., Varoquaux, G., Gramfort, A., Michel, V., Thirion, B., Grisel, O., Blondel, M., Prettenhofer, P., Weiss, R., Dubourg, V., Vanderplas, J., Passos, A., Cournapeau, D., Brucher, M., Perrot, M., & Duchesnay, É. (2011). Scikit-learn: Machine learning in Python. Journal of Machine Learning Research, 12, 2825–2830.

Peters, B., & Peters, T. (2018). Computing the Environment: Digital Design Tools for Simulation and Visualisation of Sustainable Architecture. Wiley.

Pretzsch, H., & Dieler, J. (2012). Evidence of Variant Intra- and Interspecific Scaling of Tree Crown Structure and Relevance for Allometric Theory. *Oecologia* 169 (3): 637–49. https://doi.org/10.1007/s00442-011-2240-5.

Mostapha, S.R., Pak, M., & Viola, A. (2013). Ladybug: A Parametric Environmental Plugin For Grasshopper To Help Designers Create An Environmentally-Conscious Design. Building Simulation, vol. 13: 3128–35. https://doi.org/10.26868/25222708.2013.2499.

Sharmin, M., Tjoelker, M.G., Pfautsch, S., Esperon-Rodriguez, M., Rymer, P.D., Power, S.A. (2023). Tree

Crown Traits and Planting Context Contribute to Reducing Urban Heat. *Urban Forestry & Urban Greening* 83 (May): 127913. https://doi.org/10.1016/j.ufug.2023.127913.

Singh, N., Singh, S., & Mall, R.K. (2020). Urban Ecology and Human Health: Implications of Urban Heat Island, Air Pollution and Climate Change Nexus. In *Urban Ecology*. Elsevier. https://doi.org/10.1016/B978-0-12-820730-7.00017-3.

Singh, R., & Vijaykumar, S. (2025). Kernel ridge regression inference. *arXiv preprint arXiv:2302.06578*. https://arxiv.org/abs/2302.06578

Stević, Ž., Subotić, M., Tanackov, I., Sremac, S., Ristić, B., & Simić, S. (2022). *EVALUATION OF TWO-LANE ROAD SECTIONS IN TERMS OF TRAFFIC RISK USING AN INTEGRATED MCDM MODEL*. Transport, 37(5), Article 5. https://doi.org/10.3846/transport.2022.18243

Sun, F., Zhang, J., Takeda, S., et al. (2025). Assessing the Mitigating Effects of Clustered Small Green Spaces on Urban Canyon Heatwaves: A Case Study of the Tsukiji-Gawa, Tokyo. Building and Environment 283 (September): 113373. https://doi.org/10.1016/j.buildenv.2025.113373.

Tan, J. K. N., R. N. Belcher, H. T. W. Tan, S. Menz, and T. Schroepfer. (2021). The Urban Heat Island Mitigation Potential of Vegetation Depends on Local Surface Type and Shade. *Urban Forestry & Urban Greening* 62 (July): 127128. https://doi.org/10.1016/j.ufug.2021.127128.

Thompson, V., Mitchell, D., Hegerl, G.C., Collins, M., Leach, N.J., & Slingo, J.M. (2023). The Most At-Risk Regions in the World for High-Impact Heatwaves. *Nature Communications* 14 (1): 2152. https://doi.org/10.1038/s41467-023-37554-1.

UNDRR. (2024). Nature-Based Solutions for Comprehensive Disaster and Climate Risk Management: Toolkit for Integrated Planning and Implementation of Disaster Risk Reduction and Climate Change Adaptation. https://www.undrr.org/publication/nature-based-solutions-comprehensive-disaster-and-climate-risk-management-toolkit.

United Nations. (2018). World Urbanization Prospects The 2018 Revision. https://population.un.org/wup/Publications/Files/WUP2018-Report.pdf.

Waitt, G., & Knobel, H. (2018). Embodied Geographies of Liveability and Urban Parks. *Urban Studies* 55 (14): 3151–67. https://doi.org/10.1177/0042098017740080.

Wang, Y., Cheng, Z., & Wang, Z. (2024). Multi-Output Bayesian Support Vector Regression Considering Dependent Outputs. *Mathematics*, 12(18), 2923. https://doi.org/10.3390/math12182923

Yola, L. (2020). Canyon Effects in Urban Configurations: Tropical Context Study. *IOP Conference Series: Earth and Environmental Science* 436 (1): 012028. https://doi.org/10.1088/1755-1315/436/1/012028.

Yoo, S. (2018). Investigating Important Urban Characteristics in the Formation of Urban Heat Islands: A Machine Learning Approach. *Journal of Big Data* 5 (1). https://doi.org/10.1186/s40537-018-0113-z.

Zhang, P., Ghosh, D., & Park, S. (2023). Spatial Measures and Methods in Sustainable Urban Morphology: A Systematic Review. *Landscape and Urban Planning* 237 (September): 104776. https://doi.org/10.1016/j.landurbplan.2023.104776.

Zhong, H., Feng, J., Lam, C.K.C., Hang, J., Hua, J., & Gu, Z. (2023). The Impact of Semi-Open Street Roofs on Urban Pollutant Exposure and Pedestrian-Level Thermal Comfort in 2-D Street Canyons. Building and Environment 239 (July): 110387. https://doi.org/10.1016/j.buildenv.2023.110387.

Zhou, X., & Chen, H. (2018). Impact of Urbanization-Related Land Use Land Cover Changes and Urban Morphology Changes on the Urban Heat Island Phenomenon. *Science of The Total Environment* 635 (September): 1467–76. https://doi.org/10.1016/j.scitotenv.2018.04.091.

Zhu, Z., Kleinn, C., & Nölke, N. (2021). Assessing Tree Crown Volume—a Review. *Forestry: An International Journal of Forest Research* 94 (1): 18–35. https://doi.org/10.1093/forestry/cpaa037.

Zou, J., Wang, L., Yang, S., Lacasse, M., & Wang, L.L. (2025). Predicting Long-Term Urban Overheating and Their Mitigations from Nature Based Solutions Using Machine Learning and Field Measurements." *Energy*

and Buildings 338 (July): 115720.
https://doi.org/10.1016/j.enbuild.2025.115720.

PART 4.

Conclusions

Chapter 8. Synthesis of the contribution and take-away highlights

Abstract

Cities are the defining habitats of the Anthropocene. This thesis set out to confront two intertwined threats to urban liveability, namely biodiversity loss and overheating, by advancing integrative and scalable analytical tools that bridge ecological knowledge and planning practice. Rather than refining policy frameworks from the top down, the work pursued a bottom-up strategy: exiting descriptive, decision-ready knowledge from spatial data about how cities are formed and function for both human and non-human inhabitants. Across seven chapters, the thesis developed and tested complementary methodologies: Cohabscapes for biodiversity-informed urban landscape classification, and a site-selection, downscaling, and optimization pipeline for heat mitigation with NBS, demonstrating how multi-species liveability and climatic resilience can be operationalized in planning workflows. This chapter summarizes the thesis achievements in relation to the research objectives. Subsequently, it highlights the methodological innovation and avenues for future research and applications.

Keywords

methodological innovations; future research; open data

8.1. Overall research achievements

8.1.1. Research outcomes in relation to the research objectives

This section synthesizes the empirical and methodological results of the thesis with direct reference to each of the six stated research objectives. For every objective the section describes the approach used to achieve it, the constituent subgoals and components that delivered the result, the location in the thesis where the supporting material is presented, and the principal limitations that qualify the findings.

8.1.1.1. Objective 1. Critically examine how planning systems address ecological sustainability and liveability in the Anthropocene

Objective 1 is primarily developed in chapter 1. The chapter delivers a structured analysis of contemporary planning systems that identifies four recurrent constraints: governance fragmentation, sectoral silos, inconsistent data infrastructures, and weak mechanisms for translating ecological and climatic knowledge into statutory and operational planning instruments. This analysis translates the constraints into explicit design criteria that guided the methodological work, specifically: harmonization of spatial units, open and reproducible workflows, and multiscale outputs. The thesis synthesizes policy instruments and planning practice to justify the need for tools that are interoperable across jurisdictions and scales, while noting that the analysis is comparative and normative rather than an experimental test of institutional reform, and that the diagnostic inherits the geographic and disciplinary biases present in the source literature.

8.1.1.2. Objective 2. Investigate how urban morphology and spatial analytical techniques can generate integrative, quantifiable insights into urban form

This thesis addresses Objective 2 by reviewing the state of the art in urban-morphological and spatial-analytical practice, with the goals of identifying persistent gaps in scale harmonization, methodological flexibility, as well as the integration of ecological and socio-thermal concerns. This work is conducted in chapter 2. The chapter translates the review into requirements for reproducible analytical workflows that render urban form as integrative, quantifiable knowledge. The requirements are set within existing descriptive and configurational traditions and highlights where those traditions fall short for cross-scale comparison and policy-relevant assessment. Building on that foundation, the research synthesizes morphological descriptors, configurational metrics, and spatial statistical techniques into two complementary analytical pipelines that produce harmonized, high-resolution landscape classifications and a morphometric multicriteria framework for prioritizing interventions. The resulting products convert heterogeneous vector and raster inputs into interoperable open-data layers that embed morphological, ecological, and thermal proxies within a common analytical space, enabling statistical linkage between form and function and supporting both downscaling to streetscape and building levels and upscaling to intercity comparisons. Validation against established reference datasets and independent ecological observations demonstrates the ecological and planning relevance of the outputs.

8.1.1.3. Objective 3. Define, validate, and test a biodiversity sensitive urban landscapes classification

Chapters 3 and 4 present the Cohabscapes framework: a harmonized, machine-learning classification that integrates morphological, biophysical and anthropic variables into an interpretable 10-m landscape typology through a reproducible workflow (harmonized preprocessing, PCA, unsupervised clustering, class interpretation and diagnostic outputs), and validate the framework in pilot cities using urban biodiversity occurrence records and contingency comparisons with established land-use layers. The validation and process of sensitivy analysis opens the discussion for a formal expansion of the framework toward all European cities. Specifically, Chapter 4 considers approaches to grow the classification framework by also considering its limitations, among which are class definitions and cluster sensitivity to preprocessing and sample composition, application data, and the chosen spatial resolution as well as scales.

8.1.1.4. Objective 4. Develop and validate a multiscale methodology for selecting and evaluating Nature Based Solutions for heat mitigation

Chapters 5–7 describe a multiscale decision framework that integrates SUHI mapping from thermal remote sensing, morphometric canyon typologies, multicriteria decision analysis and supervised machine-learning models to prioritize sites for Nature-Based Solutions and to estimate their likely microclimatic performance, together with a downscaling routine that translates city-level indicators into street and canyon scale guidance. SUHI derivation and morphometric diagnostics are detailed in Chapter 5, the downscaling algorithm and validation statistics are reported in Chapter 6, and the MCDM, ML training and applied site selection examples appear in Chapter 7. Methodologically, SUHI estimates are sensitive to acquisition timing and atmospheric assumptions, downscaling increases predictive uncertainty when moving from aggregate to canyon scale and requires explicit error quantification, ML model generalizability is constrained by the diversity of training data and demands retraining or domain adaptation for substantially different climates or canyon geometries, and MCDM outputs depend on criterion selection and weighting and should be interpreted as scenario-based priorities rather than definitive prescriptions. A multiscale workflow was established such that integration between thermal remote sensing, morphometric diagnostics, multicriteria decision analysis, and predictive modelling to identify priority sites for NBS was possible. The goal of this workflow, aligned with Objective 4, was to estimate NBS microclimatic performance, thus achieving a downscaling routine that translates city-level indicators into street and canyon scale guidance.

8.1.1.5. Objective 5. Bridge research and practice by producing and contextualizing tools and workflows

Chapters 3–7 deliver documented, reproducible analysis pipelines and practitioner-oriented outputs designed for integration into municipal planning workflows: packaged processing scripts, configuration files and variable dictionaries accompany Cohabscapes and the heat-mitigation pipeline. Practitioner outputs include, among others, rasterized Cohabscapes layers with class definitions, ranked priority site maps, canyon typology tables. The discussion sections orient these outputs to common planning instruments and institutional roles to support screening, prioritization and scenario testing. The limitations of this bridging effort arise from dependence on input data availability and quality, assumptions about minimum technical capacity in municipal teams (as well as the ever present knowledge gap between academic research and practice), and the fact that outputs are decision-support tools intended to inform rather than replace site-level design, monitoring and regulatory processes. The outcomes were produced to facilitate integration of the methods into planning practice. Outputs were designed to be transparent, modular, and compatible with common municipal GIS workflows.

8.1.1.6. Objective 6. Assess transferability, limitations, and future directions for the conceptual assumptions and developed methodologies

The last objective is operalized in the concluding chapter. Chapter 8 evaluates how transferable the thesis methods are, what their main limits are, and what should come next. It identifies key constraints: uneven data quality between cities, limited ecological validation across species and places, sensitivity to clustering and model choices, changing climate and remote-sensing inputs over time, and high computational costs for processing fine-resolution rasters at large scale. The chapter explains how errors can accumulate across chained steps (such as the one from chapters 5-7), which makes overall uncertainty harder to quantify. To improve transferability, it recommends practical steps such as standardizing preprocessing and variables, running sensitivity tests, and sequencing scaling through pilots, regional replication, and wider deployment based on data readiness. It also prioritizes future work, including a broaden validation to more cities and taxa, and a further optimization of computational workflows, while striving to develop clear guidance for practitioners and governance bodies. These assessments and recommendations clarify where the methods can be applied now, where more evidence is needed, and which technical and institutional actions will most increase reliable use.

8.1.2. Methodological and conceptual innovations

8.1.2.1. Conceptual reframing cities as co-habitative landscapes

Urban environments are treated as shared habitats in which human and non-human needs are negotiated through spatial form, zoning, ecological processes, ecosystem services, and socio-economic dynamics. This thesis position biodiversity and overheating as co-constitutive properties of urban fabric, rather than externalities, and reframes liveability as a multispecies and multiscale condition amenable to measurement and design (Fig. 1).

Core idea

Cities are landscapes of cohabitation where morphology, biophysical flows, and anthopic pressures jointly determine habitat quality and thermal stress.

Why it matters

It breaks the closeness between human-centric planning and ecological practice, allowing NBS to be evaluated for joint outcomes (e.g. thermal comfort, habitat value, connectivity).

Design implications

Prioritization and siting of interventions should be co-informed by species-relevant variables (e.g., tree density) and climatic risk (e.g., SUHI intensity).

Validation logic

Ecological correlations (e.g., species abundance vs. Cohabscapes classes) and microclimate performance (e.g., shading by NBS in canyons) become parallel evidence streams feeding the same planning decisions.

Trade-offs

Habitat enhancement can conflict with city-scale zoning or particular contextual needs; the reframing requires explicit multi-criteria evaluation to avoid single-goal bias.

Figure 1. Conceptual reasoning behind reframing cities as co-habitative landscapes, and consequences

8.1.2.1. Integrative analytics from heterogeneous data to interpretable deterministic decisions, oriented toward governance and practitioners

The thesis delivers methodologies that are built to be accessible to governance and planning contexts. By structuring the outputs in open formats and aligning them with policy instruments, the work reduces the gap between advanced analytics and practical implementation. The emphasis is on usability and integration into ecological and planning workflows, ensuring that results can inform and be plugged-in into dashboards, strategies, and intervention plans without requiring technical retooling (Fig. 2).

Open ad adaptable pipelines

Automated workflows with documented parameters, reproducible environments, and traceable outputs., that can function as component for existing workloads

Actionable units

Grid cells, urban tessellations, census blocks, street networks, and canyon classes allow planners to move from maps to interventions without translation overhead.

Policy alignment

Indicators and classes mapped to biodiversity strategies, adaptation plans, and governance dashboards.

Decision support clarity

Focus on heterogeneous decomposition through multi-criteria optimization and multi-parameter correlations, revealing drivers contribution and enabling targeted negotiation among urban stakeholders

Adaptable tailored to contextuality

Context-specific typologies guide multiscalar planning, such as for NBS integration, enabling inter-cities and intra-city site comparisons.

Co-benefit integration

Focus toward biodiversity and thermal comfort, parallelly evaluating primary threats for urban environments through multi-service delivery.

Capacity and knowledge building

Methodologies grant capacity for gathering documentation and case studies, as well as enabling open tooling that reduce the implementation gap for municipal teams.

Figure 2. Key take-away highlights for practical implementation of the thesis' results.

8.1.2.3. Reproducibility and openness through openly available pipelines

From a technical perspective, the thesis advances reproducibility and openness in spatial analysis by focusing on automated pipelines that bridge scales and delivers standardized outputs, from region-spanning maps and classifications to street-scale predictive designs performances. The methodological innovations lie in the integration of urban morphology theoretical knowledge together with landscape ecology, fostering two methodological pipelines that try to satisfy both academical perspectives, i.e. architecture/urban planning and urban ecology, sharing the ground framework of geospatial analysis (Fig. 3).

Data integration strategy

Cohabscapes
Stack heterogeneous layers; reduce redundancy (PCA/KPCA); cluster into species-generic classes; expose sub-classification structure to preserve interpretability.

SUHI pipeline
Encode morphometric features and contextual covariates; apply MCDM (e.g., TOPSIS/VIKOR) with objective weights (Entropy/Gini); derive typologies for targeted NBS.

Open outputs

Raster layers
For mapping and overlay

Tabular parquet datasets
For in-depth analytics and auditing

Code repositories
For reproducibility, reworking-forking the tools, and log tracebility

Automation and portability

Clear data provenance, and reproducible environments reduce friction when porting to new cities or areas

Auditability

Explicit feature modelling and diagnostics support peer review and usability confidence

Interoperability

Outputs align with common geospatial stacks and can be integrated by planning toolchains, CFD/microclimate workflows, and governance dashboards.

Robustness measures

Sensitivity checks across weighting schemes, spatial modules, and clustering parameters reduce brittleness and highlight stable signals.

Comparability vs specificity

Cohabscapes
Cohabscapes pursues cross-city comparability through common feature spaces.

SUHI pipeline
SUHI analysis accepts local heterogeneity, using typologies to tailor interventions.

Limitations and mitigations

Cohabscapes
Risk of over-aggregation; mitigated by sub-classifications and ecological validation.

SUHI pipeline
Limited thermal data resolution/temporal coverage; mitigated through modular datasets and future integration of higher-fidelity sources.

Figure 3. Key take-away highlights on the thesis outputs from a technical perspective.

8.2. Future research and implementation directions

8.2.1. The research perspective

Future work should advance the methodologies developed in this thesis along several interconnected axes.

At the continental scale, Cohabscapes requires stress-testing and refinement to ensure harmonization across European FUAs, expanding beyond the existing computed variables to incorporate richer biophysical and socio-ecological indicators. This expansion should make full use of modern HPC architectures, without sacrificing the optimization of the pipelines. The results could fully support comparative studies at the European level, coordinating ecological research and architectural practices for the development of sustainable cities.

In parallel, overheating analysis demands higher-resolution and temporally consistent SUHI datasets, enabling more reliable rankings and typologies that capture diurnal and seasonal dynamics. While this remains a critical limiting factor, alternatives for stable temperature layers or proxies exists, sacrificing the temporal specificity that EO can bring. Nonetheless, the existing architecture could already be fully scaled up to all Italian cities, and to the European scale with minor adjustments.

At finer scales, canyon-level modelling must expand beyond shading to include microclimatic indicators such as mean radiant temperature, airflow, and energy interactions, while machine learning pipelines should be strengthened through broader training datasets, hybrid physics-ML approaches, and uncertainty quantification (especially if going into CFD simulations).

Finally, future research should integrate additional ecosystem services, such as carbon sequestration, stormwater retention, air quality improvement, and biodiversity enhancement, into optimization routines, while embedding these tools into municipal workflows and governance structures to ensure uptake. A starting point could be a unified eco-climatic planning framework should be pursued, combining biodiversity and thermal risk assessments to co-prioritize interventions and design multi-benefit NBS. Together, these directions chart a pathway toward scalable, multi-species, and climate-resilient urban planning.

8.2.2. The implementation perspective

Translating research into practice requires outputs that align with governance instruments and planning workflows. The thesis already focuses on delivering outputs that satisfy these requirements from both a theoretical and technical point-of-view, such as raster maps and documented repositories, so they drop into municipal stacks and consultancy toolchains without much retooling. The focus for a thorough and effective implementation should be on slotting the tools in biodiversity strategies and adaptation plans, ensuring comparability across departments and scales. Below, the implementation pathways are tailored to three audiences that the doctorate research aims to reach: governance teams, practitioners, and ecologists/urban analysts.

8.2.2.1. Supporting governance and municipal teams in adapting cities to biodiversity loss and overheating

The primary concern is to align to current policies and support the development of the next normative generation. In doing so, indicators and typologies developed through the doctorate thesis that can map cities should be considered into adaptation plans and budget cycles, enabling different departments to track progresses within their administration, or comparing to neighbouring cities, using consistent and comparable metrics.

Dashboards are being used by governances to improve data readability and bettering the understanding of urban conditions. The units used in the technical development of the thesis aligns with actionable decisions of administrations. For example, parcels (census blocks), street networks, canyon classes, urban landscape typologies, morphological tessellation, all link maps to intervation (such as tree planting, shading strategies, upgrading the permeability of streets or connectivity of ecological corridors). Monitoring can also be supported, through the usage of indicators for addressing SUHI trends, green canopy coverage, and socioeconomic vulnerabilities.

Multicriteria optimization and decision making decomposes rankings, helping to identify main drivers' contributions (such as exposure to risk), making tailored or confronted trade-offs between different urban stakeholders more apparent and transparent for councils. This is especially relevant when the different stakeholders are not only humans, albeit vulnerable for socioeconomic conditions, but also non-humans such as plants and animals species.

Cities dashboards operate through GIS backends, and their asset management should be taken into consideration while inserting new components, permitting systems to adapt without introducing new complexities and permitting clean ingestion and supporting auditability.

8.2.2.2. Practitioners (architects, urban planners, urban designers) seeking data-driven innovation

The same spatial commitments toward design-ready spatial units are of interest for practitioners. Canyon classes, street transect, and tessellation directly translate into design briefs and support the identification of tree typologies, shading stragies, design targets, reducing the overhead burden from analysis to concept.

ML-assisted generalization provides and support the generalization of findings across different city areas, or comparison through different cities, supporting early-stage choices and reducing dependence on repeated simulation or analysis.

Toolchain compatibility is expected, especially when working with parametric design software (Rhino/Grasshopper, but also GIS or microclimate tools for CFD and airflow analysis), enabling parametric iterations tied to real urban morphologies.

8.2.2.3. *Ecologists and urban analysists advancing multispecies liveability*

Ecologists and urban analysts can use the methodologies developed in this thesis to deepen their understanding of multispecies liveability in cities. For example, the Cohabscapes classification and the canyon extraction tool provide harmonized, multiscale datasets that can link urban morphology to ecological indications such as habitat quality, species movement, or microclimatic conditions, offering analytical depth that connects ecological processes with spatial form, socioeconomic factors, and biophysical conditions.

The developed pipelines are designed with transparency in mind: data origin and scraping processes, preprocessing steps, explicit feature engineering, and diagnostics such as loadings, cluster profiles, correlation matrixes, together with rank decomposition and optimization, are fully documented, supporting replication and peer review.

The framework is also extensible, accommodating additional indicators such as ones inherent to climate analysis (e.g., mean radiant temperature or building energy interactions) and urban ecology (e.g., connectivity matrixes or species occurrence), thereby enabling richer eco-climatic analyses.

The outputs are formatted for governance dashboards and reporting systems, deliberately imagining a possible direct feed from research to policy (passing through urban design) and ensuring that ecological insights can inform evidence-based prioritization and integrated urban strategies.

8.3. Closing reflection

This thesis argues that urban resilience and cohabitations are not slogans, but practical and measurable conditions of cities. By making biodiversity and overheating legible and actionable across scales, through open and reproducible methodologies, it invites cities to move beyond fragmented and sectoral responses toward integrated and multispecies climate-aware design. The Anthropocene demands that we reimagine cities as living systems. The tools and frameworks developed in this thesis are offered as scaffolding for that reimagination of urban habitats (more specifically, for tools and applications that focuses on urban habitats), as means to describe, compare, and intervene so that cities can sustainably support the diverse forms of life they now undeniably contain.

8.4. Fundings

The author's scholarship is financed by Italian *Piano Nazionale di Ripresa e Resilienza* (PNRR), Mission 4 "Education and Research" Component 1, under Ministerial Decree No. 351 of 09/04/2022., scholarship number 1002, I.4.1 *Borse PNRR Patrimonio Culturale*.

All the commitments and conditions established under the PNRR framework and *Decreto Ministeriale* n.351/2022 have been duly satisfied. The doctoral thesis activities have been carried out in full accordance with the obligations of the scholarship, without overlapping with other funding sources, and in compliance with the expected project objectives and results. The work respects the principle of 'Do No Significant Harm' (DNSH) as defined in Regulation (EU) 2020/852, ensuring no adverse impact on climate change mitigation or adaptation, water and marine resources, circular economy, pollution prevention, or biodiversity and ecosystems. Furthermore, the doctorate project does not involve any 'brown' research activities as outlined in the European Commission Communication 2021/C 58/01, and all activities remain fully aligned with relevant EU and national environmental legislation.

The author binds his research objectives to his funding opportunities, which enabled him to fully express his personal research desires while achieving (at the very least) personally rewarding results. In this context, it important to recognize that *Patrimonio Culturale* (usually translated as "cultural heritage") encompasses a wide range of meanings, particularly within the architectural field. Together with his tutor, co-tutors, and the doctoral board, the author discussed and approved a research direction characterized by a technical and analytical approach, deepening the role of the architect as an analyst-describer who employs modern tools and methodologies. Special attention must be paid to the fact that the description of urban artifacts involves an a priori framing of their value as "cultural heritage". Such framing inevitably limits the immediate expression of judgment, yet it is precisely this foundational description that makes any subsequent evaluation possible and meaningful.

Thus, the research objectives outlined in this doctorate thesis are fully aligned with the detailed aims of the PNRR *Patrimonio Culturale* scholarships in the Architecture field (DM 351/2022, Investimento 4.1). By critically examining contemporary urban planning practices in the Anthropocene and assessing their capacity to integrate ecological sustainability and liveability, the work contributes to the valorisation and innovative interpretation of cultural heritage within urban contexts. The investigation of urban morphology through spatial analytical techniques provides quantifiable insights into urban form, thereby supporting environmentally informed planning and biodiversity-sensitive design, which are central to the sustainable management of architectural heritage. Furthermore, the development and validation of novel methodologies for describing urban

landscapes and mitigating biodiversity loss foster interdisciplinary cooperation between architects and ecologists, strengthening the analytical role of the architect as a describer of heritage conditions. Finally, the methodological framework for addressing urban heat-related risks through Nature-Based Solutions and predictive multiscale tools directly advances the PNRR objective of equipping doctoral research with innovative approaches to safeguard and enhance the resilience of cultural and architectural assets in the face of climate change.

Finanziato dall'Unione europea NextGenerationEU
Ministero dell'Università e della Ricerca
Italiadomani Piano Nazionale di Ripresa e Resilienza
Università di Genova

Borsa di dottorato cofinanziata con risorse dell'Unione europea-NextGeneration EU

Piano Nazionale di Ripresa e Resilienza Missione 4, componente 1 "Potenziamento

dell'offerta dei servizi di istruzione: dagli asili nido all'Università

PART 5

Research data and Supporting information

Data availability

The methodologies and data produced in the doctorate thesis are fully distributed in open access, as per the requirements of the fundings, of the relative projects (ECOLOPES, URBAN GENERATION), and in line with the FAIR principles (Findable, Accessible, Interoperable, and Reusable) for scientific data.

Five main repositories are built, each for a different chapter (3-7). Each repository contains the environment variables needed to reproduce the results, together with the code (mostly Jupyter commented notebooks and helper libraries) and executables, and the data output in various format.

Due to the size of the shared data and openness requirements of the research, particular care at the current stage of writing on to correctly publish the data. As of now, the five repositories are hosted in private Git repositories (gitlab/ecolopes/ for Chapter 3; github/goneto/ for Chapters 4-7), and massive data for Chapter 3 is currently hosted on a private Zenodo repository. Any request to vision the code or data will be duly met by the author will full support.

Annex A (Chapter 3) – Variable tables, methodologies, and data origin

In Chapter 3, an operative threshold of what constitutes "urban" was adopted to move beyond the immediate human-centric perspective of administrative city borders. For this purpose, the Global Human Settlement Layer definition of Functional Urban Areas (Schiavina et al., 2023) was used, as it represents urban areas more broadly by including both urban centres and peri-urban zones that economically and infrastructurally contribute to shaping cities.

An equiareal projection was selected to ensure that all grid cells in the modelling represented the same spatial extent, thereby enabling direct comparison of urban landscapes of equal size. Each city was aligned to the grid by locating the nearest corresponding points. To account for potential edge effects during computation, urban boundaries were buffered by 200 m. These boundaries were then rasterised and used as reference rasters for subsequent operations, including matching and stacking.

Datasets were primarily downloaded manually, with automated scraping applied where appropriate. The OSMNX package provided a flexible tool for extracting OSM geometries based on tags (Boeing, 2024). For each OSM-based variable, a curated set of tags was selected, and geometries were carefully pruned and cleaned. Given the variability of OSM feature tagging, an "all-or-nothing" approach was adopted: overly specific tags were disregarded, while the most widely used *areas* and *places* tags were retained. Geometries were rasterised onto the grid and stored as presence-only information. For other datasets, custom APIs were used where available to facilitate handling of large datasets and feature selection, notably the *chelsa_cmip6* package (Karger et al., 2017).

Because most datasets were distributed in tile format, constructing full mosaics would have produced very large, memory-intensive rasters and complicated computation. Instead, a feature-search approach was applied: data were extracted tile by tile within the city boundary mask, and fragments were mosaicked only afterward. The coordinate reference system (CRS) of the first tile was read to reproject the mask, after which the data were reverted to the Mollweide grid to ensure that each pixel contained information. This approach improved scalability by optimising memory usage.

The computation pipeline was structured according to variable scale. Local-scale variables were processed only for the Urban Form local sub-classification, which had native resolutions of 10 m or finer (Table A.1). Landscape-scale procedures were applied to the remaining sub-classifications, as most variables had coarser resolutions better suited to higher-scale computation (Table A.2, A.3, A.4). Landscape metrics were calculated using a rounded 21-cell diameter window, applying both kernel averages and standard deviations. The resulting data were stacked onto the reference raster, reprojected to Mollweide, and resampled to a 10 m resolution for consistency. Numerical computations were primarily conducted with *xarray* DataArrays, vector data were managed with *geopandas*, and raster writing was performed using *rasterio* and *rioxarray*. Kernel calculations and distance measures were computed with *scipy*.

Table A.1. Variables in the Local Urban Fabric subclassification

Local Urban Fabric			
Variable	**Methodology**	**Data origin**	**Native resolution**
Artificial features			
Building Height	Both sources are reprojected and matched to the reference grid using nearest neighbours. Then, UA BH 2012 layer is superimposed over MSZ Classes of building height (3<, 3-6, 6-15,15-30,>30).	Global Human Settlement Layer / Built Classification with Morphological Settlement Zones (MSZ) 10.2905/3C60DDF6-0586-4190-854B-F6AA0EDC2A30 + Copernicus / Urban Atlas Building Height 2012 https://doi.org/10.2909/42690e05-edf4-43fc-8020-33e130f62023	10 m
Built-up Fraction	The source is reprojected and matched to the reference grid using nearest neighbours.	Global Human Settlement Layer / Built Surface (Built-s) 10.2905/9F06F36F-4B11-47EC-ABB0-4F8B7B1D72EA	10 m
Mayor Transport route Presence	OSM geometries are extracted using osmnx with the base grid as a mask. The OSM geometries are then rasterized matching the reference grid, and added together with “street” layer from MSZ classification. The data is then reprojected matching the source grid.	Open Street Maps (OSM) / osm_tags = [{'highway':"motorway"}, {'highway':"motorway_link"}, {'highway':"trunk"}, {'highway':"trunk_link"}, {'highway':"primary"}, {'highway':"primary_link"}, {'highway':"secondary"}, {'highway':"secondary_link"}, {'highway':"tertiary"}, {'highway':"tertiary_link"}, {'highway':"unclassified"}, {'highway':"road"}, {'highway':"residential"}, {'railway':True}]; Global Human Settlement Layer / Built Classification with Morphological Settlement Zones (MSZ) 10.2905/3C60DDF6-0586-4190-854B-F6AA0EDC2A30	10 m
Imperviousness Density	The source is reprojected and matched to the reference grid using nearest neighbours.	Copernicus High Resolution Layer / Imperviousness https://doi.org/10.2909/3bf542bd-eebd-4d73-b53c-a0243f2ed862	10 m
Natural features			
Tree Cover Density	The source is reprojected and matched to the	Copernicus High Resolution Layer / Tree Cover Density	10 m

	reference grid using nearest neighbours.	https://doi.org/10.2909/486f77da-d605-423e-93a9-680760ab6791	
Grassland Presence	The source is reprojected and matched to the reference grid using nearest neighbours.	Copernicus High Resolution Layer / Grassland https://doi.org/10.2909/60639d5b-9164-4135-ae93-fb4132bb6d83	10 m
Shrubs Presence	The source is reprojected and matched to the reference grid using nearest neighbours.	Copernicus High Resolution Layer / Small Woody Features https://doi.org/10.2909/a8e683b1-2f96-45c8-827f-580a79413018	5 m
Agricultural Land Presence	The source layer "crop" is reprojected and matched to the reference grid using nearest neighbours.	European Space Agency / WorldCover V2 2021 https://doi.org/10.5281/zenodo.7254221	10 m
Aquatic Surface Presence	The source layer "permanent water" is reprojected and matched to the reference grid using nearest neighbours.	Copernicus High Resolution Layer / Water and Wetness Water and Wetness status 2018 (raster 10 m and 100 m), Europe, 3-yearly — Copernicus Land Monitoring Service	10 m
Other features			
Count of different land covers	Sum of land covers in cell: built-up fraction, transports, trees, grass, shrubs, agriculture		10 m

Table A.2. Variables in the Landscape Urban Fabric subclassification

Landscape Urban Fabric			
Variable	**Methodology**	**Data origin**	**Native resolution**
Class metrics			
Mean and standard deviation of each Urban Form Local Principal Component	Mean and standard deviation computed using a 21x21 (100m radius) circular kernel with scipy generic filter.	Urban Form Local classification as base mosaic	10 m
Landscape metrics			
Shannon Diversity Index	Using Fragstats 4.2, computed in a 100m radius rounded window	Urban Form Local classification as base mosaic	10 m
Contagion	Using Fragstats 4.2, computed in a 100m radius rounded window	Urban Form Local classification as base mosaic	10 m

Table A.3. Variables in the Anthropic Imprint subclassification

Anthropic Imprint			
Variable	**Methodology**	**Data origin**	**Native resolution**
Demographic			
Population Density	The source is reprojected and matched to the reference grid using nearest neighbours. Then, the average is computed in a moving window of nearest neighbour resampled value of raster; using scipy generic filter as a 21x21 round kernel (100m diameter).	Global Human Settlement Layer (GHSL)/Population Density (POP) 10.2905/2FF68A52-5B5B-4A22-8F40-C41DA8332CFE	100 m
Age Structures: 0-15	The source is divided in age groups and unified by merging female and male layers, each opportunately reprojected and matched to the reference grid, using the nearest neighbours. Then, a ratio is computed by dividing the 0-15 partition with the sum of all layers. Finally, the average is computed in a moving window using scipy generic filter as a 21x21 round kernel (100m diameter).	WorldPop / Age and gender structures, structured 10.5258/SOTON/WP00695	100 m
Age Structures: 20-35	The source is divided in age groups and unified by merging female and male layers, each opportunately reprojected and matched to the reference grid, using the nearest neighbours. Then, a ratio is computed by dividing the 20-35 partition with the sum of all layers. Finally, the average is computed in a moving window using scipy generic filter as a 21x21 round kernel (100m diameter).	WorldPop / Age and gender structures, structured 10.5258/SOTON/WP00695	100 m
Age Structures: 40-60	The source is divided in age groups and unified by merging female and male	WorldPop / Age and gender structures, structured 10.5258/SOTON/WP00695	100 m

	layers, each opportunately reprojected and matched to the reference grid, using the nearest neighbours. Then, a ratio is computed by dividing the 40-60 partition with the sum of all layers. Finally, the average is computed in a moving window using scipy generic filter as a 21x21 round kernel (100m diameter).		
Age Structures: 65-85	The source is divided in age groups and unified by merging female and male layers, each opportunately reprojected and matched to the reference grid, using the nearest neighbours. Then, a ratio is computed by dividing the 65-85 partition with the sum of all layers. Finally, the average is computed in a moving window using scipy generic filter as a 21x21 round kernel (100m diameter).	WorldPop / Age and gender structures, structured 10.5258/SOTON/WP00695	100 m
Land use: Services, accessibility, policy			
Population Density	The source is reprojected and matched to the reference grid using nearest neighbours. Then, the average is computed in a moving window of nearest neighbour resampled value of raster; using scipy generic filter as a 21x21 round kernel (100m diameter).	Global Human Settlement Layer (GHSL)/Population Density (POP) 10.2905/2FF68A52-5B5B-4A22-8F40-C41DA8332CFE	100 m
Age Structures: 0-15	The source is divided in age groups and unified by merging female and male layers, each opportunately reprojected and matched to the reference grid, using the nearest neighbours. Then, a ratio is computed by dividing the 0-15 partition with the sum of all layers. Finally, the average is computed in a moving	WorldPop / Age and gender structures, structured 10.5258/SOTON/WP00695	100 m

	window using scipy generic filter as a 21x21 round kernel (100m diameter).		
Commercial Area Ratio	The geometries are extracted using osmnx by using the base grid as a mask. The mask is reprojected to epsg:4326 to comply with OSM CRS, then the geometries are reprojected back to Mollweide before modelling. The geometries are then rasterized matching the reference grid. Finally, the ratio is computed by summing pixels with values of commercial buildings dividing by the total areas of the moving window, computed using scipy generic filter as a 21x21 round kernel (100m diameter).	osm_tags = [{'landuse':'commercial'}, {'landuse':'retail'}, {'craft':True}, {'shop':True},]	Vectoria l
Industrial Area Ratio	The geometries are extracted using osmnx by using the base grid as a mask. The mask is reprojected to epsg:4326 to comply with OSM CRS, then the geometries are reprojected back to Mollweide before modelling. The geometries are then rasterized matching the reference grid. Finally, the ratio is computed by summing pixels with values of industrial buildings dividing by the total areas of the moving window, computed using scipy generic filter as a 21x21 round kernel (100m diameter).	osm_tags = [{'landuse':'industrial'}, {'landuse':'depot'}, {'landuse':'garages'}, {'man_made':'works'}, {'man_made':'beacon'}, {'man_made':'bunker_silo'}, {'man_made':'chimney'}, {'man_made':'communications_tower'}, {'man_made':'crane'}, {'man_made':'gasometer'}, {'man_made':'goods_conveyor'}, {'man_made':'kiln'}, {'man_made':'lighthouse'}, {'man_made':'mast'}, {'man_made':'mineshaft'}, {'man_made':'monitoring_station'}, {'man_made':'observatory'}, {'man_made':'pumping_station'}, {'man_made':'pipeline'}, {'man_made':'reservoir_covered'}, {'man_made':'silo'}, {'man_made':'storage_tank'}, {'man_made':'tailings_pond'}, {'man_made':'tower'}, {'man_made':'wastewater_plant'}, {'man_made':'watermill'}, {'man_made':'water_tower'},	Vectoria l

		{'man_made':'windmill'},]	
Public Services Area Ratio	The geometries are extracted using osmnx by using the base grid as a mask. The mask is reprojected to epsg:4326 to comply with OSM CRS, then the geometries are reprojected back to Mollweide before modelling. The geometries are then rasterized matching the reference grid. Finally, the ratio is computed by summing pixels with values of public service buildings dividing by the total areas of the moving window, computed using scipy generic filter as a 21x21 round kernel (100m diameter).	osm_tags = [{'landuse':'institutional'}, {'landuse':'educational'}, # education {'amenity':'college'}, {'amenity':'dancing_school'}, {'amenity':'driving_school'}, {'amenity':'first_aid_school'}, {'amenity':'kindergarten'}, {'amenity':'language_school'}, {'amenity':'library'}, {'amenity':'surf_school'}, {'amenity':'toy_library'}, {'amenity':'research_institute'}, {'amenity':'training'}, {'amenity':'music_school'}, {'amenity':'school'}, {'amenity':'traffic_park'}, {'amenity':'university'}, # financial {'amenity':'atm'}, {'amenity':'payment_terminal'}, {'amenity':'bank'}, {'amenity':'bureau_de_change'}, {'amenity':'money_transfer'}, {'amenity':'payment_centre'}, # healthcare {'amenity':'baby_hatch'}, {'amenity':'clinic'}, {'amenity':'dentist'}, {'amenity':'doctors'}, {'amenity':'hospital'}, {'amenity':'nursing_home'}, {'amenity':'pharmacy'}, {'amenity':'social_facility'}, {'amenity':'veterinary'}, # public service {'amenity':'courthouse'}, {'amenity':'fire_station'}, {'amenity':'police'}, {'amenity':'post_box'}, {'amenity':'post_depot'}, {'amenity':'post_office'}, {'amenity':'prison'}, {'amenity':'ranger_station'}, {'amenity':'townhall'},]	Vectorial
Recreational Area Ratio	The geometries are extracted using osmnx by using the	osm_tags = [{'landuse':'recreation_ground'},	Vectorial

	base grid as a mask. The mask is reprojected to epsg:4326 to comply with OSM CRS, then the geometries are reprojected back to Mollweide before modelling. The geometries are then rasterized matching the reference grid. Finally, the ratio is computed by summing pixels with values of recreational areas dividing by the total areas of the moving window, computed using scipy generic filter as a 21x21 round kernel (100m diameter).	{'landuse':'religious'}, {'leisure':True}, {'sport':True}, # sustenance {'amenity':'bar'}, {'amenity':'biergarten'}, {'amenity':'cafe'}, {'amenity':'fast_food'}, {'amenity':'food_court'}, {'amenity':'ice_cream'}, {'amenity':'pub'}, {'amenity':'restaurant'}, # entertainment {'amenity':'arts_centre'}, {'amenity':'brothel'}, {'amenity':'casino'}, {'amenity':'cinema'}, {'amenity':'community_centre'}, {'amenity':'conference_centre'}, {'amenity':'events_venue'}, {'amenity':'exhibition_centre'}, {'amenity':'fountain'}, {'amenity':'gambling'}, {'amenity':'love_hotel'}, {'amenity':'music_venue'}, {'amenity':'nightclub'}, {'amenity':'planetarium'}, {'amenity':'public_bookcase'}, {'amenity':'social_centre'}, {'amenity':'stripclub'}, {'amenity':'studio'}, {'amenity':'swingerclub'}, {'amenity':'theatre'},]	
Cultural Location Ratio	The geometries are extracted using osmnx by using the base grid as a mask. The mask is reprojected to epsg:4326 to comply with OSM CRS, then the geometries are reprojected back to Mollweide before modelling. The geometries are then rasterized matching the reference grid. Finally, the ratio is computed by summing pixels with values of cultural locations dividing by the total areas of the moving window, computed using scipy generic filter as a	osm_tags = [{'historic':True}, {'tourism':"alpine_hut"}, {'tourism':"aquarium"}, {'tourism':"artwork"}, {'tourism':"attraction"}, {'tourism':"gallery"}, {'tourism':"museum"}, {'tourism':"yes"}, {'heritage':True},]	Vectorial

	21x21 round kernel (100m diameter).		
Public Green Proportion	The geometries are extracted using osmnx by using the base grid as a mask. The mask is reprojected to epsg:4326 to comply with OSM CRS, then the geometries are reprojected back to Mollweide before modelling. The geometries are then rasterized matching the reference grid. Then, presence values (as in, Boolean 1/0) from Grass, Shrubs, and Trees (same as the local layers) are summed together to create the total amount of green. The public green is produced firstly by using the total amount of green as a mask for the OSM geometries, then the proportion is computed by dividing the remaining osm green pixels by the total amount of green in the moving window, computed using scipy generic filter as a 21x21 round kernel (100m diameter).	osm_tags = [{'leisure':"park"}, {'leisure':"garden"}, {'leisure':"common"}, {'leisure':"playground"},]	Vectorial
Preservation Policy Ratio	The source vector geometries are rasterized on the base grid and projected to Mollweide CRS (esri 54009). Then, the ratio is calculated by using a moving window, computed using scipy generic filter as a 21x21 round kernel (100m diameter), by dividing the source data by the total area of the window.	World Database of Protected Areas (WDPA)/Other Effective Area-Based Conservation Measures (WDOECM) and International Union for Conservation of Nature (IUCN) WDPA_WDOECM_Manual_1_6.pdf	Vectorial
Average Distance to Public Transport	The OSM geometry is extracted using osmnx by masking with the base grid. The grid is projected to epsg 4326 to comply with OSM native CRS, then the geometries are reprojected back to Mollweide. The data	osm_tags = [{'public_transport':True}]	Vectorial

	is rasterized matching the reference grid. Then, for each pixel of public transport, the distance matrix is computed using scipy ndimage.distance_transform _edt sampling [10,10], equal to the reference grid. Having the distance matrix, the final average is computed by moving window using scipy generic filter as a 21x21 round kernel (100m diameter).		
Anthropic emissions			
Nighttime light Pollution	The source raster is reprojected matching the reference grid using nearest neighbours.	Wuhan University / Luojia 1-A Nighttime Lights http://59.175.109.173:8888/app/login_en.html	130
Anthropogenic Heat Flux	The source raster is reprojected matching the reference grid using nearest neighbours.	Varquez et al. (2021)/Average Anthropic Heat Emission (AHE) 2010 10.1038/s41597-021-00850-w	1000

Table A.4. Variables in the Biophysical Conditions subclassification

Biophysical Conditions			
Variable	**Methodology**	**Data origin**	**Native resolution**
Hydrology			
Permanent water ratio	The source layer "permanent water" is reprojected and matched to the reference grid using nearest neighbours. Then, the ratio is computed using a moving window with scipy generic filter as a 21x21 round kernel (100m diameter), dividing the source data by the total area of the window.	Copernicus High Resolution Layer / Water and Wetness [Water and Wetness status 2018 (raster 10 m and 100 m), Europe, 3-yearly — Copernicus Land Monitoring Service]	10 m
Temporary water ratio	The source layer "temporary water" is reprojected and matched to the reference grid using nearest neighbours. Then, the ratio is computed using a moving window with scipy generic filter as a 21x21 round kernel (100m diameter), dividing the source data by the total area of the window.	As before	10 m
Topography			
Mean Altitude	The source DEM is reprojected and matched to the reference grid using nearest neighbours. The mean is computed using a moving window with scipy generic filter as a 21x21 round kernel (100m diameter).	EOC Geo service / TanDEM-X 30m Edited Digital Elevation Model (EDEM) https://download.geoservice.dlr.de/TDM30_EDEM/	30 m
Standard deviation Altitude	As before, but the filter computes the standard deviation	As before	30 m
Mean Slope	The source DEM is reprojected and matched to the reference grid using nearest neighbours. Then, using xdem terrain.get_terrain_attribute, the slope is computed. The mean is computed using a moving window with scipy generic filter as a 21x21 round kernel (100m diameter).	EOC Geo service / TanDEM-X 30m Edited Digital Elevation Model (EDEM) https://download.geoservice.dlr.de/TDM30_EDEM/	30 m
Standard deviation Slope	As before, but the filter computes the standard deviation	As before	30 m
Mean Aspect	The source DEM is reprojected and matched to the reference grid using nearest neighbours. Then, using xdem terrain.get_terrain_attribute, the aspect is computed. The mean is	EOC Geo service / TanDEM-X 30m Edited Digital Elevation Model (EDEM) https://download.geoservice.dlr.de/TDM30_EDEM/	30 m

	computed using a moving window with scipy generic filter as a 21x21 round kernel (100m diameter).		
Standard deviation Aspect	As before, but the filter computes the standard deviation	As before	30 m
Mean Curvature	The source DEM is reprojected and matched to the reference grid using nearest neighbours. Then, using xdem terrain.get_terrain_attribute, the curvature is computed. The mean is computed using a moving window with scipy generic filter as a 21x21 round kernel (100m diameter).	EOC Geo service / TanDEM-X 30m Edited Digital Elevation Model (EDEM) https://download.geoservice.dlr.de/TDM30_EDEM/	30 m
Standard deviation Curvature	As before, but the filter computes the standard deviation	As before	30 m
Soil			
Soil wetness ratio	The source layers "permanent and temporary wetness" are reprojected and matched to the reference grid using nearest neighbours. Then, the ratio is computed using a moving window with scipy generic filter as a 21x21 round kernel (100m diameter), dividing the source data by the total area of the window.	Copernicus High Resolution Layer / Water and Wetness Water and Wetness status 2018 (raster 10 m and 100 m), Europe, 3-yearly — Copernicus Land Monitoring Service	10 m
Climate			
Absolute max of air temperature, mean value	Chelsa cmip6 is used to extract data for a specific period. From the variable bio5, I extract the scenarios ssp126, ssp370, and ssp585 and average the results for Average Warmest Month Air Temperature in the period 2014-2023. Then, the data is reprojected matching the reference grid. The mean is computed using a moving window with scipy generic filter as a 21x21 round kernel (100m diameter).	CHELSA BIOCLIM + v2.1 Bioclim – Chelsa Climate (chelsa-climate.org)	1000 m
Relative max of air temperature, mean value	From the result above, the relative is computed by dividing every pixel by the raster mean value.	As above	1000 m
Absolute min of air temperature	Chelsa cmip6 is used to extract data for a specific period. From the variable bio6, I extract the scenarios ssp126, ssp370, and ssp585 and	CHELSA BIOCLIM + v2.1 Bioclim – Chelsa Climate (chelsa-climate.org)	1000 m

, mean value	average the results for Average Coldest Month Air Temperature in the period 2014-2023. Then, the data is reprojected matching the reference grid. The mean is computed using a moving window with scipy generic filter as a 21x21 round kernel (100m diameter).		
Relative min of air temperature , mean value	From the result above, the relative is computed by dividing every pixel by the raster mean value.	As above	1000 m
Absolute precipitations, mean value	Chelsa cmip6 is used to extract data for a specific period. From the variable bio12, I extract the scenarios ssp126, ssp370, and ssp585 and average the results for Average Annual Precipitations in the period 2014-2023. Then, the data is reprojected matching the reference grid. The mean is computed using a moving window with scipy generic filter as a 21x21 round kernel (100m diameter).	CHELSA BIOCLIM + v2.1 Bioclim – Chelsa Climate (chelsa-climate.org)	1000 m
Relative precipitations, mean value	From the result above, the relative is computed by dividing every pixel by the raster mean value.	As above	1000 m
Wind speed at 10m, mean value	The source raster is extracted using the reference grid as mask, then reprojected matching the grid. Then, the mean is computed using a moving window with scipy generic filter as a 21x21 round kernel (100m diameter).	Global Wind Atlas / Wind speed 10m https://globalwindatlas.info/en/	300 m
Wind speed at 200m, mean value	The source raster is extracted using the reference grid as mask, then reprojected matching the grid. Then, the mean is computed using a moving window with scipy generic filter as a 21x21 round kernel (100m diameter).	Global Wind Atlas / Wind speed 200m https://globalwindatlas.info/en/	300 m

Annex B (Chapter 3) - Principal Component Analysis (PCA) for the four layers

A target variance of 0.95 was set for the Principal Components (PCs) to explain. The minimum number of PCs was determined from the smallest set of eigenvalues required to reach this threshold. A high variance threshold was chosen to ensure that even minor contributions from less influential variables were retained in the analysis.

Both Principal Component Analysis (PCA) and Kernel Principal Component Analysis (KPCA) were compared, with kernel approximations computed using the *Nystroem* method. The analyses were implemented in *scikit-learn*, employing the PCA, Nystroem, and *gridsearchcv* modules for computation and optimisation.

The resulting comparison matrices displayed the covariance between the original features and the PC axes, with values ranging from 1 (strong positive correlation) to –1 (strong negative correlation). These matrices were visualised using *matplotlib* and the *seaborn* heatmap function, facilitating interpretation of the relationships between variables and principal components.

B.1. Local Urban Fabric

The analysis compared PCA and KPCA, yielding broadly similar results. PCA explained 0.95 of the variance with six principal components (PCs) (Fig. B.1), while the best-performing KPCA kernel explained 0.98 of the variance with the same number of PCs (Fig. B.2). Based on the comparative plot (Fig. B.3), the KPCA solution was selected.

The kernel behaviour was effectively linear, though it required different hyperparameters and was derived from an approximation of 50 features. The six selected PCs are defined in Table B.1, with contributions below a covariance threshold of 0.1 excluded from interpretation.

Table B.1: Correlations between Local Urban Fabric features and Principal Components

Principal Component	**Strong correlation (|cov| > 0.6)**	**Medium correlation (0.3 < |cov| <= 0.6)**	**Weak correlation (0.1 < |cov| <= 0.3)**
PC1	tree cover density (-), agriculture presence (+)		
PC2	built up fraction (+), impervious density (+)	building height (+), traffic routes (+), trees (-), agriculture (-)	grassland (+)
PC3	grassland (+)	built up fraction (-), impervious density (-)	building height (-), traffic routes (-)
PC4	shrubland (+)	diversity (+)	
PC5	traffic routes (+)	diversity (+)	building height (-), built up fraction (-)
PC6	traffic routes (+)	diversity (+), built up fraction (-), impervious density (-)	traffic routes (+), building height (-)

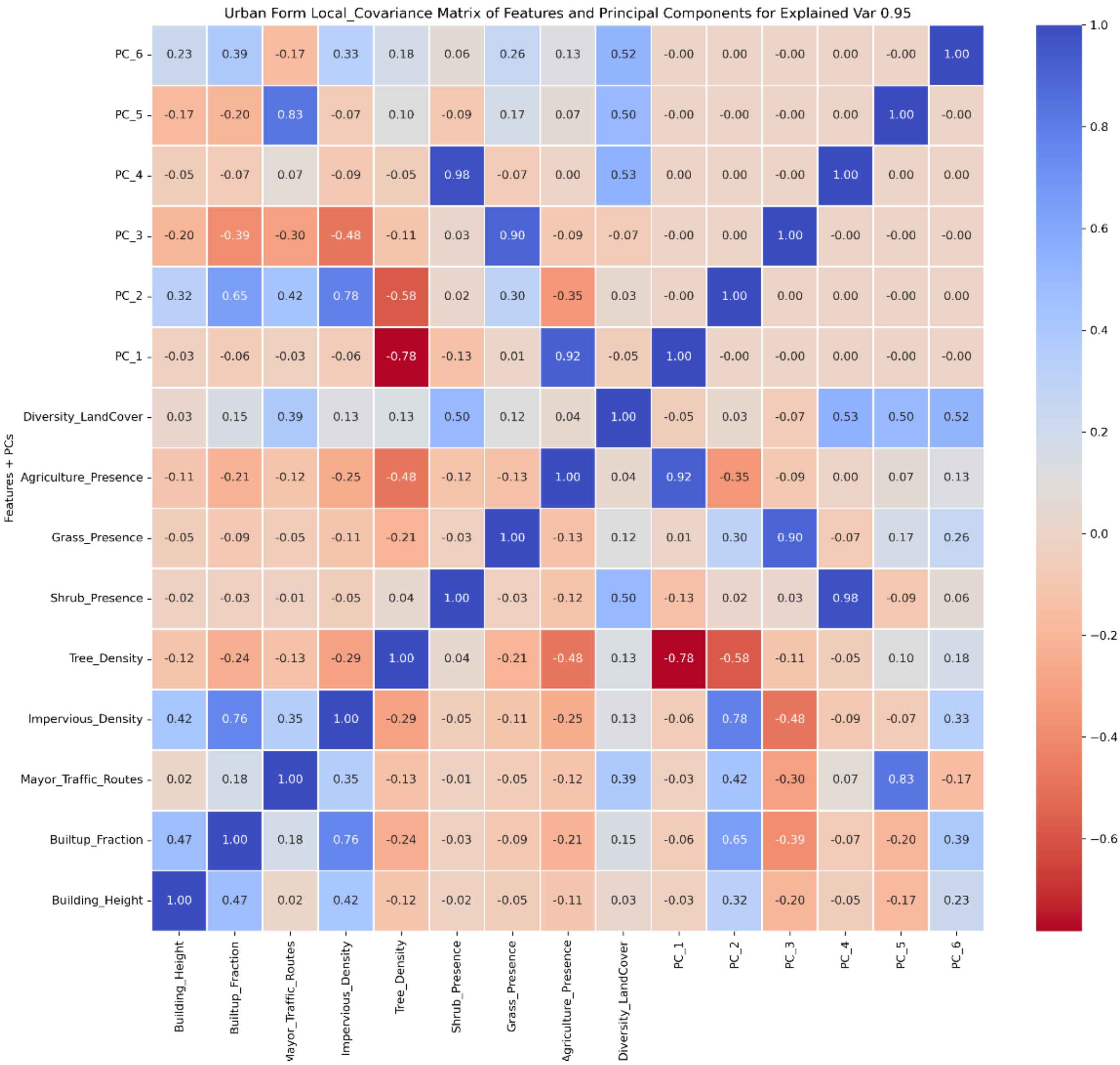

Fig. B.1: Local Urban Fabric PCA-features covariance matrix

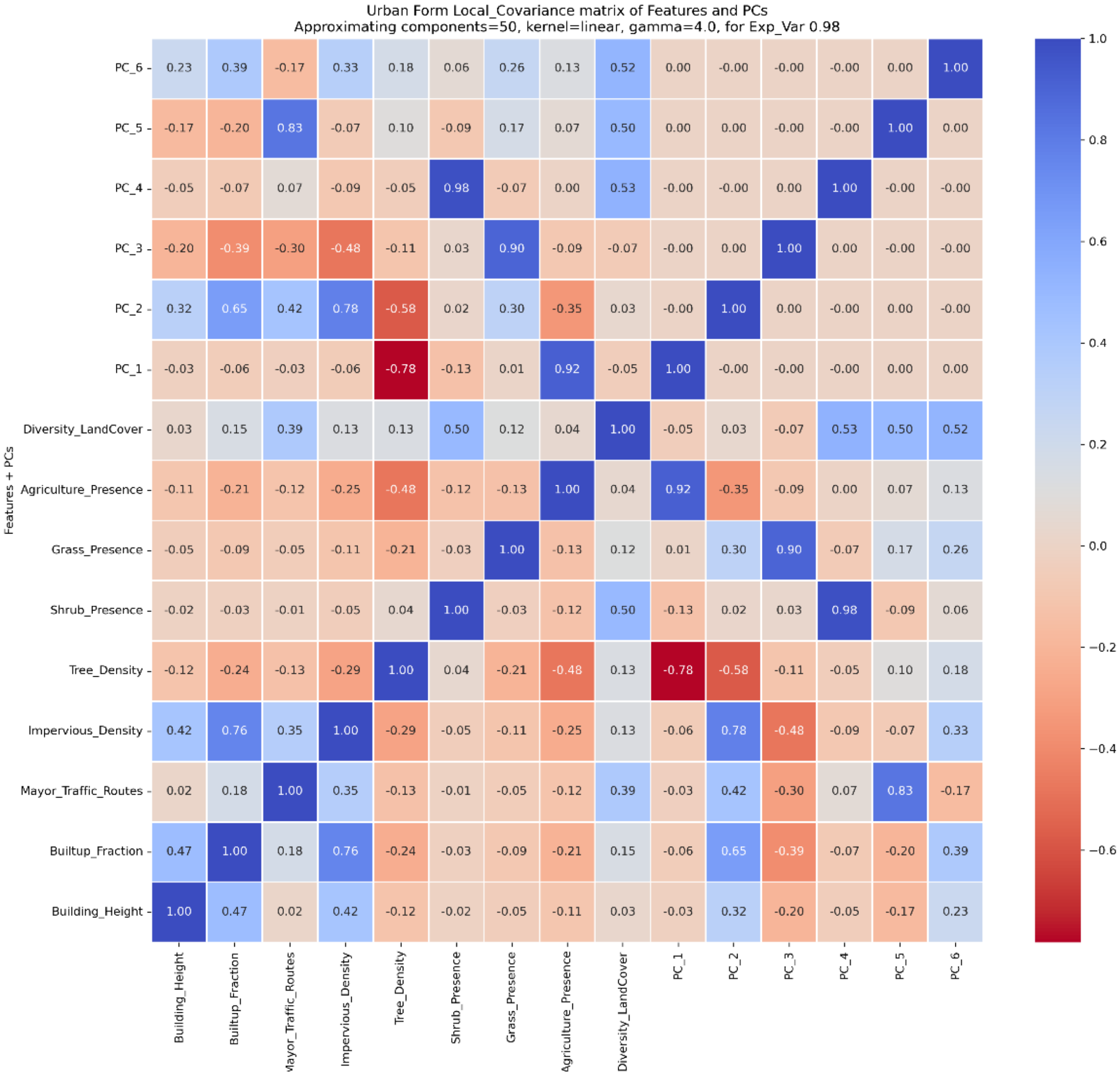

Fig. B.2: Local Urban Fabric KPCA-features covariance matrix

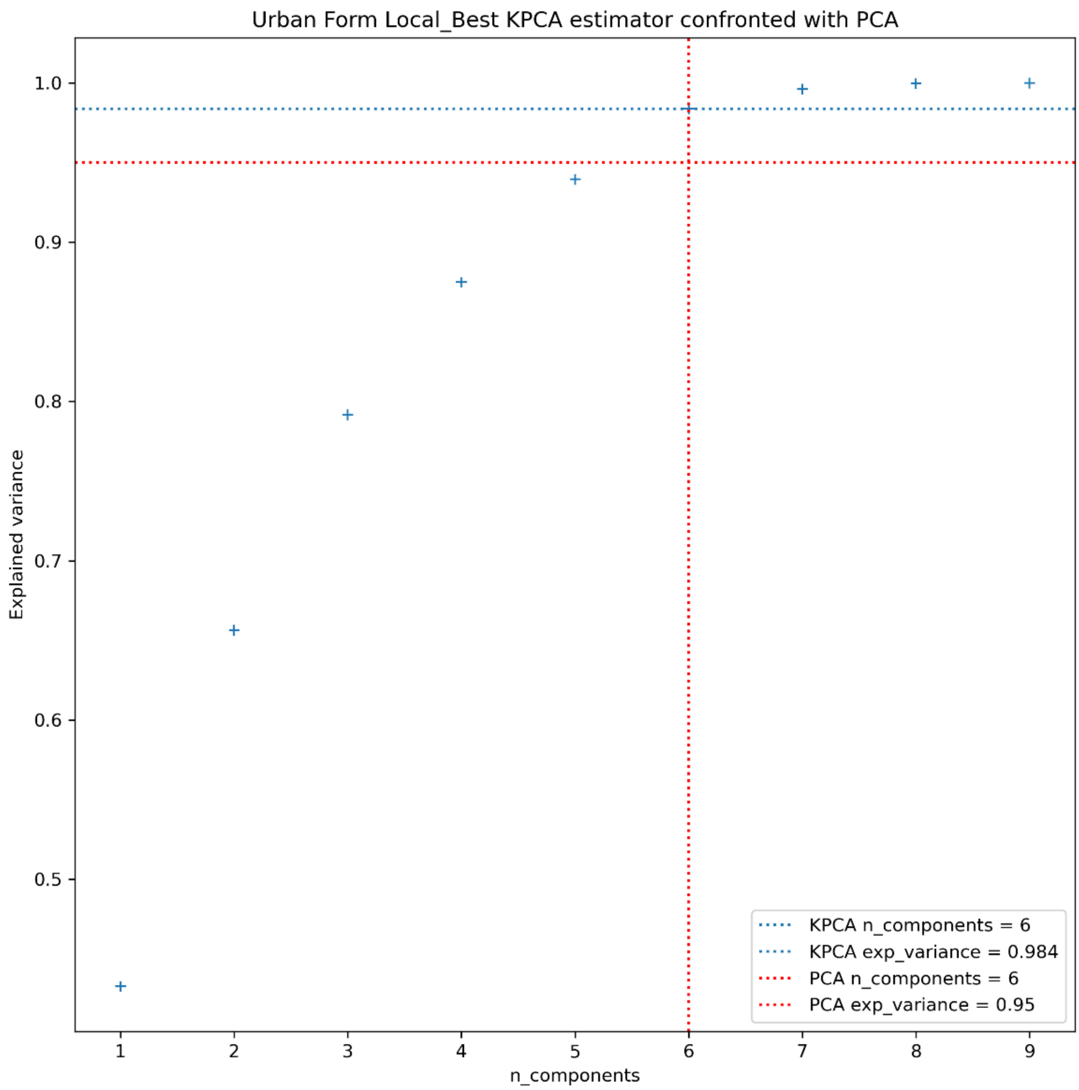

Fig. B.3: Local Urban Fabric best KPCA approximation confronted with PCA explained variance and number of components needed.

B.2. Landscape Urban Fabric

The analysis compared PCA and KPCA, producing broadly similar outcomes. PCA explained 0.95 of the variance with seven principal components (PCs) (Fig. B.4), while the best-performing KPCA kernel explained 0.944 of the variance with six components (Fig. B.5). Given the very small margin of difference, the PCA solution was selected, as also indicated by the comparative plot (Fig. B.6).

The seven selected PCs are defined in Table B.2, with contributions below a covariance threshold of 0.1 excluded from interpretation. For the local scale, PC axes were used as reference. Shannon's Diversity Index was employed to represent diversity within the kernel window, contrasting with local diversity, while Contagion was used as a measure of spatial aggregation within the kernel.

Table B.2: Correlations between Landscape Urban Fabric features and Principal Components

Principal Component	**Strong correlation (∣cov∣ > 0.6)**	**Medium correlation (0.3 < ∣cov∣ <= 0.6)**	**Weak correlation (0.1 < ∣cov∣ <= 0.3)**
PC1	Diversity index (+), mean and std PC2 (+), std PC3 (+), std PC5 (+), std PC6 (+)	Mean PC1 (+), mean and std PC4 (+)	Mean PC3 (+), mean PC5 (-), mean PC6 (-)
PC2	Mean PC1 (+)	Contagion (+), std PC1 (+)	Mean PC3 (+), mean PC4 (+)
PC3	Contagion (-)	Mean PC1 (+), std PC1 (-), mean PC2 (+)	Std PC2 (-), Mean and std PC3 (-), mean and std PC4 (+)
PC4	Mean PC3 (-)	Std PC1 (-), mean PC2 (+), std PC3 (-), std PC5 (+)	Contagion (+), mean PC6 (+)
PC5		Std PC3 (-), Mean and std PC4 (+)	Mean and std PC2 (-), Mean PC3 (-), mean and std PC5 (-), mean and std PC6 (-)
PC6		Std PC1 (-), mean and std PC3 (+)	Mean (+) and std PC2 (-), mean and std PC4 (+), std PC5 (-)
PC7	Mean PC5 (-)		Mean PC2 (+), Mean PC4 (-), std PC5 (-), mean (-) and std PC6 (+)

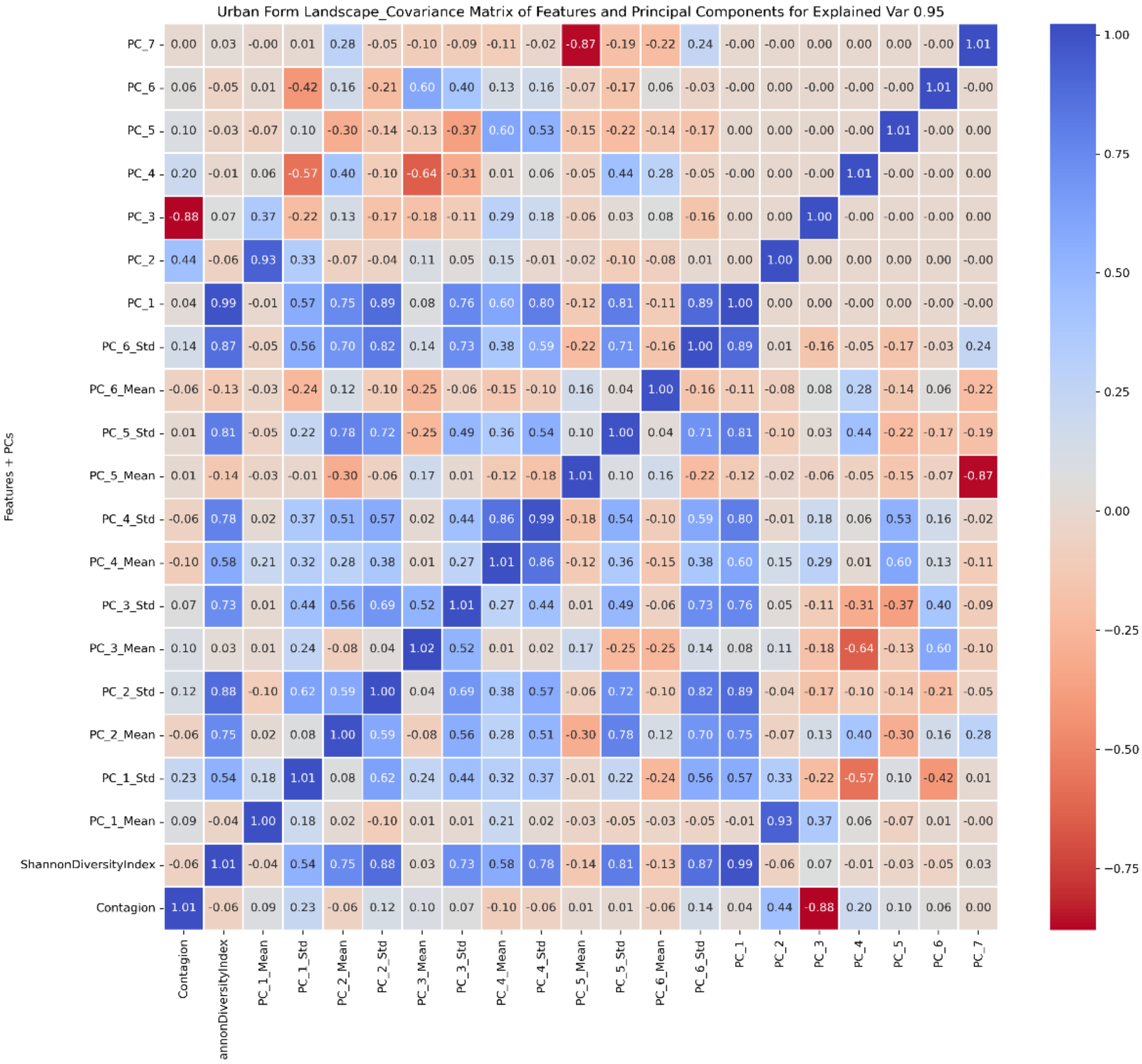

Fig. B.4: Landscape Urban Fabric PCA-features covariance matrix

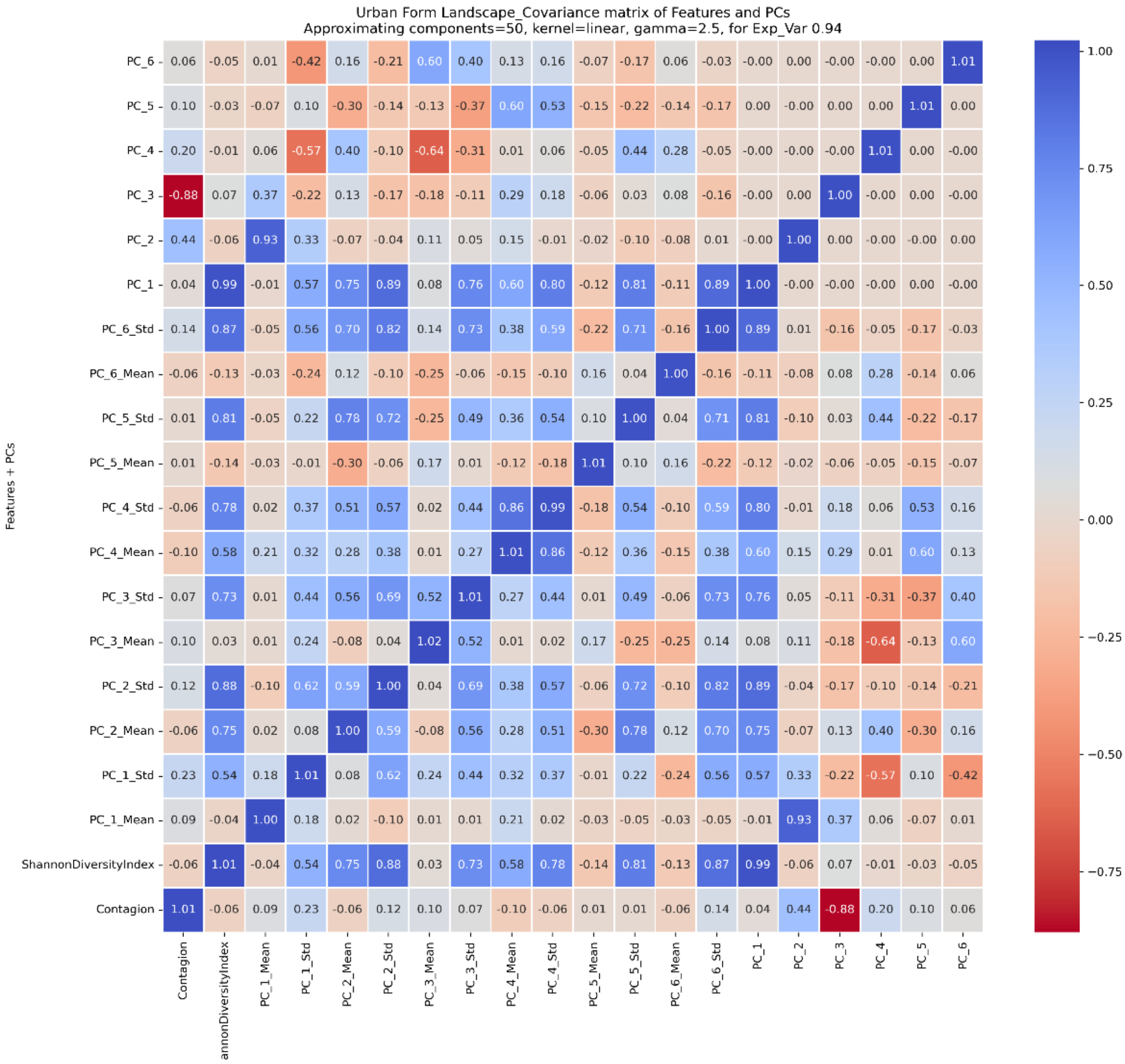

Fig. B.5: Landscape Urban Fabric KPCA-features covariance matrix

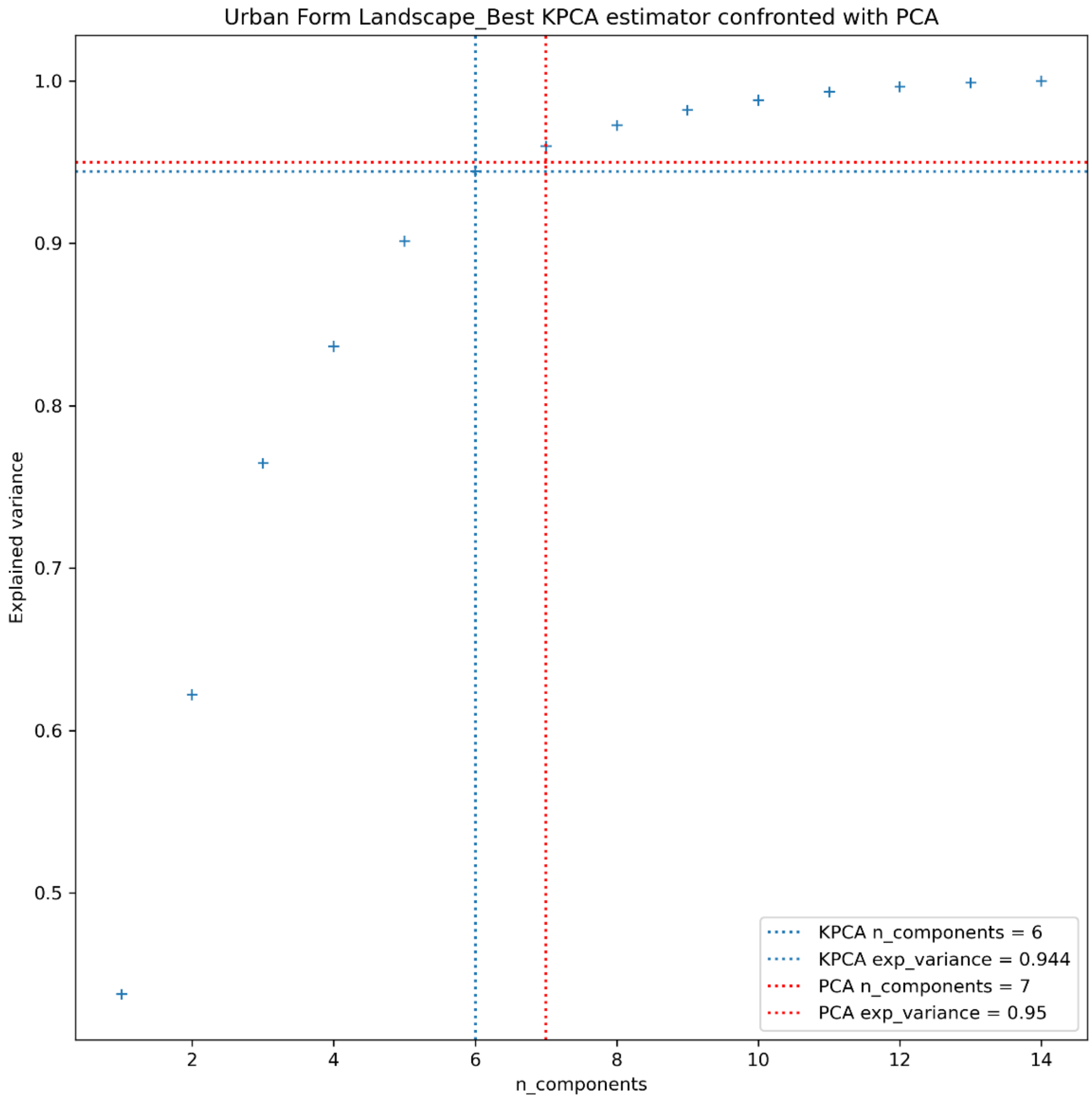

Fig. B.6: Landscape Urban Fabric best KPCA approximation confronted with PCA explained variance and number of components needed.

B.3. Anthropic Imprint

The analysis compared PCA and KPCA, producing broadly similar results. PCA explained 0.95 of the variance with five components (Fig. B.7), while the best-performing KPCA kernel explained 0.969 of the variance with six components (Fig. B.8). Despite KPCA capturing slightly more variation, PCA was selected because it achieved the minimum variance threshold of 0.95 with fewer components (Fig. B.9).

The five selected components are defined in Table B.3, with contributions below a covariance threshold of 0.1 excluded from interpretation.

Table B.3: Correlations between Anthropic Imprint features and Principal Components

Principal Component	**Strong correlation (|cov| > 0.6)**	**Medium correlation (0.3 < |cov| <= 0.6)**	**Weak correlation (0.1 < |cov| <= 0.3)**
PC1	Population density (+), Age groups 0-15, 20-35, 40-60, 65+ (+)	Public green (+), preservation policy (-), public transport (-), nighttime light (+), heat emission (+)	Commercial area (+), industrial area (+), public service (+),
PC2	Preservation policy (+)		Age groups (+), recreation area (+)
PC3	Recreation area (+)	Public green (+)	Heat emission (+)
PC4	Public green (+)		Population density (+), recreation area (-), cultural area (+), public transport (-), nighttime light (+), heat emission (+)
PC5	Public transport (+)		Public green (+)

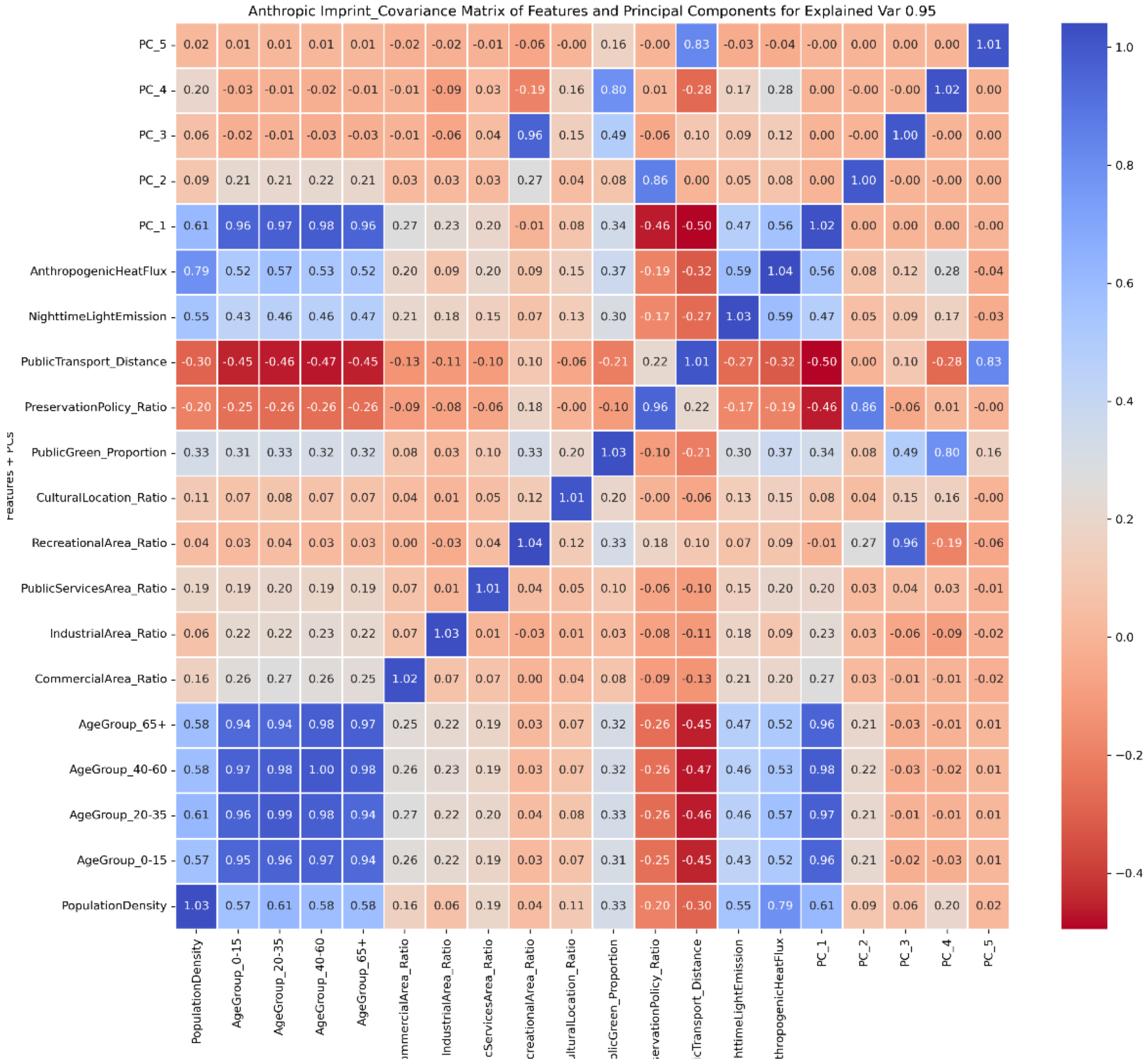

Fig. B.7: Anthropic Imprint PCA-features covariance matrix

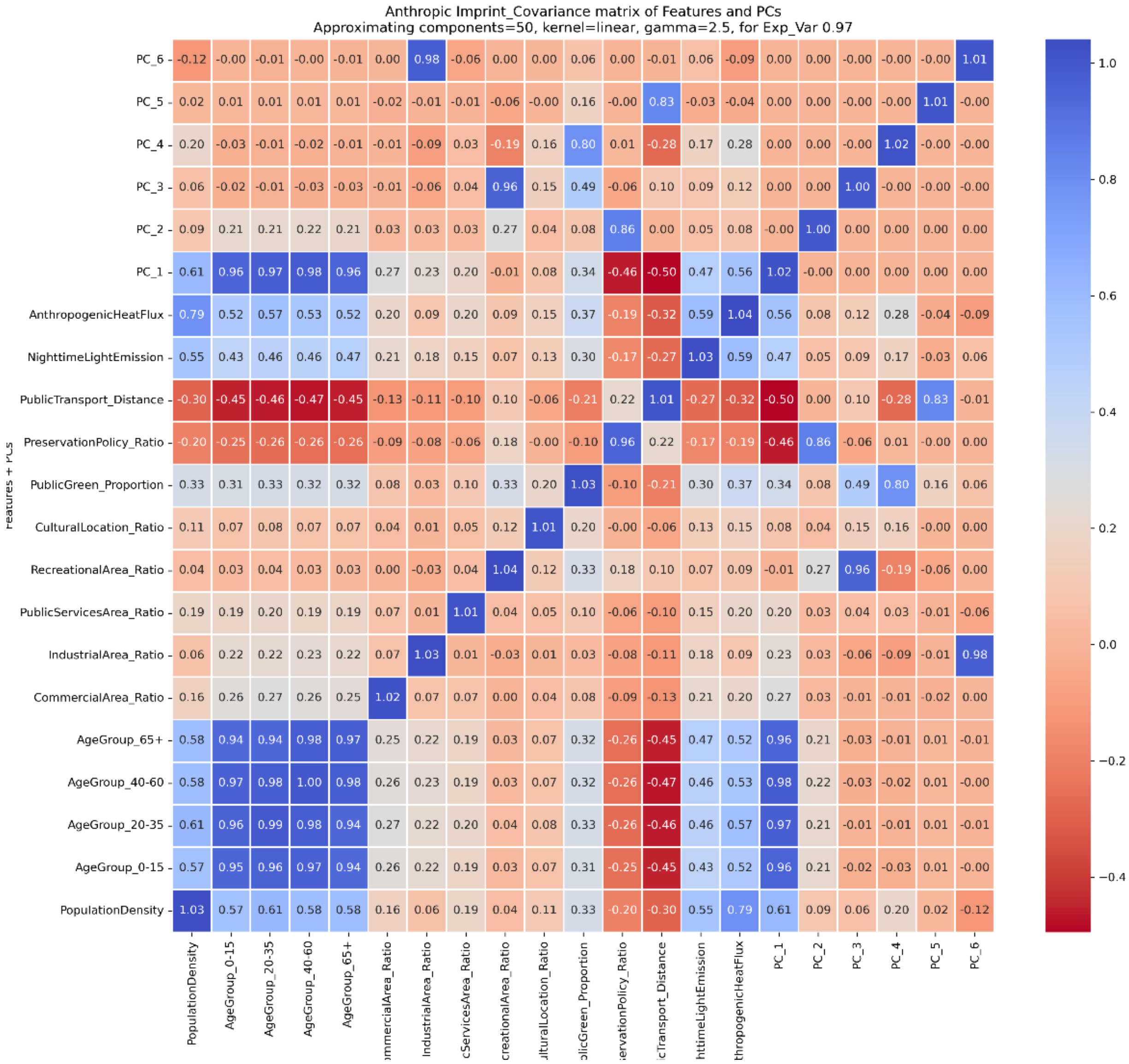

Fig. B.8: Anthropic Imprint KPCA-features covariance matrix

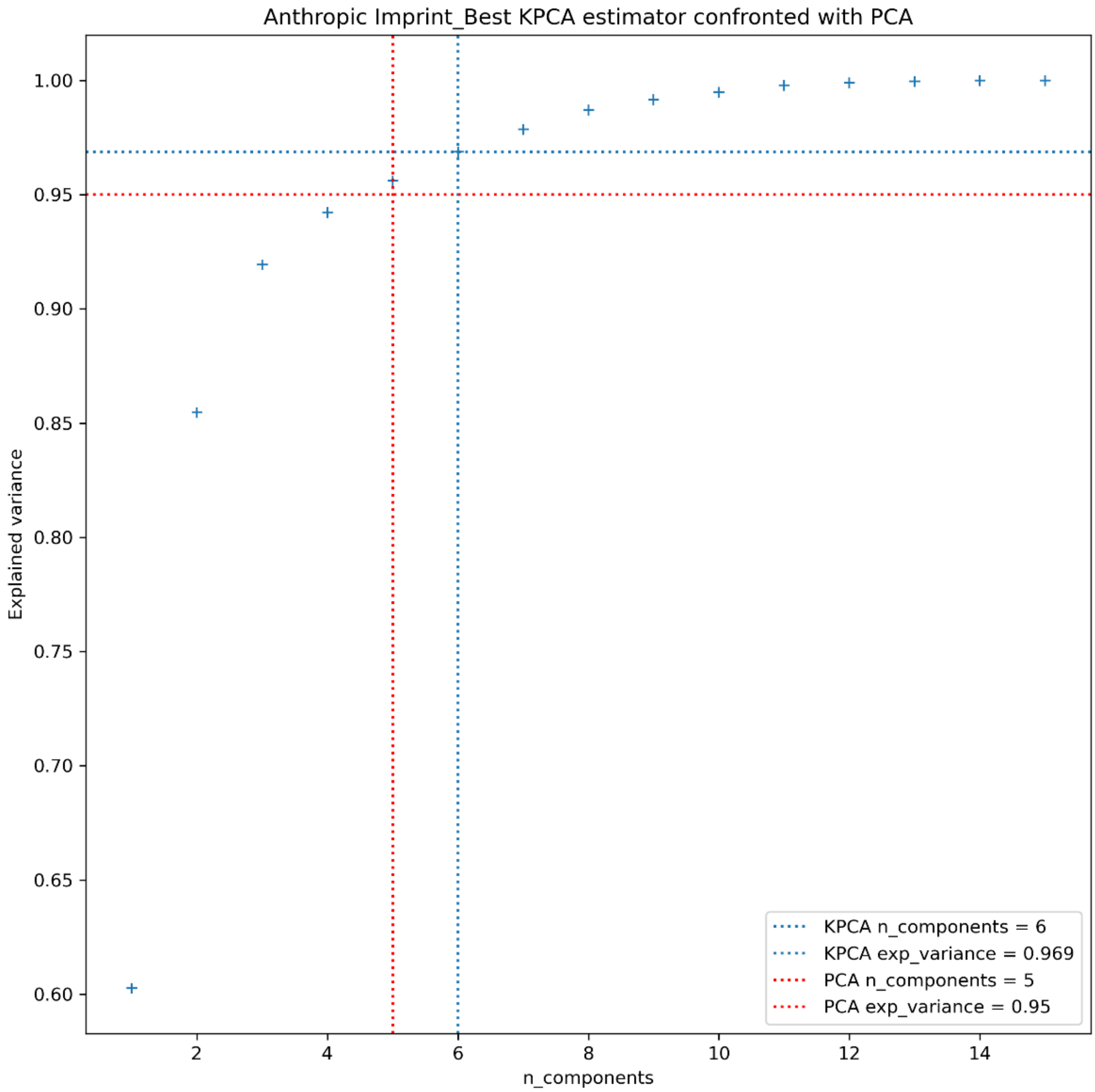

Fig. B.9: Anthropic Imprint best KPCA approximation confronted with PCA explained variance and number of components needed.

B.4. Biophysical Conditions

The analysis compared PCA and KPCA, producing similar but not equivalent results. PCA explained 0.95 of the variance with eight components (Fig. B.10), while the best-performing KPCA kernel explained 0.908 of the variance with six components (Fig. B.11). Since the KPCA solution did not reach the minimum variance threshold, it was discarded in favour of the PCA (Fig. B.12).

The eight selected PCs are defined in Table B.4, with contributions below a covariance threshold of 0.1 excluded from interpretation. Notably, surface water and soil wetness exhibited perfect correspondence, as did wind speed at 10 m and 200 m. Values greater than 1 should be interpreted as 1, as they result from approximations inherent in the algorithm.

Table B.4: Correlations between Biophysical Conditions features and Principal Components

Principal Component	**Strong correlation (|cov| > 0.6)**	**Medium correlation (0.3 < |cov| <= 0.6)**	**Weak correlation (0.1 < |cov| <= 0.3)**
PC1	Altitude mean (+), temperature max and min relative and absolute (-), precipitations absolute (+)	Precipitations relative (+)	Altitude std (+), slope (+), aspect mean (+), curvature std (+), wind speed (-)
PC2	Altitude std (+), slope (+), curvature std (+)	Precipitations absolute and relative (+)	Soil wetness (-), temperature max and min relative (-) max and min absolute (+)
PC3		Aspect (-), temperature max and min relative (-), precipitations absolute (-) and relative (+),wind speed (+)	Slope mean (-), curvature std (-)
PC4	Aspect std (-)	Permanent and temporary water (+), aspect mean (-), temperature max and min relative (+)	Precipitations absolute (+), wind speed (-)
PC5	Permanent and temporary water (+)		Aspect (+), wind speed (+)
PC6	Aspect mean (+)	Aspect std (-)	
PC7	Soil wetness (+)	Wind speed (+)	Precipitations absolute (+)
PC8		Soil wetness (+), precipitations relative (-), wind speed (-)	Precipitations absolute (-)

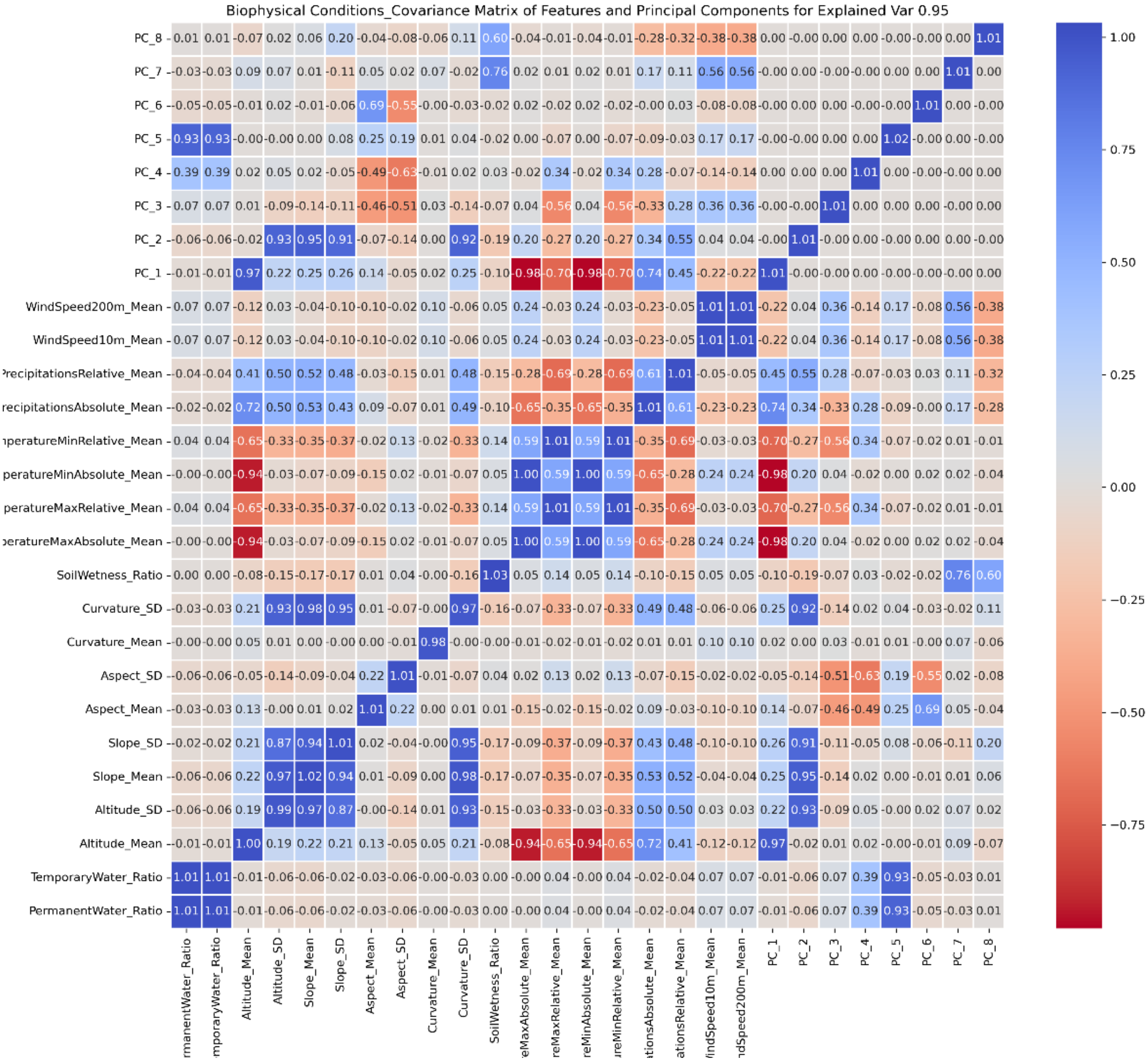

Fig. B.10: Biophysical Conditions PCA-features covariance matrix

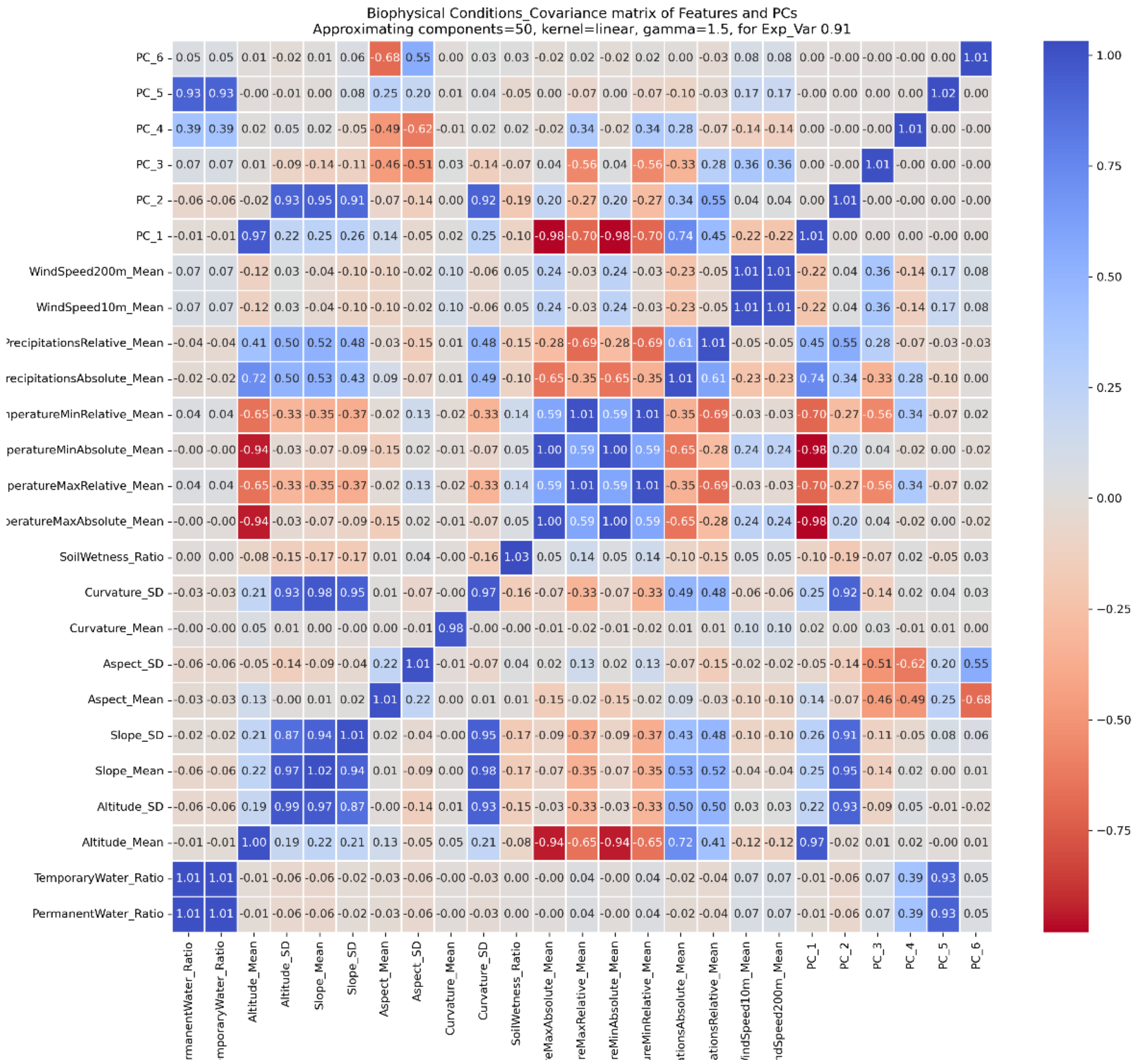

Fig. B.11: Biophysical Conditions KPCA-features covariance matrix

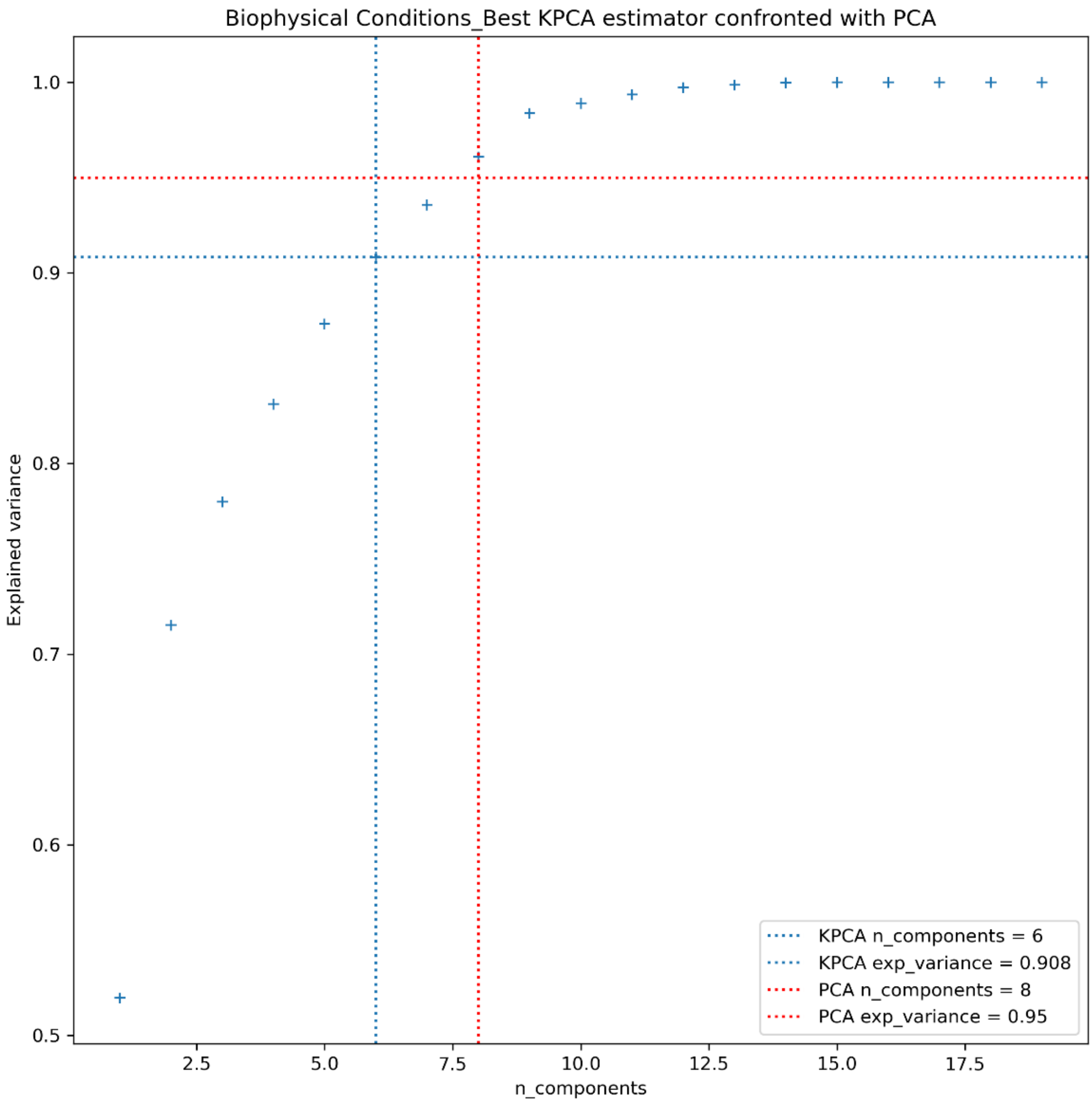

Fig. B.12: Biophysical Conditions best KPCA approximation confronted with PCA explained variance and number of components needed.

Annex C (Chapter 3) – Unsupervised Classification scores

Initial tests explored several clustering approaches. Hierarchical Clustering was considered first, as agglomerative methods are commonly applied in urban landscape classifications (Paumelle et al., 2023). Additional algorithms such as DBSCAN, HDBSCAN, OPTICS, Random Forest, and Unsupervised Neural Networks were also evaluated for their flexibility, reduced time complexity, or potential improvements in clustering quality. However, computational complexity remained a major challenge, as the sub-classification datasets contained more than 60 million cells due to the extensive spatial coverage and fine resolution.

Subsequent tests focused on the KMeans family of algorithms. Variants such as Fuzzy and Bisecting KMeans were discarded because of their consistently weaker performance compared to the traditional Lloyd implementation. The analysis was therefore limited to three flavours (Lloyd, Elkan, and MiniBatch) using sklearn implementations for all.

Each sub-classification was processed with these three KMeans variants. To identify the most effective clustering and determine the optimal number of classes (k), three evaluation metrics recommended in the literature were applied: Silhouette score (SIL), Calinski–Harabasz index (CH), and Davies–Bouldin index (DB) (Palacio-Niño and Berzal, 2019). The objective was to maximise clustering performance while applying an automatic criterion for k selection. For each k value (ranging from 6 to 30), all three scores were calculated. The maximum score across the range was identified, and for each k the difference between its score and the maximum was computed. These differences were normalised, summed across the three indices, and used to identify the k value closest to the combined maxima.

This procedure was repeated for each algorithm, with results plotted to highlight the maximum values for Silhouette and Davies–Bouldin indices and the minimum for Calinski–Harabasz. To further validate the predictions, inertia was plotted and the Elbow Method applied to visualise the curvature of inertia as k increased.

C.1. Local Urban Fabric

The classifier was executed twice, extracting a subset of data related to the built environment in order to generate additional classes. In the first run (Fig. C.1, C.2, C.3), the Elkan implementation with k = 10 was selected, yielding scores of SIL = 0.819, CH = 1.742×10^7, and DB = 0.485. In the second run (Fig. C.4, C.5, C.6), the Elkan implementation with k = 4 was chosen, producing scores of SIL = 0.689, CH = 1.631×10^6, and DB = 0.619.

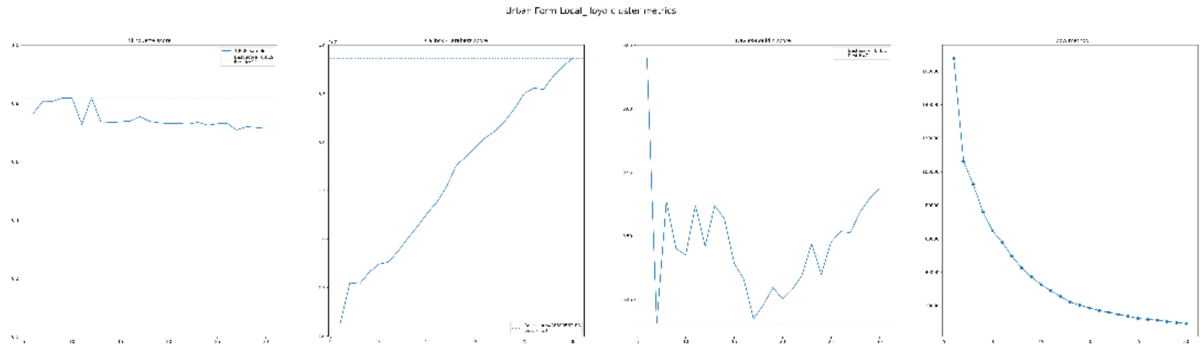

Fig. C.1: Local Urban Fabric (first run) Lloyd KMeans score plots.

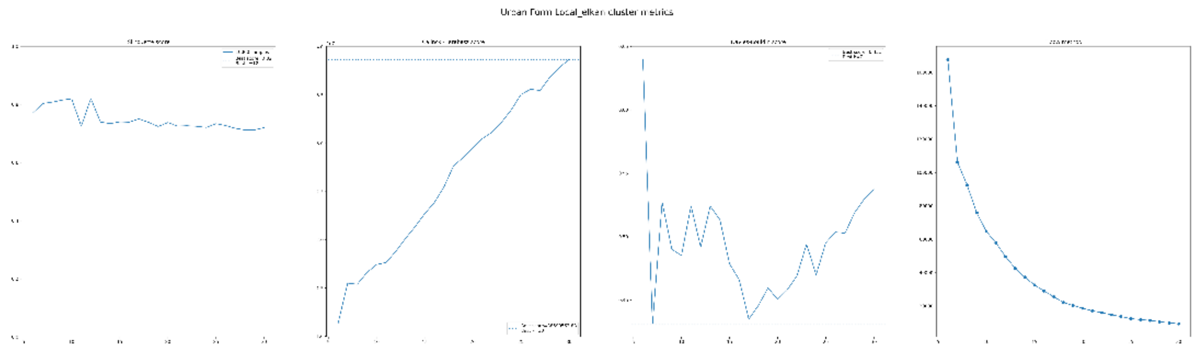

Fig. C.2: Local Urban Fabric (first run) Elkan KMeans score plots.

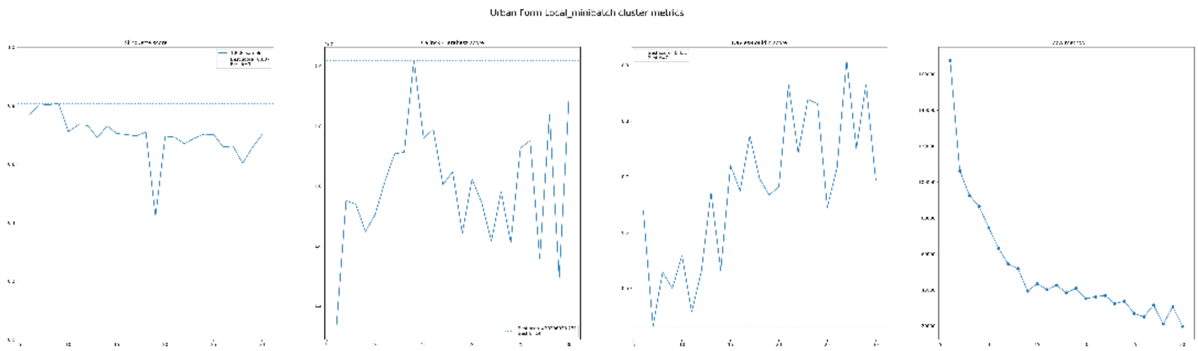

Fig. C.3: Local Urban Fabric (first run) MiniBatch KMeans score plots.

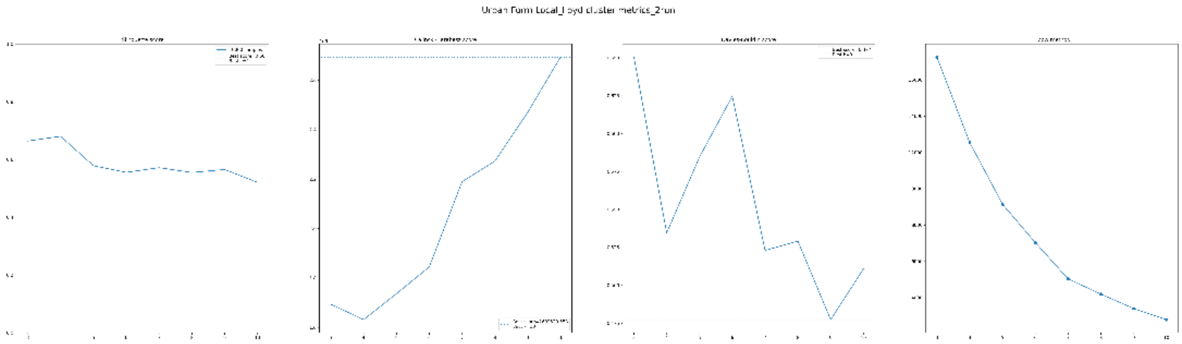

Fig. C.4: Local Urban Fabric (second run) Lloyd KMeans score plots.

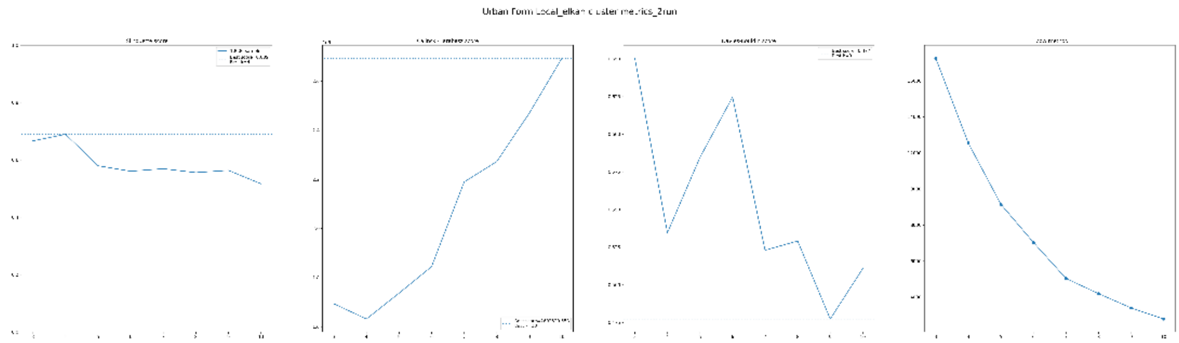

Fig. C.5: Local Urban Fabric (second run) Elkan KMeans score plots.

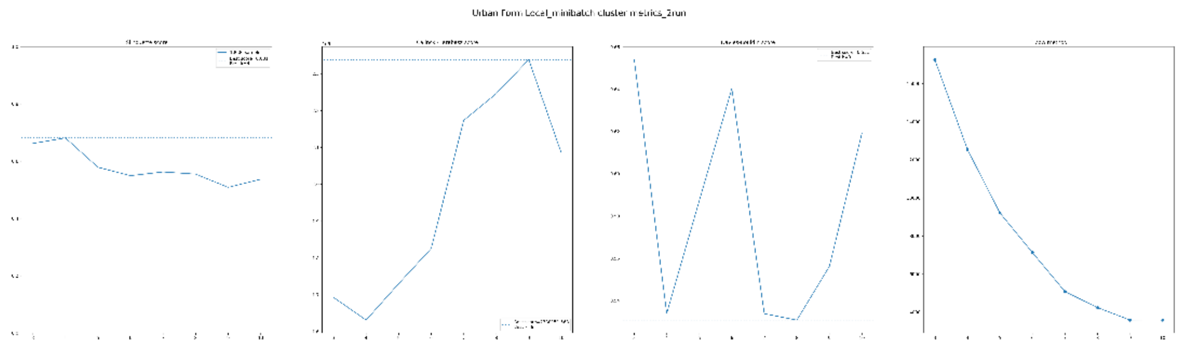

Fig. C.6: Local Urban Fabric (second run) MiniBatch KMeans score plots.

C.2. Landscape Urban Fabric

The classifier was executed once, and the optimal configuration was identified with the Elkan implementation at k = 6. This solution achieved scores of SIL = 0.440, CH = 3.035 × 10^6, and DB = 0.990 (Fig. C.7, C.8, C.9).

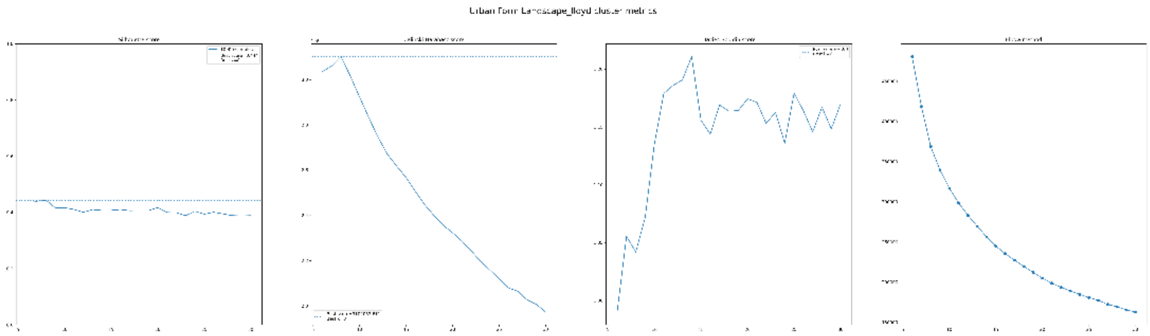

Fig. C.7: Landscape Urban Fabric Lloyd KMeans scores plots.

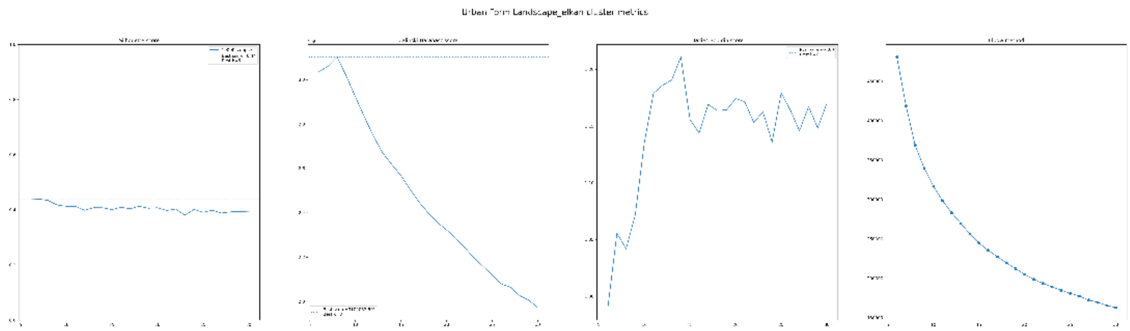

Fig. C.8: Landscape Urban Fabric Elkan KMeans scores plots.

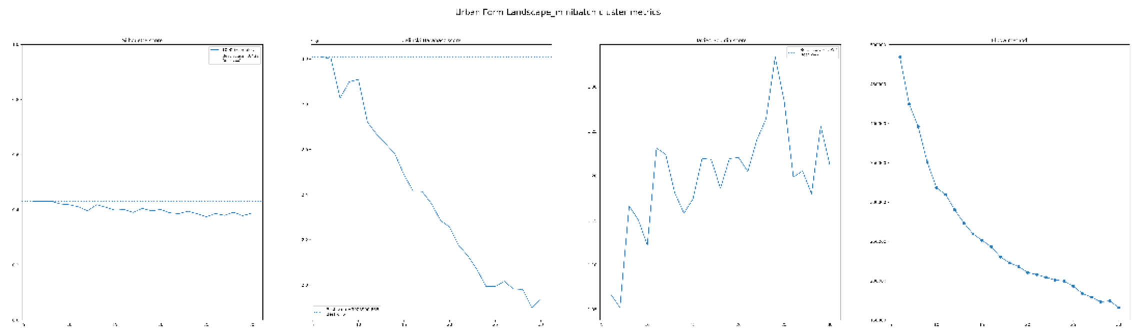

Fig. C.9: Landscape Urban Form MiniBatch KMeans scores plots.

C.3. Anthropic Imprint

The classification was executed once, and the grid search identified the optimal configuration with the Elkan implementation at $k = 6$. This solution achieved scores of SIL = 0.662, CH = 6.846×10^6, and DB = 0.723 (Fig. C.10, C.11, C.12).

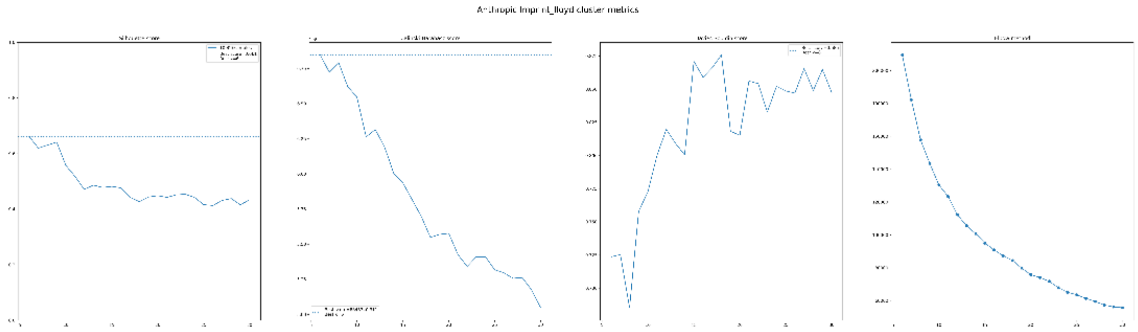

Fig. C.10: Anthropic Imprint Lloyd KMeans scores plots.

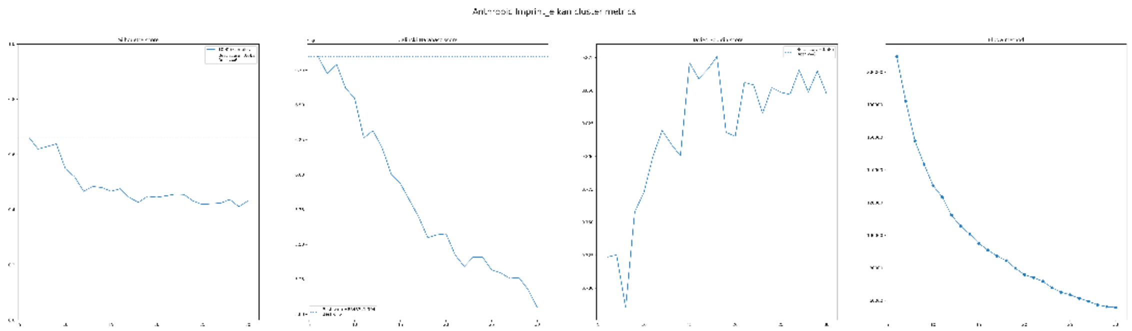

Fig. C.11: Anthropic Imprint Elkan KMeans scores plots.

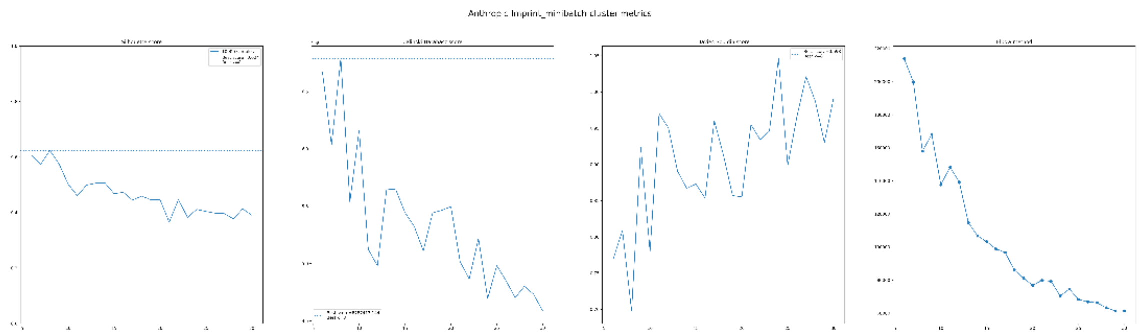

Fig. C.12: Anthropic Imprint MiniBatch KMeans scores plots.

C.4. Biophysical Conditions

The classifier pipeline was executed once, and the optimal configuration was identified with the Lloyd implementation at $k = 6$. This solution achieved scores of $SIL = 0.371$, $CH = 1.713 \times 10^6$, and $DB = 1.318$ (Fig. C.13, C.14, C.15).

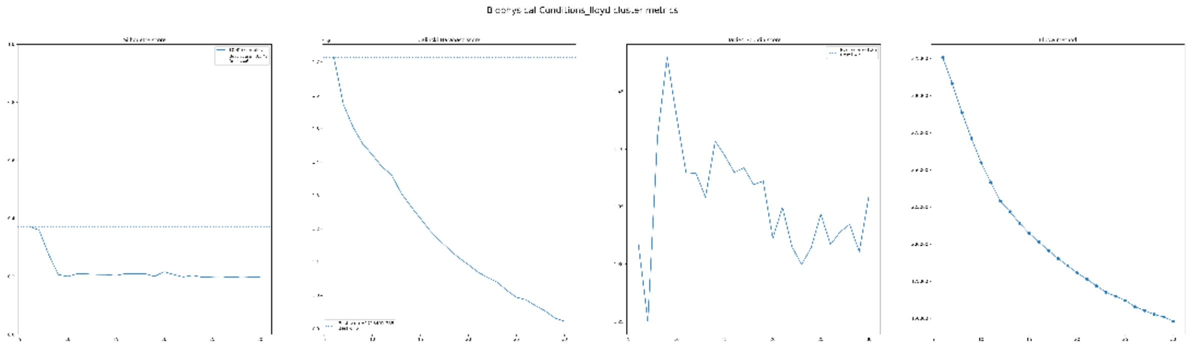

Fig. C.13: Biophysical Conditions Lloyd KMeans scores plots.

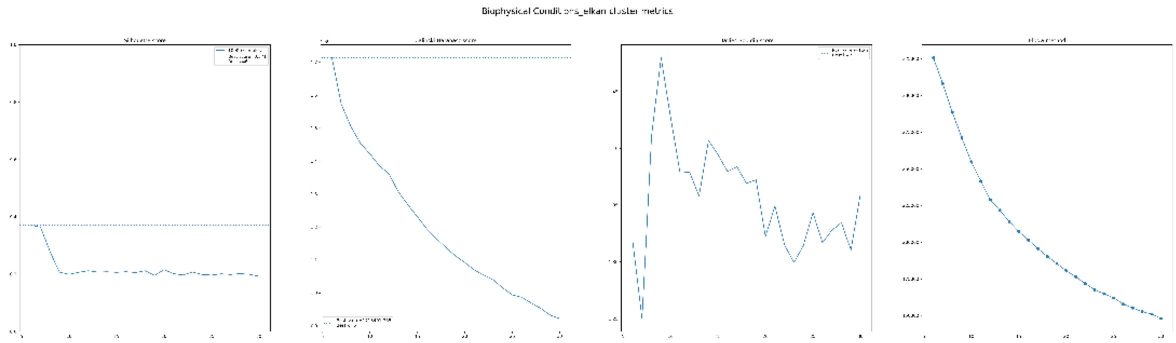

Fig. C.14: Biophysical Conditions Elkan KMeans scores plots.

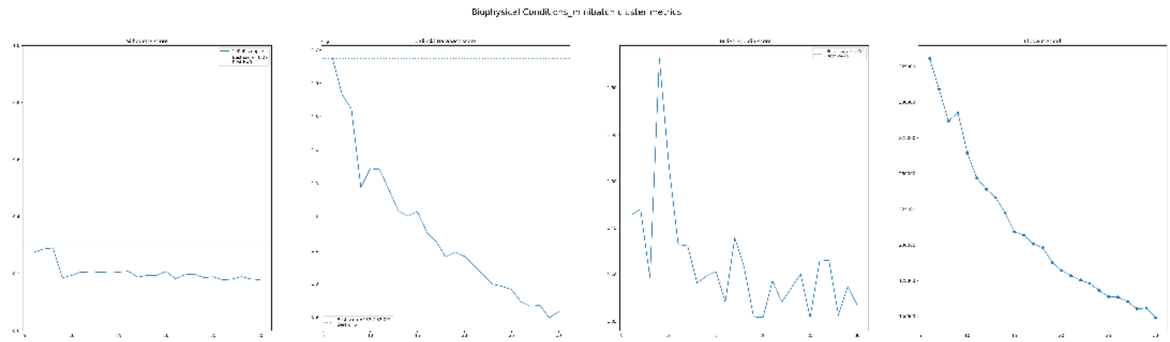

Fig. C.15: Biophysical Conditions MiniBatch KMeans scores plots.

Annex D (Chapter 3) - Clusters definitions

Having established the optimal k for the unsupervised classification, the next step was to interpret the contents of each class based on its defining features. To achieve this, Principal Component (PC) values for each cluster were visualised using boxplots. The components were rescaled to a range of –1 to 1, allowing higher and lower values to be compared on a consistent scale while reducing the influence of extreme spikes.

All plots were generated with matplotlib. To aid interpretation, four ranges of 0.5 (from maximum to minimum) were highlighted with different colours, improving the readability of the graphs. Particular attention was given to PC median values falling within the intervals (0.3, 1) and (–1, –0.3), as these indicated stronger contributions. Greater weight was also assigned to PC axes with narrower interquartile ranges, since these reflected more consistent and discriminative contributions across clusters.

D.1. Local Urban Fabric

Homogeneous water was not represented in the PCA at the local scale, as the modelling treated water as a negative presence. Consequently, patterns of water occurrence within the city boundary were derived from this negative space, resulting in the definition of a final 13th cluster.

Across the modelled pixels, 12 additional clusters of heterogeneous size were identified. The smallest cluster (Cluster 4) accounted for 0.34% of all modelled cells, while the largest (Cluster 3) represented 33.44% (Fig. D.1). These clusters were defined according to the PC values reported in Table D.1.

Table D.1: Description of Local Urban Fabric classes based on PC values, highlighting dependencies based on boxplot spread and median position within the range of each component dominion.

Cluster	Notable PC dependencies	Description
1	Agriculture (PC1)	Agriculture dominance
2	Shrubs (PC4), agriculture (PC1)	Agriculture with hedges
3	Agriculture (PC1), grass (PC3), diversity (PC5, PC6)	Fields diversified
4	Grassland (PC2), building height (PC5, 6), built-up (PC5)	Grasslands dominance
5	Building height, streets (PC2), grasslands (PC3)	Grasslands and infrastructure
6	Trees (PC1)	Trees dominance
7	Trees (PC1), Streets and railways (PC5)	Trees and infrastructure
8	Shrubs (PC4)	Shrubland dominance
9	Built-up fraction, impervious density (PC2, PC3), building height, streets (PC3)	High built-up dominance
10	Building height, streets (PC2)	Low built-up dominance
11	Built-up fraction, impervious density (PC2, PC3), streets (PC5)	Infrastructure dominance
12	Building height (PC2, 3, 6), streets (PC2), built-up (PC3), streets (PC5)	Infrastructure with built-up
13		Water

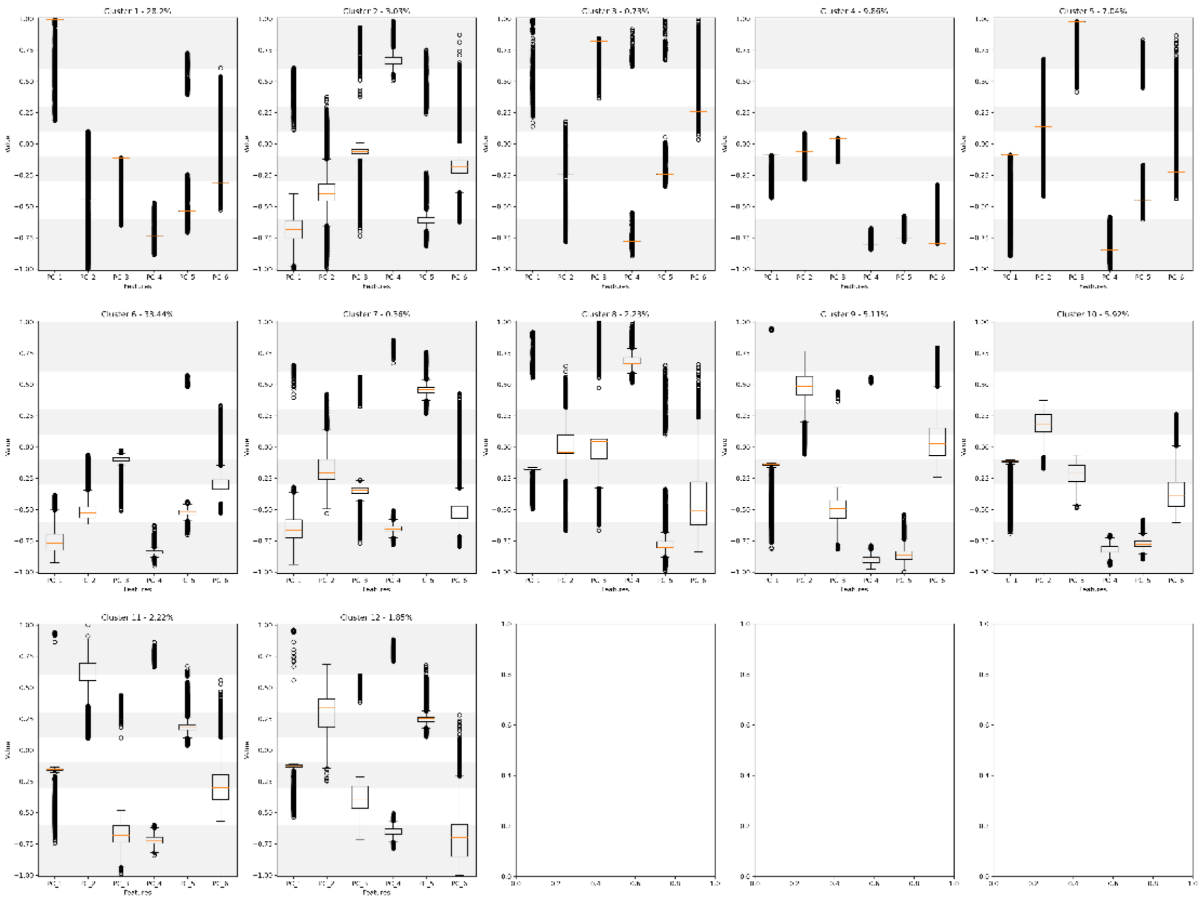

Figure D.1: Boxplot of each cluster values for Local Urban Fabric layer, with ranges for each corresponding Principal Component spread.

D.2. Landscape Urban Fabric

As with the local scale, water was not represented in the PCA and was therefore treated as a negative presence, subsequently added as a final class. From the modelled values, six homogeneous clusters were identified, ranging in size from 8.05% (Cluster 3) to 23.5% (Cluster 6) of all cells (Fig. D.2). These clusters are defined in Table D.2 based on the boxplot analysis.

A trend emerged in which core clusters (3, 5, 6) were accompanied by heterogeneous edge patches generated by disruptive elements (Clusters 1, 2, 4). This pattern highlights the structural differentiation between stable core areas and transitional edge conditions within the urban landscape.

Table D.2: Description of Landscape Urban Fabric classes based on PC values, highlighting dependencies based on boxplot spread and median position within the range of each component dominion. The dependencies refer to local mean and std PC axis, keeping in parentheses the corresponding landscape components. Additional notes are added to help interpretation.

Cluster	Notable PC dependencies	Description
1	Contagion (PC2), std PC1 (PC2), PC2 (PC5), mean PC3 (PC5), std PC5 (PC6) PC5 (PC5), PC6 (PC5, 7), mean PC4 (PC7); most agriculture and diversity coming from aggregate areas where agriculture is present	Core agriculture patches
2	Mean PC1 (PC2), std PC2 (PC3), PC3 (PC3)	Edge agriculture patches
3	PC4 (PC3), std PC1 (PC4), std PC3 (PC4), std PC2 (PC6), std PC5 (PC6, 7), PC6 (PC7); trees and urban greenery with few disturbances	Core tree patches
4	Contagion (PC3), PC2, mean PC3, PC5, PC6 (PC5, PC6, PC7); trees with numerous disruptions coming from different sources	Edge tree patches
5	Mean PC1 (PC1), PC4 (PC1, PC3); mostly impervious and built-up areas	Core impervious patches
6	Mean PC3 (PC1, PC2), mean PC4 (PC2,7), std PC2 (PC3, 6), PC3 (PC3), std PC1 (PC4), std PC3 (PC5), std PC5 (PC6, 7), PC6 (PC7)	Edge impervious patches
7		Water patches

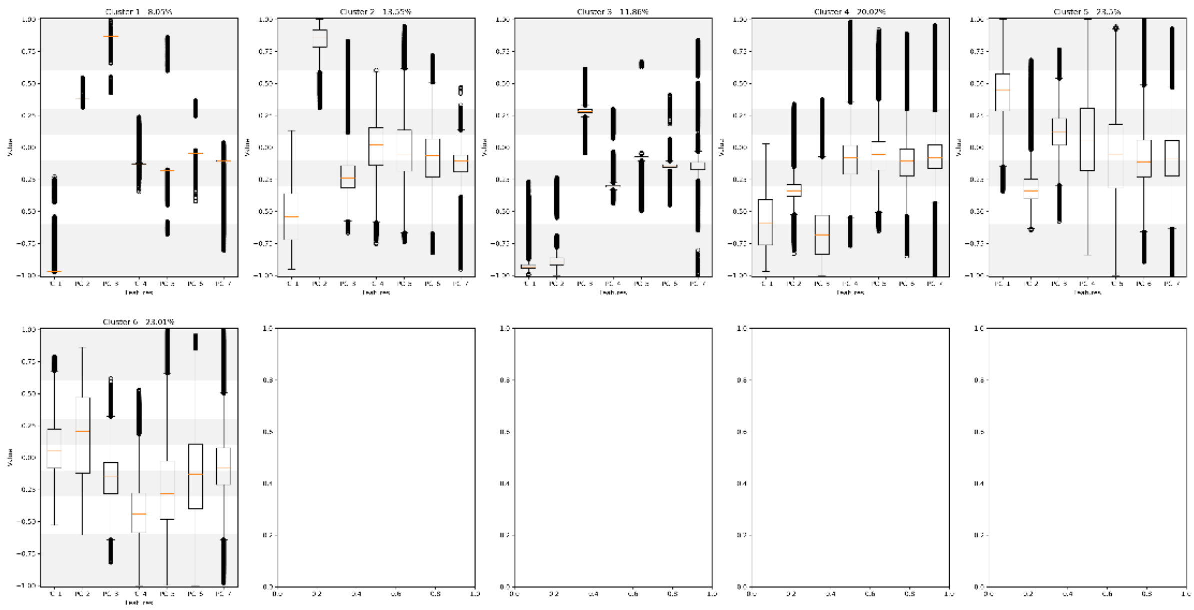

Figure D.2: Boxplot of each cluster values for Landscape Urban Fabric layer, with ranges for each corresponding Principal Component spread.

D.3. Anthropic Imprint

We modelled the entire collection of pixels without removing classes prior to preprocessing. From the modelled values, six highly inhomogeneous clusters were identified, ranging from the smallest (Cluster 3, 3.13% of all cells) to the largest (Cluster 1, 42.08%) (Fig. D.3). These clusters are defined in Table D.3 based on the boxplot analysis (Fig. D.3).

Table D.3: Description of Anthropic Imprint classes based on PC values, highlighting dependencies based on boxplot spread and median position within the range of each component dominion.

Cluster	Notable PC dependencies	Description
1	Public green (PC1), commercial area (PC1), industrial area (PC1), public service (PC1), preservation policy (PC2)	Conservation natural areas
2	Age groups (PC2), public green (PC3), recreation area (PC2, 4), transports (PC4); places without human presence and no significant services, but very high distance to public transports	Un-protected natural areas
3	Population density (PC1), age groups (PC1),	Regulated natural areas
4	Commercial area (PC1), industrial area (PC1), public service (PC1), transports (PC4)	Edge human living areas
5	Age groups (PC2), recreation area (PC2)	Core human living areas
6	Commercial area (PC1), industrial area (PC1), public service (PC1); dense industrial and commercial activities	Industrial and commercial areas

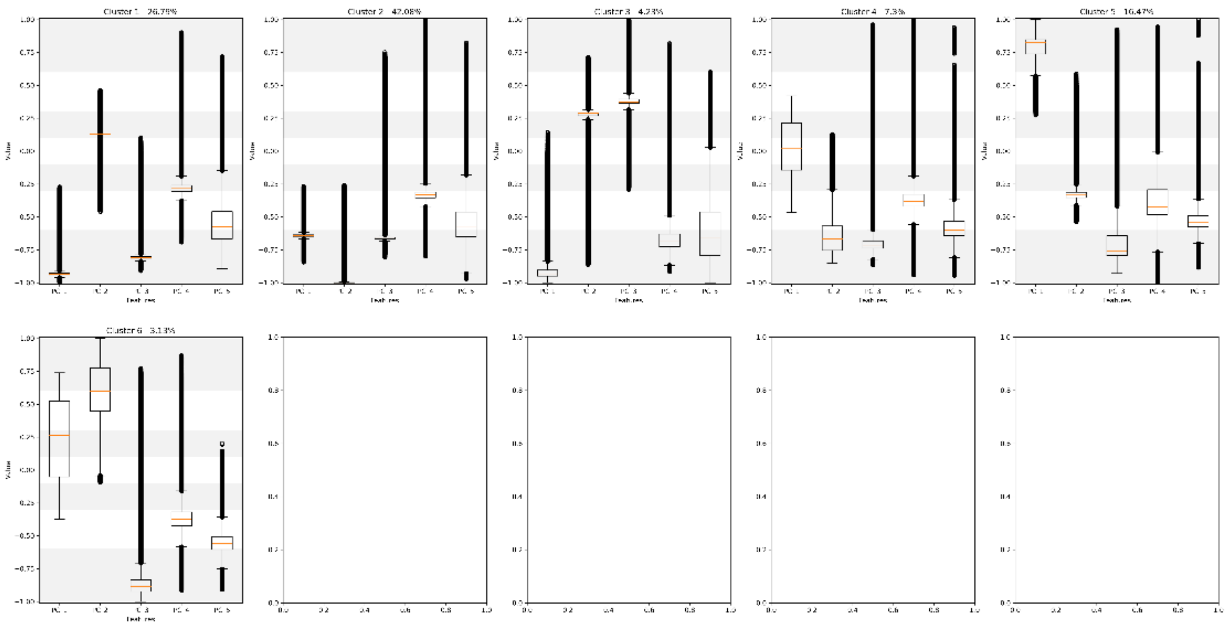

Figure D.3: Boxplot of each cluster values for Anthropic Imprint layer, with ranges for each corresponding Principal Component spread.

D.4. Biophysical Conditions

The entire collection of pixels was modelled without removing classes prior to preprocessing. From the modelled values, six clusters were identified, ranging in size from 7.53% (Cluster 6) to 33.32% (Cluster 2) of all cells (Fig. D.4). These clusters are defined in Table D.4 based on the boxplot analysis.

Regional differences posed significant challenges in distinguishing between clusters, particularly in separating temperature-related behaviour from soil constitution. This complexity made the Biophysical Conditions layer unique among the sub-classifications, as it was the only one to produce clusters absent from specific cities. Specifically, Cluster 3 was not present in Munich, while Cluster 2 was not found in Vienna.

Table D.4: Description of Biophysical Conditions classes based on PC values, highlighting dependencies based on boxplot spread and median position within the range of each component dominion. Under PC dependencies, some comments were added to improve understanding.

Cluster	Notable PC dependencies	Description
1	Temperature max and min relative (PC1), wind speed (PC1), precipitations absolute (PC8)	Local warm basin
2	Altitude std (PC1, 2), slope mean (PC1, 2, 3) and std (PC3), aspect mean (PC1), curvature std (PC1, 2, 3), precipitations absolute (PC8)	Local wet basin
3	Altitude std (PC1), slope (PC1, 3), aspect mean (PC1, 3) and std (PC6), curvature std (PC1, 3), temperature max and min absolute (PC2, 3)	Reliefs warmer
4	Wind speed (PC1, 4), soil wetness (PC2), temperature max and min relative (PC2), precipitations absolute (-)	Reliefs cold
5	Precipitations relative (PC1, 2) and absolute (PC2, 8), slope mean (PC3), curvature std (PC3), wind speed (PC4)	Reliefs colder and rainy
6	Wind speed (PC1), permanent and temporary water (PC4, 5), temperature max and min relative (PC4), precipitations absolute (PC8)	Water dominated areas

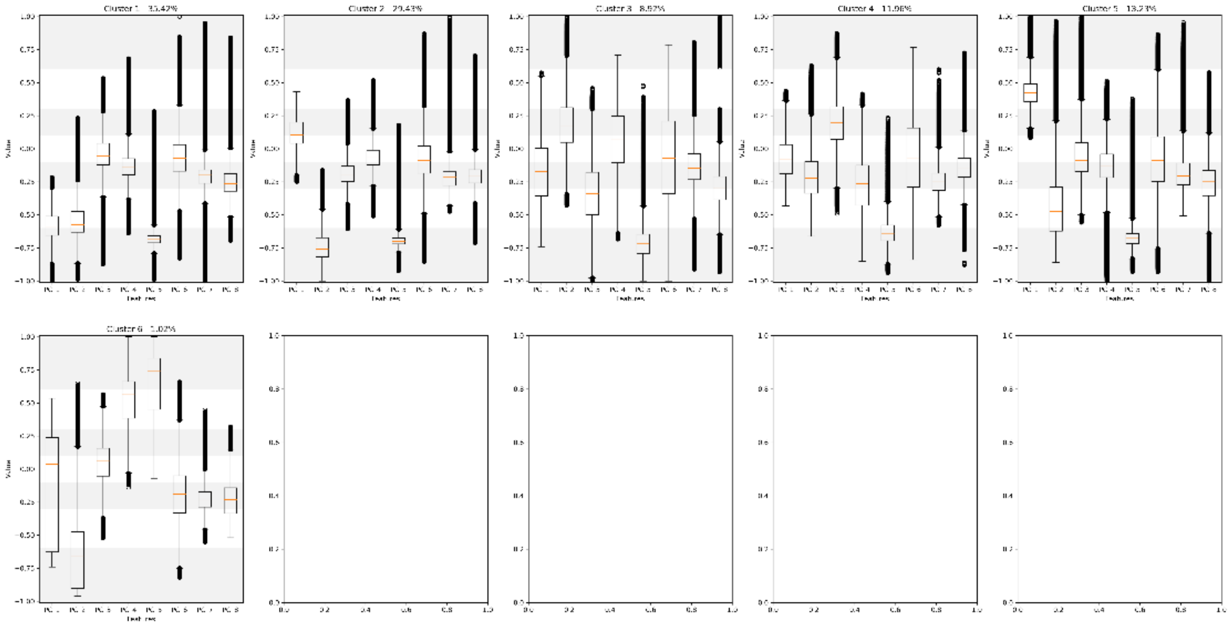

Figure D.4: Boxplot of each cluster values for Biophysical Conditions layer, with ranges for each corresponding Principal Component spread.

Annex E (Chapter 3) – External validation, contingency matrixes

This Annex presents the contingency matrices used for external validation, comparing the classification results with two established reference datasets: the Urban Atlas (UA) (EEA, 2021) and the Morphological Settlement Zones (MSZ) (Pesaresi & Panagiotis, 2023).

E.1. Cohabscapes vs Urban Atlas

The values in the UA matrixes are as follows: 1: Continuous Urban Fabric (S.L. > 80%); 2: Discontinuous Dense Urban Fabric (S.L. : 50% - 80%); 3: Discontinuous Medium Density Urban Fabric (S.L. : 30% - 50%); 4: Discontinuous Low Density Urban Fabric (S.L. : 10% - 30%); 5: Discontinuous Very Low Density Urban Fabric (S.L. < 10%); 6: Isolated Structures; 7: Industrial, commercial, public, military and private units; 8: Fast transit roads and associated land; 9: Other roads and associated land; 10: Railways and associated land; 11: Port areas; 12. Airports; 13: Mineral extraction and dump sites; 14: Construction sites; 15: Land without current use; 16: Green urban areas; 17: Sports and leisure facilities; 18: Arable land (annual crops); 19: Permanent crops (vineyards, fruit trees, olive groves); 20: Pastures; 21: Complex and mixed cultivation patterns; 22: Orchards at the fringe of urban classes; 23: Forests; 24: Herbaceous vegetation associations (natural grassland, moors...); 25: Open spaces with little or no vegetations (beaches, dunes, bare rocks, glaciers); 26: Wetland; 27: Water bodies.

E.1.1. Local Urban Fabric vs UA

The contingency matrix (Fig. E.1) highlights several strong correspondences between Cohabscapes classes (UC) and UA categories:

i. Agriculture dominance (UC-1) shows the strongest alignment overall, with 91% of its cells corresponding to Arable land (UA-18).

ii. Low built-up dominance (UC-10) is most frequently associated with Discontinuous Dense Urban Fabric (UA-2), accounting for 33% of its cells. This reflects the prevalence of moderately dense urban fabric in areas with lower built-up intensity.

iii. High built-up dominance (UC-9) aligns most strongly with Continuous Urban Fabric (UA-1), at 13%, consistent with expectations for highly urbanised zones.

iv. Trees dominance (UC-6) overlaps prominently with Complex and mixed cultivation patterns (UA-21) at 38% and Forests (UA-23) at 51%, indicating strong spatial coherence between tree-dominated landscapes and these land cover types.

v. Water (UC-13) is overwhelmingly associated with Open spaces with little or no vegetation (UA-25) at 43% and Water bodies (UA-27) at 53%, reinforcing the consistency of aquatic and barren land categories across both classifications.

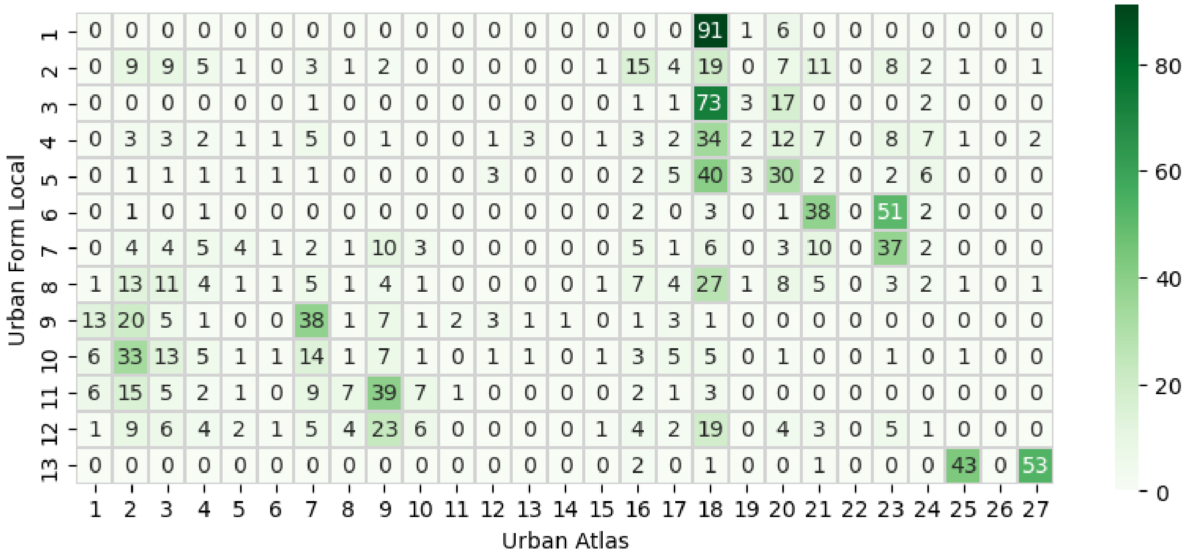

Fig. E.1: Contingency matrix of Local Urban Fabric vs Urban Atlas. The Local Urban Form values are: 1: Agriculture dominance; 2: Agriculture with hedges; 3: Fields diversified; 4: Grasslands dominance; 5: Grasslands and infrastructure; 6: Trees dominance; 7: Trees and infrastructure; 8: Shrubland dominance; 9: High built-up dominance; 10: Low built-up dominance; 11: Infrastructure dominance; 12: Infrastructure with built-up; 13: Water.

E.1.2. Landscape Urban Fabric vs UA

The contingency matrix comparing Landscape Urban Form with Urban Atlas (UA) classes (Fig. E.2) reveals several strong associations.

i. Core agriculture patches (UC-1) are most frequently linked with Arable land (annual crops) (UA-18), with a high correspondence of 94%.

ii. Edge agriculture patches (UC-2) also align closely with Arable land (UA-18), at 92%. These values highlight the strong spatial match between agricultural landscape cores and UA's agricultural land categories.

iii. Core tree patches (UC-3) and Edge tree patches (UC-4) are both strongly associated with Forests (UA-23), at 49% and 50% respectively, while also showing notable links to Complex and mixed cultivation patterns (UA-21) (48% and 31%). This reflects the mixed natural and semi-natural character of these areas.

iv. Core impervious patches (UC-5) are most associated with Discontinuous Dense Urban Fabric (50–80%) (UA-2) (19%) and Industrial, commercial, public, military and private units (UA-7) (13%), indicating their urbanised nature.

v. Edge impervious patches (UC-6) show a strong presence in Arable land (UA-18) (52%), but also appear across several urban and semi-urban categories, reflecting their transitional character.

vi. Water patches (UC-7) are clearly linked with Water bodies (UA-27) (28%) and Open spaces with little or no vegetation (UA-25) (22%), confirming their alignment with aquatic and barren land types in the UA classification.

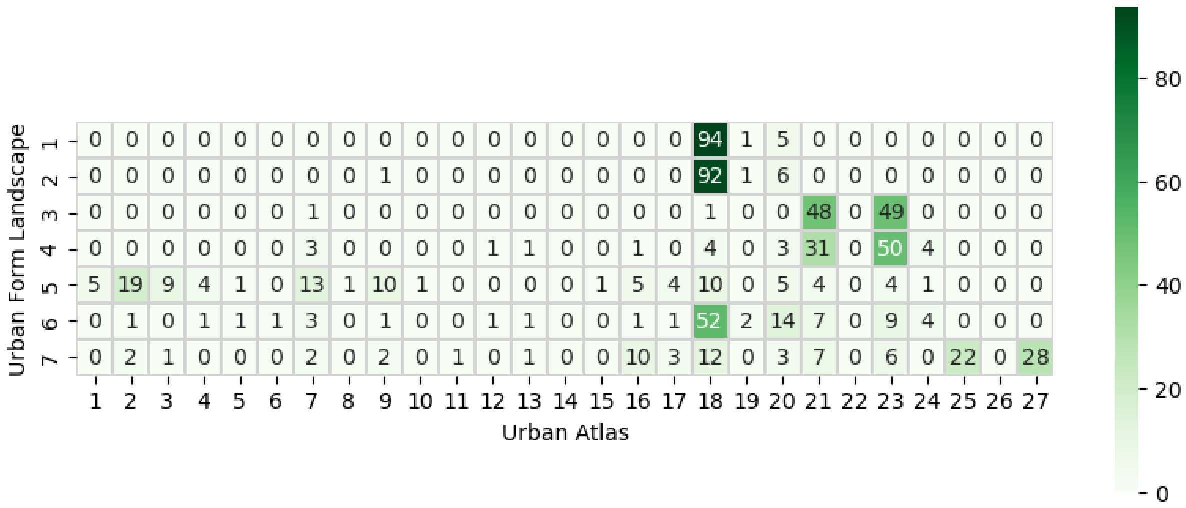

Fig. E.2: Contingency matrix of Landscape Urban Fabric vs Urban Atlas. The Landscape Urban Form values are: 1: Core agriculture patches; 2: Edge agriculture patches; 3: Core tree patches; 4: Edge tree patches; 5: Core impervious patches; 6: Edge impervious patches; 7: Water patches.

E.1.3. Anthropic Imprint vs UA

The Anthropic Imprint classification was compared with Urban Atlas (UA) categories to explore spatial associations across urban–natural gradients (Fig. E.3). The contingency matrix highlights several strong alignments:

i. Conservation natural areas (UC-1) are most associated with Permanent crops (UA-19) (19%), Complex and mixed cultivation patterns (UA-21) (32%), and Forests (UA-23) (28%), suggesting that protected zones are embedded within structured agricultural and ecological landscapes.

ii. Unprotected natural areas (UC-2) show a similar pattern, with high correspondence to Arable land (UA-18) (57%) and Forests (UA-23) (22%), indicating that these areas, while not formally conserved, remain strongly tied to natural and cultivated land covers.

iii. Regulated natural areas (UC-3) align most with Complex and mixed cultivation patterns (UA-21) (45%), Green urban areas (UA-16) (8%), and Permanent crops (UA-19) (12%), reflecting a hybrid character between ecological regulation and peri-urban land uses.

iv. Edge human living areas (UC-4) show notable associations with Arable land (UA-18) (46%), Discontinuous dense urban fabric (UA-2) (24%), and Discontinuous medium density urban fabric (UA-3) (9%), suggesting transitional zones between urban and rural forms.

v. Core human living areas (UC-5) are most strongly linked to Discontinuous dense urban fabric (UA-2) (24%), Discontinuous medium density urban fabric (UA-3) (9%), and Industrial, commercial, public, military and private units (UA-7) (17%), consistent with dense residential and functional urban cores.

vi. Industrial and commercial areas (UC-6) align with Arable land (UA-18) (18%), Discontinuous medium and low-density urban fabric (UA-3, UA-4) (9%, 11%), and Industrial units (UA-7) (7%), reflecting the integration of productive zones within mixed urban–rural contexts.

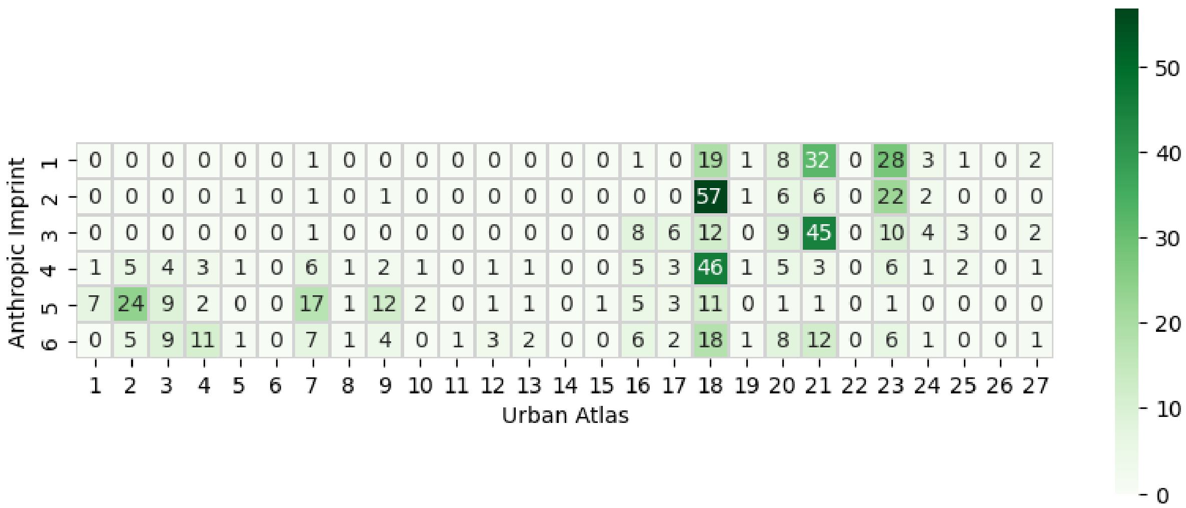

Fig. E.3: Contingency matrix of Anthropic Imprint vs Urban Atlas. The Anthropic Imprint values are: 1: Conservation natural areas; 2: Un-protected natural areas; 3: Regulated natural areas; 4: Edge human living areas; 5: Core human living areas; 6: Industrial and commercial areas.

E.1.4. Biophysical Conditions vs UA

The Biophysical Conditions classification was compared with Urban Atlas (UA) categories to identify dominant spatial associations. The contingency matrix highlights several clear patterns:

i. Local warm basin (UC-1) is most strongly associated with Arable land (annual crops) (UA-18) (50%).

ii. Local wet basin (UC-2) is also most strongly associated with Arable land (UA-18) (46%).

iii. Reliefs warmer (UC-3) aligns most closely with Forests (UA-23) (62%).

iv. Reliefs cold (UC-4) is most strongly associated with Complex and mixed cultivation patterns (UA-21) (73%).

v. Reliefs colder and rainy (UC-5) shows its strongest association with Forests (UA-23) (66%).

vi. Water-dominated areas (UC-6) are most strongly associated with Water bodies (UA-27) (56%).

These associations underscore the spatial coherence between ecological gradients and urban land-cover structures, with natural conditions aligning predictably with specific land uses. The large spatial extent of agricultural areas, particularly in Vienna and Munich, exerts a strong influence on the overall correlations observed.

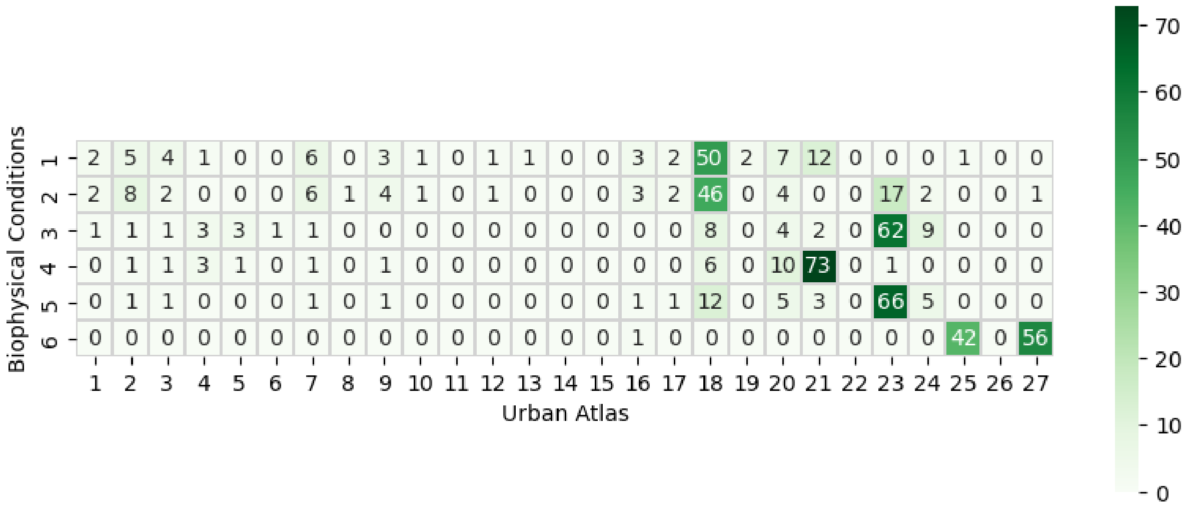

Fig. E.4: Contingency matrix of Biophysical Conditions vs Urban Atlas. Biophysical Conditions values are: 1: Local warm basin; 2: Local wet basin; 3: Reliefs warmer; 4: Reliefs cold; 5: Reliefs colder and rainy; 6: Water dominated areas.

E.2. Cohabscapes vs Morphological Settlement Zones

The values in the MSZ matrixes are as follows: 1: Open spaces, low vegetation surfaces NDVI <= 0.3; 2: Open spaces, medium vegetation surfaces 0.3 < NDVI <=0.5; 3: Open spaces, high vegetation surfaces NDVI > 0.5; 4: Open spaces, water surfaces LAND < 0.5; 5: Open spaces, road surfaces; 11: Built spaces, residential, building height <= 3m; 12: Built spaces, residential, 3m < building height <= 6m; 13: Built spaces, residential, 6m < building height <= 15m; 14: Built spaces, residential, 15m < building height <= 30m; 15: Built spaces, residential, building height > 30m; 21: Built spaces, non-residential, building height <= 3m; 22: Built spaces, non-residential, 3m < building height <= 6m; 23: Built spaces, non-residential, 6m < building height <= 15m; 24: Built spaces, non-residential, 15m < building height <= 30m; 25: Built spaces, non-residential, building height > 30m.

E.2.1. Local Urban Fabric vs MSZ

The comparison between Local Urban Fabric categories and Morphological Settlement Zones (MSZ) (Fig. E.5) reveals several strong associations.

i. Vegetated urban forms such as Agriculture dominance (UC-1), Agriculture with hedges (UC-2), Fields diversified (UC-3), Grasslands dominance (UC-4), Grasslands and infrastructure (UC-5), Trees dominance (UC-6), Trees and infrastructure (UC-7), and Shrubland dominance (UC-8), are overwhelmingly associated with Open spaces, high vegetation (NDVI > 0.5) (MSZ-3), with values ranging from 50% to 73%. This strong alignment underscores the ecological coherence of these classes, where vegetation cover is the defining spatial feature, and NDVI serves as a reliable proxy for distinguishing them.

ii. High built-up dominance (UC-9) is most strongly associated with Built residential 6–15 m (MSZ-13) (26%), reflecting the prevalence of mid-rise structures in densely urbanised zones.

iii. Low built-up dominance (UC-10), while still showing a notable share in Open spaces, high vegetation (MSZ-3) (35%), also reflects a transitional morphology between built and green areas.

iv. Infrastructure dominance (UC-11) aligns most with Open spaces, medium vegetation (0.3 < NDVI ≤ 0.5) (MSZ-2) (20%), suggesting a mix of engineered surfaces and semi-natural surroundings, such as road verges or utility corridors.

v. Infrastructure with built-up (UC-12) also leans toward Open spaces, high vegetation (MSZ-3) (34%), indicating that even infrastructural zones can be embedded within or adjacent to green patches.

vi. Water (UC-13) is most strongly associated with Open spaces, water surfaces (LAND < 0.5) (MSZ-4) (28%), confirming the spatial accuracy of the classification in capturing hydrological features.

Overall, the comparison demonstrates a strong thematic and spatial consistency between Local Urban Fabric and MSZ. Vegetation cover and building height emerge as the key discriminators across the urban–rural spectrum, reinforcing the robustness of the classification in capturing both ecological and morphological gradients.

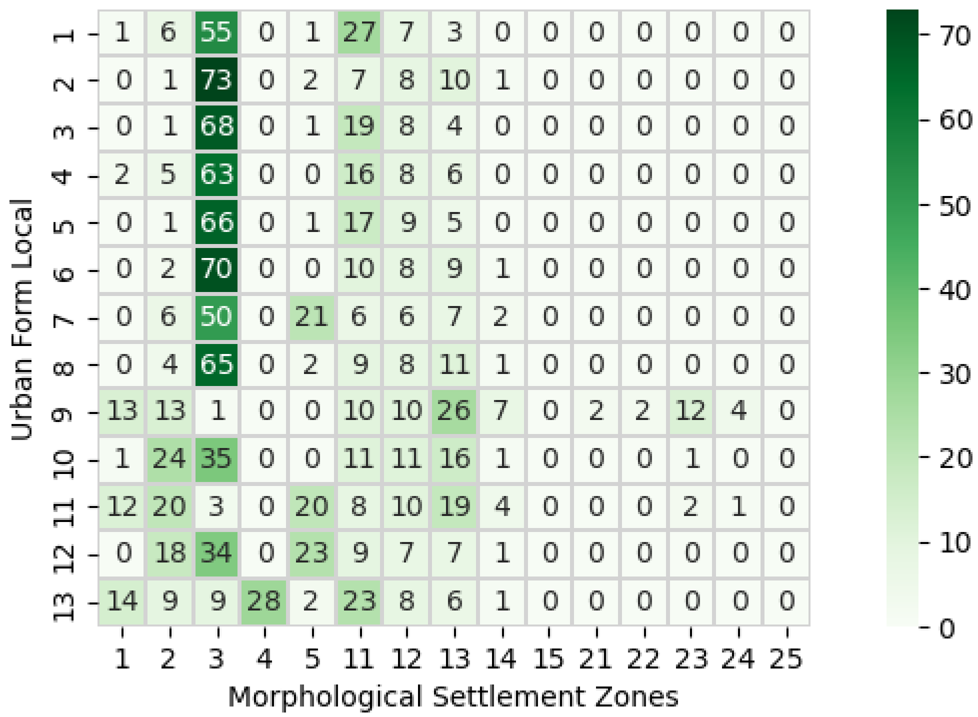

Fig. E.5: Contingency matrix of Local Urban Fabric vs Morphological Settlement Zones. The Local Urban Form values are: 1: Agriculture dominance; 2: Agriculture with hedges; 3: Fields diversified; 4: Grasslands dominance; 5: Grasslands and infrastructure; 6: Trees dominance; 7: Trees and infrastructure; 8: Shrubland dominance; 9: High built-up dominance; 10: Low built-up dominance; 11: Infrastructure dominance; 12: Infrastructure with built-up; 13: Water.

E.2.2. Landscape Urban Fabric vs MSZ

The comparison between Landscape Urban Fabric and Morphological Settlement Zones (MSZ) (Fig. E.6) reveals several distinct associations:

i. Core agriculture patches (UC-1) are most strongly linked with High vegetation open spaces (NDVI > 0.5) (MSZ-3) (65%), while also showing a notable presence in Low-rise residential areas (≤ 3 m) (MSZ-11).

ii. Edge agriculture patches (UC-2) follow a similar pattern, with high values in High vegetation (MSZ-3) (43%) and Low-rise residential (MSZ-11) (44%).

iii. Core tree patches (UC-3) are more evenly distributed but show strong associations with Low vegetation surfaces (MSZ-1) (38%) and a mix of Non-residential built spaces in the 6–30 m height range (MSZ-23, MSZ-24).

iv. Edge tree patches (UC-4) also span both vegetated and built areas, with notable counts in Non-residential buildings and Medium-rise residential zones (MSZ-14).

v. Core impervious patches (UC-5) and Edge impervious patches (UC-6) are concentrated in Residential buildings between 3–15 m in height (MSZ-12, MSZ-13), reflecting their urbanised character.

vi. Water patches (UC-7) are mostly found in High vegetation surfaces (MSZ-3) (26%), Low vegetation surfaces (MSZ-1) (6%), and Residential buildings up to 15 m (MSZ-12, MSZ-13), suggesting adjacency or overlap between aquatic features and surrounding vegetated or built environments.

Overall, the comparison demonstrates that Landscape Urban Fabric categories capture both ecological and morphological gradients, with agricultural and tree-dominated patches aligning strongly with vegetation-based MSZ classes, while impervious patches correspond closely to residential building height categories.

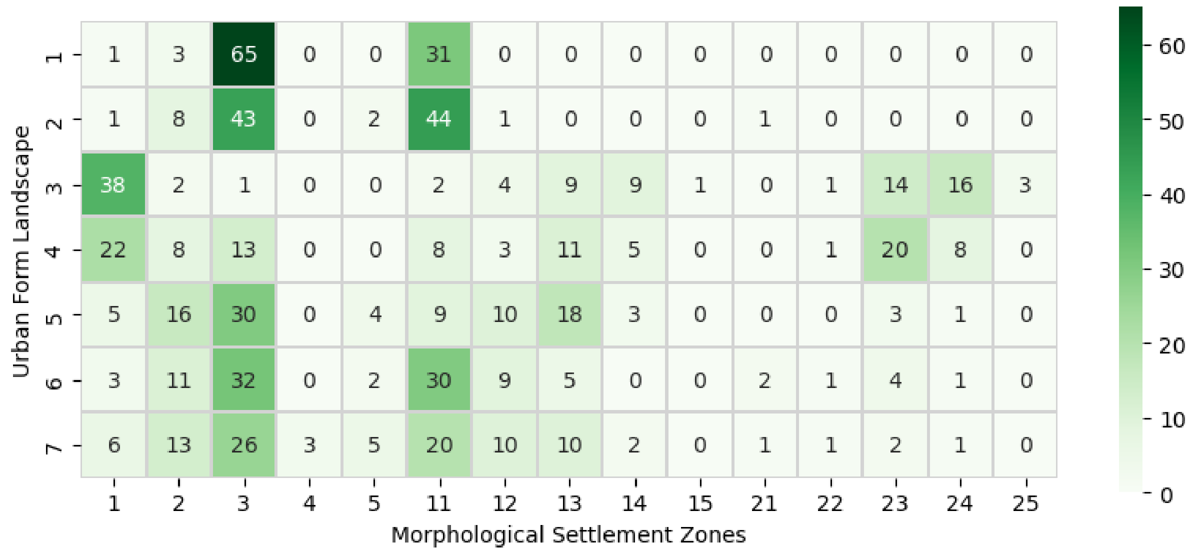

Fig. E.6: Contingency matrix of Landscape Urban Form vs Morphological Settlement Zones. The Landscape Urban Form values are: 1: Core agriculture patches; 2: Edge agriculture patches; 3: Core tree patches; 4: Edge tree patches; 5: Core impervious patches; 6: Edge impervious patches; 7: Water patches.

E.2.3. Anthropic Imprint vs MSZ

The comparison between Anthropic Imprint categories and Morphological Settlement Zones (MSZ) (Fig. E.7) reveals several noteworthy associations:

i. Conservation natural areas (UC-1) are most frequently associated with Built residential ≤ 3 m (MSZ-12) (41%). This somewhat unexpected alignment may reflect rural settlements embedded within conservation landscapes.

ii. Unprotected natural areas (UC-2) show their strongest association with Open spaces, high vegetation (NDVI > 0.5) (MSZ-3) (36%), suggesting that even without formal protection, these areas maintain a strong vegetated character, likely due to limited development pressure.

iii. Regulated natural areas (UC-3) are also most strongly linked to Open spaces, high vegetation (MSZ-3) (52%), reinforcing both their ecological structure and the effectiveness of regulatory frameworks in preserving vegetative cover.

iv. Edge human living areas (UC-4) present a more mixed profile but are most associated with Open spaces, high vegetation (MSZ-3) (32%). This reflects their transitional nature between built-up and natural zones, where peri-urban areas retain significant green cover due to lower building densities or interspersed natural features.

v. Core human living areas (UC-5), while more urbanised, still show their strongest association with Open spaces, high vegetation (MSZ-3) (28%), highlighting the persistence of green infrastructure or tree-lined residential zones even in denser urban cores.

vi. Industrial and commercial areas (UC-6) are also most strongly associated with Open spaces, high vegetation (MSZ-3) (36%), indicating that these zones may include landscaped buffers, green roofs, or undeveloped parcels within industrial estates.

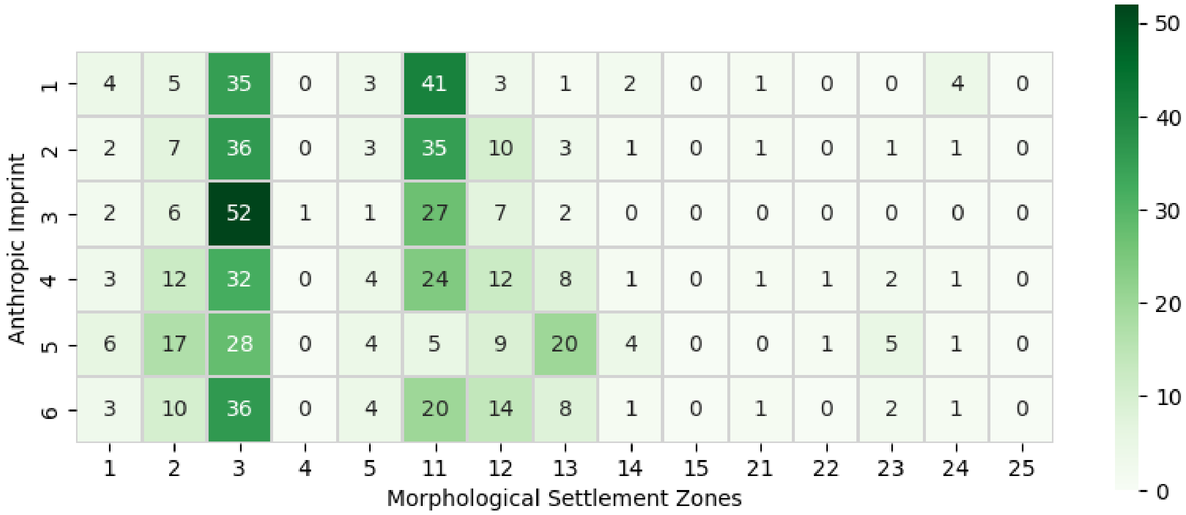

Fig. E.7: Contingency matrix of Anthropic Imprint vs Morphological Settlement Zones. The Anthropic Imprint values are: 1: Conservation natural areas; 2: Un-protected natural areas; 3: Regulated natural areas; 4: Edge human living areas; 5: Core human living areas; 6: Industrial and commercial areas.

E.2.4. Biophysical Conditions vs MSZ

The comparison between Biophysical Conditions and Morphological Settlement Zones (MSZ) (Fig. E.8) reveals a consistent pattern across most classes.

i. Local warm basin (UC-1), Local wet basin (UC-2), Reliefs warmer (UC-3), Reliefs cold (UC-4), and Reliefs colder and rainy (UC-5) are all most strongly associated with Open spaces, high vegetation (NDVI > 0.5) (MSZ-3), with values ranging from 26% to 41%. This indicates that these zones are predominantly characterised by dense vegetative cover, regardless of their climatic or topographic variation.

ii. The highest correspondence is observed in Reliefs cold (UC-4) (41%), followed closely by Reliefs colder and rainy (UC-5) (39%), suggesting that vegetation remains a dominant spatial feature even in colder and wetter conditions.

iii. In contrast, Water-dominated areas (UC-6) display a different pattern, with the strongest association found in Built residential ≤ 3 m (MSZ-12) (32%). This reflects a distinct morphological structure compared to the other biophysical categories, where built environments play a more prominent role.

iv. Open spaces, water surfaces (MSZ-4) also contribute significantly to UC-6 (21%), reinforcing its hydrological character.

Overall, the results highlight the robust role of vegetation as a unifying spatial feature across diverse biophysical conditions, while water-dominated areas diverge by showing stronger ties to build morphologies and hydrological surfaces.

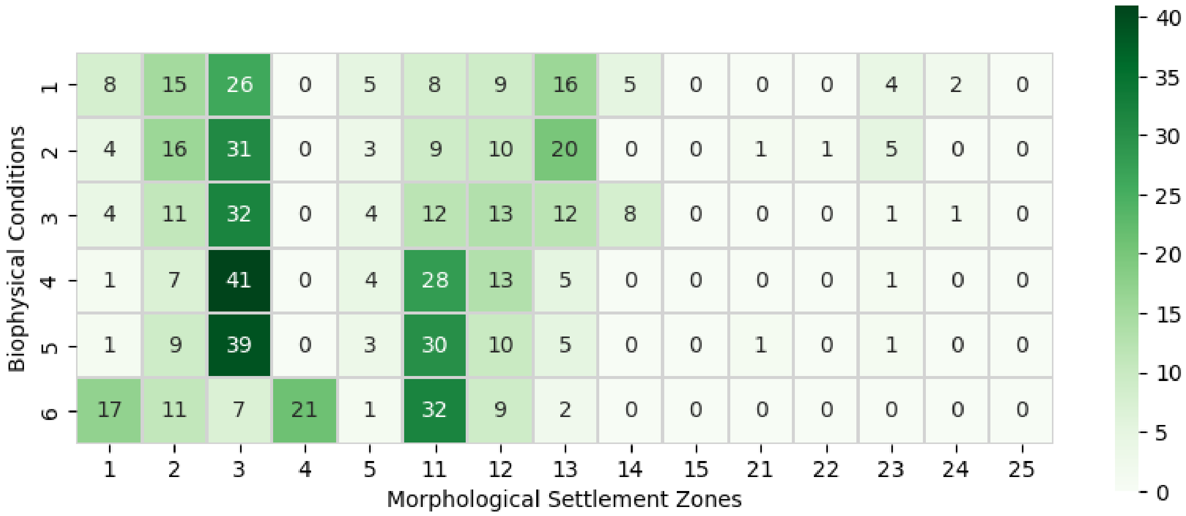

Fig. E.8: Contingency matrix of Biophysical Conditions vs Morphological Settlement Zones. Biophysical Conditions values are: 1: Local warm basin; 2: Local wet basin; 3: Reliefs warmer; 4: Reliefs cold; 5: Reliefs colder and rainy; 6: Water dominated areas.

Annex F (Chapter 3) – Birds species data in-depth analysis

This Annex documents the data-driven reasoning behind the selection of birds' species, and the consequential extensive analysis run. Additional diagnostics are performed to evaluate rasterization, sampling depth, and the statistical robustness of Jacobs' D electivity estimates across Genoa, Munich and Vienna. The evidence shows Genoa is underpowered for per-class electivity for most species; the Annex therefore prioritizes Vienna and Munich for full D interpretation and uses a small, curated simple species set for cross-city comparisons (in the main text). The annex is structured as follows:

i. F.1. Bird data selection and availability;

ii. F.2. Species lists and robustness flags;

iii. F.3. Species acculumation and sample size diagnostics;

iv. F.4. Bootstrap undertainty and valid class coverage;

v. F.5. Jacobs' D heatmaps (extended birds data coverage);

vi. F.6. Correlations, variance, and D values (extended birds data coverage), and relevance for ecology-planning.

F.1. Bird data selection and availability

This study uses occurrence records derived from GBIF.org as the primary source of bird observations. The GBIF dataset was filtered, cleaned, and georeferenced before rasterization and analysis. The following short analysis explains how the GBIF data selection and availability affect downstream results. and where the occurrence records from eBird Observation Dataset (EOD) were filtered to retain only bird observations with valid coordinates and dates (data from Vienna, Genoa, and Munich from 2004-2024 from EOD repository), then projected to the analysis CRS and rasterized to the study grid (Fig. F.1).

As key filters applied, the presence of decimal latitude/longitude, non-null taxon identifiers (family, species), and basic quality flags (georeferenced, not flagged as doubtful) were considered. Records were then clipped to GHS-FUA boundaries and rasterized to match the Cohabscapes grid.

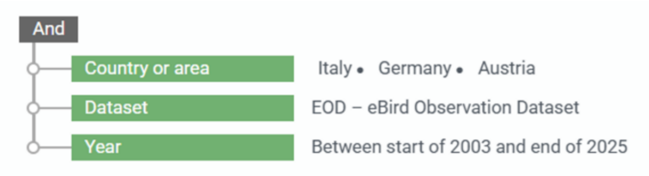

Fig. F.1: Download query for EOD data.

Using EOD allows broad taxonomic coverage and reproducibility. However, EOD is an opportunistic compilation of many data sources (citizen science, museum specimens, monitoring programs), so it carries known biases that must be diagnosed and reported. As far as data availability and representativeness diagnostics, EOD records vary in taxonomic resolution. The dataset used categorical fields family and species and encoded them as categorical IDs; species with ambiguous or unresolved names were retained only if a stable species_id existed. Although EOD provides many point records, it low counts for Genoa present a critical factor. Inside the Genoa polygon (4,262 vector points), only a small fraction survived or aligned to the raster grid used for electivity (233 non-null raster pixels). This indicates a rasterization or alignment loss that reduces usable data for per-class electivity in Genoa.

Four diagnostic plots were produced, considering the connotation of Genoa's data (Fig. F.2, F.3, F.4, and F.5). Because EOD supplies many vector points that do not translate into raster pixels for Genoa, electivity results for Genoa are unreliable for most species. The analysis therefore treats Genoa primarily as a diagnostic case (showing rasterization issues and sampling shortfall) and relies on Vienna and Munich for robust per-class Jacobs' D matrices and bootstrap uncertainty estimates.

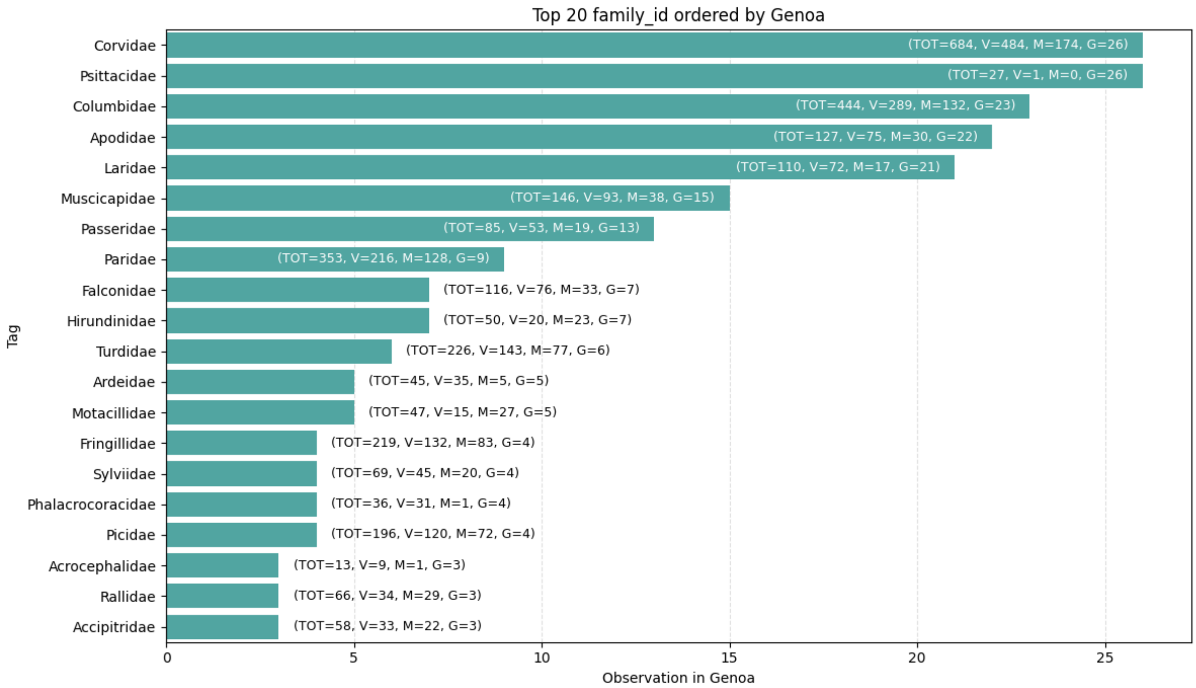

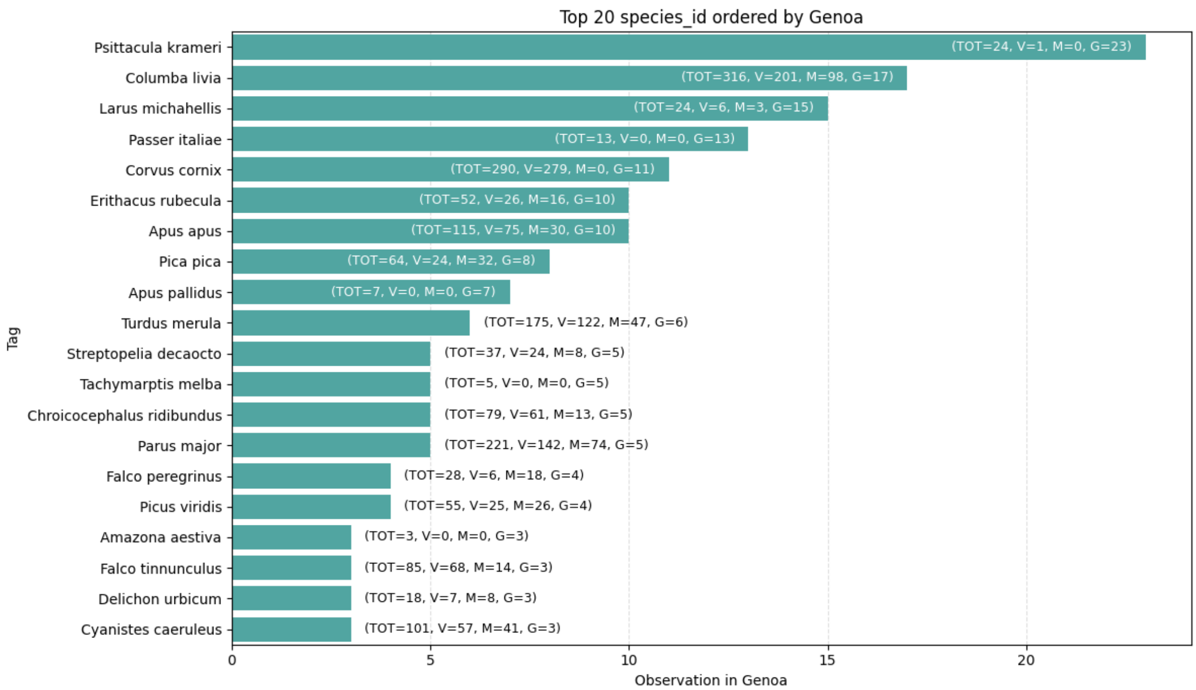

Fig. F.2 and F.3: Top 20 families/species ordered by Genoa. Each bar annotated with TOT, V, M, G counts for reference.

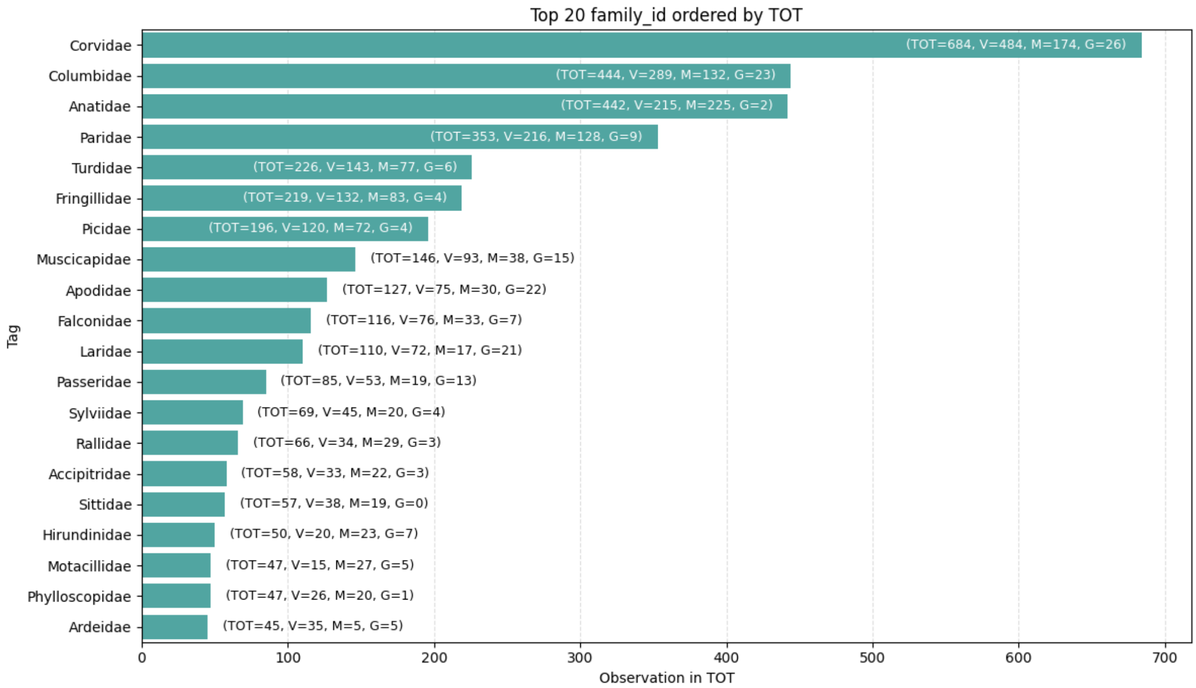

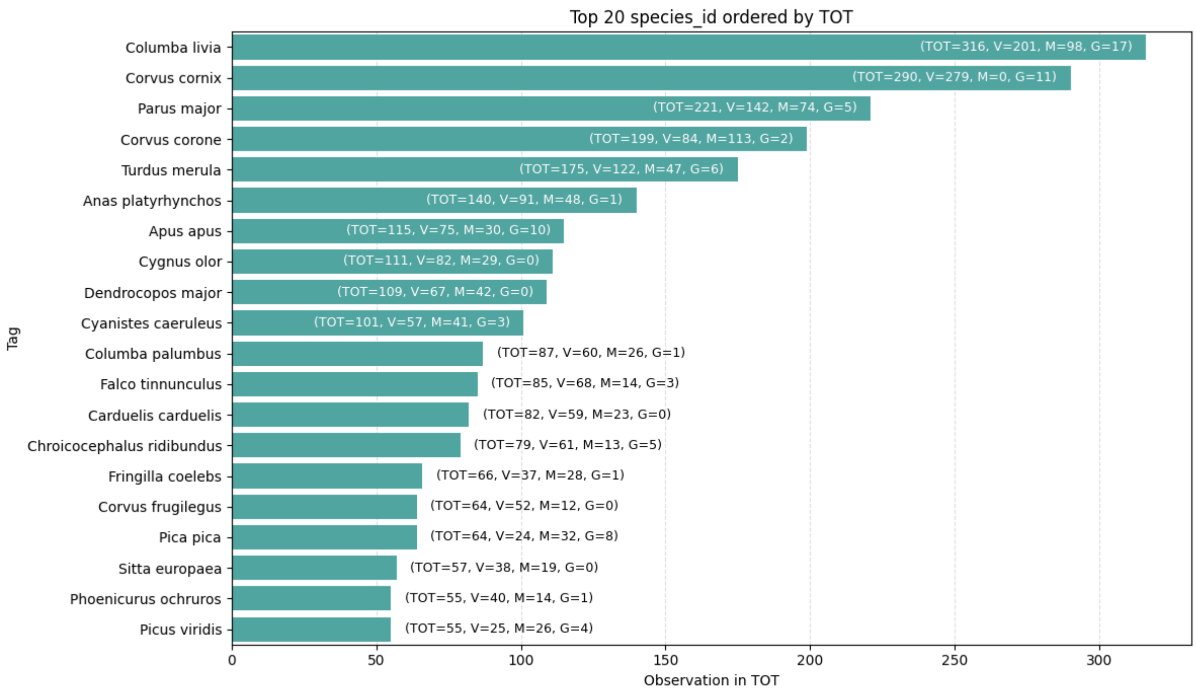

Fig. F.4 and F.5: Top 20 families/species ordered by TOT. Each bar annotated with TOT, V, M, G counts for reference.

The Genoa family and species charts show a concentration of observations in a small number of taxa. This concentration is consistent with urban sampling bias and with the presence of introduced or commensal species. The disparity between vector point counts and raster pixels suggests grid alignment or resolution choices removed many observations from the rasterized dataset; this must be addressed before treating Genoa as equivalent to Vienna or Munich for electivity inference.

Genoa's families show high representation of Corvidae, Columbidae and Paridae, indicating urban-adapted and conspicuous taxa dominate the Genoa record. As for Genoa's species, instead, several species are introduced or synanthropic (e.g., Psittacula krameri, Columba livia), which inflates local counts relative to other cities.

In the total plot, many species that are abundant are concentrated in Vienna and Munich. Genoa contributes relatively few raster pixels for those species. Families such as Anatidae and Paridae appear strongly in TOT but are under-represented in Genoa's raster grid. Conversely, some taxa (e.g., Psittacidae) are disproportionately represented in Genoa due to local introductions. Thus, cross-city comparisons must account for these imbalances: raw counts are insufficient for electivity inference without weighting or restricting to robustly sampled species.

In summary, the Chapter focused on species analysis and counted 195 individual species from which the five species in the main text were selected.

F.2. Species lists and robustness flags

Looking in depth for species data we obtained for the complete set of 195 bird species (Table F.1), species were extracted and flagged as underpowered considering Genoa's observations from which robustness can be inferred.

Table F.1: Complete list of observations in Vienna, Munich, and Genoa, with columns showing the EOD species identifier, names, total observations, pixel counts in the three cities, mean std in all cities (where common in the three cities), genoa validity flag (underpowered vs robust).

Species ID	Species name	Total obs.	V pixels	M pixels	G pixels	G validity	Mean std for all cities
3	*Accipiter gentilis*	1	0	1	0	Underpowered	n/a
4	*Accipiter nisus*	31	18	13	0	Underpowered	n/a
7	*Acrocephalus arundinaceus*	3	2	1	0	Underpowered	n/a
12	*Acrocephalus schoenobaenus*	1	0	0	1	Underpowered	n/a
13	*Acrocephalus scirpaceus*	5	5	0	0	Underpowered	n/a
14	*Actitis hypoleucos*	2	2	0	0	Underpowered	n/a
16	*Aegithalos caudatus*	29	20	8	1	Underpowered	n/a
23	*Aix galericulata*	28	6	22	0	Underpowered	n/a
24	*Aix sponsa*	1	1	0	0	Underpowered	n/a
25	*Alauda arvensis*	6	2	3	1	Underpowered	n/a
27	*Alcedo atthis*	28	10	18	0	Underpowered	n/a
31	*Alectoris rufa*	1	0	0	1	Underpowered	n/a
33	*Alopochen aegyptiaca*	2	0	2	0	Underpowered	n/a
35	*Amazona aestiva*	3	0	0	3	Underpowered	n/a
43	*Anas crecca*	2	1	1	0	Underpowered	n/a
46	*Anas platyrhynchos*	140	91	48	1	Robust	0.10784
49	*Anas undulata*	1	0	1	0	Underpowered	n/a
51	*Anser anser*	38	1	37	0	Robust	0.10432
58	*Anser indicus*	19	0	19	0	Underpowered	n/a
62	*Anthus campestris*	1	0	1	0	Underpowered	n/a
67	*Anthus pratensis*	1	0	1	0	Underpowered	n/a
71	*Anthus trivialis*	1	0	1	0	Underpowered	n/a
73	*Apus apus*	115	75	30	10	Robust	0.08744
75	*Apus pallidus*	7	0	0	7	Underpowered	n/a
84	*Ardea alba*	2	2	0	0	Underpowered	n/a
85	*Ardea cinerea*	38	31	4	3	Robust	0.10711

87	*Ardeola ralloides*	1	1	0	0	Underpowered	n/a
90	*Asio otus*	6	4	2	0	Underpowered	n/a
91	*Athene noctua*	1	0	0	1	Underpowered	n/a
96	*Aythya ferina*	8	3	5	0	Underpowered	n/a
97	*Aythya fuligula*	19	9	10	0	Underpowered	n/a
99	*Aythya nyroca*	4	0	4	0	Underpowered	n/a
101	*Bombycilla garrulus*	8	3	5	0	Underpowered	n/a
104	*Branta canadensis*	10	3	7	0	Underpowered	n/a
106	*Branta leucopsis*	11	0	11	0	Underpowered	n/a
110	*Bubulcus ibis*	1	0	0	1	Underpowered	n/a
113	*Bucephala clangula*	1	1	0	0	Underpowered	n/a
116	*Buteo buteo*	14	7	7	0	Underpowered	n/a
120	*Cairina moschata*	1	1	0	0	Underpowered	n/a
146	*Carduelis carduelis*	82	59	23	0	Robust	0.11917
153	*Certhia brachydactyla*	27	8	19	0	Underpowered	n/a
154	*Certhia familiaris*	7	5	2	0	Underpowered	n/a
158	*Charadrius dubius*	4	0	4	0	Underpowered	n/a
170	*Chloris chloris*	38	19	18	1	Underpowered	n/a
174	*Chroicocephalus ridibundus*	79	61	13	5	Robust	0.09989
176	*Ciconia ciconia*	4	2	2	0	Underpowered	n/a
177	*Ciconia nigra*	1	1	0	0	Underpowered	n/a
178	*Cinclus cinclus*	9	0	9	0	Underpowered	n/a
179	*Circaetus gallicus*	1	0	0	1	Underpowered	n/a
181	*Circus cyaneus*	1	1	0	0	Underpowered	n/a
186	*Clangula hyemalis*	3	3	0	0	Underpowered	n/a
187	*Coccothraustes coccothraustes*	4	2	2	0	Underpowered	n/a
189	*Coloeus monedula*	25	22	1	2	Underpowered	n/a
191	*Columba livia*	316	201	98	17	Robust	0.09491
192	*Columba oenas*	3	3	0	0	Underpowered	n/a
193	*Columba palumbus*	87	60	26	1	Robust	0.1137
196	*Corvus corax*	9	3	6	0	Underpowered	n/a
197	*Corvus cornix*	290	279	0	11	Robust	0.09483
198	*Corvus corone*	199	84	113	2	Robust	0.12944
199	*Corvus frugilegus*	64	52	12	0	Robust	0.09897
201	*Coturnix coturnix*	1	1	0	0	Underpowered	n/a
204	*Cuculus canorus*	5	3	1	1	Underpowered	n/a
205	*Curruca cantillans*	3	3	0	0	Underpowered	n/a
209	*Cyanistes caeruleus*	101	57	41	3	Robust	0.10305

211	*Cygnus atratus*	2	0	2	0	Underpowered	n/a
216	*Cygnus olor*	111	82	29	0	Robust	0.08783
217	*Delichon urbicum*	18	7	8	3	Underpowered	n/a
219	*Dendrocopos major*	109	67	42	0	Robust	0.09908
220	*Dendrocopos syriacus*	3	3	0	0	Underpowered	n/a
221	*Dendrocoptes medius*	16	15	1	0	Underpowered	n/a
226	*Dryobates minor*	1	0	1	0	Underpowered	n/a
227	*Dryocopus martius*	12	10	2	0	Underpowered	n/a
230	*Egretta garzetta*	2	0	1	1	Underpowered	n/a
237	*Emberiza cia*	1	0	0	1	Underpowered	n/a
238	*Emberiza cirlus*	1	0	0	1	Underpowered	n/a
239	*Emberiza citrinella*	12	5	7	0	Underpowered	n/a
245	*Emberiza rustica*	1	1	0	0	Underpowered	n/a
249	*Erithacus rubecula*	52	26	16	10	Underpowered	n/a
259	*Falco peregrinus*	28	6	18	4	Underpowered	n/a
261	*Falco subbuteo*	2	2	0	0	Underpowered	n/a
262	*Falco tinnunculus*	85	68	14	3	Robust	0.09639
263	*Falco vespertinus*	1	0	1	0	Underpowered	n/a
264	*Ficedula albicollis*	8	7	0	1	Underpowered	n/a
265	*Ficedula hypoleuca*	7	6	1	0	Underpowered	n/a
273	*Fringilla coelebs*	66	37	28	1	Robust	0.10561
274	*Fringilla montifringilla*	4	1	2	1	Underpowered	n/a
275	*Fulica atra*	34	12	22	0	Underpowered	n/a
277	*Galerida cristata*	4	4	0	0	Underpowered	n/a
280	*Gallinula chloropus*	30	22	6	2	Underpowered	n/a
282	*Garrulus glandarius*	32	20	9	3	Underpowered	n/a
283	*Gavia adamsii*	2	2	0	0	Underpowered	n/a
285	*Gavia immer*	4	3	1	0	Underpowered	n/a
286	*Gavia stellata*	1	1	0	0	Underpowered	n/a
299	*Haematopus ostralegus*	2	2	0	0	Underpowered	n/a
301	*Haliaeetus albicilla*	1	1	0	0	Underpowered	n/a
302	*Hieraaetus pennatus*	2	1	0	1	Underpowered	n/a
303	*Himantopus himantopus*	1	0	0	1	Underpowered	n/a
304	*Hippolais icterina*	4	2	0	2	Underpowered	n/a
306	*Hirundo rustica*	31	13	15	3	Underpowered	n/a

312	*Ichthyaetus melanocephalus*	1	1	0	0	Underpowered	n/a
316	*Ixobrychus minutus*	1	1	0	0	Underpowered	n/a
331	*Larus cachinnans*	2	1	1	0	Underpowered	n/a
338	*Larus michahellis*	24	6	3	15	Underpowered	n/a
346	*Linaria cannabina*	2	0	2	0	Underpowered	n/a
355	*Lophophanes cristatus*	2	0	2	0	Underpowered	n/a
363	*Luscinia megarhynchos*	7	5	1	1	Underpowered	n/a
364	*Luscinia svecica*	1	0	0	1	Underpowered	n/a
365	*Lymnocryptes minimus*	1	1	0	0	Underpowered	n/a
371	*Mareca strepera*	5	1	4	0	Underpowered	n/a
375	*Melanitta fusca*	1	1	0	0	Underpowered	n/a
376	*Melanitta nigra*	1	1	0	0	Underpowered	n/a
383	*Mergellus albellus*	2	2	0	0	Underpowered	n/a
384	*Mergus merganser*	21	4	17	0	Underpowered	n/a
385	*Mergus serrator*	2	2	0	0	Underpowered	n/a
386	*Merops apiaster*	3	2	1	0	Underpowered	n/a
388	*Microcarbo pygmaeus*	2	2	0	0	Underpowered	n/a
389	*Milvus migrans*	2	2	0	0	Underpowered	n/a
390	*Milvus milvus*	1	0	1	0	Underpowered	n/a
395	*Motacilla alba*	18	9	8	1	Underpowered	n/a
396	*Motacilla cinerea*	23	5	15	3	Underpowered	n/a
398	*Motacilla flava*	3	1	1	1	Underpowered	n/a
400	*Muscicapa striata*	4	2	2	0	Underpowered	n/a
405	*Netta rufina*	7	1	6	0	Underpowered	n/a
406	*Nucifraga caryocatactes*	1	0	1	0	Underpowered	n/a
418	*Oenanthe oenanthe*	1	0	0	1	Underpowered	n/a
420	*Oriolus oriolus*	3	3	0	0	Underpowered	n/a
422	*Otus scops*	1	0	0	1	Underpowered	n/a
426	*Pandion haliaetus*	1	1	0	0	Underpowered	n/a
429	*Parus major*	221	142	74	5	Robust	0.12313
430	*Passer domesticus*	50	38	12	0	Robust	0.10045
432	*Passer italiae*	13	0	0	13	Underpowered	n/a
433	*Passer montanus*	22	15	7	0	Underpowered	n/a
434	*Pastor roseus*	1	1	0	0	Underpowered	n/a
439	*Perdix perdix*	1	1	0	0	Underpowered	n/a
440	*Periparus ater*	13	8	4	1	Underpowered	n/a
441	*Pernis apivorus*	4	3	0	1	Underpowered	n/a

443	*Phalacrocorax aristotelis*	1	0	0	1	Underpowered	n/a
444	*Phalacrocorax carbo*	33	29	1	3	Underpowered	n/a
448	*Phasianus colchicus*	7	4	2	1	Underpowered	n/a
455	*Phoenicurus ochruros*	55	40	14	1	Robust	0.0966
456	*Phoenicurus phoenicurus*	10	7	3	0	Underpowered	n/a
459	*Phylloscopus collybita*	33	15	18	0	Underpowered	n/a
467	*Phylloscopus proregulus*	8	8	0	0	Underpowered	n/a
469	*Phylloscopus sibillatrix*	3	3	0	0	Underpowered	n/a
471	*Phylloscopus trochilus*	3	0	2	1	Underpowered	n/a
472	*Pica pica*	64	24	32	8	Robust	0.09825
475	*Picus viridis*	55	25	26	4	Underpowered	n/a
476	*Platalea leucorodia*	1	1	0	0	Underpowered	n/a
485	*Podiceps auritus*	2	2	0	0	Underpowered	n/a
486	*Podiceps cristatus*	10	1	9	0	Underpowered	n/a
488	*Podiceps nigricollis*	1	0	0	1	Underpowered	n/a
489	*Poecile montanus*	4	2	2	0	Underpowered	n/a
490	*Poecile palustris*	12	7	5	0	Underpowered	n/a
496	*Porzana porzana*	1	0	0	1	Underpowered	n/a
500	*Prunella modularis*	1	1	0	0	Underpowered	n/a
504	*Psittacula krameri*	24	1	0	23	Underpowered	n/a
506	*Ptyonoprogne rupestris*	1	0	0	1	Underpowered	n/a
514	*Pyrrhula pyrrhula*	10	6	4	0	Underpowered	n/a
516	*Rallus aquaticus*	1	0	1	0	Underpowered	n/a
518	*Regulus ignicapilla*	4	0	2	2	Underpowered	n/a
519	*Regulus regulus*	13	8	5	0	Underpowered	n/a
520	*Remiz pendulinus*	5	5	0	0	Underpowered	n/a
523	*Rissa tridactyla*	1	1	0	0	Underpowered	n/a
525	*Saxicola rubetra*	1	0	1	0	Underpowered	n/a
527	*Scolopax rusticola*	2	2	0	0	Underpowered	n/a
529	*Serinus serinus*	4	3	0	1	Underpowered	n/a
534	*Sitta europaea*	57	38	19	0	Robust	0.10524
535	*Somateria mollissima*	1	1	0	0	Underpowered	n/a

541	*Spatula querquedula*	1	0	0	1	Underpowered	n/a
544	*Spinus spinus*	9	5	4	0	Underpowered	n/a
545	*Stercorarius longicaudus*	1	0	0	1	Underpowered	n/a
550	*Sterna paradisaea*	1	1	0	0	Underpowered	n/a
552	*Streptopelia decaocto*	37	24	8	5	Underpowered	n/a
555	*Streptopelia turtur*	1	1	0	0	Underpowered	n/a
556	*Strix aluco*	25	5	19	1	Underpowered	n/a
558	*Sturnus vulgaris*	33	25	7	1	Underpowered	n/a
559	*Sula leucogaster*	2	0	0	2	Underpowered	n/a
560	*Sylvia atricapilla*	51	33	16	2	Robust	0.10679
561	*Sylvia borin*	3	0	3	0	Underpowered	n/a
562	*Sylvia communis*	4	2	1	1	Underpowered	n/a
565	*Sylvia curruca*	7	7	0	0	Underpowered	n/a
572	*Sylvia undata*	1	0	0	1	Underpowered	n/a
574	*Tachybaptus ruficollis*	8	4	4	0	Underpowered	n/a
575	*Tachymarptis melba*	5	0	0	5	Underpowered	n/a
588	*Thalasseus sandvicensis*	1	0	0	1	Underpowered	n/a
590	*Threskiornis aethiopicus*	1	0	0	1	Underpowered	n/a
599	*Troglodytes troglodytes*	23	11	11	1	Underpowered	n/a
602	*Turdus iliacus*	4	3	1	0	Underpowered	
603	*Turdus merula*	175	122	47	6	Robust	0.11797
605	*Turdus philomelos*	9	6	3	0	Underpowered	n/a
606	*Turdus pilaris*	26	7	19	0	Underpowered	n/a
608	*Turdus viscivorus*	12	5	7	0	Underpowered	n/a
610	*Upupa epops*	2	1	1	0	Underpowered	n/a
615	*Vanellus vanellus*	1	0	1	0	Underpowered	n/a
617	*Xema sabini*	1	1	0	0	Underpowered	n/a

F.3. Species accumulation and sample size diagnostics

The results were further interpreted by using (species) accumulation curves (Fig. F.6, F.7, F.8). These plots show how the number of species increases as sampling effort increases. They are a standard diagnostic tool for detecting under-sampling. Accumulation curves and histograms confirm that Genoa is under-sampled relative to the other cities. This under-sampling reduces the number of species with sufficient per-class counts (≥4) and prevents reliable bootstrap estimation of Jacobs' D for most species in Genoa. Vienna (Fig. F.6) and Munich (Fig. F.7) show higher sampling depth and a clearer asymptomatic approach. Genoa (Fig. F.8), instead, show slow accumulation and high variance, consistent with low raster sample size.

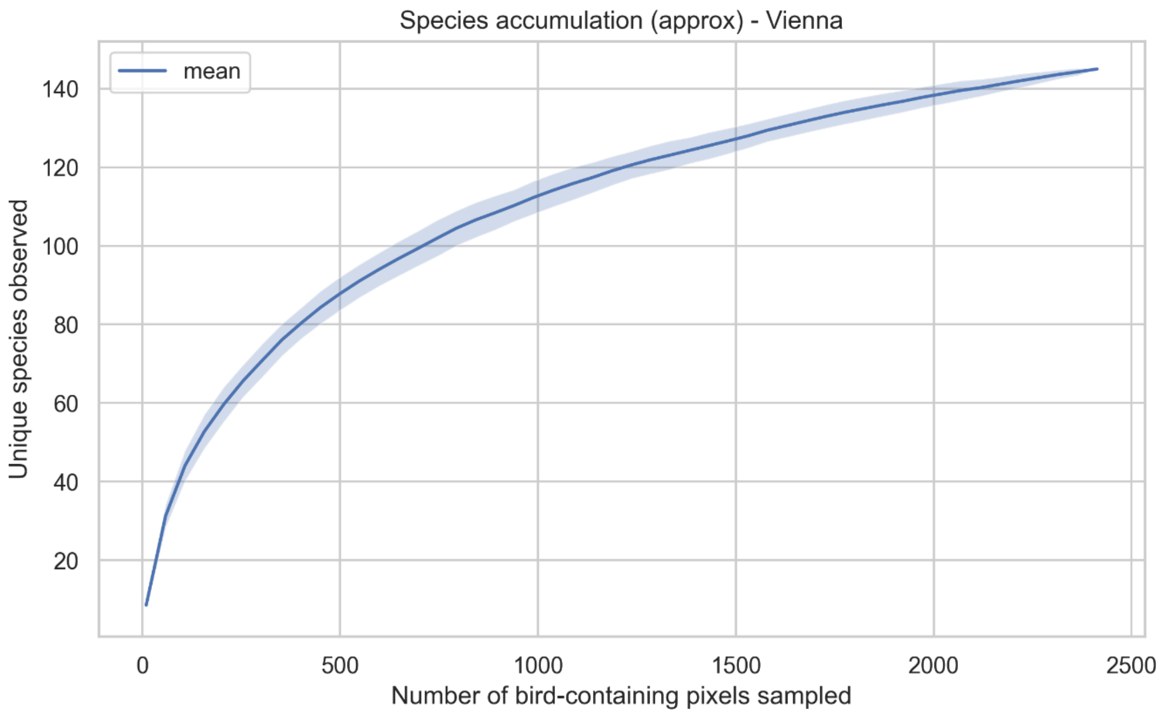

Fig. F.6: Species accumulation curve for Vienna observations.

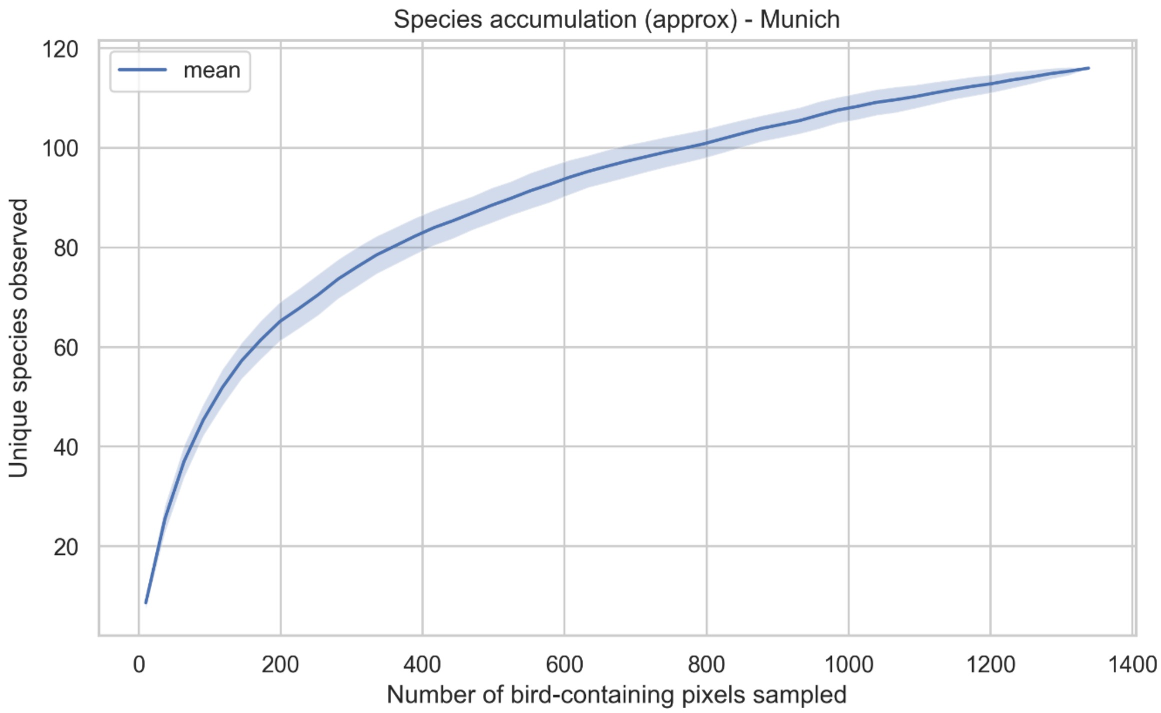

Fig. F.7: Species accumulation curve for Munich observations.

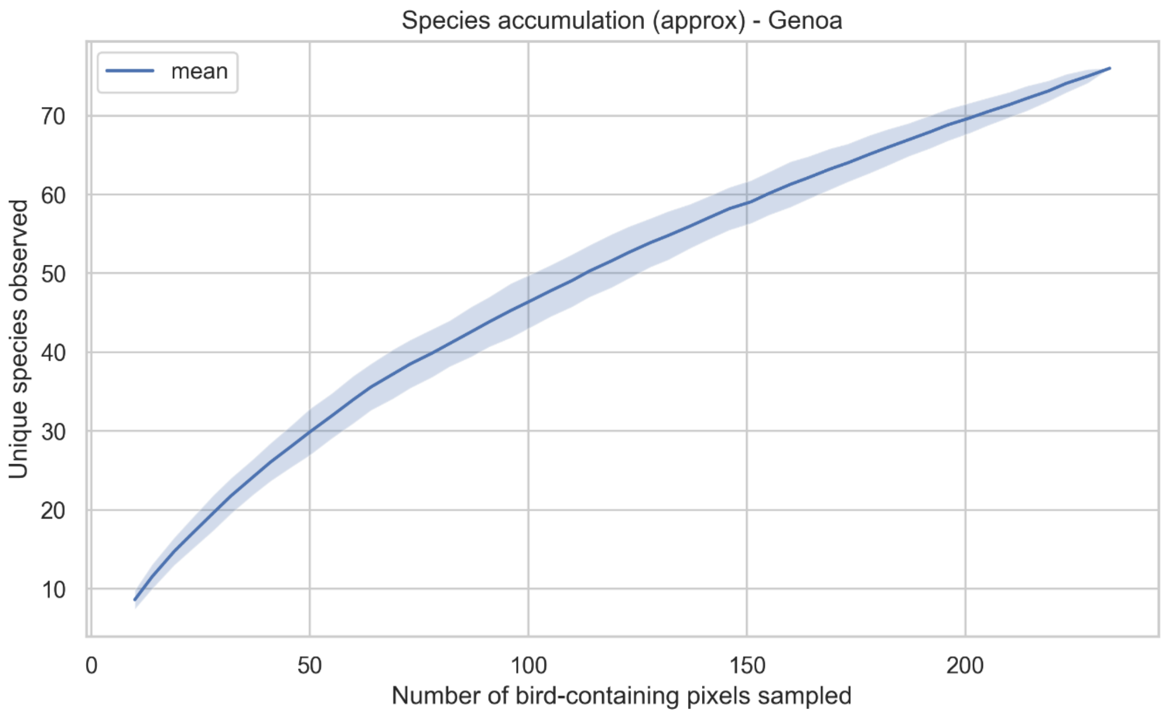

Fig. F.8: Species accumulation curve for Genoa observations.

F.4. Bootstrap uncertainty and valid class coverage

To better understand uncertainty, bootstrap standard deviations were used, produced by bootstrap resampling of Jacobs' D (we repeatedly resample the pixel-level data for a species; we recalculate D each time. The spread of those bootstrap value gives bootstrap SD). A small SD signals that D is stable, conversely it means D is noisy and unstable. The distribution of SD is shown by using a histogram (Fig. F.9). This data is informative for Vienna and Munich, but largely unavailable for Genoa because again few species meet the minimum pixel threshold for bootstrapping.

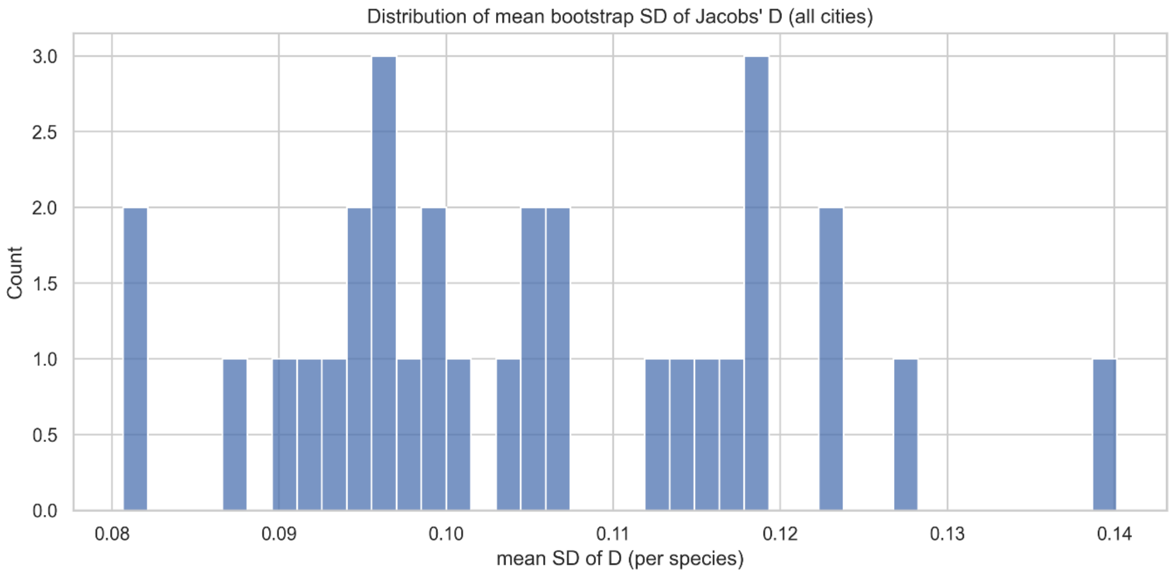

Fig. F.9: Distribution of mean bootstrap SD of Jacobs' D across species and cities. Values converge around 0.09–0.13 for well-sampled species, indicating moderate variability.

F.5. Jacobs' D heatmaps (extended birds data coverage)

The main text presents the heatmaps of detection for five selected species. Here the extended heatmaps for Vienna (Fig. F.10) and Munich (Fig. F.11) are shown, limiting to the 30 most abundant species. Particularly, blue/red hatched cells show positive/negative values found at the same time in both cities, showing consistent patterns of detection level across the cities. As the masking rule, the cells with counts <4 were set to NaN and are shown as empty; hatched cells are only drawn when the species×class cell is non-NaN in the two cities and the plotted city has at least four presences.

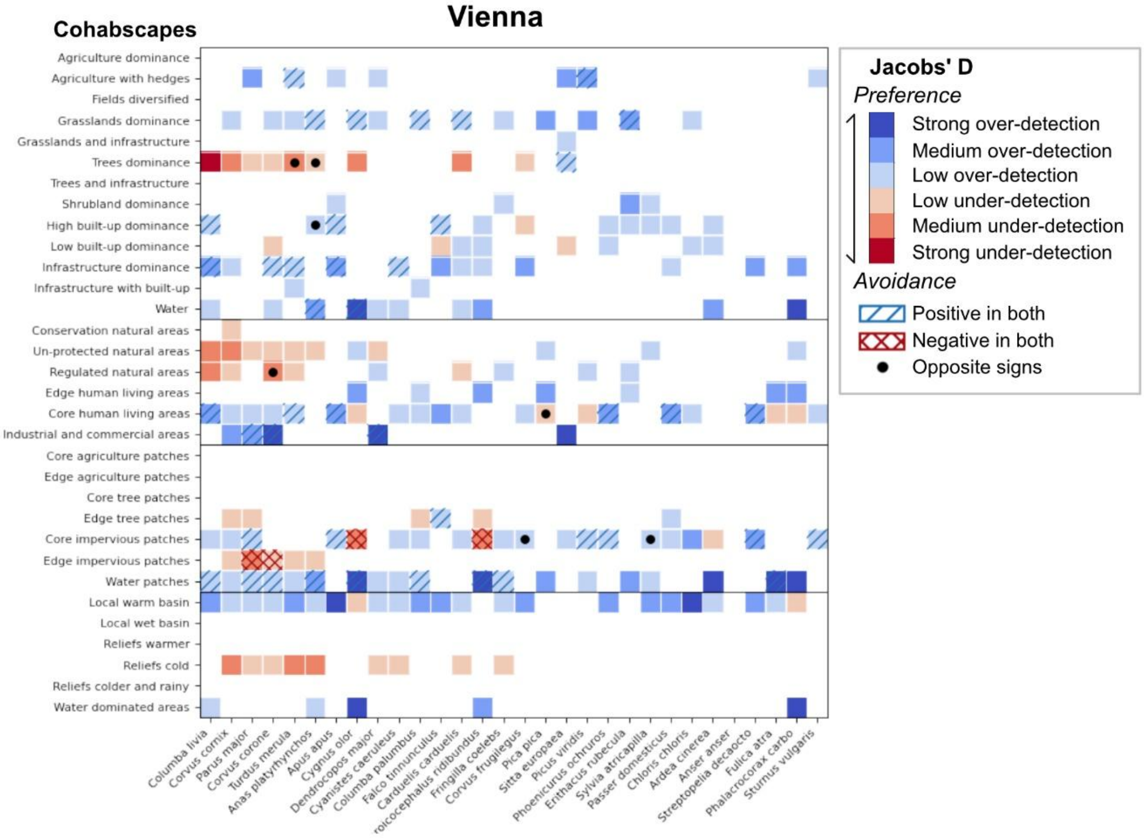

Fig. F.10: Complete species×class heatmap with Jacobs' D values in Vienna.

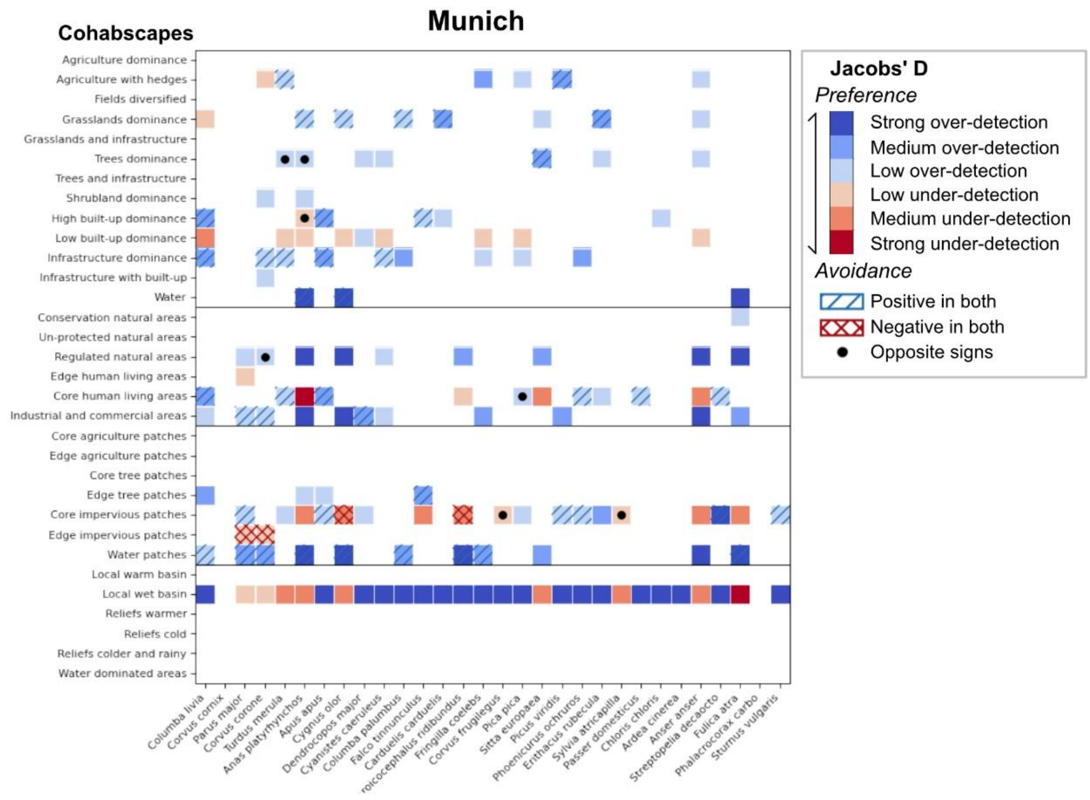

Fig. F.11: Complete species×class heatmap with Jacobs' D values in Munich.

F.6. Correlations, variance, and D values (extended birds data coverage), and relevance for ecology and planning

As for the previous point, the table for correlations, variances, and D values for the extended list of birds are shown (Table F.2). The table condenses three complementary diagnostics for each species: Pearson's ϱ, which quantifies how similarly a species' Jacobs' D profile is expressed between Vienna and Munich; variance of D across habitat classes, which indicates whether habitat use is concentrated in a few classes or spread heterogeneously; and mean Jacobs' D, which summarizes net selection versus avoidance. High Pearson's ϱ values near one identify species with highly repeatable habitat associations across the two cities and therefore robust, generalizable urban habitat use. Low Pearson's ϱ values reveal weak cross-city agreement or noisy signals, and NaN correlations flag insufficient overlapping data or near-absence in one city. Variance and mean D together refine interpretation: low variance with a positive mean D signals a consistent, moderate preference across many classes; high variance with a positive mean D signals strong selection in some classes and avoidance in others, indicating a heterogeneous, class-specific pattern; negative mean D or mixed signs indicate net avoidance or balanced selection and avoidance across classes.

From an ecological and urban-planning perspective, these diagnostics help identifying priorities. Species with high ϱ and positive mean D are reliable indicators of urban features that consistently support birds and can inform conservation or enhancement of those features across cities, for example by protecting or expanding the habitat elements they select. Species with low ϱ or NaN require scrutiny of sampling effort and local context before ecological conclusions are drawn. Where differences are real, they point to context dependence and suggest targeted, city-specific management. High-variance species should be examined at the class level to identify which habitat types drive strong selection or avoidance, because interventions that amplify favore classes or mitigate avoided ones will have disproportionate effects. Practically, use the analysis identifies species for additional follow-up research. This could be done by prioritizing high-ϱ species for cross-city policy recommendations, investigating low-ϱ and NaN cases for data gaps or local drivers, and mapping class-level D for high-variance species to design precise habitat interventions that align biodiversity goals with urban planning objectives such as green infrastructure placement, zoning for mixed vegetation, and targeted restoration.

Fig. F.12: Complete table of species abundance, variance, and D values in the combined Vienna-Munich set.

Species	**Paired cells**	**Pearson's ϱ (abs.)**	**Pearson p**	**Variance (abs.)**	**Variance (rel.)**	**Mean D**	**Mean |D|**	**Median |D|**
Corvus corone	17	0.381	0.132	0.100	0.288	0.064	0.267	0.210
Parus major	14	0.578	0.030	0.074	0.214	0.091	0.231	0.171
Anas platyrhynchos	12	0.431	0.162	0.230	0.664	0.120	0.400	0.341
Columba livia	9	0.789	0.011	0.139	0.403	0.216	0.365	0.439
Turdus merula	9	0.157	0.686	0.079	0.229	0.121	0.278	0.283
Cyanistes caeruleus	9	0.072	0.853	0.042	0.120	0.067	0.175	0.148
Cygnus olor	6	0.992	0.000	0.347	1.004	0.227	0.531	0.516
Dendrocopos major	6	0.959	0.002	0.087	0.251	0.197	0.253	0.140
Columba palumbus	6	0.117	0.825	0.067	0.194	0.206	0.259	0.246
Apus apus	5	0.721	0.169	0.056	0.160	0.476	0.477	0.516
Carduelis carduelis	5	0.545	0.343	0.044	0.127	0.191	0.234	0.254
Sitta europaea	5	0.101	0.871	0.118	0.342	0.170	0.307	0.286
Fringilla coelebs	5	0.542	0.345	0.081	0.233	0.076	0.201	0.147
Pica pica	4	0.312	0.688	0.109	0.314	0.116	0.294	0.283
Erithacus rubecula	4	0.068	0.932	0.095	0.274	0.290	0.352	0.371
Falco tinnunculus	4	0.613	0.387	0.136	0.394	0.265	0.404	0.455
Chroicocephalus ridibundus	3	0.990	0.089	0.344	0.993	0.077	0.504	0.516
Picus viridis	3	0.944	0.215	0.145	0.419	0.234	0.409	0.438
Phoenicurus ochruros	3	0.980	0.127	0.029	0.084	0.435	0.435	0.416
Streptopelia decaocto	2	1.000	1.000	0.075	0.216	0.681	0.681	0.736
Passer domesticus	2	1.000	1.000	0.083	0.239	0.271	0.340	0.273
Chloris chloris	2	1.000	1.000	0.048	0.138	0.259	0.262	0.221
Corvus frugilegus	2	1.000	1.000	0.118	0.341	0.122	0.337	0.376
Sylvia atricapilla	2	1.000	1.000	0.047	0.135	-0.022	0.188	0.195

Sturnus vulgaris	2	1.000	1.000	0.043	0.125	0.202	0.276	0.283
Fulica atra	1	NaN	NaN	0.000	0.000	0.925	0.925	0.925
Ardea cinerea	0	NaN	NaN	NaN	NaN	NaN	NaN	NaN
Anser anser	0	NaN	NaN	NaN	NaN	NaN	NaN	NaN
Corvus cornix	0	NaN	NaN	NaN	NaN	NaN	NaN	NaN
Phalacrocorax carbo	0	NaN	NaN	NaN	NaN	NaN	NaN	NaN

Annex G (Chapter 5) - SUHI analysis from remote sensing data

Surface Urban Heat Island (SUHI) was calculated separately and imported into the workflow in raster format. The temporal framework for the analysis was Summer 2022, a period marked by anomalously high temperatures and heatwaves in Northern Italy (NOAA, 2023).

SUHI characterization was based on Land Surface Temperature (LST) data acquired by the Landsat 8 and 9 satellites under near clear-sky conditions over Genoa and Turin between 01/07/2022 and 15/08/2022. Landsat was selected due to its higher spatial resolution compared to other missions capable of providing LST data (e.g., Sentinel-3, which offers daily coverage but at 1 km resolution). The Thermal Infrared Sensor (TIRS) onboard Landsat 8 and 9 acquires thermal data with a Ground Sampling Distance (GSD) of 100 m, distributed as LST products with a pixel size of 30 m. With a revisit time of 16 days per satellite, the combined use of Landsat 8 and 9 provides an effective temporal resolution of 8 days, which can be further reduced depending on orbital configuration and acquisition geometry. All images used in this study were acquired in the morning (10:00–10:30 GMT).

Data were downloaded as Collection 2 Level 2 Science Products from the USGS Earth Explorer portal, with reference system EPSG 32632. Cloud and shadow contamination was removed using the QA_PIXEL band, and the images were subsetted over an Area of Interest (AOI) defined as the administrative boundaries of each city plus a buffer. Administrative boundaries were obtained from official repositories (Genoa: Regione Liguria Open Data; Turin: Comune di Torino Geoportal). The buffer was defined using the Global Human Settlement – Functional Urban Areas (GHS-FUA) layer (Schiavina et al., 2023), which delineates commuting areas and thus extends beyond nominal city limits.

Landsat LST data were converted to °C, stacked, and the 50th percentile was calculated for each pixel. This percentile map was used to characterize SUHI as the difference between urban LST and mean rural LST, following the "Buffer area around the city" approach (Sarath Raj & Geun Young Yun, 2023). This method requires distinguishing between urban and rural pixels within the AOI:

i. Urban = CLC 2018 Level 1 "Artificial Surfaces"

ii. Rural = CLC 2018 Level 1 "Agricultural Areas" and "Forest and Semi-natural Areas"

iii. Wetlands and Water Bodies were excluded.

The CLC 2018 dataset was downloaded as a raster with 100 m resolution. After aggregation of thematic classes, the data were resampled to 30 m and reprojected from EPSG 3035 to EPSG 32632 using the

Nearest Neighbour algorithm, then aligned to the Landsat grid.

SUHI was then calculated independently for each city by subtracting, from each urban pixel within the administrative boundaries, the mean LST of rural pixels located within the AOI. The same mean value was also subtracted for rural pixels inside the administrative boundaries. All pixels outside the administrative boundaries were masked out in the final SUHI maps.

Annex H (Chapter 5) - Correlation analysis for MCDM-derived risk

This Annex contains the full correlation matrixes obtained from computing Pearson's ϱ between Risk, Hazard, Exposure, and Vulnerability, and all variables, after processing with the selected combination of ET, TOPSIS, and entropy weights. The results are presented for Genoa (Table H.1) and Turin (Table H.2).

Table H.1. Correlation analysis results in Genoa.

	Risk	**Hazard**	**Exposure**	**Vulnerability**
Risk	1.00	0.57	0.96	0.73
Hazard	0.57	1.00	0.38	0.24
Exposure	0.96	0.38	1.00	0.67
Vulnerability	0.73	0.24	0.67	1.00
Climate_SUHI_50perc_mean	0.80	0.42	0.79	0.56
Climate_WindSpeed10m_mean	-0.45	-0.81	-0.30	-0.18
Climate_WindSpeed50m_mean	-0.28	-0.87	-0.09	-0.04
Climate_WindSpeed100m_mean	-0.25	-0.84	-0.06	-0.01
Climate_WindSpeed150m_mean	-0.25	-0.79	-0.07	-0.00
Climate_WindSpeed200m_mean	-0.24	-0.74	-0.07	0.01
DemographyIndirect_Population0to5_mean	0.57	0.11	0.58	0.69
DemographyIndirect_Population65+_mean	0.57	0.11	0.58	0.69
DemographyIndirect_PopulationDensity_mean	0.69	0.22	0.72	0.56
DemographyDirect_PopulationResident_majority	0.06	0.02	-0.00	0.05
DemographyDirect_Citizen0to5yo_majority	0.08	0.04	0.01	0.12
DemographyDirect_Citizen65+_majority	0.03	0.01	-0.02	0.00
DemographyDirect_CitizenNoEducationQualification_majority	0.13	0.05	0.04	0.24
DemographyDirect_CitizenWithLowEducation_majority	0.17	0.08	0.08	0.26
DemographyDirect_CitizenWithDegree_majority	-0.17	-0.08	-0.17	-0.31
DemographyDirect_CitizenEmployed_majority	0.05	0.02	-0.01	0.01
DemographyDirect_CitizenExtraEU_majority	0.11	0.03	0.03	0.28

DemographyDirect_CitizenAlone_majority	0.04	0.02	-0.03	0.07
Morphology_Elevation_mean	-0.74	-0.48	-0.71	-0.44
Morphology_Slope_mean	-0.71	-0.36	-0.73	-0.35
Morphology_Roughness_mean	-0.71	-0.35	-0.73	-0.35
Morphology_Rugosity_mean	-0.65	-0.32	-0.66	-0.32
Morphology_BuildingHeight_mean	0.61	0.13	0.70	0.56
Morphology_BuiltUpRatio_Average	0.68	0.20	0.74	0.57
LandCover_ImperviousDensity_mean	0.84	0.32	0.87	0.62
LandCover_TreeCoverDensity_mean	-0.74	-0.33	-0.75	-0.50
LandCover_ShrubsRatio_mean	-0.70	-0.31	-0.70	-0.46
LandCover_GrasslandRatio_mean	-0.37	-0.08	-0.38	-0.32
LandUse_DistanceFromTransports	-0.51	-0.29	-0.47	-0.43
LandUse_DistanceFromServices	-0.62	-0.28	-0.62	-0.43
LandUse_DistanceFromEmergency	-0.56	-0.23	-0.58	-0.35
LandUse_DistanceFromGreenAmenities	-0.58	-0.25	-0.57	-0.43
LandUse_DistanceFromNonGreenAmenities	-0.60	-0.26	-0.59	-0.49

Table H.2. Correlation analysis results in Turin.

	Risk	**Hazard**	**Exposure**	**Vulnerability**
Risk	1.00	0.65	0.96	0.64
Hazard	0.65	1.00	0.56	0.16
Exposure	0.96	0.56	1.00	0.48
Vulnerability	0.64	0.16	0.48	1.00
Climate_SUHI_50perc_mean	0.83	0.56	0.83	0.37
Climate_WindSpeed10m_mean	-0.31	-0.67	-0.23	-0.06
Climate_WindSpeed50m_mean	-0.14	-0.62	-0.06	0.08
Climate_WindSpeed100m_mean	-0.11	-0.59	-0.03	0.11
Climate_WindSpeed150m_mean	-0.12	-0.58	-0.03	0.09
Climate_WindSpeed200m_mean	-0.10	-0.54	-0.01	0.08
DemographyIndirect_Population0to5_mean	0.53	0.17	0.52	0.54
DemographyIndirect_Population65+_mean	0.53	0.17	0.52	0.54
DemographyIndirect_PopulationDensity_mean	0.66	0.34	0.69	0.45
DemographyDirect_PopulationResident_majority	0.25	0.06	0.10	0.42

DemographyDirect_Citizen0to5yo_majority	0.21	0.03	0.06	0.42
DemographyDirect_Citizen65+_majority	0.18	0.03	0.08	0.28
DemographyDirect_CitizenNoEducationQualification_majority	0.27	0.04	0.11	0.51
DemographyDirect_CitizenWithLowEducation_majority	0.28	0.06	0.12	0.50
DemographyDirect_CitizenWithDegree_majority	0.05	0.05	-0.01	0.00
DemographyDirect_CitizenEmployed_majority	0.24	0.07	0.10	0.36
DemographyDirect_CitizenExtraEU_majority	0.21	0.05	0.07	0.48
DemographyDirect_CitizenAlone_majority	0.20	0.06	0.06	0.39
Morphology_Elevation_mean	-0.62	-0.66	-0.64	-0.08
Morphology_Slope_mean	-0.83	-0.52	-0.84	-0.34
Morphology_Roughness_mean	-0.82	-0.52	-0.84	-0.34
Morphology_Rugosity_mean	-0.76	-0.46	-0.77	-0.31
Morphology_BuildingHeight_mean	0.50	0.17	0.57	0.39
Morphology_BuiltUpRatio_Average	0.61	0.26	0.66	0.44
LandCover_ImperviousDensity_mean	0.79	0.46	0.82	0.44
LandCover_TreeCoverDensity_mean	-0.78	-0.50	-0.80	-0.35
LandCover_ShrubsRatio_mean	-0.78	-0.51	-0.80	-0.29
LandCover_GrasslandRatio_mean	-0.34	-0.19	-0.36	-0.20
LandUse_DistanceFromTransports	-0.44	-0.21	-0.43	-0.39
LandUse_DistanceFromServices	-0.41	-0.18	-0.50	-0.13
LandUse_DistanceFromEmergency	-0.53	-0.37	-0.60	-0.15
LandUse_DistanceFromGreenAmenities	-0.46	-0.24	-0.54	-0.15
LandUse_DistanceFromNonGreenAmenities	-0.46	-0.24	-0.54	-0.15

Annex I (Chapter 5) - Cluster analysis (k value)

This Annex presents the analysis used to determine the optimal number of clusters (k) in the Hierarchical Agglomerative Clustering (HAC). The HAC procedure was applied to the PCA-reduced dataset across a range of k = 2 to 30. Two complementary approaches were used: the Silhouette Score (SS) and a clustergram, which plots the distance of each cluster to the mean of the corresponding principal components.

The SS plot (Fig. I.1) shows that the score values degrade rapidly as *k*increases, with only two notable peaks: the first value (k = 2) and k = 8. Although k = 2 yields the highest SS, this solution was disregarded because it produces only two clusters, which would be overly coarse and uninformative for the purposes of site characterisation. Instead, k = 2 was retained solely as a reference point.

Based on the balance between statistical performance and interpretive usefulness, k = 8 selected as the most appropriate number of clusters. This choice provides sufficient differentiation to capture meaningful urban typologies while avoiding excessive fragmentation.

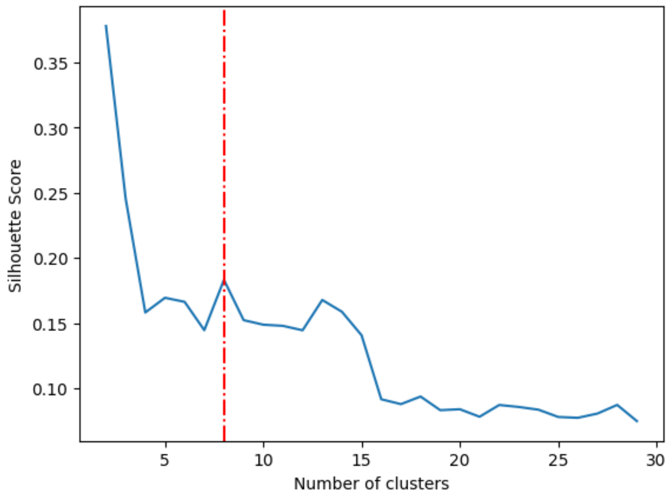

Fig. I.1. SS plot for HAC in the range k=2-30. The red dotted line highlights k=8.

Secondly, the selection of k = 8 can be further supported by examining the clustergram (Fig. I.2). The chosen solution is distant from any major splits, such as the one observed at k = 3, and can therefore be considered a stable representation of the clustering structure. At higher values of k, the divisions originating from k = 8 are progressively reduced without introducing substantial differences. Only when k exceeds 13 do new splits appear with sufficient distinction. However, these additional splits are always contained within larger clusters that belong to single cities and thus do not provide further insight for cross-city comparison. Although increasing k also produces subdivisions within the sole cluster shared by both cities (Cluster 8, as described in the main text), this remains a relatively small cluster and does not alter the overall interpretation.

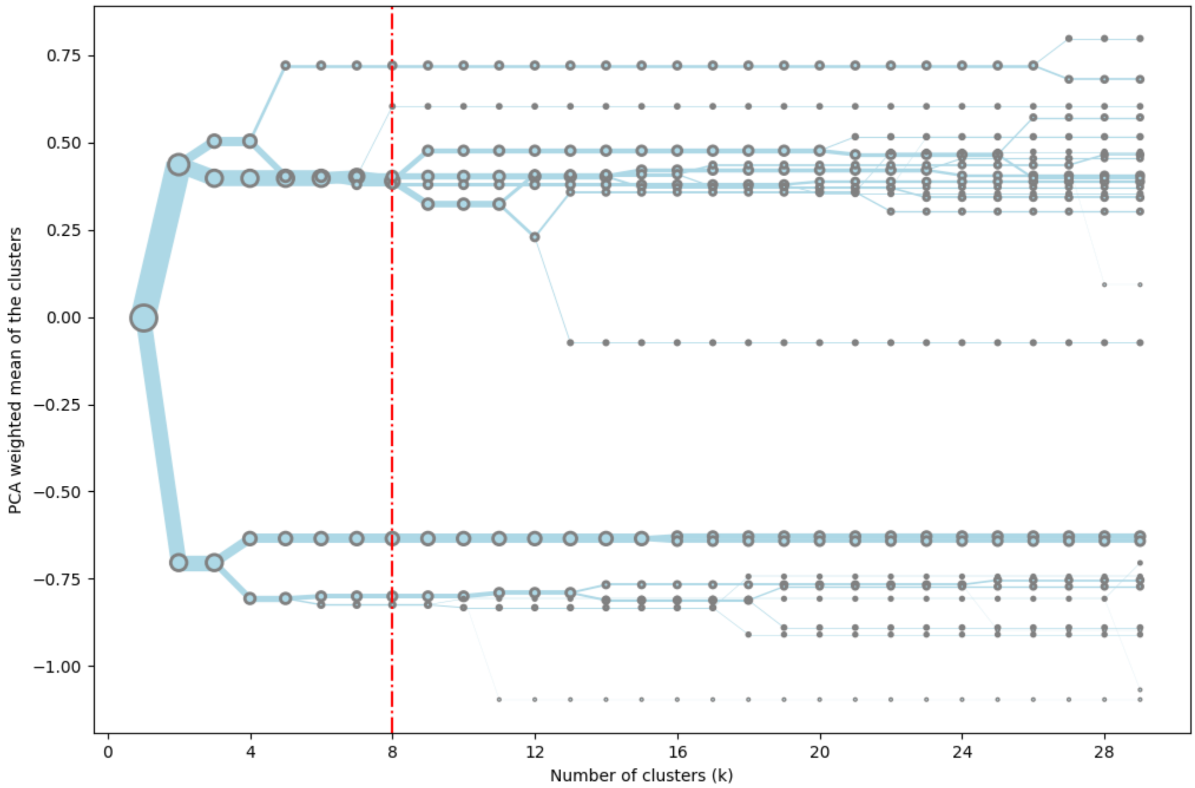

Fig. I.2. Clustergram obtained from HAC values in the range 2-30, highlighting the k=8.

Annex J (Chapter 5) - Cluster analysis (cluster content)

This Annex presents the analysis of the content of each cluster. For every cluster label and variable, the mean (Table J.1), standard deviation (Table J.2), and correlation using Pearson's ϱ (Table J.3) were computed. These statistics allow both the central tendencies and the variability within clusters to be assessed, as well as the strength of associations between variables.

The findings can be synthesised into a qualitative attribution of cluster content. Only one cluster (C3) is present in both cities, while Genoa has five exclusive clusters (C1, C2, C5, C7, C8) and Turin has two exclusive clusters (C4, C6). The argumentation is organised according to the variable structure: Climate, Demography, Morphology, Land Cover, and Land Use.

J.1. Climate variables

J.1.1. Surface Urban Heat Island (SUHI)

i. Means: C6 (10.78 °C) and C4 (10.57 °C) show the highest daytime surface warming, while C1 (7.67 °C) and C3 (7.92 °C) show the lowest.

ii. Variability: C3 displays the greatest heterogeneity (std = 3.43 °C), suggesting mixed land-cover patches, while C4 is the most uniform (std = 1.13 °C).

iii. Correlations: In C4, higher SUHI strongly increases the outcome (ϱ = +0.39), reflecting sensitivity in its consistent urban core. In contrast, C1 shows a pronounced inverse relationship (ϱ = –0.45), where cooler microclimates align with higher responses.

J.1.2. Wind speed

i. Means: Near-surface winds are calmest in C3 (0.70 m/s) and strongest in C5 (2.54 m/s). At 200 m elevation, all clusters converge around 6 m/s.

ii. Variability: Low-level wind speed is most variable in suburban C1 (std = 0.57 m/s) and C2 (0.46 m/s), while C4 remains uniform (std = 0.06 m/s). At 200 m, C3 shows the widest spread (std = 0.91 m/s), while C4 again remains consistent (std = 0.09 m/s).

Correlations: In C4, both near-surface and high-altitude winds strongly dampen the response (ϱ ≈ –0.56 to –0.63). In contrast, C1 (ϱ ≈ +0.38 to +0.42) and C5 (ϱ ≈ +0.28 to +0.29) show positive associations, indicating that breezier fringes elevate outcomes.

J.2. Demography variables

J.2.1. Indirect demographics

i. Means: Children (0–5 yrs) are most numerous in C5 (7.11 %) and C4 (6.05 %). Elderly citizens (65+) are highest in C5 (15.67 %) and lowest in C3 (4.89 %). Population density peaks in C4 (47.66 pop/ha) and C2 (44.36 pop/ha).

ii. Variability: Children are most dispersed in C2 (std = 2.79 %) and C8 (2.72 %), but uniform in C3 (0.80 %). Elderly citizens are most dispersed in C2 (std = 6.14 %) and most uniform in C3 (1.65 %).

iii. Correlations: C4 shows consistent positive correlations with children (ϱ = +0.35), elderly (ϱ = +0.19), and population density (ϱ = +0.39). C1 is moderately inversely correlated with population density (ϱ = –0.37).

J.2.2. Direct demographics

i. Means: The highest number of residents occurs in C6 (593), the lowest in C5 (135). C6 also records the highest employed population (980) and the largest counts of Extra-EU citizens (113) and single-person households (222).

ii. Variability: Resident counts vary most in C3 (std = 219) and least in C5 (std = 110). Citizens with degrees are most dispersed in C3 (62), while employment spread is highest in C6 (98). Extra-EU and single-household counts in C6 also show very high variance, indicating strong immigrant and single-person presence.

iii. Correlations: C6 shows strong positive correlations across all demographic variables (population ϱ = +0.62; no-qualification ϱ = +0.65; low-education ϱ = +0.62; degree ϱ = +0.42; employed ϱ = +0.60; extra-EU ϱ = +0.39; alone ϱ = +0.40). Clusters C1, C2, C5, C7, and C8 show mild negative correlations (ϱ ≈ –0.10 to –0.17), suggesting saturation effects in smaller or mid-sized contexts. C4 shows weak or negligible ties, while C3 highlights higher education as the only notable correlation (ϱ = +0.19).

J.3. Morphology variables

J.3.1. Topographic features

i. Means: Highest elevations are in C6 (248 m) and C4 (245 m); lowest in C2 (15 m) and C7 (14 m).

ii. Variability: Elevation spread peaks in C8 (std = 1.48 m) and is minimal in C4 (std = 0.14 m). Slope and roughness are steepest in C5 (mean = 4.69°, std = 1.69) and C8 (mean = 5.32°, std = 1.99), while C4 is essentially flat (0.56°).

iii. Correlations: Elevation in C4 correlates strongly positively (ϱ = +0.69), while in C1 it is inverse (ϱ = –0.43). Slope and roughness in C5 are strong positive drivers (ϱ ≈ +0.58), contrasting with negative ties in C4 (ϱ ≈ –0.36).

J.3.2. Built form

i. Means: Building height is highest in C2 (10.74 m) and C5 (9.43 m), and lowest in C3 (1.47 m). The built-up ratio is highest in C2 (0.814) and lowest in C4 (0.094); C3 is the most fragmented (0.181).

ii. Variability: Height variability is greatest in C8 (std = 3.20 m), indicating a mixed skyline, and lowest in C3 (1.70 m). Built-up ratio is most heterogeneous in C3 (0.24) and C7 (0.19), while C2 is the most consistent (0.13).

Correlations: Height in C2 is positively linked (ϱ = +0.48), while in C3 it is negative (ϱ = –0.31). Built-up ratios in C2 (UA ϱ = +0.35; OSM ϱ = +0.39) confirm its association with dense urban fabric. C7 shows negative ties (ϱ ≈ –0.44), reflecting mixed condition.

J.4. Land Cover

i. Means: Impervious density is highest in C2 (95.8 %) and C7 (93.3 %). Tree cover density is highest in C1 (3.25 %) and C8 (2.52 %). Shrubs and grasslands are negligible (<0.03 %).

ii. Variability: Impervious density variability is greatest in C3 (8.04 %) and lowest in C2 (5.96 %). Tree cover density variability is highest in C1 (6.50 %) and lowest in C2 (1.85 %). Shrubs and grasslands show the widest spread in C3 (0.03–0.04).

iii. Correlations: C2 correlates positively with impervious areas (ϱ = +0.37), while C1 shows the opposite (ϱ = –0.37). In C1, tree cover density is moderately correlated (ϱ = +0.31), while other vegetation ties are negligible.

J.5. Land Use

i. Means: Cluster 3 (C3) is the most remote from key amenities, with average distances of 1,176 m to services, 816 m to emergency facilities, and 546 m to green amenities. By contrast, Clusters 5 (C5) and 8 (C8) are the closest, with mean distances of approximately 60–100 m.

ii. Variability: C3 again shows the widest spreads in distances, indicating heterogeneous accessibility conditions, while Cluster 4 (C4) is the most uniform, with standard deviations ranging between 42 and 62 m.

iii. Correlations: In C3, distances to services (ϱ = +0.74), green amenities (ϱ = +0.65), and emergency facilities (ϱ = +0.52) act as strong positive drivers, highlighting the influence of remoteness on cluster outcomes. In other clusters, correlations are weakly negative or near zero (ϱ ≈ –0.02 to –0.13), suggesting that accessibility plays a less decisive role in shaping their profiles.

J.6. Cluster means, standard deviations (variability), and correlations

Table I.1. Mean values of cluster data, divided by cluster labels.

Variable (mean values)	C1	C2	C3	C4	C5	C6	C7	C8
Climate_SUHI_50perc_mean_lag	7.669	8.958	7.918	10.567	7.973	10.780	9.824	8.233
Climate_SUHI_50perc_std_lag	0.458	0.318	1.264	0.377	0.332	0.492	0.735	0.470
Climate_WindSpeed10m_mean_lag	2.220	2.245	0.700	0.959	2.542	0.955	2.156	2.416
Climate_WindSpeed10m_std_lag	0.085	0.049	0.009	0.008	0.113	0.007	0.082	0.431
Climate_WindSpeed50m_mean_lag	3.964	4.216	1.247	1.728	4.532	1.734	4.082	4.081
Climate_WindSpeed50m_std_lag	0.046	0.026	0.004	0.005	0.063	0.004	0.044	0.285
Climate_WindSpeed100m_mean_lag	4.984	5.249	1.548	2.174	5.554	2.174	5.107	5.092
Climate_WindSpeed100m_std_lag	0.032	0.019	0.002	0.004	0.043	0.003	0.033	0.207
Climate_WindSpeed150m_mean_lag	5.459	5.703	1.726	2.423	6.013	2.402	5.572	5.601
Climate_WindSpeed150m_std_lag	0.024	0.014	0.002	0.003	0.033	0.002	0.025	0.153
Climate_WindSpeed200m_mean_lag	5.756	5.999	1.896	2.618	6.313	2.575	5.876	5.932
Climate_WindSpeed200m_std_lag	0.019	0.011	0.002	0.003	0.026	0.002	0.021	0.117
DemographyIndirect_Population0to5_mean_lag	3.295	4.935	0.649	6.052	7.112	3.723	1.505	3.485
DemographyIndirect_Population0to5_std_lag	1.114	1.608	0.260	1.937	1.957	1.244	0.833	1.372
DemographyIndirect_Population65+_mean_lag	7.260	10.872	1.265	10.507	15.668	6.462	3.316	7.677
DemographyIndirect_Population65+_std_lag	2.455	3.542	0.531	3.362	4.311	2.159	1.835	3.022
DemographyIndirect_PopulationDensity_mean_lag	34.495	44.359	38.203	47.657	39.254	42.086	35.694	33.907
DemographyIndirect_PopulationDensity_std_lag	20.098	18.392	20.799	17.674	19.176	18.837	21.287	20.737

DemographyDirect_PopulationResident_majority_lag	210.049	188.459	313.650	220.183	135.426	593.480	138.531	183.779
DemographyDirect_PopulationResident_majority_lag	210.049	188.459	313.650	220.183	135.426	593.480	138.531	183.779
DemographyDirect_PopulationResident_majority_lag	210.049	188.459	313.650	220.183	135.426	593.480	138.531	183.779
DemographyDirect_PopulationResident_majority_lag	210.049	188.459	313.650	220.183	135.426	593.480	138.531	183.779
DemographyDirect_Citizen0to5yo_majority_lag	6.922	6.041	9.944	7.827	3.840	21.177	4.806	5.938
DemographyDirect_Citizen65+_majority_lag	33.592	29.800	44.428	31.558	21.464	82.989	21.733	28.548
DemographyDirect_CitizenNoEducationQualification_majority_lag	6.681	5.795	10.885	8.147	3.638	23.969	4.233	5.586
DemographyDirect_CitizenWithLowEducation_majority_lag	34.070	29.474	44.416	34.307	20.377	96.920	21.902	29.364
DemographyDirect_CitizenWithDegree_majority_lag	31.039	29.989	73.849	40.045	23.652	81.351	21.036	26.017
DemographyDirect_CitizenEmployed_majority_lag	81.319	74.368	132.101	90.296	52.799	227.155	54.649	74.310
DemographyDirect_CitizenExtraEU_majority_lag	22.295	18.807	28.228	20.955	9.302	80.039	13.991	20.223
DemographyDirect_CitizenAlone_majority_lag	52.411	43.210	86.481	52.970	31.772	163.954	32.511	46.151
Morphology_Elevation_mean_lag	36.334	15.242	171.939	244.592	42.714	248.221	14.307	41.514
Morphology_Elevation_std_lag	1.860	0.811	0.661	0.202	3.695	0.223	0.805	2.485
Morphology_Slope_mean_lag	7.100	3.209	2.283	0.559	14.653	0.660	2.363	8.487
Morphology_Slope_std_lag	1.888	0.738	0.655	0.076	4.504	0.092	0.671	2.783
Morphology_Roughness_mean_lag	3.273	1.464	1.062	0.248	7.007	0.293	1.069	4.006
Morphology_Roughness_std_lag	0.856	0.334	0.296	0.034	2.101	0.041	0.296	1.319
Morphology_BuildingHeight_mean_lag	5.578	10.741	2.341	7.056	9.428	4.733	3.460	5.305
Morphology_BuildingHeight_std_lag	7.644	9.769	3.095	8.231	10.912	6.409	5.217	7.514

Morphology_BuiltUpRatio_UA_lag	0.560	0.814	0.507	0.752	0.723	0.658	0.351	0.509
Morphology_BuiltUpRatio_OSM_lag	0.300	0.450	0.286	0.382	0.384	0.312	0.223	0.291
Morphology_BuiltUpRatio_Average_lag	0.430	0.632	0.396	0.567	0.553	0.485	0.287	0.400
LandCover_ImperviousDensity_mean_lag	78.216	95.843	78.555	87.132	87.168	80.295	93.349	83.594
LandCover_ImperviousDensity_std_lag	18.589	5.817	14.572	12.843	14.010	16.092	10.336	16.356
LandCover_TreeCoverDensity_mean_lag	3.249	0.229	1.716	1.242	1.549	2.260	0.328	2.523
LandCover_TreeCoverDensity_std_lag	6.243	0.645	2.689	3.062	3.435	4.632	1.014	5.339
LandCover_ShrubsRatio_mean_lag	0.001	0.000	0.003	0.000	0.000	0.000	0.000	0.001
LandCover_ShrubsRatio_std_lag	0.002	0.000	0.004	0.000	0.000	0.000	0.000	0.003
LandCover_GrasslandRatio_mean_lag	0.002	0.000	0.006	0.000	0.000	0.001	0.001	0.002
LandCover_GrasslandRatio_std_lag	0.007	0.000	0.014	0.000	0.000	0.003	0.004	0.008
LandCover_SurfaceWetnessCapacityRatio_mean_lag	0.000	0.000	0.000	0.000	0.000	0.000	0.000	0.000
LandCover_SurfaceWetnessCapacityRatio_std_lag	0.000	0.000	0.000	0.000	0.000	0.000	0.000	0.000
LandCover_SurfaceWaterCapacity_mean_lag	0.000	0.000	0.000	0.000	0.000	0.000	0.000	0.000
LandCover_SurfaceWaterCapacity_std_lag	0.000	0.000	0.000	0.000	0.000	0.000	0.000	0.000
LandUse_DistanceFromTransports_lag	71.898	95.683	163.199	97.560	60.950	105.184	98.852	61.750
LandUse_DistanceFromServices_lag	118.649	96.206	1176.005	142.814	91.067	196.002	177.381	142.121
LandUse_DistanceFromEmergency_lag	162.816	115.279	786.095	139.210	121.754	221.311	205.620	193.844
LandUse_DistanceFromGreenAmenities_lag	151.981	156.456	832.360	188.734	136.419	178.303	232.131	163.199
LandUse_DistanceFromNonGreenAmenities_lag	153.718	149.234	847.402	188.734	142.767	178.303	215.564	171.41

Table I.2. Standard deviation values of cluster data, divided by cluster labels.

Variable (standard deviation values)	**C1**	**C2**	**C3**	**C4**	**C5**	**C6**	**C7**	**C8**
Climate_SUHI_50perc_mean_lag	1.649	1.340	3.429	1.134	1.281	1.585	1.659	1.304
Climate_SUHI_50perc_std_lag	0.398	0.233	1.234	0.258	0.163	0.477	0.634	0.270
Climate_WindSpeed10m_mean_lag	0.573	0.459	0.341	0.060	0.526	0.116	0.312	0.467
Climate_WindSpeed10m_std_lag	0.104	0.072	0.017	0.011	0.120	0.008	0.082	0.196
Climate_WindSpeed50m_mean_lag	0.791	0.407	0.595	0.085	0.364	0.201	0.390	0.510
Climate_WindSpeed50m_std_lag	0.055	0.037	0.009	0.006	0.065	0.005	0.042	0.091
Climate_WindSpeed100m_mean_lag	0.769	0.455	0.736	0.098	0.319	0.248	0.386	0.461
Climate_WindSpeed100m_std_lag	0.038	0.027	0.006	0.005	0.045	0.004	0.030	0.063
Climate_WindSpeed150m_mean_lag	0.716	0.417	0.818	0.100	0.273	0.272	0.355	0.407
Climate_WindSpeed150m_std_lag	0.029	0.019	0.005	0.005	0.033	0.003	0.023	0.047
Climate_WindSpeed200m_mean_lag	0.688	0.392	0.906	0.091	0.255	0.289	0.356	0.377
Climate_WindSpeed200m_std_lag	0.023	0.015	0.004	0.004	0.026	0.003	0.020	0.037
DemographyIndirect_Population0to5_mean_lag	2.087	2.785	0.796	2.037	2.617	2.156	1.678	2.724
DemographyIndirect_Population0to5_std_lag	0.922	1.199	0.483	1.304	1.400	1.008	0.876	1.304
DemographyIndirect_Population65+_mean_lag	4.598	6.135	1.652	3.535	5.765	3.742	3.696	6.002
DemographyIndirect_Population65+_std_lag	2.031	2.642	1.023	2.264	3.083	1.750	1.929	2.872
DemographyIndirect_PopulationDensity_mean_lag	7.779	9.504	14.046	6.365	6.721	7.976	12.062	9.280
DemographyIndirect_PopulationDensity_std_lag	3.922	3.687	6.649	3.082	2.872	3.655	5.580	4.429

DemographyDirect_PopulationResident_majority_lag	145.909	134.165	219.233	110.043	101.173	269.129	115.381	127.795
DemographyDirect_PopulationResident_majority_lag	145.909	134.165	219.233	110.043	101.173	269.129	115.381	127.795
DemographyDirect_PopulationResident_majority_lag	145.909	134.165	219.233	110.043	101.173	269.129	115.381	127.795
DemographyDirect_PopulationResident_majority_lag	145.909	134.165	219.233	110.043	101.173	269.129	115.381	127.795
DemographyDirect_Citizen0to5yo_majority_lag	6.524	5.153	8.342	4.683	3.284	8.707	5.461	4.913
DemographyDirect_Citizen65+_majority_lag	27.537	24.439	33.607	21.053	17.785	50.258	19.447	21.697
DemographyDirect_CitizenNoEducationQualification_majority_lag	5.770	4.781	8.109	4.790	3.313	12.188	3.881	4.441
DemographyDirect_CitizenWithLowEducation_majority_lag	26.029	23.763	32.957	20.049	16.358	42.176	19.603	21.282
DemographyDirect_CitizenWithDegree_majority_lag	26.633	27.995	62.595	25.187	23.268	51.615	19.762	22.802
DemographyDirect_CitizenEmployed_majority_lag	55.085	52.748	96.170	45.869	39.972	97.997	46.572	52.710
DemographyDirect_CitizenExtraEU_majority_lag	32.070	25.574	31.546	20.642	13.143	113.337	22.678	24.380
DemographyDirect_CitizenAlone_majority_lag	52.456	33.121	64.596	27.264	24.285	222.064	29.289	35.696
Morphology_Elevation_mean_lag	28.064	14.867	90.860	12.630	28.138	15.241	15.897	25.456
Morphology_Elevation_std_lag	1.156	0.639	1.240	0.143	1.231	0.194	0.532	1.484
Morphology_Slope_mean_lag	4.651	2.570	4.411	0.346	4.693	0.601	1.787	5.317
Morphology_Slope_std_lag	1.475	0.779	1.644	0.117	1.693	0.160	0.692	1.995
Morphology_Roughness_mean_lag	2.236	1.182	2.128	0.155	2.413	0.279	0.823	2.555
Morphology_Roughness_std_lag	0.686	0.351	0.762	0.052	0.842	0.069	0.304	1.025
Morphology_BuildingHeight_mean_lag	2.745	4.549	1.467	2.307	2.589	1.929	2.360	2.937
Morphology_BuildingHeight_std_lag	2.939	2.504	1.698	2.048	2.104	2.393	2.818	3.200

Morphology_BuiltUpRatio_UA_lag	0.164	0.130	0.236	0.136	0.130	0.190	0.186	0.188
Morphology_BuiltUpRatio_OSM_lag	0.085	0.110	0.152	0.107	0.065	0.091	0.112	0.102
Morphology_BuiltUpRatio_Average_lag	0.115	0.107	0.181	0.094	0.087	0.121	0.143	0.138
LandCover_ImperviousDensity_mean_lag	12.311	5.599	21.902	7.024	8.525	11.095	6.141	11.103
LandCover_ImperviousDensity_std_lag	6.467	5.955	8.041	5.486	6.323	6.114	6.314	7.489
LandCover_TreeCoverDensity_mean_lag	4.502	0.830	4.895	2.135	2.689	3.868	0.888	3.746
LandCover_TreeCoverDensity_std_lag	6.497	1.850	5.752	4.078	4.791	5.867	2.114	6.095
LandCover_ShrubsRatio_mean_lag	0.010	0.001	0.033	0.000	0.002	0.000	0.001	0.007
LandCover_ShrubsRatio_std_lag	0.013	0.002	0.026	0.000	0.006	0.000	0.004	0.014
LandCover_GrasslandRatio_mean_lag	0.011	0.001	0.020	0.002	0.001	0.006	0.009	0.007
LandCover_GrasslandRatio_std_lag	0.025	0.003	0.040	0.003	0.003	0.017	0.019	0.025
LandCover_SurfaceWetnessCapacityRatio_mean_lag	0.000	0.000	0.000	0.000	0.000	0.000	0.000	0.000
LandCover_SurfaceWetnessCapacityRatio_std_lag	0.000	0.000	0.000	0.000	0.000	0.000	0.000	0.000
LandCover_SurfaceWaterCapacity_mean_lag	0.000	0.000	0.000	0.002	0.000	0.000	0.000	0.000
LandCover_SurfaceWaterCapacity_std_lag	0.000	0.000	0.000	0.004	0.000	0.000	0.000	0.000
LandUse_DistanceFromTransports_lag	41.129	81.750	155.445	42.333	26.687	53.751	68.723	29.150
LandUse_DistanceFromServices_lag	111.153	114.596	774.681	71.179	46.900	114.664	136.694	122.488
LandUse_DistanceFromEmergency_lag	146.527	114.309	816.283	61.646	65.030	151.658	136.750	129.705
LandUse_DistanceFromGreenAmenities_lag	92.381	115.921	545.554	100.583	56.657	97.365	141.679	86.804
LandUse_DistanceFromNonGreenAmenities_lag	99.504	91.726	544.219	100.583	61.496	97.365	129.859	109.743

Table I.3. Pearson correlation values of cluster data, divided by cluster labels.

Variable (Pearson's ϱ)	C1	C2	C3	C4	C5	C6	C7	C8
Climate_SUHI_50perc_mean_lag	-0.45	-0.03	-0.12	0.39	-0.16	0.29	0.11	-0.06
Climate_SUHI_50perc_std_lag	-0.02	-0.13	0.34	-0.10	-0.08	0.02	0.17	0.00
Climate_WindSpeed10m_mean_lag	0.38	0.27	-0.28	-0.56	0.29	-0.37	0.16	0.12
Climate_WindSpeed10m_std_lag	0.17	-0.04	-0.10	-0.27	0.15	-0.18	0.07	0.51
Climate_WindSpeed50m_mean_lag	0.38	0.34	-0.30	-0.61	0.29	-0.40	0.22	0.10
Climate_WindSpeed50m_std_lag	0.14	-0.05	-0.10	-0.26	0.15	-0.18	0.06	0.61
Climate_WindSpeed100m_mean_lag	0.40	0.35	-0.32	-0.63	0.28	-0.41	0.22	0.10
Climate_WindSpeed100m_std_lag	0.14	-0.05	-0.10	-0.26	0.14	-0.18	0.07	0.62
Climate_WindSpeed150m_mean_lag	0.41	0.35	-0.32	-0.63	0.28	-0.42	0.23	0.10
Climate_WindSpeed150m_std_lag	0.13	-0.05	-0.10	-0.25	0.14	-0.18	0.08	0.62
Climate_WindSpeed200m_mean_lag	0.42	0.35	-0.32	-0.63	0.28	-0.43	0.23	0.11
Climate_WindSpeed200m_std_lag	0.13	-0.05	-0.10	-0.26	0.14	-0.18	0.09	0.60
DemographyIndirect_Population0to5_mean_lag	-0.21	0.11	-0.26	0.35	0.29	-0.07	-0.31	-0.04
DemographyIndirect_Population0to5_std_lag	-0.15	0.07	-0.19	0.25	0.13	-0.05	-0.15	-0.00
DemographyIndirect_Population65+_mean_lag	-0.14	0.18	-0.26	0.19	0.36	-0.13	-0.29	-0.02
DemographyIndirect_Population65+_std_lag	-0.09	0.13	-0.19	0.13	0.18	-0.10	-0.13	0.01
DemographyIndirect_PopulationDensity_mean_lag	-0.37	0.17	-0.05	0.39	-0.03	0.06	-0.15	-0.09
DemographyIndirect_PopulationDensity_std_lag	0.13	-0.09	0.08	-0.20	-0.00	-0.03	0.16	0.05
DemographyDirect_PopulationResident_majority_lag	-0.11	-0.12	0.07	-0.07	-0.15	0.62	-0.16	-0.04

DemographyDirect_PopulationResident_majority_lag	-0.11	-0.12	0.07	-0.07	-0.15	0.62	-0.16	-0.04
DemographyDirect_PopulationResident_majority_lag	-0.11	-0.12	0.07	-0.07	-0.15	0.62	-0.16	-0.04
DemographyDirect_PopulationResident_majority_lag	-0.11	-0.12	0.07	-0.07	-0.15	0.62	-0.16	-0.04
DemographyDirect_Citizen0to5yo_majority_lag	-0.11	-0.13	0.04	-0.03	-0.16	0.60	-0.14	-0.04
DemographyDirect_Citizen65+_majority_lag	-0.06	-0.09	0.05	-0.08	-0.13	0.50	-0.14	-0.03
DemographyDirect_CitizenNoEducationQualification_majority_lag	-0.14	-0.14	0.06	-0.03	-0.16	0.65	-0.16	-0.05
DemographyDirect_CitizenWithLowEducation_majority_lag	-0.09	-0.12	0.03	-0.07	-0.15	0.62	-0.16	-0.04
DemographyDirect_CitizenWithDegree_majority_lag	-0.13	-0.10	0.19	0.02	-0.12	0.42	-0.15	-0.05
DemographyDirect_CitizenEmployed_majority_lag	-0.12	-0.12	0.09	-0.04	-0.16	0.60	-0.17	-0.04
DemographyDirect_CitizenExtraEU_majority_lag	-0.05	-0.07	0.01	-0.06	-0.10	0.39	-0.08	-0.02
DemographyDirect_CitizenAlone_majority_lag	-0.06	-0.09	0.05	-0.05	-0.09	0.40	-0.10	-0.02
Morphology_Elevation_mean_lag	-0.43	-0.38	0.12	0.69	-0.17	0.47	-0.28	-0.09
Morphology_Elevation_std_lag	0.35	-0.11	-0.07	-0.39	0.55	-0.25	-0.08	0.14
Morphology_Slope_mean_lag	0.35	-0.09	-0.08	-0.39	0.57	-0.25	-0.11	0.12
Morphology_Slope_std_lag	0.29	-0.11	-0.06	-0.36	0.58	-0.23	-0.09	0.14
Morphology_Roughness_mean_lag	0.34	-0.09	-0.07	-0.38	0.58	-0.24	-0.11	0.12
Morphology_Roughness_std_lag	0.28	-0.11	-0.06	-0.35	0.58	-0.23	-0.09	0.15
Morphology_BuildingHeight_mean_lag	-0.17	0.48	-0.23	0.07	0.21	-0.18	-0.26	-0.05
Morphology_BuildingHeight_std_lag	-0.03	0.27	-0.31	0.08	0.28	-0.16	-0.26	-0.01
Morphology_BuiltUpRatio_UA_lag	-0.25	0.35	-0.13	0.28	0.10	0.02	-0.44	-0.09

Morphology_BuiltUpRatio_OSM_lag	-0.22	0.39	-0.10	0.18	0.10	-0.09	-0.31	-0.06
Morphology_BuiltUpRatio_Average_lag	-0.26	0.39	-0.13	0.26	0.11	-0.02	-0.42	-0.08
LandCover_ImperviousDensity_mean_lag	-0.37	0.37	-0.11	0.08	0.04	-0.15	0.21	-0.02
LandCover_ImperviousDensity_std_lag	0.40	-0.45	0.02	-0.06	0.01	0.11	-0.14	0.05
LandCover_TreeCoverDensity_mean_lag	0.28	-0.19	-0.00	-0.08	-0.02	0.05	-0.13	0.03
LandCover_TreeCoverDensity_std_lag	0.31	-0.24	-0.04	-0.06	-0.01	0.07	-0.15	0.04
LandCover_ShrubsRatio_mean_lag	0.04	-0.02	0.05	-0.03	-0.01	-0.02	-0.01	0.01
LandCover_ShrubsRatio_std_lag	0.06	-0.03	0.07	-0.04	-0.01	-0.03	-0.02	0.03
LandCover_GrasslandRatio_mean_lag	0.08	-0.06	0.12	-0.07	-0.04	-0.01	0.01	0.02
LandCover_GrasslandRatio_std_lag	0.11	-0.08	0.12	-0.10	-0.05	-0.00	0.01	0.04
LandCover_SurfaceWetnessCapacityRatio_mean_lag	0.01	-0.00	-0.00	-0.00	-0.00	-0.00	-0.00	-0.00
LandCover_SurfaceWetnessCapacityRatio_std_lag	0.01	-0.00	-0.00	-0.00	-0.00	-0.00	-0.00	-0.00
LandCover_SurfaceWaterCapacity_mean_lag	-0.01	-0.01	-0.00	0.03	-0.00	-0.00	-0.00	-0.00
LandCover_SurfaceWaterCapacity_std_lag	-0.01	-0.01	-0.00	0.03	-0.00	-0.01	-0.00	-0.00
LandUse_DistanceFromTransports_lag	-0.18	0.04	0.23	0.06	-0.13	0.08	0.04	-0.06
LandUse_DistanceFromServices_lag	-0.13	-0.12	0.74	-0.06	-0.08	0.03	0.00	-0.02
LandUse_DistanceFromEmergency_lag	-0.05	-0.12	0.52	-0.10	-0.07	0.06	0.03	0.01
LandUse_DistanceFromGreenAmenities_lag	-0.14	-0.09	0.65	-0.02	-0.09	-0.03	0.05	-0.02
LandUse_DistanceFromNonGreenAmenities_lag	-0.14	-0.10	0.67	-0.02	-0.08	-0.03	0.03	-0.02

Annex K (Chapter 7) – Optimization and ML algorithms comparison

This Annex contains information relating to the overall performance of all trained ML models. Additionally, in this context the performance of ML models is covered, whose training sets are composed by TOPSIS preferences (as shown in the Main text) and by VIKOR preferences (referred to as sensitivity test). This is done to ascertain the accuracy and robustness of the methodology in two phases, i.e. the optimization and the learning. In the training, the data is divided between:

i. Two canyon orientations (0°, 90°).

ii. Two MCDM scoring algorithms (TOPSIS, VIKOR).

And trained through five ML models: Linear Regression (LR), Kernel Ridge Regression (KRR), Random Forest (RF), Support Vector Regression (SVR), Multi-Layer Perceptron Regression (MLP).

The Annex is structured as follows:

i. K.1. Comparison of optimization algorithms.

ii. K.2. ML algorithm selection.

iii. K.3. Confront of R2 scores.

K.1. Comparison of optimization algorithms.

K.1.1. Optimization with VIKOR

First, the difference between choosing TOPSIS / VIKOR is quantified by selecting the most performing NBS for the ML training set. Each step done for TOPSIS in the main Chapter is emulated for VIKOR, starting with plotting all simulated solutions regarding their rankings and scores with VIKOR (Fig. K.1).

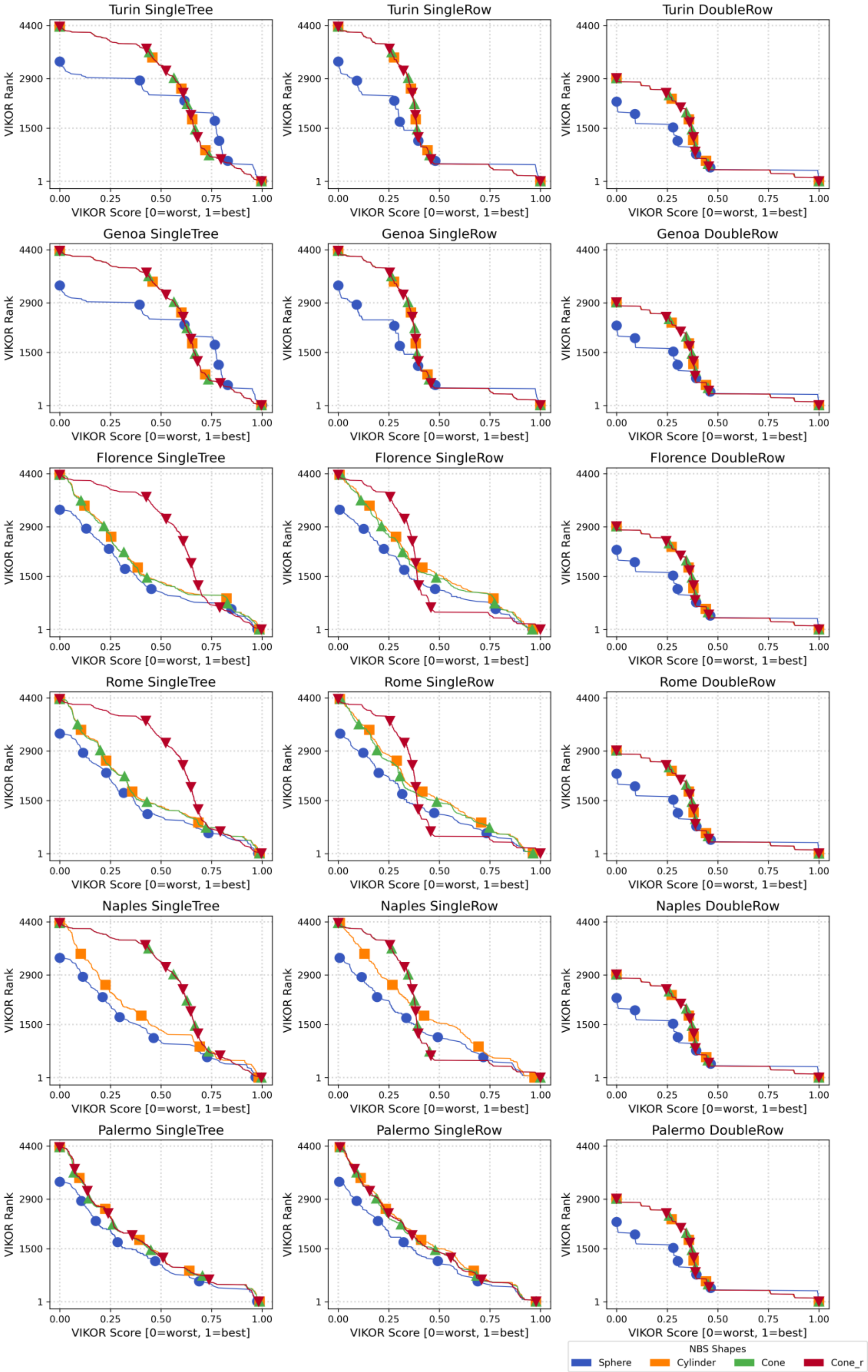

Figure K.1. NBS simulated data, divided in 72 scenarios of different city, NBS Shape (Sphere, Cylinder, Cone, Reversed cone), and NBS Type (Single Tree, Single Row, Double Row). A VIKOR Score of "1" is equal to the ideal solution, and a Rank of "1" is the highest ranking.

The VIKOR-based feature influence analysis reveals a performance structure that parallels the TOPSIS results but with notable inversions and attenuations consistent with VIKOR's compromise-oriented formulation (Figure K.2). Building Distance and Crown Radius display strong positive deviations at low values (Z ≈ +1.14 and +1.09, respectively), followed by a monotonic decline into negative territory as the feature increases, indicating that smaller distances and crown radii are favoured under VIKOR, opposite to the trend observed in TOPSIS. Conversely, Building Height and Crown Height transition from negative to positive Z-scores, suggesting that greater heights contribute more positively to the compromise solution. Several categorical variables exhibit pronounced contrasts: NBS Type shows a two-standard-deviation advantage for the "Single tree" category, while NBS Shape reverses the TOPSIS ordering, with "Cone Reversed" emerging as the strongest performer (Z ≈ +1.43). City Latitude also displays a widespread, ranging from –1.49 to +1.10, underscoring its sensitivity to the VIKOR aggregation. Compared to the TOPSIS results, the VIKOR curves redistribute influence across the feature space, emphasizing trade-offs rather than strict proximity to an ideal point.

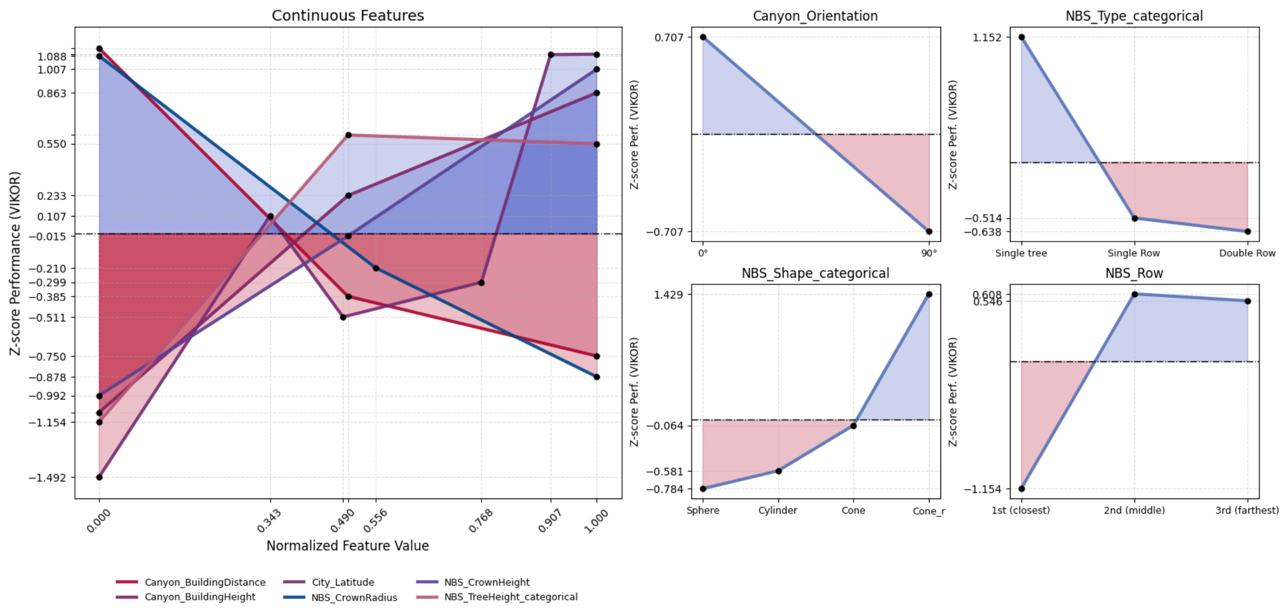

Figure K.2. Influencing factors trends over VIKOR-based standardized performance using the Z-Score. A Z-Score of 0 indicates average performance, while values around +1 or –1 reflect substantially better- or worse-than-average behaviour, respectively.

The differences between different canyon conditions are further analysed (Fig. K.3). Here, the main differences between this image and the result with TOPSIS is the higher values for Palermo in the narrowest canyons. In fact, with TOPSIS that configuration scored very low (< 0.5 both orientations). Additionally, the scores for all other configurations are higher than the TOPSIS equivalent.

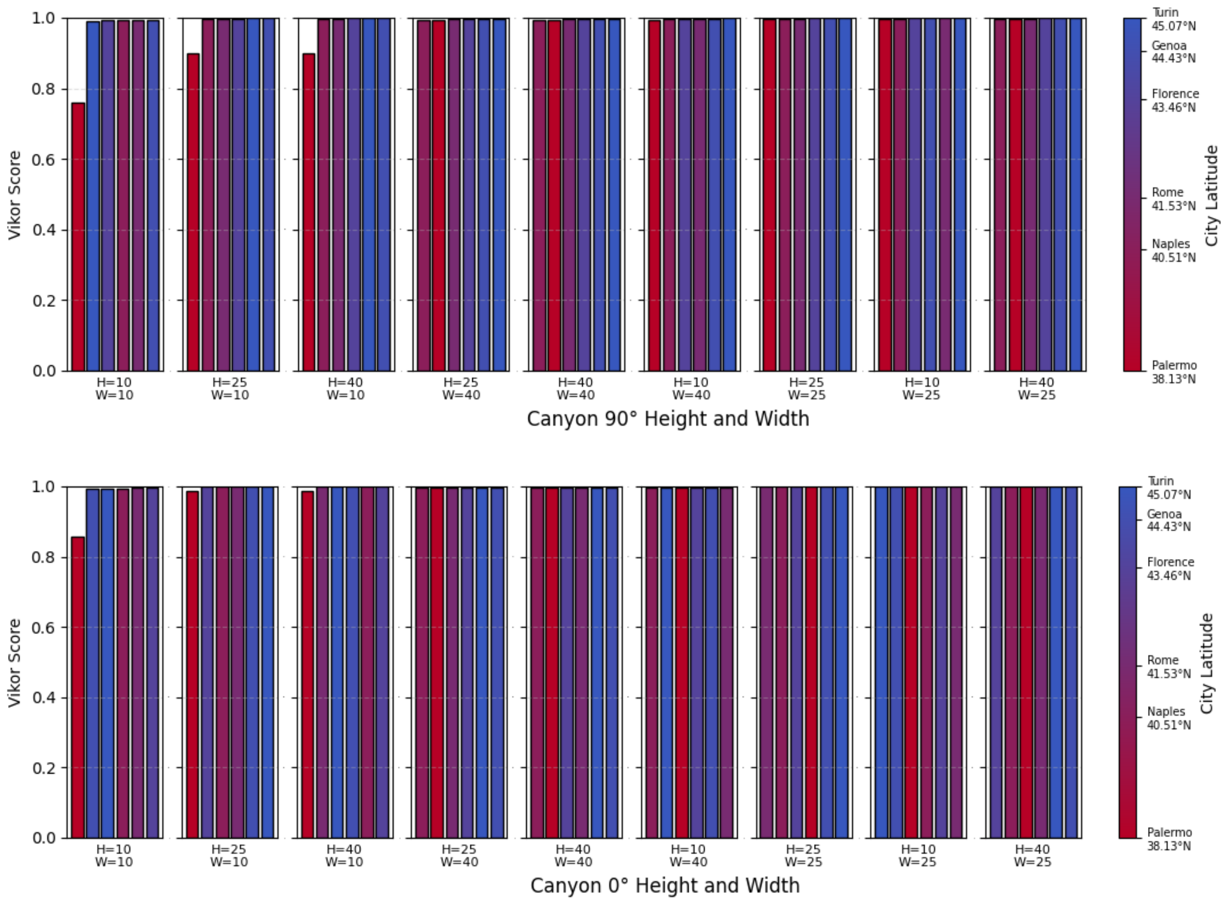

Fig. K.3. Bar graph of the best NBS from each canyon configuration data for each city. The upper Figure refers to canyons with 90° orientation, the lower Figure refers to canyons with 0° orientation.

K.2. ML algorithm selection

The quality of the different ML models is assessed by predicting a matrix consisting of n-combinations between canyon depths, heights, and city latitude, to determine the best NBS by TOPSIS value. Specifically, the variables are indicated as indicated in Table K.1. The mean value for the remaining variables is necessary to give a value for the X, since the models have been trained on all variables but here, we are only interested in predicting by the four variables.

Table K.1. Prediction array for evaluation of ML performance.

Variable	**Prediction array**
Canyon depth	[min(x), max(x), 10 steps]
Canyon height	
City latitude	
TOPSIS Score	
Street shading	mean(x)
Building shading	
Crown volume	
Trunk volume	

The following figures (Fig. K.4-K.27) plot the results into a 3D space as surfaces, each defined by different latitude. This criterion is repeated for the next sections (K.2.1-K.2.4), addressing different combinations of Canyon orientation (90°, 0°) and MCDM optimization (TOPSIS, VIKOR), in which for each the models were retrained.

K.2.1. ML Performance of TOPSIS optimized data / Canyons 90°

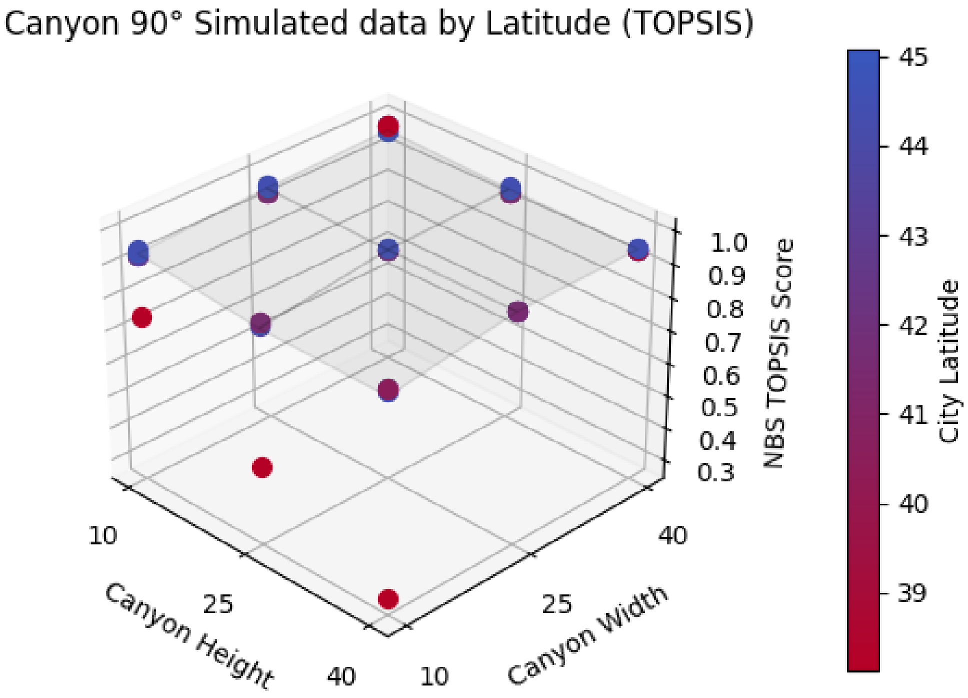

Fig. K.4. Simulated values for TOPSIS optimized data in canyons with 90° orientation, distributed by Canyon Height, Canyon Width, and TOPSIS Score.

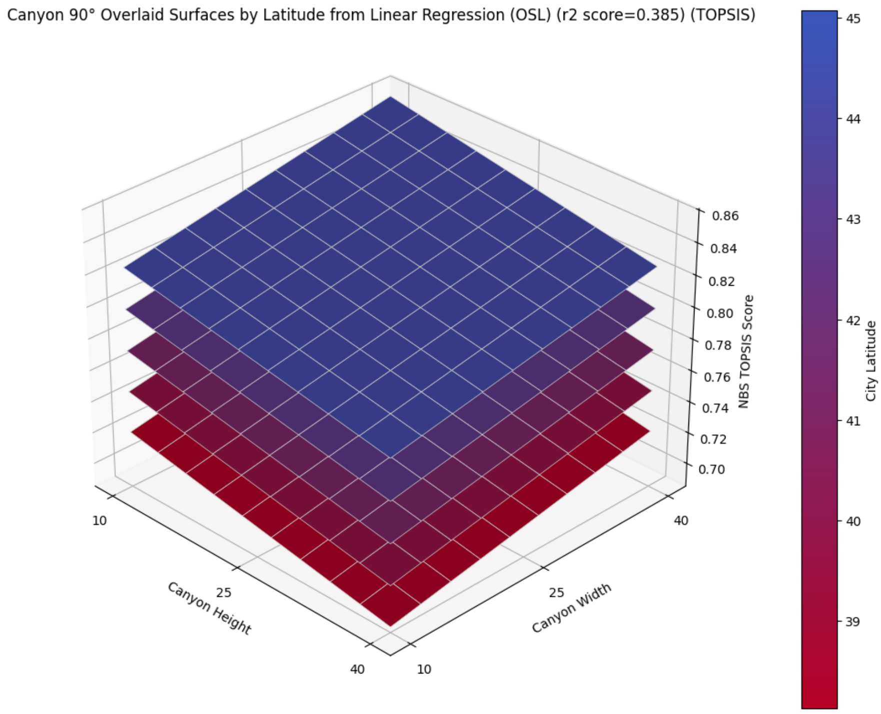

Fig. K.5. Predicted values for TOPSIS optimized data in canyons with 90° orientation with Linear Regression ML model, achieving R^2 Score = 0.385.

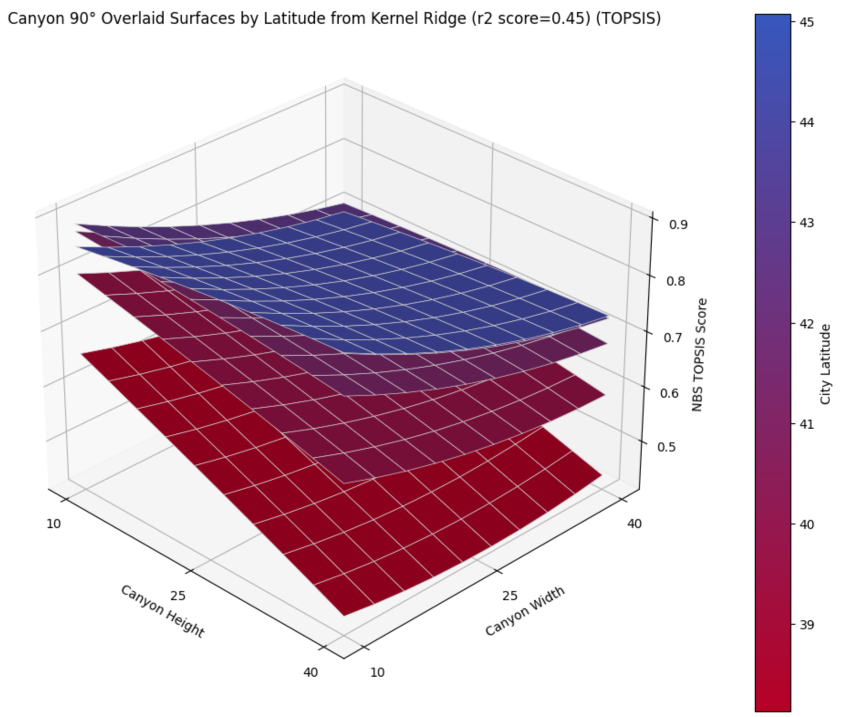

Fig. K.6. Predicted values for TOPSIS optimized data in canyons with 90° orientation with Kernel Ridge Regression ML model, achieving R^2 Score = 0.450.

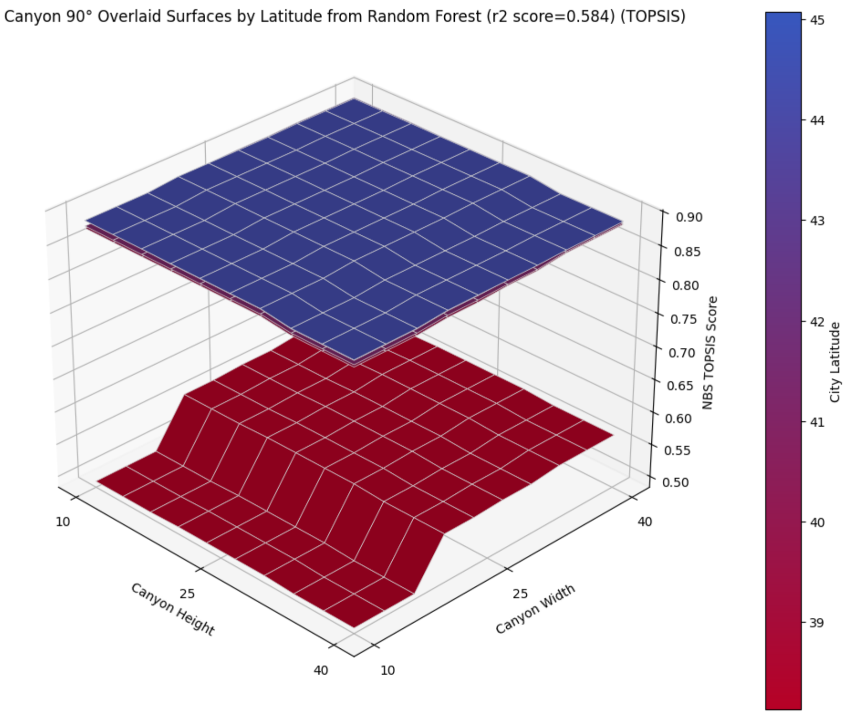

Fig. K.7. Predicted values for TOPSIS optimized data in canyons with 90° orientation with Random Forest Regression ML model, achieving R^2 Score = 0.584.

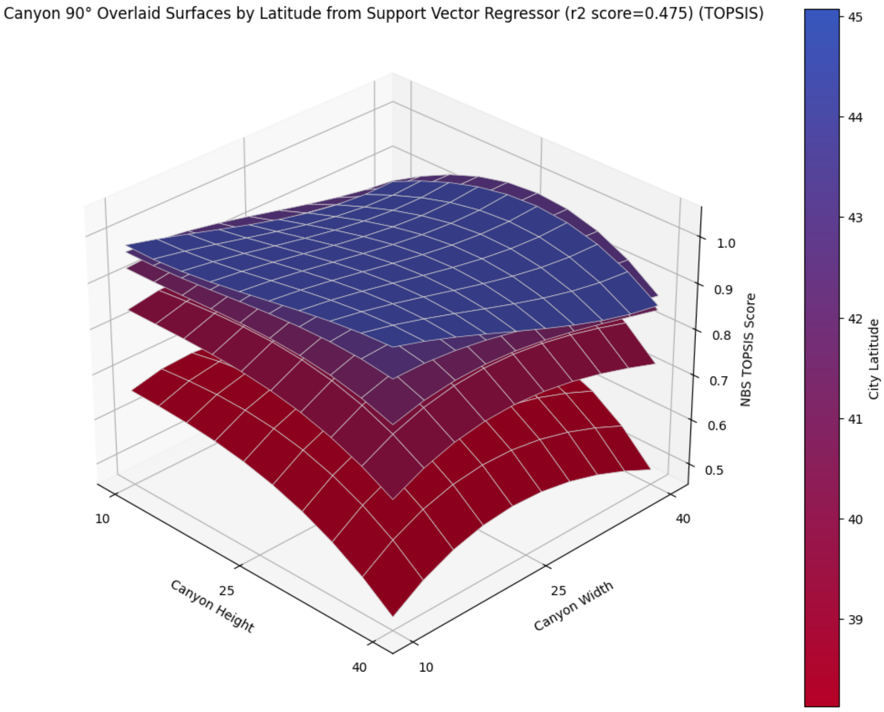

Fig. K.8. Predicted values for TOPSIS optimized data in canyons with 90° orientation with Support Vector Regression ML model, achieving R^2 Score = 0.475.

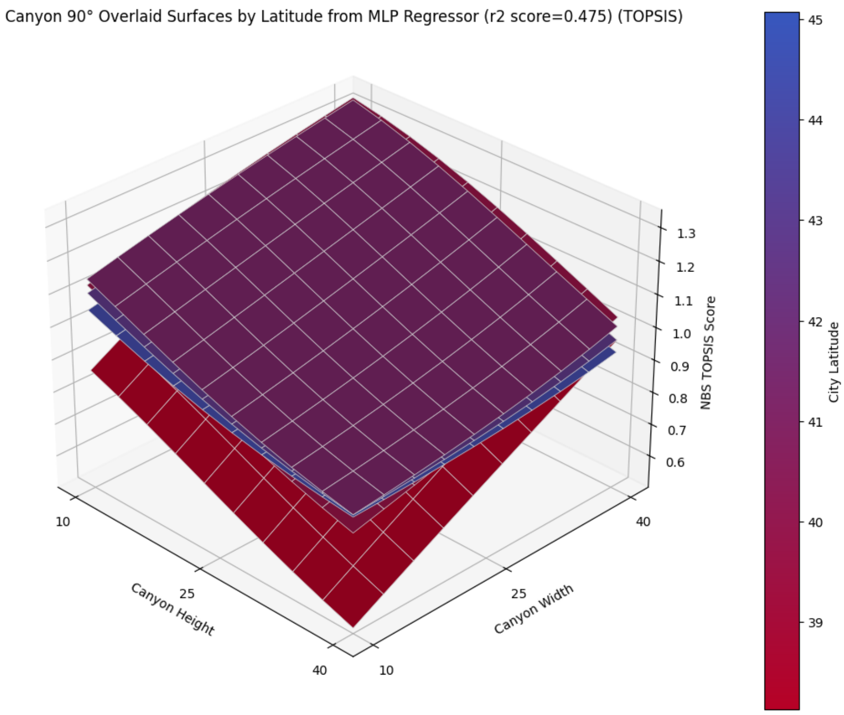

Fig. K.9. Predicted values for TOPSIS optimized data in canyons with 90° orientation with MLP Regression ML model, achieving R^2 Score = 0.475.

K.2.2. ML Performance of TOPSIS optimized data / Canyons 0°

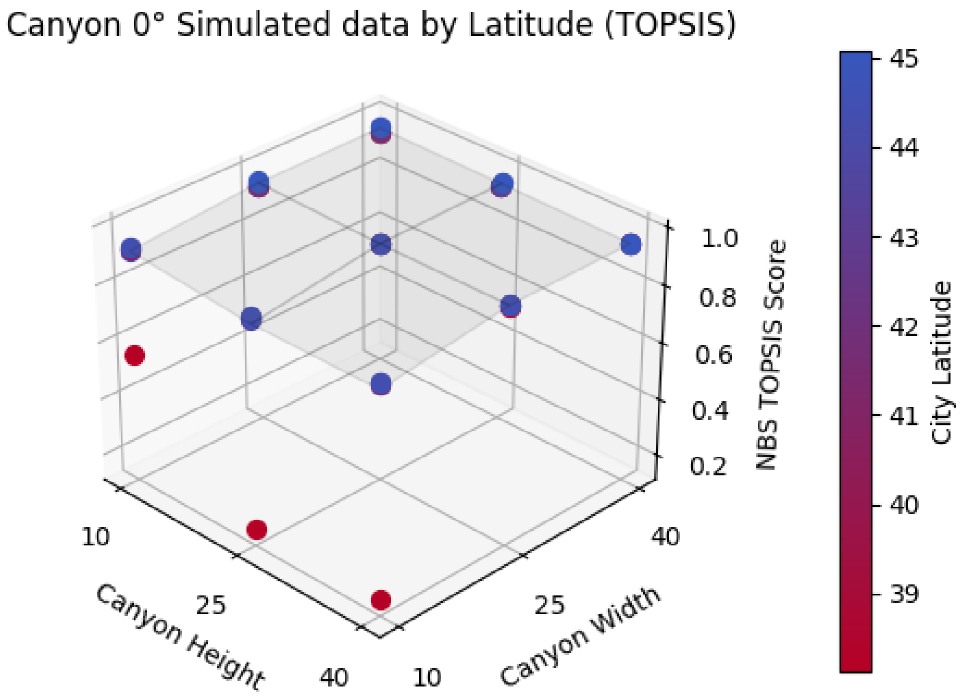

Fig. K.10. Simulated values for TOPSIS optimized data in canyons with 0° orientation, distributed by Canyon Height, Canyon Width, and TOPSIS Score.

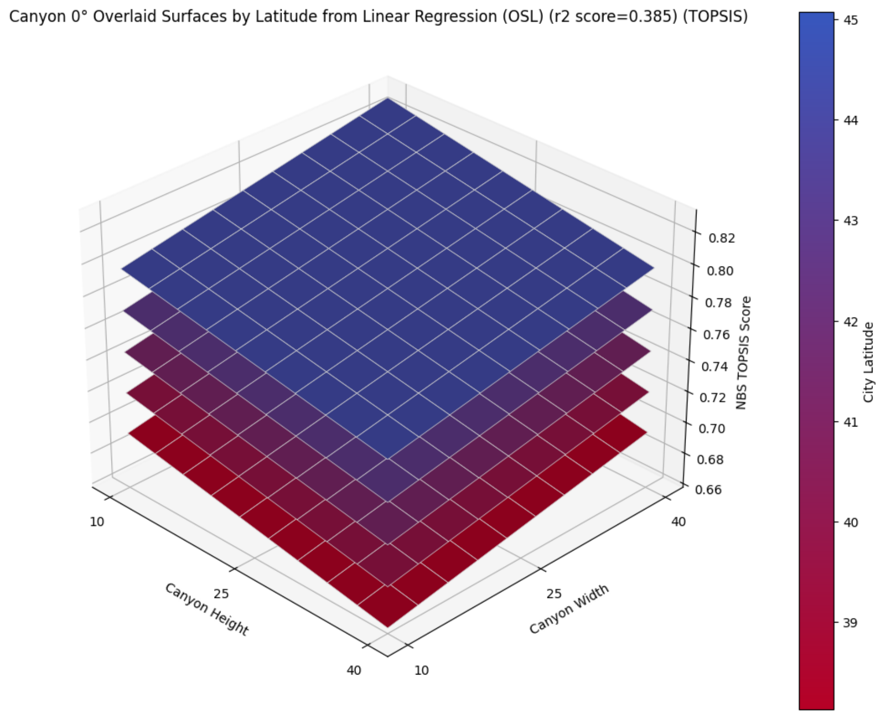

Fig. K.11. Predicted values for TOPSIS optimized data in canyons with 0° orientation with Linear Regression ML model, achieving R^2 Score = 0.385.

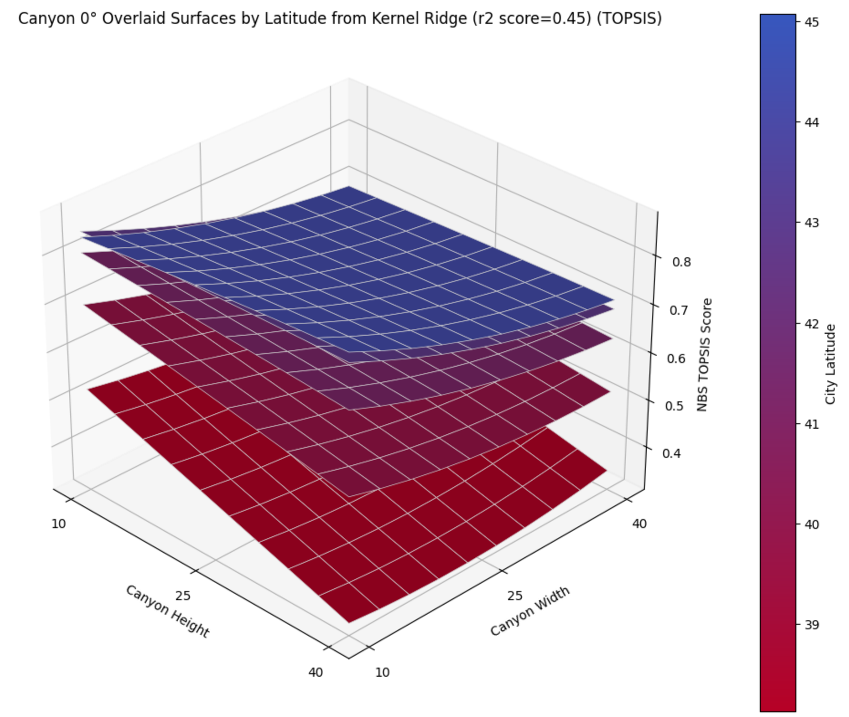

Fig. K.12. Predicted values for TOPSIS optimized data in canyons with 0° orientation with Kernel Ridge Regression ML model, achieving R^2 Score = 0.450.

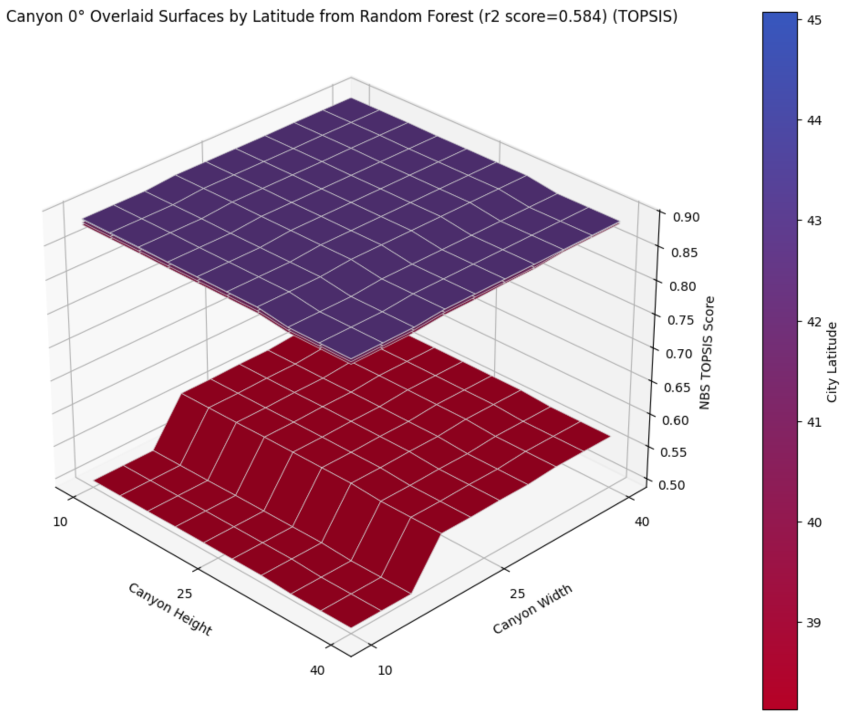

Fig. K.13. Predicted values for TOPSIS optimized data in canyons with 0° orientation with Random Forest Regression ML model, achieving R^2 Score = 0.584.

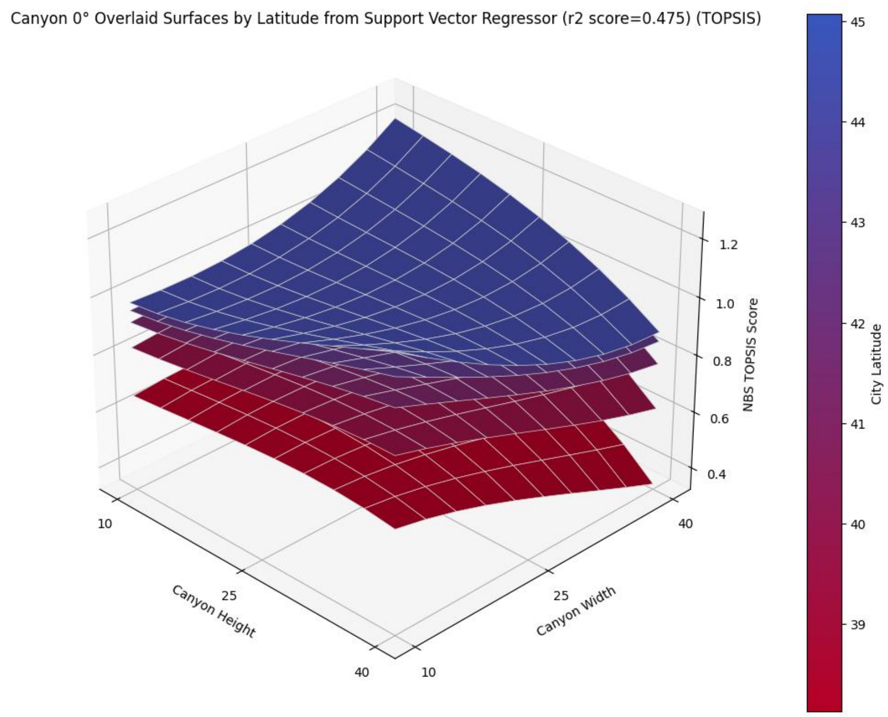

Fig. K.14. Predicted values for TOPSIS optimized data in canyons with 0° orientation with Support Vector Regression ML model, achieving R^2 Score = 0.475.

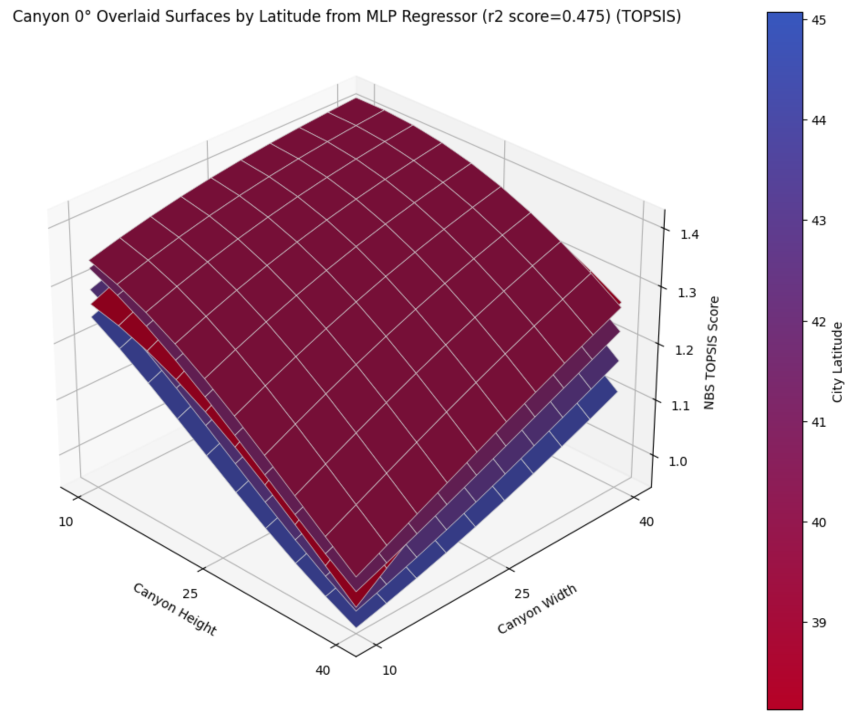

Fig. K.15. Predicted values for TOPSIS optimized data in canyons with 0° orientation with MLP Regression ML model, achieving R^2 Score = 0.475.

K.2.3. Performance of VIKOR optimized data / Canyons 90°

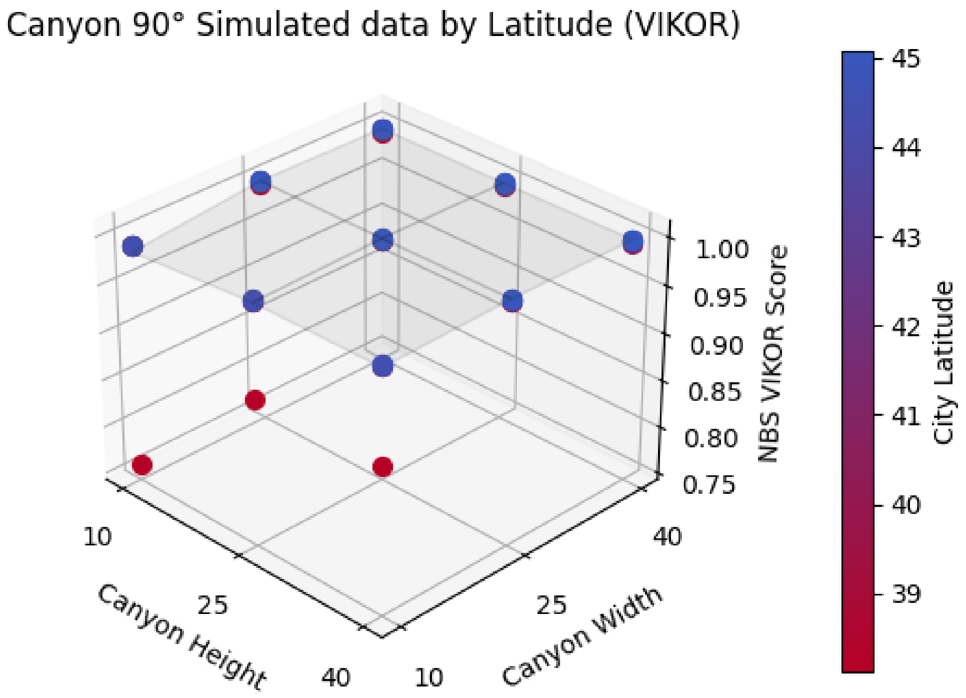

Fig. K.16. Simulated values for VIKOR optimized data in canyons with 90° orientation, distributed by Canyon Height, Canyon Width, and TOPSIS Score.

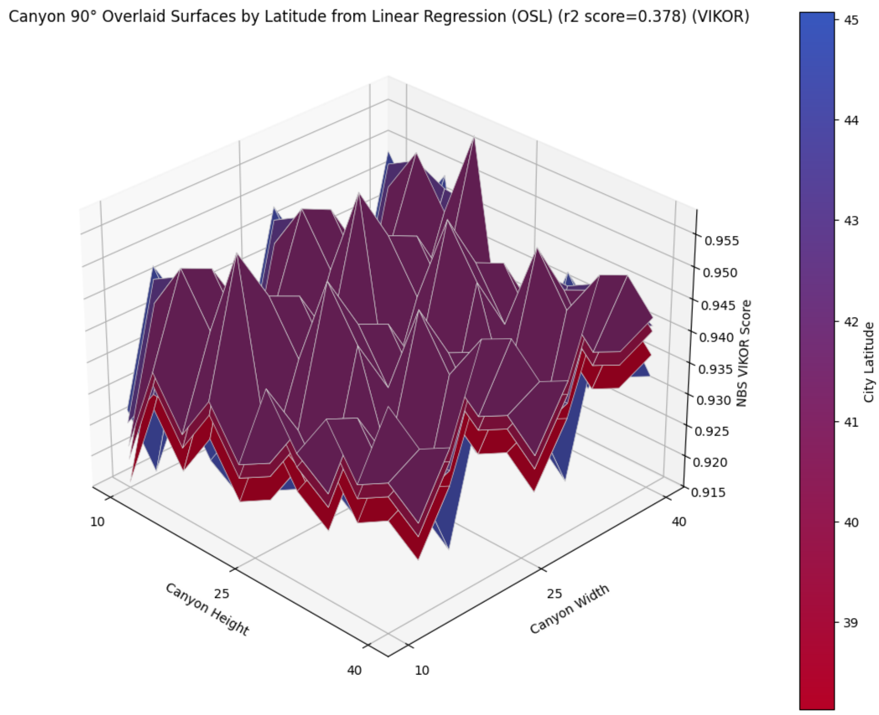

Fig. K.17. Predicted values for VIKOR optimized data in canyons with 90° orientation with Linear Regression ML model, achieving R^2 Score = 0.378.

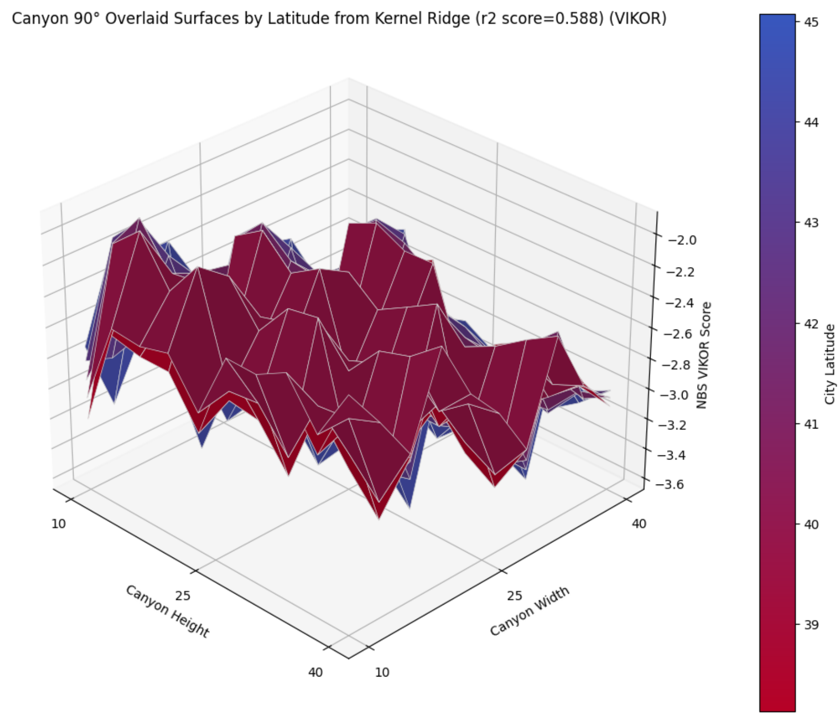

Fig. K.18. Predicted values for VIKOR optimized data in canyons with 90° orientation with Kernel Ridge Regression ML model, achieving R^2 Score = 0.588.

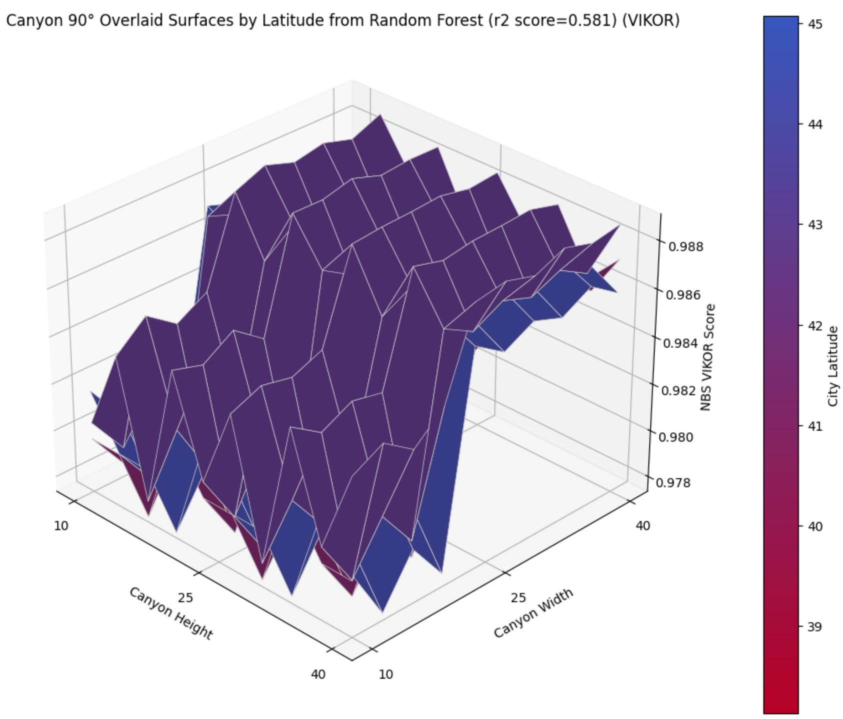

Fig. K.19. Predicted values for VIKOR optimized data in canyons with 90° orientation with Random Forest Regression ML model, achieving R^2 Score = 0.581.

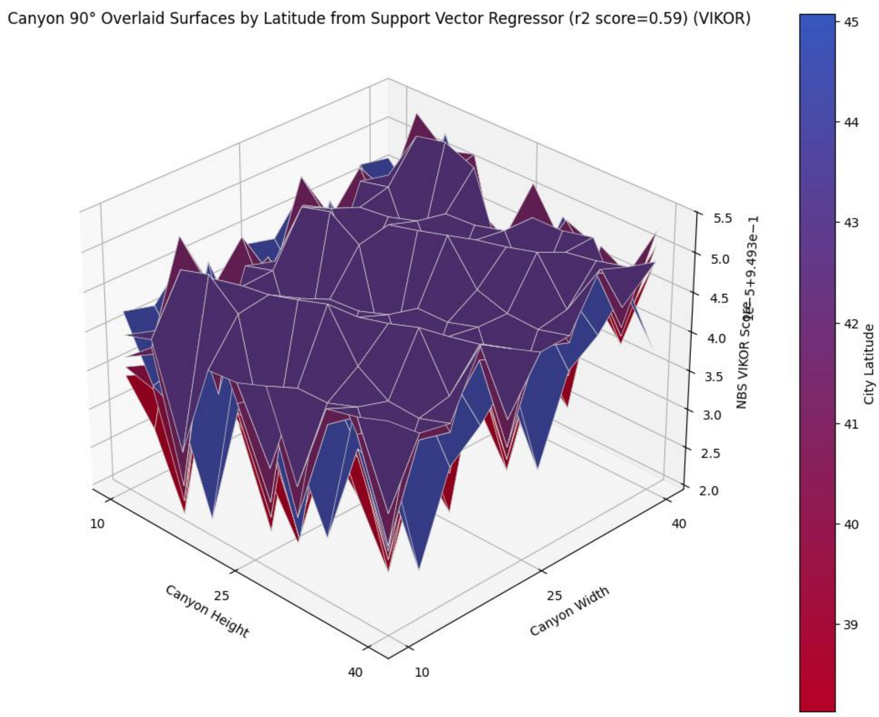

Fig. K.20. Predicted values for VIKOR optimized data in canyons with 90° orientation with Support Vector Regression ML model, achieving R^2 Score = 0.590.

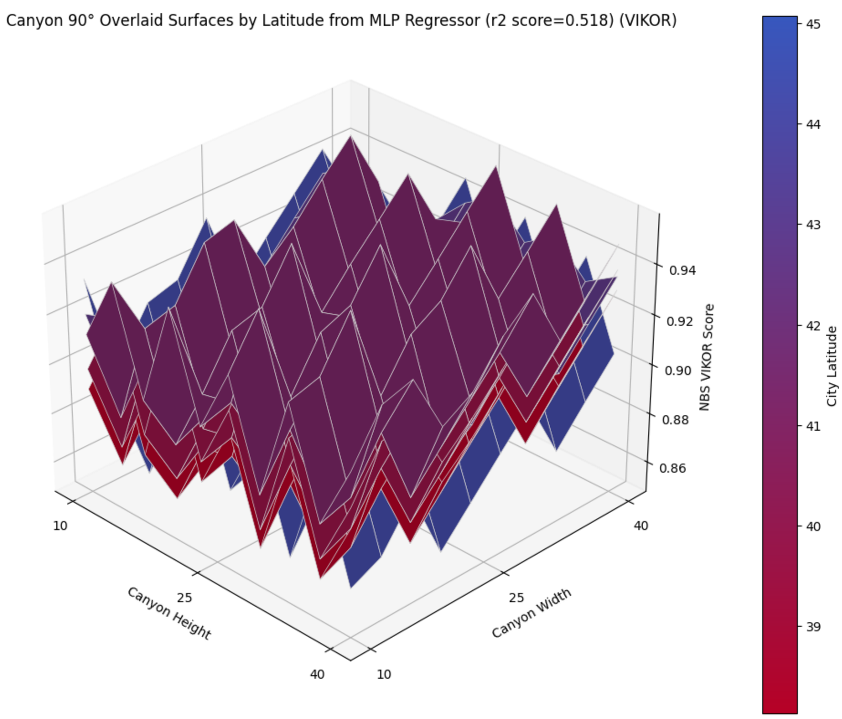

Figure K.21. Predicted values for VIKOR optimized data in canyons with 90° orientation with MLP Regression ML model, achieving R^2 Score = 0.518.

K.2.4. Performance of VIKOR optimized data / Canyons 0°

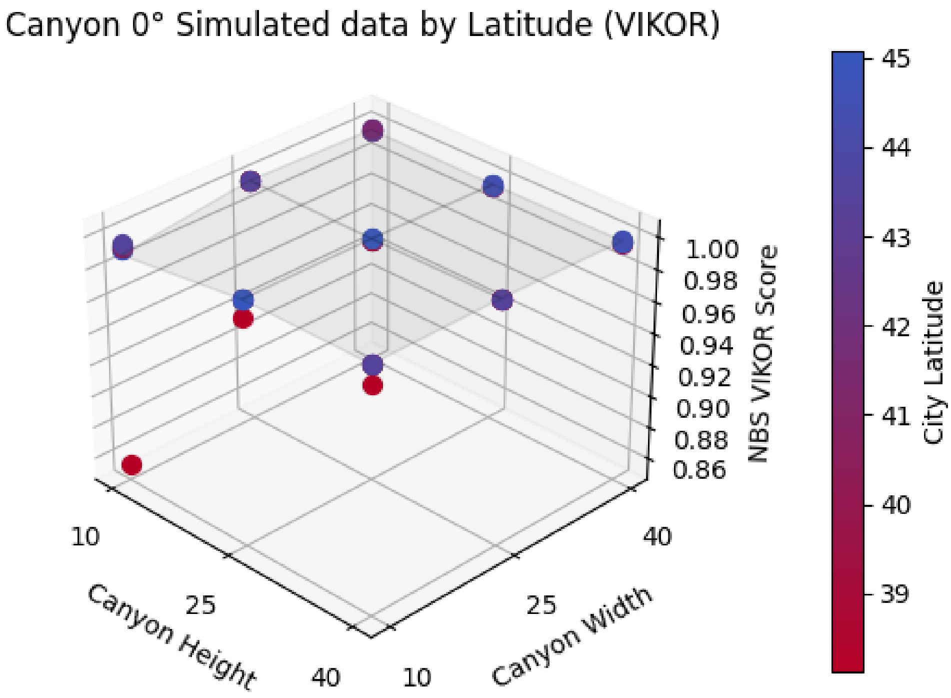

Fig. K.22. Simulated values for VIKOR optimized data in canyons with 0° orientation, distributed by Canyon Height, Canyon Width, and TOPSIS Score.

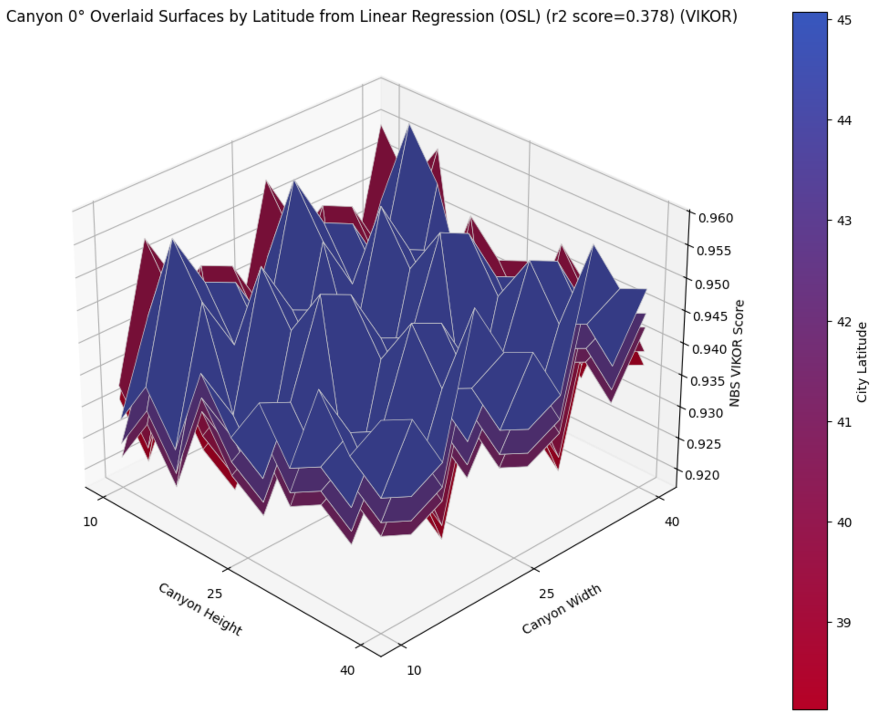

Fig. K.23. Predicted values for VIKOR optimized data in canyons with 0° orientation with Linear Regression ML model, achieving R^2 Score = 0.378.

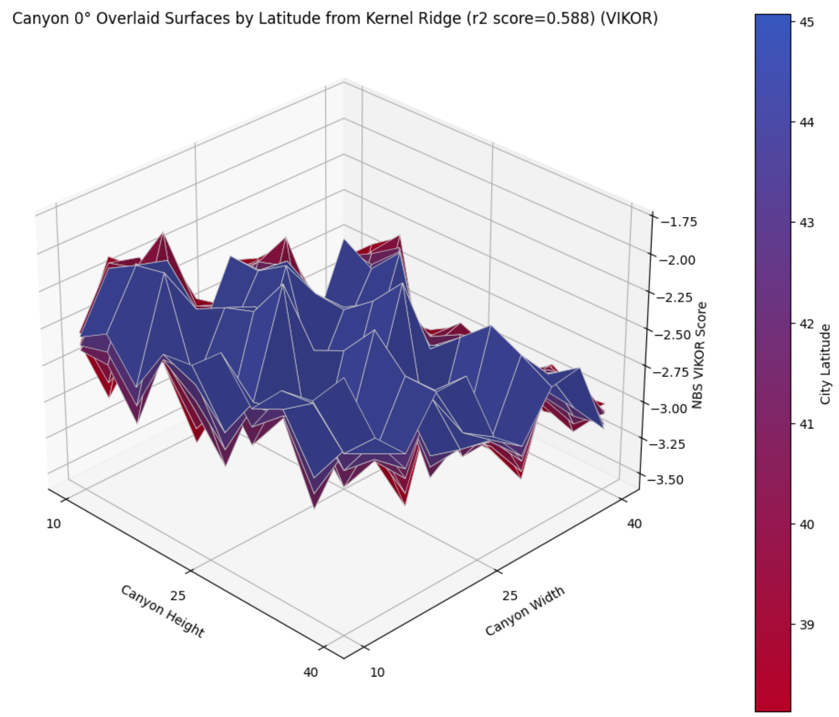

Fig. K.24. Predicted values for VIKOR optimized data in canyons with 0° orientation with Kernel Ridge Regression ML model, achieving R^2 Score = 0.588.

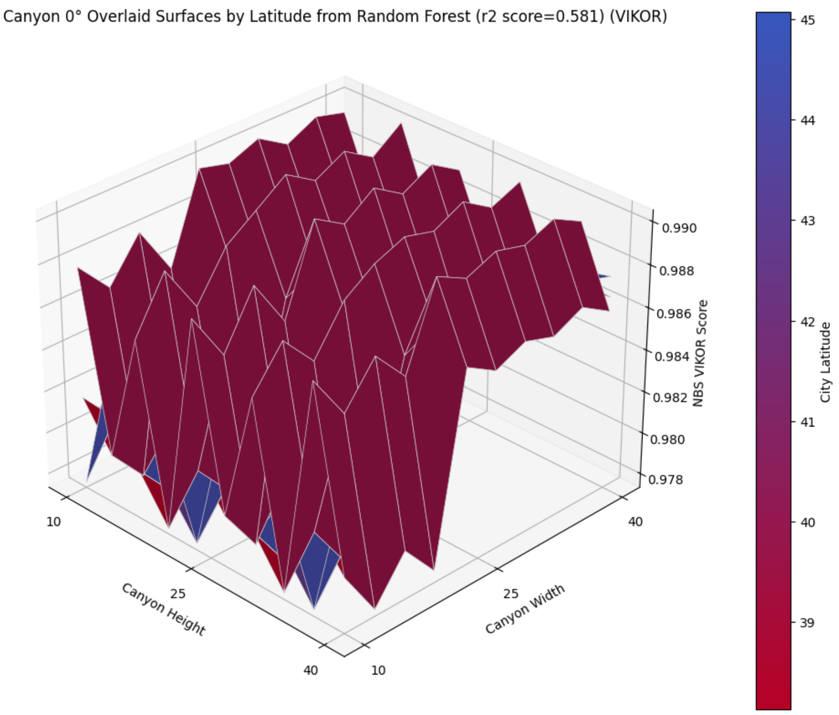

Fig. K.25. Predicted values for VIKOR optimized data in canyons with 0° orientation with Random Forest Regression ML model, achieving R^2 Score = 0.581.

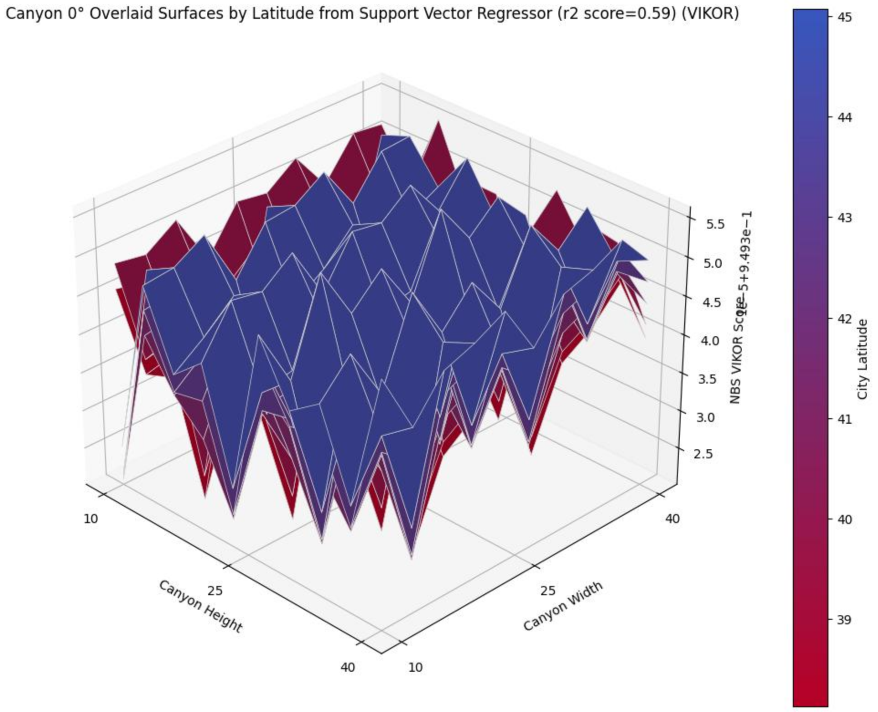

Fig. K.26. Predicted values for VIKOR optimized data in canyons with 0° orientation with Support Vector Regression ML model, achieving R^2 Score = 0.590.

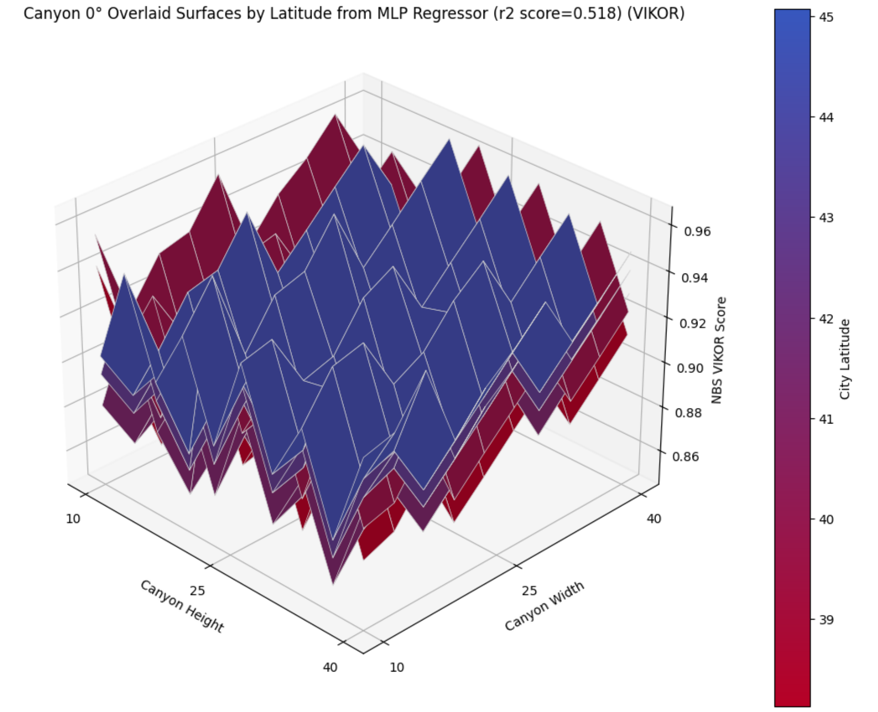

Figure K.27. Predicted values for VIKOR optimized data in canyons with 0° orientation with MLP Regression ML model, achieving R^2 Score = 0.518.

K.3. Confront of R2 scores

The performance of all ML models is confronted by using the testing set as threshold, for both TOPSIS (Fig. K.28) and VIKOR (Fig. K.29) including both Canyon orientations. With this assessment it is possible to compare and discuss the overall performance of the models and choose, considering the previous distributions and their scores. Notably, the scores are sensitive to the limited sample size, evidencing from the fact that higher scores were obtained during the hyperparameter optimization phase due to the k-folding procedure. A higher testing (and prediction) sets may yield to less discrepancies.

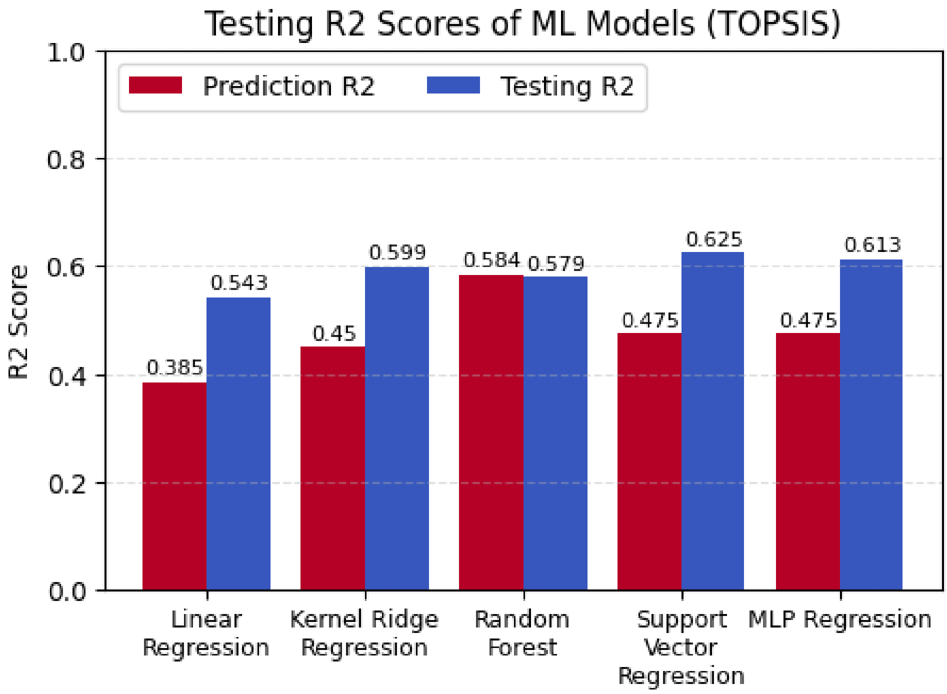

Figure K.28. Comparison of R^2 scores between the Prediction sets (in red) and Testing sets (in blue) trained using TOPSIS scores. A higher value of R^2 corresponds to a higher degree of robustness of the ML model. A closer difference between Prediction and Testing R^2 signifies relative accuracy for each specific model.

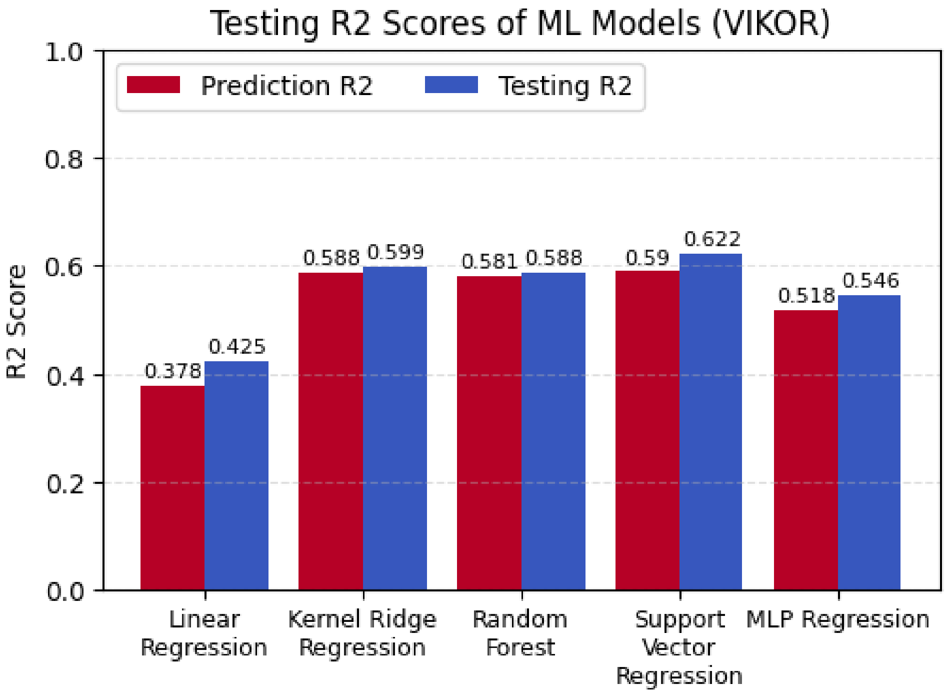

Figure K.29. Comparison of R^2 scores between the Prediction sets (in red) and Testing sets (in blue) trained using VIKOR scores. A higher value of R^2 corresponds to a higher degree of robustness of the ML model. A closer difference between Prediction and Testing R^2 signifies relative accuracy for each specific model.